THE DEACTIVATION OF ZEOLITE-Y AND MORDENITE DURING HEXANE CRACKING AND PROPENE OLIGOMERISATION

BY

Klaus Peter Möller
BSc(Chem. Eng.) (Cape Town)

Submitted to the University of Cape Town in fulfilment of the requirements for the degree of

Doctor of Philosophy

Department of Chemical Engineering
University of Cape Town
Rondebosch
Cape Town
South Africa

MT 660 MOEL
89/11/95

Acknowledgements

I would like to thank my supervisors, Dr Masami Kojima and Professor Cyril T. O'Connor for their guidance, encouragement and friendship over the years. A special thanks to Dr Masami Kojima for her assistance with some of the mathematics.

I would also like to thank staff members, members of the catalysis research group and postgraduate students for their assistance and friendship through the duration of this work.

I wish to thank Messrs E.W. Randall and G. de la Cruz for their assistance and helpfulness with the computing and electronics.

All the technical staff, Messrs A. Barker, R. Senekal, K. Wheeler and J. Daniels of the Chemical Engineering workshop, as well as other departmental assistants for their friendship and assistance.

The following people and institutions are also acknowledged:

SASOL and the CSIR for financial and technical assistance, in particular Dr B.M. van Vliet of the CSIR for the porosimetry analyses and J. Vink of the CSIR for the BET analyses.

Norton International Inc. (USA) for supplying H-Mordenite.

To my parents, Jutta and Rudolf,
and special friends, Sarah and Dianne

SUMMARY

The objective of this study was to determine the effect that the type of catalyst and reaction would have on the rate of deactivation, properties of coke and transport properties of the catalyst. HY and HM were chosen because of their different pore structures and acid site distributions. Hexane cracking at 1 atmosphere and high pressure propene oligomerisation provided two different reaction types. The transport properties of the catalysts were compared by measuring adsorption and diffusion using the GC technique with ancillary information obtained from ammonia TPD, mercury porosimetry and BET surface area measurements.

It was confirmed that a knowledge of the crystallite size distribution was necessary to predict the adsorption and diffusion of light hydrocarbons in HY and HM. The adsorption constants and heats of sorption were found to be much greater in HM than in HY, in agreement with the presence of a greater number of strong acid sites detected in HM by ammonia TPD. The diffusivities of the light hydrocarbons were too large to measure in HY. In HM only methane diffusion was too fast to measure. Diffusivities decreased and adsorption constant increased with increasing molecular size.

HY had greater activity and slower deactivation than HM towards hexane cracking. The reaction as well as coking took place in the micro-pores. The graphitic coke content of HY was much greater than in HM. The introduction of the macro-pore adsorption term was necessary to predict diffusion in coked samples, emphasizing the severity of the diffusional resistance. While hydrocarbon diffusivities decreased after cracking, adsorption constants were found to increase in the presence of graphitic coke in HY. In HM the deactivation took place primarily by pore blockage, with strong acid sites being preferentially removed. Both diffusivities and adsorption constants decreased in the presence of coke in HM.

In HY and HM deactivated by oligomerisation, macro-pore adsorption had to be taken into account, again emphasizing the severe diffusional resistance. Reaction as well as graphitic coke occurred predominantly in the micro-pores in HY. High boiling point hydrocarbons were able to migrate into the meso-pores where they closed the mouths of the micro-pores in HY. Strongly adsorbed high boiling point hydrocarbons which deactivated the catalyst presented far less diffusional resistance in HY than the equivalent mass of graphitic coke. These high boiling point hydrocarbons also markedly lowered the adsorption constants. Graphitic coke was responsible for the

modification of the catalyst selectivity. Temperature runaway in HY caused severe coking and hence deactivation. The inactivity of HM below 200°C was caused by strong adsorption and high diffusional resistance of reactant and product. Pore blockage was the dominant deactivation mechanism in HM, while in HY it was partial pore blockage by graphitic coke and pore mouth closure by high boiling point hydrocarbons. It was possible to restore the activity of HY for oligomerisation by flushing the high boiling point hydrocarbons in flowing nitrogen.

TABLE OF CONTENTS

List of Tables

LIST OF FIGURES

NOMENCLATURE FOR CHAPTER 5

A_m	defined by equation 5.42	
B	defined by equation 5.27	
C	concentration	mol/cm^3
C	defined by equation 5.28	
C_x	concentration in the micro-pores	mol/cm^3
C_y	concentration in the macro-pores	mol/cm^3
C_z	concentration in the column	mol/cm^3
D	defined by equation 5.29	
D	dispersion number in a blank column	cm^2/s
D_c	micro-pore diffusivity	cm^2/s
D_{co}	pre-exponential factor, equation 5.48	
D_m	molecular diffusion	cm^2/s
d_p	diameter of catalyst particle	cm
d_t	diameter of column	cm
D_x	two phase model diffusivity in micro-pores	cm^2/s
D_y	macro-pore diffusivity	cm^2/s
D_z	axial dispersion coefficient	cm^2/s
E^*	dimensionless residence time distribution function	
E_{Dc}	diffusional activation energy for micro-pore diffusion	kJ/mol
E_{Kc}	heat of sorption in the micro-particles	kJ/mol
E_{Ky}	heat of sorption in the macro-pores	kJ/mol
error	defined by equation 5.35	
G	defined by equation 5.5	
H	defined by equation 5.9	
HETP	height equivalent of a theoreical plate, equation 5.38	cm
Im(ω)	imaginery part of Fourier transformed response curve, equation 5.34	
k_a	adsorption rate constant	cm/s
K_c	micro-pore adsorption constant	
K_{co}	pre-exponential factor, equation 5.47	
K_f	gas film mass transfer coefficient	cm/s
K_x	two phase model micro-pores adsorption constant	
K_y	macro-pore adsorption constant	
K_{yo}	pre-exponential factor, equation 5.46	
L	bed length	cm

N_1	dimensionless parameter, equation 5.20	
N_2	dimensionless parameter, equation 5.21	
N_3	dimensionless parameter, equation 5.22	
N_4	dimensionless parameter, equation 5.23	
$p(R_x)$	crystallite size distribution on a number basis equation 5.18	
P_0	dummy parameter, initial value	
P_1	dummy parameter, current value	
Pe	Péclet number	
R	universal gas constant	J/gmol/K
Re	Reynolds number	
$Re(\omega)$	real part of Fourier transformed response curve, equation 5.33	
RTD	residence time distribution curve	
R_x	crystallite radius	cm
$\overline{R_x^3}$	$\exp(3\mu + 9\sigma^2/2)$	cm^3
R_y	catalyst particle radius	cm
s	Laplace transform variable	
Sc	Schmidt number	
T	temperature	K
t	time	s
t^*	dimensionless time, t/τ	
v	superficial carrier gas velocity	cm/s
V	volume	cm^3
W	defined by equation 5.17	
x	radial distance from centre of crystallite particle	cm
X_{opt}	defined by equation 5.37	
y	radial distance from centre of catalyst particle	cm
z	axial distance from column entrance	cm

Subscripts

exp	experimental data
model	model data
pulse	reference to injection pulse
system	reference to packed column
x	micro-particle quantity
y	catalyst particle quantity
z	column quantity

Greek letters

α	defined by equations 5.16 and 5.40	
α'	defined by equation 5.43	
β	defined by equations 5.15 and 5.40	
β'	defined by equation 5.44	
$s\gamma$	defined by equations 5.14 and 5.40	
γ'	defined by equation 5.45	
$\delta(t)$	Dirac delta function	
θ_x	micro-pore porosity (cm^3 micro-pores / cm^3 crystallite)	
θ_y	macro-pore porosity (cm^3 macro-pores / cm^3 catalyst particle)	
θ_z	bed porosity (cm^3 voids / cm^3 bed)	
μ	parameter in crystallite size distribution function, equation 5.18	
μ^*	dimensionless mean of RTD curve, equation 5.30	
σ	parameter in crystallite size distribution function, equation 5.18	
σ^*	dimensionless variance of RTD curve, equation 5.31	
τ	bed residence time, L/v	s
ω	frequency	s^{-1}

1. INTRODUCTION

1.1 Deactivation of catalysts due to the formation of coke

Observations of important chemical processes (e.g., cracking, hydrotreatment, reforming, hydrogenation) have shown that coke formation in acid catalysis depends on the amount, nature and strength of acidity, type of chemical reaction, on the structure of the catalyst, type of reactor used and reaction conditions. Good reviews have been given on deactivation with reference to experimental data and modelling by Butt (1978) and Trimm (1982), the latter concentrating on supported metal catalysts. Froment (1976, 1980, 1982) reviewed the rigorous "coke on catalyst" approach to modelling of catalyst deactivation and its application to reactor design.

In this section the factors which affect coke formation, the mode of deactivation and the nature of coke will be briefly discussed.

1.1.1 Factors which affect the formation of coke

The factors which affect the formation of coke in acid catalysis - pore structure, catalyst acidity, nature of the reactants and the reaction conditions - are considered in this section, with a particular emphasis on zeolites as catalysts.

1.1.1.1 Pore structure

It was postulated by Rollmann (1977) that the ease of coke formation was an intrinsic property of the zeolite, whereby the formation of the coke and its precursors are inhibited by the spatial restrictions of the small pores in zeolites. This was expected in view of the size of the bulky polyalkylaromatics which are known to be the coke precursors. Rollmann and Walsh (1979) obtained a correlation between coking tendency and shape selectivity of a large number of zeolite samples differing in structure, composition and crystal size, and hence were able to substantiate the above postulate. However, effects of crystal size and catalyst acidity could not be wholly neglected.

Dejaifve et al. (1981) observed the deactivation of HZSM-5, H-mordenite (HM) and H-offretite (HO) during the methanol conversion and found that coking and ageing depended on pore size and on the nature of the channel network. Intracrystalline coking was observed on HM (one dimensional) and HO (two dimensional) with associated pore blockage, while ZSM-5 appeared to produce little coke in the intracrystalline volume but rather on the outside of the crystallites causing very slow deactivation. These workers proposed that in the case of ZSM-5 large coke precursors had to migrate to the outside before they could be transformed into coke due to pore restrictions.

Langner (1982) found for methanol conversion over zeolites of varying pore structures that the rate of deactivation increased in the order HZSM-5 < NaH-Y < H-T < H-L, while the amount of coke increased as HZSM-5 < H-T < H-L < NaH-Y. These findings illustrate the tendency of large pore zeolite for rapid coke formation. The amount of coke deposited suggested that in small pore zeolites the reaction took place primarily on the exterior surface and the small channels were easily blocked even when little coke was deposited. Large pore volumes increased lifetime by being able to accommodate more coke. Langner reported that oligoaromatics were not formed in the pores of ZSM-5 because of steric hindrance, thereby reducing coking. However, pore blockage was observed with all the zeolites.

A more recent study by Magnoux et al. (1987b) of heptane cracking over HY, HZSM-5 and HM showed that large pores underwent partial pore blockage making sites inaccessible to the reactant. In the case of HZSM-5, in disagreement with the findings of Dejaifve et al. (1981), coke molecules formed at the channel intersections at low coke content and pore blockage occurred on the external surface at higher coke contents. HM on the other hand, due to its one-dimensional structure, underwent pore blockage at low coke content.

1.1.1.2 Acidity of the catalyst

It would be expected that the increase in number and strength of the acid sites would increase the rate of coke formation. Walsh and Rollmann (1977) showed that the contribution of aromatic reactant to coking increased to a limiting value as the Al content (giving rise to acidity) increased. Eisenbach and Gallei (1979) found that for HY the highest coking activity was shown by the OH groups in the supercages corresponding to strong acid sites

and the external OH groups had very low activity below 300°C. Other workers, Itoh et al. (1984), Kubelkova et al. (1985) and Karge et al. (1984) have also found that the coking activity was dependent on the strong acid sites and the Si/Al ratio.

Langner and Meyer (1980) found that for the reaction of butadiene over NH_4Y coke formation was a strong function of calcination temperature with a maximum at 450°C which showed that both Lewis sites and Bronsted sites participated in the coking reaction. They postulated that cyclic compounds were first produced by Diels-Alder addition on Lewis sites which then underwent hydride transfer reaction on Bronsted sites to produce more cyclic double bonds for Diels-Alder additions forming an autocatalytic cycle, increasing the rate of coke formation. The maximum was observed because increased diffusional resistance due to coke would slow down autocatalysis. Similar observations but different mechanisms were proposed by Blackmond et al. (1982) who found that coke formation was linearly proportional to the consumption of Bronsted acid hydroxyl groups, and that the interaction of these sites with Lewis sites was also important for partially dehydroxylated catalyst. A dual site mechanism was proposed in which the active sites of the dehydroxylated sample were produced through the inductive effect of the Lewis sites on the few remaining supercage hydroxyl groups.

Dejaifve et al. (1981) found that coking poisoned strong and medium acid sites in HZSM-5, but variation in acid concentration could not explain their data as the initial coking rates per acid site in HZSM-5, offretite, HM were all the same. They suggested that coke precursors formed everywhere in the intracrystalline voids. McLellan et al. (1986) found by means of ammonia temperature programmed desorption (TPD) that coke on HZSM-5 greatly reduced the number of acid sites available with no measurable change in the strength or distribution of the remaining sites. They postulated two modes of deactivation, viz., (i) at low coke content one acid site is lost for every five carbon atoms (e.g., two sites for C_{10}) which corresponded to localized coke formation on internal acid sites; and (ii) above 9.5 wt% coke one acid site was lost for every 100 carbon atoms which corresponded to the formation of coke on the outer surface and/or topological blocking of zeolite channels. The order of coke formation is in disagreement with that proposed by Dejaifve et al. (1981).

Magnoux et al. (1987b) showed that the increase in strength and number of acid sites increased the coking rate in large pore zeolites, while on smaller pore zeolites channel structure and pore volume also played a roll.

1.1.1.3 Nature of reactant

It is clear from considerations of pore structure and acidity that different reactants would have different coking tendencies due to varying activities and/or stabilities of reactants in acid medium and pore restrictions. Indeed Appleby et al. (1962) showed that on silica alumina aromatic and olefins had the largest coke formation tendency, with the olefins forming coke via the formation of aromatic intermediates. Coke formation increased with an increase in molecular weight and basicity of the aromatic. The structure of the aromatic compound which played a large role in its interaction with acidic surface was also an important parameter. Interactions between olefins and aromatics speeded up the rate of coking.

The tendency of olefins and aromatics to increase the coke formation has also been observed by Walsh and Rollmann (1977), Eisenbach and Gallei (1979) and Fetting et al. (1984). The last authors also found that the coke composition from aromatics and olefins were different from that formed from alkanes. Similar observations were made by Furimsky (1978) for the catalytic hydrotreatment of bitumen and heavy gas oil.

A recent study by Abbot and Wojciechowski (1987) showed that the rate of decay of HY during n-paraffin cracking increased with increasing chain length, the reaction being strongly inhibited by olefinic product molecules. Two decay processes were postulated: two site decay observed for cumene cracking and multi-site decay involving pore blocking. Pore blocking tendencies increased with the increasing length of the feed molecule.

1.1.1.4 Reaction conditions

As coke formation is a chemical reaction it would be expected to depend on reaction conditions. Eberly et al. (1966) found that the coke formation on silica alumina in fixed beds was a complex function of the length of the cracking cycle and the feed rate.

Eisenbach and Gallei (1979) found that increasing temperature increased the intensity of the infrared (IR) coke band. Langner and Meyer (1980) and Langner (1981) found that the deactivation of NH_4Na-Y by 1-butene and propene was more rapid at low temperature which favoured polymerisation over cracking and hydride transfer. The C/H ratio of coke increased with increasing reaction temperature. A change of mechanism for coke formation was proposed. At low temperatures deactivation was due to strongly adsorbed compounds such as cyclic olefins and dienes in the pores of the zeolites, the size of which are limited by the pore structure. At high temperatures (above 300°C) aromatization of oligoaromatic compounds by hydride transfer reactions take place and these aromatics are able to diffuse to the exterior surface. The high coking tendency of these oligoaromatic compounds causes growth to macromolecular, graphite-like species on the exterior of the catalyst, possibly starting at the pore mouth, causing pore blockage.

Langner (1982) showed for methanol conversion on zeolites that in large pore zeolites the amount of coke deposited increased with increasing temperature, in small pore zeolites coke content was independent of temperature, and in intermediate pore zeolites coke level decreased with temperature. However, at low temperatures deactivation was more rapid than at higher temperatures and accompanied by pore blocking for all the zeolites. Fetting et al. (1984) made similar observations on HM where no graphitic coke formed below 230°C, but increased sharply in content at 250°C and levelled off at 300°C.

1.1.2 Mode of deactivation

Generally there are three modes of deactivation, namely poisoning of the accessible active sites, blockage of the available pore voidage by the formation of carbonaceous material and sintering of the active surface of the coke catalyst. The first mode is caused by strong adsorption of reactant or product. The second and third mechanisms cause a change in the pore structure or size of the catalyst. In this section, the mechanisms of deactivation by hydrocarbon reaction on acid catalysts will be discussed. In particular, sintering will not be considered since it is an important mode of deactivation for metal catalysts.

Langner and Meyer (1980) and Langner (1981, 1982) observed for dienes and light olefins over NH_4Y that coke formation was related to a decrease in adsorption capacity with pore blockage being the main cause of deactivation. At low reaction temperatures strong adsorption of coke precursors on the acid sites in the pores caused deactivation while at high temperatures growth of macromolecular graphite-like material on the exterior surface blocked the zeolite pores. Dadyburjor (1983), using constant coke Arrehenius plots, was able to distinguish between site poisoning and pore blockage by making use of the variation of diffusion and reaction rate. As mentioned earlier, McLellan et al. (1986) proposed a two stage mechanism for coking during methanol conversion over HZSM-5, loss of acid sites followed by pore blockage. Magnoux et al. (1987b) made similar observations for HZSM-5. In contrast HM underwent immediate pore blockage while in HY only partial blockage occurred.

In an attempt to obtain a better understanding of the mode of deactivation, mathematical models of coke formation have been proposed, the first of which was given by Voorhies (1945). A serious limitation of this process time dependent model, although widely used, is that it is specific to a particular reacting system and the reactor operating conditions.

The coke on catalyst approach has been proposed as an alternative to the Voorhies type analysis. Froment and Bischoff (1961) presented a convective model for parallel and consecutive coking in which the deactivation function multiplying the activity of the catalyst was linearly, exponentially or hyperbolically related to the coke content on the catalyst. Ozawa and Bischoff (1968a,b) found that the above model applied to the ethylene reaction over silica alumina but not to n-hexadecane cracking. Using Langmuir-Hinshelwood kinetics, Chu (1968) was able to show that increased coke precursor adsorption or concentration at the external catalyst surface increased the rate of deactivation.

Beeckman and Froment (1979, 1980, 1982) analysed active site coverage and pore blockage (due to growth of coke molecules from a precursor covering a site) using probability theory in single ended pores, pores open at both ends and various pore networks including the effects of finite rate of growth of coke molecule and diffusional resistance. Lin et al. (1983) applied this theory successfully to cumene cracking over lanthanum exchanged Y. The advantages of this approach are the allowance for pore structure and the ease of solutions by a computer. The drawbacks are that the "tree like structure"

lacks interconnectivity (e.g., if the neck of the tree is blocked then the whole tree is blocked) and the solutions imply that the coking reactions are zero order while observations do not show this.

Mann and Thompson (1987) modelled coke accumulation (wedge layer mechanism) using time as an independent parameter on both zeolite and support including the interactions of support pore volume and coke deposits. The disadvantage of the method was the representation of the pore structure as a parallel bundle. Applications to cumene cracking at 500°C showed rapid loss of activity followed by slower support pore deactivation which included plugging of pores up to 150 Å.

Shah and Ottino (1987) modelled the changing morphology due to the deposition of solid residue causing deactivation. The morphology was assumed to be completely disordered throughout the process and was represented by a site percolation model. The model accounted for effects of accessible void area and volume fraction, accessible intermaterial density and the effective diffusivity.

1.1.3 Nature of coke

The deposition of coke in most commerical organic reaction systems is of a complex nature dependent on the type of reaction, feed, reactor and catalyst. It is therefore clear that the nature of coke is specific to a reacting system. However, coke has been observed to consist of a soluble fraction (which can be removed by extraction with a good solvent), an insoluble fraction (graphite-like substance which can only be removed by ignition in oxygen) and an ash fraction (due to inorganic residues which can never be removed).

Appleby et al. (1962) classified the "coke" on silica alumina deactivated by gas oil cracking as follows:

(i) a heterogeneous mixture of metal oxide left behind from prior regeneration;

(ii) a growing solid/semi-liquid mixture of polynuclear aromatic molecules (e.g. dimers and trimers of naphthalene and chrysene); and

(iii) more strongly adsorbed components of reaction product.

The coke was analysed as having 2-8 wt% ash, while X-ray data showed that the radius for the assumed spherical particles was less than 100 Å with a turbostratic graphite structure similar to that of carbon black. Eberly (1966) observed IR spectra of the same catalyst and found aromatic skeletal vibrations which corresponded to a low hydrogen content and a high degree of condensation which tended towards a pseudo-graphitic structure.

Furimsky (1978, 1979) observed for bitumen and gas oil cracking that the coke was high in nitrogen and oxygen content from heterocyclic feed components. Metals in the feed were also found to concentrate in the coke. Beuther et al. (1980) proposed that coke deposits in large pore catalysts consisted of several monolayers and the effective pore diameter became smaller. Coke formation by ordered stacking of aromatic molecules was proposed in the processing of bitumous feed, similar to the mechanism of meso-pore formation. Wukasch and Rase (1982) analysed commercial hydrotreater catalysts and found that the inner portion of the catalyst contained material of a high nitrogen to carbon ratio, higher molecular weight and hydrogen saturation than the exterior portion. However, most of the deposits were predominantly on the exterior of the catalyst, preferentially fouling the 50-70 Å diameter pores. The interior carbon was found to increase with severity of treatment and was more difficult to burn-off.

Langner and Meyer (1980) found that for butadiene and NH4-Y calcined below 600°C, coke precursors were mainly alkylated mono- and oligoaromatics, while at calcination temperatures above 650°C coke precursors were mainly cyclic, often non-aromatic hydrocarbons with the formula $C_{4n}H_{6n-x}$. Langner (1981) observed carbon to hydrogen ratios from 0.7 at a reaction temperature of 200°C to 1.8 at a reaction temperature of 450°C. At the latter temperature coke was fused, possibly alkylated aromatic systems of up to 6 rings of high molecular weight and approximately 2% solubility. At low reaction temperatures cyclic polyolefinic hydrocarbons with a high proportion of conjugated double bonds was observed. Blackmond et al. (1982) also observed on NH_4-Y that coke was a highly dehydrogenated structure with some aliphatic residue. The composition of coke was found to be similar for each type of acid site, with possibly a higher aromatic content on the Bronsted acid hydroxyls.

Shiring et al. (1983) proposed, using IR analysis, a complex polycyclic structure with no aromatic hydrogen for C_6, C_7 cracking on ReY and HY. From the observation that interparticulate coke formed far from the primary catalytic site they postulated that coke itself provided active sites for more coke formation. Fetting et al. (1984) observed the characteristic IR coke band for polycyclic aromatics with low hydrogen content on HM. They also observed that the coke formed from olefins and aromatics was different from that formed from alkanes. Alkylated naphthalenes were the most probable constituents of the coke while higher temperatures appeared to favour some anthracene-like molecules.

Magnoux et al. (1987b) observed for heptane cracking on HY a chloro-methane soluble fraction of light polyaromatics of 3-7 rings with small alkyl groups and an insoluble fraction of heavy polyaromatics of more than 7 rings. The degree of aromaticity, represented by the insoluble content, was found to increase with reaction time (coke content).

1.2 Temperature programmed desorption (TPD)

TPD is a common technique used to evaluate the number and strength of acid sites. The technique involves desorbing a base, commonly ammonia or pyridine, at a constant heating rate. The base is previously adsorbed under controlled conditions. The desorption of the base is monitored as a function of temperature using a suitable detector, usually a thermal conductivity cell (ammonia) or flame ionisation detector (pyridine) but infra-red spectroscopy and mass spectrometry has also been used. The concentration of the acid sites is given by the area under the peak while the strength of the acid sites is indicated by the temperature at which maximum rate of desorption occurs.

Classical TPD theory was originally presented by Cvetanovic and Amenomiya (1967) for first order desorption from a uniformly packed ideal CSTR, neglecting the effects of axial dispersion and diffusion. It was, however, shown by Brenner and Hucul (1979) that even for a system in which the desorption was first order, classical TPD theory yielded erroneous values for the kinetic parameters due to the sensitivity of the model to small experimental errors.

Gorte (1982) developed a generalized TPD model. Dimensional analysis of the model yielded criteria for determining the intrusion of effects from sample lag time, diffusion lag time, concentration gradients and readsorption. It was also shown that readsorption can raise peak temperatures by several hundred degrees. Jones and Griffin (1983) showed, under Langmuir equilibrium sorption with gas phase diffusion being the rate limiting process, up to a 5% negative shift in the peak maximum temperature due to variations in initial coverage for TPD from a porous catalyst.

Rieck and Bell (1984) modelled TPD from a bed of catalyst with flowing carrier gas either as a CSTR or a series of CSTR's. Simulations showed that the position and shape of the spectra were sensitive functions of catalyst particle size, catalyst bed depth, carrier gas flowrate and composition; the effects were similar for both first and second order desorption. For large particles, distortions due to non-uniform adsorbate distribution were expected while extensive readsorption of gas occurred within the catalyst particles with the local adsorbate coverage governed by equilibrium adsorption. Intra-particle concentration gradients were minimized by reducing catalyst size and carrier gas flowrate which also validated Gorte's criteria.

Notwithstanding the above problems, TPD has been used to provide quantitative information on the desorption process for a porous catalyst. Tronconi and Forzatti (1985) observed that variation in the peak temperature and desorption rate constant with particle size provided a good criterion for detecting diffusion limitations, in accordance with Gorte's criterion. Model predictions coupled with pore diffusion and readsorption were successful.

All the above modelling applies only to a single uniform pore system similar to silica alumina. Zeolites used in TPD would have bidisperse pore systems if particle sizes of the order of 0.2 mm are used. As many assumptions are required to model single pore systems, the application to zeolites would seem rather doubtful. Nevertheless quantitative experimental information about acid site distribution and strength as well as heats of desorption has been reported. In what follows, mainly the use of TPD to study deactivated catalyst samples will be discussed.

Topsøe et al. (1981) analysed the effect of methanol conversion on the acid sites of HZSM-5 and observed a considerable reduction in acid sites with

deactivation. It was postulated that active acid sites were related to the aluminium content and most probably located at the channel intersections, while the weaker acid sites correspond to terminal silanol groups on the external surface or non-zeolitc impurities. The weak sites were most easily poisoned and regenerated.

Itoh et al. (1984) found that methanol conversion activity and product distribution were a function of Si/Al ratio, with catalyst activity depending on the amount of strong acid sites. However the low temperature peak (l-peak) was inactive for methanol conversion over HZSM-5. Post and van Hoof (1984) found a threshold level of acid strength for hexane cracking over HZSM-5 but were not able to relate strong or weak acid sites to discrete lattice positions.

Kubelkova et al. (1985) found that coke on HY and HZSM-5 changed the shape of the ammonia desorption spectrum, the effect being most pronounced during the initial stage of coking. Coked samples adsorbed less ammonia with lower peak heights. In HY and HZSM-5 peaks were found to shift to higher temperatures because of the hindered ammonia desorption due to pore blockage, while in dealuminated HY the peaks shifted to lower temperatures because of poisoning of most of the acid sites. In contrast, McLellan et al. (1986) found that coke on HZSM-5 reduced the number of acid sites for ammonia desorption without any measurable change in the strength and/or distribution of the acid sites.

In order to examine the degree to which TPD data from different laboratories can be compared, Niwa et al. (1986) considered the effect of experimental conditions on ammonia TPD from HM and HY. They found that the peak maximum was related to the contact time, with the l-peak in particular being dependent on a number of experimental conditions. They found large variations between different laboratories, but the data from each laboratory were internally consistent. It was recommended that only the high temperature peak (h-peak) would be needed to account for the acidity of the catalyst.

1.3 Diffusion in catalysts

Changes in diffusivity with reaction can throw some light on the type of deactivation mechanism. Diffusivities in catalysts may be measured by means of diffusion cell, sorption apparatus, nuclear magnetic resonance (NMR) or gas chromatograph (GC). Each of these methods will be reviewed as well as the effect of chemical reaction on diffusivity and the reasons for choosing the GC technique.

1.3.1 Experimental measurements

1.3.1.1 The diffusion cell technique

The steady state technique, originally developed by Wicke and Kallenbach (1941) in which a stagnant gas was allowed to diffuse through a porous catalyst pellet under the influence of a concentration gradient, was modified into a flow system by Weisz (1957). This technique has been extensively used to measure effective diffusivities in silica alumina pellets (Weisz and Schwartz, 1962; Henry et al., 1961; Wakao and Smith, 1962). The technique was further modified into a pulse-response system (Dogu and Smith, 1975, 1976) and applied to silica alumina. Hashimoto et al. (1976) showed that only macro-pore diffusivity could be obtained from the first moment, while the introduction of the second moment was necessary to evaluate micro-pore diffusivity in a bidisperse catalyst. In addition, a rigorous theoretical analysis of the system (Burghardt and Smith, 1979) showed that large, specially prepared pellets which would have different physical properties to the actual industrial pellets would have to be used.

Recently Dogu and Ercan (1983) successfully measured micro- and macro-pore diffusivities in α-alumina. Their moment analysis technique was criticised by Biswas et al. (1987a) who extended the mono-disperse time domain solutions of Do and Smith (1984) to bidisperse solids. Although the theoretical considerations of this technique have shown it to be suitable for measuring diffusivities, Biswas et al. (1987b) were unable to measure micro-pore diffusion because crystallites had to be large (>40 μm) and/or diffusivity had to be small, while the pellet length could not be reduced to a length necessary to make the response sensitive to micro-pore diffusion. The technique was not recommended for the evaluation of micro-pore diffusivity.

It therefore follows that the advantages of this technique, e.g., the response being dependent only on adsorption, micro- and macro-pore diffusivity, are offset by practical limitations.

1.3.1.2 Sorption rate measurements

One of the most widely used methods of determining diffusivity is measuring gravimetrically, volumetrically or piezometrically the sorption rate of a sorbate on adsorbent particles under the influence of a step change in local sorbate concentration. Most of the early work was carried out assuming isothermal operation with instantaneous equilibrium at the particle surface, which was a good approximation for slow diffusing systems. By taking sorption rate measurements at various concentrations it was possible to determine isotherms and diffusivities as a function of concentration.

Early work on the sorption of light gaseous hydrocarbons on synthetic mordenite (Satterfield and Frabetti, 1967) showed that equilibrium sorption and diffusion was affected by synthesis conditions and mechanical treatment such as grinding, while the diffusivity was also concentration dependent and varied by orders of magnitude between adsorption and desorption. Ruckenstein et al. (1971) developed theory for the isothermal sorption on a bidisperse pore structure, separating the effects of macro- and micro-pore diffusion. A similar model using a rectangular adsorption isotherm (Lee and Ruthven, 1979) was shown by Lee et al. (1979) to be valid for cis-2-butene and n-heptane sorption in 5A molecular sieves.

Ruthven and Loughlin (1971a,b) showed the importance of crystallite size and shape in determining the diffusivity of C_1 to C_4 alkanes in 5A sieves. The Darken equation together with Dubinin-Polanyi potential theory was used to explain the concentration dependence of the diffusivity. This was extended to 4A sieves (Loughlin et al., 1971), 5A pellets with binder (Ruthven and Loughlin, 1971c) and the effect of cation exchange in type A zeolites (Loughlin and Ruthven, 1972). Results showed that there was no difference between pellets and crystals, and the effect of cation exchange on the diffusion followed the expected trend. The statistical model isotherm used to interpret the sorption of light paraffins in 4A and 5A (Ruthven and Loughlin, 1972) was extended to the sorption of ethane, propane and

cyclopropane in 5A (Derrah et al., 1972). The rise in isosteric heat of sorption with concentration was explained by the effect of sorbate-sorbate repulsion, while the stronger adsorption of olefins relative to paraffins was attributed to the greater energy of sorption arising from specific electrostatic interactions.

The diffusion of mono- and di-atomics in 4A (Ruthven and Derrah, 1975) was explained by transition state theory, while in 5A the inverse concentration dependence in the Henry's law region suggested a collisional transport mechanism which appeared to be related to the magnitude of the energy barrier at the sieve window. C_6 and C_7 hydrocarbons in 13X (Ruthven and Doetsch, 1976) showed similar behaviour to the above gases in 5A.

Chihara et al. (1976), using an approximate analysis, was able to show that accounting for non-isothermal effects could increase the diffusivity by two-fold. A more detailed analysis of non-isothermal behaviour in rapidly diffusing systems (Lee and Ruthven, 1979), in which the main resistance to heat transfer was at the external surface, has been used to explain the anomalous dependence of diffusivity on crystal size and concentration in a previous study by Ruthven and Doetsch (1976). This analysis was applied to CO_2 in 4A, and CO_2 and n-pentane in 5A (Ruthven et al., 1980), confirming the validity of the model. Further application to N_2, CH_4 and C_2H_6 in 4A (Yucel and Ruthven, 1980a,b) showed that the sorption kinetics was controlled by diffusion rather than the surface barrier, while for CF_4 and n-pentane in 5A, heat effects as well as diffusion were controlling. Diffusion was found to be independent of crystal size, while large variations were observed between different batches of the same catalyst. Heat effects were also observed for methanol adsorption on ZSM-5 by Kmiotek (1982). In contrast, Ruthven and Lee found that for C_5, C_6 and C_8 hydrocarbons in 10X and 13X, bed diffusion and heat effects were controlling and that for these systems intra-particle crystalline diffusion was too fast to be determined.

Much of the early work using sorption was plagued by incorrect analysis of the experimental sorption rate experiments and the failure to correctly access the controlling mass transport mechanism. Self-diffusivities can, however, be measured by tracer exchange experiments using an isotopically labelled species for which heat effects are non-existent (Goddard and Ruthven, 1986).

1.3.1.3 Nuclear magnetic resonance (NMR)

Self-diffusivities may be easily measured by NMR methods, although the technique is restricted to molecules which have a sufficiently high concentration of unpaired electrons. Initially the self-diffusivities were obtained directly from measurements of the spin lattice relaxation time by estimating the mean square jump distance in Einstein equation. However, the estimation of the mean square jump distance proved to be unreliable.

Alternatively the pulsed field gradient technique (a modification of the above) allows the direct measurement of the mean square displacement during the known time between the two gradient pulses at a 90°C phase difference. However, limitations of the technique have set the lower limit of the diffusivity at 10^{-8} cm^2/s (i.e., rapidly diffusing systems) with a crystallite size of about 20 μm. Fast tracer desorption (Kärger, 1982), which was another modification, allowed the use of crystals down to 1 μm and diffusivities down to 10^{-11} cm^2/s. A combination of both these techniques allows a quantitative evaluation of surface barrier effects. These techniques also provide a means of studying multi-component sorption.

Many systems have been studied, a summary of which are given by Kärger et al. (1983). The refinements of both NMR and sorption techniques have narrowed the difference between the measured diffusivities. NMR generally gives values greater by a few orders of magnitude (Yucel and Ruthven, 1980a,b) although the data obtained by each technique are self-consistent. In a recent study Goddard and Ruthven (1986) have shown that although sorption and tracer exchange gave similar results, NMR gave diffusivities two orders of magnitude larger which could not be attributed to the use of different samples or calcination conditions. It is therefore clear that although NMR offers a good alternative for measuring diffusivities, the discrepancies arising from the use of different methods have not yet been resolved.

1.3.1.4 Gas chromatography (GC)

The non-idealities in gas chromatography, which has been used as an analytical tool for many years (see Choudary, 1974), were analysed by van Deemter et al. (1956) as being due to longitudinal dispersion and mass

transfer, from which the well know HETP theory emerged. Since the development of Kubin-Kucéra model (Kucéra, 1965), the method has provided an alternative in diffusivity measurements. The technique involves measuring the response of a small packed bed of porous particles to a pulse or a step change in concentration of suitable tracer gas. The position and spread of the response peak is a function of adsorption equilibrium constant, axial dispersion, external mass transfer and macro and/or micro pore diffusion.

Initially the measurement of diffusivity was performed by the HETP method - Eberly (1969) measured diffusivities of inert gases in 3A and 5A molecular sieves, zeolite-Y, mordenite and silica alumina; Ma and Mancel (1972) measured CO_2, NO, NO_2 and SO_2 diffusivities in 5A, 13X molecular sieves and mordenite; MacDonald and Habgood (1972) measured benzene, octane and decane diffusivities in NaX; and Butt et al. (1975) measured SF_6 diffusivity in coked mordenite. The method has been shown to be sufficiently accurate for determining variations in diffusivity between catalysts as well as verifying that diffusion in zeolites is an activated process dependent on the sieve window size and sorption equilibrium.

The Kubin-Kucéra model, which was an improvement on the HETP method, has been applied extensively, primarily to macro-porous structures. The measurement of diffusivities of ethane, propane and n-butane in silica-gel by Schneider and Smith (1968a) using moment analysis was extended to measurement of surface diffusion (Schneider and Smith, 1968b) at estimated surface coverages of 10^{-4} fraction of the monolayer. It was also shown that tracer gas concentration fell rapidly during the initial 10% of the column length. Thermal effects were used to explain the variation in n-butane adsorption constants in silica-gel (Cerro and Smith, 1969), while the diffusivities of non-adsorbed gases were also determined (Cerro and Smith, 1970).

Gangwal et al. (1971, 1979, 1980) have extensively analysed the experimental operating conditions and limitations of the Kubin-Kucéra model. Results showed that reproducibility was excellent and the model adequately represented the experimental data. However, physical sorption rates could not be measured and external gas mass transfer was measurable only under severely restricted conditions. Fourier analysis was used and recommended. The variation of diffusivity with velocity which was observed with the Kubin-Kucéra models using moment, time domain and Fourier analysis (Boersma-Klein

and Moulijn, 1979) was explained by taking the effect of intra-particle forced convection into account (Rodrigues et al., 1982).

The bidisperse pore model developed for chromatography (Haynes and Sarma, 1973), which was an extension of the Kubin-Kucéra model, was applied to measurement of diffusivities of argon in 3A and 5A molecular sieves (Sarma and Haynes, 1974). Good agreement between experiment and model was found. Time domain solutions (Haynes, 1975) were obtained to determine operating conditions for good parameter evaluation. The addition of the crystallite size distribution to the model (Hsu and Haynes, 1981) was found to be essential for predictions, while the results of n-butane and n-hexane in NaY were plagued by non-linearities. More sensitive detectors overcame the non-linearities (Fu et al., 1986), while the diffusion model and surface barrier model proved to be indistinguishable. The surface barrier approach appeared, however, to be physically more likely. The variation of pulse size to ensure system linearity was sufficient to ensure no heat effects, which were shown to be negligible (Haynes, 1986). Fourier analysis was the preferred method of analysis. The bidisperse model with moment analysis was also used by Hashimoto and Smith (1973, 1974) to determine macro-pore diffusivity of n-butane in 5A molecular sieves and silica alumina pellets, the accuracy of the diffusivity being estimated at 25%.

Carg and Ruthven (1974) determined micro-pore diffusivity from break-through curves with N_2, ethane and ethene in 4A and 5A molecular sieves which compared favourably with gravimetric data even though axial dispersion was neglected. Shah and Ruthven (1977) found good agreement with gravimetric data of methane, ethane, propane and cyclopropane diffusivities in 5A molecular sieves. The technique was extended to binary diffusion of N_2-CH_4 in 4A molecular sieves by Ruthven and Kumar (1979). Orthogonal collocation solution of the model equations (Raghavan and Ruthven, 1985), provided good representation of the diffusivity of argon in 5A and 10X molecular sieves. Boniface and Ruthven (1985) developed the model analysis up to the fourth moment including crystallite size distribution which was applied to light gases in HM, Na-M and Ca-X, while the simplified model (no crystallite size distribution, first and second moments) was used to analyse the diffusivities of O_2, N_2, CH_4 and CO_2 in 4A and of O_2, N_2, CH_4, CO_2, cyclopropane and cis-butane in 5A molecular sieves (Haq and Ruthven, 1986a,b). The effect of water was to slow diffusion substantially in 4A while O_2, N_2, CH_4 and CO_2 diffusion was too fast to measure in 5A.

Non-isobaric conditions have been analysed (Carleton et al., 1978) using the Kubin-Kucéra model with the Blake-Kozeny pressure drop correlation. First moment analysis of C_3 to C_6 hydrocarbons showed that the accuracy was improved by high pressure. Chiang et al. (1984a) have extended this technique to zeolite powder packed in a GC column with simulations to show the effects of pressure drop and dead volume. Measurement of propane and butane diffusivities in 5A molecular sieves and silicalite (Chiang et al., 1984b) by means of moment and Fourier analysis showed that pressure drop had to be determined independently while results were in broad agreement with those reported in the literature. Forni et al. (1986a,b) have developed and applied a similar model using moment analysis to determine the diffusivity of aromatics in zeolite-Y and ZSM-5. These analyses have not taken crystallite size distribution into account.

A number of methods of analysis are available, namely, time domain, Fourier, transfer function, weighted moment and moment analysis, which have been evaluated by Hays et al. (1967), Anderssen and White (1970), Wakao and Tanaka (1973), Wakao et al. (1979, 1980) and Fahim and Wakao (1982). Results show that time domain analysis was the most accurate, but due to extensive computing time Fourier analysis was preferred while the moment analysis was subject to tailing errors as well as the assumption that the model represented the data well. The literature shows that moment analysis is the most popular but there has been a shift to the more accurate Fourier analysis.

It has been shown in the literature that there are limitations with the GC technique. Heat effects are typically negligible but crystallite size distribution should be taken into account. The linear isotherm assumption is easily checked by varying the pulse size. It is often not possible to determine which mass transfer process is dominant from a single experiment, and use of different particle sizes, tracer gases and flowrates is necessary.

1.3.2 The effect of chemical reaction

All the analyses of the preceding sections have been for inert catalysts in which the tracer gas does not undergo reactions. It is important to know what effect reaction or reaction products would have on the measured

diffusivity. To date there have been numerous theoretical studies based on diffusion and reaction, but experimental measurements have been few.

Mingle and Smith (1961) showed that the pore size distribution could not affect the micro-pore effectiveness factor by more than 10%, but that values >1 were possible for highly exothermic reactions and reasonably sized particles. Wakao and Smith (1964) and Raja et al. (1964) used a simplified pore structure model to relate diffusivity to the micro-pore effectiveness factor and found the theory to be satisfactory in predicting the ortho-para-hydrogen conversion using a single catalyst of NiO and Al_2O_3. Similar observations for the micro-pore effectivness factor to those of Mingle and Smith were obtained. Suzuki and Smith (1971) developed Laplace domain solutions for a GC fixed bed reactor as well as moment analysis. Furusawa and Smith (1974) showed that for a bidisperse pore catalyst where the micro-pore effectiveness was unity, the overall effectiveness factor should be a function of macro-pore diffusivity only.

Wakao et al. (1978) have shown that dispersion coefficients determined under first order reaction conditions were found to be very large and depended not only on the intraparticle diffusivities but also on the Thiele modulus, while the centre symmetric intraparticle concentration assumption was valid, provided the reaction was first order. Gangwal et al. (1978) have shown that the centre symmetric intraparticle concentration assumption was not valid at low flowrates. Leung and Haynes (1984) have bridged the gap between two popular diffusion models, whereby the effect of rapid chemical reaction in the micro-pores converts the micro-pore model (which includes micro-pore contribution to the overall diffusive flux) into the macro model (in which no account is taken of diffusion in the micro-pores). The moments of the effluent curves for a reacting system in a CSTR were applied to diffusivity measurement under reacting conditions (Park and Kim, 1986a,b). Results showed that for the active catalyst the diffusivity was an order of magnitude smaller than in the absence of reaction.

Most of the above workers have modelled or measured diffusivity under reaction conditions but have not taken into account that catalysts deactivate, causing changes in pore structure and nature of the active surface. Diffusivity would therefore be a function of coke content and/or process time. Attempts to account for the changing pore structure have been presented by Mann and Thompson (1987) and Shah and Ottino (1987). The above

analyses do, however, allow some estimate of diffusivity under reaction conditions.

1.3.3 Reasons for choosing the GC technique

In this section reasons for the choice of GC techniques are given in view of the techniques outlined in the foregoing sections. The advantages and disadvantages of the different methods are discussed to emphasise the choice of system.

The equipment required for the sorption technique is a reasonably sophisticated vacuum micro-balance which is subject to strict operating conditions. Heat effects are almost always present, while small samples used may not be representative. The technique owes its popularity to the simpler analysis of experimental results although accounting for heat effects and bed diffusion introduces complications.

The diffusion cell technique has been analysed by Smith and co-workers. The governing equations and boundary conditions for the dynamic response of a single pellet are complicated while the pellet shapes and sizes are unrealistic and the apparatus must be sophisticated to prevent leaks. The technique does offer the advantages of no axial dispersion and gas mass transfer, but has been found to be unsuitable for measuring micro-pore diffusivity (Biswas et al., 1987a,b).

The NMR technique is relatively new and has been used by Kärger and co-workers. It is the only technique whereby the motion of hydrocarbons in the micro-pores is reliably monitored, this motion being clearly distinguished from axial dispersion or inter-crystalline diffusion. The equipment required is sophisticated and expensive. It has been shown that diffusivities obtained by NMR are several orders of magnitude greater than values obtained by other techniques. This discrepancy has not been satisfactorily explained.

The GC technique has been extensively studied by Haynes and co-workers, Ruthven and co-workers, Smith and co-workers and a host of others. The apparatus required is inexpensive, simple, quick, robust and easy to use. It does, however, require careful tuning to eliminate as much of the extra column effects as possible. A representative sample is analysed at one time.

The system has been shown to be isothermal, but system linearity must always be checked. The solution of the governing equations is complicated, but computerised numerical solutions provide a quick analysis. Catalyst size used can be representative of that used in industry. The use of the packed column does introduce additional factors such as axial dispersion and external gas mass transfer which to date offer problems. However, careful experimentation should minimise the effects of these parameters.

There is an abundance of studies using the GC technique in the literature and this method is hence possibly a logical engineering choice. This technique with careful experimentation has shown the most promise and therefore is the chosen method in this work.

1.4 Zeolites HY and HM

The sodium exchanged zeolite-Y, a sketch of which is shown in Figure 1.1, has the unit cell formula $Na_{56}Al_{56}Si_{136}O_{384}\cdot 265H_2O$. The primary structural unit is the sodalite cage which consists of a truncated octahedron containing 24 silicon and aluminium tetrahedra. The supercage is produced by joining the sodalite cages in a tetrahedral arrangement through hexagonal prisms, with each such prism being joined to a 6-ring face of a sodalite cage. This produces a 3-dimensional, open pore structure with the free diameter in the supercage of approximately 1.30 nm. The pore diameter is 0.8 nm which allows the entry of aromatic compounds and some branched hydrocarbons. The volume of the supercage can hold 24 water molecules.

Sodium exchanged mordenite has the unit cell formula $Na_8Al_8Si_{40}O_{96}\cdot 24H_2O$, and is shown in Figure 1.2. The main building blocks of mordenite are five membered rings composed of SiO_4 and AlO_4 tetrahedra. The rings form a one dimensional system of elliptical channels with a major and minor axis of 0.70 and 0.67 nm, respectively. These rings are stacked to form a tetrahedral chain which are further side-linked to other tetrahedral chains to form the main channel structure. The unit cell volume of a channel is 0.480 nm^3. These channels open into smaller elliptical side channels with a major and minor axis of 0.57 and 0.29 nm, respectively, with the volume per unit cell of 0.428 nm^3. Each side channel branches through two distorted 8-membered rings of 0.28 nm minimum free diameter into two similar side channels opening into the next main channel with a Na ion at the centre of each distorted 8-

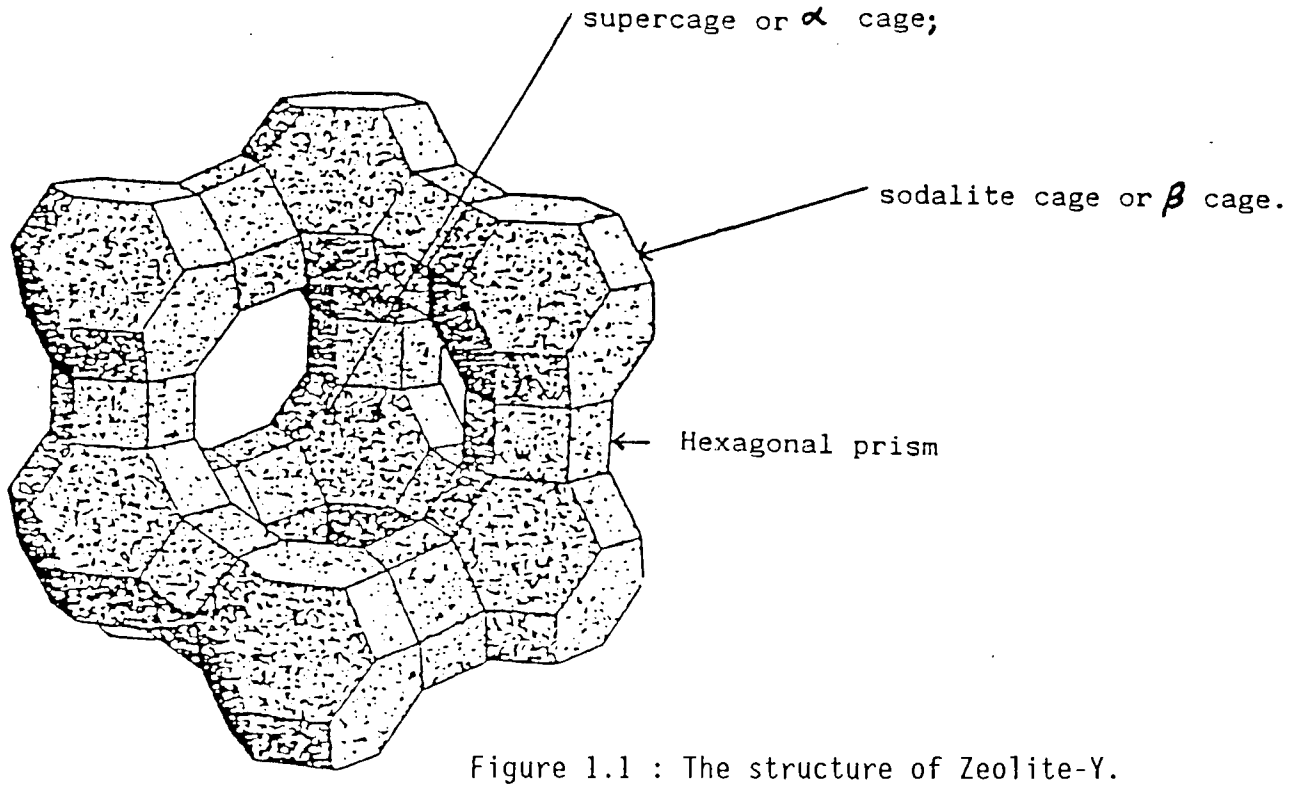

Figure 1.1 : The structure of Zeolite-Y.

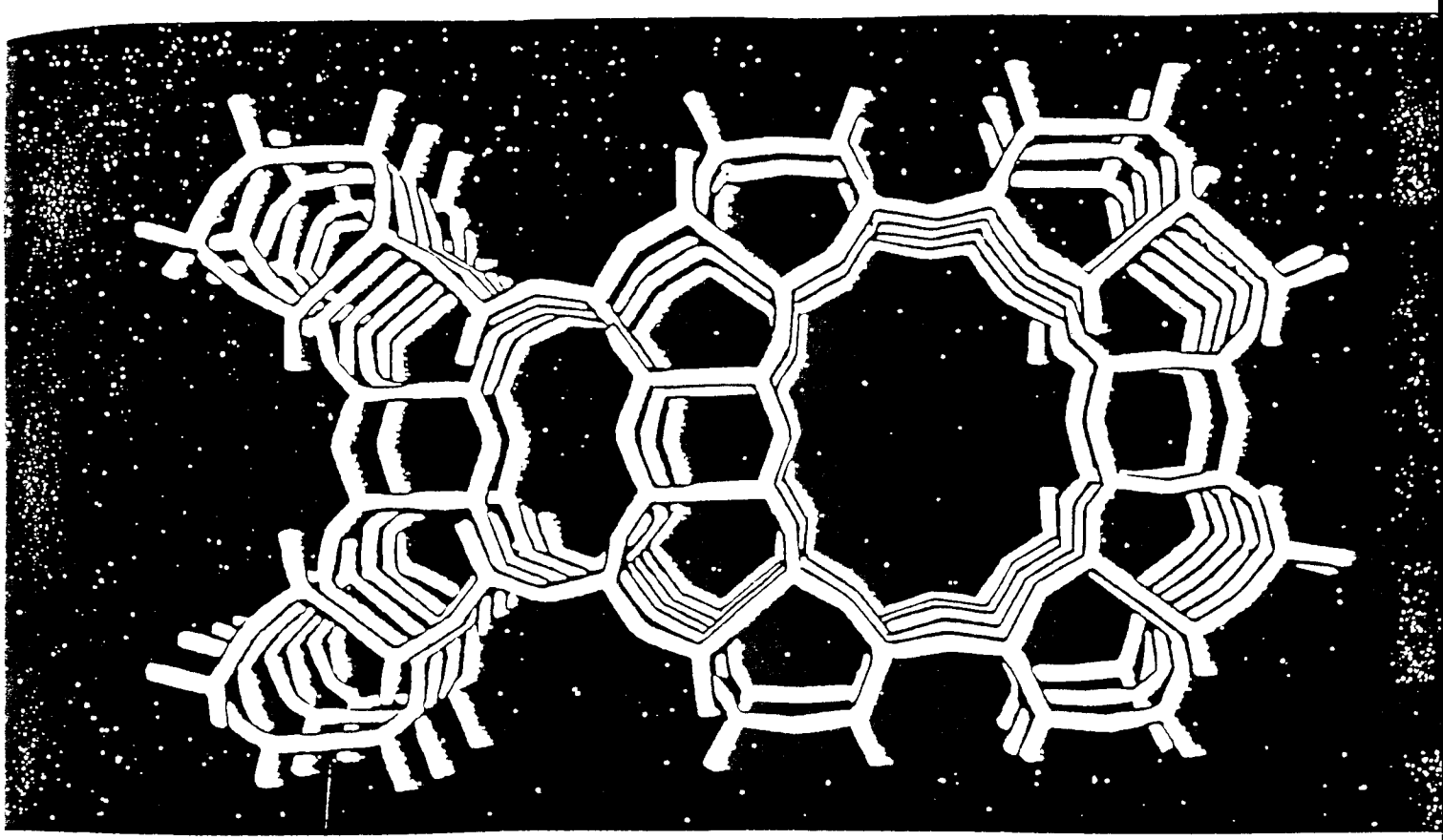

Figure 1.2 : Spatial arrangement of mordenite viewed along the c-axis.

member ring. This creates the one dimensional structure with the main channels lined with two rows of side pockets.

1.5 Objectives of this study

The primary objective of this study was to determine the effect that the type of catalyst and reaction would have on the rate of deactivation, properties of coke and transport properties of the catalyst. For this purpose the following factors were considered :

(a) HY and HM were choosen to examine the effect of type of catalyst in terms of pore structure and acid site distribution.

(b) The effect of type of reaction was analysed by comparing atmospheric cracking and high pressure oligomerisation.

(c) The transport properties of the catalyst were compared by determining diffusion and adsorption with ancillary information being obtained from ammonia TPD, TG/DTA, mercury porosimetry and BET surface measurements.

2 HEXANE CRACKING AND PROPENE OLIGOMERISATION REACTIONS

2.1 INTRODUCTION

The aim of this section was to determine the effect of the nature of the reactant and reaction conditions on the deactivation of HY and HM, with a view to generating coked catalyst samples for analysis by means of of TG/DTA, BET, ammonia TPD, and GC diffusion parameter determination. For this purpose hexane cracking and propene oligomerisation reactions were choosen on account of their different reaction conditions and feed molecules. Hexane cracking is well known to deactivate HY and HM rapidly, while propene oligomerisation at high pressure has not been studied widely in terms of deactivation.

A fixed bed reactor configuration was used for both the reactions. However, in order to achieve a uniform coke profile required for the purpose of measuring adsorption, diffusion and other properties, graphitic coke content of less than 7 wt% could not be achieved in either reaction with the exception of hexane cracking over HM. When the coke content was less, visual inspection of the coked catalyst bed immediately revealed the presence of coke profile in the reactor, whereas for the GC diffusion experiments to be valid catalyst particles of identical physical properties had to be packed into the diffusion column. Coke in this study is defined as any product or reactant which remains on the catalyst subsequent to reaction after the deactivated catalyst is flushed overnight in flowing nitrogen *at the reaction temperature*. In Chapter 3 it will be shown that two types of coke were detected by TG/DTA. The first could be removed by flowing nitrogen and will be referred to as high boiling point hydrocarbons. The second could be removed in air in the vicinity of 500°C and will be referred to as graphitic coke. A detailed treatment of the coke analysis is presented in Chapter 3.

Hexane cracking was carried out at constant reactor operating conditions which were easily achieved, with time on stream being the only variable. The data thus obtained were modelled according to the time on stream approach of Wojciechowski (1968) to understand more about the deactivation mechanism. The change in product distribution and conversion was monitored as a function of time on stream in order to observe the effects of deactivation.

Propene oligomerisation was considered as a function of temperature and pressure, but temperature runaway during start-up and fluctuating WHSV introduced additional variables affecting deactivation. Modelling of these data was not attempted due to the unsteady behaviour of the reacting system. Product distribution and conversion were monitored as a function of time on stream, were considered in the light of WHSV and temperature runaway, and were correlated with coke content.

The chapter is divided into two sections, viz., hexane cracking and propene oligomerisation, with each section describing first the apparatus and procedure, followed by the results and a discussion.

2.2 HEXANE CRACKING

2.2.1 Apparatus and Procedure

Figure 2.1 shows a sketch of the apparatus for hexane cracking. The flow rate of the high purity nitrogen was controlled by a metering needle valve at 350 mℓ/min. A constant composition (13 mol%) of hexane (AR grade 99.5%) in nitrogen was achieved by a double stage saturator (saturation at 40°C followed by condensation at 15°C). All piping was made of 1/8" stainless steel.

A reactor specially designed with 12 aluminium longitudinal fins (dimensions 10 cm x 3 cm x 3 mm) was mounted in a forced draft oven which was capable of achieving 500°C. The inlet to the reactor served as a feed preheater. This reactor was used because preliminary experiments showed that an ordinary fixed bed reactor had significant temperature and coke profiles. This was because the catalyst bed (10 mℓ) was large and without dilution. The diffusion experiment required a large amount of undiluted catalyst. The finned reactor was found to have a much smaller axial temperature profile (maximum being 30°C during start-up) and the coke profile was uniform by visual inspection. It was possible to cool the finned reactor from 500°C to 50°C in approximately 30 min, the cooling rate between 500°C and 150°C being very fast, and this feature enabled temperature runaways to be controlled. The thermowell down the centre of the bed allowed the bed temperature to be accurately measured.

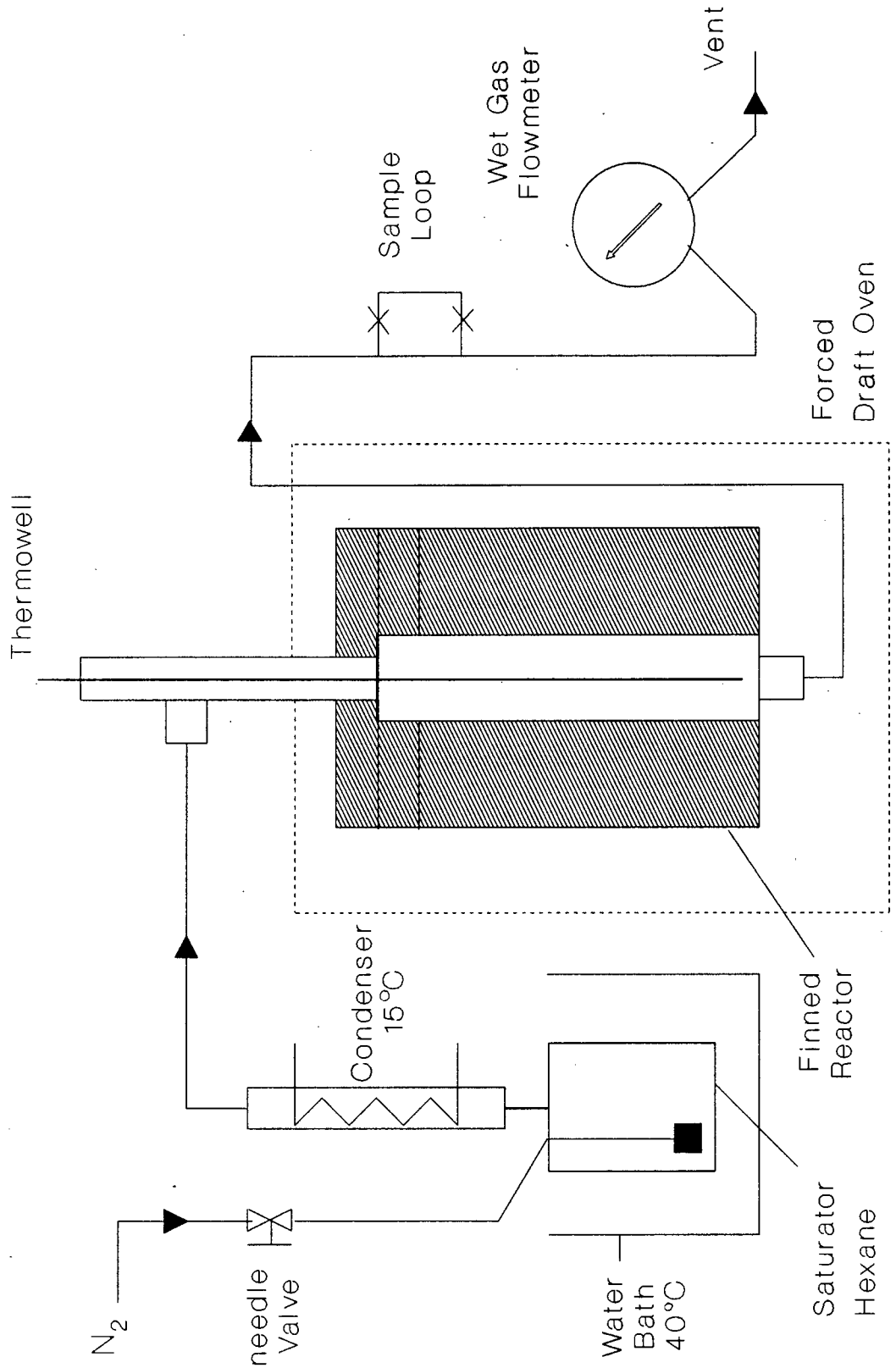

Figure 2.1 : Sketch of hexane cracking apparatus

The condenser at 15°C ensured that the feed to the reactor would always be gaseous so that conversion could be determined by standard GC gas analysis. The total volume of the outlet gas was monitored by a wet gas flowmeter.

The operating conditions of the reactor system are summarised in Table 2.1. Hydrogen mordenite (tradename : Zeolon 900-H, lot 37 248) was supplied by Norton Company (Norton International Inc., Chemical Process Products, Akron, Ohio, USA) in the form of 1/16" binderless extrudates, referred to as HM hereafter. Ultrastable hydrogen zeolite-Y (tradename : LZY82) was supplied by Union Carbide Corporation (USA) in the form of 1/16" extrudates bonded with 20% of acid-washed inorganic oxide, referred to as HY hereafter. Prior to use both catalysts were crushed with mortar and pestle and sieved to $250 < d_p < 500$ μm. This size fraction made it possible to use the catalyst particles for all the subsequent analyses without any further mechanical treatment.

Table 2.1 : Reaction conditions for HY and HM

Pretreatment	400°C in air, overnight
Feed	13 mol% hexane in N_2
Catalyst volume	10 ml (ca. 6g)
WHSV	2g/g cat·h

After calcination and setting the N_2 flowrate through a saturator bypass line, hexane was introduced into the reactor at 400°C. Except for an initial temperature rise of 30°C the system was isothermal. Barring the initial conversion, the average conversion for most of the run was between 10-20%. Low conversions and isothermal operation contributed to the near-constant coke profile.

The first analysis was performed on a sample taken within the first 2 minutes after start-up, and from then on sampling intervals of between ½ to 2 h were chosen depending on the length of the run. The mass of hexane used was determined by weighing the saturator before and after reaction. This agreed well with the estimated hexane used from flowmeter readings and gas composition data. The catalyst was flushed in flowing nitrogen at 400°C overnight after the reaction.

2.2.2 Data analysis

Conversion was based on the GC gas analysis. Gas analysis was performed isothermally at 80°C on a 3 m n-octane/Porasil C column. In the analysis the C_4-hydrocarbons were grouped into alkanes and alkenes and the C_5-hydrocarbons as a single group. Results from the GC analysis were converted to mol% based on the above groupings for the purpose of selectivity data interpretations. The WHSV defined as (g hexane)/(g cat·h) was calculated from the mass of hexane used by difference in the weight of the saturator.

The conversion vs time on stream was modelled using first order and Langmuir kinetics by including the hyperbolic time on stream decay function of Wojciechowski (1968),

$$-d\theta/dt = k_d\,\theta^m. \quad \ldots\ldots\ldots\ldots\ldots\ldots\ldots\ldots \quad 2.1$$

Integrating the above from θ=1 at t=0 to $\theta=\theta$ at t gives

$$\theta(t) = (1 + (m-1)k_d t)^{-(1/(m-1))} \quad \ldots\ldots\ldots\ldots \quad 2.2$$

where t - time on stream,

θ - fraction of active sites at time t,

m - number of active sites lost per decay event,

k_d - deactivation rate constant.

The first order rate equation,

$$\frac{dX}{d\tau} = k\,(1 + Gt)^{-N}\,\frac{(1 - X)}{(1 + \epsilon X)}\,, \quad \ldots\ldots\ldots\ldots\ldots \quad 2.3$$

where X - fractional conversion at t,

τ - space time,

k - first order rate constant,

ϵ - volume expansion correction,

G, N - decay parameters;

with G and N in turn given by

$$G = (m-1)\,k_d, \quad \ldots\ldots\ldots\ldots\ldots\ldots\ldots\ldots \quad 2.4$$

$$N = n/(m-1), \quad \ldots\ldots\ldots\ldots\ldots\ldots\ldots\ldots \quad 2.5$$

were n is the number of active sites used for reaction, yields the following relationship between conversion and time on stream upon integration:

$$k\tau(1 + Gt)^{-N} = -(1 + \epsilon)\,\ell n\,(1 - X) - \epsilon X\,. \quad \ldots\ldots\ldots\ldots \quad 2.6$$

The Langmuir rate equation,

$$\frac{dX}{d\tau} = (1 + Gt)^{-N} \frac{A(1 - X)/(1 + \epsilon X)}{1 + B(1 - X)/(1 + \epsilon X)} , \quad \ldots\ldots\ldots 2.7$$

where A and B are Langmuir rate constants, upon integration yields

$$A\tau(1 + Gt)^{-N} = (B - \epsilon)X - (1 + \epsilon)\, \ell n(1 - X) . \quad \ldots\ldots 2.8$$

Equations 2.6 and 2.8 allow explicit solution of time on stream as a function of conversion. Using a Nelder and Mead simplex routine, estimations of the model parameters were obtained. It was found, however, that the objective function for the optimisation which was based on the least squares error criterion weighted the data towards long time on stream. This led to poor estimation of rate parameters. Alternatively equations 2.6 and 2.8 may be solved for conversion as a function of time by Newton's method. Use of the conversion least squares error as the objective function provided a much more reliable parameter estimation. As the catalyst deactivated very rapidly the initial part of the conversion vs time curve was most important. Another analysis technique, used by Pachovsky and Wojciechowski (1971), Best et al. (1973), and Abbott and Wojciechowski (1987), requires data as a function of τ. The method outlined above is simpler and gave acceptable results.

2.2.3 Results of hexane cracking

The conversion vs time profiles for hexane cracking at 400°C over HY and HM are shown in Figures 2.2a and b. The wt% coke content of each sample determined by TG/DTA (as discussed in Chapter 3) is indicated in parentheses in all figures. It was difficult to obtain accurate initial conversions due to the rapid deactivation of the catalysts. It is evident however that HM deactivated faster than HY. Because of its high rate of deactivation and low coke content, only one run was performed using HM. Figure 2.3 shows that the coke build-up was rapid during the initial ½ h, and levelled off subsequently.

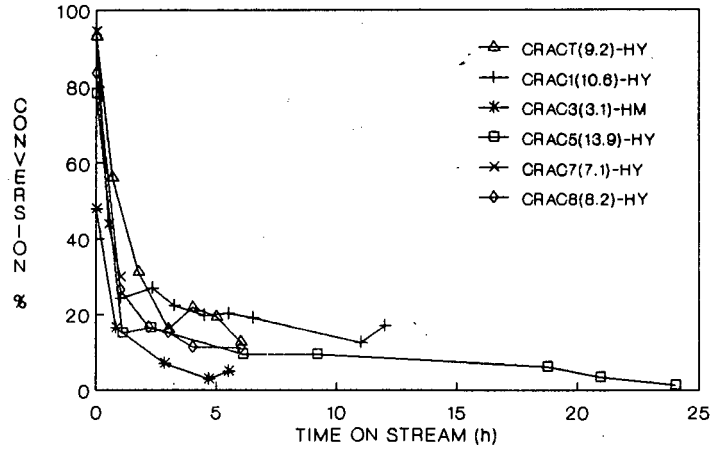

Figure 2.2a : Conversion vs time on stream for hexane cracking over HY & HM ; wt% coke in parentheses.

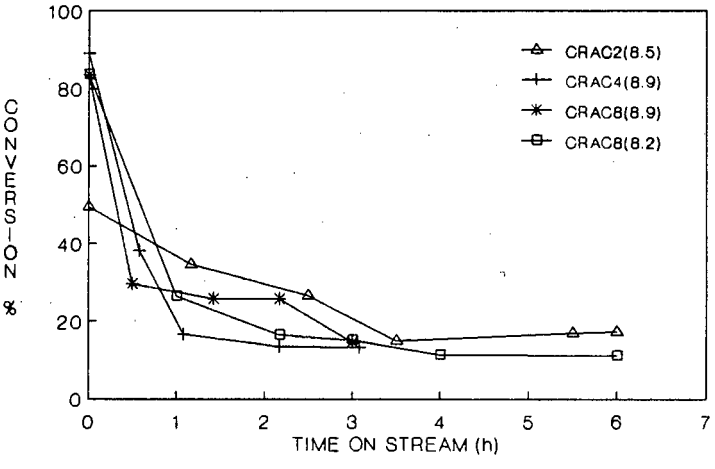

Figure 2.2b : Conversion vs time on stream for hexane cracking over HY & HM ; samples with similar coke content.

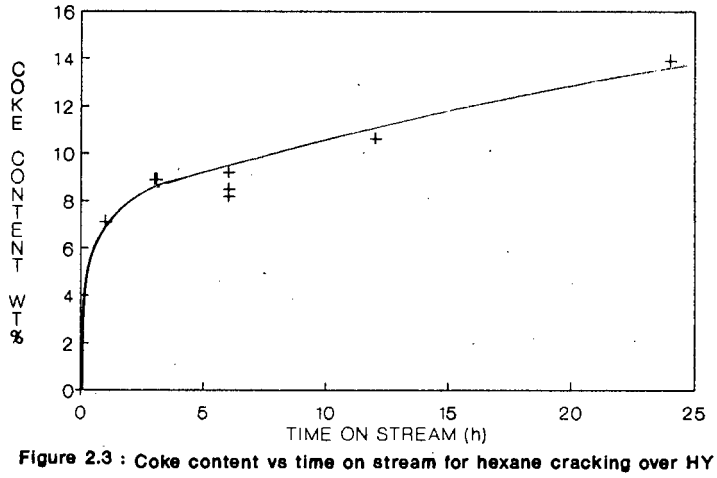

Figure 2.3 : Coke content vs time on stream for hexane cracking over HY

The initial product distribution as shown in Figures 2.4a-d consisted mainly of paraffins with propane constituting the largest fraction. The maximum temperature reached during temperature runaway (T_{max}) is also shown in these figures. However, as the coke content increased (coke increased with time on stream), the ratio of olefins to paraffins increased as shown in Figures 2.5a and b. The largest olefin to paraffin ratio was observed at the highest coke content. The olefin to paraffin ratio at small time on stream varied between 0.1 and 0.2 and tended to unity as the extent of deactivation increased. The ratio of C_4/C_3 decreased from 0.7 to 0.2 as the coke content of the catalyst increased as shown in Figure 2.5c. Figure 2.6 shows the product distribution as a function of coke content on the catalyst, using the last product sample at the end of each run as being representative of that particular coke content.

The deactivation function of Wojciechowski (1968), first order and Langmuir kinetics, represented the data well as shown in Figure 2.7. The model parameters are summarised in Table 2.2 (see section 2.2.2 for model equations). The parameters for the decay function are shown in Table 2.3 for first order and Langmuir kinetics. The parameters m and k_d are evaluated from the assumption that one active site is used per reaction event (n=1) (Pachovsky et al., 1973). Steady state conversions assuming no deactivation are also shown. The decay function using the model parameters in Table 2.3 are shown in Figure 2.8.

TABLE 2.2 : Summary of model parameters.

First order kinetics			
Catalyst	$G(h^{-1})$	N	k (g hexane/g cat•h)
HY	96.8	0.41	4.20
HM	3.81	0.94	1.40

Langmuir kinetics				
Catalyst	$G(h^{-1})$	N	A (g hexane/g cat•h)	B
HY	5.26	1.89	1.41	-1.09
HM	4.29	0.875	1.53	0.156

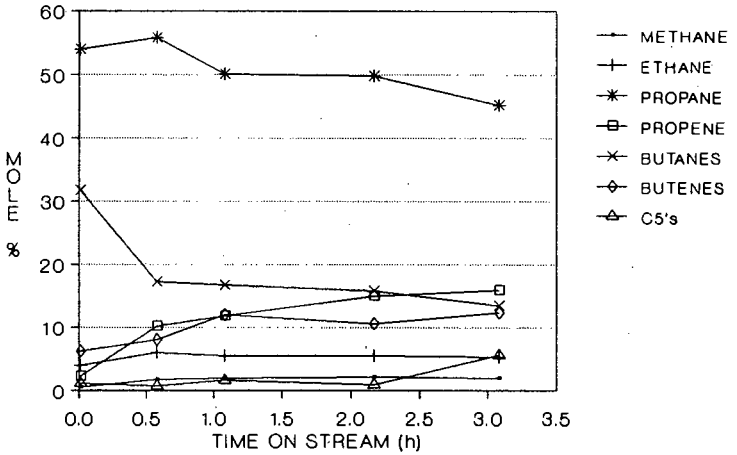

Figure 2.4a : Product distribution vs time on stream for hexane cracking over HY - CRAC4 , Tmax = 420°C.

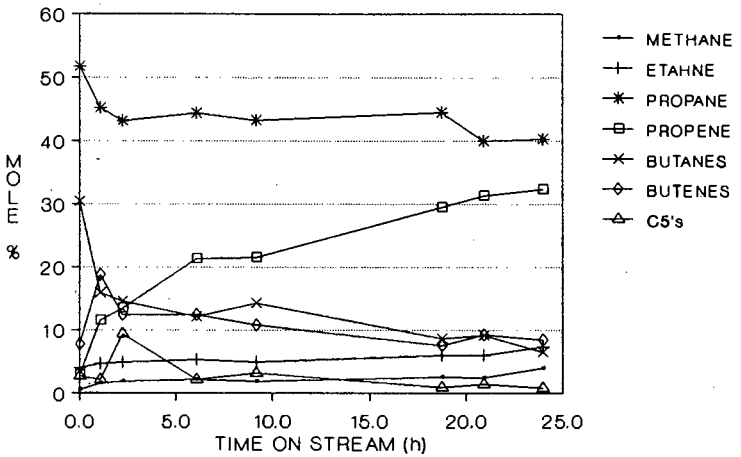

Figure 2.4b : Product distribution vs time on stream for hexane cracking over HY - CRAC5 , Tmax = 410°C.

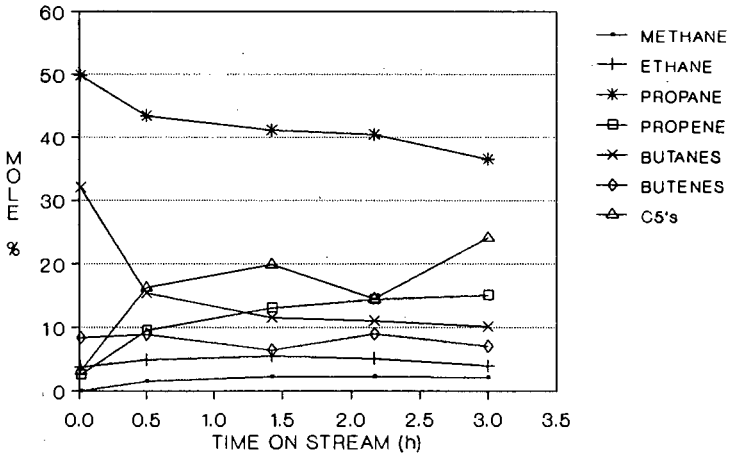

Figure 2.4c : Product distribution vs time on stream for hexane cracking over HY - CRAC6 , Tmax = 430°C

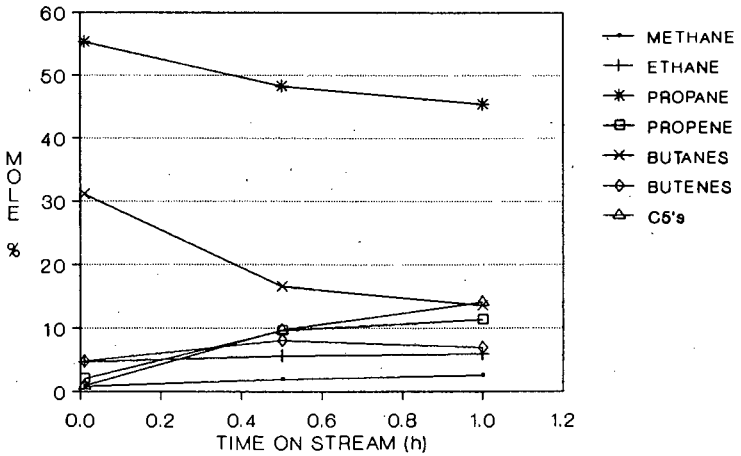

Figure 2.4d : Product distribution vs time on stream for hexane cracking over HY - CRAC7 , Tmax = 430°C.

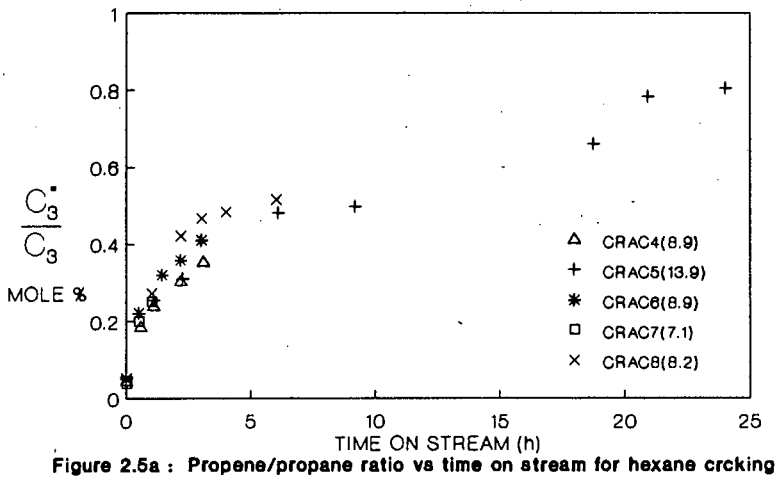

Figure 2.5a : Propene/propane ratio vs time on stream for hexane crcking over HY.

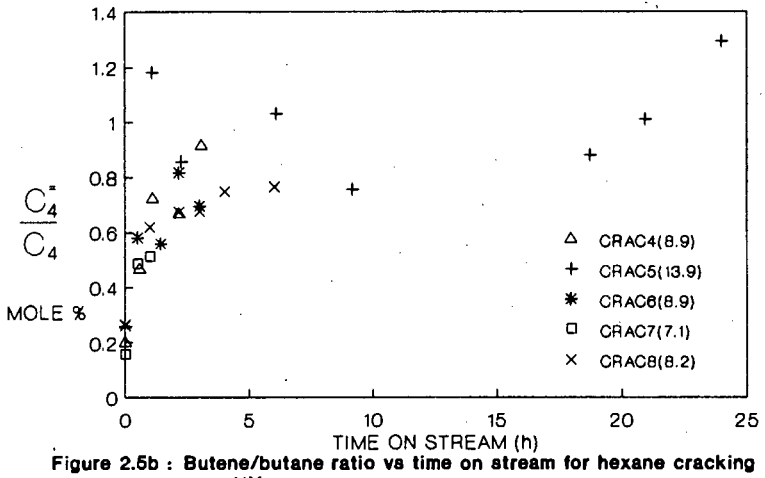

Figure 2.5b : Butene/butane ratio vs time on stream for hexane cracking over HY.

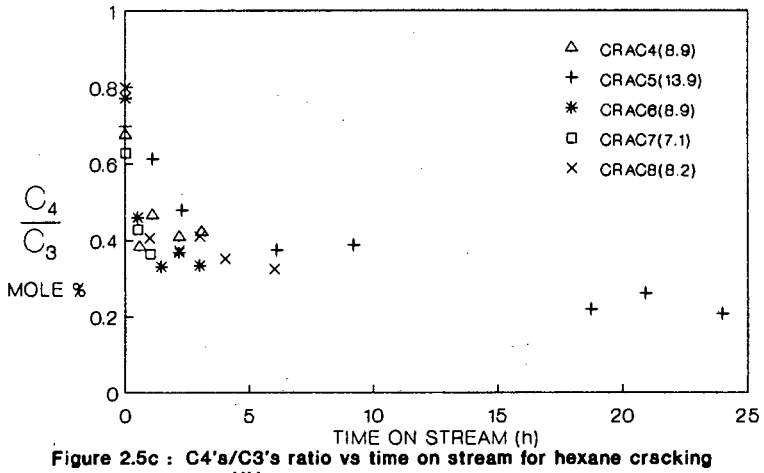

Figure 2.5c : C4's/C3's ratio vs time on stream for hexane cracking over HY

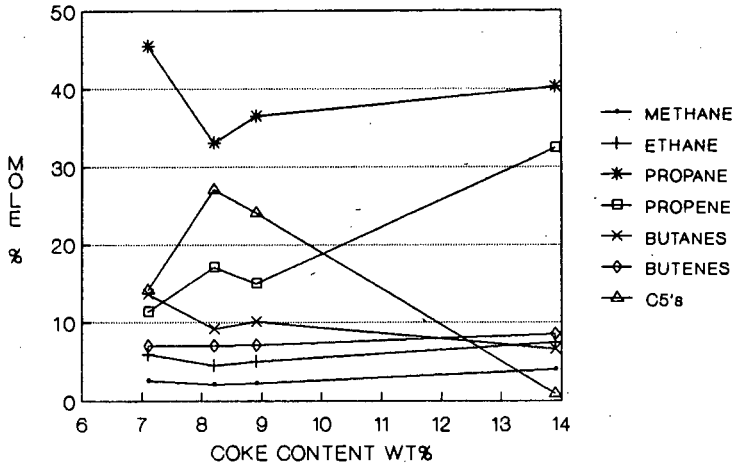

Figure 2.6 : Product distribution vs coke content for hexane cracking over HY.

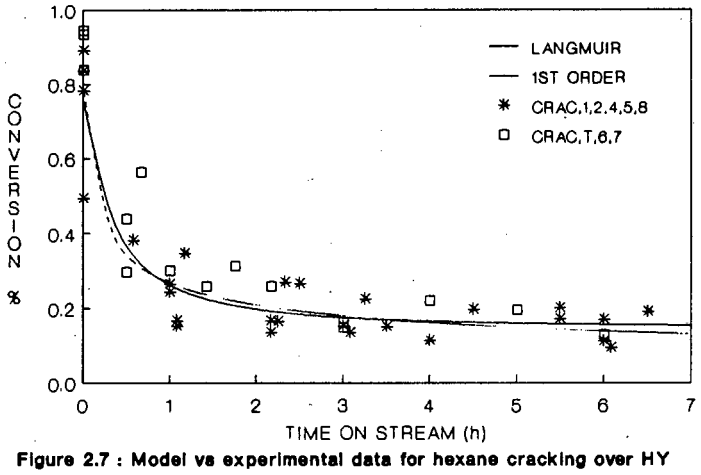

Figure 2.7 : Model vs experimental data for hexane cracking over HY

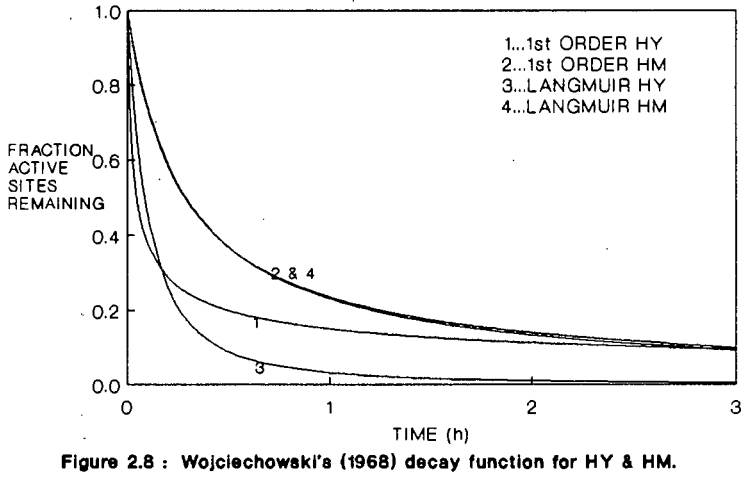

Figure 2.8 : Wojciechowski's (1968) decay function for HY & HM.

TABLE 2.3 : Decay function parameters

Catalyst	Model	k_d (h^{-1})	m	n	$X_{steady\ state}$
HY	First order	40.0	3.42	1	86%
HM	First order	3.59	2.06	1	49%
HY	Langmuir	9.92	1.53	1	77%
HM	Langmuir	3.76	2.14	1	49%

2.2.4 Discussion of hexane cracking results

Magnoux et al. (1987a,b) obtained similar trends in product distribution for the cracking of heptane over HY and HM. The temperature runaway (410-430°C for HY) did not appear to have appreciable effect on the initial product distributions shown in Figures 2.4a-d. Comparing the coke content with temperature runaway, no apparent trend was observed. This suggests that the data were comparable in terms of product distribution and coke content. The product distributions can be explained by the usual mechanism of carbenium ion formation of C_6, isomerisation, cracking into two C_3 fractions and the secondary transformation of olefinic products by alkylation and hydride transfer. The secondary transformations of the olefins are initially very rapid giving rise to the low olefin to paraffin ratios. This is because the olefins are adsorbed much more strongly than the paraffins and spend longer time in the pores of the catalyst, thereby increasing the probability of undergoing transformations. Transformations would occur in the catalyst micro-pores in the presence of a large number of strong acid sites. Once the catalyst is deactivated, the probability of olefins undergoing transformations is reduced, and more olefins are desorbed before undergoing further reactions. Coke could reduce the effective pore size, which would restrict the formation of bulky intermediates formed during the olefin transformations. Alternatively the pores could be partially blocked, resulting in fewer accessible acid sites, and this would produce a similar effect. To determine the cause of the shift in product distribution with coke content, it is essential to understand more about the effect of coke on the structure and acidity of the catalyst pores.

Individual determination of the hexane cracking model parameters for each run yielded erratic estimations due primarily to inaccurate measurement of

initial conversion and insufficient data points in the time on stream region of 0 to 1 h where most of the deactivation took place. The temperature runaway was also responsible for differences in the initial conversion. However, when all the data for HY at a WHSV = 2 were used and model parameters optimised simultaneously, there was better consistency between theory and experiment than when optimisation was carried out individually for each run. Based on the analysis of Wojciechowski (1968), who distinguished three classes of catalyst depending on the value of N, the values of N indicate that HM is a class I catalyst (N<1). However in light of the fact that only one run was performed over HM, any interpretation of the results is speculative since there were not enough data points. HY on the other hand is either class I or class III (N>1) catalyst depending on the kinetics. As the value of N becomes small the ideal non-aging catalyst is obtained. In the case of HY, first order kinetics yields N = 0.41, which is not likely as HY deactivates rapidly. It is therefore more likely that HY is a class III catalyst for which Langmuir kinetics is applicable. This indicates that there may be a difference in hexane cracking mechanism between HM and HY. Interestingly one cannot distinguish between the two kinetics from a goodness of fit shown in Figure 2.7. However, when fluidized and moving bed reactors were modelled (Pachovsky et al., 1973), all catalysts were found to behave as class II (N=1).

For the Langmuir kinetics the parameter B = -1.09 for HY was obtained, similar to the value obtained by Abbot and Wojciechowski (1987). The value of B = -1 indicates high surface coverage and strong adsorption. This suggests that hexane cracking is greatly inhibited by olefinic products which adsorb strongly. Abbot and Wojciechowski (1987) also showed that Langmuir kinetics would better describe paraffin cracking and that the first order model would apply only to the case in which the number of molecular species remains constant during reaction, such as in isomerisation, and in which reactant molecules have similar adsorption constants to those of the product molecules. The data of Abbot and Wojciechowski (1987) show much faster deactivation rates for n-octane, n-dodecane and n-hexadecane, indicated by large values of G and k_d, as expected. It is, however, felt that their data do not contain sufficient points in the initial reaction stages to evaluate the model parameters accurately.

In the case of HM both types of kinetics yield the same deactivation function and steady state conversion. Hence first order kinetics describes the

reaction just as well as Langmuir kinetics. This is not in agreement with the work of Abbott and Wojciechowski (1987) who found that first order kinetics could not fit their data. In this work the squared error residuals were similar for both types of kinetics over HM. In other words the squared error residuals were not a good criterion of the applicability of each model due to the nature of the data. However the expansion coefficient ϵ in this work was 0.1 (from the product distribution data) while Abbott and Wojciechowski had $\epsilon > 1$. A small value of ϵ would favour first order kinetics (e.g., for isomerisation $\epsilon = 0$). It should be recalled that in the present study only one run was carried out over HM owing to its fast deactivation. Hence there are not sufficient data points to draw clear conclusions on the deactivation of HM. For HY different deactivation functions and steady state conversions were obtained for each model. The values of m are expected to be smaller than those for larger molecules (n-octane m = 2.25, Abbott and Wojciechowski), and hence m = 1.53 is more likely (less sites lost per deactivating event for small molecules). This suggests that Langmuir kinetics is applicable to HY.

The decay function shows that HY loses active sites at a greater rate than HM (see Figure 2.8). However, the drop in conversion with time on stream for HY was slower than for HM. This suggests that HY must have more active sites which are used for cracking than HM. It has been proposed by Abbott and Wojciechowski (1987) that for $2 < m < 3$ pore blocking is the prevalent mechanism. Therefore, pore blockage may have been dominant in HM but not in HY. HM was nearly inactive after 5 h on stream with 6% of active remaining sites, while HY had approximately 15% conversion after 5 h on stream with only 0.2% active sites according to Langmuir kinetics (For the first order kinetics HY has 7.7% of active sites remaining). This may be an indication of pore blockage in HM, due to its one dimensional pore structure. Other techniques would have to be used to investigate this phenomenon further.

2.3 HIGH PRESSURE PROPENE OLIGOMERISATION

2.3.1 Apparatus and procedure

Figure 2.9 shows a schematic diagram of the high pressure reactor system. Feed gas, a mixture containing 79 mol% propene and the balance consisting of propane and ethane (see Appendix A, Table A3) obtained from Sasol, was supplied from a No.7 CADAC cylinder held at 40°C (approx. 15 atm) to ensure enough suction head for the pump. The feed was dried by 3A molecular sieves and any particulate matter was removed by a 0.5 μm physical filter. A Lewa diaphragm pump was used to pump the feed to 30-65 atm pressure. The pump head was kept at 5°C to prevent any flashing. Inlet to the pump was 1/4" stainless steel tubing, whereas all other tubing was 1/8" stainless steel.

Feed to the catalyst bed was preheated by a bed of 2 mm glass beads. The temperature profile in the catalyst bed could be obtained from a thermocouple in the thermowell axially positioned at the centre of the reactor. Temperature control of the reactor was accurate to within ± 1°C at 200°C. The two 500 W cartridge heaters were able to power the reactor to over 500°C. The cooling rate of the reactor was poor, and to minimize temperature runaway the insulation was used only during calcination. The product from the reactor passed through a 0.5 μm physical filter and a condenser at 5°C to protect the back pressure regulator from any entrained catalyst particles and overheating, respectively. The back pressure regulator was capable of handling gas and liquid. The back pressure regulator was kept at 40°C to prevent the flashing product from freezing.

The liquid and vapour were separated in a double walled glass catch-pot kept at 5°C. Liquid product could be tapped off at the bottom while the gas passed through a sampling loop and a wet gas meter. For calcination and purging the system after reaction a side line through which either air or N_2 could be passed was used. During calcination the reactor was disconnected from the product line. The operating conditions for the reactor system are outlined in Table 2.4.

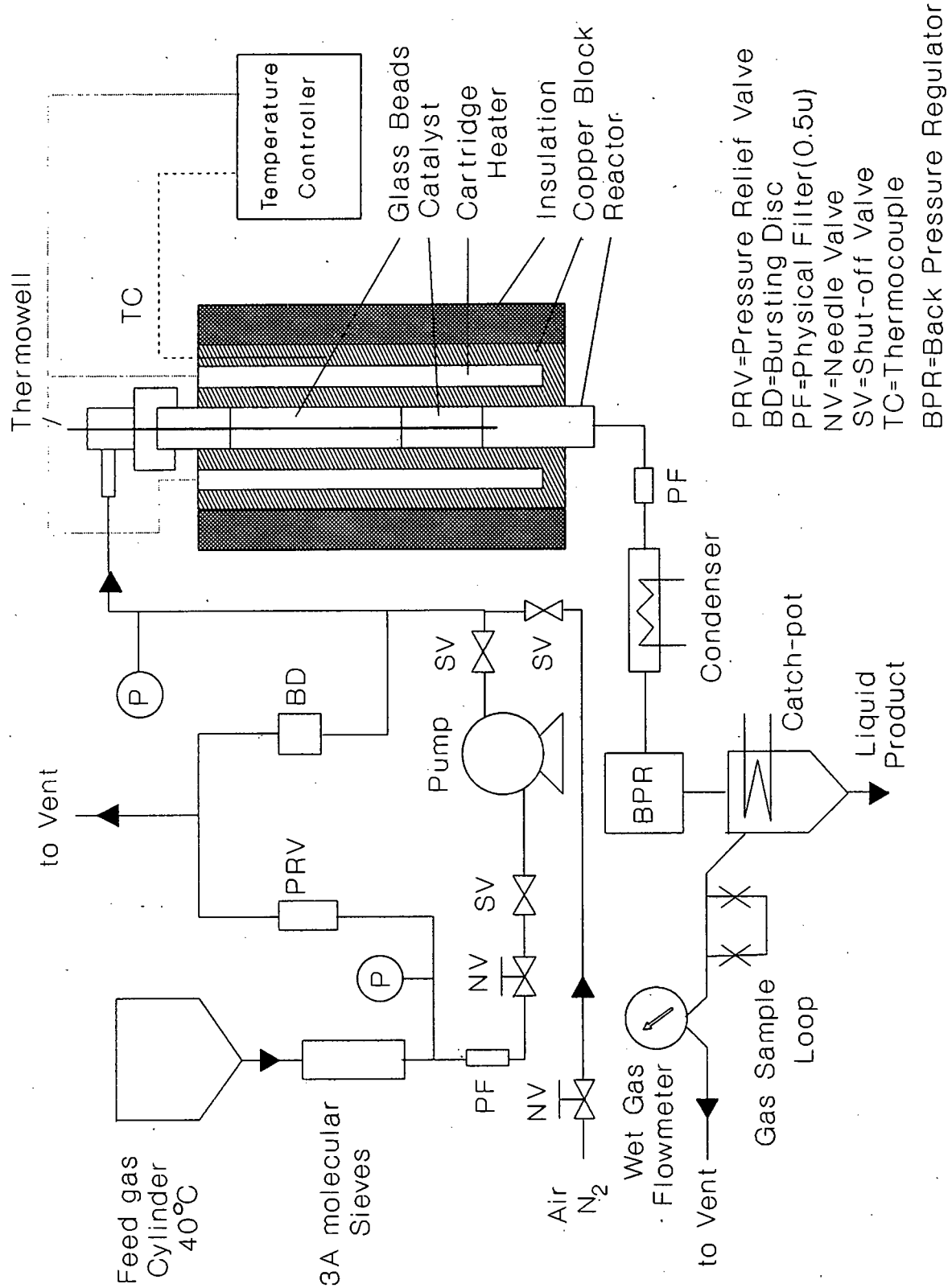

Figure 2.9 : Propene oligomerisation high pressure reactor system

TABLE 2.4 : Reactor operating conditions

Pre-treatment	Calcination at 400°C HY/350°C HM in air
Feed	79% propene
Catalyst volume	10 mℓ, ca. 6 g
WHSV	1-4 g propene /g cat·h
Pressure	30, 50 and 65 atm, gauge

The start-up procedure and operation are summarised below. Before starting the pump the following checks were made: the feed gas cylinder stable at 40°C, the 3A molecular sieves regenerated, the back pressure regulator at 40°C and the coolant to the pump and condensers at 5°C. Prior to operation the system was checked for leaks with high pressure nitrogen. The reactor was then pressurised with 8 atm of nitrogen. Propene feed was slowly passed into the system through a needle valve until bottle pressure (ca. 15 atm) was reached. The system was then pumped to pressure. At this point the temperature controller was turned on and the system was slowly heated. It was found that HY always had a temperature runaway at the flash point of the feed (≈ 90°C). This was not controllable with this reactor system. The effect was reduced by approaching the flash point temperature slowly. Temperature runaway was not observed in the case of HM.

Once a reasonably stable temperature had been obtained the first sample was taken. The product gas analysis showed that the gaseous effluent consisted primarily of unreacted feed as most of the dimer was condensed as a liquid. Liquid product was collected in sealed bottles, weighed and analysed by GC. Once the catalyst had deactivated sufficiently the pump was stopped and the residual gas flowed slowly through the system. The system was then flushed with nitrogen at the reaction temperature overnight and any residual liquid was collected.

The mass of propene was obtained by weight difference of the feed gas cylinder. The initial mass of the cylinder was taken after the line up to the shut-off valve before the pump was filled. The final mass of the cylinder was measured after the run. This was compared to the total volume of gas plus the total liquid obtained after flaring the system for the purpose of checking the mass balance.

2.3.2 Data analysis

The mass balance calculations were based on the average product gas density which varied by less than 1% (see Appendix A, Table A4) for an entire run. The mass balances for all the runs were good to within 5%. The start time of a run was taken as zero when the propene feed was passed onto the catalyst.

The WHSV was based on the feed rate of propene. The total mass of feed passing through the system was calculated by accounting for product gas and liquid in a time increment. Hence by knowing the feed composition (from gas analysis), the feed rate of propene was calculated. The average conversion for a time increment could then be calculated by dividing the amount of liquid produced by the mass of propene fed.

The average liquid production rate (g liq/g cat•h) was a good measure of the catalyst activity but was dependent on the feed rate. Liquid compositions were analysed on a 3.8 m column packed with 3% OV-101 on Chromosorb W-HP. The peaks were grouped into oligomers of propene as dimer (C_5-C_7), trimer (C_8-C_{10}), tetramer, pentamer, hexamer and heptamer+. The sampling interval depended on the activity of the catalyst (i.e., the amount of liquid produced) and ranged from ½ to 2 h.

As the catalyst deactivated rapidly none of the runs were continued for more than 12 h. Steady state was never achieved. The WHSV also varied from run to run, because the pump was operated near its lower flowrate limit causing unsteady behaviour. Flowrate adjustments were not attempted because some runs were only six hours long. Experience showed that any flowrate adjustments would cause even greater unsteady behaviour. All the above factors contributed to making the comparison of runs difficult as reaction parameters varied from run to run. One indicator of how hard a catalyst has worked is the total amount of liquid produced per gram of catalyst. For the purpose of determining trends such as the variation of product composition with deactivation, and the effect of reaction temperature and pressure on reaction rate and deactivation, the data were reasonable.

2.3.3 Results

The oligomerisation data are considered in terms of the hourly rate at which liquid product is formed per gram catalyst (LPR - liquid production rate), composition of the oligomer product, activity which is based on the total amount of liquid formed per gram of catalyst divided by the total time on stream in hours (LPR(ave)), rate of deactiviation, and the coke content of the catalyst. The effects of temperature, pressure and regeneration on propene oligomerisation over HY and HM were investigated.

2.3.3.1 Constant reaction conditions (reproducibility)

Figures 2.10a and 2.11a show the results of propene oligomerisation reactions at 200°C and 300°C over HY and HM, respectively. The corresponding WHSV's as a function of time on stream are plotted in Figures 2.10b and 2.11b. During start-up, the temperature of the reactor rose considerably above the set temperature in the case of HY. The maximum temperature observed during such a temperature runaway is shown in parentheses in Figure 2.10a. For HY the differences in LPR from run to run are caused by differences in WHSV as shown in Figure 2.10b. Comparison of OLIGT with OLIG2, and of OLIG1 with OLIG5 shows that the data are fairly reproducible for a given flow rate, particularly in light of rapid deactivation and temperature runaway observed during start-up. The product composition for two runs over HY are shown in Figures 2.12a and b. Two numbers given in parentheses for coke correspond to wt% high boiling point hydrocarbons and graphitic coke which will be discussed in Chapter 3. The variation of liquid composition was greater in the case of OLIG18 than in OLIG5. In the former, the initial composition contained more dimer and less heavier fractions than in OLIG5, but with increasing time on stream the heavier fractions increased significantly at the expense of dimer, approaching the product composition in OLIG5. For OLIG5 there were only marginal increases in tetramer and pentamer. Besides having a lower WHSV, OLIG5 had a temperature runaway to 320°C during start-up, while for OLIG18 the maximum temperature during start-up was 250°C. The final coke compositions for OLIG5 were 4.4 wt% high boiling point hydrocarbons and 16.7% graphitic coke. The corresponding values for OLIG18 were 4.3% and 16.9%, respectively. Figure 2.10a shows that the rate of deactivation was not significantly dependent on temperature runaway and was primarily a function of WHSV, viz., deactivation was rapid at high WHSV.

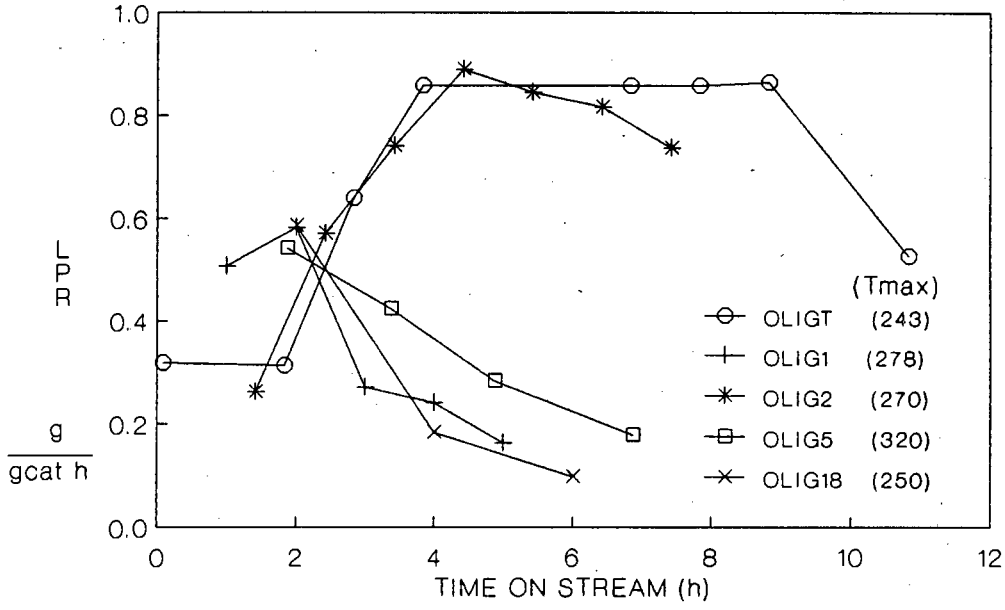

Figure 2.10a : LPR vs time on stream for propene oligomerisation over HY, T = 200°C, P = 50 atm

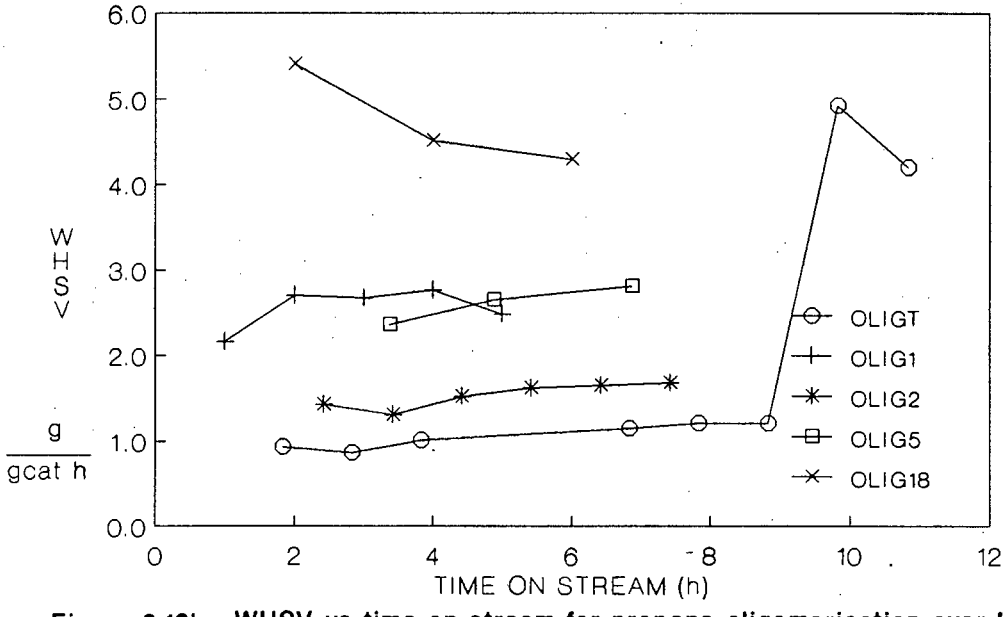

Figure 2.10b : WHSV vs time on stream for propene oligomerisation over HY, T = 200°C, P = 50 atm.

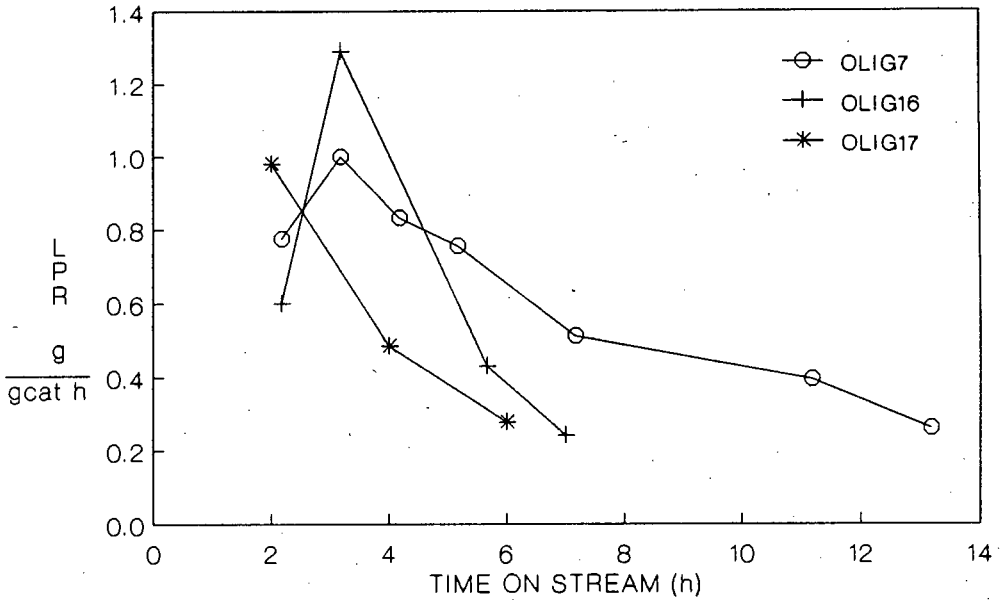

Figure 2.11a : LPR vs time on stream for propene oligomerisation over HM, T = 300°C, P = 50 atm

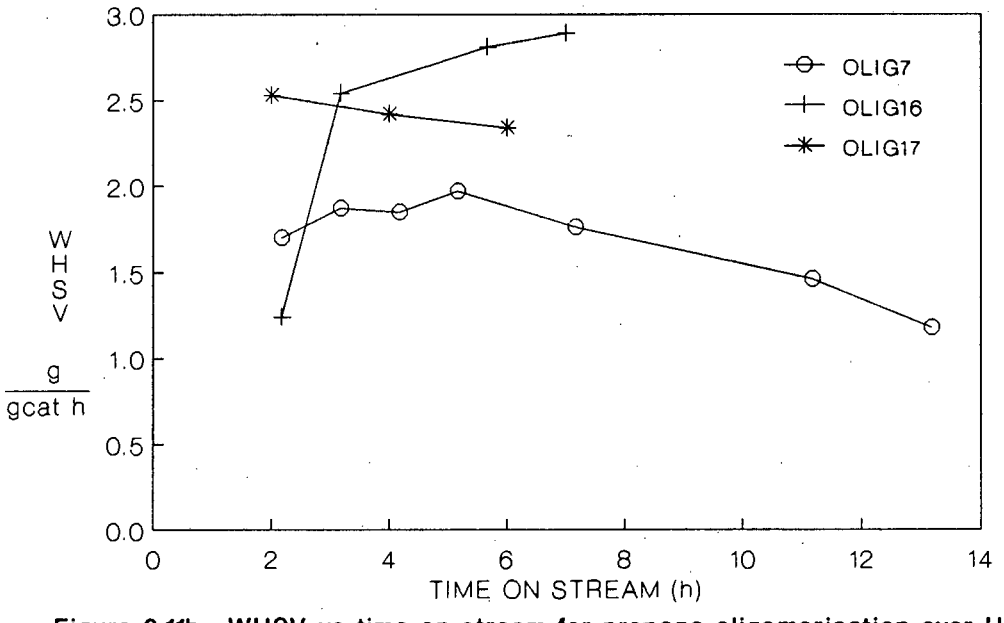

Figure 2.11b : WHSV vs time on stream for propene oligomerisation over HM, T = 300°C, P = 50 atm

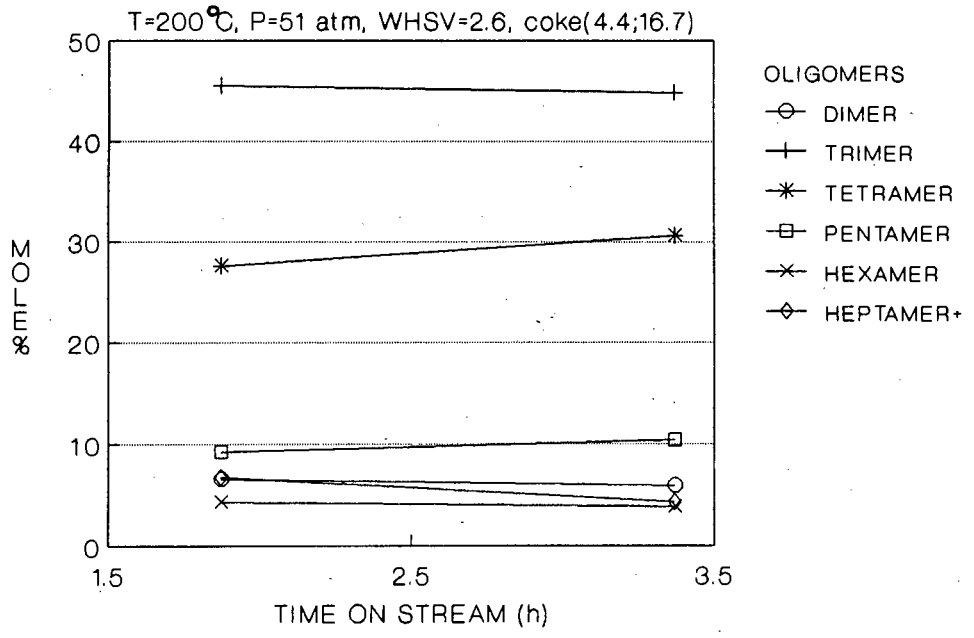

Figure 2.12a : Product distribution vs time on stream for propene oligomerisation over HY - OLIG5

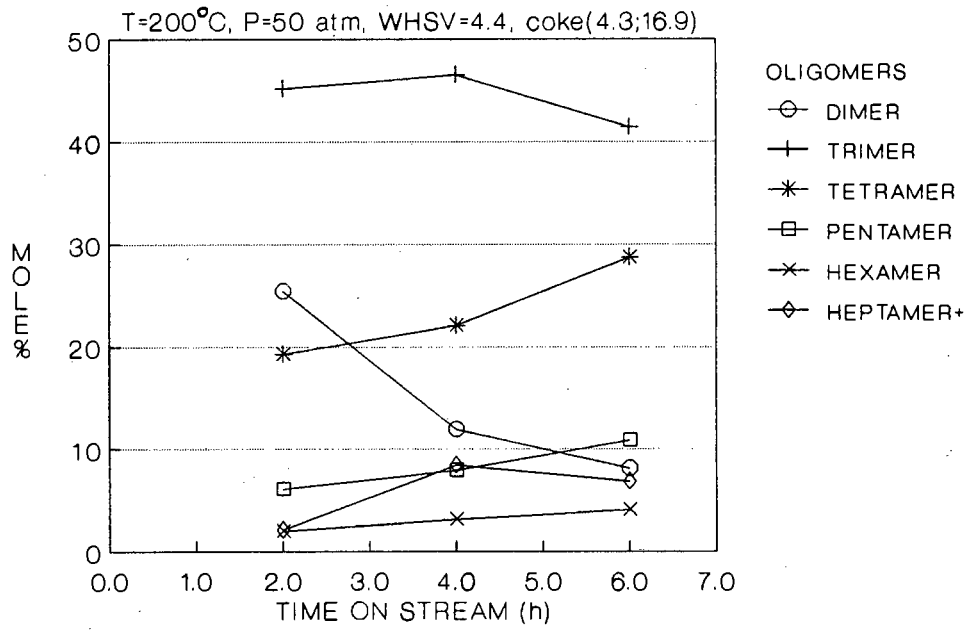

Figure 2.12b : Product distribution vs time on stream for propene oligomerisation over HY - OLIG18.

Figures 2.11a and b show that HM had a high initial LPR, but deactivated rapidly, particularly at high WHSV. The reaction temperature was steady and no temperature runaway was observed during start-up. Monotonically increasing WHSV in OLIG16 resulted in the maximum LPR after 3.2 h on stream. A similar variation of LPR with WHSV was observed in OLIG7. Initial variations in LPR were primarily due to the variations in WHSV, but as previously discussed any on-line adjustments would have caused greater variations.

Figures 2.13a-c show the product compositions for HM. In all three cases the product composition shifted to heavier fractions with increasing deactivation. There was a maximum in the dimer and a minimum in the heptamer+ (OLIG7) and tetramer and pentamer (OLIG16) contents which corresponded to the maximum LPR in Figure 2.11a.

2.3.3.2 The effect of reaction temperature

Figure 2.14a shows that increasing temperature increased LPR at the expense of catalyst lifetime for HY. In all the runs the reactant was in the gas phase as the flash point of the feed was approximately 90°C at 50 atm. The effect of temperature can be seen when comparing OLIG12 with OLIG3 and OLIG4 with OLIG2, both sets of which had similar WHSV. The liquid product composition in Figures 2.14b and 2.12b shows that low temperature favoured trimer and tetramer.

HM was found to be inactive for propene oligomerisation below 200°C, in contrast to HY which showed activity even at room temperature. Figure 2.15a shows that the activity was low even at 250°C and high WHSV. The LPR at 300°C was significantly greater than that at 250°C, but deactivation was more pronounced, particularly at small time on stream. The LPR at 350°C followed the same trend as that at 300°C. This run was hampered by fluctuating low WHSV. Given that the WHSV was less than ½ of those in the other two runs, the activity was considerably higher. Figures 2.15b and c and Figure 2.13a show that as the reaction temperature was increased there was an increase in the amount of dimer formed. Taking product distribution at small time on stream as representing a low coke content catalyst (there was no temperature runaway), at 250°C trimer and tetramer constituted over 60% of the liquid

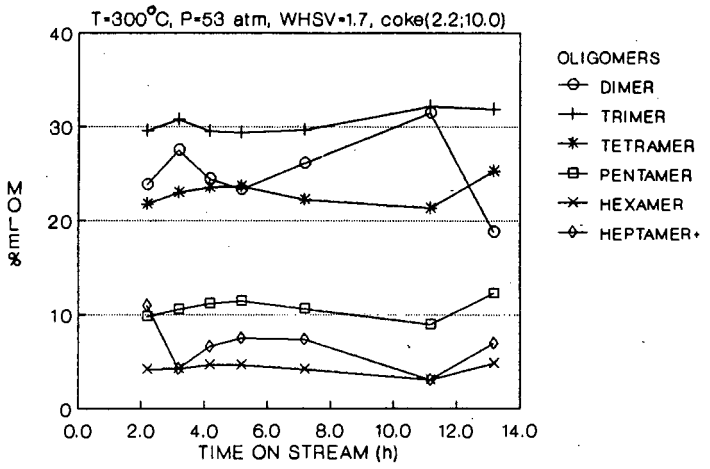

Figure 2.13a : Product distribution vs time on stream for propene oligomerisation over HM - OLIG7.

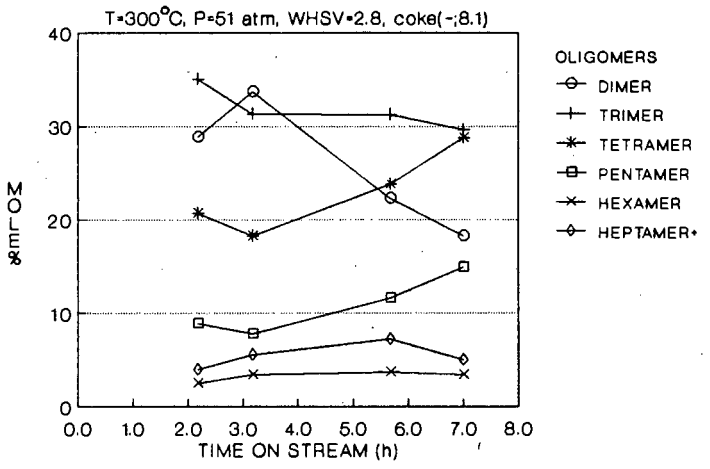

Figure 2.13b : Product distribution vs time on stream for propene oligomerisation over HM - OLIG16.

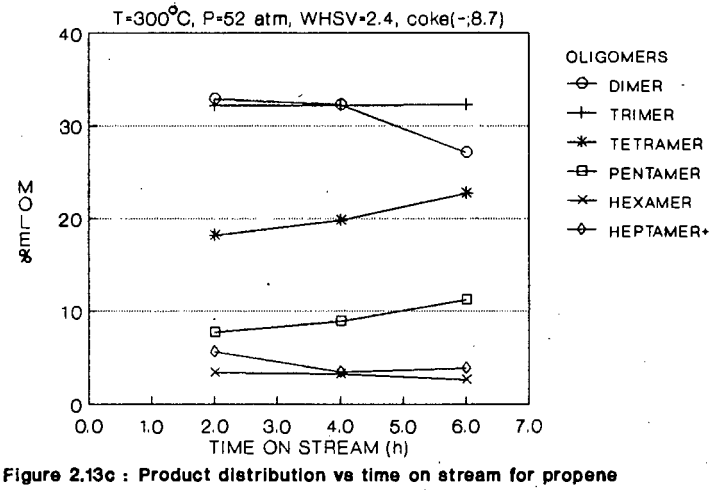

Figure 2.13c : Product distribution vs time on stream for propene oligomerisation over HM - OLIG17.

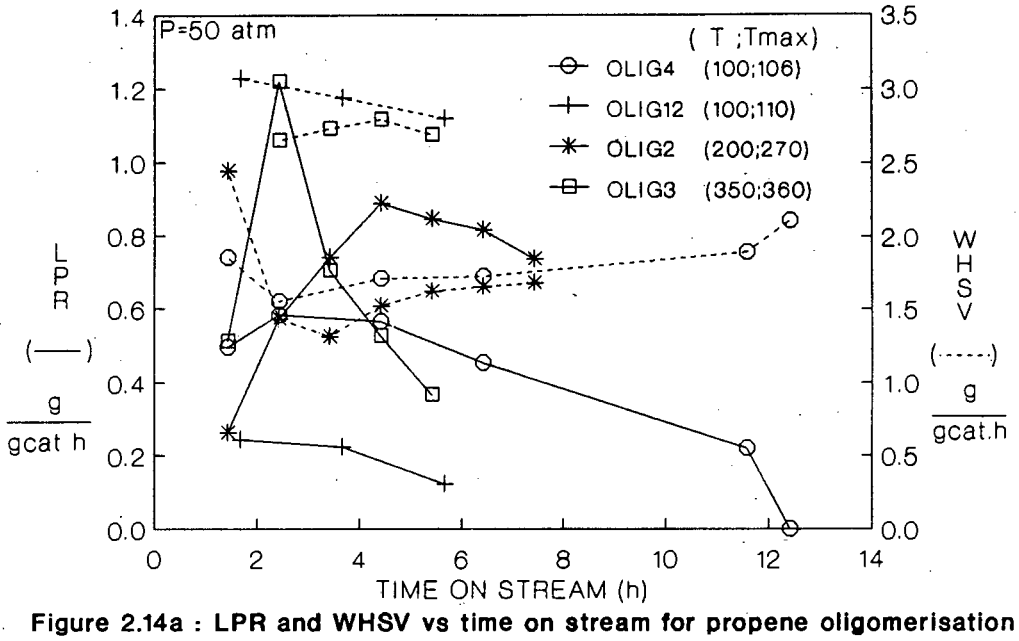

Figure 2.14a : LPR and WHSV vs time on stream for propene oligomerisation over HY; effect of reaction temperature.

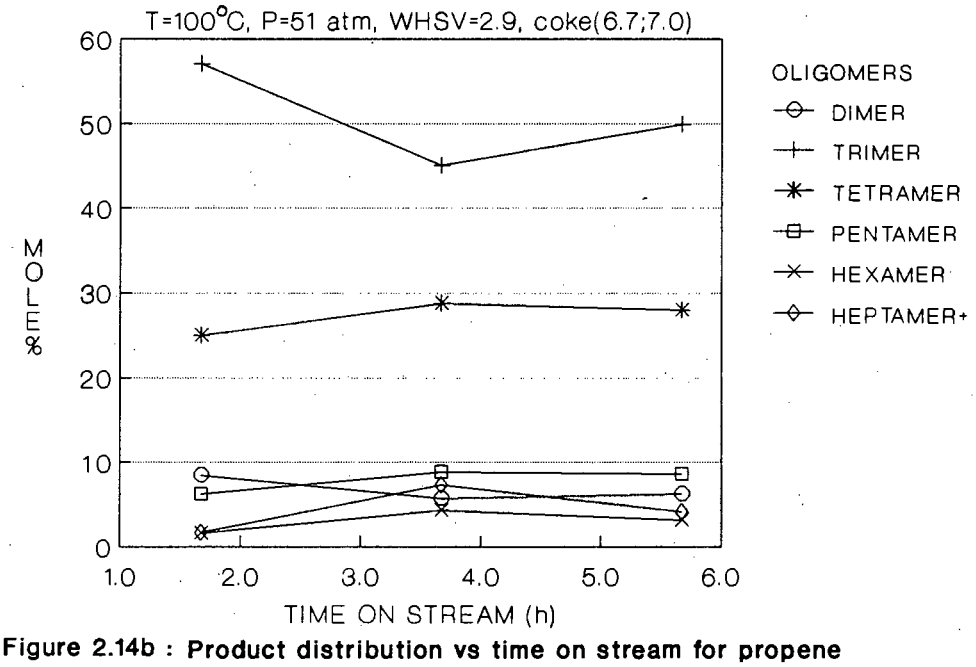

Figure 2.14b : Product distribution vs time on stream for propene oligomerisation over HY - OLIG12.

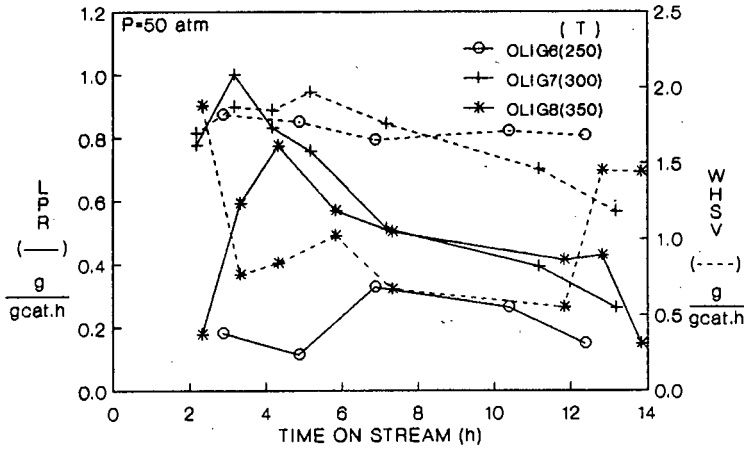

Figure 2.15a : LPR and WHSV vs time on stream for propene oligomerisation over HM; the effect of reaction temperature.

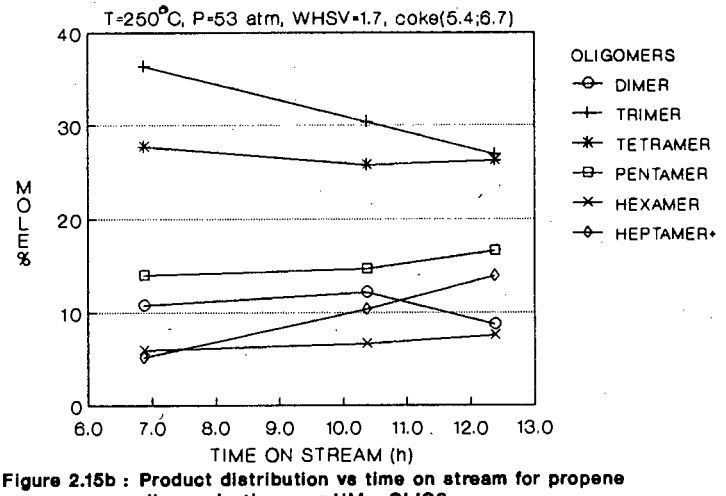

Figure 2.15b : Product distribution vs time on stream for propene oligomerisation over HM - OLIG6

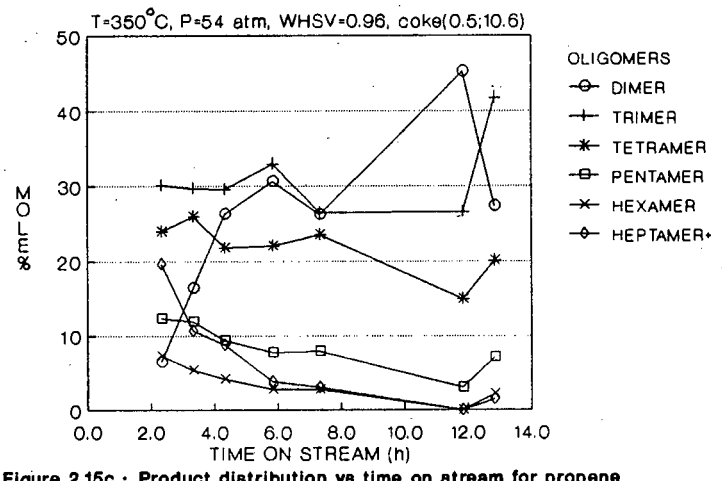

Figure 2.15c : Product distribution vs time on stream for propene oligomerisation over HM - OLIG8

product. At 300°C the dimer content became substantial. At 350°C, because of the low WHSV (and hence longer residence time) the dimer content was low and trimer and tetramer constituted about 50% of the total product. With increasing time on stream the product spectrum shifted to heavier fractions at 250°C. However at 300 and 350°C the product distributions shifted to lighter fractions.

Figure 2.16 shows that the activity of HY increased with increasing reaction temperature. The data points were taken at varying WHSV, but the effect of WHSV was less pronounced than the effect of reaction temperature. The coking rate at 350°C was not high enough to cause a reduction in LPR(ave) within the reaction time examined. Lighter fractions were produced during initial reaction stages when the activity was high. As the activity fell longer chain length products were detected by the GC. Figure 2.17 shows that graphitic coke increased with increasing reaction temperature. HY produced more graphitic coke than HM. This was also observed in the case of hexane cracking. As the reaction temperature was increased, the coking rate of HY increased faster than that of HM.

2.3.3.3 The effect of reaction pressure

Figure 2.18a shows that high pressure markedly enhanced the LPR and lifetime of HY. The deactivation at high pressure became significant only after 10 h. At 30 atm the LPR was low with rapid deactivation. Figures 2.18b-d show that at high pressure the formation of heavier fractions was favoured towards the end of the reaction. Considering the initial samples which are assumed to correspond to low coke content, 65 atm produced considerably less dimer with more heptamer+. However the next sample of the 65 atm run showed a large increase in dimer with a corresponding decrease in heptamer+. Comparison of the liquid compositions towards the end of each run which represented deactivated catalyst shows that at 30 atm more pentamer, hexamer and heptamer+ were produced at the expense of dimer. Comparing the runs over long periods of time was difficult because the low LPR at 30 atm produced enough liquid for only two analyses. The WHSV at 65 atm was 1.6/h while at 30 atm it was 2.2/h.

Figure 2.19a shows that for HM the increased LPR at high pressure was followed by rapid deactivation after 6 h on stream. At 30 atm the LPR was

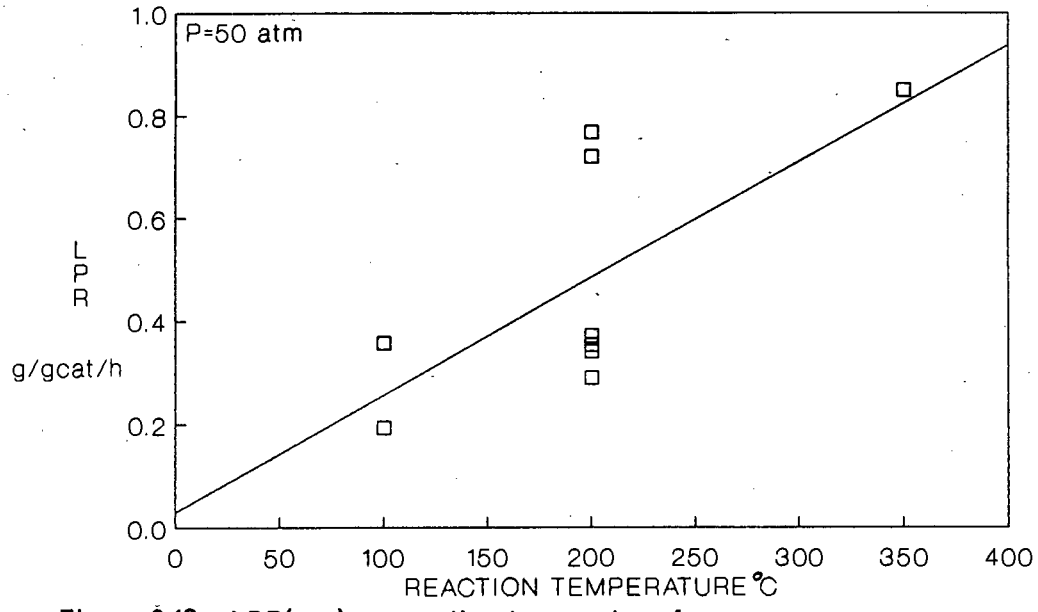

Figure 2.16 : LPR(ave) vs reaction temperature for propene oligomerisation over HY.

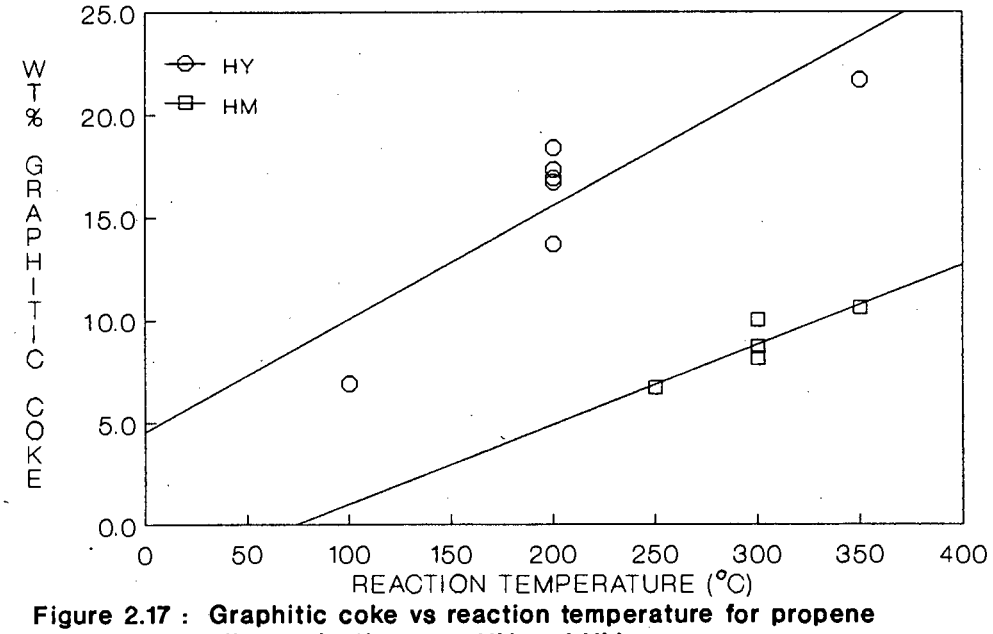

Figure 2.17 : Graphitic coke vs reaction temperature for propene oligomerisation over HY and HM.

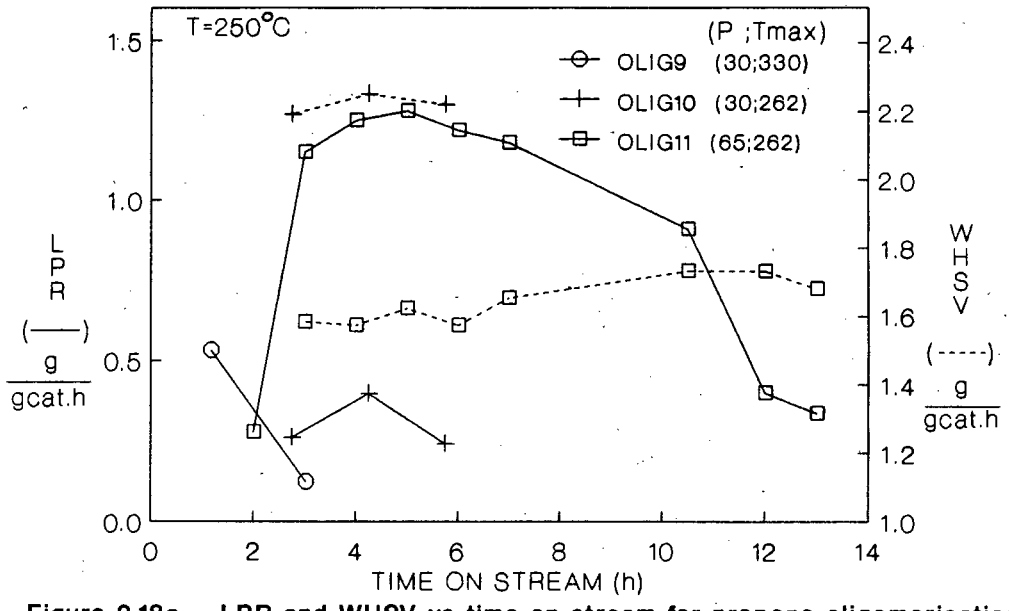

Figure 2.18a : LPR and WHSV vs time on stream for propene oligomerisation over HY; the effect of reaction pressure.

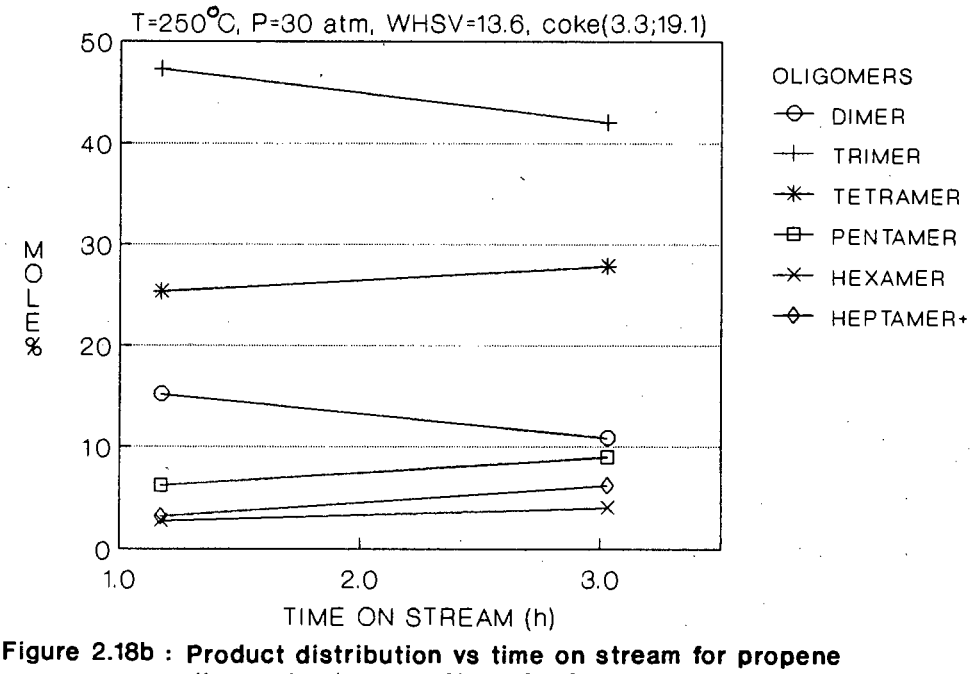

Figure 2.18b : Product distribution vs time on stream for propene oligomerisation over HY - OLIG9.

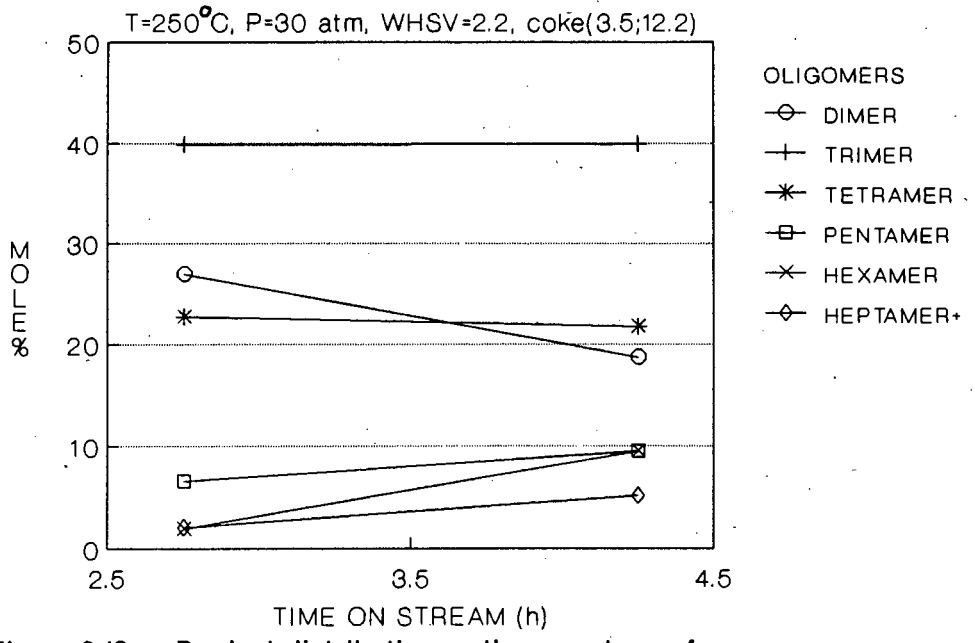

Figure 2.18c : Product distribution vs time on stream for propene oligomerisation over HY - OLIG10.

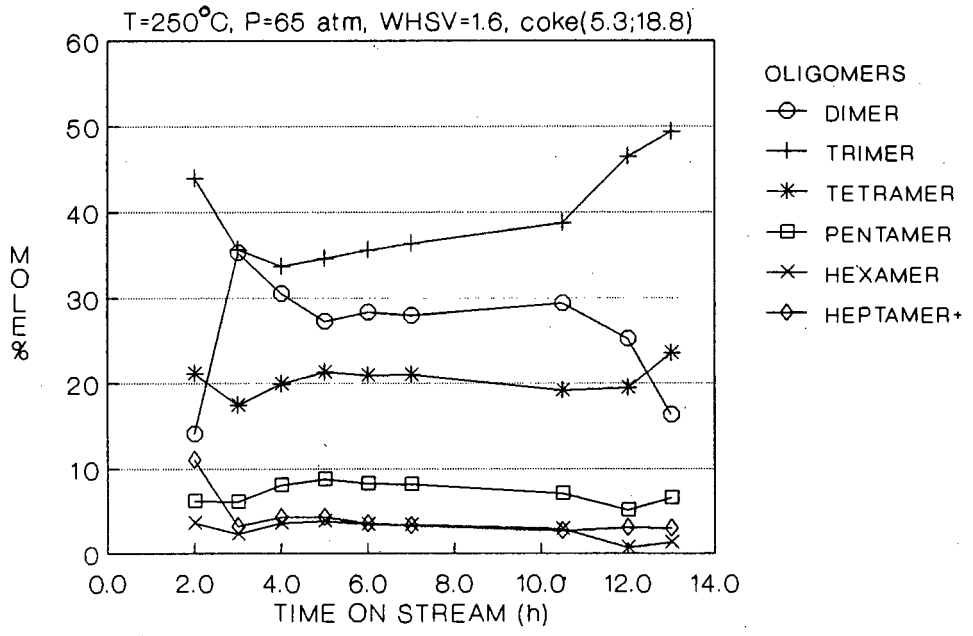

Figure 2.18d : Product distribution vs time on stream for propene oligomerisation over HY - OLIG11.

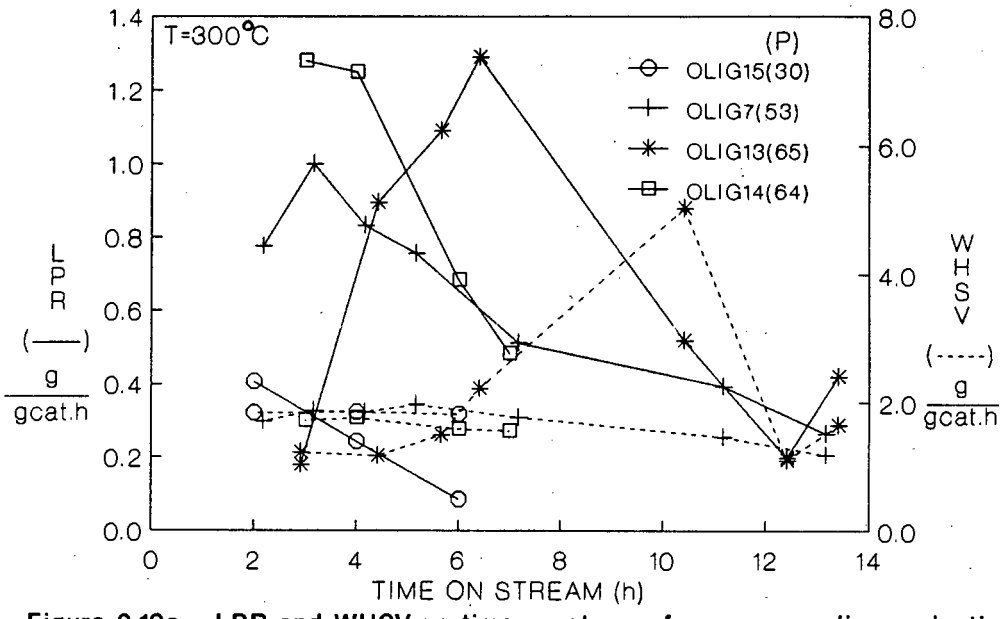

Figure 2.19a : LPR and WHSV vs time on stream for propene oligomerisation over HM; the effect of reaction pressure.

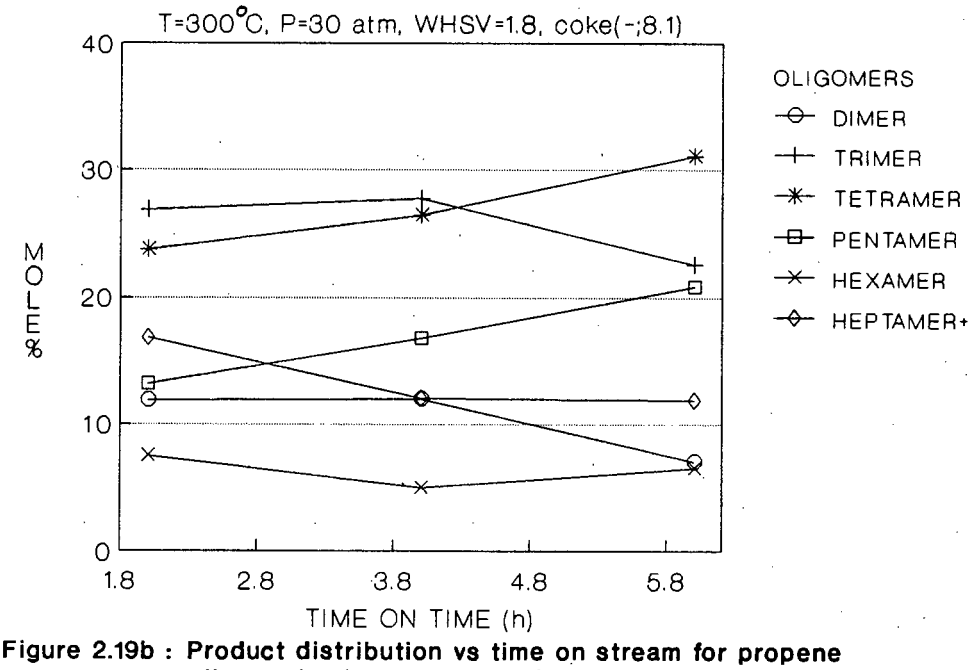

Figure 2.19b : Product distribution vs time on stream for propene oligomerisation over HM - OLIG15.

low with approximately the same deactivation behaviour as that at 50 atm. Figures 2.19b-d and Figure 2.13a show that high pressure favoured the formation of lighter liquid product. With the exception of OLIG13 all the WHSV's were similar. Considering the initial samples (i.e., low coke content) at 30 atm there was a substantial amount of pentamer and heptamer+. With increasing pressure the dimer content increased at the expense of pentamer+.

Figure 2.20 shows that the activity (LPR(ave)) was not only higher for HY than for HM, but also increased faster with increasing pressure. In contrast Figure 2.21 shows that the graphitic coke content for HY increased with increasing pressure while for HM graphitic coke content remained relatively constant. In other words, the rate of liquid product formation increased more with increasing pressure for HY than HM in spite of the greater deposition of coke.

2.3.3.4 The effect of regeneration

HM samples used in OLIG16 and OLIG17 were flushed in flowing nitrogen overnight and tested again for propene oligomerisation. TG/DTA experiments showed that this temperature would allow most of the high boiling point hydrocarbons to desorb. However, no liquid product formation was observed after this treatment. In contrast, HY was found to regain its initial activity as shown in Figure 2.22a. Both reactions showed a temperature runaway to 250°C. Figures 2.22b and 2.12b show that the regenerated HY favoured slightly lighter liquid fractions, but differences were small. Comparing initial samples it can be seen that the regenerated catalyst had low dimer content and more trimer. This is expected if coke causes a shift to heavier fractions as was observed with previous data. However, when comparing the liquid composition of the last product sample it is seen that OLIG18 (fresh) produced less dimer and more tetramer and pentamer than OLIG18 (regenerated). The WHSV in OLIG18 was higher, causing faster deactivation, and this could have caused a shift to longer chain length hydrocarbons.

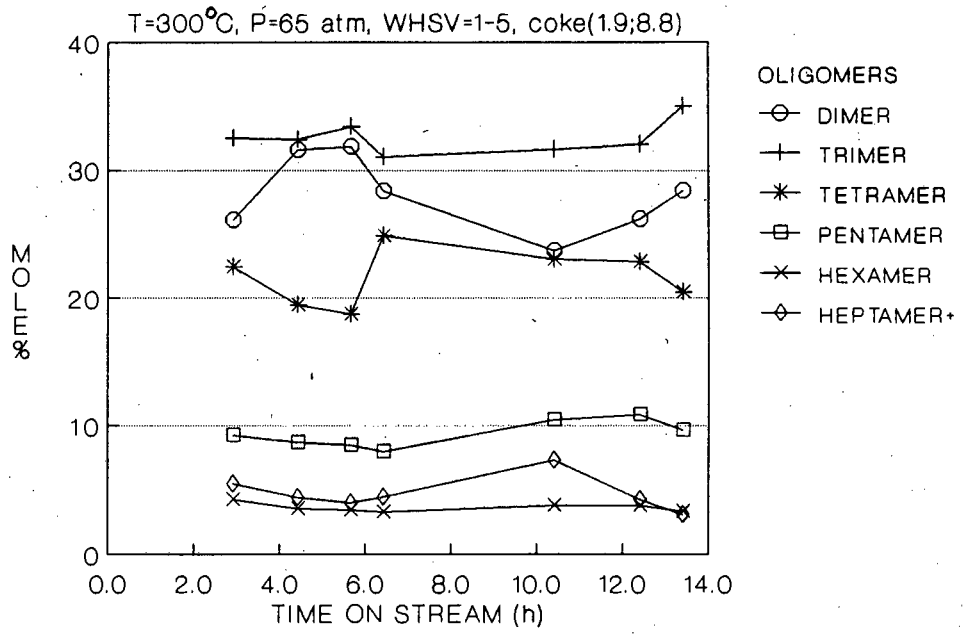

Figure 2.19c : Product distribution vs time on stream for propene oligomerisation over HM - OLIG13.

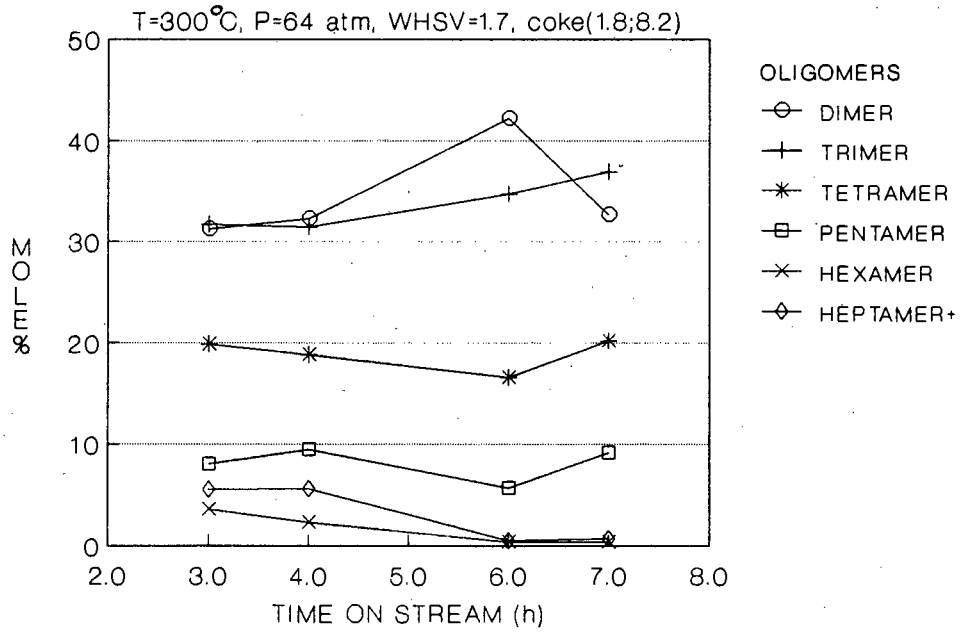

Figure 2.19d : Product distribution vs time on stream for propene oligomerisation over HM - OLIG14.

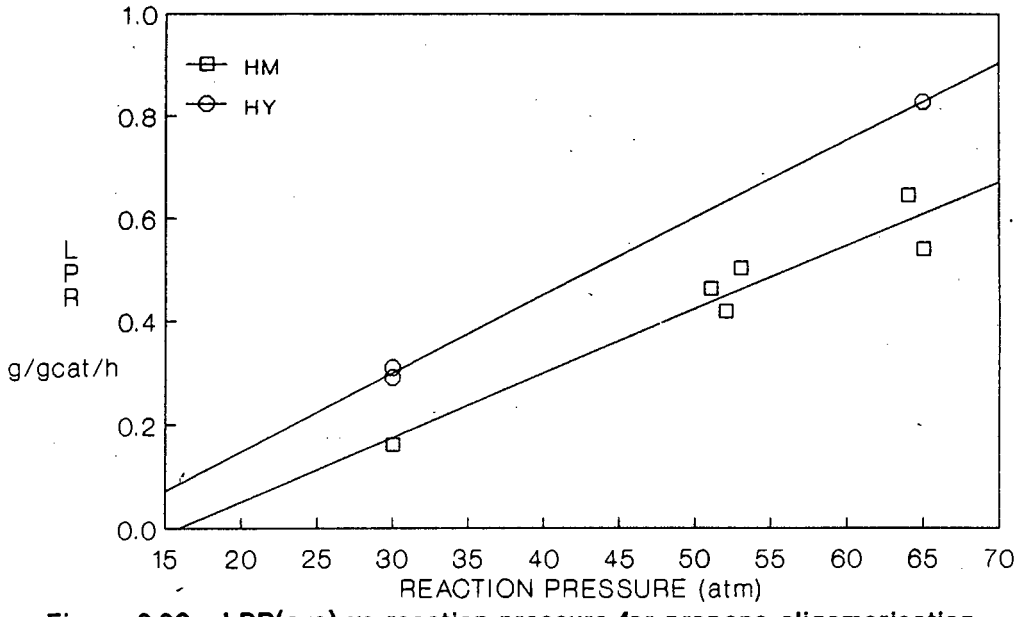

Figure 2.20 : LPR(ave) vs reaction pressure for propene oligomerisation over HY at 200°C and HM at 300°C.

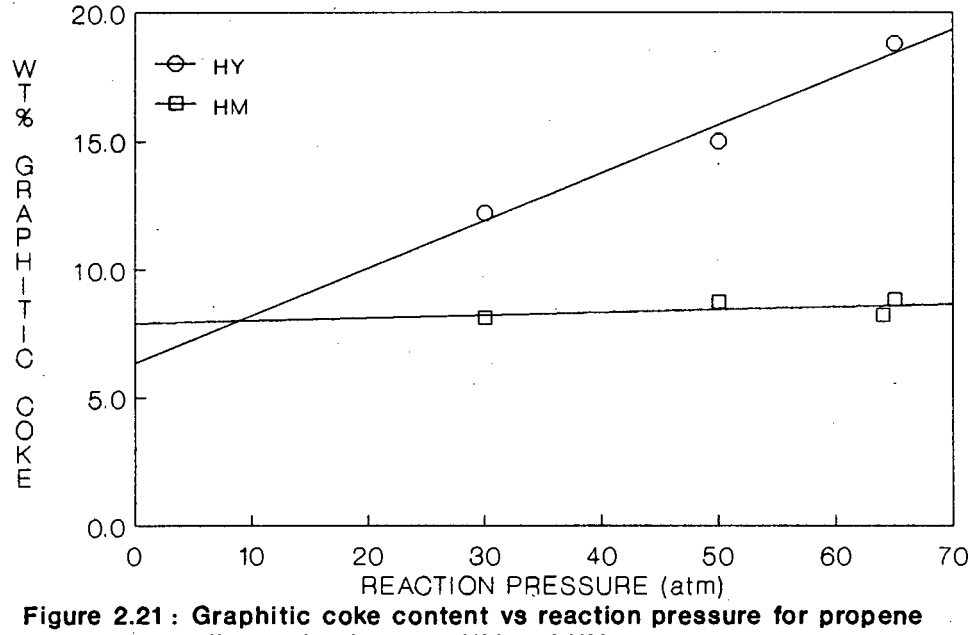

Figure 2.21 : Graphitic coke content vs reaction pressure for propene oligomerisation over HM and HY.

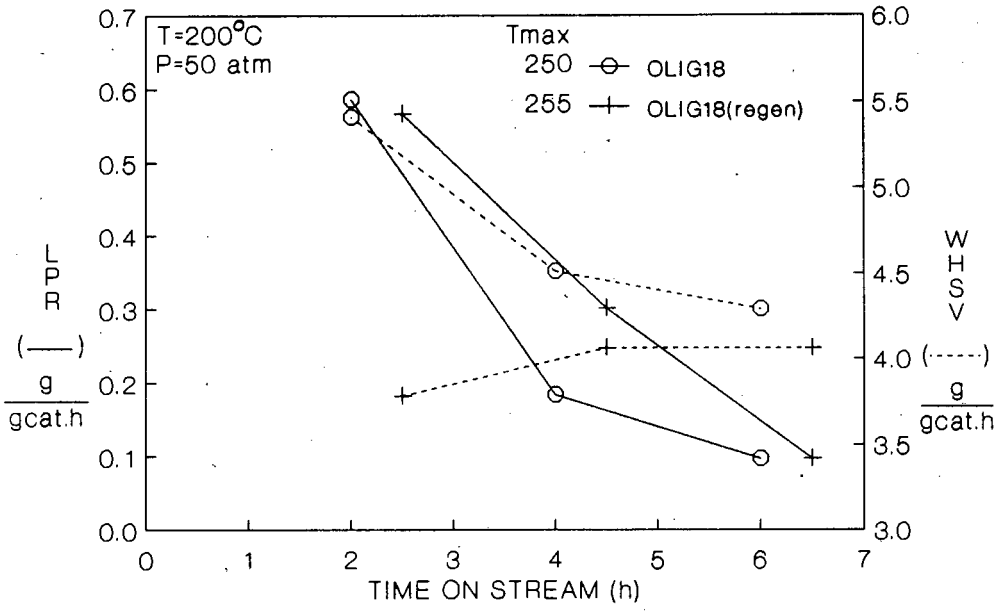

Figure 2.22a : LPR and WHSV vs time on stream for propene oligomerisation over HY; the effect of regeneration.

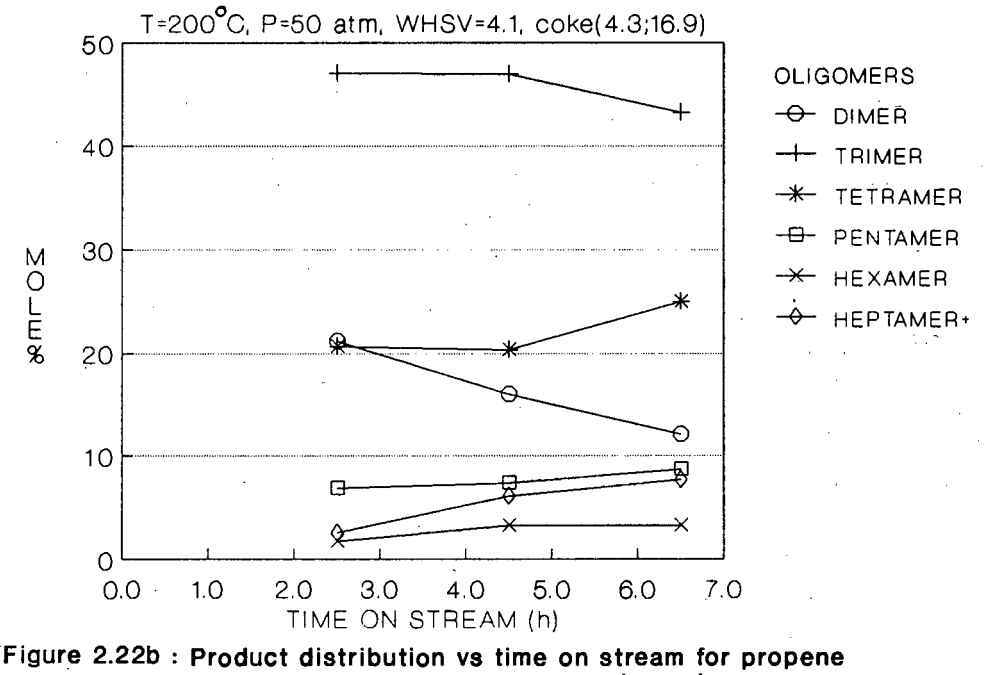

Figure 2.22b : Product distribution vs time on stream for propene oligomerisation over HY - OLIG18(regen).

2.3.4 Discussion

This section presents a discussion of the results obtained from propene oligomerisation over HY and HM. The catalyst deactivation is considered in terms of WHSV, coke content and temperature runaway, and the possibility that the latter two may cause pore blockage and/or site poisoning.

2.3.4.1 Constant reaction conditions

For HY the results showed that a high WHSV caused rapid deactivation with a low average LPR and short lifetime. In the absence of deactivation a high WHSV typically resulted in a high LPR. The final coke contents of the catalysts showed no simple correlation with the total time on stream or WHSV. OLIGT which had the lowest WHSV had the lowest coke content (13.7% graphitic). OLIGT also showed a reasonably steady LPR until the WHSV increased after which the LPR immediately decreased. This suggests that high WHSV causes rapid coking of the catalyst, diminishing the activity of the catalyst to such an extent that the overall activity of the catalyst decreases with increasing WHSV. It follows that under these operating conditions there exists an optimum WHSV which will give the highest LPR and the largest amount of liquid produced per gram of catalyst. The temperature runaway does not appear to have a significant effect on the LPR or the lifetime.

However, when considering the initial compositions of OLIG5 and OLIG18, it appears that temperature runaway in OLIG5 (T_{max}=320°C) caused a rapid build-up of coke, which modified the selectivity of the catalyst even before the first sample was taken. In OLIG18, the coke build-up gradually modified the selectivity of the catalyst as the reaction proceeded, finally tending to that of OLIG5. Langner (1981) has given evidence for the reaction of propene over $NaNH_4$-Y at atmospheric conditions that below 300°C the deactivation is caused by strong adsorption of compounds in the pores, but above 300°C deactivation is caused by graphitic coke which blocks the catalyst pores. Lin et al. (1983) have shown that propene is a coke precusor in cumene cracking over lanthanum exchanged Zeolite-Y. The above reported findings together with the data obtained in this work suggest that coke (possibly graphitic coke only) is responsible for modifying the selectivity and that temperature runaway is an important parameter when comparing data, as it

modifies selectivity by causing initial coke build-up and determining, at least in part, the nature of the coke. Nevertheless, this initial build-up of coke does not appear to affect the rate of deactivation markedly, as seen from the fact that OLIG1 and OLIG5, with essentially equal WHSV's but different extents of temperature runaway, had similar LPR's and lifetime.

In the case of HM, a high WHSV produced a high LPR initially followed by rapid deactivation. There was no temperature runaway. In OLIG7 the generally low WHSV gradually decreasing with reaction time prolonged the lifetime by reducing the deactivation rate. The data indicate that a low WHSV and resulting low activity led to slow deactivation notwithstanding longer residence time (low WHSV) which could cause greater deactivation.

High WHSV appeared to favour the production of lighter fractions which is consistent with shorter residence time. On the other hand, as coke content increased, heavier fractions were obtained. This is contrary to the data reported by Rautenbach (1986) who found that, for butene oligomerisation over HM at 200°C and 50 atm, the dimer increased while tetramer and pentamer decreased with increasing time on stream.

The coke content of the HM samples covered a narrow range (8.1% - 10.0 wt% graphitic). Hexane cracking resulted in fast deactivation and the catalyst was nearly inactive at 3 wt% coke. However, deactivation during oligomerisation was slower with higher coke levels. This could indicate that the acid sites used for oligomerisation are weaker than those required for hexane cracking as the strong active sites would deactivate first (hexane cracking requires strong active sites). Alternatively pore blockage could have occurred in hexane cracking to a much greater extent than in propene oligomerisation, viz., the location of coke due to cracking may be different from that due to oligomerisation.

2.3.4.2 The effect of reaction temperature

Only gas phase reactions were considered as Fasol (1983) has shown that liquid phase reactions over HY have low activity and favour dimer production. The temperature runaway, probably by virtue of short duration, did not significantly affect the activity. The effect of reaction temperature runaway will be discussed at the end of this section. High temperature

caused a high LPR with rapid deactivation. This is probably due to the rapid coke build-up at high temperature which is shown by the high graphitic coke content of 21.7 wt% at 350°C. Comparison of initial sample compositions (presumably containing low wt% coke) between OLIG12 and OLIG18 shows that high temperature favoured lighter fractions. However, as the catalyst deactivated, OLIG12 (100°C) showed very little variation in product composition, while the final sample in OLIG18 (200°C) contained heavier fractions than those in OLIG12. The graphitic coke content of OLIG12 was 7% while that of OLIG18 was 16.9%, thus indicating that graphitic coke may be responsible for causing large changes in product distribution.

After reaction at 100°C HY had a brownish appearance. This suggests that the residue had a low aromatic content favouring polymerisation. This was also found by Langner (1980). There was no temperature runaway in the runs at 100°C to cause initial coke build-up on the catalyst. Clearly high boiling point hydrocarbon residues on the catalyst did not significantly affect the product distribution.

HM was inactive below 200°C while HY was active even at room temperature, even though HM has been shown to possess stronger acid sites than HY (Hilgado et al., 1984). It is possible that because of the strong acid sites the hydrocarbon molecules are strongly (or irreversibly) adsorbed on HM at low temperatures. This is particularly possible in the case of unsaturated product oligomers, and this would prevent any further reaction from taking place.

With increasing time on stream, the reaction at 250°C over HM favoured the formation of heavier hydrocarbons while those at 300 and 350°C favoured the formation of lighter fractions, particularly in OLIG8. The graphitic coke contents of OLIG6, OLIG7 and OLIG8 were 6.7, 10.0, and 10.6%, respectively, with OLIG6 having 5.4% high boiling point hydrocarbons. The coke level in OLIG6 may not be high enough to cause a significant production of lighter fractions. At 300 and 350°C the coke build-up was rapid with less adsorbed high boiling point hydrocarbons (viz., similar to hexane cracking). In this case the graphitic coke could be responsible for deactivation and change in product distribution to lighter fractions. Towards the end of the run OLIG7 and OLIG8 showed sudden changes to heavier fractions. This was also observed in OLIG14. One possible explanation is that above a certain critical coke content the macro-pores may become restricted, increasing residence time, but

still large enough to desorb large product species. It is possible that in the one dimensional pore structure of HM the micro-pores are rapidly blocked (recall that in the case of hexane cracking deactivation was nearly complete at only 3.1% coke), and that the macro-pores play a significant role in determining the product composition. More detailed investigations of the pore properties might explain some of the phenomena observed.

The graphitic coke content increased with increasing reaction temperature, as expected. HY had higher coke content than HM at the same reaction temperature. Extrapolation of the data in Figure 2.17 suggests that HY is probably active below 100°C. When the feed was introduced slowly into the reactor at 15 atm and 25°C, HY generated heat of adsorption which raised the bed temperature by between 45 and 125°C. In contrast, the rise in bed temperature owing to the heat of adsorption was between 5 and 25°C for HM. Although this temperature rise lasted less than 5 min, it would be possible for HY to deactivate during this initial period because the actual temperature inside the zeolite pore was most probably much higher than the measured bed temperature. In addition, once the reactor containing HY had been pumped to pressure at room temperature, a few drops of liquid product always appeared. In the case of HM, liquid appeared only once the system was at set temperature and pressure for 30 minutes. This suggests that HY could be more active if initial coking could be prevented. HM suffers severe deactivation at low coke levels which must be attributed to the one-dimensional pore structure.

The temperature runaway during start-up, which was unavoidable, had an effect on the product distribution. The two cases of severe runaway, OLIG5 (Figure 2.12a) to 320°C and OLIG9 (Figure 2.18b) to 330°C, can be compared to the equivalent reactions with smaller temperature runaway, OLIG18 (Figure 2.12b) and OLIG10 (Figure 2.18c), respectively. OLIG5 and OLIG18 have already been discussed in section 2.3.4.1 where it was noted that temperature runaway caused the product distribution to shift to heavier fractions by causing premature coking.

2.3.4.3 The effect of reaction pressure

High pressure favoured high LPR and good lifetime for HY which is expected from thermodynamic considerations. The reaction at 30 atm had a low LPR notwithstanding the high WHSV. For the reaction at 65 atm, LPR was high even

at low WHSV with the effect of coke on the catalyst becoming noticeable only after 10 h on stream.

Reaction at 65 atm over HY appeared to favour lighter fractions, even though WHSV was relatively low. However, the composition of the initial sample indicates that high pressure may favour heavier products on a fresh catalyst in accordance with thermodynamic consideration. Liquid compositions at high pressure remained steady between 4 and 10 h on stream, corresponding to approximately steady LPR, but after 10 h when the catalyst started deactivating the product composition became heavier. It is possible that at high pressure the increased propene concentration increased the formation of liquid fractions, but because of the higher pressure only the lighter fractions were able to leave the catalyst rapidly, the heavier fractions being more strongly adsorbed. This means that the high pressure reaction should have longer chain length hydrocarbons in the final sample obtained during the purge. Unfortunately this sample was not analysed. The final composition of OLIG10 taken during the run had substantially more pentamer and hexamer than OLIG11. The graphitic coke content of the catalysts were 12.2% and 18.8% for 30 and 65 atm, respectively. Comparison of product distributions of OLIG18 and OLIG11 shows that temperature has a greater effect on the product distribution than pressure. Finally it appears that in the case of HY coke content of the catalyst will dictate the product composition more than pressure or temperature.

Turning to HM, OLIG15 at 30 atm had the lowest LPR and the shortest lifetime. Comparing reactions at 50 and 65 atm, OLIG7 at 53 atm and OLIG13 at 65 atm had comparable lifetime. The LPR of OLIG13 was initially higher, but unfortunately after 6.4 h on stream the WHSV more than doubled to 5/h as a result of the coolant pump failure. The high WHSV was followed by rapid deactivation. OLIG14, also at 65 atm, had a steady feed flow rate but much shorter lifetime. The reason for the poor performance in this run is not clear.

Comparison of initial samples in OLIG14 and OLIG15 shows that low pressure favoured heavier fractions. There appears to be no significant overall correlation between the coke content and the liquid composition. High pressure would raise the boiling point of heavier fractions, and together with the resulting diffusional limitations in the one-dimensional main channels of HM, heavier fractions might not have been able to desorb and

diffuse out of HM pores. This is consistent with the fact that an insignificant amount of high boiling point hydrocarbons were observed by TG/DTA for OLIG15 (30 atm) while for OLIG7 and OLIG14, 2.2 and 1.8% high boiling point hydrocarbons, respectively, were detected.

The LPR(ave) under the conditions of these experiments increased with an increase in pressure. The data in Figure 2.20 at 30 atm for HY and 50 and 65 atm for HM include the effects of varying WHSV and reaction times. The figure shows that HY was more active than HM and that the activity of HY increased more rapidly than that of HM with increasing pressure. Extrapolation to lower pressures indicates that HY may well be active for oligomerisation at atmospheric conditions which has been shown by Langner (1981). Interestingly the graphitic coke content of HY increased with increasing reaction pressure together with the LPR(ave) while for HM the graphitic coke content remained constant with increasing pressure. The greater tolerance for higher coke levels in HY could lead to longer lifetime.

2.3.4.4 The effect of regeneration in nitrogen

The inactivity of HM after regeneration in nitrogen shows that high boiling point hydrocarbons partially converted to graphitic coke at 350°C in nitrogen together with the residual graphitic coke on HM had eliminated all the sites active for oligomerisation. On the other hand HY regained its initial activity indicating that the deactivation must be due to high boiling point hydrocarbons a large portion of which can be desorbed from the surface, although some cracking would always take place. It is surprising that residual graphitic coke had little effect on the product distribution of the catalyst, especially given that OLIG18(regenerated) had 17 wt% graphitic coke. This is little evidence that graphitic coke poisoned sites or presented diffusional resistance to large product molecules. This in turn may indicate that actual graphitic coke is much lower than that given by TG/DTA, and that much of what is detected as graphitic coke is actually high boiling point hydrocarbons which are converted to "graphitic coke" during temperature programming in flowing air as will be discussed in Chapter 3.

2.4 SUMMARY

Coke formation in hexane cracking caused rapid deactivation which reduced the rate of olefin transformations, thus changing the product spectrum. Initial coke formation was rapid but levelled off after long time on stream. Modelling of the experimental data suggested that deactivation in HM was caused by pore blockage, while in HY partial pore blockage was more dominant. The mode of deactivation in HM and HY was not conclusive from the data. HM deactivated more rapidly than HY and required much less coke content for reduced activity.

In oligomerisation coke formation and deactivation are much slower than in cracking. High temperature and WHSV caused rapid coking. At high temperature more graphitic coke was formed causing rapid deactivation at the expense of higher initial activity, while at low temperature deactivation was primarily caused by the strong adsorption of product molecules. High pressure increased the activity for HY and HM and resulted in long lifetime for HY. Reaction at 30 atm gave poor performance for both catalysts. Graphitic coke formation caused the product distribution to favour heavier fractions. Overall, the graphitic coke content dictated the product composition to a greater extent than either reaction temperature or pressure. HY regained its initial activity after regeneration in nitrogen, while HM was innactive.

The results suggest that the acid sites used by oligomerisation are much weaker than those used by cracking. HM deactivated at very low coke levels when compared to HY, suggesting that pore blockage may be the dominant deactivation mechanism. These results however do not offer unambiguous interpretation of the deactivation mechanisms.

3 TG/DTA, MERCURY POROSIMETRY AND BET SURFACE AREA MEASUREMENTS

3.1 Introduction

The aim of this section was to determine the amount and nature of coke and its effect on the morphology of a few representative deactivated samples. For this purpose thermogravimetric/differential thermal analysis (TG/DTA), helium pycnometry, mecury porosimetry and BET techniques were employed. This work was carried out with a view to enhancing the understanding of deactivation mechanisms and of the results obtained in Chapters 4 and 5.

The monitoring of mass loss and temperature difference during the removal of coke on catalyst samples in the TG/DTA apparatus enabled a distinction to be made between carbonaceous deposits due to cracking and oligomerisation. The former contained only a "graphite-like" fraction, while the latter consisted of both high boiling point hydrocarbons and a graphitic fraction. Thus coke was broadly classified into the above two catagories.

Porosity distribution, macro-pore surface area, and the BET surface area measurements of selected samples were then related to the quantity of each fraction, thus establishing the effects of coke on the morphology of the catalyst. These trends would aid interpretation of results from Chapters 2, 4 and 5.

The apparatus and procedure of the techniques used are treated briefly first, followed by the presentation of the results obtained and finally a discussion.

3.2 Apparatus and procedure

TG/DTA determinations were carried out on a Stanton Redcroft Thermal Analyser model 780. The system was interfaced to an IBM compatible PC using a high gain amplifier and a multiplexed 12-bit ADC. The PC recorded time, temperature, DTG, DTA and TG signals in addition to controlling the temperatures and gas flows of the TG analyser.

The coke on the catalyst was determined by placing approximately 20 mg of sample in the furnace and heating at 10°C/min from 40 to 700°C in 60 ml/min of flowing air. The TG and DTA curves were then plotted as a function of sample temperature. From the plots the amount of water was estimated by observing the endotherm which ended at approximately 200°C. In cracking samples a large exothermic peak due to coke burn off was present and the mass loss corresponding to this peak gave the amount of coke on the catalyst. For oligomerisation samples two or more peaks were observed in the DTA curve, the low temperature peaks being due to "high boiling point hydrocarbons" and the high temperature peak due to "graphitic coke". The relative amount of each coke type was given by considering the mass losses corresponding to the DTA peaks. The coke content was then calculated on a clean catalyst basis.

In a few TG/DTA runs deactivated catalyst samples were heated in flowing nitrogen at 10°C/min. At 700°C the flowing nitrogen was switched to air, causing sudden exothermicity and large mass loss.

Pore size distribution data were obtained under the supervision of Dr B.M. van Vliet at the CSIR using Micromeritics auto-pore 9200. Skeleton density was determined by helium pycnometry . The standard mercury-solid contact angle of 130° was used in all the calculations. The pre-treatment of the samples was to dry them in flowing nitrogen at the reaction temperature, so as to prevent any of the high boiling point hydrocarbons or the coke from being removed.

BET surface area measurements were performed at the Energy Technology Division of the CSIR using the Langmiur method under the supervision of Mr. J. Vink. Unfortunately the samples were pretreated at 10^{-2} bar and 100°C which possibly caused some of the high boiling point hydrocarbons to be removed.

3.3 Results of TG/DTA, mercury porosimetry and BET surface area measurements on coked HY and HM

Table 3.1 summarises the estimated coke content based on the mass of catalyst oxidized in flowing air at 700°C as determined by TG/DTA. When nitrogen was passed over catalyst samples deactivated by hexane cracking, the TG showed no weight loss except for adsorbed moisture (<200°C). However, in the presence

TABLE 3.1 : ESTIMATION OF COKE CONTENT FROM TG/DTA.

Run ID	Catalyst	Clean sample weight(mg)	Total coke(wt%)	hbph	Graphitic (wt%)
CRACT	HY	-	9.2	-	9.2
CRAC1	"	-	10.6	-	10.6
CRAC2	"	-	8.5	-	8.5
CRAC3	HM	-	3.1	-	3.1
CRAC4	HY	-	8.9	-	8.9
CRAC5	"	-	13.9	-	13.9
CRAC6	"	-	8.9	-	8.9
CRAC7	"	-	7.1	-	7.1
CRAC8	"	-	8.2	-	8.2
OLIGT	HY	16.6	19.1	5.4	13.7
OLIG1	"	16.1	17.3	4.3	13.0
OLIG2	"	16.9	18.4	5.2	13.2
OLIG3	"	16.0	23.0	1.3	21.7
OLIG4	"	16.2	14.8	7.9	6.9
OLIG5	"	16.0	21.1	4.4	16.7
OLIG6	HM	17.3	12.1	5.4	6.7
OLIG7	"	17.4	12.2	2.2	10.0
OLIG8	"	17.0	11.1	0.5	10.6
OLIG9	HY	15.6	22.4	3.3	19.1
OLIG10	"	16.9	25.7	3.5	12.2
OLIG11	"	15.9	24.1	5.3	18.8
OLIG12	"	16.1	13.7	6.7	7.0
OLIG13	HM	17.1	10.7	1.9	8.8
OLIG14	"	17.5	10.0	1.8	8.2
OLIG15	"	17.7	8.1	-	8.1
OLIG16	"	17.5	8.1	-	8.1
OLIG17	"	17.3	8.7	-	8.7
OLIG18	HY	16.5	21.1	4.3	16.9

weight% coke based on mass of clean catalyst
Total sample mass = weight clean catalyst + weight coke
hbph - high boiling point hydrocarbons

of air a strong exotherm in the DTA at approximately 500°C was observed with the associated burn-off of the graphitic coke. The TG/DTA of oligomerisation samples in the presence of nitrogen showed continuous endothermic desorption until residual coke was burnt off at 700°C (Figures 3.1a and b) when the flow was switched to air. In the presence of air, however, desorption of water was endothermic (below 200°C) while at higher temperatures the coke burn-off yielded two distinct exotherms at approximately 350°C and 500°C (taking into account sample temperature lag) which were tentatively assigned to high boiling point hydrocarbons and graphitic coke, respectively. By comparing the DTA peaks with the TG it was possible to estimate the mass loss due to water, to high boiling point hydrocarbons and to graphitic coke. Comparison with cracking samples which gave only one DTA peak at 500°C confirmed the tentative assignment of graphitic coke. In contrast, using nitrogen as a carrier gas did not allow distinction between adsorbed water and high boiling point hydrocarbons.

Table 3.1 shows that increasing reaction time length for hexane cracking yielded more graphitic coke. Figures 3.2a and b show that increasing the reaction temperature of oligomerization over HY yielded more graphitic coke as seen by the increase in the intensity of the exotherm at ca. 500°C and associated mass loss. High reaction temperatures (and hence flushing the spent catalyst in the reactor at high temperatures after the reaction) gave less high boiling point hydrocarbons shown by the near absence of an exotherm at ca. 350°C in the case of OLIG3, sharp exotherm in this region for OLIG2, and the broad exotherm of OLIG4. The same trends were observed in HM and illustrated in Figures 3.3a and b. Here a smaller range of reaction temperatures was scanned owing to the inactivity of HM below 250°C. The intensities of exothermic peaks were smaller than those of HY. In addition, the peak temperature of the second exotherm above 500°C shifted to higher values with increasing reaction temperature. This shift was far more pronounced than that observed in the case of HY.

Increasing oligomerization reaction pressure over HY increased the amount of coke with a substantial increase in the first exotherm at ca. 350°C (Figures 3.4a and b, curves 3 and 4). OLIG9 (curve 2) had greater exothermicity and mass loss than OLIG10. During the start-up of OLIG9 a temperature runaway took the reactor temperature up to 330°C, while in OLIG10 the maximum measured temperature was 262°C. In addition OLIG9 had WHSV > 10, while that of OLIG10 was for the most part in the neighbourhood of 2. These differences

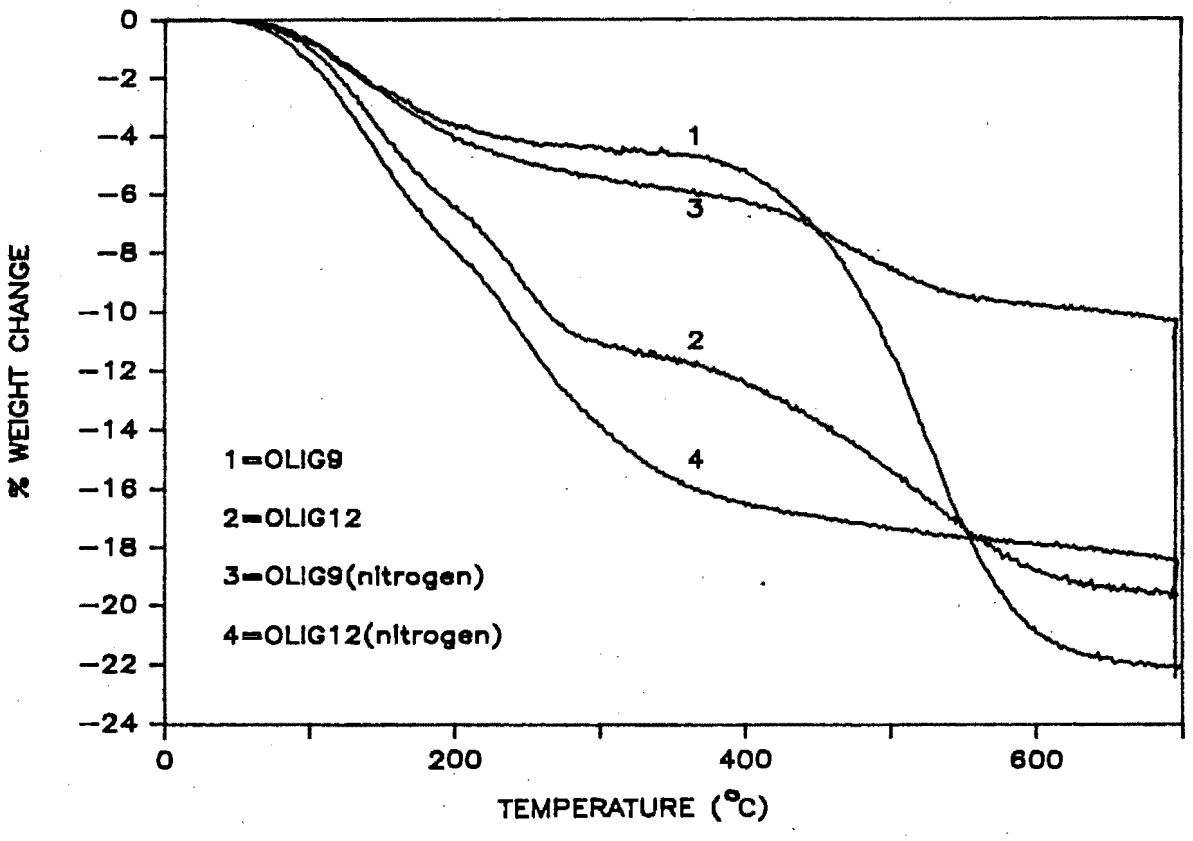

Figure 3.1a : TG of HY after propene oligomerisation : the effect of using nitrogen or air as a carrier gas.

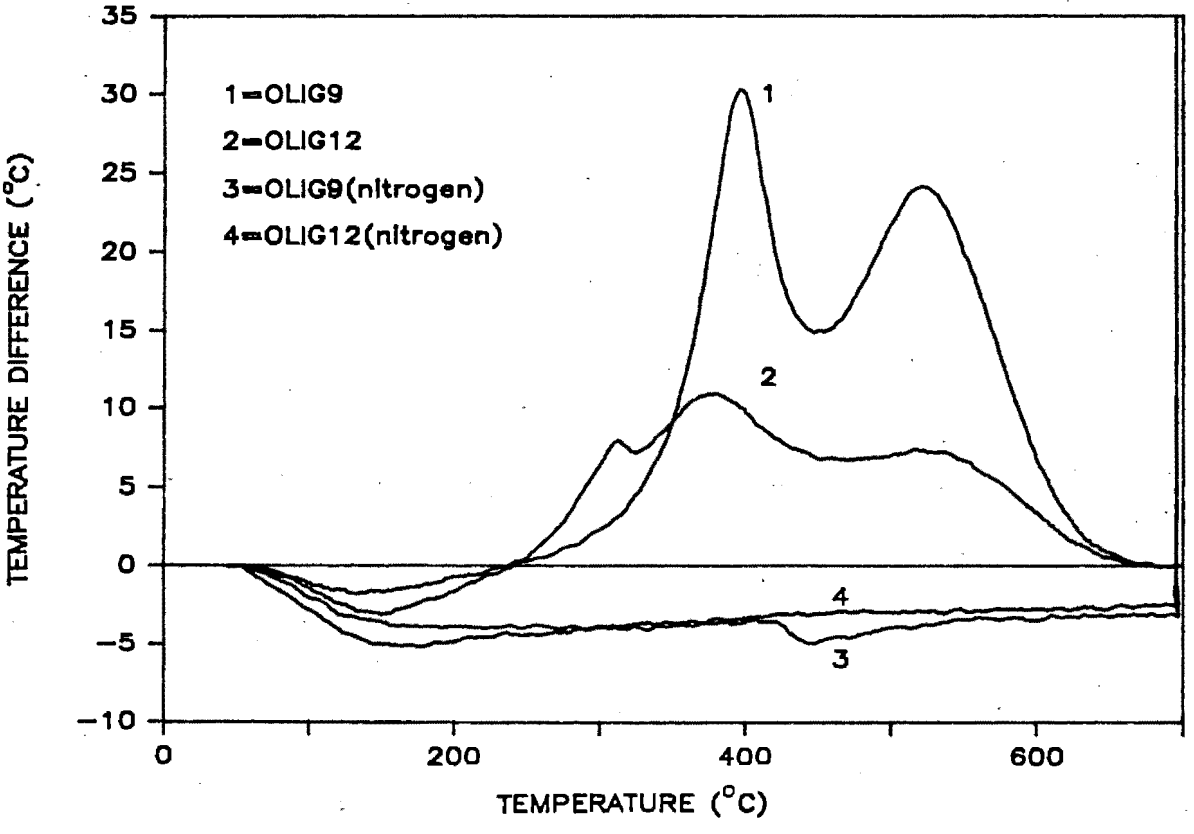

Figure 3.1b : DTA for HY after propene oligomerisation : the effect of using nitrogen or air as a carrier gas.

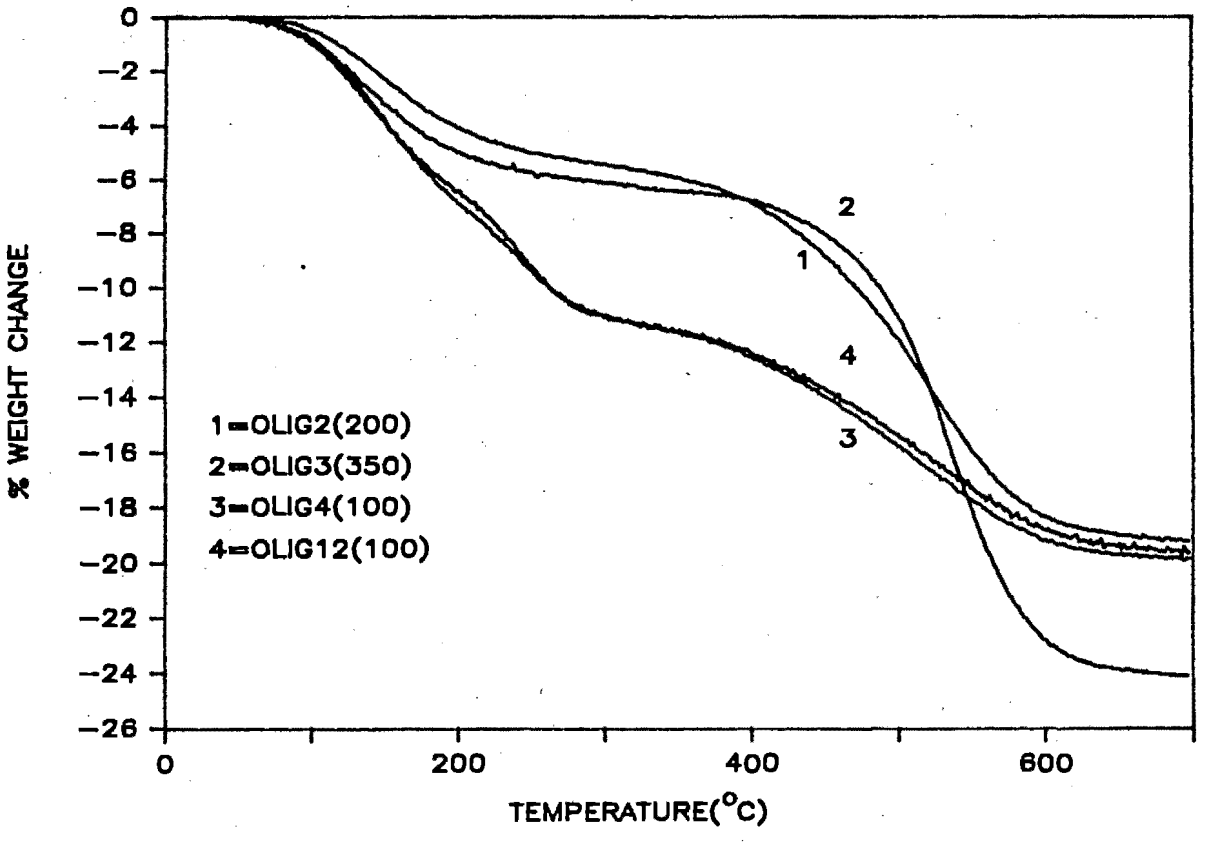

Figure 3.2a : TG for HY after propene oligomerisation : the effect of varying reaction temprature, shown in parentheses in °C.

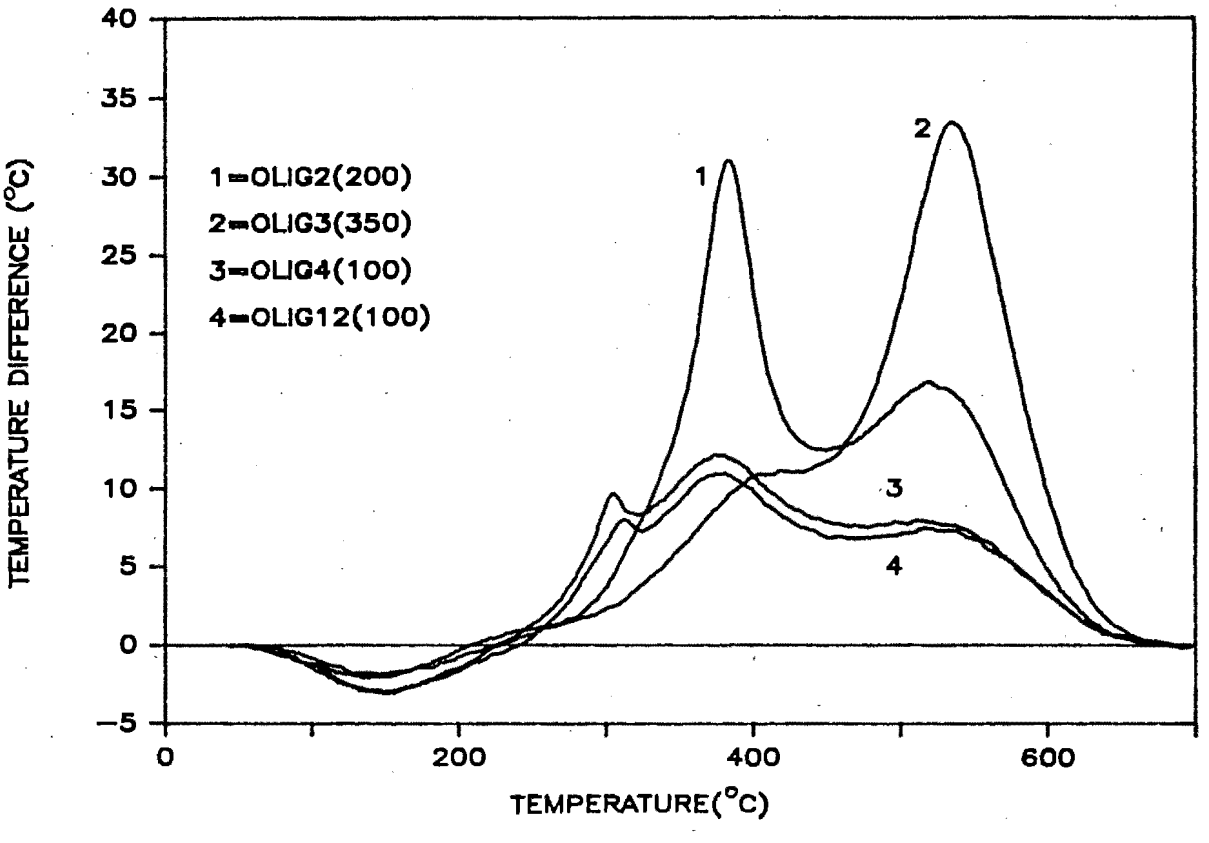

Figure 3.2b : DTA for HY after propene oligomerisation : the effect of varying the reaction temperature.

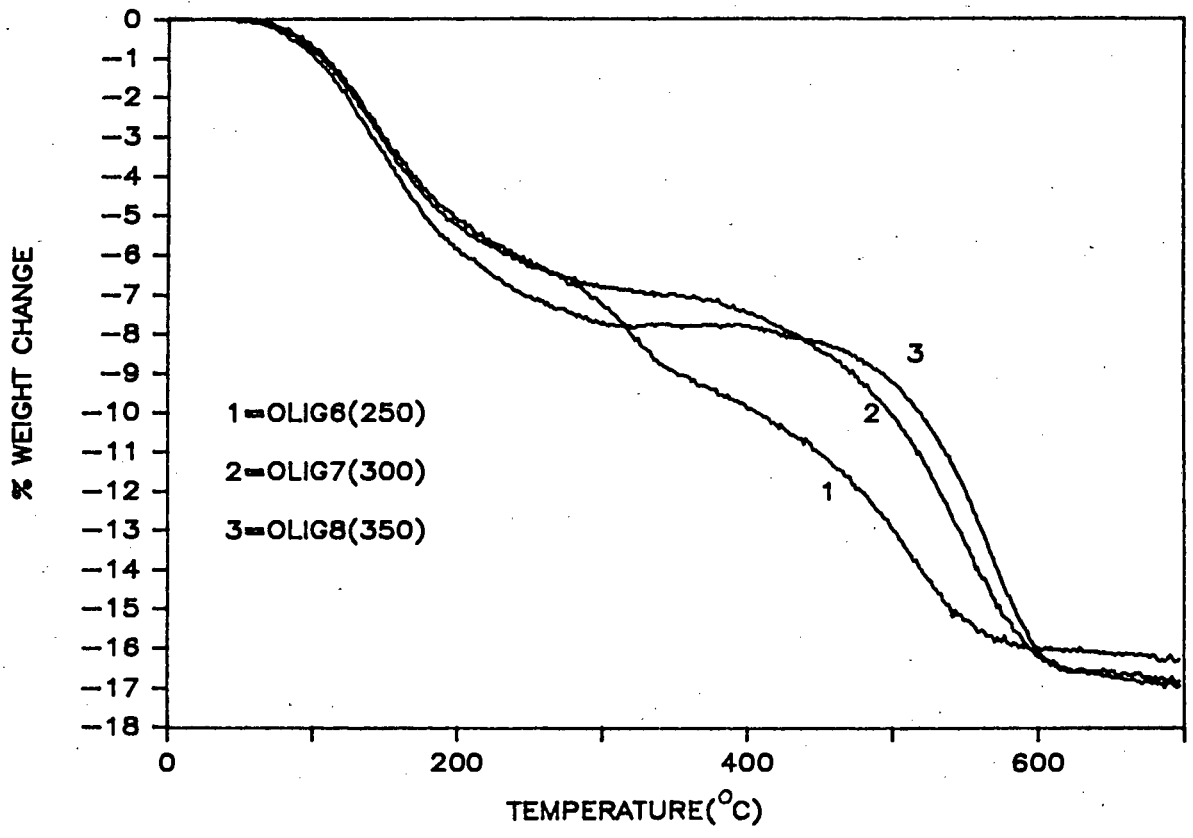

Figure 3.3a : TG for HM after propene oligomerisation : the effect of varying the reaction temperature.

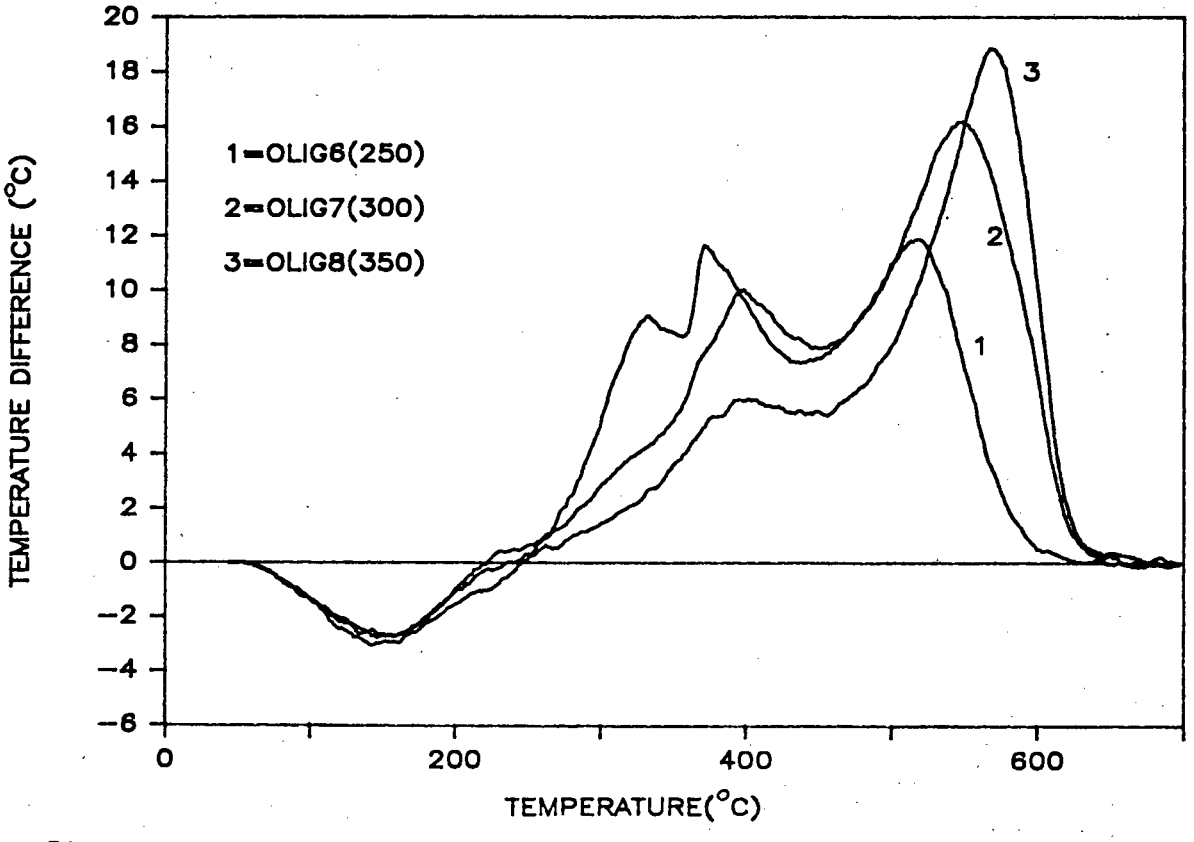

Figure 3.3b : DTA for HM after propene oligomerisation : the effect of varying the reaction temperature.

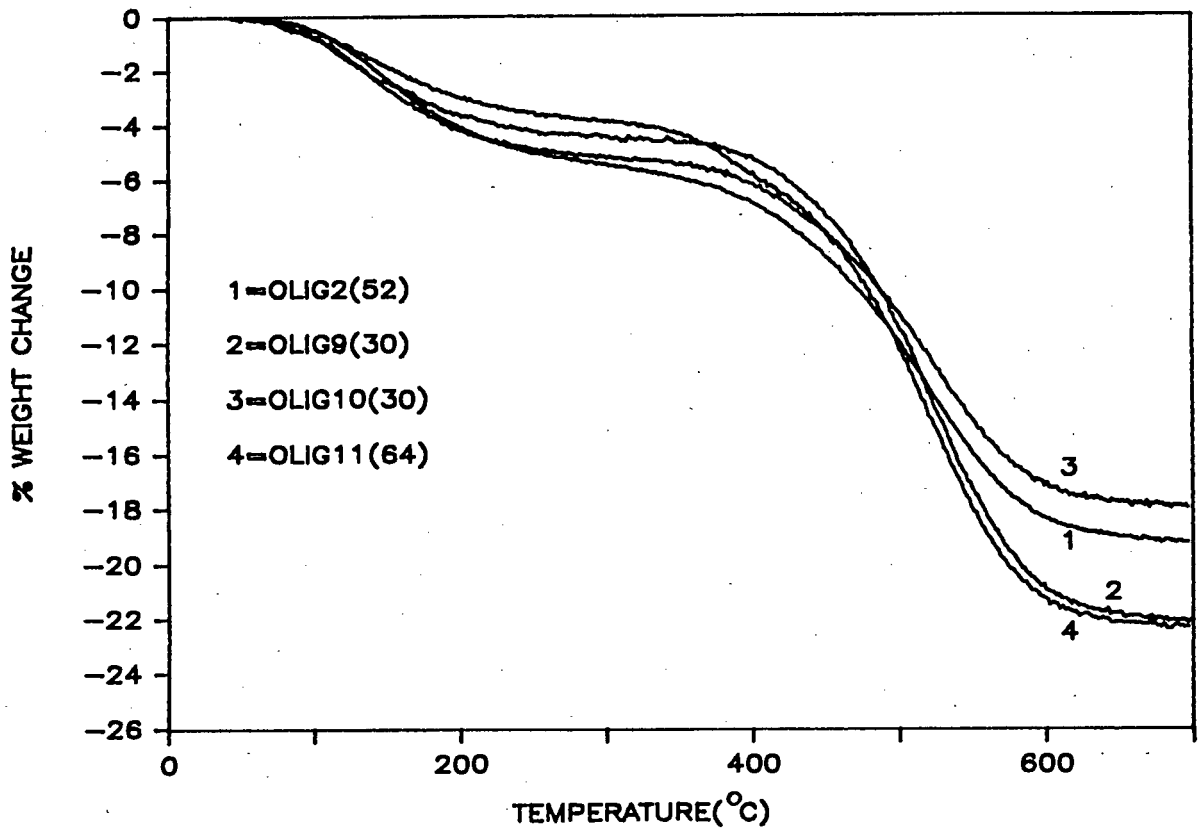

Figure 3.4a : TG for HY after propene oligomerisation : the effect of varying the reaction pressure shown in parentheses in atm.

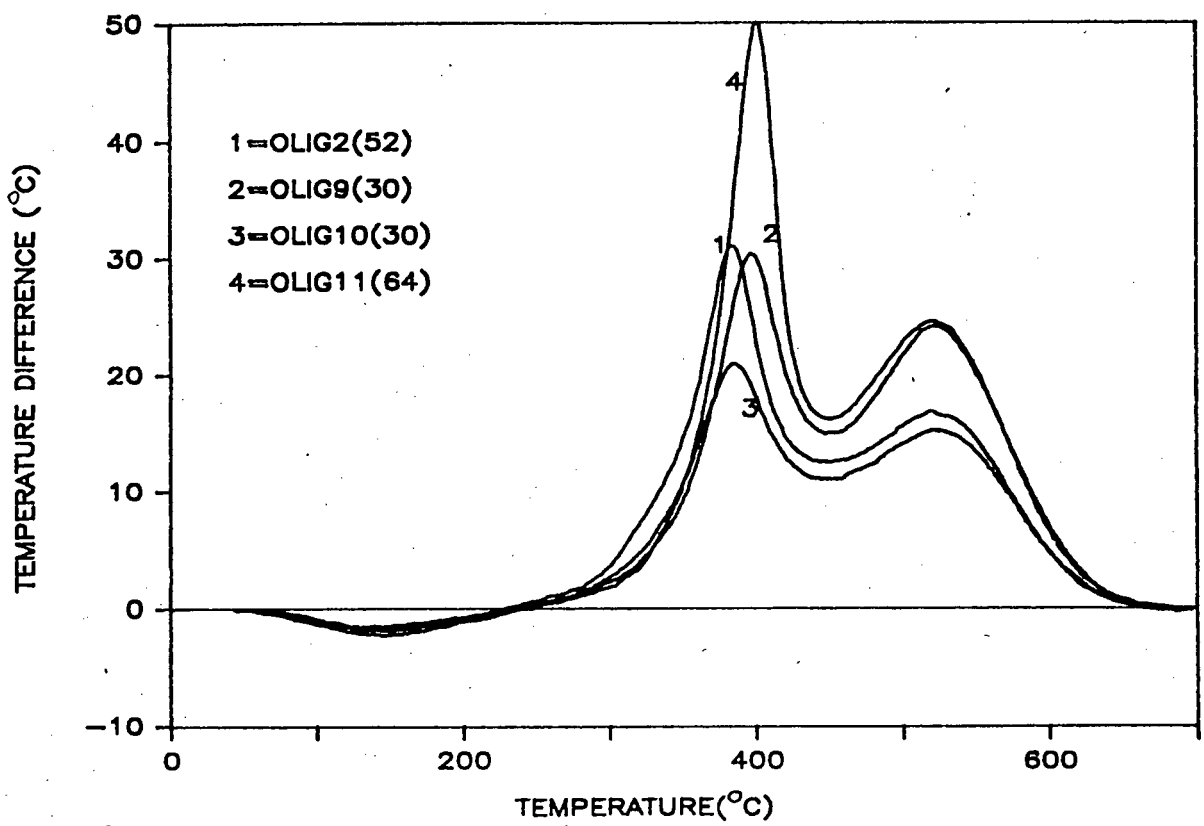

Figure 3.4b : DTA for HY after propene oligomerisation : the effect of varying the reaction pressure.

are most probably responsible for the different TG/DTA spectra. In HM, increasing the oligomerization reaction pressure did not produce significantly more high boiling point hydrocarbons or graphitic coke, nor did the position of exothermic peaks change (Figures 3.5a and b). It appears that reaction pressure was not as important a parameter as temperature and the observed differences were probably due to variations in the degree of deactivation, although curves 2 and 3, both corresponding to 64 atm, were very reproducible even with the varying WHSV observed in OLIG13. DTA exotherms of HM were considerably smaller in intensity than those of HY.

It was assumed that high boiling point hydrocarbons had an approximate density of 1 g/cm^3 by considering hydrocarbons with boiling points between 300-350°C, the approximate exotherm peak temperature. Graphitic coke was assumed to have a density of 2 g/cm^3 (density of amorphous graphite 1.8-2.1 g/cm^3). From these assumptions the volume of coke per gram of clean catalyst was estimated as well as void volume fractions and the estimations are given in Table 3.2.

The skeleton density, determined by helium pycnometry, mercury porosimetry results and BET surface areas are shown in Table 3.3. Reproducibility of the mercury porosimetry data was good as shown in Figures 3.6a and b for HY and HM, respectively. Comparison of HY and HM (Figure 3.6c) shows that HM had a true bi-porous structure with macro-pores of 10000 Å diameter. HY on the other hand showed macro-pores of 1000 Å diameter with significant meso-pores of 60 Å diameter, the effect of which was seen in the six-fold increase in the total macro-pore surface area of HY over HM ("total macro-pores" were considered to consist of "meso-pores" and "macro-pores").

Increasing coke content was found to decrease the skeleton density and increase the bulk density (Table 3.3). Figure 3.7a shows that hexane cracking did not significantly affect the macro-pore size distribution and caused almost no change in the macro-pore void fraction. Nevertheless, the macro-pore surface area was reduced by about 25%. Micro-pore void fraction decreased between 55 and 67% while the BET surface area decreased between 41 and 86%. Oligomerization over HY showed a larger change in macro-pore distribution than hexane cracking (Figure 3.7b), splitting the macro-pores into pores of two distinct diameters (700 Å and 1000 Å) but with the same total void fraction. The considerable change in the meso-pore distribution was reflected in the 30% reduction in meso-pore void fraction and the 50%

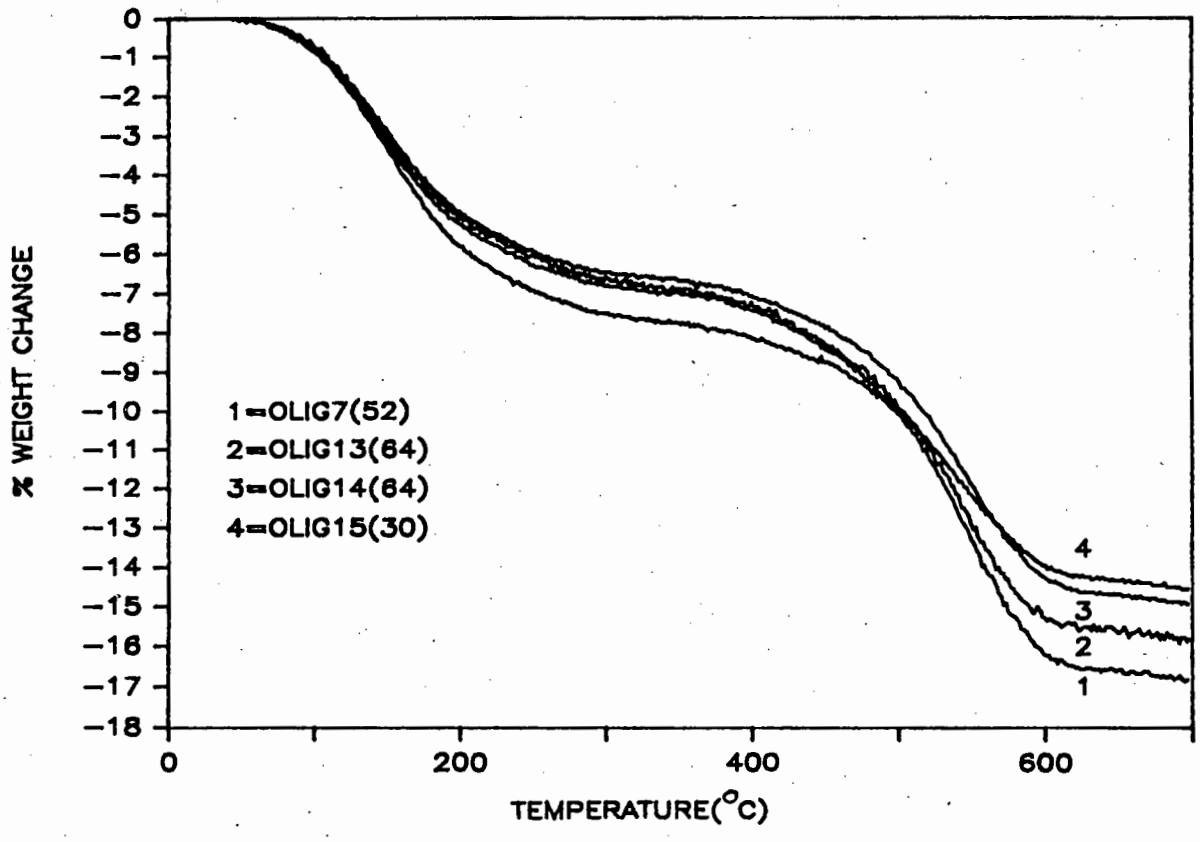

Figure 3.5a : TG for HM after propene oligomerisation : the effect of varying the reaction pressure.

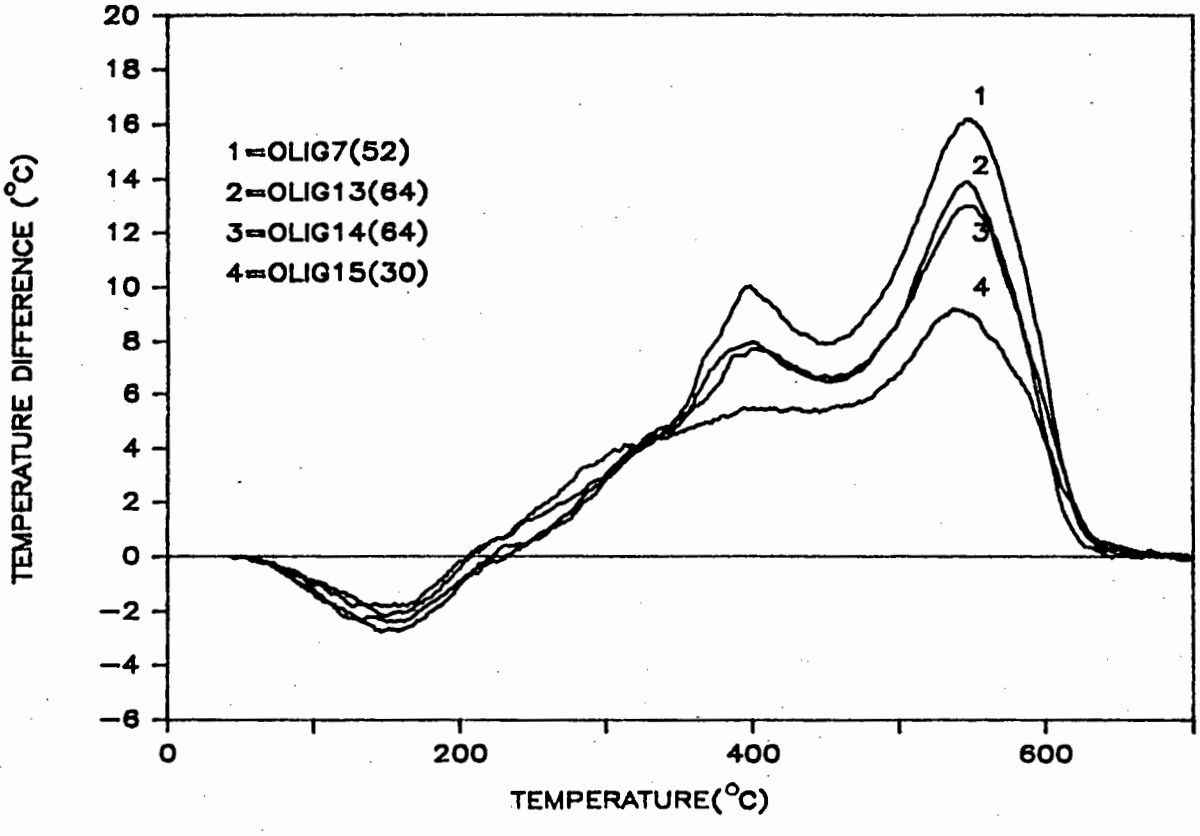

Figure 3.5b : DTA for HM after propene oligomerisation : the effect of varying the reaction pressure.

TABLE 3.2 : VOID FRACTION OCCUPIED BY COKE ESTIMATED FROM TG/DTA.

For 1 g of clean catalyst:

Catalyst	Void volume (cm^3)		
	Total(V_t)	Macro(V_{mac})	Micro(V_{mic})
HM	0.363	0.244	0.118
HY	0.536	0.360	0.176

Assumptions: Density of high boiling point hydrocarbons = $1 g/cm^3$
: Density of graphitic coke = $2 g/cm^3$

Run ID	Catalyst	Volume Coke $V_c(cm^3)$	$1-V_c/V_t$	$1-V_c/V_{mic}$
CRACT	HY	0.046	0.914	0.739
CRAC1	"	0.053	0.901	0.699
CRAC2	"	0.043	0.920	0.756
CRAC3	HM	0.016	0.956	0.866
CRAC4	HY	0.045	0.916	0.744
CRAC5	"	0.070	0.869	0.602
CRAC6	"	0.045	0.916	0.744
CRAC7	"	0.036	0.933	0.795
CRAC8	"	0.041	0.924	0.767
OLIGT	HY	0.123	0.771	0.301
OLIG1	"	0.108	0.799	0.386
OLIG2	"	0.118	0.780	0.330
OLIG3	"	0.122	0.772	0.307
OLIG4	"	0.114	0.787	0.352
OLIG5	"	0.127	0.763	0.218
OLIG6	HM	0.088	0.758	0.254
OLIG7	"	0.072	0.811	0.390
OLIG8	"	0.058	0.840	0.308
OLIG9	HY	0.129	0.759	0.267
OLIG10	"	0.096	0.821	0.455
OLIG11	"	0.147	0.726	0.165
OLIG12	"	0.120	0.776	0.318
OLIG13	HM	0.063	0.816	0.466
OLIG14	"	0.059	0.837	0.500
OLIG15	"	0.041	0.887	0.653
OLIG16	"	0.041	0.887	0.653
OLIG17	"	0.044	0.879	0.627
OLIG18	HY	0.128	0.741	0.673

$1-V_c/V_t$ - Total volume fraction not occupied by coke.
$1-V_c/V_{mic}$ - Micro-volume fraction not occupied by coke, assuming all coke is deposited in micropores.
Table is based on 1g of clean catalyst.

TABLE 3.3 : PARTICLE DENSITY, PORE SIZE DISTRIBUTION AND BET SURFACE AREA.

Run ID	Cat	Coke Content		Skeleton	Bulk	Voidage				macro surface	BET surface
		hbph	gc	density	density	Total	Macro	Meso	Micro	area	area
-	HY	-	-	2.441	1.057	0.567	0.200	0.180	0.187	97.7	525
-	HM	-	-	2.301	1.254	0.455	0.267	0.039	0.149	17.3	460
CRAC1	HY	-	10.6	2.215	1.261	0.431	0.190	0.180	0.061	70.5	160
CRAC5	"	-	13.9	2.307	1.268	0.450	0.192	0.182	0.076	71.0	73
CRAC7	"	-	7.1	2.231	1.180	0.471	0.196	0.191	0.084	81.9	310
OLIG2	HY	5.2	13.2	2.099	1.276	0.392	0.208	0.125	0.059	50.8	62
OLIG3	"	1.3	21.7	2.105	1.290	0.387	0.211	0.124	0.052	50.7	34
OLIG4	"	7.9	6.9	2.363	1.281	0.458	0.214	0.138	0.106	57.2	78
OLIG6	HM	5.4	6.7	1.943	1.417	0.271	0.271	-	-	20.6	<5
OLIG7	"	2.2	10.0	2.001	1.635	0.183	0.183	-	-	16.6	<5
OLIG8	"	0.5	10.6	2.079	1.427	0.314	0.314	-	-	19.9	<5

hbph = high boiling point hydrocarbons, gc = graphitic coke
density in g/cm^3particle; voidage in cm^3/cm^3particle
total macro pore volume taken as macro+meso pores for diffusion analysis
surface area - m^2/g
600 < macro pore diameter < 100 000 A
30 < meso pore diameter < 600 A
micro pore diameter < 30 A

TABLE 3.4 : DISTRIBUTION OF COKE VOLUME(cm^3) PER g OF CLEAN CATALYST AS DETERMINED FROM MERCURY POROSIMETRY.

Run ID	Cat	total pore volume	macro pore volume	micro pore volume	total coke volume	coke volume macro pores	coke volume micro pores
-	HY	0.536	0.360	0.177	-	-	-
-	HM	0.363	0.244	0.119	-	-	-
CRAC1	HY	0.408	0.350	0.058	0.129	0.010	0.119
CRAC5	HY	0.426	0.366	0.072	0.111	0.006	0.105
CRAC7	HY	0.445	0.366	0.079	0.090	-0.006	0.096
OLIG2	HY	0.371	0.315	0.056	0.166	0.045	0.121
OLIG3	HY	0.366	0.317	0.049	0.170	0.043	0.127
OLIG4	HY	0.433	0.333	0.101	0.103	0.027	0.076
OLIG6	HM	0.216	0.216	-	0.147	0.028	-
OLIG7	HM	0.146	0.146	-	0.217	0.098	-
OLIG8	HM	0.250	0.250	-	0.113	-0.006	-

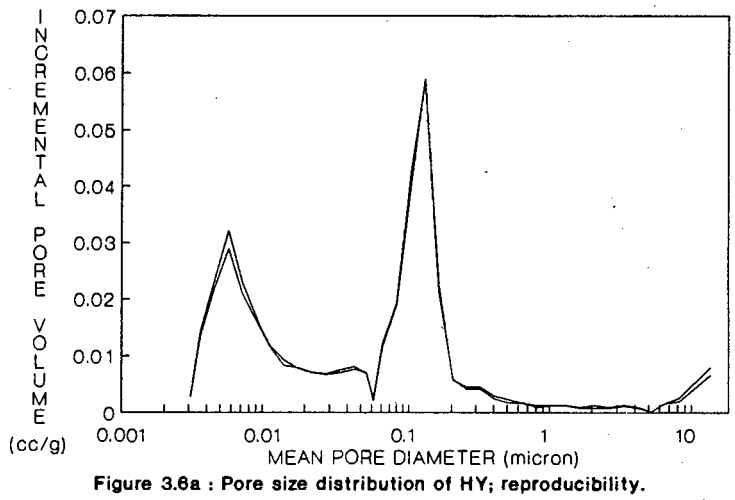

Figure 3.6a : Pore size distribution of HY; reproducibility.

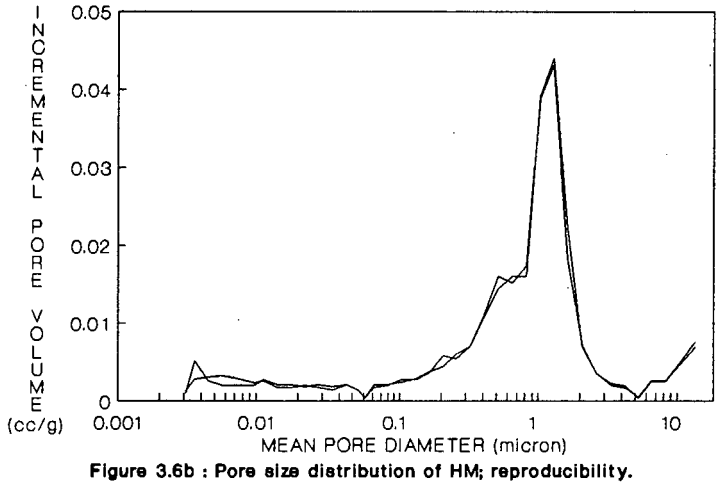

Figure 3.6b : Pore size distribution of HM; reproducibility.

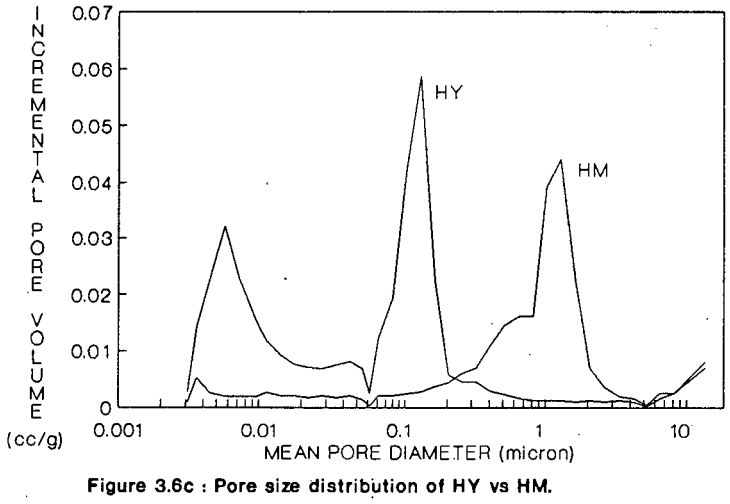

Figure 3.6c : Pore size distribution of HY vs HM.

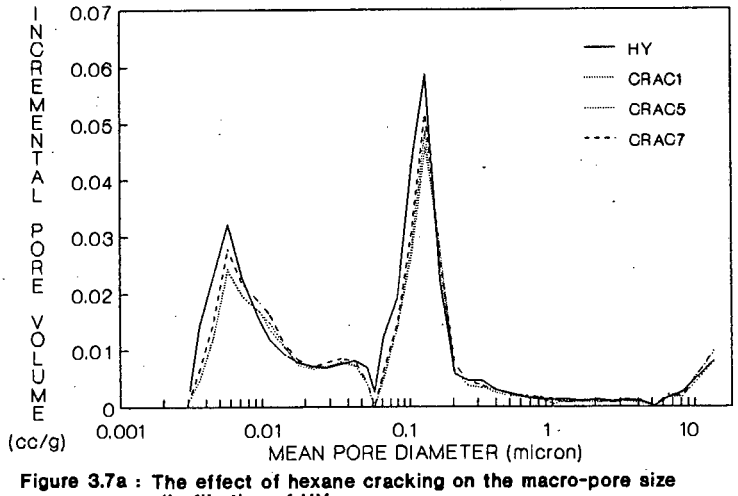

Figure 3.7a : The effect of hexane cracking on the macro-pore size disrfibution of HY.

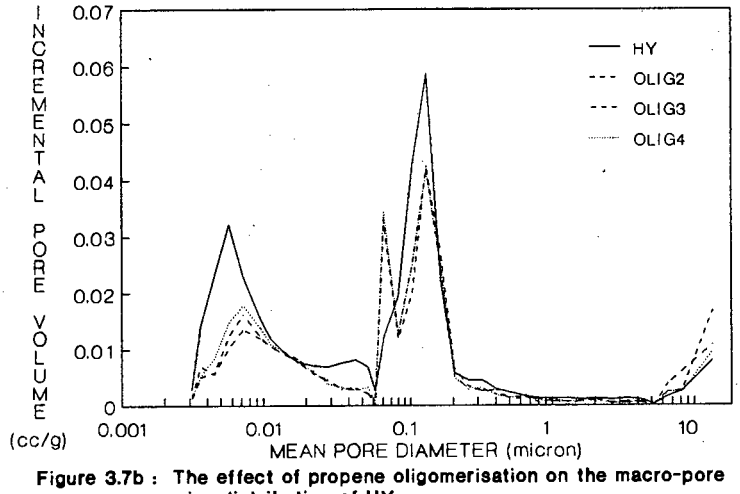

Figure 3.7b : The effect of propene oligomerisation on the macro-pore size distribution of HY.

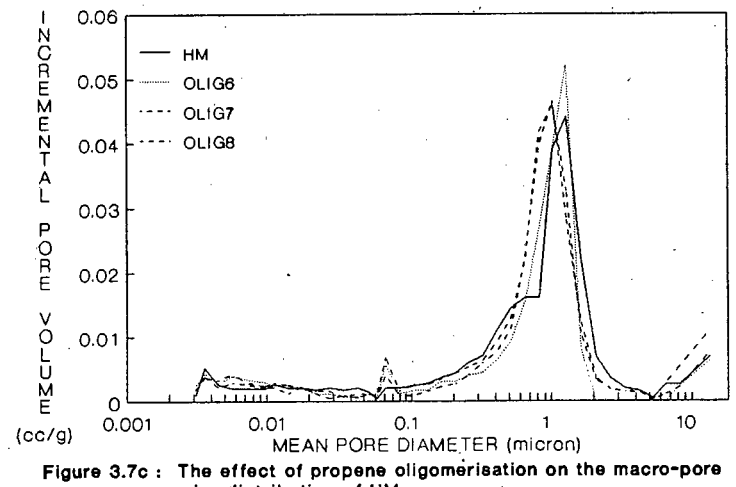

Figure 3.7c : The effect of propene oligomerisation on the macro-pore size distribution of HM

reduction in macro-pore surface area. Micro-pore voidage decreased by between 43 and 72% while the BET surface area decreased between 85 and 94%.

In reporting results obtained from deactivated HM samples, it should be noted that mercury porosimetry was difficult to carry out. The time it took to reach equilibrium at each step was long, possibly on account of desorbing hydrocarbons. As a result helium pycnometry and mercury porosimetry data were inconsistent in that the pore volume filled by mercury exceeded slightly the total pore volume computed from skeleton and bulk densities. Hence these limitations must be taken into account when examining the data.

Deactivated HM was found to have no measurable micro-pores according to BET surface area measurements. Figure 3.7c shows that macro-pore distribution and voidage were changed but no systematic trends with coke content or reaction conditions were observed. Macro-pore surface area also showed no marked variation. There was a small peak at approximately 600Å similar in position to, but smaller than, that observed in HY deactivated by oligomerization (part of the macro-pore double peak). This peak was not observed in the case of cracking.

Figure 3.8a shows that θ_x (see Nomenclature for Chapter 5) in HY for both oligomerization and cracking decreased with increasing graphitic coke content. In HY, θ_y showed only subtle change (larger in oligomerisation samples) with graphitic coke content, while for HM no pattern in θ_y was observed. Figure 3.8b shows that the actual decrease in total pore volume was always greater (particularly for HM) than the estimated decrease in total pore volume, except for OLIG4. The total volume ratio is defined as:

$$\text{Total volume ratio} = \frac{\text{total pore volume of coked catalyst based on 1 g of clean catalyst}}{\text{total pore volume of 1 g of clean catalyst}}$$

A similar trend was observed in the micro-pore volume ratio (Figure 3.8c), except that the ratios of the HY samples used in oligomerization runs were much closer to the estimated values. Table 3.4 shows the measured pore distribution and volume of coke. It follows from the negative values determined for coke in the macro-pores that the accuracy of coke volume estimations is low.

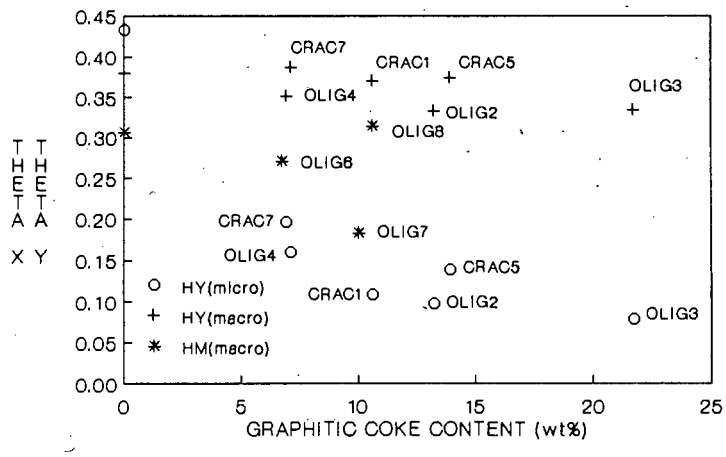

Figure 3.8a : Voidage vs graphitic coke content in HY and HM

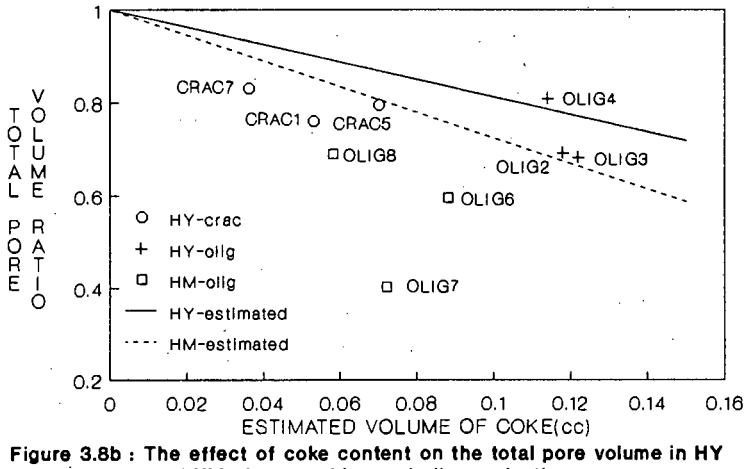

Figure 3.8b : The effect of coke content on the total pore volume in HY and HM after cracking and oligomerisation.

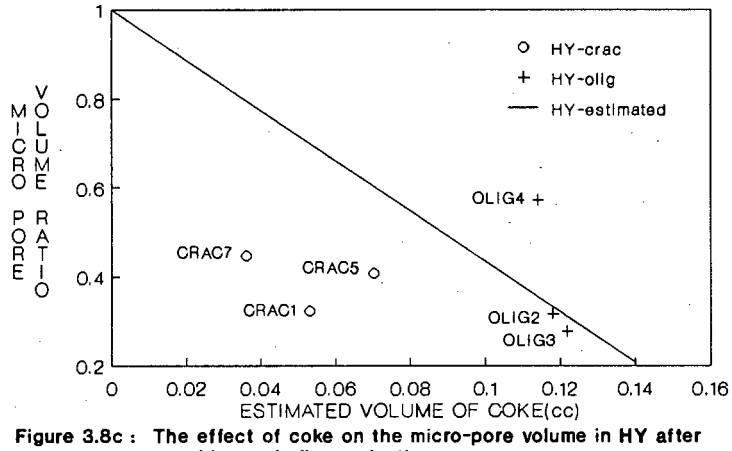

Figure 3.8c : The effect of coke on the micro-pore volume in HY after cracking and oligomerisation.

3.4 Discussion

Since high boiling point hydrocarbons should ignite at a lower temperature than graphitic coke, the low temperature exotherm was assigned to high boiling point hydrocarbons. After TG/DTA the catalyst was white which showed that all the coke had been removed. As this was an acid catalyst, the cracking of high boiling point hydrocarbons to lighter fractions and simultaneously aromatization to graphitic coke must have occurred during heating to 700°C in the presence of air. This was supported by the observed endotherm up to 700°C during the mass loss in the presence of nitrogen, although some baseline drift may have occurred. As cracking is endothermic, the observed endotherm was probably not solely due to high boiling point hydrocarbon desorption, but also due to heat of reaction. The observed exotherms in the presence of air must be due to coke burn-off. This heat of reaction in turn could accelerate cracking and desorption autothermally. This was also supported by TG/DTA analysis of OLIG4 and OLIG12 which showed approximately 7% graphitic coke, although in each case the catalyst had a brownish colour suggesting the presence predominantly of high boiling point coke (Langner, 1981). The TG/DTA method should therefore overestimate the graphitic coke content and in turn underestimate the volume occupied by coke.

On catalyst samples subjected to reaction temperatures above 200°C, all the adsorbed water was removed below 200°C as seen from the endotherm. However, for oligomerisation at 100°C (OLIG4, OLIG12) high boiling point hydrocarbons would be expected to desorb below 200°C simultaneously with the adsorbed water. The separation of water and high boiling point hydrocarbons, taken at the cross-over of endotherm to exotherm, was probably not reliable and possibly led to further underestimation of high boiling point hydrocarbons in OLIG4 and OLIG12. The estimation of the density of each coke fraction was in accordance with the values reported by Magnoux et al. (1987a) who for heptane cracking at 450°C took the density of the soluble coke fraction (polyaromatics) to be 1.3 g/cm^3 and the insoluble fraction (graphite) to be 2.2 g/cm^3. They also found that the soluble fraction was negligible after more than 6 h on stream.

The shift in the 500°C exotherm in HM was possibly due to the increased diffusional resistance of the one-dimensional pore structure, which would delay the burn-off process as graphitic coke increased (Weisz and Goodwin,

1963). This was not observed in HY, presumably because of faster diffusion in the three-dimensional pore structure. The more exothermic behaviour of HY as opposed to HM appeared to be directly proportional to the increase in coke content as would be expected. However, contradictory behaviour was observed in HY in which OLIG4, which had more high boiling point hydrocarbons than OLIG11 (250°C, 64 atm), had a considerably smaller exotherm. A similar pattern was also observed with OLIG4 and OLIG2. This suggests that the nature of high boiling point hydrocarbons was dependent on reaction conditions and the extent of deactivation as seen from the liquid product distribution data. Such a difference would affect the nature of the high boiling point hydrocarbons, and in turn would affect the approximations of the coke fractions, as high boiling point hydrocarbons for each oligomerization run would crack to a different degree during the temperature programming of the TG/DTA. Diffusion effects were also expected to contribute towards variable high boiling point hydrocarbon exotherms as low diffusional resistance might lead to less cracking by increasing the residence time of high boiling point hydrocarbons inside the pores. Once the hydrocarbons diffuse out of the zeolite pores, they can burn-off more easily in air (with possibly a greater exotherm), and this would counteract the above effects.

It is clear from the TG/DTA results that reaction temperature had a more significant effect on coke than reaction pressure. The small effect of pressure on the amount of high boiling point hydrocarbons in HM at 300°C appears to be due to the high reaction temperature which tended to generate predominantly graphitic coke. High reaction pressure should produce more residual high boiling point hydrocarbons due to the increase in boiling point at a fixed reaction temperature. However, as the product distribution in HM was not pressure dependent and contained lighter fractions than HY, the reaction temperature might have been high enough to desorb most of the residual high boiling point hydrocarbons, even at high pressure. In contrast, more high boiling point hydrocarbons remained behind in HY at high pressure and 250°C.

The order of magnitude greater macro-pore diameter in HM could be due to different extrusion pressures and the 20 wt% inorganic oxide binder used in HY. The large meso-pore fraction in HY could arise from the binder, as they were not observed in HM which was binderless. The meso-pores in HY could become a significant parameter during adsorption and diffusion of small

aliphatics in the GC diffusion experiments of coked samples in Chapter 5, as the surface area was greatly reduced after deactivation. It has been shown by Androutsopoulos and Mann (1976) that skin effects (arising from the more dense layer of catalyst found on the surface of extrudates) can cause over-estimation of macro-pore surface area and shift the pore size distribution determined by mercury porosimetry in favour of smaller pores. In this work the 1/16" extrudates of HY and HM were crushed to $250 < d_p < 500$ μm size fraction, so that skin effects in these samples were expected to be negligible. On the other hand, any blockage resulting in "bottle necks" at the meso-pore mouth would lead to the same effect in mercury porosimetry, the theoretical basis of which applies only to the case of perfectly cylindrical pores.

The decrease in skeleton density with increasing coke content suggested that coke filled pores were inaccessible to helium. Coke and inaccessible pores had a lower density than the zeolite framework and therefore the skeleton density of deactivated samples decreased. The bulk particle density increased with increasing coke content as the void space was now occupied by more dense coke. The pore volume determined from these density measurements would not necessarily be accessible to larger molecules such as nitrogen and hydrocarbons, but ammonia used in TPD should be able to access most of it. Hence the total pore volume per gram of catalyst should approximately follow the change in acid site concentration per g of catalyst unless acid sites are poisoned without the introduction of diffusional limitations. Such similarities were observed particularly in the case of HY (see Chapter 4).

If only pore blockage took place, then the reduction in BET surface area should be approximately proportional to the reduction in micro-pore volume, which was observed in HM. That macro-pore surface area was greater than the BET surface area may be due to skin effects (over-estimation) caused by coke. In addition, BET may not be applicable to such large pores (10000 Å). However, if the BET surface area decreased more rapidly than the micro-pore volume, partial pore blockage occurred because helium can access more pore volume than nitrogen. This was observed in HY oligomerization data, but cracking results were anomalous. Cracking over HY showed partial pore blockage for high graphitic coke content, while at low coke level more surface area was measured than expected. This could still be explained by partial pore blockage, for the pores in CRAC7 may be just large enough to

admit nitrogen, hence accessing a much larger surface area with little change in micro-pore volume.

As was the case with HM, macro-pore surface areas for the high coke content HY samples were larger than or comparable to the BET surface area. The significantly smaller change in the macro-pore surface area was expected because coke should have less effect on the total macro-pores than on micro-pores. It is possible that skin effects caused overestimation of macro-pore surface area, particularly in light of the small meso-pores. Macro-pores (> 600 Å) were not expected to be affected significantly because coke molecules are much smaller in dimension. Furthermore the BET technique is based on adsorption of nitrogen and it is not clear how the coke on the samples affects the BET area measurements. Care must be taken when comparing the surface area of the coked samples.

The inconsistent behaviour in the macro-pore voidage of HM shows that the macro-pore volume of OLIG7 may well be too small, which could be caused by the larger particle density (see Table 3.3). The particle densities of the HM samples are expected to be similar. Thus if the particle density of OLIG7 is assumed to be 1.42 g/cm^3, then the macro-pore voidage would be 0.29, which is more consistent with the values of the other HM samples, all being within experimental error of the values of fresh HM (meso- and macro-pores). One source of error in all measurements is the standard mercury contact angle of 130° which was used throughout.

The macro-pore peak observed around 600 Å in HY and HM after oligomerization was not observed in the HY cracking samples and must therefore have been caused by high boiling point hydrocarbons. It is not clear what effect high boiling point hydrocarbons would have on mercury porosimetry, but it is possible that high boiling point hydrocarbons restrict penetration of mercury until a certain pressure, after which additional macro-pores may appear as the high boiling point hydrocarbons are forced into the micro-pores.

The effect of high boiling point hydrocarbons on catalyst properties is seen by comparing CRAC7 with OLIG4, both of which had similar estimated graphitic coke contents (although OLIG4 may actually have had considerably less), from which it is clear that high boiling point hydrocarbons reduced BET surface area considerably. The skeleton density of OLIG4 was greater than that of CRAC7. This is most unlikely since OLIG4 contained considerably more coke

which was lighter than the zeolite framework. The skeleton density of OLIG4 is thus probably in error. A lower value of the OLIG4 skeleton density than CRAC7 would lower the micro-pore volume to below that of CRAC7. The graphitic coke (CRAC7) appeared not to affect the (macro+meso)-pores, while in OLIG4 (macro+meso)-pores were significantly reduced. This is clearly due to the larger coke content and the greater volume occupied by high boiling point hydrocarbons which are less dense. Estimated coke volume indicated that all the oligomerization coke could be accomodated in the micro-pores. This means that it is possible for the mercury to compress some of the high boiling point hydrocarbons into the micro-pores, thereby giving an overestimation of the macro-pores. Additionally θ_y measured in cracking samples was not signifigantly affected by coke, while in the case of oligomerisation samples the change was larger. One model which incorporates the above features is that graphitic coke is located predominatly in the micro-pores, causing pore blockage, and high boiling point hydrocarbons are mobile and occur in both the macro-pores and micro-pores.

θ_x decreased rapidly with increasing coke content. The estimated reduction in pore volume due to coke (based on the density of coke) was always less than the actual reduction determined by porosimetry, which suggests pore blockage, particularly for HM. The anomalous behaviour of OLIG4 has been suggested in the above to be due to incorrect skeleton density. If the skeleton density is reduced, OLIG4 would follow the trend of the other samples. Similar results based on estimated coke volume were obtained by Magnoux et al. (1987b). It follows that results are subject to experimental errors but observed trends are generally valid.

3.5 SUMMARY

The TG/DTA method was able to distinguish the high boiling point hydrocarbons and graphitic coke, but overestimated the amount of the latter, leading to an underestimation of the volume of coke. The TG/DTA results were affected by diffusional limitations and differences in the nature of coke. Increasing the reaction temperature had a more significant effect on the formation of the graphitic coke than increasing the pressure.

Skeleton density decreased while bulk density increased with increasing graphitic coke content. In all cases the micro-pore volume decreased with

increasing coke content. However macro- and meso-pore volume showed no change in HY after cracking. Macro-pore volume in HY after oligomerisation remained the same, while the meso-pore volume showed subtle decreases with increasing graphitic coke content. Due to experimental difficulties, information on porosity of deactivated HM samples was inconclusive. BET surface area decreased for both HY and HM in all cases. In particular, the sharp reduction in the BET surface areas of deactivated HM samples demonstrated clearly the inaccessibility of the mordenite main channels to nitrogen molecules. Macro-pore surface area in HY decreased while in HM it remained unchanged with increasing coke content. The meso-pore volume in HY played a significant role in the residual pore volume and surface area after coking. The reduction in pore volume based on estimated coke volume was always less than the actual pore volume determined from porosimetry.

Results showed that total pore blockage was the dominant deactivation mechanism in HM, while in HY partial pore blockage occurred, with the meso-pores playing an important role. In all cases it can be postulated that graphitic coke was predominantly located in the micro-pores while high boiling point hydrocarbons were located in both micro- and macro-pores. These results were subject to limitations of the analytical techniques such as the assumed contact angle of 130° for mercury, skin effects, compression of high boiling point hydrocarbons into the micro-pores by mercury at high pressure, high boiling point hydrocarbons restricting the access of mercury and the possible effect of coke on the BET technique was not known.

4 AMMONIA TEMPERATURE PROGRAMMED DESORPTION

4.1 INTRODUCTION

The aim of this section was to determine the effect of coke on the strength and distribution of acid sites on a catalyst as measured by ammonia temperature programmed desorption (TPD). These results should aid the prediction of a mode of deactivation, viz., site poisoning as opposed to pore blockage. Therefore the results should complement the understanding of the results of Chapters 2 and 5.

TPD is a common technique used for determining the strength and distribution of acid sites from ammonia desorption, previously adsorbed under controlled conditions, from an acid catalyst subject to a constant heating rate. The modelling of TPD, the validity of assumptions and the determination of good operating conditions have been extensively studied (Cvetenovic and Amenomiya, (1967); Gorte, (1982); Jones and Griffin, (1983); Rieck and Bell, (1984); and Tronconi and Forzatti, (1985, 1988)). Numerous studies have also been conducted on fresh (Topsøe et al. (1981) and Hidalgo et al. (1984)) and deactivated catalysts (Itoh et al. (1984); Kubelkova et al. (1985) and McLellan et al. (1986)). Niwa et al. (1986) showed that quatitative comparison of data between various laboratories was not possible, but that the data obtained using the same apparatus were internally consistent.

In this section attempts are made to correlate the change of acid site distribution with the coke content of the catalyst determined from TG/DTA. Ammonia TPD is shown to qualitatively and quantitatively predict the acidity of HY and HM. Catalyst after hexane cracking proved to follow a simple trend with graphitic coke content, while the analysis of catalysts after propene oligomerisation was complicated by the desorption of high boiling point hydrocarbons.

This chapter firstly considers the apparatus and procedure, outlining the apparatus used, the experimental technique and the operating conditions. The accuracy of the data is also discussed. This is follwed by the results and discusion.

4.2 APPARATUS AND PROCEDURE

4.2.1 TPD apparatus

Figure 4.1 shows a schematic diagram of the TPD apparatus. A thermal conductivity detector was used to detect desorbing NH_3. The helium and NH_3/He (ca. 4% NH_3) were set at a back pressure of 200 kPa to ensure as constant a flowrate as possible at 60 ml/min through the controlling needle valve. A 3-way shut-off valve was used to switch to either gas. Helium was dried by 3A molecular sieves. A more detailed sketch of the quartz/glass sample cell is shown in Figure 4.2. The inlet tube acted as a preheat. The catalyst was held by a sintered disc and a thermowell in the centre of the catalyst bed was used to monitor the temperature changes in the sample. Three stopcocks allowed the sample to be bypassed. All piping was 1/8" (316) stainless steel and glass to metal fittings were used. The exit line from the cell was heated to 100°C.

The core of the furnace was made of phosphorus-bronze. The four 350 W cartridge heaters were able to power the furnace to above 600°C at a linear rate greater than 15°C/min. The furnace was well insulated and brass filings were used as a packing to improve the heat transfer between the sample cell and the furnace. The heating rate was linear at 15°C/min except for the end points (± 10°C). There was a temperature lag of 15°C. The Eurotherm temperature controller and programmer combination was able to control the furnace to ±0.5°C.

Dead volume from the sample cell to the TCD was kept to a minimum. To improve sensitivity and stability of the TCD (Gowmac Model) a constant temperature waterjacket at 40°C was used. This also ensured fast stabilization after start-up. Helium at 50 ml/min was used as the reference. The exit gas from the TCD passed through a saturator where NH_3 was removed by reaction with 0.1N H_2SO_4 solution. The H_2SO_4 solution was then back titrated using 0.1N NaOH to determine the total amount of ammonia desorbing from the catalyst. The flowrate through the system was monitored by a soap bubble meter.

The signal from the Gowmac control unit was amplified 100x, 50x and 25x. These three signals together with the cell thermocouple output were sent to a PC through an 8-bit serial interface. The PC monitored samples every second

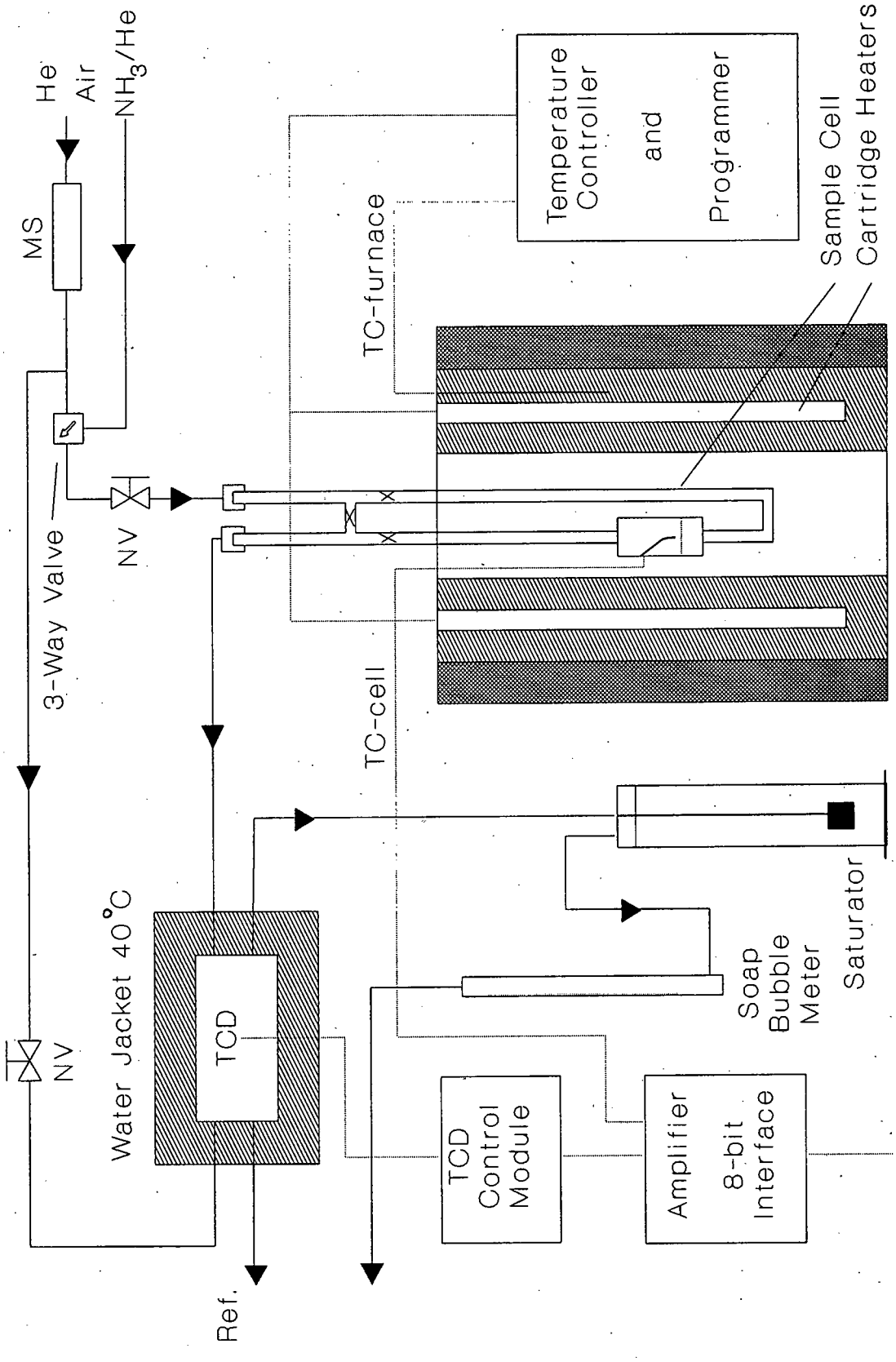

Figue 4.1 : Schemmatic diagram of TPD apparatus.

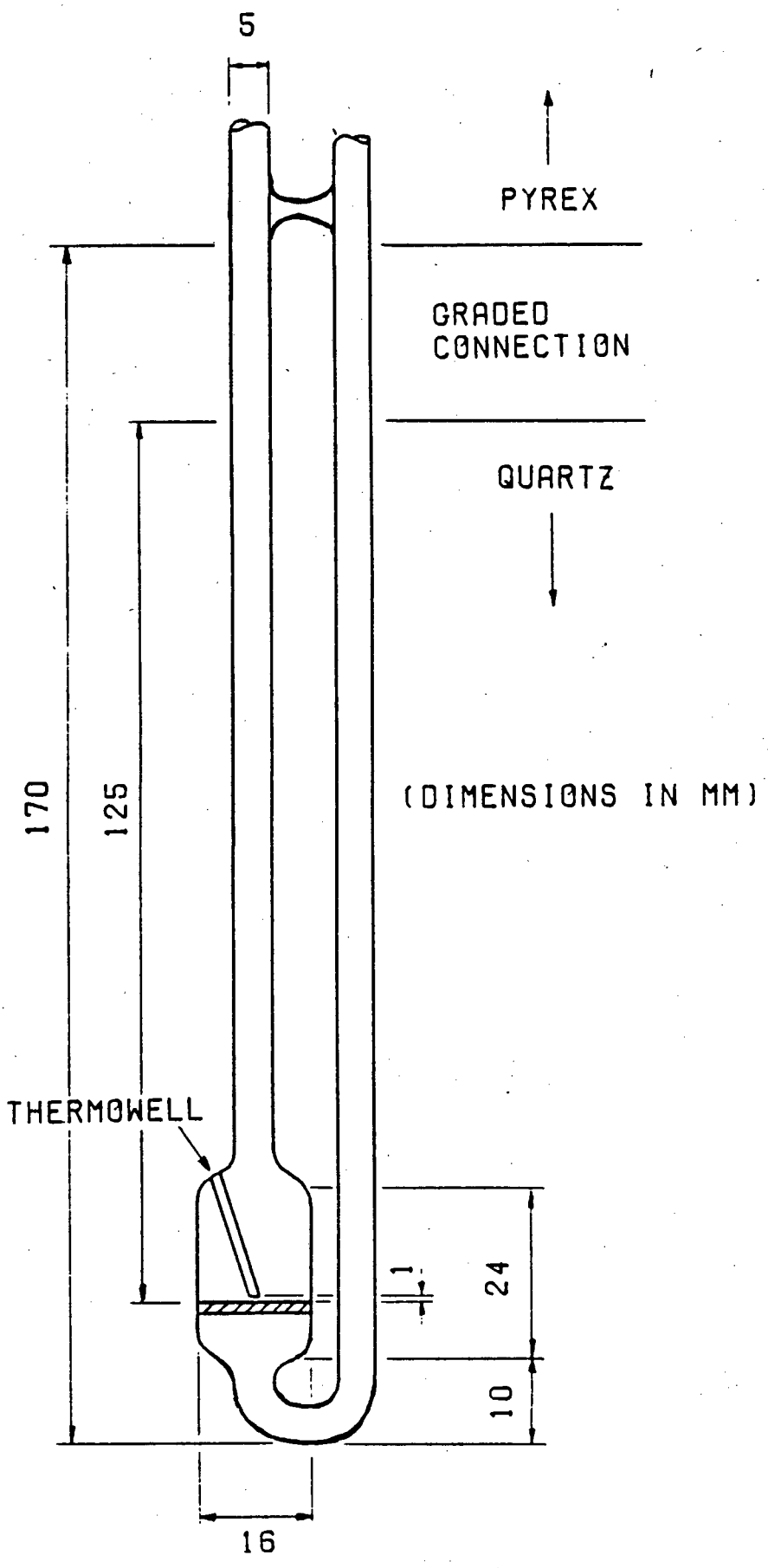

FIG 4.2 TPD SAMPLE CELL

and logged 10 second sample averages (as real numbers for improved resolution) of these signals together with the time on disk. Temperature conversion from ADC to °C was performed in the logging program from 25°C to 620°C.

4.2.2 Experimental conditions and procedures

0.5 g of catalyst in size fraction range 0.25 - 0.50 mm was packed into the sample cell. This amount of catalyst was required to obtain a good signal with the TCD. The sample was calcined in-situ in air at 400°C for fresh HY and 350°C for HM for 6 h. The deactivated samples were heated to 200°C in flowing nitrogen except for OLIG4 and OLIG12 which were heated to 100°C (i.e., reaction temperature) for 6 h. The sample cell was then sealed and cooled to 100°C. Once the TCD was stable with helium flow passing over the catalyst sample, the 3-way valve was switched to introduce the NH_3/He mixture to the catalyst. Simultaneously the data logging program was started. When the adsorption curve was steady the 3-way valve was switched back to helium. Desorption at 100°C of weakly held ammonia was complete when the signal from the TCD had returned to the baseline (or close to it). The temperature programmer (5°C/min) was started and the saturator was put on line. When 600°C was reached and the spectrum had returned to the baseline the TPD was complete. The data logging program was terminated and the back titration with methyl orange indicator performed.

In order to correct the baseline for the desorption of water and hydrocarbons, or any baseline drift, the sample was calcined as before and the TCD stabilized in flowing helium. The programmer (5°C/min) and the data logging program were then started to record any desorption of moisture or detector drift with temperature increase. In the case of the oligomerisation samples this incorporated the desorption of high boiling point hydrocarbons. Typical TPD spectra showed that the adsorption curve oscillated at saturation. These oscillations were in phase with the 0.5 °C temperature oscillations of the sample bed.

The operating conditions can be summarised by considering the dimensionless parameters of Gorte (1982). Rieck and Bell (1984) and Tronconi and Forzatti (1988) have verified the validity of these parameters for a packed bed. The parameters and these estimated values are shown in Table 4.1. The parameters

TABLE 4.1 : TPD EXPERIMENTAL SYSTEM PARAMETERS.

Parameter	Physical description	Significance	Estimated value HY	Estimated value HM
$\frac{V\beta}{Q(T_f-T_o)}$	Average residence time for the cell (parameter 1)	<0.01 for the cell to follow net desorption rate	0.0012	0.0012
$\frac{\beta r^2 \epsilon}{D(T_f-T_o)}$	Accumulation of the gas in the catalyst pore (parameter 2)	<0.01 for the cell to follow net desorption rate	0.0026	0.129
$\frac{Qr}{DA}$	Effect of carrier gas flowrate (parameter 3)	<0.1 concentration gradients are negligible. >20 flowrate is essentially infinite and the concentration at the catalyst edge is effectively zero	24.6	1800
$\frac{\alpha \delta s F r^2}{\pi^2 D}$	Ratio of adsorption to diffusion rate at infinite carrier gas flowrate (parameter 4)	>1 readsorption is important, even at high carrier gas flowrates	2.37E11 * s	1.27E13 * s

where

Parameter	HY	HM
V-system volume (ml)	9.48	9.48
β-heating rate (°C/sec)	0.083	0.083
Q-volume flowrate of carrier gas(ml/sec)	1.27	1.27
T_f-final temperature (°C)	600	600
T_o-initial temperature (°C)	100	100
r-catalyst particle radius (cm)	0.01875	0.01875
ϵ-catalyst porosity	0.567	0.455
D-effective diffusivity (cm^2/sec)	1.29E-5	2.06E-7
A-external surface area (cm^2)	75	64
α-active surface area (cm^2/g)	4.77E6	3.47E6
δ-catalyst particle density (g/cm^3)	1.06	1.25
$F=(RT/2\pi M)^{\frac{1}{2}}$ (cm/sec)	17000	17000
s-sticking factor	-	-
R-gas constant ($cm^2g/sec^2/mol/K$)	8.314E7	8.314E7

were evaluated at the worst case, i.e., 100°C. The porosity was obtained by mercury porosimetry and helium pycnometry as discussed in Chapter 3.

The external surface area was calculated from 3*(weight catalyst)/$r\rho$ where ρ is the bulk density of the catalyst. The effective diffusivity of NH_3 was assumed to be close to that of methane and hence the values obtained in Chapter 5 were used. Crystallite sizes were assumed to be $3x10^{-4}$ cm (Hsu and Haynes, 1981) for HY and $2.5x10^{-4}$ cm (Satterfield and Frabetti, 1967) for HM. The active surface area (α) was calculated from α = 2*(micro-pore porosity)/($r_p\rho$) giving 477 m^2/g and 347m^2/g for HY and HM, respectively. The pore radius r_p was taken to be 7.4 Å for HY and 6.85 Å for HM. The system volume included the dead volume of the exit tubing.

Table 4.1 shows that the cell time lag (parameter 1) is negligible and the detector will monitor the net desorption rate. The accumulation of gas in the catalyst pore (parameter 2) is negligible for HY but not for HM. This is because the diffusion of NH_3 in HM is slower than in HY. The TPD from HM is therefore subject to error. The only means of reducing this effect would be to reduce the heating rate by an order of magnitude (not practical) or to use much smaller catalyst particles (not desirable, since the catalyst particles would not be fully supported by the sintered disc). Concentration gradients in the pellet can, however, also occur independently of this group (Gorte, 1982), but such a phenomenon has been shown to be unimportant in most cases (Gorte, 1982). Parameter 3 shows that concentration gradients in the catalyst exist, especially for HM, the concentration at the catalyst edge being essentially zero. Readsorption (parameter 4) is important because the sticking coefficient (s) would have to be 10^{-11} and 10^{-13} for HY and HM, respectively, to make readsorption insignificant.

Finally evaluating the dispersion number (D/vL = 0.0003) in the exit pipe from correlations given by Levenspiel (1972) indicates that plug flow was well approximated. This suggests that peak spreading in the exit pipe was negligible. However, the calculation does not include the pipe fittings for which peak spreading was assumed to be negligibly small.

4.2.3 Ammonia calibration and data analysis

Each analysis includes an adsorption curve, the maximum ADC reading of which corresponds to the concentration of ammonia in the NH_3/He mixture. This procedure can account for any change in detector sensitivity from run to run. The NH_3 mixture was standardised by titration with H_2SO_4 and NaOH using a saturator. The ammonia content was 4.08 ± 0.10% NH_3/He (see Appendix D, Table D1 for details).

Data analysis and integration were performed on an IBM compatible PC. The ADC ranges were chosen to obtain maximum sensitivity from the logged data. The baseline correction was carried out by curvefitting the baseline ADC data as a function of temperature (100 - 600°C) using between 30 - 40 cubic spline nodes. Excellent curve fits were obtained over the entire temperature range. This was then subtracted from the actual TPD spectra, making corrections for slight flowrate differences between analysis and baseline data (always <2%). The mean of the last three concentration oscillations was taken as the ADC value equivalent to the initial feed concentration (1.82 μmol $NH_3/m\ell$). After data smoothing, integration limits could be chosen manually from a graphical display and the peaks integrated after accounting for the different flowrates. The data were logged in a way which was suitable for plotting with a graphics package. The heating rate was correlated with a linear regression ($r^2 > 0.999$) between 110 and 590°C.

4.2.4 Data accuracy

The data accuracy was limited by the sensitivity of the TCD. Linearity of the detector was not a problem as the concentration was always lower than the NH_3/He feed, which was in the linear range. Due to the corrosive nature of NH_3 there always tended to be a slight baseline drift. This had very little effect on adsorption but desorption and TPD were more sensitive to this drift. The baseline correction noted earlier was not able to correct for this effect entirely, although it was possible to use the analysis program to approximate the baseline drift as a linear function of temperature.

The accuracy was also limited by the 8-bit ADC. Although three ranges of the output signal were processed, some of the TPD runs which had very low ammonia adsorption were in the lower range of the lowest ADC signal, while the feed

gas concentration was in the upper region of the highest signal. The signals were affected by inherent oscillations in the ADC. The use of 10 point averages improved the resolution of the ADC. However, these improvements were hampered by the ADC oscillations and only a 1/800, as opposed to the expected 1/2500, resolution was possible.

TCD detects not only ammonia but also water and hydrocarbons. The latter was particularly a problem in the case of oligomerisation samples where large desorption peaks from the high boiling point hydrocarbons were present. The ammonia adsorption for these samples was small, and therefore when the baseline was subtracted small errors would be magnified by the resulting signal. Any change in the desorption of the high boiling point hydrocarbons between analysis and baseline runs would result in the NH_3 desorption spectrum being indistinguishable from hydrocarbon peaks. The excellent cubic spline curve fit of the baseline would not be able to circumvent this difficulty.

4.3 RESULTS

A typical TPD response curve obtained using fresh HY is shown in Figure 4.3 which illustrates adsorption and desorption at 100°C followed by temperature programmed desorption. The oscillations in the spectrum in the neighbourhood of 20-60 min were due to 0.5°C temperature oscillations in the sample cell held "isothermally" at 100°C during that time and did not affect the rest of the experiment in any way. The heating rate of 5°C/min was clearly linear except at the end points which had negligible influence on the TPD peak positions. The heating rate varied within 1.5% between experiments (see Table 4.2).

Table 4.2 summarises the relevant TPD parameters for fresh HY, HM and their deactivated counterparts. In the case of fresh HM, there were two distinct desorption peaks, one in the vicinity of 200°C and the other above 500°C. They will be referred to as the l-peak and h-peak, respectively, hereafter. As mentioned in the description of the procedure, the sample holder was maintained at 600°C until no more desorption of ammonia was registered by TCD. When plotted against temperature, the desorption rate gave the appearance of falling steeply at 600°C. The integration of the area under the desorption spectrum was performed in the time domain. The amount of

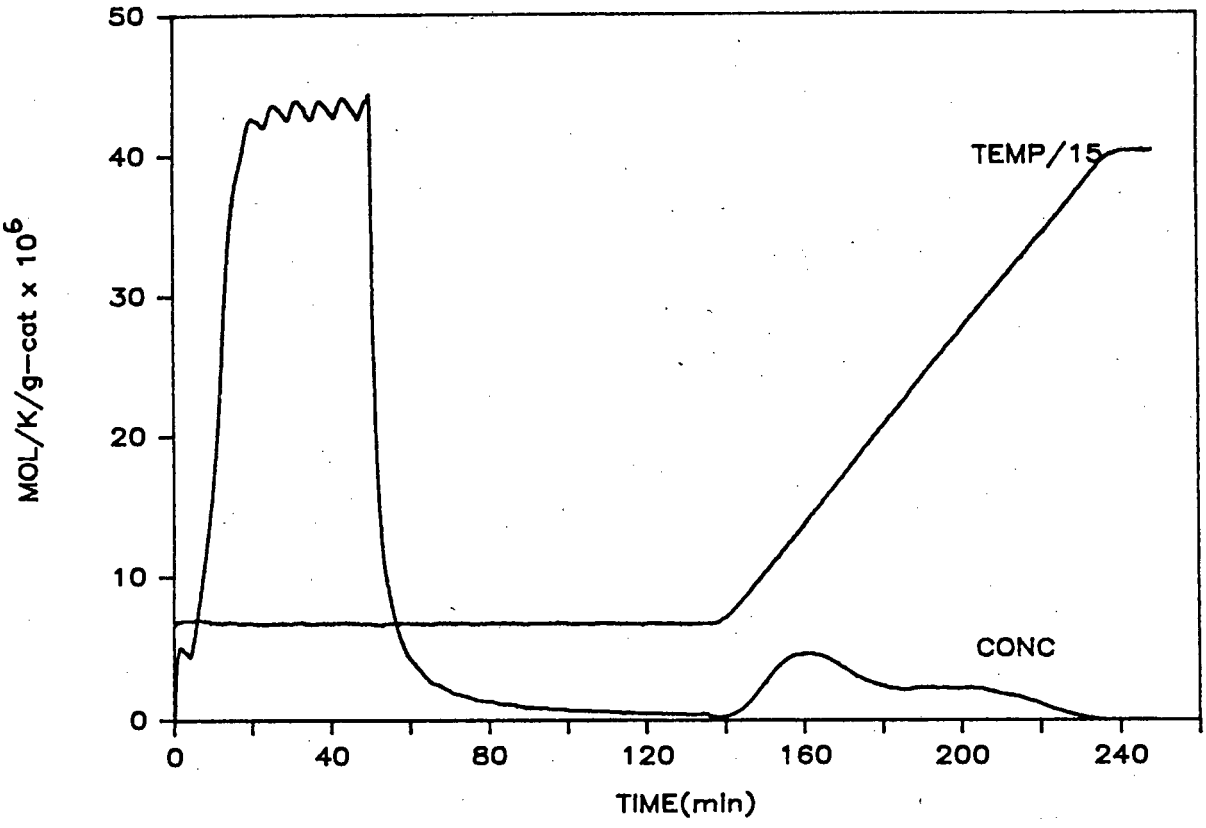

Figure 4.3 : Typical ammonia TPD run with HY; calcined at 400°C

TABLE 4.2 : SUMMARY OF TPD DATA.

Run ID	Catalyst	Coke Content hpb	Coke Content gc	Pretreatment	Heating Rate	T_i °C	T_h °C
LZY82	HY	-	-	Air/400°C	5.14	210	368
100HM	HM	-	-	Air/350°C	4.99	212	570
97HM	97%NH_4-M	-	-	Air/500°C	5.02	218	522
97HMC	97%NH_4-M	-	-	"	5.01	213	498
HM1	HM	-	-	Air/350°C	5.03	213	557
HM2	"	-	-	"	5.02	218	565
CRACT	HY	-	9.2	N_2/400°C	5.13	209	364
CRAC1	"	-	10.6	"	5.15	205	350
CRAC2	"	-	8.5	"	5.16	210	365
CRAC3	HM	-	3.1	N_2/350°C	5.09	212	576
CRAC4	HY	-	8.9	N_2/400°C	5.13	207	363
CRAC5	"	-	13.9	"	5.12	208	-
CRAC6	"	-	8.9	"	5.10	212	352
CRAC7	"	-	7.1	"	5.09	215	365
OLIGT	HY	5.4	13.7	N_2/200°C	5.13	195	368
OLIG1	"	4.3	13.0	"	5.10	177	372
OLIG2	"	5.2	13.2	"	5.07	183	368
OLIG3	"	1.3	21.7	"	5.09	186	-
OLIG4	"	7.9	6.9	N_2/100°C	5.11	298	373
OLIG5	"	4.4	16.7	N_2/200°C	5.08	179	356
OLIG6	HM	5.4	6.7	"	5.06	200	464
OLIG7	"	2.2	10.0	"	5.02	195	547
OLIG8	"	0.5	10.6	"	5.04	208	570
OLIG9	HY	3.3	19.1	"	5.08	173	-
OLIG10	"	3.5	12.2	"	5.08	176	380
OLIG11	"	5.3	18.8	"	5.05	168	372
OLIG12	"	6.7	7.0	N_2/100°C	5.09	301	380
OLIG13	HM	1.9	8.8	N_2/200°C	5.08	195	487
OLIG14	"	1.8	8.2	"	5.05	200	379
OLIG15	"	-	8.1	"	5.03	200	548
OLIG16	"	-	8.1	"	5.03	205	546
OLIG17	"	-	8.7	"	5.03	201	572
OLIG18	HY	4.3	16.9	"	5.05	176	365

hpb - high boiling point hydrocarbons
gc - graphitic coke wt%
Heating Rate - °C/min

TABLE 4.2 : continued

Run ID	ads	des	TPD integration			TPD titre. total	h-peak total	Ratio
	mmol/g	mmol/g	total	l-peak	h-peak			
LZY82	2.23	0.97	1.01	0.64	0.37	1.34	0.37	-
100HM	3.18	1.11	1.72	0.92	0.81	2.32	0.47	-
97HM	3.61	1.12	1.98	1.34	0.64	2.50	0.32	-
97HMC	3.27	1.12	1.87	1.35	0.52	2.44	0.28	-
HM1	3.39	0.99	1.75	0.97	0.78	2.34	0.45	-
HM2	3.40	1.12	1.79	0.94	0.85	2.32	0.48	-
CRACT	1.95	0.90	0.87	0.61	0.26	1.02	0.30	0.87
CRAC1	1.74	0.82	0.78	0.55	0.23	1.04	0.29	0.78
CRAC2	1.85	0.91	0.85	0.61	0.25	1.28	0.29	0.83
CRAC3	2.99	0.92	1.47	0.86	0.61	2.08	0.42	0.94
CRAC4	1.98	0.86	0.96	0.64	0.32	1.12	0.33	0.89
CRAC5	1.98	0.79	0.78	0.57	0.21	1.06	0.26	0.76
CRAC6	1.97	0.88	0.85	0.59	0.27	1.08	0.31	0.88
CRAC7	2.01	0.85	0.91	0.61	0.30	1.36	0.33	0.90
OLIGT	1.24	0.62	0.46	0.25	0.21	0.70	0.46	0.56
OLIG1	1.31	0.69	0.41	0.37	0.04	0.73	0.10	0.59
OLIG2	1.14	0.62	0.56	0.29	0.27	0.69	0.49	0.51
OLIG3	1.27	0.63	0.41	0.41	-	0.64	-	0.57
OLIG4	1.28	0.60	1.19	0.40	0.79	0.94	0.66	0.57
OLIG5	1.05	0.54	0.44	0.26	0.17	0.62	0.39	0.47
OLIG6	2.38	0.68	1.36	0.54	0.82	1.63	0.60	0.73
OLIG7	2.32	0.50	1.03	0.60	0.44	1.86	0.42	0.73
OLIG8	2.40	0.77	1.12	0.67	0.45	1.94	0.40	0.76
OLIG9	1.07	0.46	0.29	0.29	-	0.68	-	0.48
OLIG10	1.04	0.54	0.31	0.24	0.07	0.70	0.21	0.47
OLIG11	0.82	0.42	0.35	0.20	0.15	0.64	0.42	0.37
OLIG12	1.34	0.62	1.10	0.38	0.72	1.16	0.66	0.60
OLIG13	2.34	0.48	1.14	0.67	0.47	2.30	0.41	0.73
OLIG14	2.35	0.62	1.21	0.65	0.56	1.80	0.47	0.74
OLIG15	2.60	0.73	1.18	0.64	0.54	1.84	0.46	0.82
OLIG16	2.45	0.71	1.12	0.72	0.39	1.83	0.35	0.77
OLIG17	2.47	0.72	1.15	0.66	0.49	1.83	0.43	0.78
OLIG18	1.09	0.46	0.53	0.29	0.24	0.71	0.45	0.49

Ratio - adsorption with coke/adsorption without coke
Total, l-peak, h-peak - mmol/g
TPD titration total - mmol/g

ammonia adsorbed initially at 100°C, that desorbed at 100°C in flowing He, and that desorbed during TPD were all obtained by integration. Comparison of runs 100HM, HM1 and HM2 (Figure 4.4), in which the total amount of ammonia desorbed agreed to within 2% with slightly larger variations in the l-peak (2.6%) and h-peak(4.4%), showed that the reproducibility was good. 97% NH_4^+ exchanged NaM (97HM) showed a larger l-peak and smaller h-peak with 20% more ammonia adsorbed in total than HM. HM in turn had 70% greater total adsorption with a 43% greater l-peak and 117% greater h-peak than HY. The h-peak fraction, defined as the ratio of the quantity of ammonia corresponding to the h-peak to the total amount desorbed, of HM was 27% greater than that of HY. It is clear from Figure 4.5 that the h- and l-peaks of HM were better separated than those of HY which showed a broad diffuse acid site distribution above 300°C. The maximum desorption rate of the h-peak for HM occurred at a much higher temperature than that for HY while the temperatures at which the maximum desorption rate of the l-peak were observed were comparable.

Hexane cracking over HY had only marginal effects on the acid site distribution as measured by ammonia. The decrease in acid sites of the h-peak was greater than that of the l-peak (Figures 4.6a and b). A similar trend was observed for HM (Figure 4.6c). Figure 4.7a shows that 14% graphitic coke in HY reduced the ammonia adsorption capacity by 25% while a 6% reduction was observed for 3.1% coke on HM. The HY data scattered in the 9% coke region but the amount of ammonia adsorbed clearly decreased with increasing coke content. The TPD ratio plotted in Figure 4.7b, the ratio of the total amount of ammonia desorbed from deactivated catalyst to that desorbed from fresh catalyst, also showed a decrease of over 20% in acid sites at <10% coke on HY with considerable scatter in the 9% coke region, while HM showed a 10% decrease at 3.1% coke.

Table 4.2 shows that the quantity of desorbed ammonia determined from titration was always greater than the integrated amount. This indicated that although baseline subtraction was performed which accounted for flowrate variations and additional water desorption at higher temperatures, baseline variation must still have occurred during the TPD experiment. The TCD baseline recorded in the absence of ammonia desorption was found to be extremely stable. While errors introduced by inaccurate calibration of TCD and baseline drifts might have made determination by integration of the quantity of ammonia desorbing somewhat unreliable, the TPD ratio computed

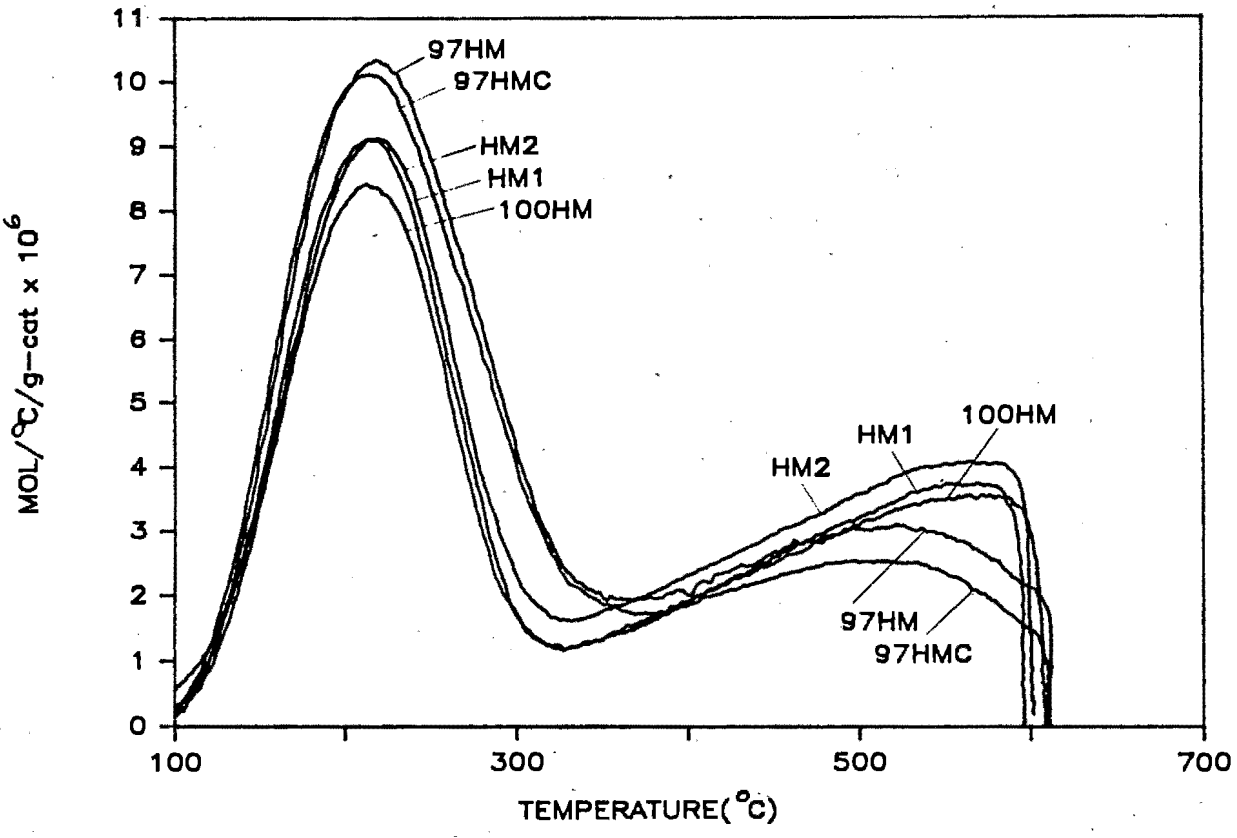

Figure 4.4 : Ammonia TPD HM and NH_4-M; reproducibility of data.

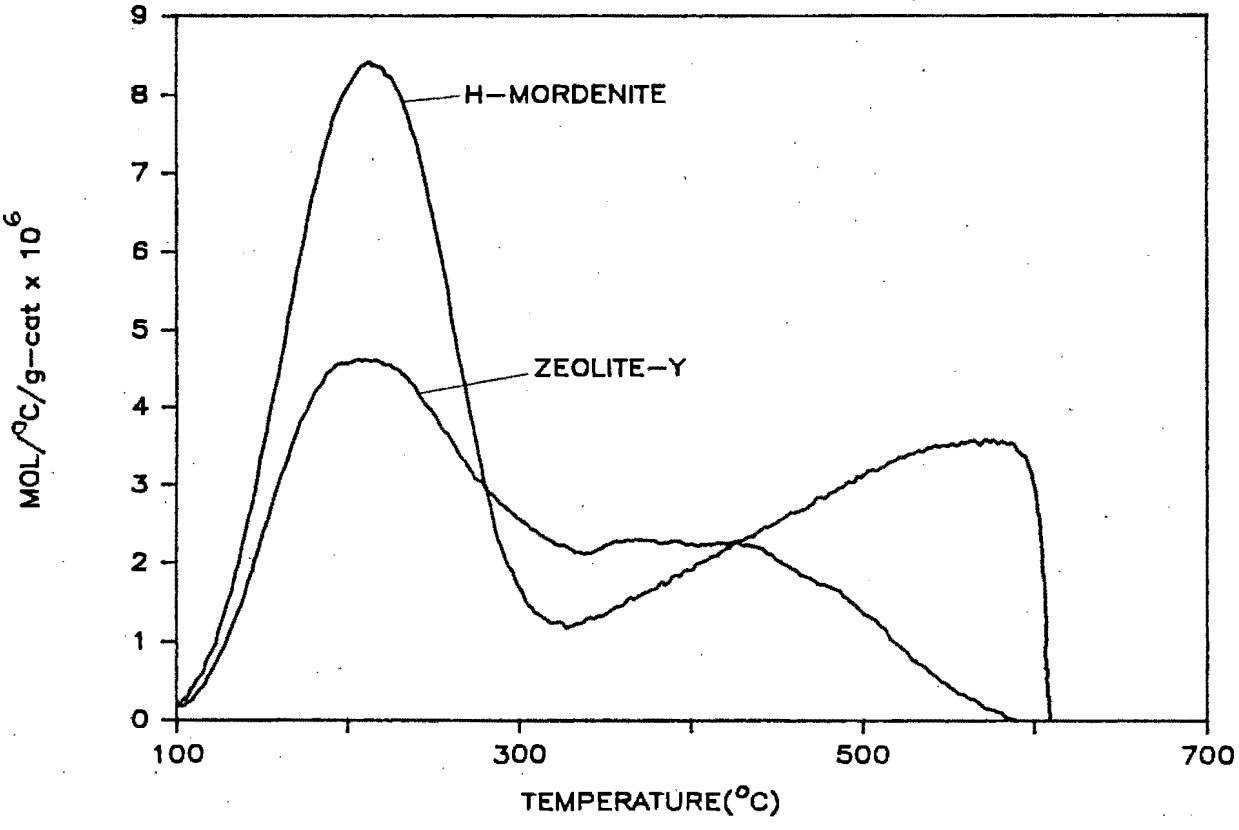

Figure 4.5 : Ammonia TPD from HY vs HM

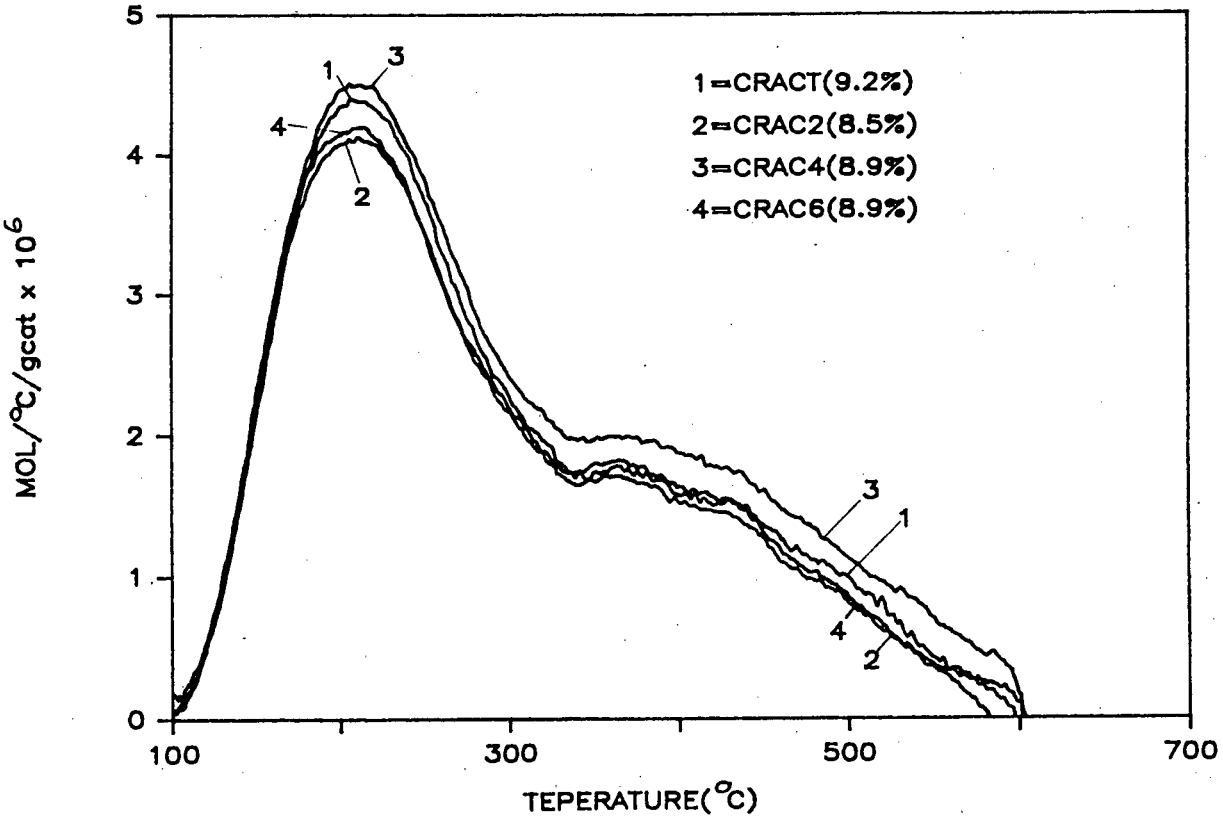

Figure 4.6a : Ammonia TPD from HY; cracking vs HY at caparable coke levels shown in parentheses.

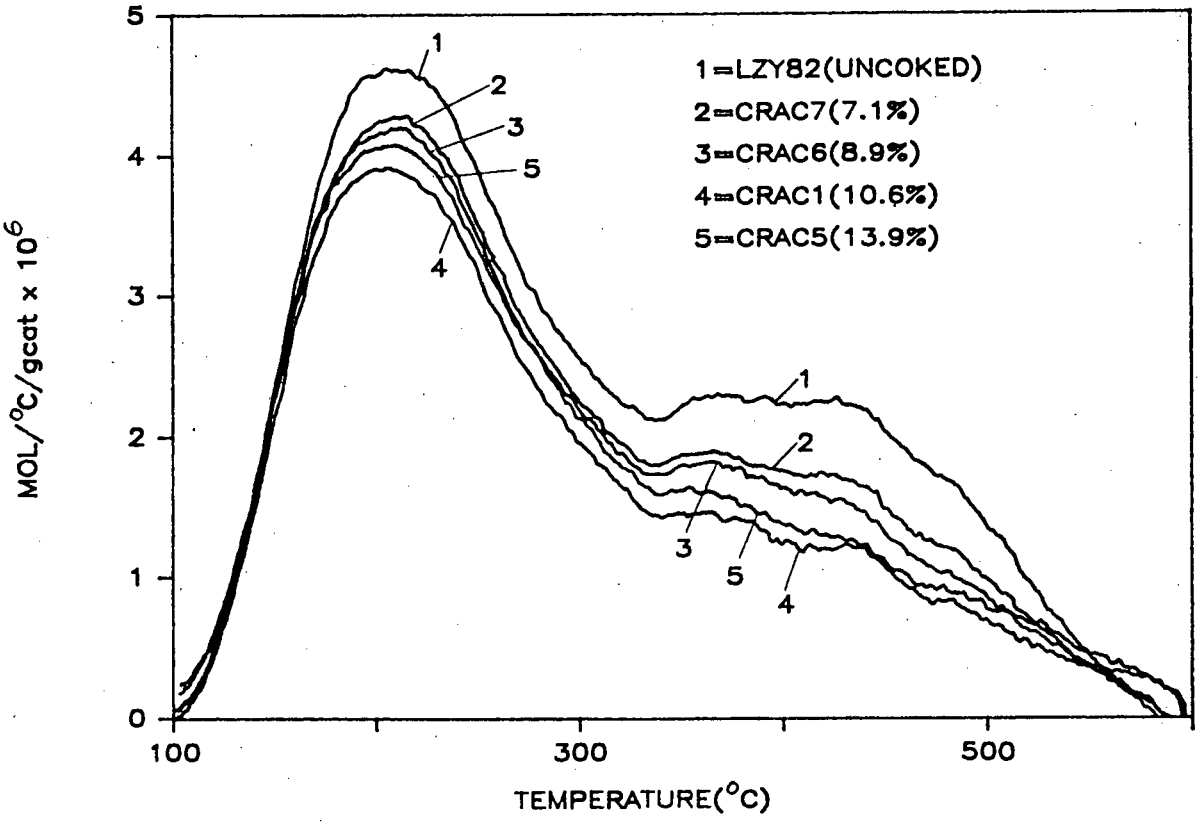

Figure 4.6b : Ammonia TPD from HY; cracking vs HY at various coke levels parentheses.

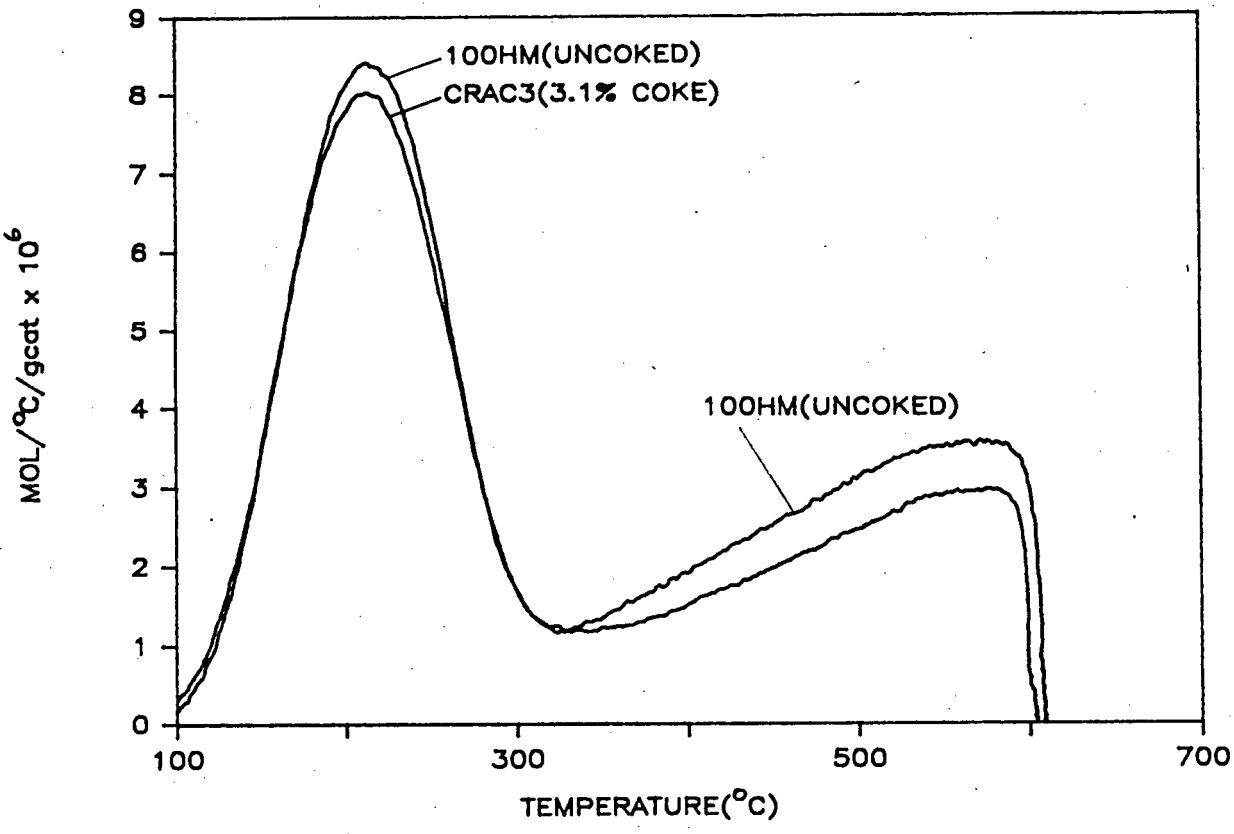

Figure 4.6c : Ammonia TPD from HM; CRAC3 vs uncoked HM.

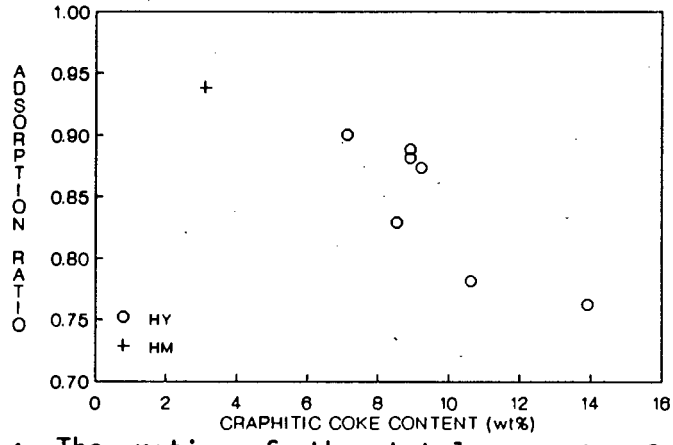

Figure 4.7a : The ratio of the total amount of ammonia adsorbed (physisorbed and chemisorbed) on deactivated catalyst to that adsorbed on fresh catalyst as a function on graphitic coke content of HY and HM after hexane cracking.

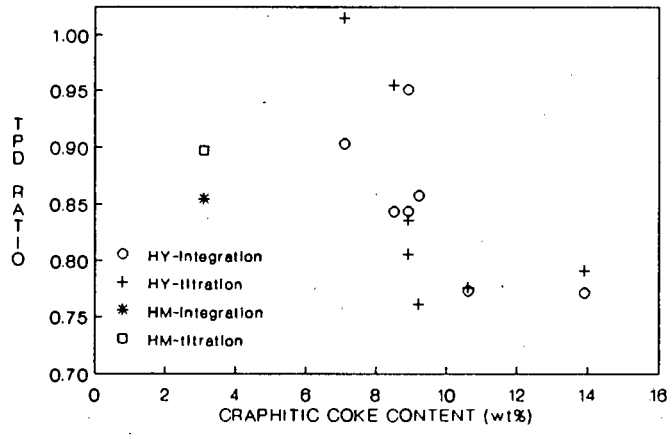

Figure 4.7b : The ratio of ammonia desorbed during TPD from deativated catalyst to that desorbed from fresh catalyst as a function of graphitic coke content for HY and HM after hexane cracking.

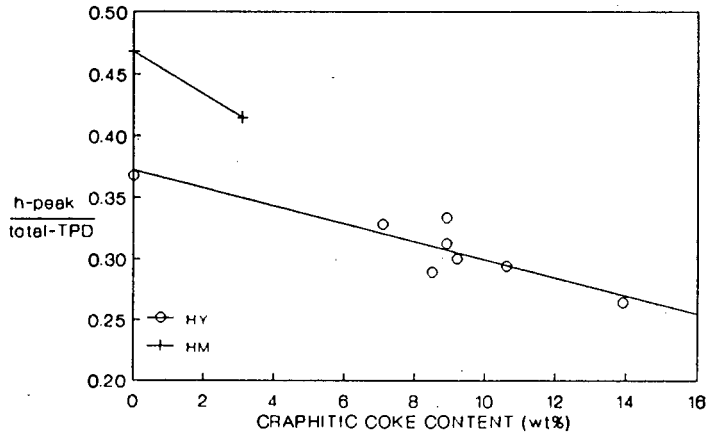

Figure 4.7c : The ratio of the amount of ammonia desorbing in the h-peak from deactivated catalyst to that desorbing from fresh catalyst as a function of grapitic coke content of HY and HM after hexane cracking.

from integration gave a trend similar to that given by titration. The h-peak ratio (h-peak coked/h-peak uncoked) showed a decrease of 40% at 13% coke in HY and a 25% decrease at 3.1% coke in HM (Figure 4.7c). The ratio was approximately linearly related to the graphitic coke content of HY. In addition, the h-peak of HM decreased more rapidly with coke content than that of HY. It must be noted that the estimation of the h-peak in HY was only an approximation and was defined to be ammonia desorbing above 340°C, while for HM the distinction between l- and h-peaks was much sharper. Furthermore, l- and h-peaks could be computed only from integration of TCD spectra which was subject to experimental errors described above.

The determination by integration of ammonia desorption from catalysts deactivated by oligomerisation was found to be unreliable. A "baseline" run was performed for each deactivated sample whereby helium was passed over the catalyst during temperature programming without adsorbed ammonia and desorption of hydrocarbons was monitored by TCD. In addition titration was performed to ensure that no basic substance was desorbing. When TPD of ammonia was performed with a new sample of the same deactivated catalyst, it was evident that the desorption of hydrocarbons was affected by the presence of ammonia. The influence of ammonia was most pronounced in the case of HY deactivated at 100°C. Figures 4.8a and b clearly illustrate the shift of high boiling point hydrocarbon desorption to higher temperatures in the presence of ammonia for OLIG4 and OLIG12, yielding more "acid sites" than uncoked HY between 250 and 450°C. However, the amount of ammonia adsorbed should be independent of high boiling point hydrocarbon desorption. A further source of error lay in the fact that the amount of ammonia adsorbed was small compared to the amount of high boiling point hydrocarbons desorbing, and subtraction of one large value from another to yield a small value as in the case of baseline subtraction inevitably led to large errors in the computation of ammonia desorbed during the TPD. The same problem was observed with HM, particularly OLIG6, as shown in Figures 4.9a and b. However, for OLIG8 and OLIG15, which had almost no high boiling point hydrocarbons, the ammonia had less effect on the baseline, while the regenerated runs OLIG16 and OLIG17 desorbed essentially no high boiling point hydrocarbons. Titration showed that no basic substance desorbed from deactivated catalysts, and hence titration values should correspond to the amount of chemisorbed ammonia.

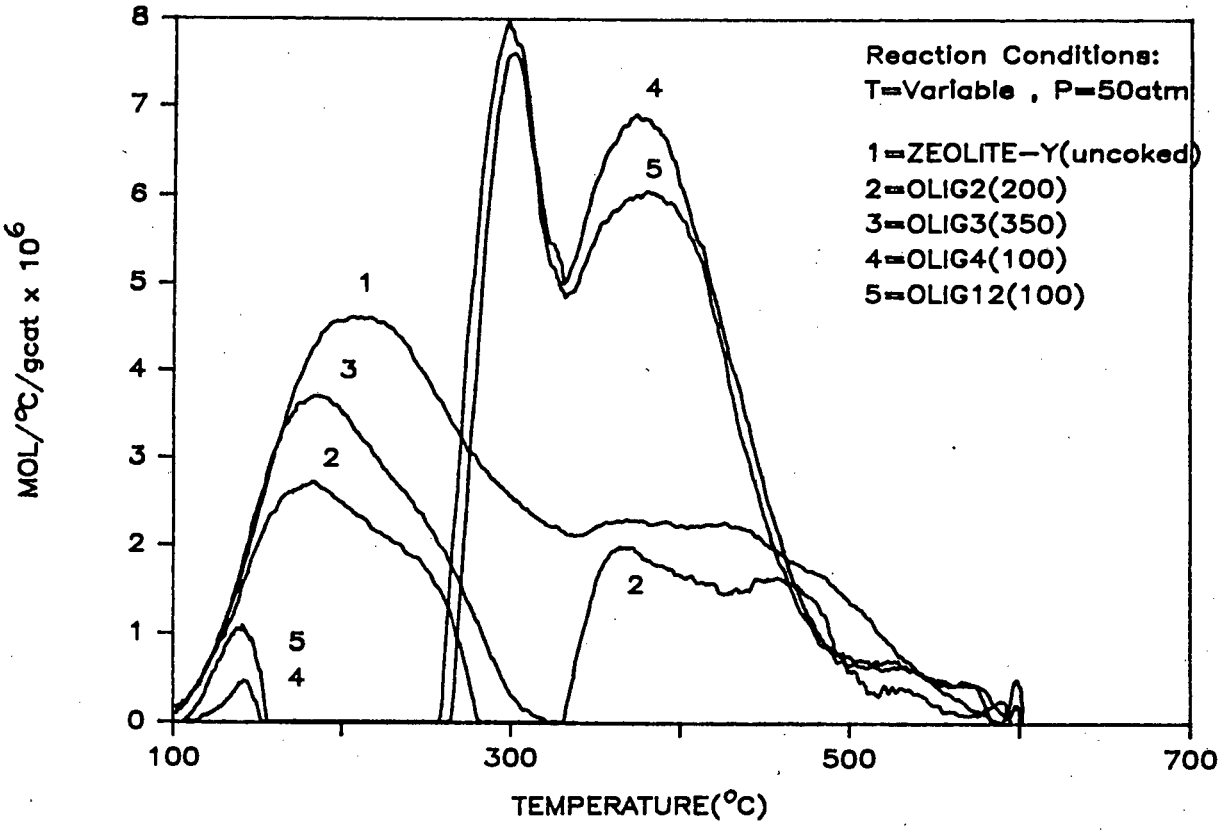

Figure 4.8a : Ammonia TPD from HY; oligomerisation.

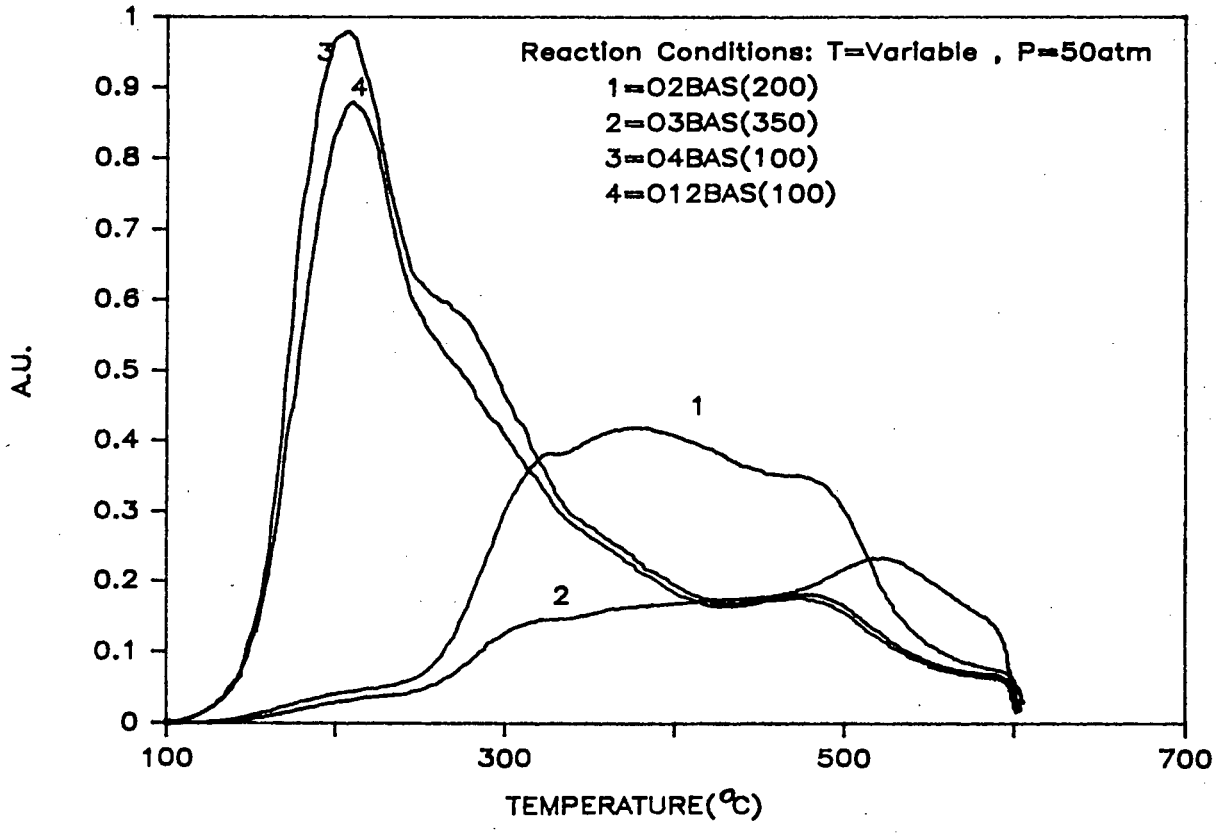

Figure 4.8b : Desorption of high boiling point hydrocarbons from HY, deactivated by oligomerisation.

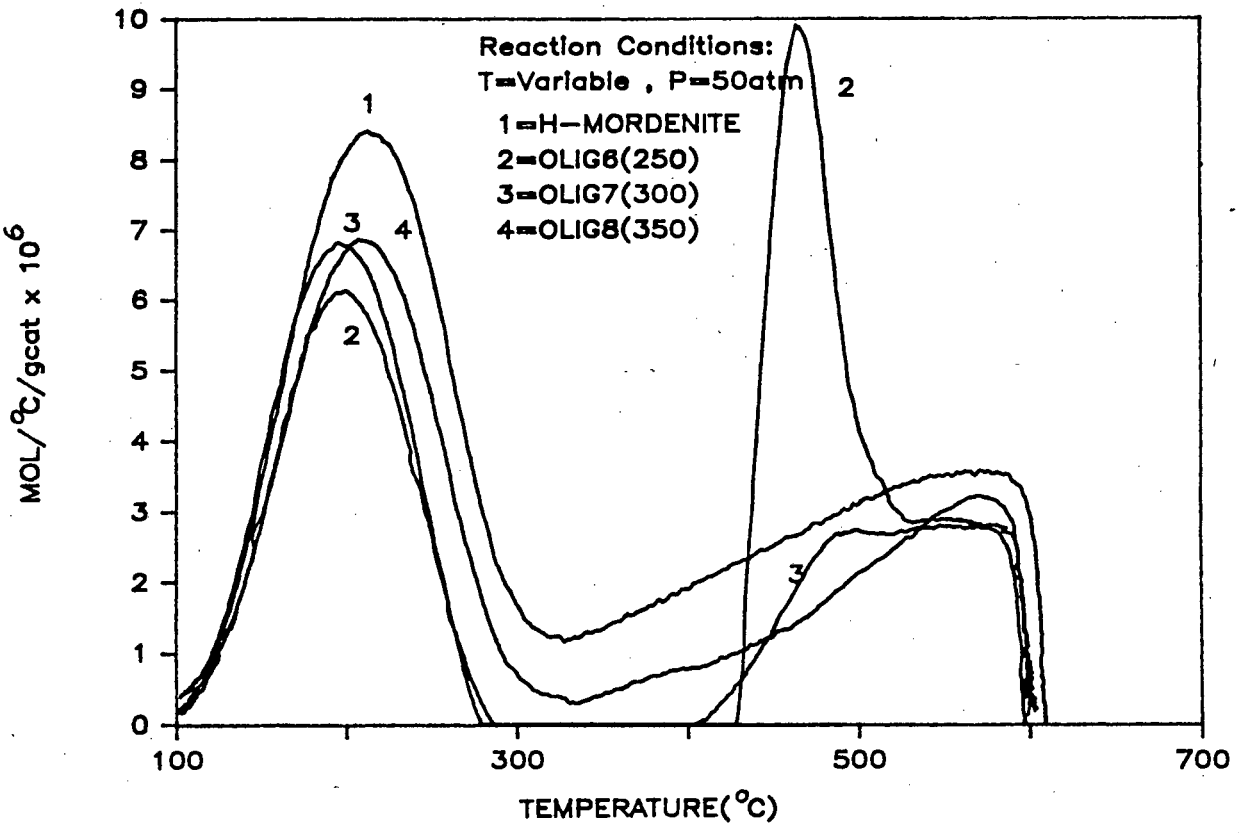

Figure 4.9a : Ammonia TPD from HM; oligomerisation.

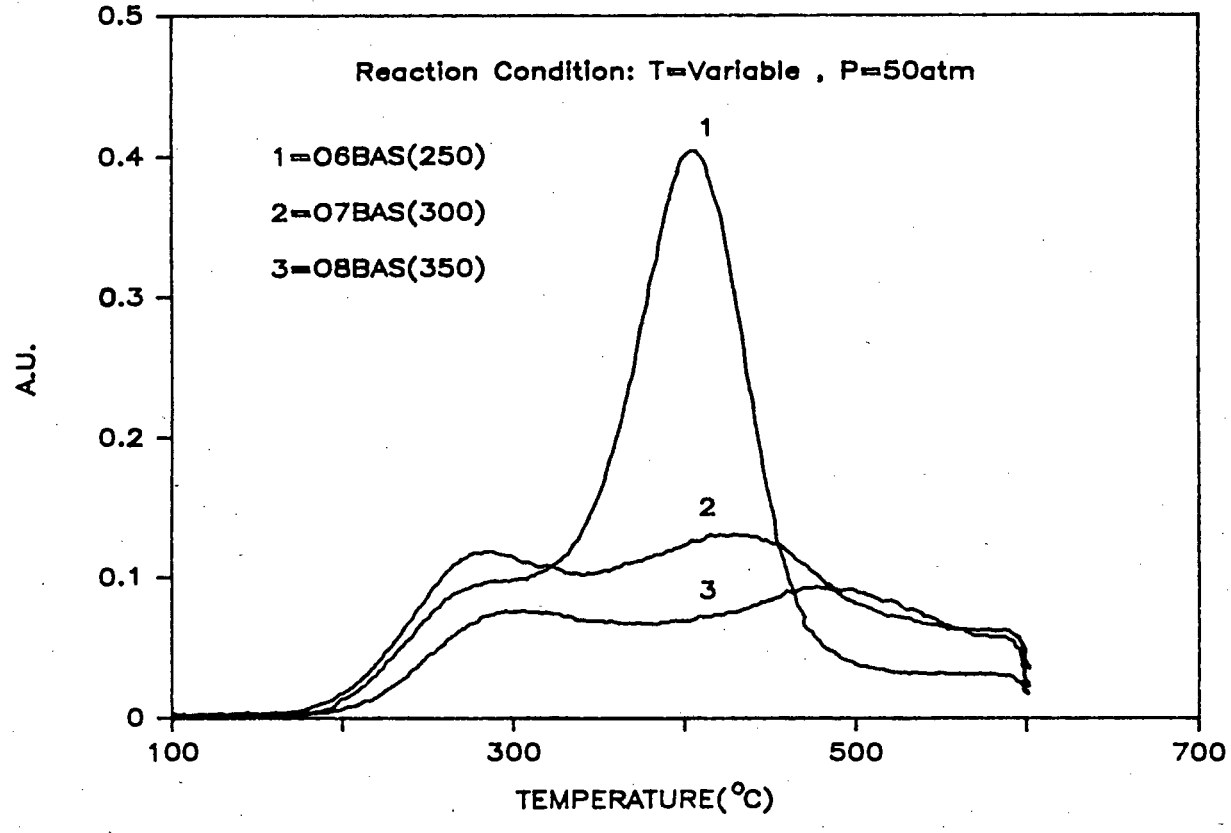

Figure 4.9b : Desorption of high boiling point hydrocarbons from HM, deactivated by oligomerisation.

Adsorption of ammonia was reduced by 40% and 25% in HY and HM, respectively, at similar coke contents as seen in Figure 4.10a. A closer look at the HM data revealed that both high boiling point hydrocarbons and graphitic coke reduced the adsorption capacity, although to different extents. Similarly, adsorption on HY decreased with both increasing graphitic coke content and increasing high boiling point hydrocarbons, although this pattern was not strictly adhered to around 13% graphitic coke. The effect of high boiling point hydrocarbons was less dominant in HY. As shown in Figure 4.10b, the amount of ammonia desorbed decreased for both HM and HY after oligomerisation. In HY desorbed ammonia decreased with increasing graphitic coke content. The difference between OLIG4 and OLIG12 which had nearly identical graphitic coke content must be due to high boiling point hydrocarbons. The effect of the presence of high boiling point hydrocarbons was less significant at higher graphitic coke content. HM on the other hand showed increased chemisorbed ammonia with increasing graphitic coke content. Although the range of wt% coke was narrow it appeared that high boiling point hydrocarbons reduced the quantity of chemisorbed ammonia, the effect being more significant than for HY.

4.4 DISCUSSION

The reproducibility of the TPD runs performed on HM and NH_4M samples was good. The total amount of ammonia adsorbed on 97% NH_4M was expected to be similar to that adsorbed on HM because of similarity in their Si/Al ratio. The results however showed that 97% NH_4M had more total acid sites, although less strong, than HM. This difference can be attributed to different calcination temperatures employed, and to the possibility that HM supplied by Norton already contained a large number of Lewis sites prior to calcination as observed by other investigators (Karge 1977; Kojima et al. 1988b). The maximum thoeretical amount of acid sites on HY (Si/Al = 2.69) assuming 22% water and HM (Si/Al = 5) assuming 13% water are 3.71 and 2.42 mmol/g, respectively. Therefore the total desorbed amount was slightly less and slightly greater than the maximum theoretical number of Bronsted sites for HM and 97% NH_4M, respectively, which indicated that ammonia was able to access most of the acid sites. In contrast, Kojima et al (1988a) showed that for HM the number of acid sites accessible to pyridine increased with calcination temperature, reaching a maximum at 500°C. Hidalgo et al. (1984) reported only 1.28 mmol/g (70% of the theoretical maximum) of ammonia desorbing from

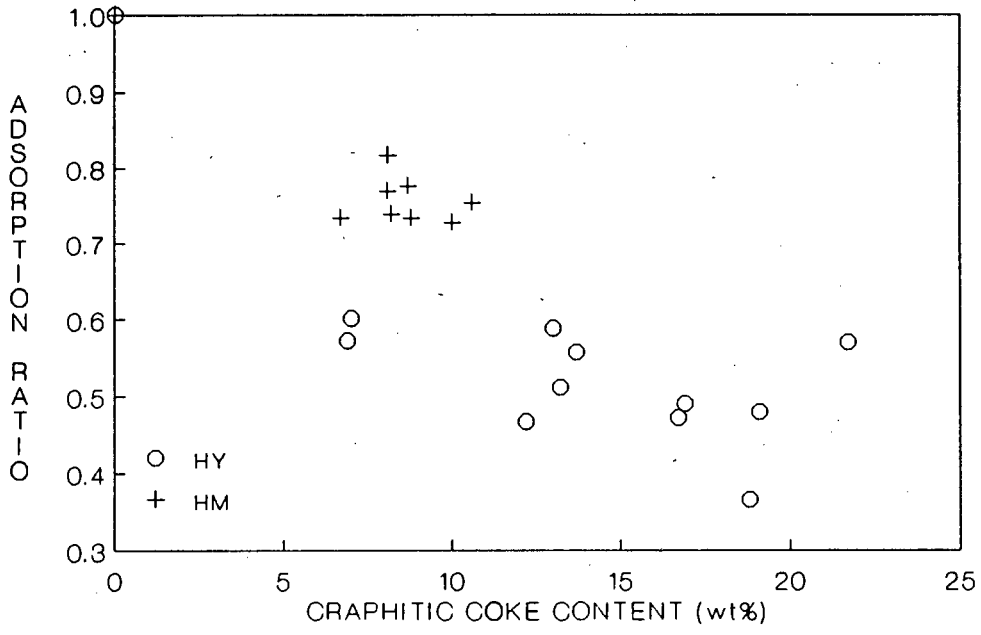

Figure 4.10a : The ratio of total amount of ammonia adsorbed (physisorbed and chemisorbed) on deactivated catalyst to that adsorbed on fresh catalyst as a function of graphitic coke content in HY and HM after propene oligomerisation.

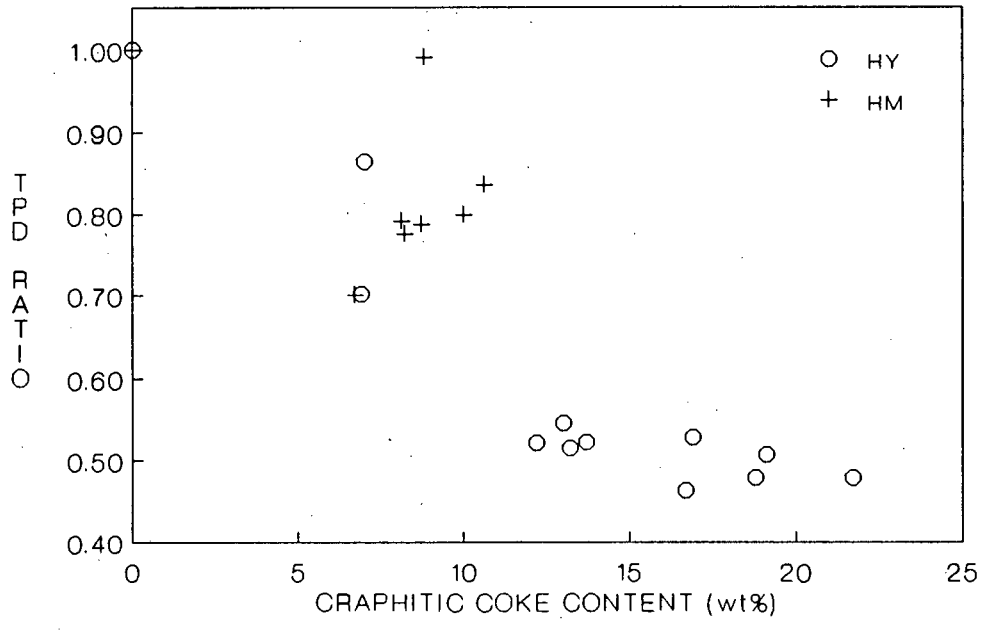

Figure 4.10b : The ratio of ammonia desorbed during TPD from deactivated catalyst to that from fresh catalyst as a function of graphpitic coke content in HY and HM after propene oligomerisation.

HM (Si/Al = 6.8) after calcination at 500°C in vacuum followed by evacuation of ammonia at 100°C. The evacuation at 100°C was expected to remove considerably more l-peak ammonia than the 100°C helium purge used in this work. The value that they obtained for the h-peak (0.87 mmol/g) was in closer agreement with that observed in this work (1.06 mmol/g), taking into account the different Si/Al ratios. The positions of the peaks, however, would be different due to different heating rates.

From the results it is clear that HM had stronger and more acid sites than HY as detected by ammonia TPD, although HY had 50% more theoretical number of acid sites. The acid sites measured by ammonia desorption in HY represented only 30% of the theoretical maximum and together with low initial ammonia adsorption this suggests, in addition to dehydroxylation, that a large number of the acid sites are weak. The positions of l-peaks of HY and HM were essentially the same. The h-peak of HM was however much more prominent with its maximum above 500°C.

The acid site distribution of HY was broad with a poorly resolved h-peak. This was also observed by Hidalgo et al. (1984) who measured only 36% of the theoretical amount of acid sites. Niwa et al. (1986), investigating the effects of experimental conditions on ammonia TPD, found that 1.87 mmol/g with a broad spectrum desorbed from HY, while quantities ranging from 1.09 to 3.18 and 0.21 to 1.87 mmol/g for the h- and l-peak, respectively, were reported by various workers for the same sample of HM (Si/Al = 7.5). These findings point to difficulties involved in comparing experimental data of different workers but the results obtained with the same apparatus were internally consistent.

Cracking activity decreased with a decrease in acid sites. Although the catalyst activity was reduced to below 20%, a large portion of the acid sites (>75%) were still available for ammonia adsorption. A slightly greater decrease in the intensity of the h-peak was in agreement with the finding of Magnoux et al. (1987b) that strong acid sites were preferentially deactivated during heptane cracking. In their work, the total number of acid sites in HY decreased by 1.5 and 4%, while the strong acid sites (h-peak) decreased by 10 and 30%, for 6.5 and 16% coke, respectively. Due to the small size of the ammonia molecule it was possible to penetrate into pores not accessible to larger molecules such as n-hexane or even nitrogen. The faster decrease of the total and h-peak acid sites in HM than in HY with increasing coke content

was consistent with the faster deactivation observed during hexane cracking. The fact that hexane cracking activity was <1% while there were still >90% of the acid sites accessible to ammonia suggests severe pore restriction. The reduction in total number of acid sites (10%) and strong acid sites (24%) at 3.1% coke content in HM was comparable to the results of Magnoux et al. (1987b) who obtained a reduction of 13% and 29% for the total acid sites and strong acid sites, respectively, at 3% coke. This shows that ammonia had more difficulty in penetrating the pores of HM than those of HY.

In the case of oligomerisation it was not possible to separate unambiguously the l- and h-peaks due to the desorption of high boiling point hydrocarbons. Both adsorption and desorption of ammonia decreased with increasing coke content for HY and HM. A similar trend was also found by Topsøe et al. (1981) for ammonia TPD from HZSM-5, deactivated by methanol conversion at 370°C, using an infra-red (IR) analyser. Their finding of 93% reduction for adsorption and 96% reduction for desorption was considerably greater than that observed in this work. Regeneration in nitrogen at 600°C which removed any residual high boiling point hydrocarbons was found to increase the availability of acid sites to 26% for adsorption and 41% for desorption. As coke content was not indicated a more detailed comparison could not be made. McLellan (1986) studied ammonia and pyridine TPD from ZSM-5 after methanol conversion at 370°C using a mass spectrometer and found that increasing coke content reduced the intensity of the desorption peaks without significantly affecting the strength and distribution of the acid sites. This behaviour appeared to be similar to that observed after hexane cracking in this work. It was also found that no acidity was observed with pyridine above 9.5% coke while ammonia showed residual acidity up to 25% coke. This was attributed to partial pore blockage, and emphasized the steric hindrance that coke might present to reactant or product molecules. The decrease in acid sites was also much greater than that observed in this work. They found that by plotting the number of desorbed molecules/unit cell against the coke content, two modes of deactivation became evident. The first mode was due to internal coking and corresponded to one site lost for five carbon atoms. The second was attributed to external coke and/or topological blocking and represented one site lost for 100 carbon atoms. From this work no such observations could be made. As higher reaction temperatures and a different detector were used by the above authors, they were able to eliminate desorbing reaction products.

The high boiling point hydrocarbons (density ≈ 1 g/cm^3 for oligomeri-sation) were expected to have an effect on the accessibility of acid sites as they would occupy twice as much volume as the graphitic coke (density ≈ 2.2 g/cm^3). The ammonia adsorption on and desorption from HY after cracking appeared to have an S-shaped decrease in respect of coke content while the decrease observed after oligomerisation tended to be exponential. This is evident when Figure 4.10a is replotted in terms of total wt% coke. One possibility is that high boiling point hydrocarbons, by virtue of their volume, cover a greater number of acid sites per unit weight.

In the case of HM, ammonia TPD after cracking and after oligomerization appeared to follow the same trend, suggesting the possibility of a similar deactivation mechanism. Higher reaction temperatures in most HM oligomerisations prevented excessive formation of residual high boiling point hydrocarbons. OLIG6 was the only run with any substantial amount of high boiling point hydrocarbons. In contrast to HY, the amount of ammonia chemisorbed was not markedly less than those measured on other samples with similar total wt% coke.

In hexane cracking over HY, ammonia was able to access the bulk of acid sites although the BET surface areas were significantly reduced. After propene oligomerisation BET measurements showed virtually no surface area for HM, and an order of magnitude decrease in the surface area of HY. Yet ammonia TPD sugggested that at least half of the adsorbing sites initially present were still available. These observations call for a detailed investigation into transport and adsorption properties of the deactivated samples, the findings of which are presented in Chapter 5.

4.5 SUMMARY

TPD results showed that HM had a greater number of stronger acid sites than HY. Cracking activity decreased with a decrease in acid sites with strong acid sites being preferentially eliminated. In addition the activity decreased more rapidly than the number of acid sites. The acid sites in HM decreased at a faster rate than those in HY.

After oligomerisation desorbing hydrocarbons as well as ammonia were detected by the TCD during TPD and hence it was not possible to seperate the l- and h-

peaks. Titration showed that the amount of adsorbed ammonia decreased. In HY the removal of the acid sites after oligomerisation was faster than after cracking, indicating more severe restrictions offered by the high boiling point hydrocarbons. In HM the loss of acid sites after both oligomerisation and cracking followed a similar trend suggesting a similar deactivation mechanism.

5. ADSORPTION AND DIFFUSION IN HY AND HM AFTER HEXANE CRACKING AND PROPENE OLIGOMERISATION

5.1 INTRODUCTION

The aim of this chapter is to determine the effect of the coke on the transport properties (viz., adsorption and diffusion) of deactivated catalysts. For this purpose the gas chromatography (GC) technique was used. The results obtained should enable a distinction to be made between deactivation by pore blockage or site coverage, and together with the results of Chapters 2, 3 and 4, allow the prediction of a deactivation mechanism.

GC is a common analytical technique, but its application to the measurement of bidisperse pore model parameters (Sarma and Haynes, 1973) is more recent. Since then numerous studies have been made using this technique, notably by Hsu and Haynes (1981) and Fu et al. (1986). This technique has been shown to yield reliable results, provided the linearity of the model is satisfied (see Chapter 1). The technique is rapid and easily implemented while measurements of representative samples are easily determined at elevated temperatures. While data analysis is complicated, this is greatly simplified by the use of computers.

In this study good data analysis was obtained using Fourier analysis with frequency domain parameter optimisation. The equipment was characterised by considering the response of blank and glassbead columns. The technique was tested by measuring the adsorption and diffusion in 5A molecular sieves. The model parameters obtained for fresh and deactivated HY and HM were correlated as a function of graphitic coke content. Thus adsorption constant, diffusivity, heats of sorption and diffusional activation energy could be indirectly related to surface area, pore volume, acidity and the activity of the catalyst. This would enable the mode of deactivation to be determined.

This chapter presents the complete bidisperse pore model, common simplifications used and real time solutions. A non-dimensionalised version of the model is used to simulate typical response curves and do a sensitivity analysis of the parameters, which is followed by a discussion. Practical points about the apparatus, techniques for parameter estimation and the accuracy of these estimations are then discussed. Results and discussion from preliminary experiments using blank columns as well as columns packed with glassbeads and 5A molecular sieves show the applicability of the model.

Finally the results of the adsorption and diffusion in fresh and deactivated HY and HM are presented and followed by a discussion.

5.2 THEORETICAL MODELLING

5.2.1 Theoretical models

The complete bidisperse pore model equations can be derived by considering mass balances in the micro-pores, macro-pores and catalyst bed (Hsu and Haynes, 1981). The catalyst is taken to consist of spherical crystallites (micro-particles) which in turn constitute spherical macro-particles (crushed extrudates in this study). The mass transport processes that have to be taken into account are:

- Axial dispersion in the catalyst bed (D_z),
- Gas film mass transfer from the bulk stream to the catalyst surface (k_f),
- Adsorption in the macro-pores (K_y),
- Macro-pore diffusion (D_y),
- Finite rate of adsorption onto the outer surface of the crystallites (k_a),
- Adsorption in the micro-pores (K_c) and
- Micro-pore diffusion (D_c).

The following assumptions are made:

- The density of the fluid is constant.
- The adsorption isotherm is linear.
- Diffusion is Fickian.
- The contribution of microparticle to the radial flux is negligible.
- Diffusion is independent of concentration.

A mass balance in the micro-pores gives

$$D_c \left(\frac{\partial^2 C_x}{\partial x^2} + \frac{2}{x} \frac{\partial C_x}{\partial x} \right) = \frac{\partial C_x}{\partial t} \quad \ldots\ldots\ldots\ldots\ldots\ldots\ldots 5.1$$

with boundary conditions

$$\left. \frac{\partial C_x}{\partial x} \right|_{R_x,t} = \frac{k_a}{D_c} \left[C_y(y,t) - \frac{1}{K_c} C_x(R_x,t) \right] \quad \ldots\ldots\ldots\ldots 5.2$$

$$\left.\frac{\partial C_x}{\partial x}\right|_{0,t} = 0 \quad \ldots\ldots\ldots\

$$\gamma = \frac{\theta_z}{v} s + \frac{3(1 - \theta_z)k_f}{vR_y} \left[\frac{\beta R_y \coth(\beta R_y) - 1}{k_f R_y/D_y + \beta R_y \coth(\beta R_y) - 1} \right] \quad .. 5.14$$

$$\beta^2 = \frac{\theta_y(1 + K_y)}{D_y} s + \frac{(1 - \theta_y)}{D_y} (W) \quad . . . . . 5.15$$

$$\alpha^2 = s/D_c \quad . . . . . 5.16$$

and

$$W = \frac{3\ D_c}{R_x^3} \int_0^\infty R_x \left(\frac{\alpha R_x \coth(\alpha R_x) - 1}{\frac{D_c}{k_a R_x} \left[\alpha R_x \coth(\alpha R_x) - 1 \right] + \frac{1}{K_c}} \right) p(R_x)\ d(R_x) \quad . . . 5.17$$

where the crystallite size distribution $p(R_x)$, may be described by a log-normal function based on the number distribution,

$$p(R_x) = \frac{1}{R_x \sqrt{2\pi\sigma^2}} \exp \left[- \frac{(\ell n(R_x) - \mu)^2}{2\sigma^2} \right] \quad . . . . . 5.18$$

This completes the general model. In many cases the adsorption rate is assumed to be very large, i.e., $k_a \to \infty$. If the crystallite size is constant, these equations can be written in dimensionless forms, which are similar to those previously reported by Haynes (1975), where

$$K_c = C_{adsorbed}/C_{gas} \quad . . . . . 5.19$$

$$N_1 = \frac{vL}{D_z} \quad . . . . . 5.20$$

$$N_2 = \frac{k_f R_y}{D_y} \quad . . . . . 5.21$$

$$N_3 = \frac{D_y L^2}{D_z R_y^2} \quad . . . . . 5.22$$

$$N_4 = \frac{D_c K_c R_y^2}{D_y R_x^2} \quad . . . . . 5.23$$

$$K_c = \theta_x(1 + K_x) \quad . . . . . 5.24$$

$$D_x = K_c D_c \quad \ldots\ldots\ldots\ldots\ldots\ldots\ldots\ldots\ldots\ldots \quad 5.25$$

The model equations in the Laplace domain become

$$E^*(1,s) = \tau E = \exp\left(- \frac{N_1}{2} \left[\sqrt{(1 + 4B)} - 1 \right] \right) \quad \ldots\ldots\ldots \quad 5.26$$

$$B = \frac{\theta_z}{N_1} s + \frac{3(1 - \theta_z)N_2N_3}{N_1^2} \left[\frac{C \coth(C) - 1}{N_2 + C \coth(C) - 1} \right] \quad \ldots\ldots \quad 5.27$$

$$C = \sqrt{\left[\frac{\theta_y N_1}{N_3} (1 + K_y)s + 3(1 - \theta_y)N_4(D \coth(D) - 1) \right]} \quad \ldots \quad 5.28$$

$$D = \sqrt{\left[\frac{N_1 K_c}{N_3 N_4} \right] s} \quad \ldots\ldots\ldots\ldots\ldots\ldots\ldots\ldots\ldots \quad 5.29$$

The dimensionless mean and variance of the output signal for constant crystallite size are

$$\mu^* = \int t^* E^* \, dt^* = \theta_z + (1 - \theta_z)\theta_y + (1 - \theta_z)(1 - \theta_y)K_c \quad \ldots \quad 5.30$$

$$(\sigma^*)^2 = \int (t^*)^2 E^* \, dt^* - (\mu^*)^2 = \frac{2}{N_1}(\mu^*)^2$$

$$+ \frac{2 N_1}{3N_2N_3}(1 - \theta_z)\left[\theta_y + (1 - \theta_y)K_c\right]^2$$

$$+ \frac{2 N_1}{15N_3}(1 - \theta_z)\left[\theta_y + (1 - \theta_y)K_c\right]^2$$

$$+ \frac{2 N_1}{15N_3N_4}(1 - \theta_z)(1 - \theta_y)K_c^2 \quad \ldots\ldots\ldots\ldots\ldots \quad 5.31$$

The above equations are used in the parameter sensitivity analysis.

5.2.2 Assumptions of model parameters

It is clear from the model equations that there are too many variables to determine (this will be shown in the sensitivity analysis), and thus further simplifying assumptions need to be made. Commonly made assumptions (Hsu and Haynes, 1981; Fu et al. 1986) are to neglect macro-pore diffusional resistance ($D_y \rightarrow \infty$), adsorption in the macro-pores ($K_y \rightarrow \infty$), and gas phase mass transfer resistance ($k_f \rightarrow \infty$). The assumption in the crystallite size distribution model of either infinite sorption rate ($k_a \rightarrow \infty$) or infinite diffusivity ($D_c \rightarrow \infty$) is necessary because the two effects cannot be distinguished (Fu et al. 1986). These assumptions may be easily incorporated in the the above models by taking the limits of the relevant parameters.

In this work the simplifying models used are defined as follows,

- The constant R_x model with constant crystallite size, $k_f \rightarrow \infty$, $K_y \rightarrow 0$, $D_y \rightarrow \infty$, $k_a \rightarrow \infty$.
- The R_x(constant,K_y) model with constant crystallite size, $k_f \rightarrow \infty$, $D_y \rightarrow \infty$, $k_a \rightarrow \infty$ (i.e., macro-pore adsorption included).
- The R_x model with log-normal crystallite size distribution, $k_f \rightarrow \infty$, $K_y \rightarrow 0$, $D_y \rightarrow \infty$, $k_a \rightarrow \infty$.
- The R_xK_y model with log-normal crystallite size distribution, $k_f \rightarrow \infty$, $D_y \rightarrow \infty$, $k_a \rightarrow \infty$ (i.e., macro-pore adsorption included).
- The macro model where $k_f \rightarrow \infty$, $\theta_x=0$ (i.e., no micro-pores, hence no micro-pore model parameters).
- The dispersion model where $k_f \rightarrow \infty$, $D_y \rightarrow \infty$, $K_y \rightarrow 0$, $K_c \rightarrow 0$, $D_c \rightarrow \infty$, $k_a \rightarrow \infty$, (i.e., adsorption and diffusion resistance neglegible in both macro- and micro-pores).

5.2.3 Real time solutions

Provided that all processes are linear and setting $s = i\omega$, the complex inversion formula yields the real time solution as discussed by Haynes (1975) for the constant R_x and R_x(constant,K_y) model. Inversion using Simpson integration was performed on an IBM compatible PC using a Maths Co-processor.

For inert non-porous glass beads the analytical solution yields the dispersion model

$$E^* = \frac{1}{2}\sqrt{\frac{\theta_z N_1}{\pi (t^*)^3}}\ \exp\left[-\frac{N_1\,(t^* - \theta_z)^2}{4\theta_z t^*}\right] \quad \ldots\ldots 5.32$$

For the crystallite size distribution model Filon integration and Gauss-Hermite quadrature (Handbook of Mathematical Functions with Formulas, Graphs and Mathematical Tables, 1965) was employed as suggested by Hsu and Haynes (1981). For the Filon integration it was necessary to divide the frequency response range into a number of equally spaced intervals starting with a suitably small value of ω and ending at a maximum value of ω which caused the integrand to be close to zero. For the Gauss-Hermite quadrature it was necessary to use 30 abscissa points to get good integration results over the whole frequency range.

5.2.4 Results of modelling and sensitivity analysis

Figures 5.1 to 5.10 show typical RTD (residence time distribution) curves obtained from modelling. Figures 5.1 to 5.6 represent the complete non-dimensional model and show the independent variation of the parameters K_x (Figure 5.2), N_1 (Figure 5.3), N_2 (Figure 5.4), N_3 (Figure 5.5), and N_4 (Figure 5.6). Typical system parameter values are given in Table 5.1. Parameters are estimated from standard correlations, viz., for dispersion (D_z) (Edwards and Richardson, 1968), for mass transfer (k_f) (Wakao et al.., 1958), for molecular diffusion (D_m) (Fuller et al., 1966), and for macro-pore diffusion ($D_m/2$) (Shah and Ruthven, 1977). The adsorption constant K_c = 50 (K_x = 125) and diffusivity $D_c = 1 \times 10^{-6}$ cm^2/s ($D_x = 5 \times 10^{-5}$ cm^2/s) have been chosen arbitrarily as typical values.

Figures 5.7 to 5.10 compare other variations of the model. Typical model parameters are shown in the third column of Table 5.1. Figure 5.7 compares the constant R_x model with the R_x model showing the variation of D_c. Figure 5.8 compares the surface barrier model (i.e., finite k_a with $D_c \rightarrow \infty$) with the diffusion model ($k_a \rightarrow \infty$, finite D_c), using a log-normal crystallite size distribution. Figure 5.9 shows the effect that K_y has on the RTD curve when D_c is varied. Figure 5.10 shows the variation of D_c when comparing the constant R_x model with the R_x model when K_y is significant. Table 5.2 shows the individual contributions of each mass transfer process to the second moment given by the dimensionless model (Equation 5.31).

TABLE 5.1 : Typical System Parameters

Parameter	Value (Fig 5.1-5.6)	Value (Fig 5.7-5.10)
L (cm)	30	30
v (cm/s)	5	5
θ_x	0.40	0.43
θ_y	0.20	0.31
θ_z	0.40	0.40
R_y (cm)	0.01875	-
R_x (cm)	2.0×10^{-4}	1.72×10^{-5}
μ (#)	-	-11.38
σ (#)	-	0.9036
K_c	50	50
K_y	0	40
D_z (cm^2/s)	0.17	0.25
k_f (cm/s)	15	∞
D_y (cm^2/s)	0.08	∞
D_c (cm^2/s)	1.0×10^{-6}	1.0×10^{-10}

(#) Parameters from Fu et al. (1986)

5.2.5 Discussion

The modelling results show that a near Gaussian curve is obtained for a typical response curve (Figure 5.1). The moment contribution shows that D_z is dominant. Figure 5.2 shows that the response curve is very sensitive to variations in K_x, which is dependent on temperature. K_x decreases exponentially with increasing temperature (Arrehenius law). However, adsorption has very little effect on the individual contribution to moments of the response curve. Figure 5.3 shows that small values of N_1 result in spreading of the response curve. This is also seen in Table 5.2. To have a small contribution from dispersion (N_1 large), a high velocity is needed, but this causes a high pressure drop, thereby making the model inapplicable. Reducing the value of D_z (viz., increasing N_1) can be achieved by operating at low temperature since $D_z \propto D_m$, but this increases K_x which could make the response curve (concentration) immeasurable. It can be shown by considering the first moment that for the assumption of infinite bed length, an error of less that 1% when compared to the Dankwerts (1953) boundary conditions is achieved if $N_1 > 100$.

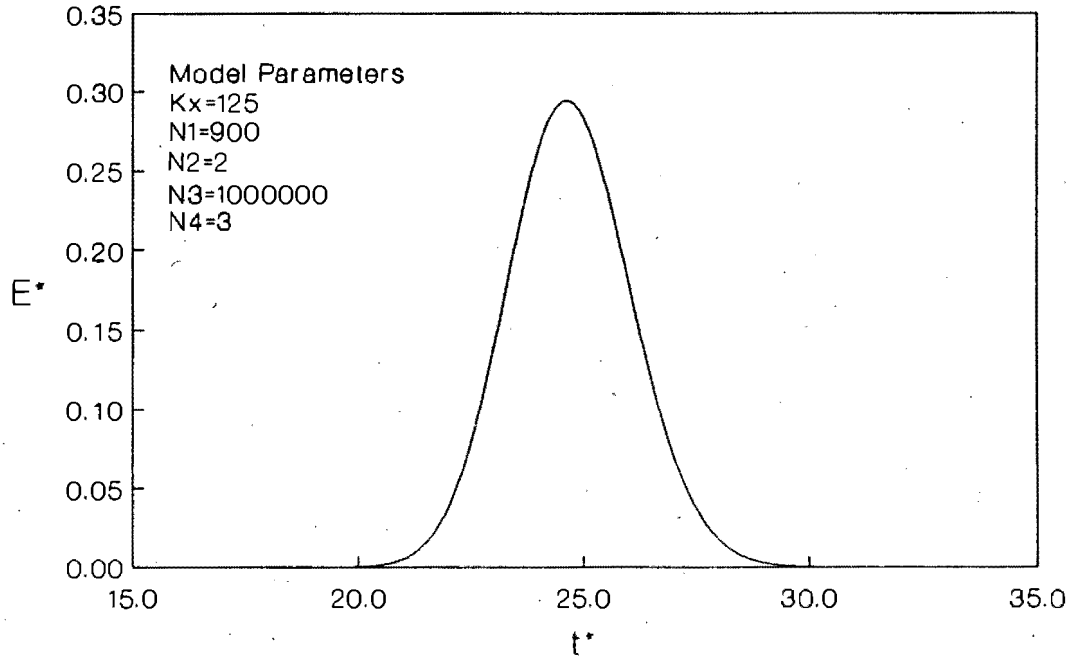

Figure 5.1 : Typical simulated RTD curve for the constant Rx model.

TABLE 5.2 : INDIVIDUAL CONTRIBUTIONS OF THE MASS TRANSFER PROCESSES TO THE SECOND MOMENT.

Figure	Parameter Values					%Contribution			
No.	K_x	N_1	N_2	N_3	N_4	σ^{*}_{Dz}	σ^{*}_{kf}	σ^{*}_{Dr}	σ^{*}_{Dc}
5.1	125	900	2	10^6	3	87.2	6.9	2.8	3.1
5.2	10	900	2	10^6	3	90.0	5.6	2.2	2.2
	100	900	2	10^6	3	87.3	6.8	2.7	3.1
	500	900	2	10^6	3	87.0	7.0	2.8	3.2
5.3	125	100	2	10^6	3	99.8	0.1	-	-
	125	300	2	10^6	3	98.4	0.9	0.3	0.4
	125	900	2	10^6	3	87.2	6.9	2.8	3.1
	125	1500	2	10^6	3	71.1	15.6	6.2	7.1
5.4	125	900	0.1	10^6	3	37.8	59.7	1.2	1.4
	125	900	1	10^6	3	81.6	12.9	2.6	2.9
	125	900	10	10^6	3	92.3	1.5	2.9	3.3
	125	900	100	10^6	3	93.5	0.1	3.0	3.4
5.5	125	900	2	10^4	3	6.4	50.5	20.2	23.0
	125	900	2	10^5	3	40.6	32.0	12.8	14.6
	125	900	2	10^6	3	87.2	6.9	2.8	3.1
	125	900	2	10^7	3	98.6	0.8	0.3	0.4
5.6	125	900	2	10^6	0.001	0.9	0.1	-	99.0
	125	900	2	10^6	0.01	8.4	0.7	0.3	90.7
	125	900	2	10^6	0.1	45.7	3.6	1.4	49.3
	125	900	2	10^6	1	82.1	6.5	2.6	8.8
	125	900	2	10^6	10	89.2	7.0	2.8	1.0
	125	900	2	10^6	100	90.0	7.1	2.8	0.1

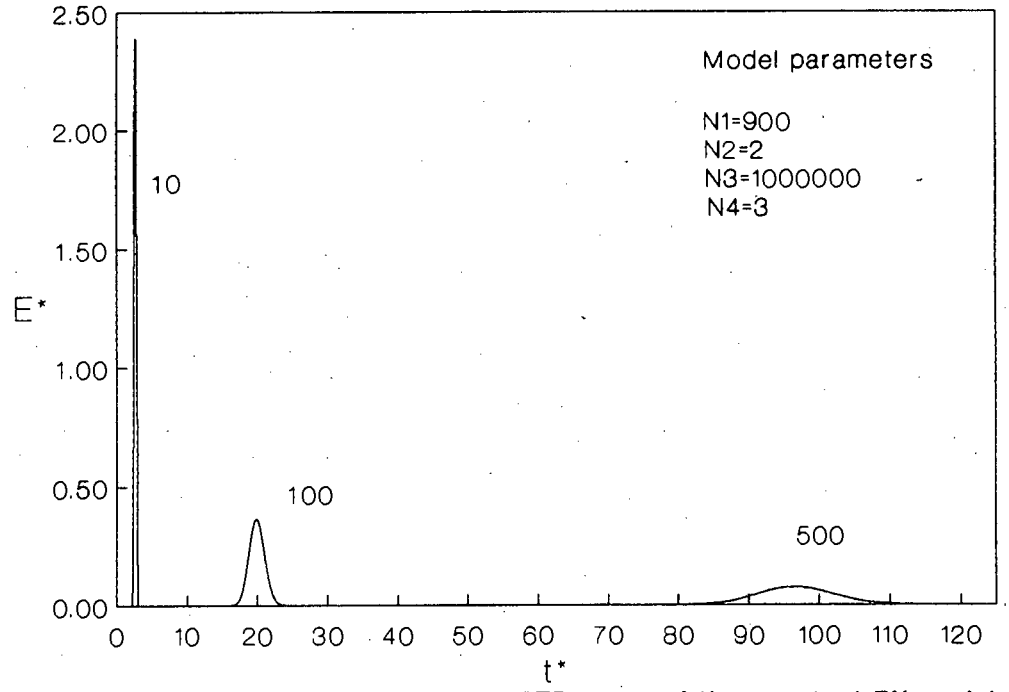

Figure 5.2 : The effect of Kx on the RTD curve of the constant RX model

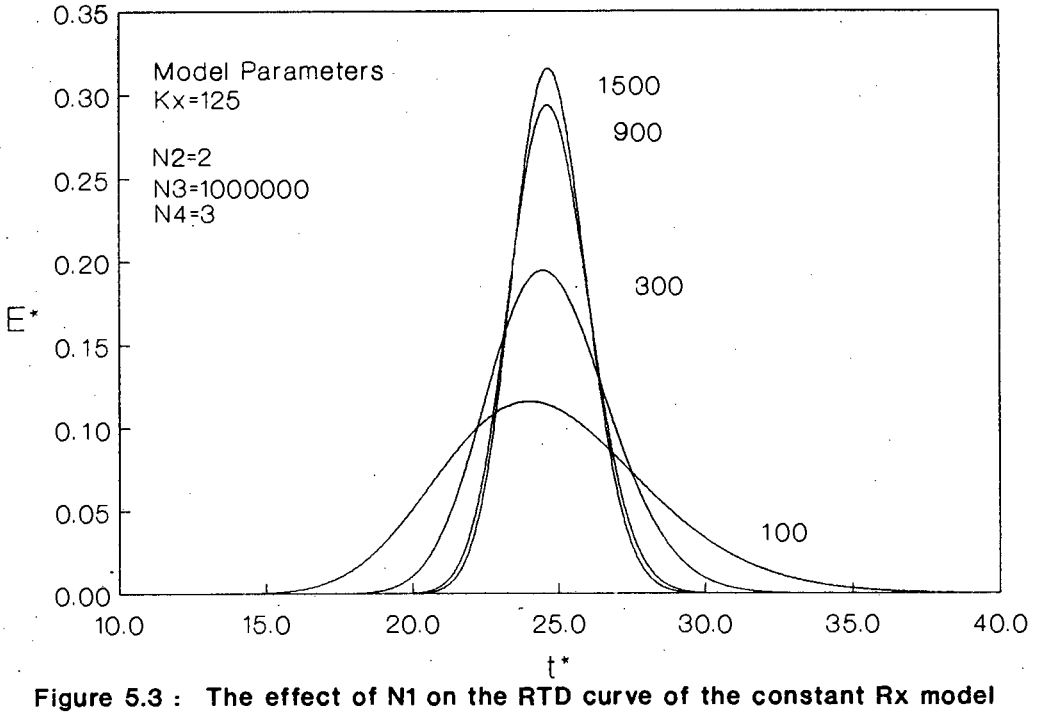

Figure 5.3 : The effect of N1 on the RTD curve of the constant Rx model

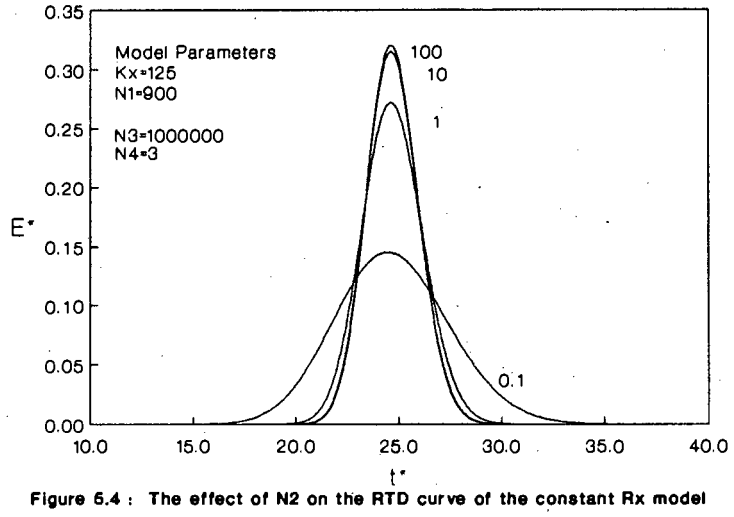

Figure 5.4 : The effect of N2 on the RTD curve of the constant Rx model

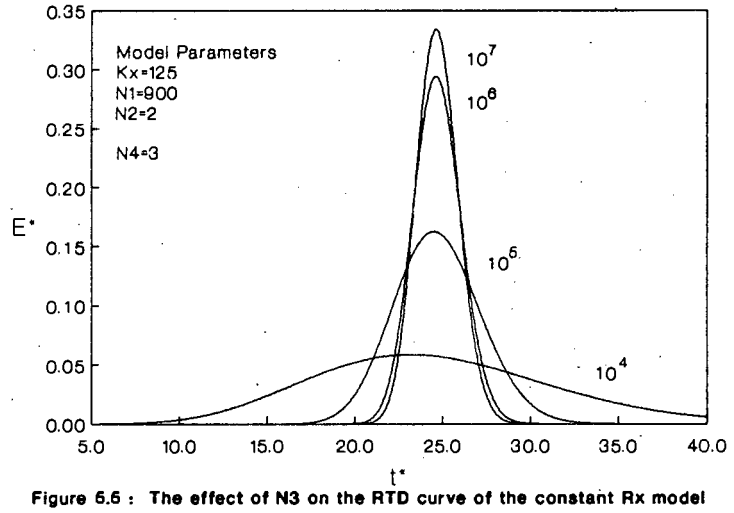

Figure 5.5 : The effect of N3 on the RTD curve of the constant Rx model

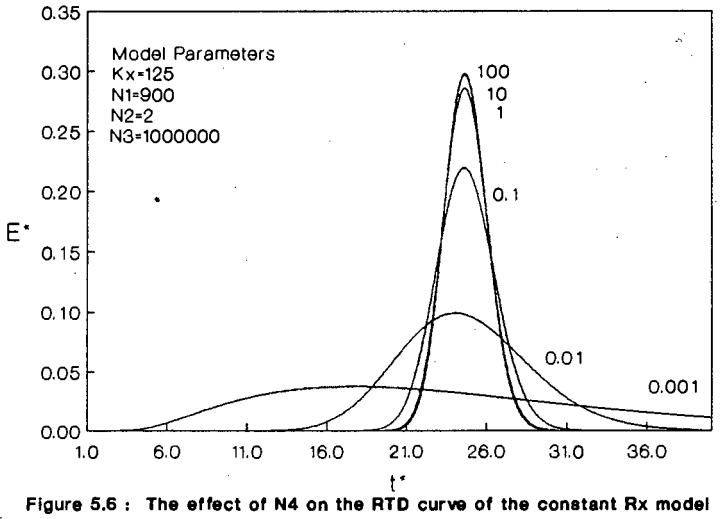

Figure 5.6 : The effect of N4 on the RTD curve of the constant Rx model

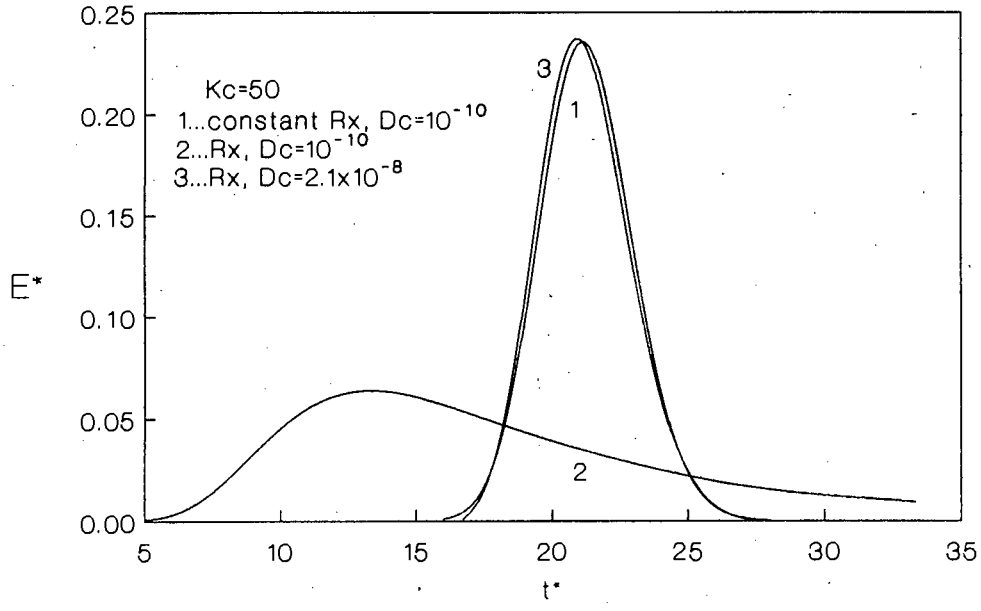

Figure 5.7 : Comparison of the diffusivities of the constant Rx model with the Rx model.

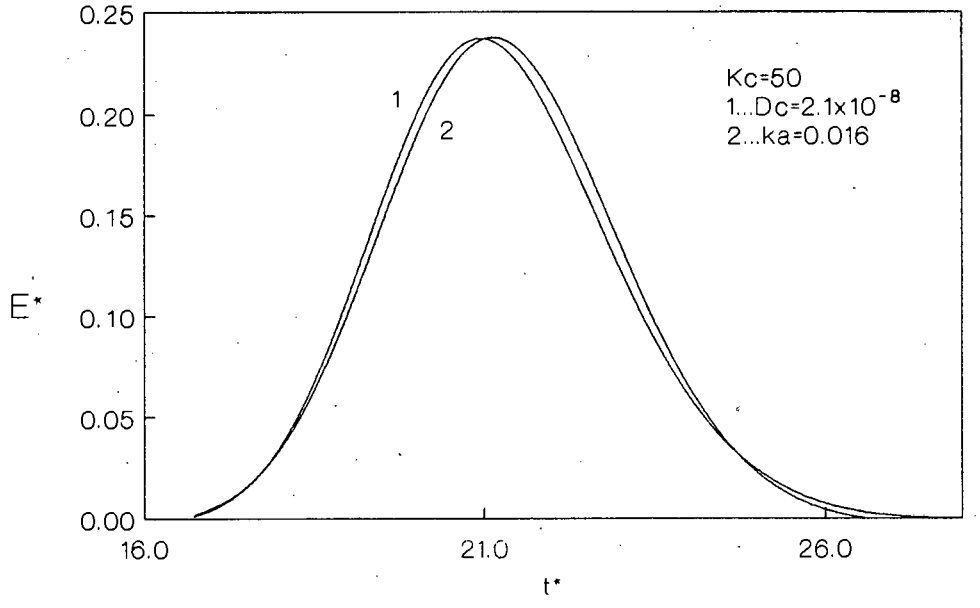

Figure 5.8 : Comparison of Dc vs Ka in the Rx model

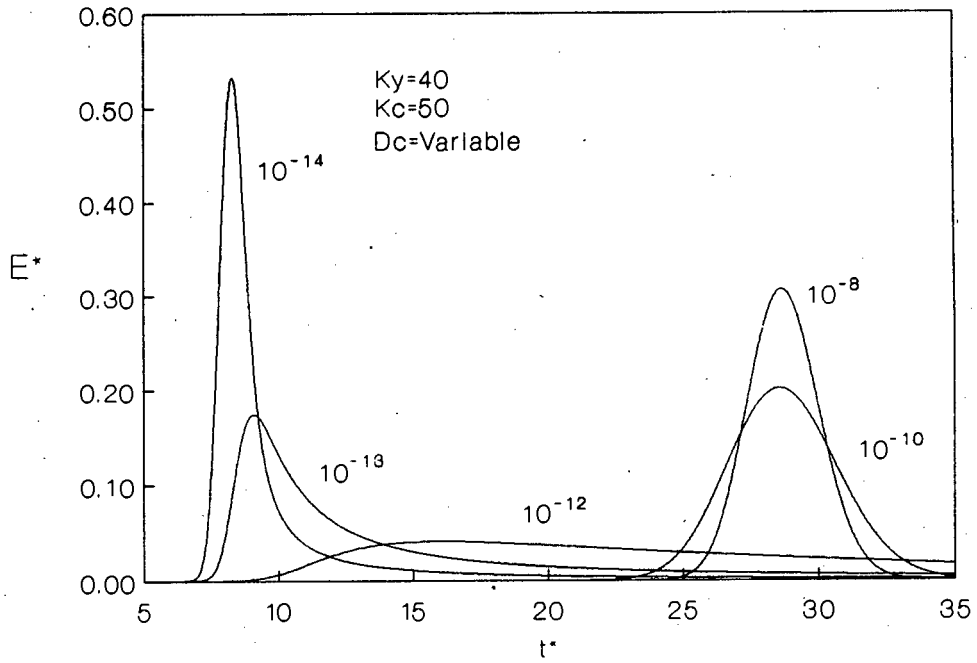

Figure 5.9 : The effect of including Ky in the constant Rx model

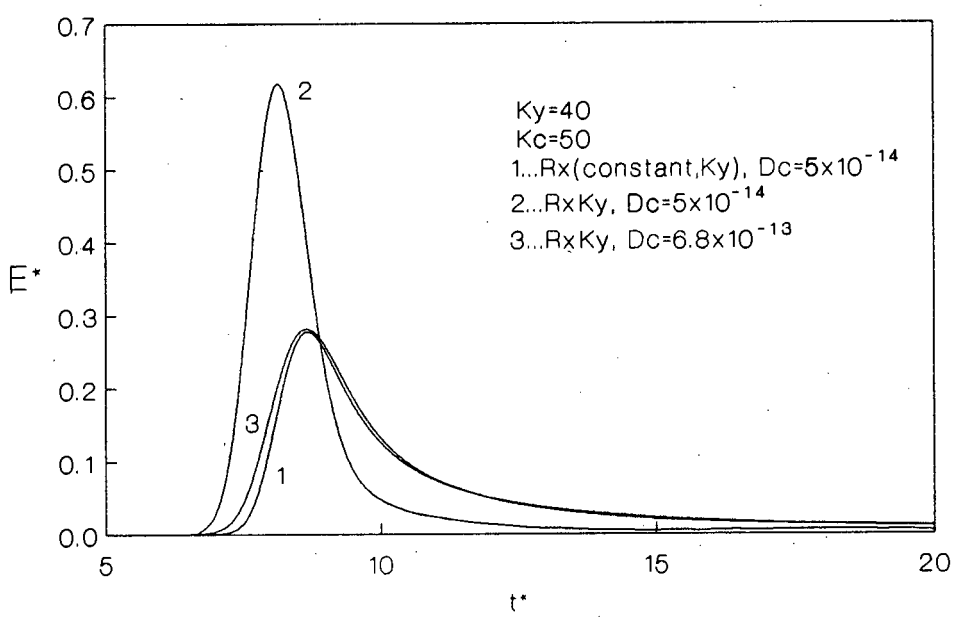

Figure 5.10 : Comparison of the diffusivities of the Rx(constant,Ky) model with the RxKy model.

Variation of N_2 (Figure 5.4) shows the same effect on the response curve as N_1. The resistance to mass transfer which is normally neglected becomes significant for $N_2 < 1$ (Table 5.2). There appears to be some disagreement among workers regarding correlations for k_f at low Reynolds numbers, making accurate evaluation of N_2 difficult. Variation of the macro-pore diffusion term (N_3) also shows the same trend in the response curve as N_1 as demonstrated in Figure 5.5. The macro-pore diffusional resistance which is normally neglected becomes significant for $N_3 < 10^{-5}$. However, when macro-pore diffusional resistance becomes large, the contributions of both mass transfer and micro-pore diffusion to the second moment also become significant. Finally the variation of N_4 yields the same variation in the response curve as N_1, N_2, and N_3. Micro-pore diffusional resistance becomes significant at $N_4 < 1$, which is therefore the appropriate region to operate in order to estimate N_4.

It is apparent from the above simulations that K_x and only one of the other parameters, viz., N_1, N_2, N_3 and N_4, can be evaluated from GC experiments. In most cases the value of N_1 is evaluated from correlations. The contributions from mass transfer and macro-pore diffusion are typically assumed negligibly small. This would therefore allow N_4 to be determined. The accuracy of the value of N_4 is dependent on its relative contribution to the peak spreading. For a small contribution to the peak spreading, Figure 5.6 shows that N_4 can easily vary by two orders of magnitude for a small change in the shape of the curve, while for a large contribution to peak spreading N_4 would be more accurately determined. Wakao et al. (1979, 1980) showed using parameter error maps that K_x could be determined accurately from one experiment, while in order to determine N_1 and N_4, data as a function of velocity would be needed. It was also shown that when N_1 was obtained from correlations the response curve was much more insensitive to variations in N_4 than in K_x, which is easily determined from the mean residence time. They further verified that only one of N_2, N_3, and N_4 could be determined by pulse chromatography. Gangwal et al. (1979) also showed a similar problem with the Kubin-Kucéra model.

The above discussion shows that in order to determine micro-pore diffusivity accurately, an accurate dispersion correlation would be needed, together with a compromise between temperature and velocity to minimise dispersion and maximise micro-pore diffusion without losing detector response (due to strong adsorption) or causing unacceptably high pressure drop. However, it is of utmost importance to choose a tracer gas which would make the micro-pore diffusional resistance significant, thereby eliminating the above procedures.

Similar plots with similar conclusions are applicable to a macro model (with macro-pore adsorption constant K_y).

Other workers (Hsu and Haynes, 1981; Fu et al., 1986; Boniface and Ruthven, 1985) have used the R_x model when analysing their data. Figure 5.7 shows that both models give the same response curves. However the value of D_c for the R_x model is 210 times larger. The R_x model shows more tailing than the constant R_x model. The surface barrier approach, which has also received attention (Fu et al. 1986; Ruthven and Derrah, 1975; Ruthven and Doetsch, 1976), has been shown to yield a similar response curve to the diffusion model. The diffusion model shows slightly more tailing than the surface barrier model. This is apparent in the lower K_c values for the surface barrier model than those for the diffusion model in Fu et al. (1986). This difference is not significant and the two approaches are essentially identical in terms of curve fitting.

To the author's knowledge no modelling incorporating significant macro-pore adsorption has been considered in the literature to date. The commonly used assumption of negligible K_y is good when the macro-surface respresents only ≈1% of the total surface area. If the micro-pore surface area (essentially total surface area) were to drop by a factor of 10 due to catalyst fouling under reaction conditions the macro-pore surface area would now contribute ≈10% to the total surface area and K_y cannot be neglected. It was shown in Chapter 3 that the macro-pore surface area, particularly in HY, contributes significantly to the total surface area. Figure 5.9 shows that for large values of D_c (fast micro-pore diffusion) the response curves are still Gaussian, but the mean residence time has shifted to larger values. For small values of D_c (slow micro-pore diffusion, expected in fouled catalysts), a long tailing response curve with a peak maximum shifted to smaller time (i.e., tending to the mean time of the macro model) is observed. Interestingly this response curve shape was observed in many of the fouled catalyst samples studied, but not in clean catalysts. Moment analysis of these data is not possible, first, because two parameters K_c and K_y appear in the first moment, and, second, because the long tail would magnify measurement errors. It is possible that in the case of the fouled catalyst the diffusional limitations in macro-pores would be significant, but in this case the model parameter estimation would become degenerate owing to the problems stated earlier. At this stage it seems reasonable to assume infinite D_y.

Finally when the R_xK_y model with significant K_y and small D_c is compared to the R_x(constant,K_y) model, the value of D_c is only 13.6 times larger (Figure 5.10). The R_xK_y curve is also wider than the R_x(constant,K_y) curve, this effect being more significant than previously noted. However, the fact that D_c of the two models are now much closer is consistent with the theory in that both models should be identical for the case $D_c \rightarrow \infty$.

This completes the brief discussion on the models to be used in this work. For more discussion on other aspects of the models additional information is available in the following references: Raghaven and Ruthven (1985), Schneider and Smith (1968a,b), Cerro and Smith (1969), Hashimoto and Smith (1973, 1974, 1976) and Haq and Ruthven (1986a,b).

5.3 EXPERIMENTAL DIFFUSION APPARATUS

Figure 5.11 shows a schematic diagram of the diffusion apparatus which uses a GOWMAC flame ionization detector. High purity nitrogen (99.99%) was used as the carrier gas. The flow rate was measured using a rotameter which was calibrated using a typical packing so that system pressure drop would be taken into account (see Appendix C for calibration curves).

Carrier gas was passed through a heated injection port which incorporated a pre-heat coil. The injection port allowed the sample pulse to be injected just above the packing in the column, thus minimising dead volume. The injection port temperature was maintained the same as that of the furnace. The furnace was equipped with eight equally spaced 1/8" diameter x 15 cm cartridge heaters. Five thermocouples were placed axially to the centre of the heater block of length 38 cm. During a typical run they indicated a maximum deviation of 2°C at 200°C, allowing good isothermal operation. The furnace was insulated and mounted in the vertical position. This arrangement was chosen because previous experience showed that using a GC oven with coiled columns was unsatisfactory due to packings settling over days of operation, causing inconsistencies in the packing density of the bed. This was caused mainly by the particles shrinking during calcination, the vibrations of the GC forced draft oven and the difficulties in packing coiled columns. However, the system used here was vibration free, easily packed and if any bed shrinkage occurred during calcination, this only affected the packed length which was always measured after each experiment.

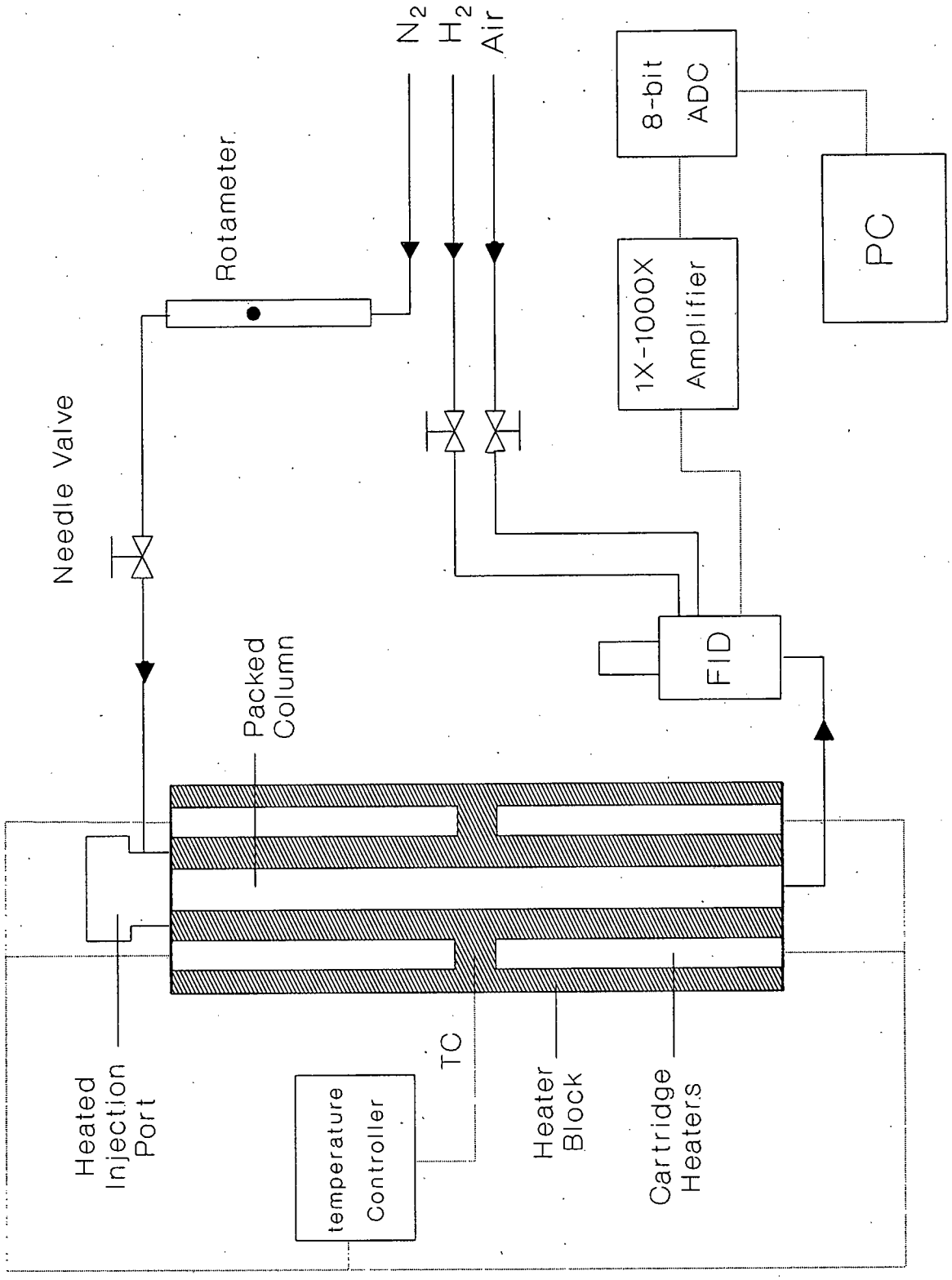

Figure 5.11 Sketch of diffusion apparatus

Two columns used in these experiments are listed in Table 5.3. Column A was made with 6 mm O.D. ends which fitted the Swagelok column connectors. Only the 6 mm I.D. section was packed. The extrudates of HY and HM were crushed to a size fraction of $250 < d_p < 500$ μm.

TABLE 5.3 : Columns used

Column	Type	I.D.(mm)	Approx. packed length (cm)
A	glass	6.0	28.0
B	stainless steel	4.6	32.4

Frequent column breakage led to the use of column B. Column B made of 1/4" S.S. tubing was more robust, had less dead volume, was easier to pack and had a lower pressure drop. System pressure drop (including that in the detector) was measured by water manometer for typically packed columns (see Appendix C for calibration curve). The packing was kept in place using glass wool plugs.

The GOWMAC FID detector was heated to 200°C. Interconnecting tubing was 1/8" S.S. due to pressure drop considerations. The GOWMAC electrometer was run at a sensitivity of 10^{-10}. However, for the experiments where the slow desorption of high boiling point hydrocarbons caused baseline instabilities, 10^{-9} was used. The detector flame was found to be stable up to flowrates of 140 mℓ/min of nitrogen, which made it unnecessary to install a bypass system which would cause extra-column dispersion.

The signal from the FID electrometer was passed through a 1-1000x variable amplifier so that an on scale signal would be received by the 8-bit ADC. Using an IBM compatible PC, data could be logged at a maximum rate of 5 samples/s. The logging rate was determined by knowing the total number of samples taken and the starting and ending time (also logged). These data files were then used to create other data files using a maximum of 200 points which contained additional information about the system (e.g., temperature, flowrate, pressure and catalyst properties). Flowrate was corrected for temperature and pressure using the ideal gas law.

Injection of sample was achieved using a gas-tight syringe (1-25 $\mu\ell$). Sampling valves available in our laboratory had injection volumes of 100 $\mu\ell$ or more and had more dead volume and dispersion effects than an injection port. Injection by a gas tight syringe was hence preferred to a sampling

valve. The sample injection and the logging program were activated simultaneously by hand. With a little practice the reproducibility of this method proved to be good.

5.4 DATA ANALYSIS TECHNIQUES

Real time analysis, frequency domain analysis and moment analysis techniques were considered. The real time analysis was found to be too time consuming due to the numerical inversion of the model equations from the frequency domain to the time domain. The other two techniques were found to be successful and are described below, together with an evaluation of parameter accuracy.

5.4.1 Frequency domain analysis

Frequency domain analysis is similar to that used by Hsu and Haynes (1981). The input pulse was approximated as a Dirac delta function in this study. The experimental data are converted into the frequency domain using the Fourier Transforms in the usual manner,

$$Re(\omega) = \int_0^t C(t) \cos(\omega t)\, dt \quad \ldots\ldots\ldots\ldots\ldots\ldots 5.33$$

$$Im(\omega) = -\int_0^t C(t) \sin(\omega t)\, dt \quad \ldots\ldots\ldots\ldots\ldots\ldots 5.34$$

where C(t) is the response of the packed bed to a pulse input. The model equations in the complex plane can then be curve fitted to the experimental data using a Nelder and Mead simplex optimisation routine. The objective function used,

$$error = \sum_1^n (Re_{model}(\omega) - Re_{exp}(\omega))^2 + (Im_{model}(\omega) - Im_{exp}(\omega))^2 \quad 5.35$$

closely approximated the real time least squares error criterion (Hays et al. 1967). For the frequency optimisation 190 equally spaced frequency values were chosen from $\omega_{start} = 0.001$ and ω_{end} given by the criterion,

$$\left\{ Re^2_{exp}(\omega_{end}) + Im^2_{exp}(\omega_{end}) \right\}^{\frac{1}{2}} \leq 0.01 \quad \ldots\ldots\ldots\ldots 5.36$$

To improve the convergence ability of the Nelder and Mead simplex optimisation, modified parameters (X_{opt}) were defined as

$$X_{opt} = P_1/P_0 \quad \ldots\ldots\ldots\ldots\ldots\ldots\ldots\ldots \quad 5.37$$

where P_1 is the current value and P_0 is the initial value of the model parameter to be optimised. The Nelder and Mead routine was found to be successful in determining the model parameters. Dispersion was estimated from an independent correlation.

5.4.2 Moment analysis

This is a very well known technique which is simpler than the frequency domain analysis. Rearranging equations 5.30 and 5.31 gives,

$$\frac{HETP}{2v} = \frac{D_z}{v^2} + \frac{R_x^2 K_c (1 - \theta_z)(1 - \theta_y)}{15 D_c \{\theta_z + (1 - \theta_z)\theta_y + (1 - \theta_z)(1 - \theta_y) K_c\}^2} \quad 5.38$$

where $$HETP = \frac{(\sigma^*)^2}{(\mu^*)^2} L \quad \ldots\ldots\ldots\ldots\ldots\ldots \quad 5.39$$

If a plot of HETP/2v vs $1/v^2$ yields a straight line then D_z is not a function of velocity. However, this would apply only at low velocities (i.e., large $1/v^2$). It has been shown (Hsu and Haynes, 1981) that the velocity dependence of D_z is given by

$$\frac{1}{Pé} = \frac{\alpha}{ReSc} + \frac{\beta}{1 + \gamma/ReSc} \quad \ldots\ldots\ldots\ldots\ldots\ldots \quad 5.40$$

where α, β and γ are constants which depend on the experimental system. It would be incorrect to use the intercept from the above plot to determine D_c. However if equation 5.40 is substituted into 5.38 and rearranged, then

$$\frac{HETP}{2v} = \frac{\alpha'}{v^2} + \frac{\beta'}{v + \gamma'} + A_m \quad \ldots\ldots\ldots\ldots\ldots\ldots \quad 5.41$$

where

$$A_m = \frac{R_x^2 (1 - \theta_z)(1 - \theta_y) K_c}{15 D_c \{\theta_z + (1 - \theta_z)\theta_y + (1 - \theta_z)(1 - \theta_y) K_c\}^2} \quad 5.42$$

$$\alpha' = \alpha \quad \ldots\ldots\ldots\ldots\ldots\ldots\ldots\ldots\ldots\ldots \quad 5.43$$

$$\beta' = \beta\, d_p \quad \ldots\ldots\ldots\ldots\ldots\ldots\ldots\ldots\ldots\ldots \quad 5.44$$

$$\gamma' = \gamma\, D_m/d_p \quad \ldots\ldots\ldots\ldots\ldots\ldots\ldots\ldots\ldots\ldots \quad 5.45$$

Here A_m is the actual intercept. Parameters α', β', γ', D_c and K_c can be determined using a Nelder and Mead simplex routine. This technique is used as a check because it averages the parameters over a range of velocities.

5.4.3 Accuracy of parameter estimates

Many workers have carried out extensive studies of different methods of data analysis (Boniface and Ruthven 1985; Kelly and Fuller 1980; Fahim and Wakao 1982; Wakao and Tanaka 1973, 1974; Anderssen and White 1970). It has been shown that real time analysis is preferred, but that frequency domain analysis is more practical with negligible loss in accuracy. The moment technique is prone to tailing errors in the second moment. The real time parameter sensitivity plots of Wakao et al. (1979, 1980) show clearly that only two parameters may be estimated from response curve with any accuracy. This was also found by Gangwal et al. (1971, 1978, 1979, 1980).

In this work moment analysis was used to get initial parameter estimates for the frequency analysis. It was found that any attempt to determine more than two model parameters reduced the accuracy of the parameters and multi-nodal behaviour was observed. Parameter determination showed that the model was most sensitive to K_c with D_c being less accurately determined. This was also observed by Wakao et al. (1979, 1980). By using good initial parameter values the model parameters could be satisfactorily determined. However in the R_xK_y model it was possible to determine three model parameters, K_y, K_c and D_c, under severe diffusional limitations. The model became insensitive to small changes in these parameters near the optimum values.

5.5 PRELIMINARY EXPERIMENTS

5.5.1 Input pulse and dead volume

Figures 5.12a and b show the exit dispersion number $(D/vL)_{out}$ as a function of the velocity through the column and injection pulse size. Additional data can be found in Appendix B, Table B1. The Bodenstein number ($Bo = vd_t/D_m$) was always less than 3 indicating that molecular diffusion was the dominant process causing dispersion in the column. The output pulse included the effects of interconnecting tubing and fittings. The graphs indicate that the extra-column dispersion effects were at minimum between 3 and 8 cm/s. These flowrates were therefore preferred when performing diffusion experiments. As seen in Figure 5.13, the column volume computed from residence time showed some scatter when determined as a function of pulse size. The system response was quick (approximately 10 s) and the scatter probably reflects the difficulty of reproducing manual injections identically from run to run at these exceptionally short residence times. Table 5.4 shows the system volume and dead volume used in further calculations. As mentioned previously the glass column had 6 mm O.D. ends which were not packed and which therefore contributed to the system dead volume.

Table 5.4 : Column and system parameters

Column Type	Diameter cm	Length cm	System Volume mℓ	Packed Volume mℓ	Dead Volume mℓ
Glass	0.6	28.5	9.16	8.06	1.10
Stainless steel	0.46	32.4	6.23	5.38	0.85

The input dispersion number (see Table B1) was found to be less than zero in more than half the experiments. In other words the input pulse and extra column effects were not easily determinable even at 10 $\mu\ell$ injections. This suggests that either the dispersion correlation for the blank column (Levenspiel, 1972) was poor or that the input pulse was close to a delta function. Levenspiel (1979) has indicated that to get Gaussian response curves from pulse experiments, $D/vL < 0.01$ and $V_{pulse}/V_{system} < 0.01$ are required. For a 10 $\mu\ell$ injection and the glass column which was used for the

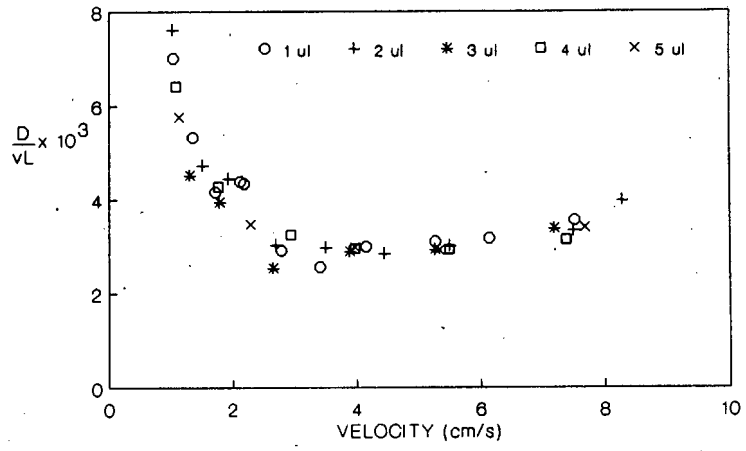

Figure 5.12a : Diepersion number vs velocity as a function of pulse size.

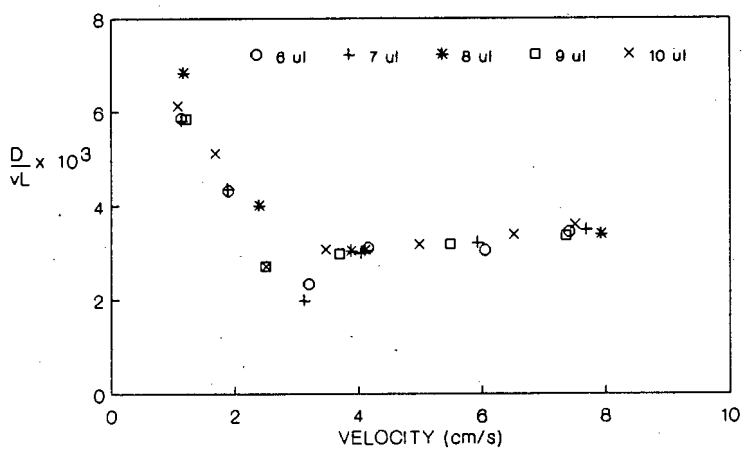

Figure 5.12b : Dispersion number vs velocity as a function of puse size.

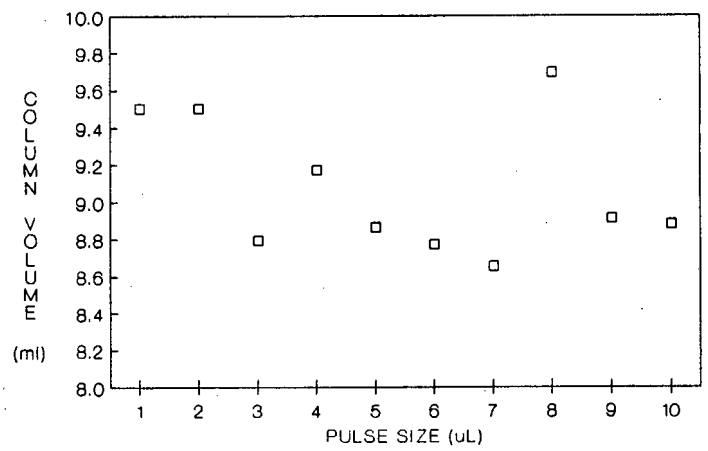

Figure 5.13 : Column volume as a function of methane pulse size.

experiments the above criterion is met since V_{pulse}/V_{system} = 0.001. The standard pulse size was 5 $\mu\ell$ and choosing the worst case of a stainless steel column packed with glass beads (θ_z = 0.36), V_{pulse}/V_{system} = 0.0018. This is still small, and as the adsorption of tracer in packings would increase the effective system volume, the effect of pulse size would be small. Other workers (Hsu and Haynes, 1981; Boniface and Ruthven, 1985; Hashimoto and Smith, 1973) used sampling valves to inject large volumes (0.5 - 0.2 mℓ) of dilute tracer gas. They have had to take into account the input pulse due to the dilution gas. In this work, since the input pulse was between 100 and 40 times smaller, it would be safe to assume an ideal pulse input.

5.5.2 Glass bead dispersion experiments

Figure 5.14 shows the variations of bed porosity of a column packed with glass beads (d_p = 0.0425 cm; d_t = 0.60 cm) calculated from response curves as a function of methane pulse size at ambient conditions. Additional data can be found in Appendix B, Table B2. The mean porosity calculated from the pulse data was θ_z = 0.353 ± 0.026. The porosity calculated from column dimensions and the density of glass beads as 2.88 g/cc (measured by water displacement) was θ_z = 0.362. Figures 5.15a and b show the dispersion number (D_z/vL) as a function of superficial velocity and methane pulse size. The values of (D_z/vL < 0.01) as a function of velocity indicate that the dispersion model is applicable (D_z/vL < 0.01). Figure 5.16 and Table 5.5 show dispersion correlations obtained for the glass bead column in relation to those obtained by other workers on a dimensionless plot of Pé vs ReSc which should be independent of temperature and tracer gas. In correlations 5 and 6 d_p was taken as 0.0375 cm. The dispersion in the glass bead column was found to be lower than those of other correlations except that of Edwards and Richardson (1968).

5.5.3 Linde 5A molecular sieve diffusion experiments

The diffusion data are available in Appendix B, Tables B3 and B4. Moment analysis of the methane pulse data using the glass column at 100°C are shown in Figure 5.17. The data gave a straight line, the slope of which gives α (see equation 5.40) in the dispersion correlation equation. The similar slopes of these lines showed that the values for both packings are similar. Theory predicts that at large v (small $1/v^2$) the line in Figure 5.17 would curve downwards. As the intercept of the linearly extrapolated line and the

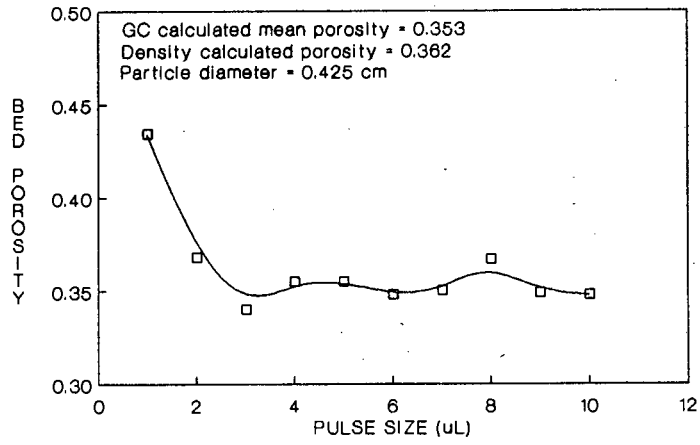

Figure 5.14 : Calculated glass bead bed porosity vs pulse size.

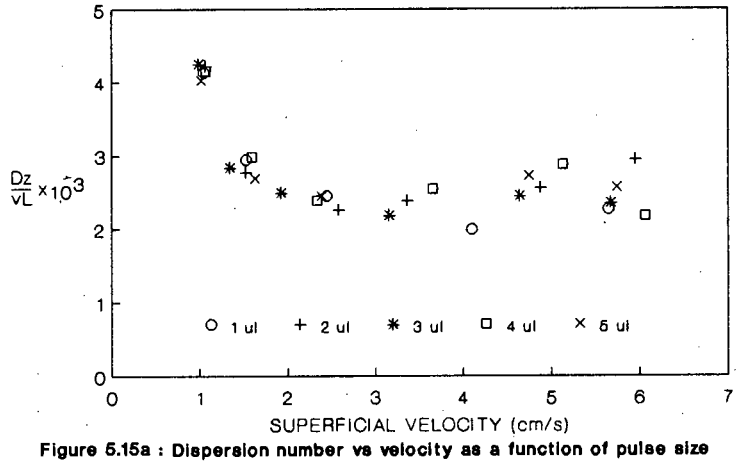

Figure 5.15a : Dispersion number vs velocity as a function of pulse size for glass beads.

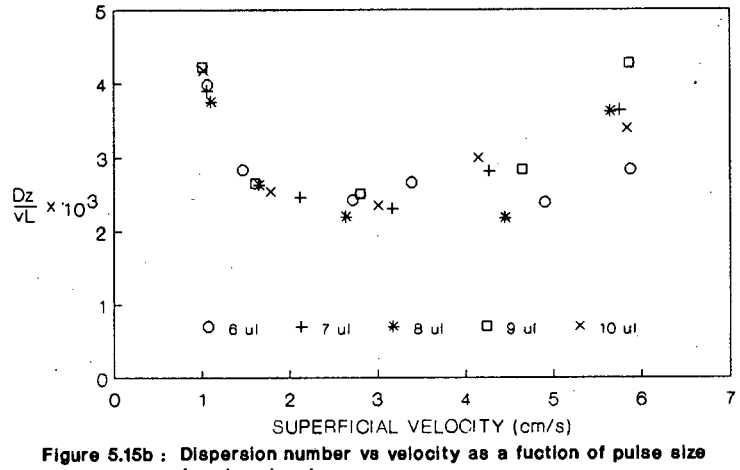

Figure 5.15b : Dispersion number vs velocity as a fuction of pulse size for glass beads.

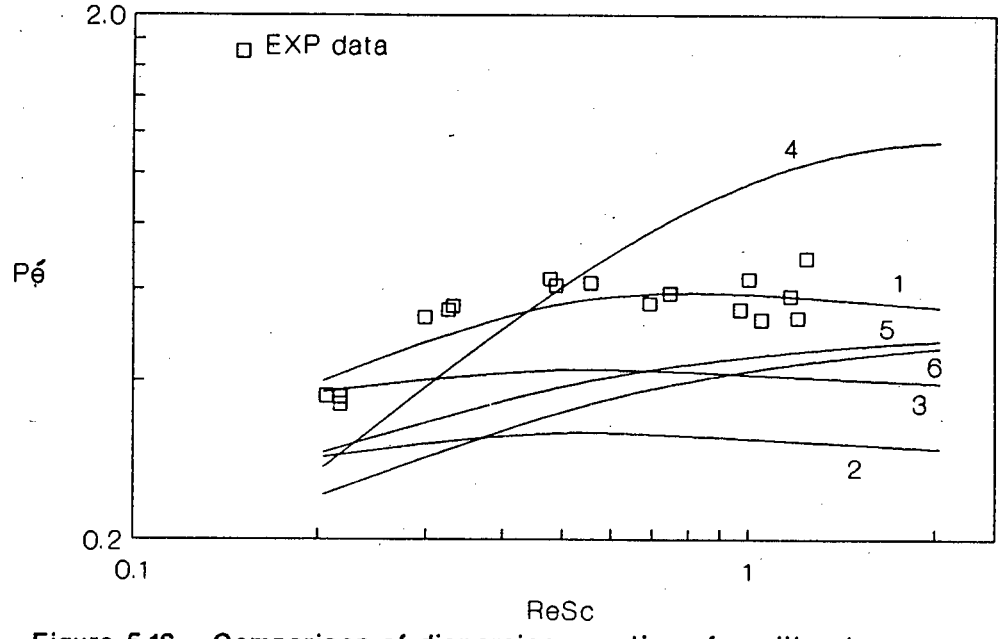

Figure 5.16 : Comparison of dispersion equations from literature.

TABLE 5.5 : DISPERSION CORRELATIONS.

Ref. in fig.	Correlation	Comments	Reference
1	$\frac{1}{Pé} = \frac{0.404}{ReSc} + \frac{2.09}{1 + 0.611/ReSc}$	40 mesh glassbeads $\theta_z = 0.36$ $d_t/d_p = 14$	This work
2	$\frac{1}{Pé} = \frac{0.394}{ReSc} + \frac{3.57}{1 + 0.27/ReSc}$	40/60 mesh catalyst particles $\theta_z = 0.44$ $d_t/d_p = 23$	Hsu and Haynes (1981)
3	$\frac{1}{Pé} = \frac{0.285}{ReSc} + \frac{2.66}{1 + 0.239/ReSc}$	20/30 mesh catalyst particles $\theta_z = 0.35$ $d_t/d_p = 15$	Fu, Ramesh, Haynes (1986)
4	$\frac{1}{Pé} = \frac{0.73}{ReSc} + \frac{1.385}{1 + 3.50/ReSc}$	Glassbeads $14 < d_t/d_p < 220$ $\theta_z = 0.36$	Edwards and Richardson (1968)
5	$\frac{1}{Pé} = \frac{0.30}{ReSc} + 0.083\ d_p$	Glassbeads $d_t/d_p = 9.6$	Suzuki and Smith (1972)
6	$\frac{1}{Pé} = \frac{0.44}{ReSc} + 0.083\ d_p$	catalyst particles $11 < d_p/d_t < 43$	"

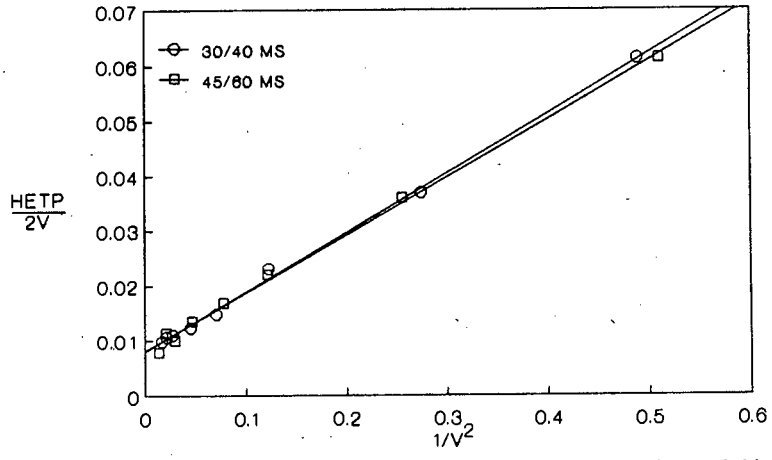

Figure 5.17 : Moment analysis for methane in 30/40 and 45/60 mesh Linde 5A molecular sieves at 100°C

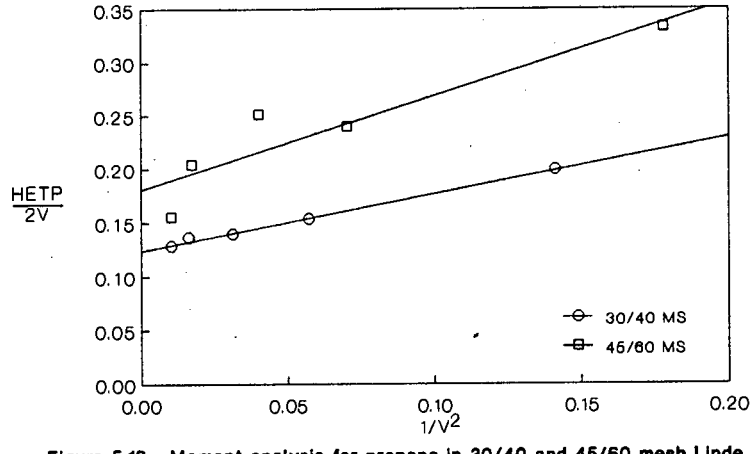

Figure 5.18 : Moment analysis for propane in 30/40 and 45/60 mesh Linde 5A molecular sieves at 200°C.

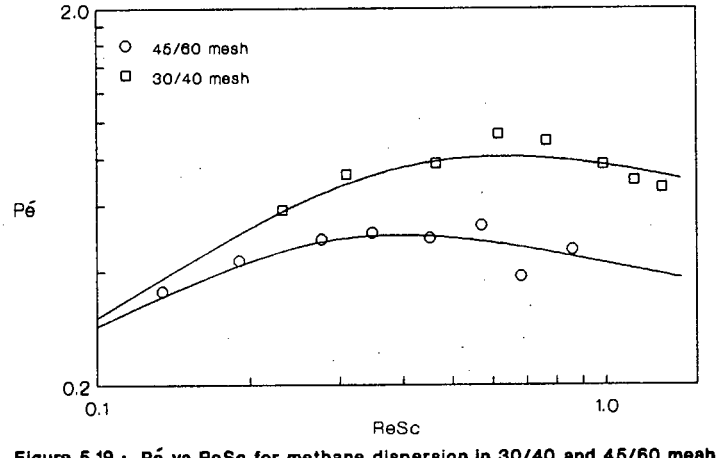

Figure 5.19 : Pé va ReSc for methane dispersion in 30/40 and 45/60 mesh Linde 5A molecular sieves at 100°C

y-axis is already small the diffusional limitations of methane in molecular sieves at 100°C are negligible.

In the case of propane diffusion in molecular sieves at 200°C shown in Figure 5.18, the moment analysis gave a much larger intercept, indicating that diffusional resistance was not negligible. The scatter of the 45/60 mesh data is due to measurement errors in determining the second moment arising from considerable tailing of the response curve. Using the assumption that methane diffusion in molecular sieves at 100°C was rapid the parameters α, β, γ in the dispersion equation could be determined and are shown in Table 5.6.

Table 5.6 Linde 5A molecular sieves dispersion correlation parameters

Packing	α	β	γ	d_p(cm)	d_t/d_p
30/40 mesh	0.316	2.47	1.50	0.0508	12
45/60 mesh	0.309	3.86	0.569	0.0302	20

The dispersion data are shown in Figure 5.19. Use of smaller particles led to a larger contribution to dispersion.

Table 5.7 gives a summary of the diffusion data obtained from three different diffusion models, namely, constant R_x model (or R_x(constant)) with parameters D_z, K_c and D_c and a constant crystallite radius, R_x model which accounts for the log-normal crystallite size distribution, and a constant R_x model which includes K_y (or R_x(constant,K_y)). The log-normal crystallite distribution parameters were estimated from the crystallite size distribution data given by Haq and Ruthven (1986a) as μ = -9.585 and σ = 0.600 after converting to a number basis. In the case of methane diffusion only an order of magnitude estimate was given as the diffusional resistance was assumed to be negligible. The diffusion and adsorption temperature dependence using the Arrhenius expressions,

$$K_y = K_{yo} \exp (E_{Ky}/RT) \quad \ldots\ldots\ldots\ldots\ldots\ldots 5.46$$

$$K_c = K_{co} \exp (E_{Kc}/RT) \quad \ldots\ldots\ldots\ldots\ldots\ldots 5.47$$

$$D_c = D_{co} \exp (-E_{Dc}/RT) \quad \ldots\ldots\ldots\ldots\ldots\ldots 5.48$$

are shown in Table 5.8 for each of the models and its parameters. The propane adsorption constants of the constant R_x model and R_x model were comparable. However, the diffusivities of the R_x model were twice as large. In the case of the R_x(constant,K_y) model the adsorption parameters cannot be

TABLE 5.7 : SUMMARY OF MOLECULAR SIEVE DIFFUSION DATA.

catalyst	tracer	T °C	model	K_y	K_c	$D_c x10^{10}$ cm^2/s
30/40 Linde 5A molecular sieves	methane	100	constant R_x	-	7.12	≈9E+8
	propane	150		-	150	3.54
		200		-	52.5	7.33
		250		-	24.2	12.5
		150	R_x	-	153	7.79
		200		-	54.2	15.0
		250		-	24.2	24.5
		150	R_x(constant,	176	70.0	1.46
		200	K_y)	55.1	27.9	3.43
		250		22.8	14.1	6.41
45/60 Linde 5A molecular sieves	methane	100	constant R_x	-	7.66	≈4E+8
	propane	150		-	145.8	2.55
		200		-	56.9	5.18
		250		-	24.7	9.59
		150	R_x	-	150.0	5.35
		200		-	61.8	10.0
		250		-	25.8	18.2
		150	R_x(constant,	182.0	65.4	0.930
		200	K_y)	61.5	13.6	2.21
		250		182.0	65.4	4.35

TABLE 5.8 : ARRHENIUS TEMPERATURE DEPENDENCE OF LINDE 5A MOLECULAR SIEVE DIFFUSION PARAMETERS FOR PROPANE.

cat.	model	$K_{y\,o}$ $x10^3$	E_{Ky} kJ/mol	r^2	$K_{c\,o}$ $x10^2$	E_{Kc} kJ/mol	r^2	$D_{c\,o}$ $x10^7$	E_{Dc} kJ/mol	r^2
30/40 mesh	constant R_x	-	-	-	1.05	33.6	1.00	2.65	23.2	1.00
	R_x	-	-	-	1.19	33.2	1.00	3.17	21.1	1.00
	R_x(constant, K_y)	3.93	37.6	1.00	1.57	29.5	1.00	3.43	27.3	1.00
45/60 mesh	R_x(constant)	-	-	-	1.34	32.7	1.00	2.56	24.3	1.00
	R_x-model	-	-	-	1.50	32.4	1.00	3.12	22.5	1.00
	R_x(constant, K_y)	6.28	36.1	1.00	1.80	28.9	1.00	2.99	28.4	1.00

compared to those of the other models. The diffusivities were half of those estimated by the constant R_x model. The adsorption constants of the 30/40 and 45/60 mesh molecular sieves compared favourably, but the diffusivities in the 45/60 mesh were found to be about 30% lower. The diffusion temperature dependence was lowest in the case of the R_x model. The adsorption activation energies of the constant R_x and R_x models were comparable, while the diffusion activation energy difference was slightly larger. The activation energies of the R_x(constant,K_y) model did not compare well to those of the other models.

Figures 5.20a-c show the accuracy of the model predictions. Clearly the R_x model gave the best agreement with the data. Table 5.9 shows the values obtained from the literature in comparison to those extrapolated from this work.

5.5.4 Discussion

5.5.4.1 Glass bead results

Computed bed porosity was independent of pulse size above 1 $\mu\ell$ and the slight variation in the data must be considered as being within experimental error for manual injections. Because the reponse of the glass bead column was fast, accurate reproducibility using manual pulse injection would be difficult. In addition, the assumption of an ideal input pulse would be less valid in the case of a very short residence time. The measured porosity and the porosity determined from the pulse experiments compared favourably, showing that the system dimensions (e.g., dead volume) determined from the blank pulse experiments were good estimates.

The dispersion number showed that the assumption of infinite column length as opposed to the more rigorous Dankwerts boundary condition was reasonable, because $D_z/vL < 0.01$ for error < 1%. It follows from the dispersion data that the velocity which would yield the smallest contribution from axial dispersion effects would lie between 2 and 4 cm/s. An order of magnitude variation in the input pulse size gave variation within the accuracy of the experimental procedure. This suggests that it is probably reasonable to assume the input pulse as ideal for the purpose of estimating dispersion.

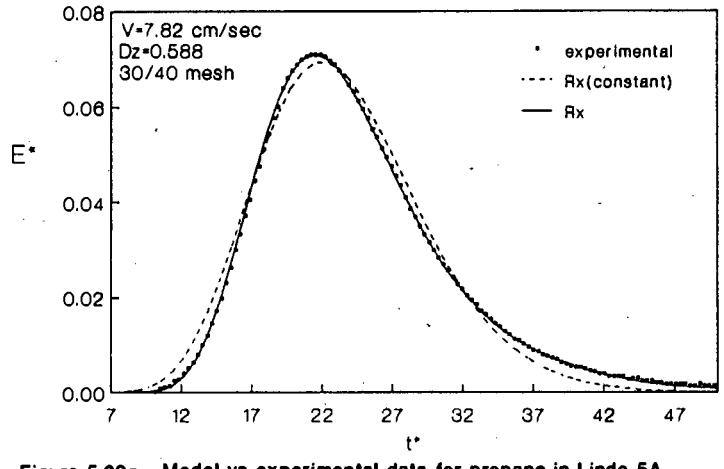

Figure 5.20a : Model vs experimental data for propane in Linde 5A molecular sieves at 200°C; run MS200-3.

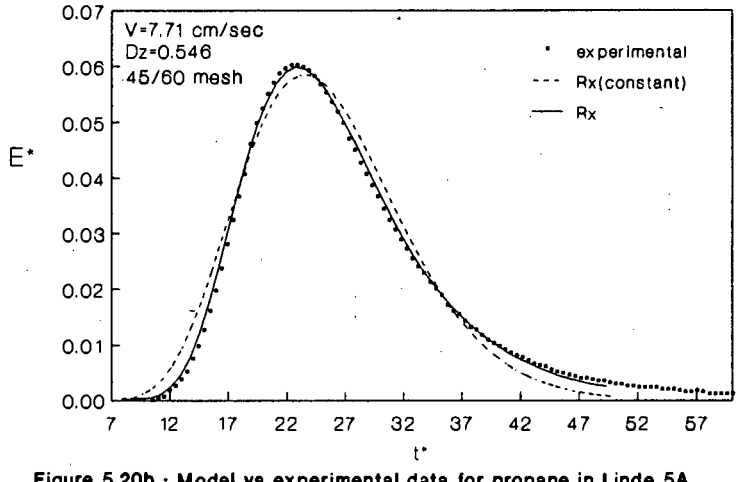

Figure 5.20b : Model vs experimental data for propane in Linde 5A molecular sieves at 200°C; run MSM20-3.

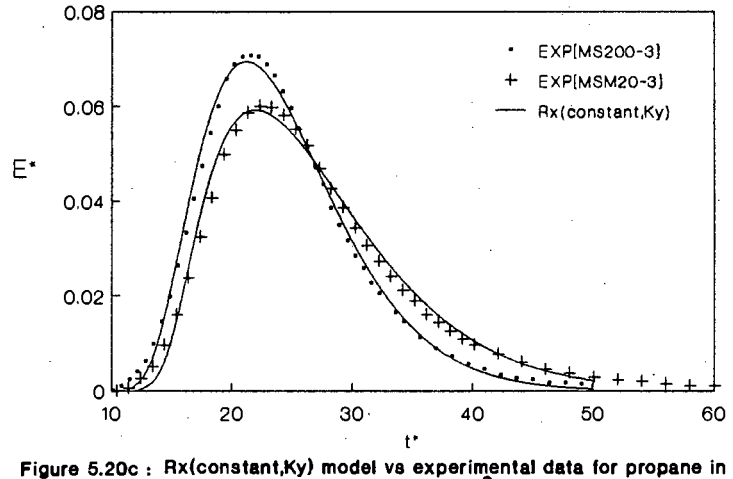

Figure 5.20c : Rx(constant,Ky) model vs experimental data for propane in Linde 5A molecular sieves at 200°C; runs MS200-3 and MSM20-3.

TABLE 5.9 : COMPARISON OF ADSORPTION AND DIFFUSION DATA TO THOSE IN THE LITERATURE FOR 5A MOLECULAR SIEVES.

reference	tracer	T °C	K_c	D_c x10^{10}	E_{Kc} kJ/mol	E_{Dc} kJ/mol	comments
Chiang, Ma, Dixon (1984)	propane	150 125 100	160 280 518	23.0 16.0 5.9	35	4.5	GC, high pressure drop, Crystallites, no size distribution, curve fit
Shah, Ruthven (1977)	methane propane	75 125	12.7 360	- 2.4-4.2	- -	- -	GC, 30/40 mesh, no size distribution, moments, account for clay binder
Ruthven, Loughlin (1972)	methane	-88 -43 0 100*	8104 455 133 11.9	- - - -	21.8	-	Gravimetric, crystallites, size distribution, concentration dependence of diffusivity
	propane	50 85 125	6470 2614 820	- - -	33.9	-	
This work extra-polated	propane	50 85 100 125 150£	2785 831 531 271 153	1.23 2.64 3.52 5.39 7.79	33.2	21.1	GC, 30/40 mesh, crystallite size distribution, frequency domain curve fit

* - Extrapolated from given data
£ - Measured data

The comparison of these dispersion data with those of other workers is restricted by the use of glass beads. However, when comparing the correlations 1, 4 and 5 in Figure 5.16, considerable variation in the data is observed. The value of d_t/d_p increased in the order 5 < 1 < 4 as shown in Table 5.5, demonstrating that axial dispersion increased with decreasing d_t/d_p. The figure also shows that a column packed with catalyst particles cannot be simulated using glass beads for the purpose of estimating axial dispersion, as seen from curves 1 and 3 in Figure 5.16 which had the same d_t/d_p. Similar conclusions were drawn by Suzuki and Smith (1972). It follows from the above that for accurate evaluation of dispersion in a packed bed, a correlation must be independently determined for each bed.

5.5.4.2 Axial dispersion in molecular sieve columns

Determination of the catalyst diffusivity (D_c) from GC pulse experiments requires that the axial dispersion be independently determined. The above section has clearly shown that generalized correlation (Edwards and Richardson, 1968) or glass bead simulation experiments are not sufficient for determining the axial dispersion accurately. Scott et al. (1974) reported that for small tube to particle diameter ratios, i.e., $d_t/d_p < 1.4$, the axial dispersion Péclet number was similar to those of $d_t/d_p > 15$. However, in the range $1.4 < d_t/d_p < 8$, Hsiang and Haynes (1977) showed that axial dispersion was greater than predicted from packed bed correlations. Ahn et al. (1986) found similar behaviour for their experiments in the range $1.9 < d_t/d_p < 4.9$. Both groups of workers have explained these observations in terms of wall effects. Oliverous and Smith (1982) were unable to predict the extent of channelling when it affected only the tail of a response curve for $d_t/d_p \approx 12$. Urban and Gomezplata (1969) showed that smoothness and a high degree of size uniformity in packed beds delayed the onset of large scale mixing in the voids. Studies of porosity profiles by Staneck and Eckert (1979) and Pillai (1977) showed that wall effects would always be present in packed beds. The findings of these other workers emphasize the difficulty of obtaining accurate dispersion correlations.

The method of Hsu and Haynes (1981) was therefore used to determine axial dispersion in the molecular sieve columns. Because of the use of FID as a detector, which does not respond to inorganics, the tracer gas was limited to methane. The correlations determined in this way clearly showed increasing axial dispersion with increasing particle size (smaller d_t/d_p) at high flowrates. It would have been incorrect to assume that the same dispersion

correlation applied to both columns. Hsu and Haynes (1981) showed that when tracer gas and temperature were varied the data fell on the same curve when Pé was plotted against ReSc for NaY, provided the intracrystalline diffusion was very rapid and the same column was used. Shah and Ruthven (1977) and Haq and Ruthven (1986a,b) were unable to determine the diffusivity of methane in 5A molecular sieves in the temperature range 35 to 200°C. The results of the moment analysis (Figure 5.17), in agreement with those of the above workers, showed that methane diffusivity was large and that this method of determing axial dispersion was valid.

5.5.4.3 Diffusion and adsorption in Linde 5A molecular sieves

In the preceding section it was shown that the diffusivity of methane was too large to be estimated. Nevertheless the adsorption constant could still be determined. The estimated adsorption constants appeared to be similar to those of Chiang et al. (1984a,b), but were lower than the values from gravimetric data (see Table 5.9). K_c at 150°C in Table 5.9 was not extrapolated but represents a measured value in the present study. The heats of sorption for methane were not calculated because methane data served to obtain dispersion correlations only.

Moment analysis showed that propane diffusion was not fast. Because of the tailing of the 45/60 mesh response curves, moment analysis would not give accurate results as shown by the scatter in Figure 5.18. In the case of significant diffusional resistance the crystallite size distribution model (R_x model) agreed with the data well (Figures 5.20a and b). The constant R_x model was not able to predict the tailing of the response curve. This in turn caused the values of K_c and D_c to be lower than otherwise (viz., less tailing would shift the mean). Comparison of the K_c and D_c between the two models showed this trend.

The tailing may be reasonably well predicted by introducing a macro-pore adsorption term (K_y) into the constant R_x model. Figure 5.20c shows that the R_x(constant,Ky) model predicted the response significantly better than the constant R_x model. The former model predicted large tailing only when the diffusional resistance was large. If there is no tailing, K_y and K_c cannot be distinguished. One limitation of the R_x(contant,K_y) model is that the parameters are sensitive to small variations in tailing and parameter sensitivity near the optimum values is poor. These trends are evident in the large variations in the parameters K_y, K_c and D_c for the R_x(constant,K_y)

model in Tables B3 and B4. In addition, in terms of surface area available for adsorption, the macro-pores would contribute approximately 1% to the total surface area. It follows then that the R_x(constant,Ky) model, while being able to predict the tailing response curve, has no physical signficance. The model, however, may become useful in cases where the macro-pore surface area may become significant as a result of serious deactivation.

Comparison of model parameters shows that the R_x(constant,K_y) model cannot be compared to the other two models because of its different transport mechanism which in the case of 5A molecular sieves does not apply. For the other two models the parameters showed similar trends. The adsorption constants showed no systematic variation with flowrate. Diffusivity showed increases of less than 20% with increasing velocity, the effect being greater in the case of the constant R_x model. Variations of less than 20% may be within the experimental error. They may also be due to the concentration dependence of the diffusivity, but in the Henry's law region this dependence is slight (Ruthven and Loughlin, 1971b). The temperature dependence of the adsorption constant of the two models compared well. However, the diffusion activation energy was greater in the constant R_x model.

Comparison between 30/40 and 45/60 mesh data using the R_x model shows that the adsorption constants of both methane and propane were similar. However, the 30/40 mesh gave propane diffusivity which was about 30% higher. Loughlin et al. (1971) have shown that the crystallite size distribution of Linde 5A molecular sieves may vary considerably from batch to batch. This would not have affected the adsorption properties of the molecular sieves, but it would significantly affect the diffusivity, the determination of which is dependent on crystallite size distribution. As the same crystallite size distribution was used in the calculation for both 30/40 and 45/60 mesh, this would possibly explain the variation obtained in diffusivity.

Comparison with literature values showed that the heats of sorption compared favourably with both gravimetric and GC data. Extrapolated K_c data for propane compared well with those of Chiang et al. (1984a,b), but not with the value given by Shah and Ruthven (1977) which was higher, perhaps in part owing to the presence of 20% inert binder which they took into account. The K_c values from gravimetric data were considerably higher but this difference may be due to temperature and concentration effects on the adsorption activation energy which would lead to poor estimation. Comparison of propane diffusivity obtained using GC showed variations by several factors (Table 5.9). Gravimetric data of Ruthven and Loughlin (1971b) showed limiting

diffusivity of 1.0 x 10^{-9} cm^2/sec at 80°C which compared well with the extrapolated value from this work. Since the work of Chiang et al. (1984a,b) and of Shah and Ruthven (1977) did not consider crystallite size distribution, the diffusivities obtained are in reasonable agreement. Another factor, when not accounting for crystallite size distribution, is the definition of the mean crystal radius. The technique used here requires the mean crystal radius to be defined from the particle number distribution as (3 x volume/area) for spherical particles. The use of the volume mean computed using the probability function on a volume basis in this case would have increased the diffusivity by two-fold.

5.6 RESULTS

SEM photographs of the HY and HM catalysts, previously dispersed in an ultrasonic bath, showed a large fraction of amorphous material, particularly HY. This could have been caused by the inorganic binder used in HY. The determination of crystallite size distribution was not possible from these photographs. The photographs showed that the HM crystallites were larger than HY the latter consisting of very small crystallites. As commercial NaY should have a similar crystallite size distribution as HY, the crystallite size parameters of Fu et al. (1986), who gave μ = -11.38 and σ = 0.9036, were used for the data analysis. For commercial HM, the data of Boniface and Ruthven (1985) gave μ = -10.43 and σ = 0.820. Although these data may not be strictly applicable, the approximation would only affect the absolute magnitude of the diffusivities, but not the trends between samples.

5.6.1 Axial dispersion in columns packed with catalysts

As discussed in the previous section the evaluation of diffusivity requires an accurate estimation of the axial dispersion contribution. The methane pulse data assuming negligible diffusional resistance using fresh as well as deactivated HM and HY are summarized in Figure 5.21, and the dispersion correlations obtained are given in Table 5.10. The moment analysis of methane pulses in HY and HM are shown in Figures 5.22a-c as a function of catalyst packing, temperature and pulse size. Figures 5.23a and b illustrate the moment analysis of the selected cracking and oligomerisation data.

The HM and HY data in Figure 5.21 show that the axial dispersion fell within a considerably broad band. There is also some scatter in Figure 5.22a. The effect of temperature (Figure 5.22b) was to increase molecular diffusion with an increase in temperature as demonstrated by increasing slope. However, the effect of temperature on the intercept is small, suggesting minimal variation in diffusional limitations. The variation of pulse size had no effect on the curves in Figure 5.22c. It follows from these plots that diffusional resistance was indeed negligibly small for methane diffusion in HY and HM. The broad band of the moments and dispersion data must be due to slight differences in packing of the columns. The data appeared to be within experimental error, as found by Chiang and Haynes (1977). The dispersion correlation obtained for HY and HM was therefore based on all the methane data including effects of varying temperature, packing and pulse size.

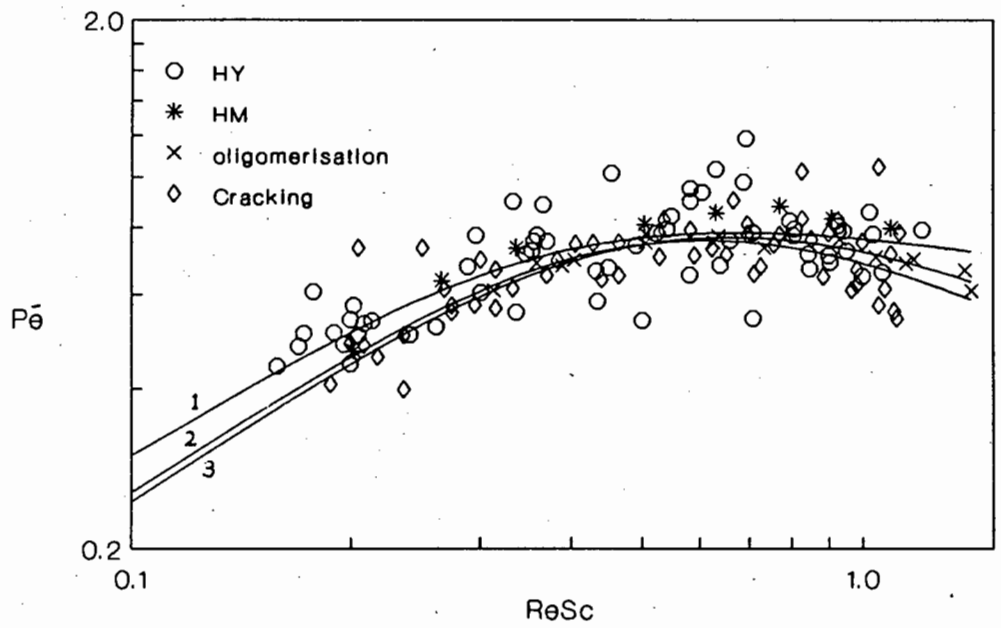

Figure 5.21 : Pē vs ReSc for methane dispersion in HY and HM.

TABLE 5.10 : DISPERSION CORRELATIONS FOR HY, HM, CRACKING AND OLIGOMERISATION GC COLUMNS.

Ref. in figure	GC packing	correlation	comments
1	HY, HM uncoked catalyst	$\frac{1}{Pé} = \frac{0.315}{ReSc} + \frac{1.93}{1 + 0.951/ReSc}$	methane data for HY at 50, 100, 150 °C with 4 repackings. HM methane on repacked column. d_t/d_p=16
2	cracking catalyst	$\frac{1}{Pé} = \frac{0.378}{ReSc} + \frac{7.74}{1 + 6.24/ReSc}$	methane runs CRAC1, CRAC2, CRAC4, CRAC6, CRAC7, CRAC8, REGEN8. d_t/d_p=16
3	oligomerisation catalyst	$\frac{1}{Pé} = \frac{0.394}{ReSc} + \frac{5.17}{1 + 4.25/ReSc}$	methane runs OLIG4, OLIG5. S.S column d_t/d_p=12

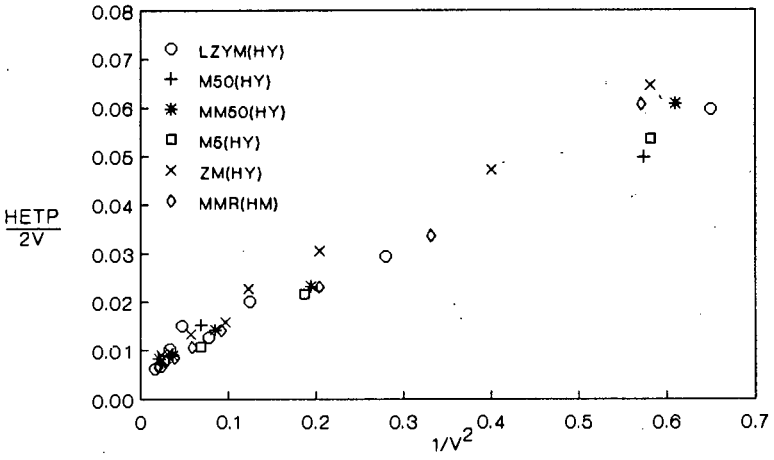

Figure 5.22a : Moment analysis of methane diffusion in HY and HM at 50°C

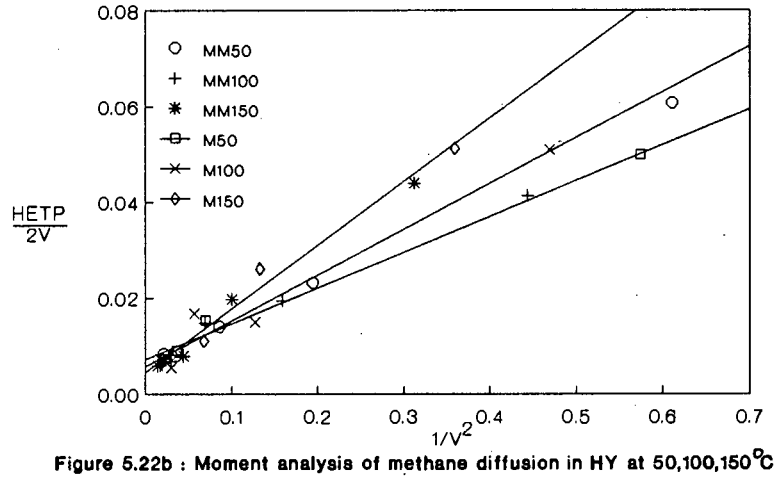

Figure 5.22b : Moment analysis of methane diffusion in HY at 50,100,150°C

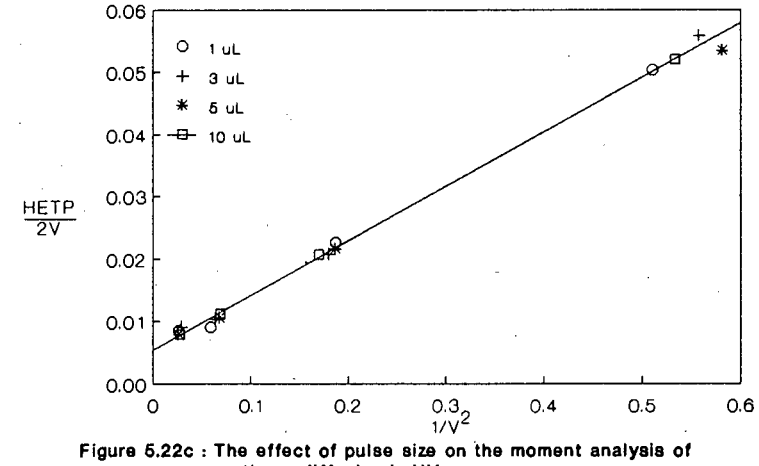

Figure 5.22c : The effect of pulse size on the moment analysis of methane diffusion in HY.

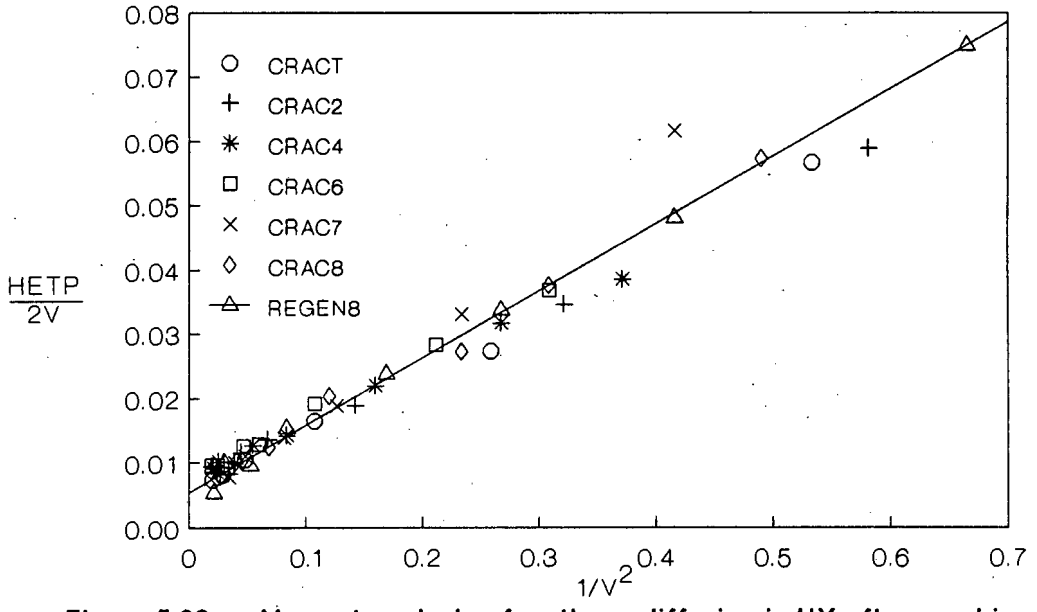

Figure 5.23a : Moment analysis of methane diffusion in HY after cracking.

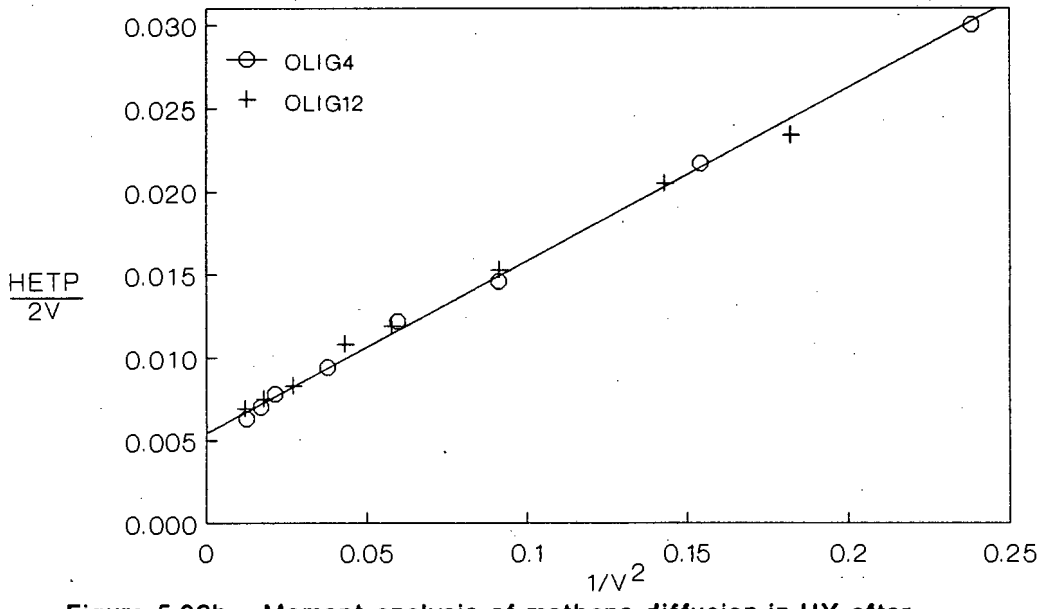

Figure 5.23b : Moment analysis of methane diffusion in HY after oligomerisation.

The dispersion data after cracking fell within the error band of the HY and HM data as seen in Figure 5.21. The moment analysis of the data after cracking plotted in Figure 5.23a had the same pattern as that of fresh HY and HM indicating that diffusional resistance was probably negligible. However, diffusional resistance was clearly evident in other data taken after cracking not shown here, viz., CRAC5 and CRAC3 (HM) whose response curves showed moderate and severe skewing, respectively. Consequently dispersion correlation for these data could not be found. The dispersion correlation based on all the cracking data yielded a curve similar to that of fresh HY and HM (Figure 5.21), but the molecular dispersion was larger.

The data collected on catalysts deactivated by oligomerisation fell in the range given in Figure 5.21 even though the s.s. column (d_t/d_p=12) was used. Moment analysis (Figure 5.23b) indicated that the data from OLIG4 and OLIG12 fell on a single curve and that diffusional resistance was negligible. However, all the other diffusion runs after oligomerization gave severe skewing, indicating significant diffusional resistance even for methane. In the latter case no dispersion correlation could be estimated.

Figure 5.21 shows that the smallest dispersion was obtained on fresh HY and HM and that all the other data, including those where there was some doubt as to whether diffusional resistance was small, fell within the experimental error band of the fresh HY and HM data. This suggests that the dispersion correlation for HY and HM may be used to estimate dispersion in the other columns.

In the absence of an alternative method for estimating the axial dispersion in the case where deactivation increased the diffusional resistance in catalyst pores even for methane, it was decided that the fresh HY and HM data gave a correlation reliable enough to be used for all the catalyst samples, fresh or deactivated, in this study.

5.6.2 Diffusion and adsorption in fresh HY

The Henry's law adsorption constants for methane, propane, n-butane and i-butane are shown in Table 5.11 together with the heats of sorption. Adsorption was found to increase in the order methane, propane, i-butane and n-butane; the heats of sorption increased in the order methane, i-butane, n-butane and propane. Data in Appendix C, Table C1 show that the variation of

TABLE 5.11 : ADSORPTION AND DIFFUSION IN FRESH HY.

tracer gas	T °C	K_c	D_c x 10^9 cm^2/sec	K_{co}	E_{Kc} kJ/mol	r^2
methane	50	6.74	-	0.180	9.62	1.00
	100	4.05	-			
	150	2.77	-			
propane	50	336	-	0.0133	27.1	0.996
	100	72.4	-			
	150	31.5	-			
n-butane	50	1216	-	0.0592	26.8	0.993
	100	399	5.0			
	150	112	-			
i-butane	50	791	-	0.199	22.5	0.983
	100	350	-			
	150	106	-			

TABLE 5.12 : ADSORPTION AND DIFFUSION IN FRESH HM.

tracer gas	T °C	K_c	D_c x10^9 cm^2/sec	K_{co} x10^3	E_{Kc} kJ/mol	r^2	D_{co} x10^3	E_{Dc} kJ/mol	r^2
methane	50	30.4	-	3.82	24.1	-	-	-	-
	100	9.12	-						
propane	50	5283	4.83	3.66	38.1	1.00	1.65	33.7	0.967
	100	784	48.9						
	150	185	88.2						
n-butane	100	6895	0.256	0.915	49.0	0.999	0.106	40.2	1.00
	150	939	1.11						
	200	247	3.98						
i-butane	100	6720	0.0910	0.653	49.9	0.999	0.393	47.5	0.999
	150	865	0.510						
	200	226	2.33						
propane[1]	100	750	2.19	-	-	-	-	-	-

1-repacked another batch of HM with different pretreatment.

pulse size from 1 to 10 $\mu\ell$ showed no systematic change in the adsoprtion constant. The variation appeared to be within experimental error.

The agreement between theory and experiment, and the magnitude of the axial dispersion contribution are shown in Figures 5.24a-d, 5.25a-d and 5.26a-d for propane, n-butane and i-butane, respectively. The data showed that for propane and i-butane diffusional resistance was negligible, although propane showed some tailing which affected the accuracy of the model prediction. The significant skewing in the n-butane response curves showed that diffusional resistance might be significant. Detector limitations became a problem for smaller pulse sizes, 1 and 3 $\mu\ell$ (see Figure 3.25c), particularly in the region of tailing, and it was not possible to curve fit the experimental data well. Larger pulse sizes (5 and 10 $\mu\ell$) showed that the axial dispersion contribution appeared to predict the peak front well, but failed to fit the trailing peak or the tail. For the same maximum peak height, the dispersion model predicted a wider bulk response than was actually observed, suggesting that dispersion may well be much smaller than estimated. The incorporation of diffusional resistance did little to improve the curvefit. However, when the axial dispersion term was decreased to an unrealistically small value (e.g., by a factor of 20), excellent curvefits of the data were obtained (see Appendix C, Table C1*), with the value of D_c of the order of 3×10^{-9} cm^2/sec. This skewing and tailing was not observed with i-butane where axial dispersion alone predicted the response curves reasonably well.

The moment analysis plotted in Figures 5.27a-c shows considerable scatter for propane and n-butane owing to the tailing. The variation of pulse size showed no trend. These graphs clearly demonstrate that reliable moment analysis is not possible in the presence of significant tailing.

Assuming negligible pore diffusional resistance, D_z was estimated from a frequency domain curvefit of D_z and K_c (dispersion model) and compared to the predicted axial dispersion in Figure 5.28. The data showed slight scatter but predicted axial dispersion for propane and i-butane was within the accuracy of the correlation. In the case of n-butane the data scattered severely due to the tailing. Recall that the dispersion model cannot predict the tailing observed and hence the estimated value of D_z (or Pé) could be an overestimate (or an underestimate for Pé). Indeed, the data with the largest tail had the smallest Pé. The data also showed that the largest value of D_c which could be determined was of the order of 10^{-7} cm^2/s. An estimated value of D_c for n-butane at 100°C is given in Table 5.11.

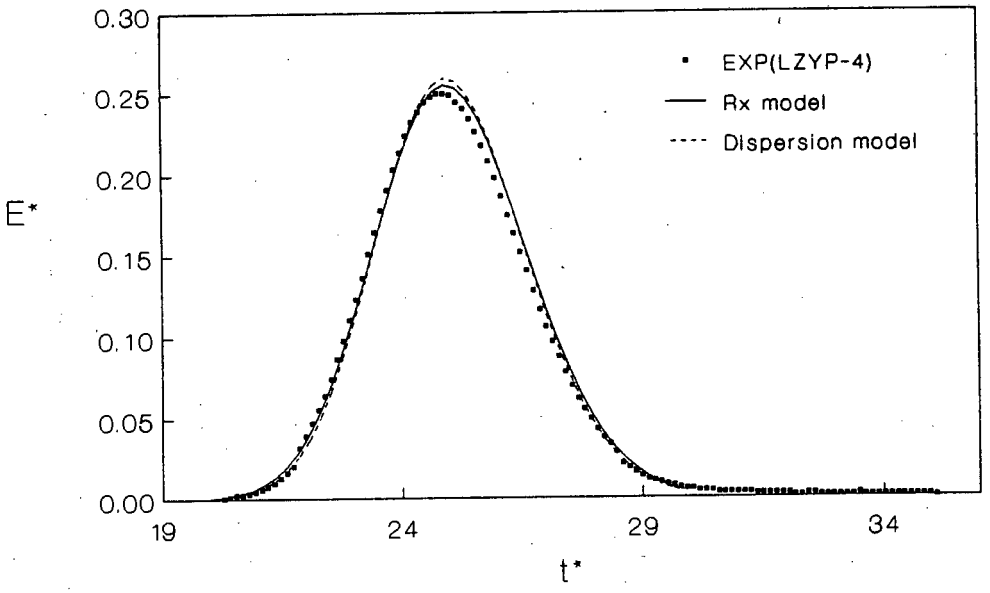

Figure 5.24a : E* vs t* of experimental data and model prediction for propane in HY; run LZYP-4.

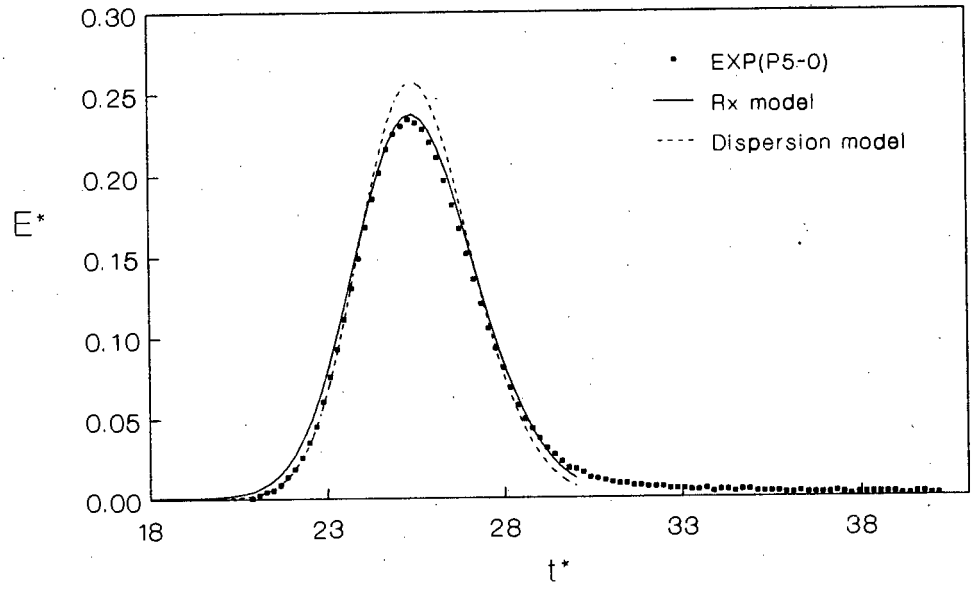

Figure 5.24b : E* vs t* of experimental data and model prediction for propane in HY; run P5-0.

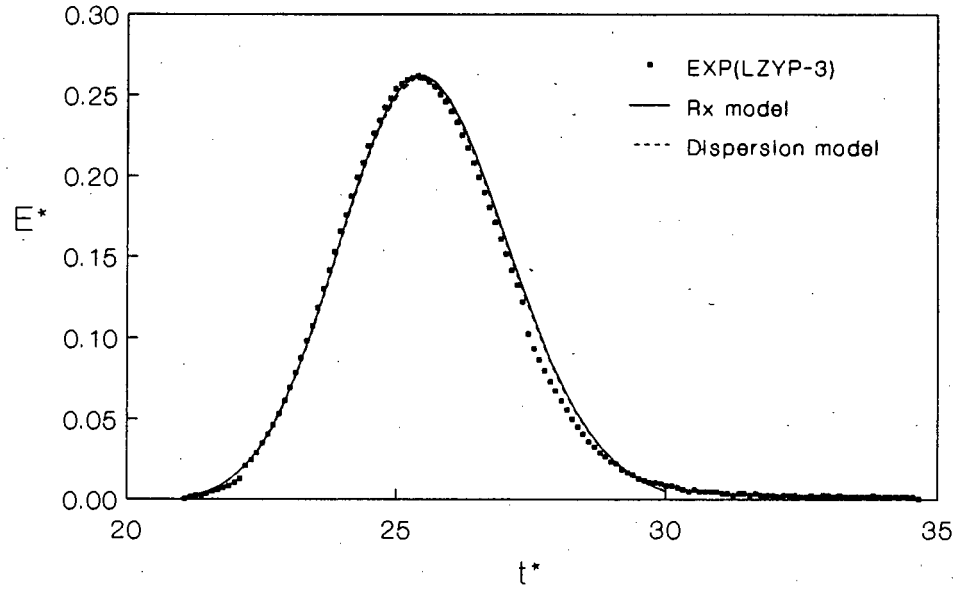

Figure 5.24c : E* vs t* of experimental data and model prediction for propane in HY; run LZYP-3.

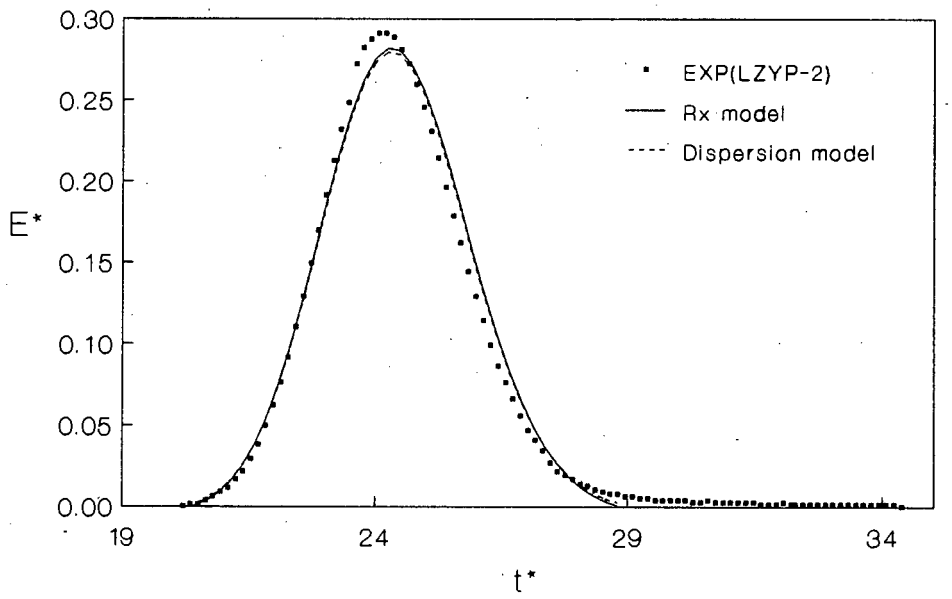

Figure 5.24d : E* vs t* of experimental data and model prediction for propane in HY; run LZYP-2.

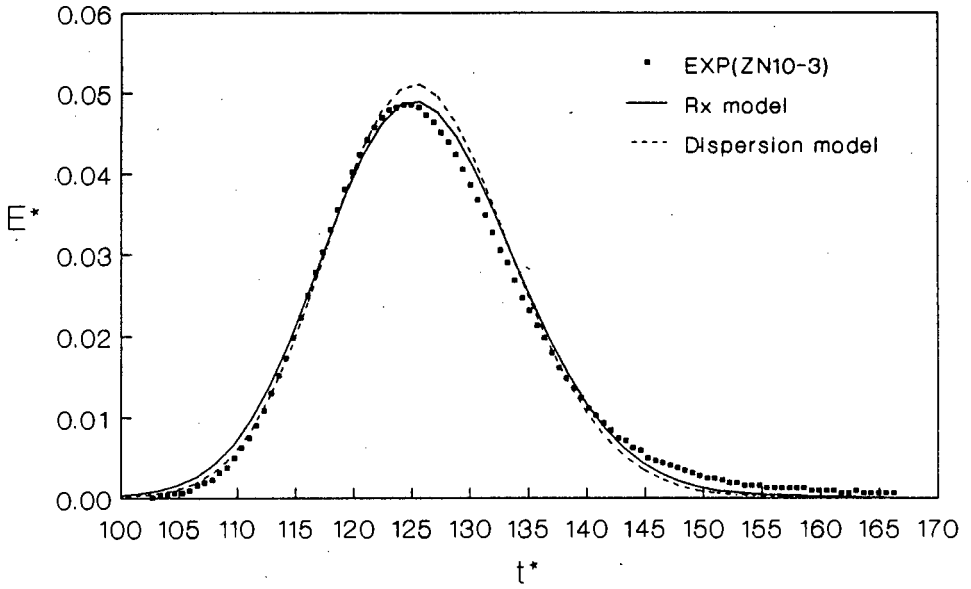

Figure 5.25a : E* vs t* of experimental data and model prediction for n-butane in HY; run ZN10-3.

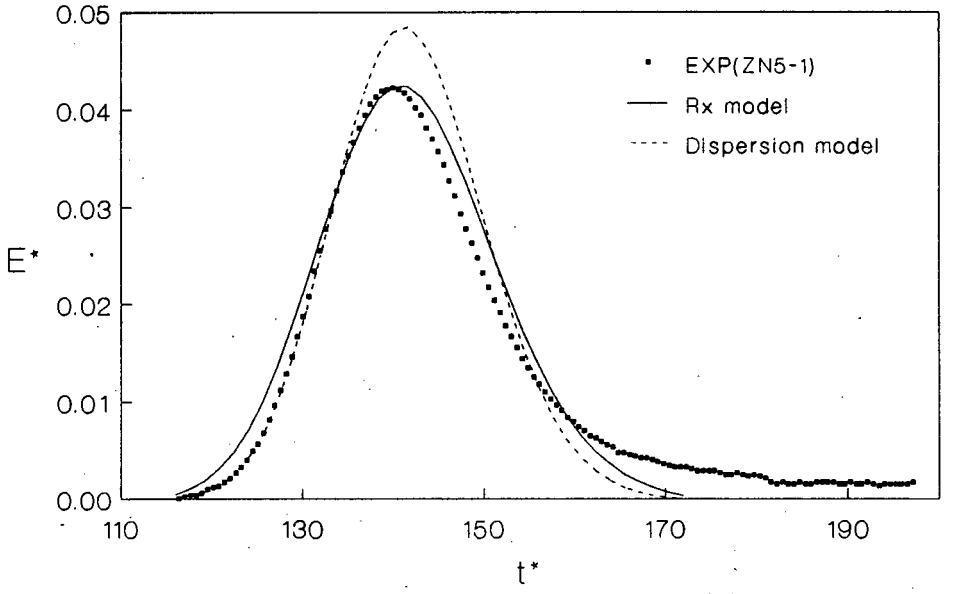

Figure 5.25b : E* vs t* of experimental data and model prediction for n-butane in HY; run ZN5-1.

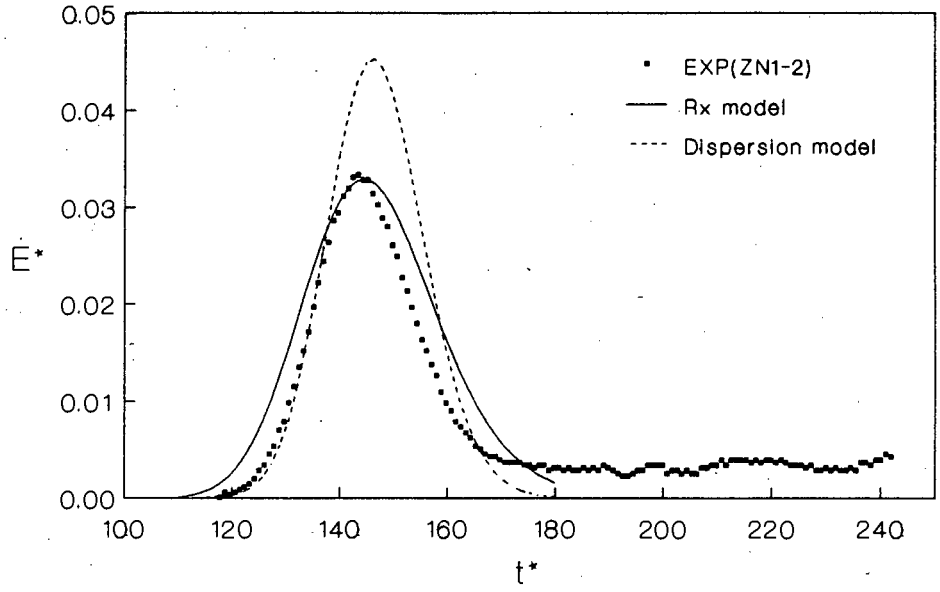

Figure 5.25c : E* vs t* of experimental data and model prediction for n-butane in HY; run ZN1-2.

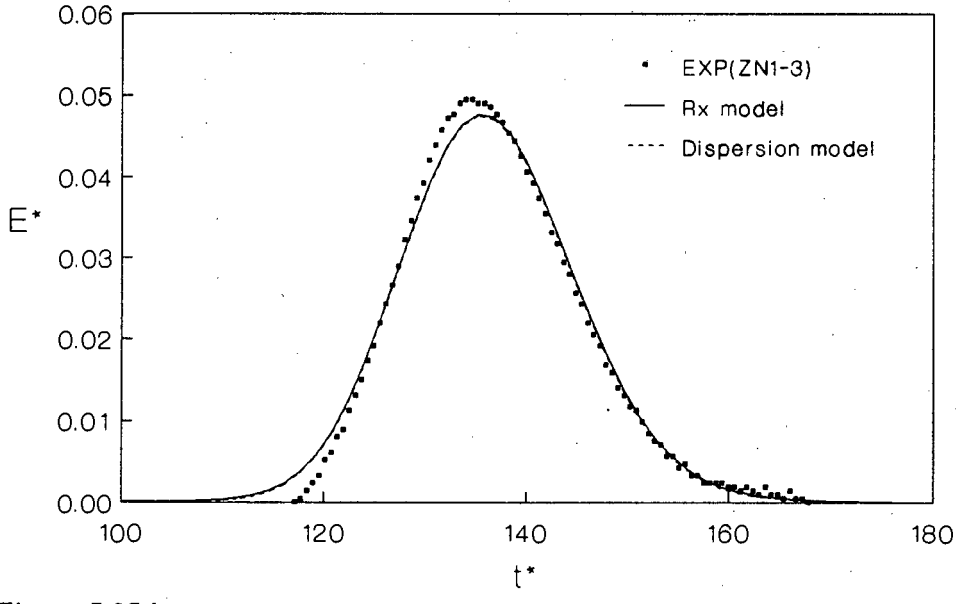

Figure 5.25d : E* vs t* of experimental data and model prediction for n-butane in HY; run ZN1-3.

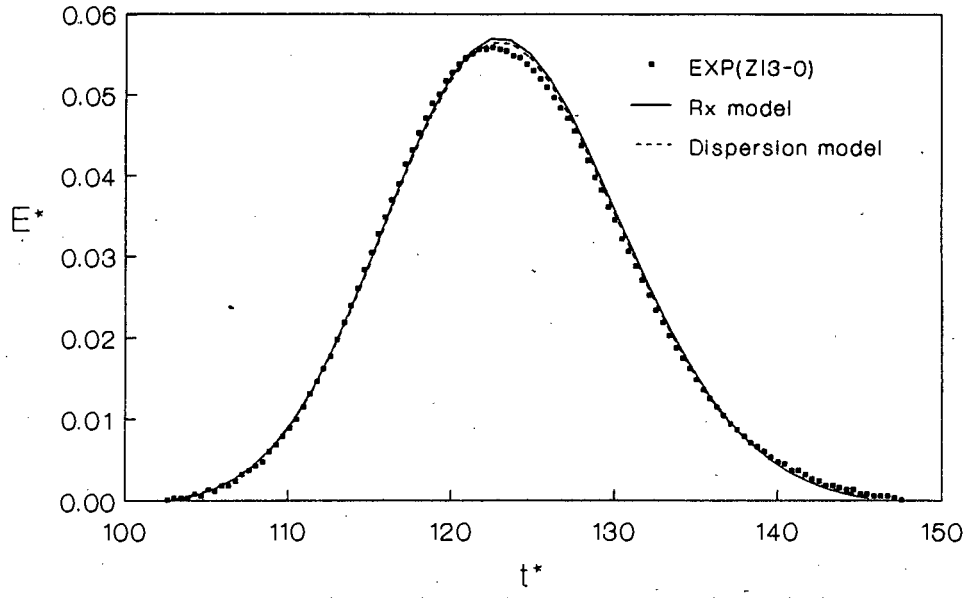

Figure 5.26a : E* vs t* of experimental data and model prediction for i-butane in HY; run ZI3-0.

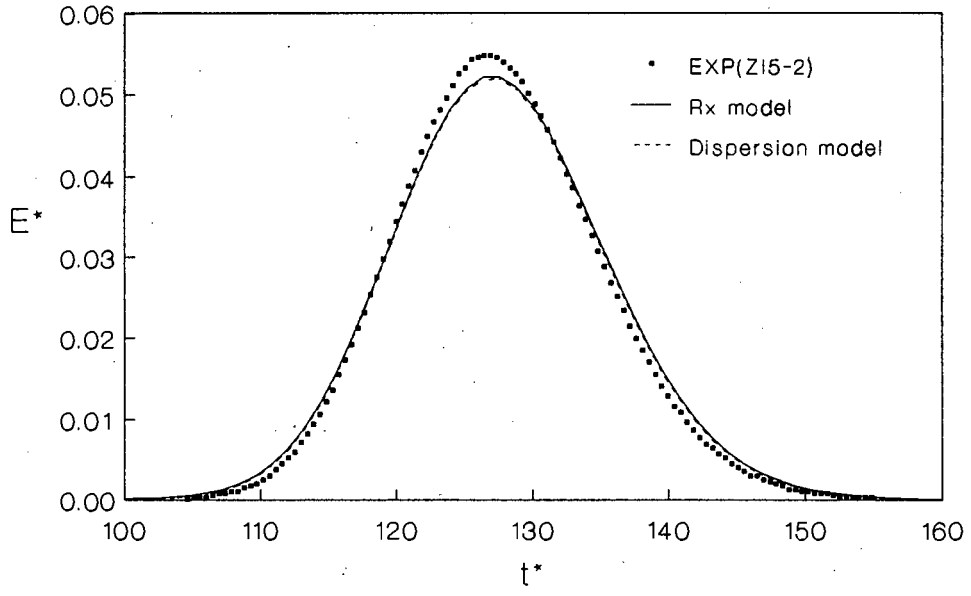

Figure 5.26b : E* vs t* of experimental data and model prediction for i-butane in HY; run ZI5-2.

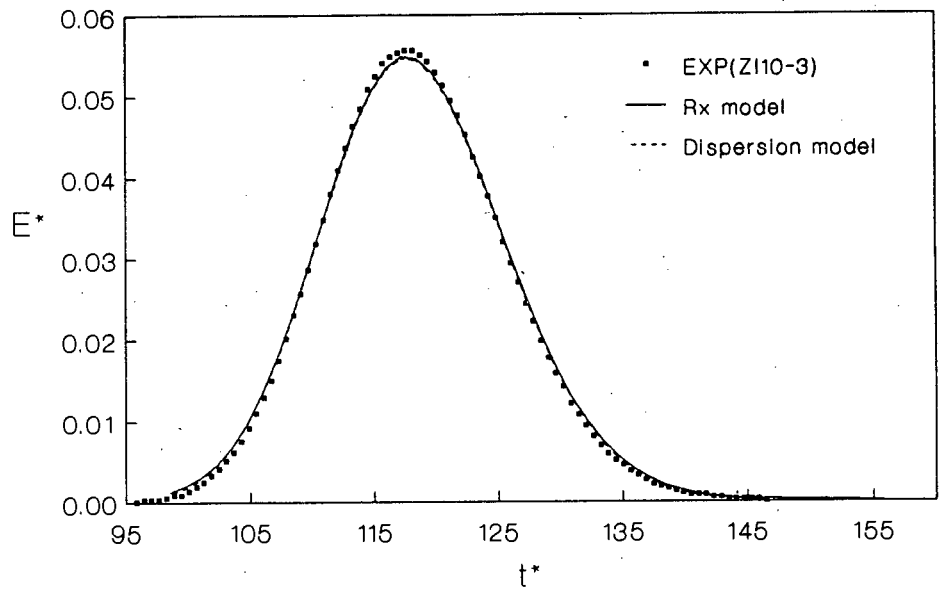

Figure 5.26c : E* vs t* of experimental data and model prediction for i-butane in HY; run ZI10-3.

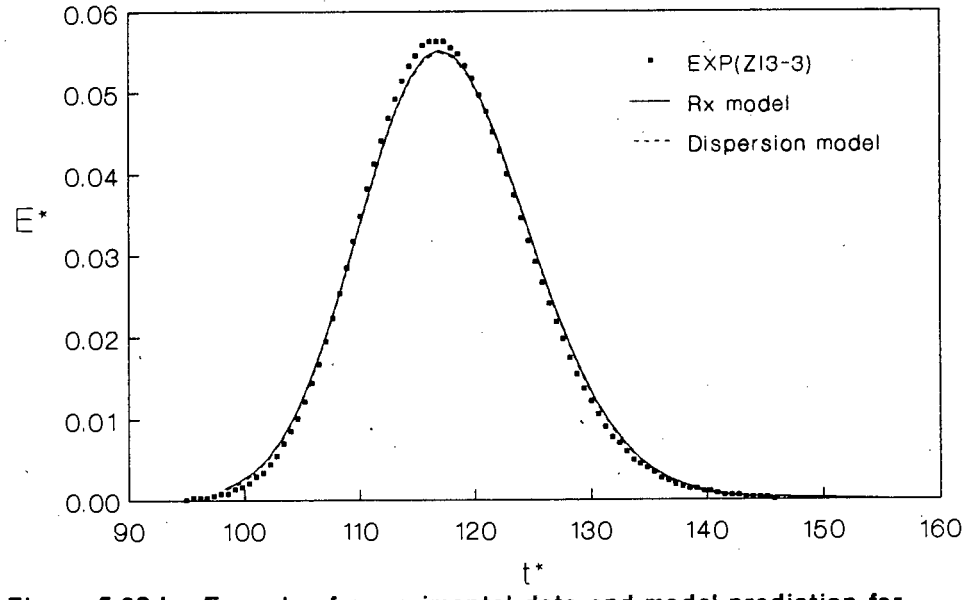

Figure 5.26d : E* vs t* of experimental data and model prediction for i-butane in HY; run ZI3-3.

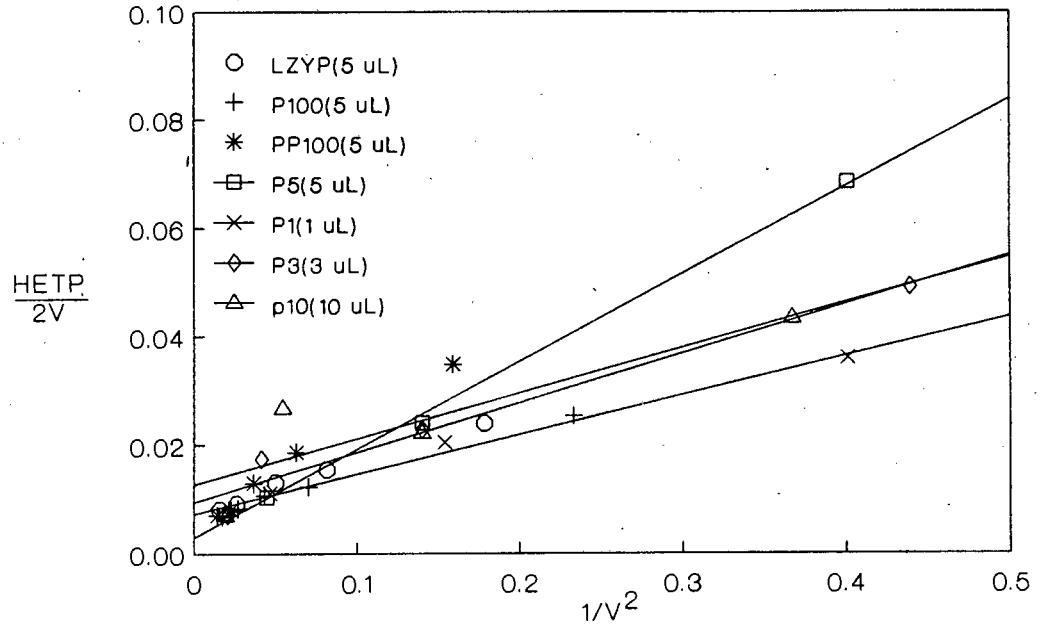

Figure 5.27a : The effect of pulse size on the moment analysis of propane diffusion in HY at 100°C

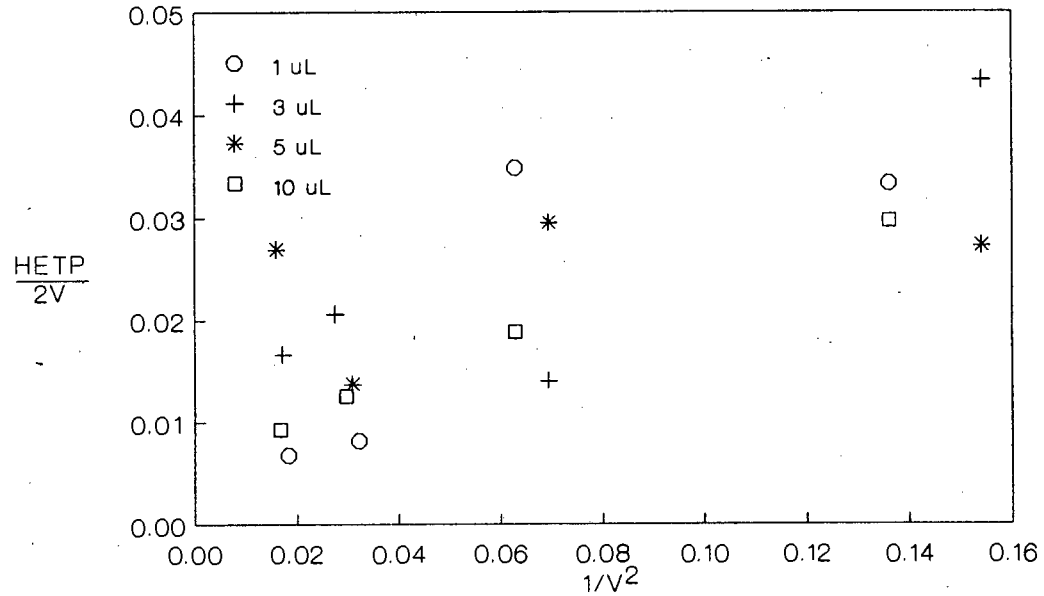

Figure 5.27b : The effect of pulse size on the moment analysis of n-butane diffusion in HY at 100°C.

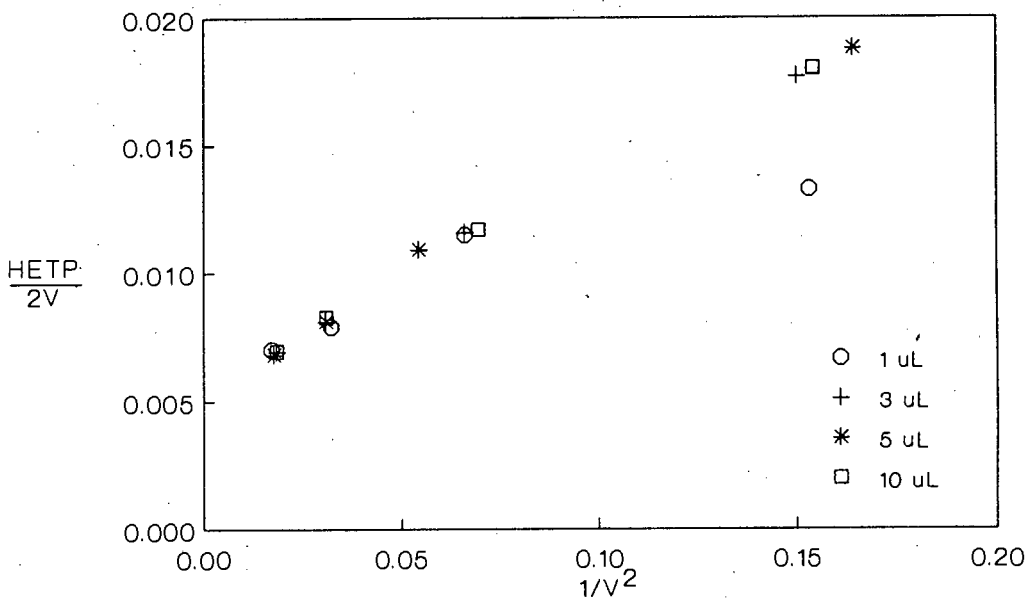

Figure 5.27c : The effect of pulse size on the moment analysis of i-butane diffusion on HY at 100°C.

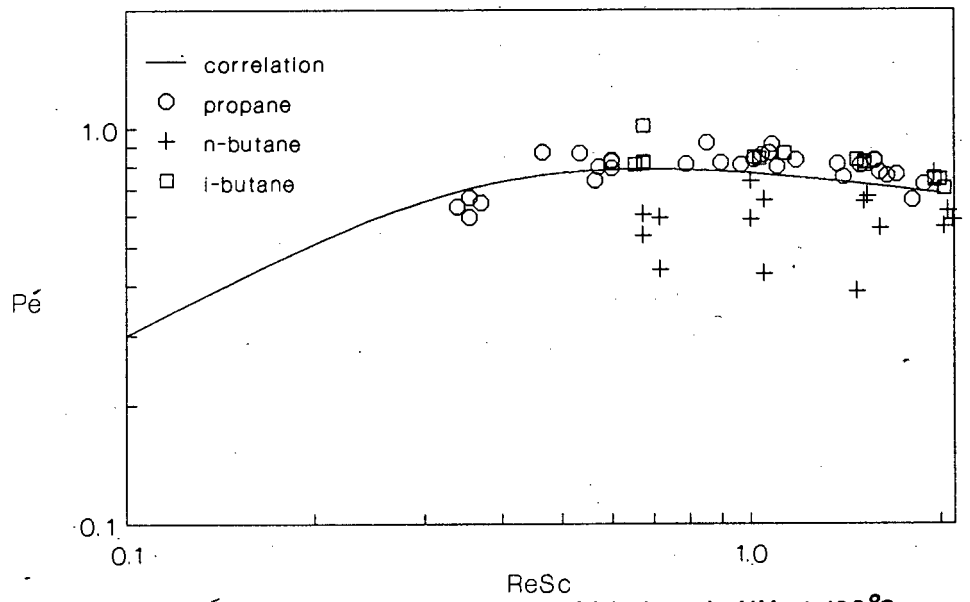

Figure 5.28 : Pé vs ReSc for propane,n- and i-butane in HY at 100°C.

5.6.3 Diffusion and adsorption in fresh HM

Henry's law adsorption constants increased with increasing molecular weights as seen in Table 5.12. Heats of sorption followed the same trend and in particular they were similar for n-butane and i-butane. Data in Table C2, Appendix C show that there appeared to be no correlation between the adsorption constant and pulse size except in the case of i-butane. From the observation that K_c increased slightly with increasing flowrate of i-butane, the drop in the mean residence time in the case of 10 $\mu\ell$ injection in run HMIP-3 was probably due to experimental error. These observations suggest that the system was overall in the linear regime.

Model predictions of experimental data for propane (Figures 5.29a and b), n-butane (Figure 5.29c) and i-butane (Figure 5.29d) showed the goodness of fit and the extent to which intracrystalline diffusional resistance caused additional peak spreading and skewing in contrast to the predicted curves taking into account axial dispersion only. The error column in Table C2 indicating discrepancy between theory and experiment shows that the crystallite size distribution had to be accounted for in order to predict the experimental data, i.e., to enable the model to fit the tailing. Figures 5.29a and b show different response curves for propane in HM. Table C2* shows that reducing the value of D_z by 20% decreased the value of D_c by a factor of four for propane. Diffusional resistance encountered by the butanes was significant with i-butane diffusing more slowly than n-butane. Moment analysis shown in Figure 5.30 is not reliable because of the tailing of the butane response curves which makes the computation of the moments inaccurate.

Table 5.12 shows that the micro-pore diffusivity decreased, and diffusional activation energy increased, with increasing molecular size, i-butane being more bulky than n-butane. The data in Appendix C, Table C2 shows there is a correlation between diffusivity and pulse size. There appeared to be an increase in diffusivity with increasing velocity for the butanes, but the variation was slight. In the case of methane and propane, slight changes in D_z led to orders of magnitude differences in D_c. Any variations in diffusivity seen here are thus probably due to inaccurate determination of D_z which would have a much greater influence than in the case of the butanes.

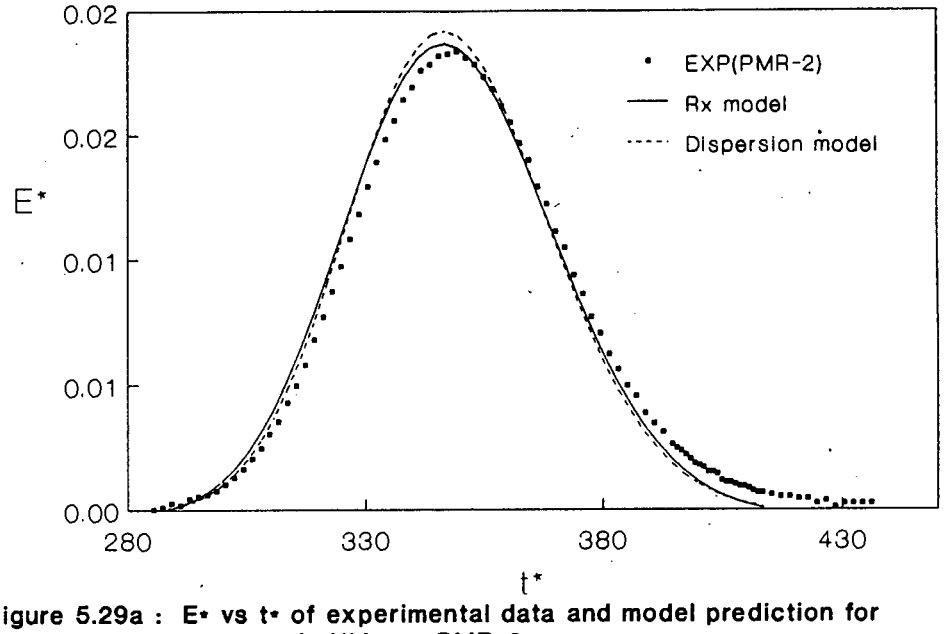

Figure 5.29a : E* vs t* of experimental data and model prediction for propane in HM; run PMR-2.

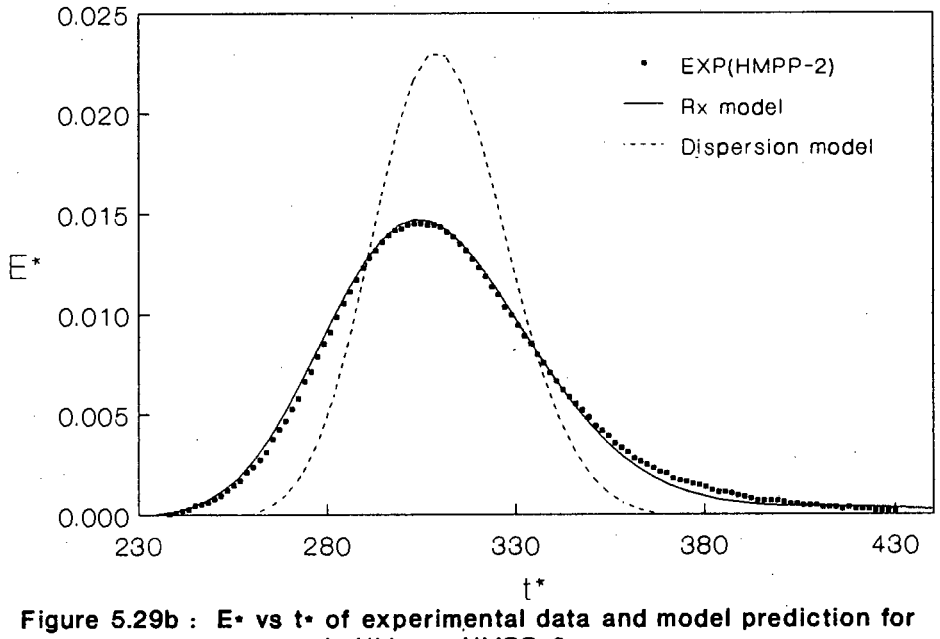

Figure 5.29b : E* vs t* of experimental data and model prediction for propane in HM; run HMPP-2.

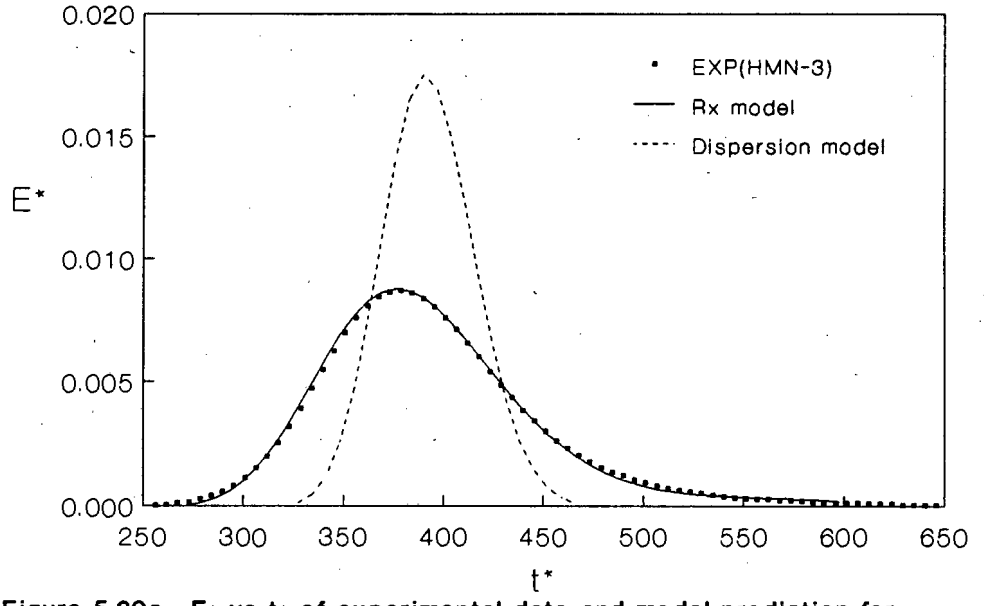

Figure 5.29c : E* vs t* of experimental data and model prediction for n-butane in HM; run HMN-3.

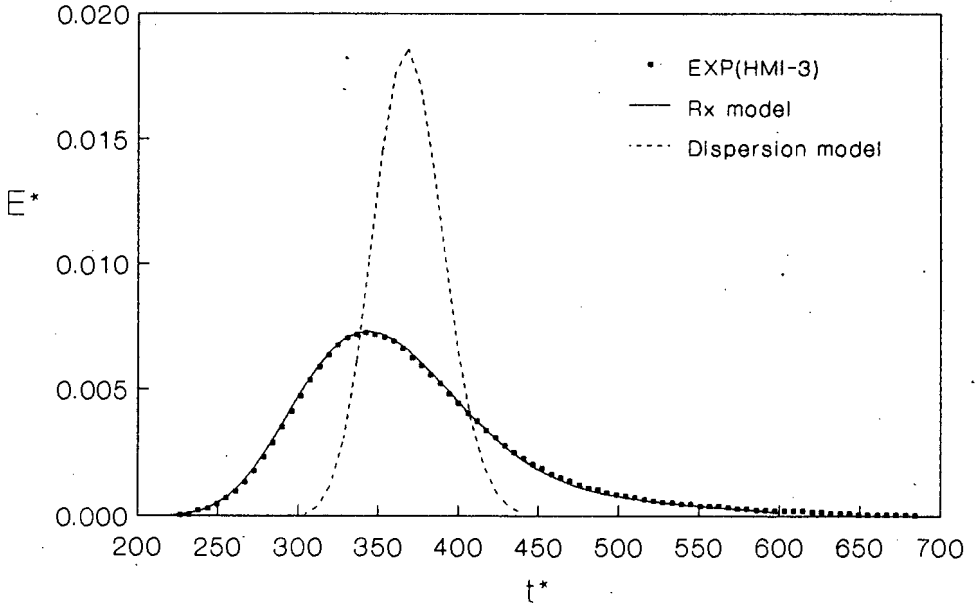

Figure 5.29d : E* vs t* of experimental data and model prediction for i-butane in HM; run HMI-3.

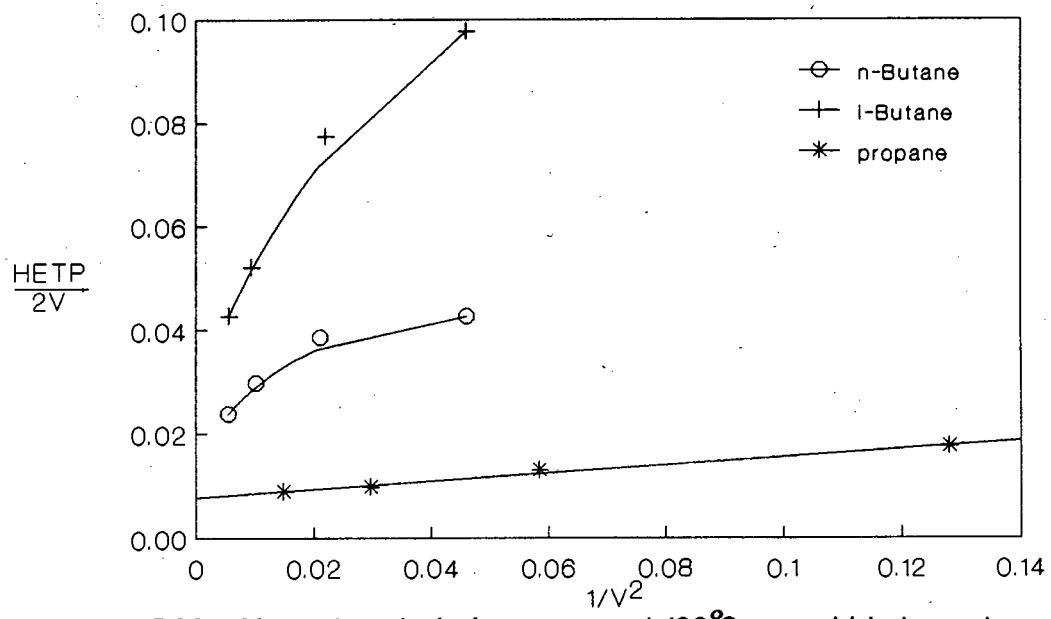

Figure 5.30 : Moment analysis for propane at 100°C, n- and i-butane at 150°C in HM.

5.6.4 Diffusion and adsorption in HY and HM after hexane cracking

Methane and propane diffusion and adsorption data for HY and HM are shown in Tables C3 to C12 in Appendix C. Measurements obtained from HY with 8-9% coke showed that propane diffusional resistance was significant and that the experimental response curves were well predicted by the R_x model. In the case of severe coking (>10%), it was necessary to introduce a macro-pore adsorption (i.e., the R_xK_y model) to predict the response curves as illustrated in Figures 5.31a and b. In contrast, at 7.1 wt% coke diffusivity was too high to be determined. Figure 5.31c shows that for cases where diffusional resistance was small even the constant R_x model was able to predict the data, although the diffusivites given by the two models differed substantially. Moment analysis of methane and propane in HY (Figures 5.32a-d) showed that diffusional resistance was small except when coke content exceeded 10 wt%. Difficulties involved in accurately recording tailing makes the applicability of the moment analysis of CRAC1 and CRAC5 doubtful.

In the case of HM response peaks showed severe tailing with a steep front, particularly for propane. As the flow rate was increased, response peaks became sharper with a steeper front, but the long tail remained. Table C6 in Appendix C shows that the R_x model could not predict the response curves well, especially for propane. The R_xK_y model gave better agreement with experiment. This is illustrated in Figures 5.33a and b. The R_x model appeared to predict the propane response curves well at low velocities, suggesting that equilibrium might not have been reached at higher velocities (i.e., the adsorption rate (k_a) may be finite). Figure 5.34a shows that moment analysis cannot be used as severe tailing introduced inaccuracy in the evaluation of the moments. The mean was found to decrease with increasing velocity (Figures 5.34b and c) which could be due to a non-linear adsorption isotherm. A similar trend was observed for K_c and D_c when determined from either the R_x or R_xK_y model. However, part of this variation was due to inaccuracies in measuring the severe tailing present, especially at high velocity.

Table 5.13 shows the variation of K_c and D_c after cracking using the R_x model, evaluated at 50, 100 and 150°C at approximately the same velocity (within 10% variation). Run REGEN8 represents the catalyst sample of run CRAC8 regenerated in air at 400°C overnight. Table 5.14 shows the same data in case of severe diffusional limitations using the R_xK_y model. The heats of sorption and diffusional activation energies for HY using the R_x and R_xK_y models are shown in Tables 5.15 and 5.16, respectively.

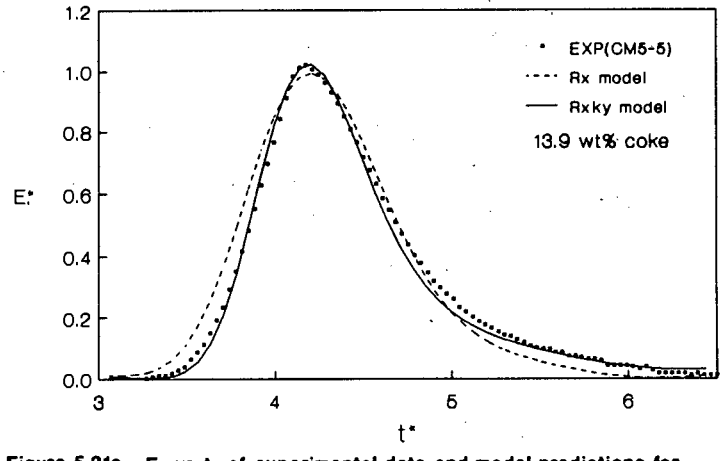

Figure 5.31a : E* vs t* of experimental data and model predictions for methane in HY at 50°C, after hexane cracking; run CM5-5.

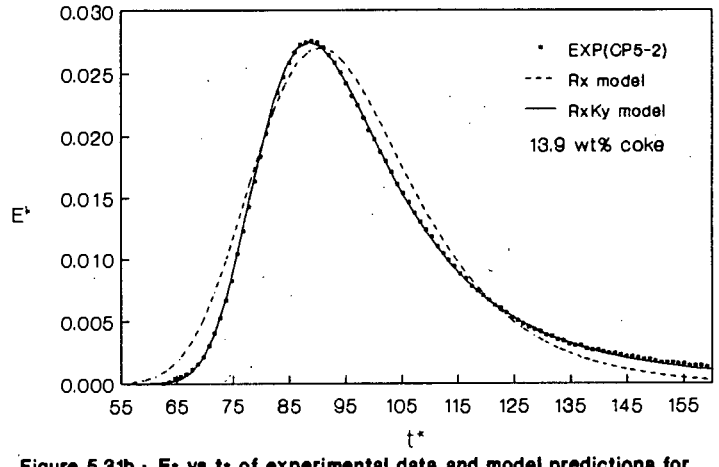

Figure 5.31b : E* vs t* of experimental data and model predictions for propane in HY at 100°C, after hexane cracking; run CP5-2.

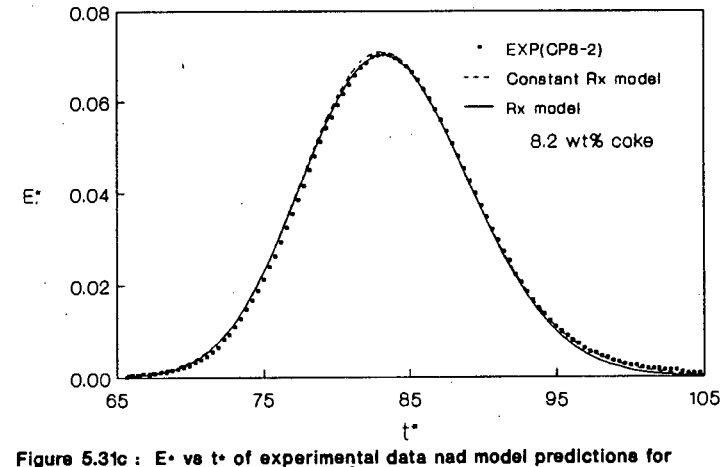

Figure 5.31c : E* vs t* of experimental data nad model predictions for propane in HY at 100°C, after hexane cracking; run CP8-2.

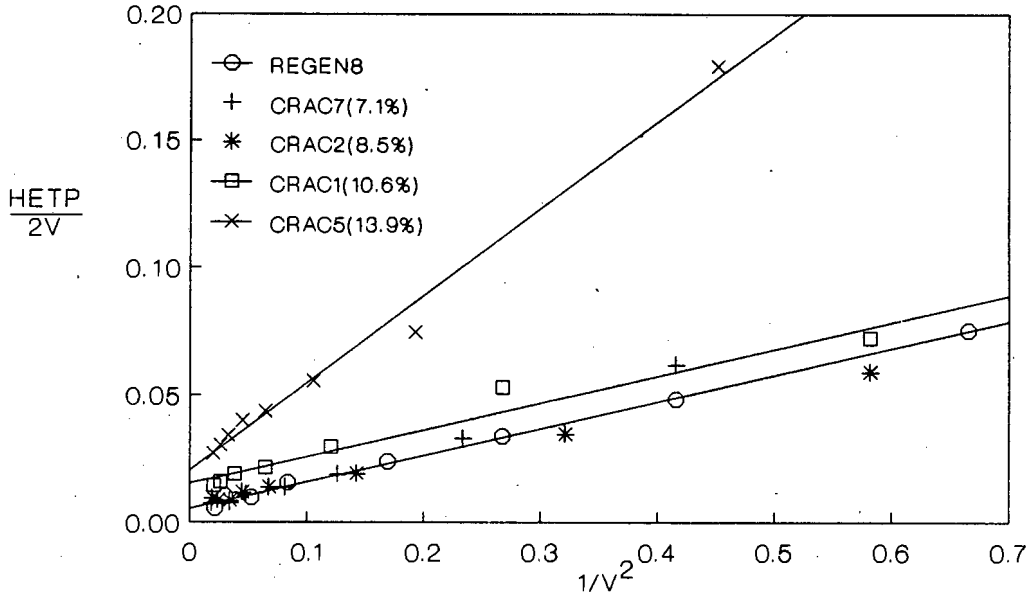

Figure 5.32a : Moment analysis of methane in HY at 50°C after hexane cracking; the effect of coke content and regeneration.

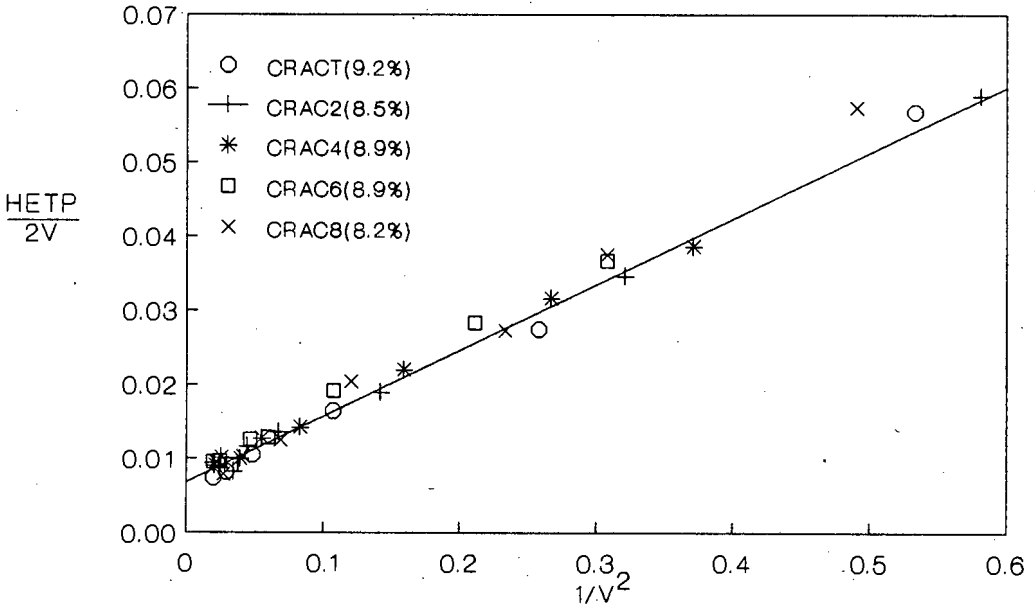

Figure 5.32b : Moment analysis of methane in HY at 50°C after hexane cracking; catalyst samples with similar coke contents.

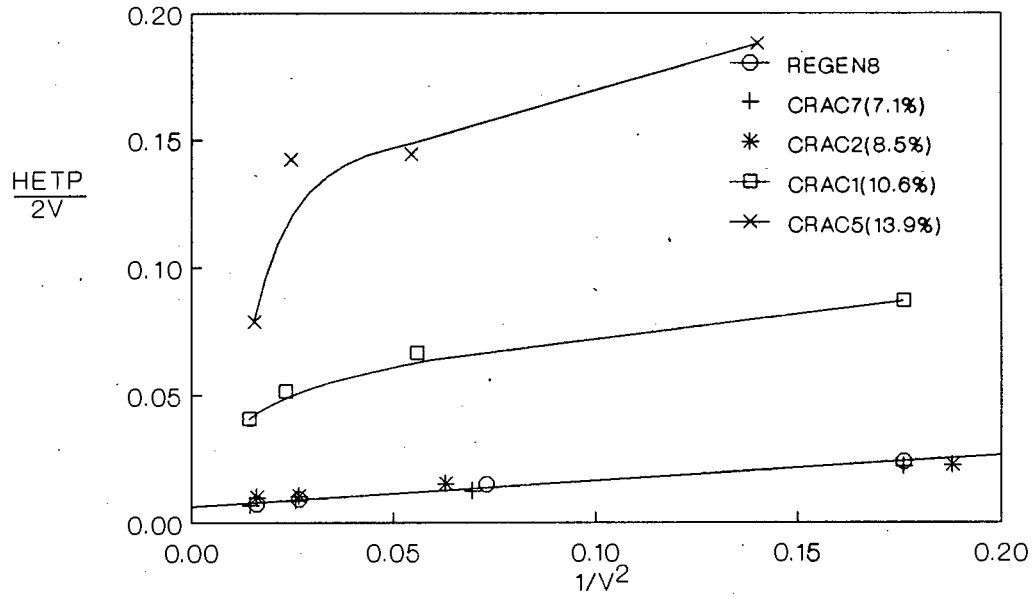

Figure 5.32c : Moment analysis of propane in HY at 100°C after hexane cracking; the effect of coke and regeneration.

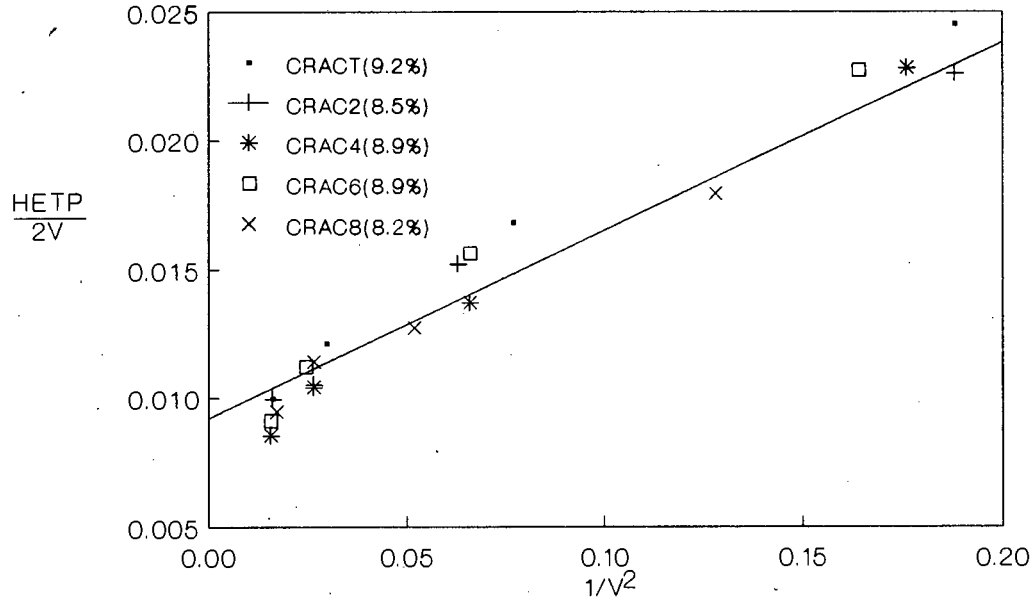

Figure 5.32d : Moment analysis of propane in HY at 100°C after hexane cracking; catalyst samples with similar coke content.

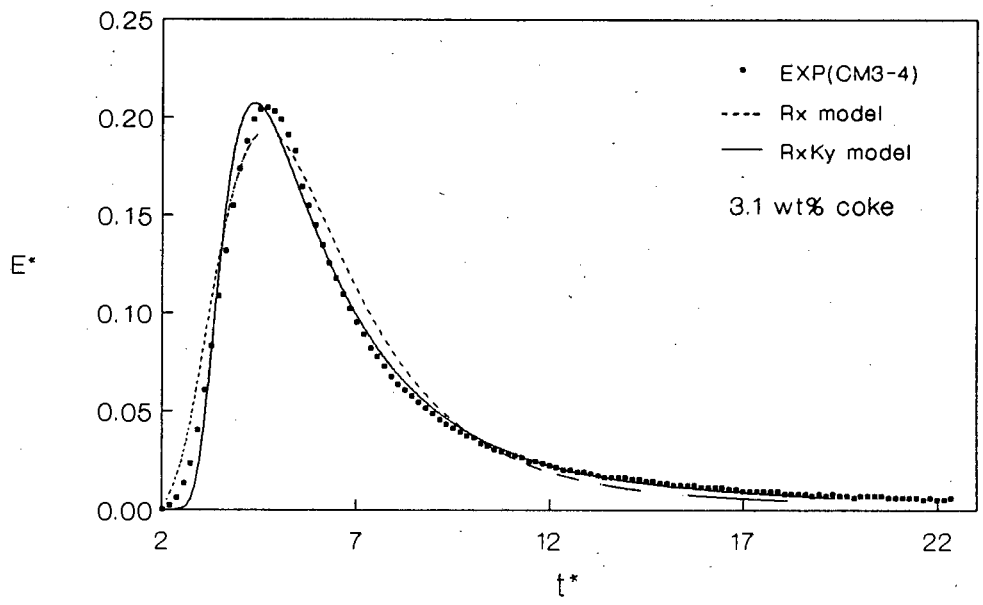

Figure 5.33a : E* vs t* of experimental data and model prediction for methane in HM at 50°C after hexane cracking; run CM3-4.

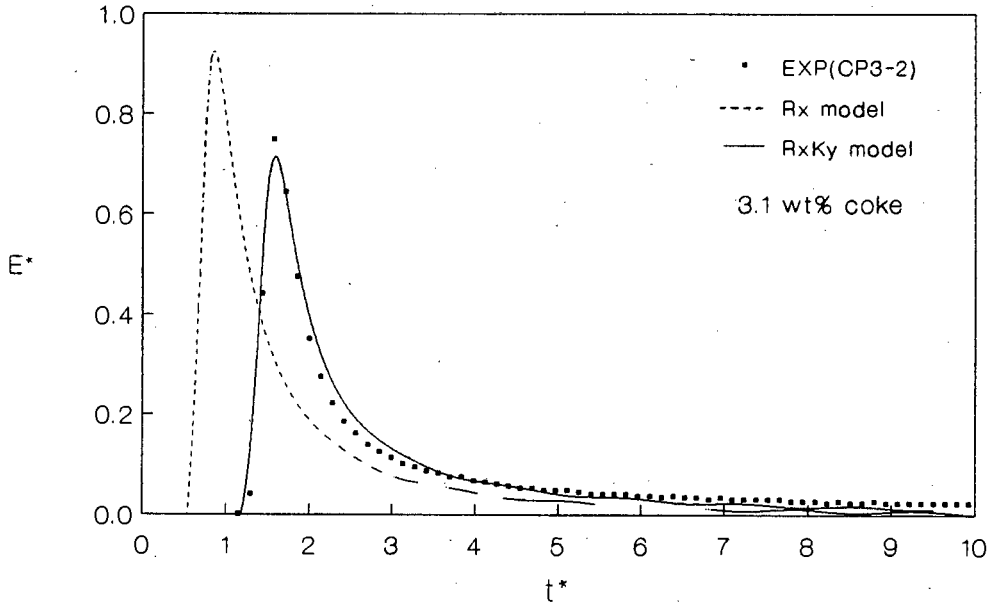

Figure 5.33b : E* vs t* of experimental data and model prediction for propane in HM at 100°C after hexane cracking; run CP3-2.

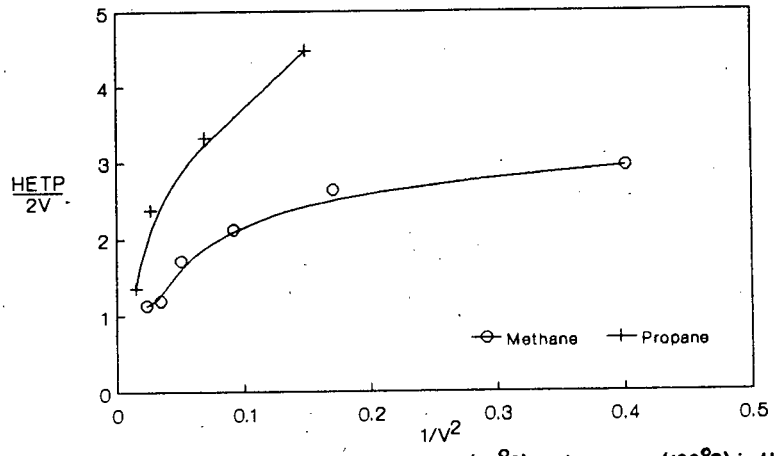

Figure 5.34a : Moment analysis of methane (50°C) and propane (100°C) in HM after hexane cracking; run CRAC3.

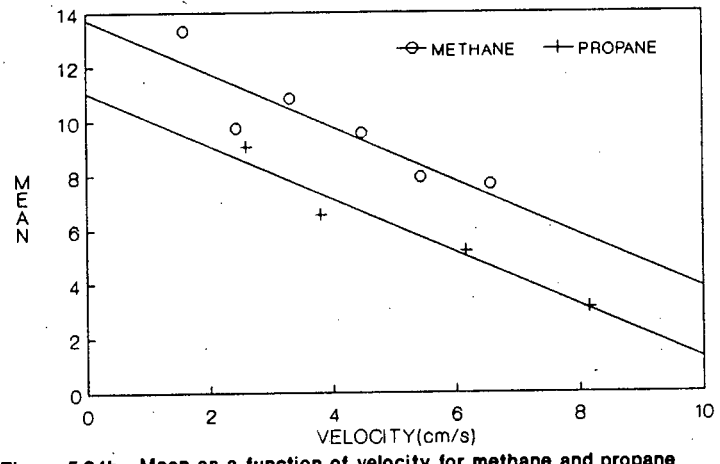

Figure 5.34b : Mean as a function of velocity for methane and propane diffusion in HM after hexane cracking; run CRAC3.

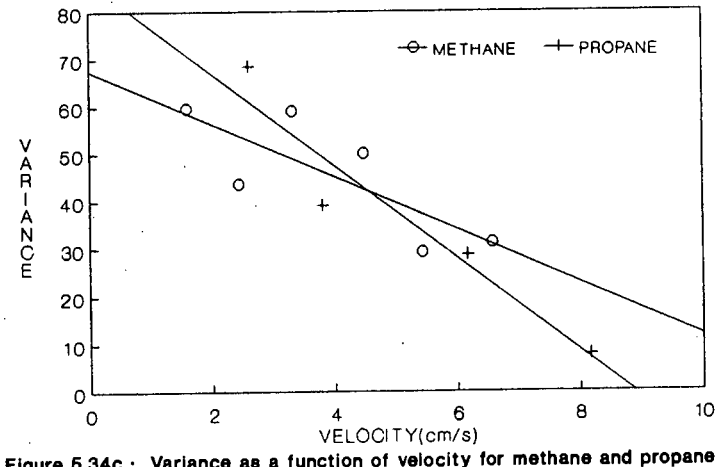

Figure 5.34c : Variance as a function of velocity for methane and propane diffusion in HM after hexane cracking; run CRAC3.

TABLE 5.13 : ADSORPTION AND DIFFUSION IN HY AND HM AFTER HEXANE CRACKING; R_x MODEL.

Run ID	tracer gas	coke content wt%	K_c			$D_c \times 10^9$		
			50 °C	100 °C	150 °C	50 °C	100 °C	150 °C
CRACT	methane	9.2	11.6	-	-	-	-	-
CRAC1		10.6	10.3	-	-	118	-	-
CRAC2		8.5	9.59	-	-	-	-	-
CRAC3£		3.1	16.0	-	-	1.01	-	-
CRAC4		8.9	7.69	-	-	-	-	-
CRAC5		13.9	10.4	-	-	51.4	-	-
CRAC6		8.9	8.98	-	-	-	-	-
CRAC7		7.1	9.07	-	-	-	-	-
CRAC8		8.2	9.31	-	-	-	-	-
REGEN8		0.0	6.41	-	-	-	-	-
CRACT	propane	9.2	2315	325	72.8	4.96	27.0	133
CRAC1		10.6	2148	294	59.5	0.153	1.14	6.60
CRAC2		8.5	2017	254	62.6	3.20	29.3	149
CRAC3£		3.1	-	5.5	-	-	0.163	-
CRAC4		8.9	1256	185	48.4	19.8	62.5	409
CRAC5		13.9	2226	279	57.5	0.0775	0.585	3.57
CRAC6		8.9	1304	206	52.0	4.99	32.7	172
CRAC7		7.1	1164	198	50.7	-	-	-
CRAC8		8.2	1638	231	51.2	5.55	30.4	157
REGEN8		0.0	289	76.4	27.1	-	-	-

TABLE 5.14 : ADSORPTION AND DIFFUSION IN HY AND HM AFTER HEXANE CRACKING; $R_x K_y$ MODEL.

Run ID	tracer gas	K_y			K_c			$D_c \times 10^{10}$		
		50 °C	100 °C	150 °C	50 °C	100 °C	150 °C	50 °C	100 °C	150 °C
CRAC3£	methane	10.7	-	-	14.9	-	-	2.04	-	-
CRAC5		15.3	-	-	2.09	-	-	3.61	-	-
CRAC1	propane	400	250	49.8	1907	146	29.9	1.28	3.20	19.9
CRAC3£		-	4.13	-	-	22.4	-	-	0.086	-
CRAC5		1707	294	62.0	1236	117	22.8	0.225	0.550	3.29

£-HM

TABLE 5.15 : ARRHENIUS TEMPERATURE DEPENDENCE OF DIFFUSION AND ADSORPTION FOR PROPANE IN HY AFTER HEXANE CRACKING; R_x MODEL.

Run ID	coke content	K_{co} x 10^3	E_{Kc} kJ/mol	r^2	D_{co} x 10^3	E_{Dc} kJ/mol	r^2
CRACT	9.2	1.02	39.3	1.00	4.88	37.2	0.998
CRAC1	10.6	0.571	40.7	1.00	1.16	42.6	0.999
CRAC2	8.5	0.786	39.6	0.999	37.3	43.7	1.00
CRAC4	8.9	1.25	37.1	1.00	4.97	33.8	0.977
CRAC5	13.9	0.426	41.5	1.00	0.762	43.4	0.999
CRAC6	8.9	1.55	36.6	1.00	14.6	40.1	0.999
CRAC7	7.1	2.05	35.6	1.00	-	-	-
CRAC8	8.2	0.708	39.4	1.00	6.74	37.8	0.998
REGEN8	-	17.8	26.0	0.999	-	-	-

TABLE 5.16 : ARRHENIUS TEMPERATURE DEPENDENCE OF DIFFUSION AND ADSORPTION FOR PROPANE IN HY AFTER HEXANE CRACKING; R_xK_y MODEL.

Run ID	K_{yo} x 10^3	E_{Ky} kJ/mol	r^2	K_{co} x 10^5	E_{Kc} kJ/mol	r^2	D_{co} x 10^6	E_{Dc} kJ/mol	r^2
CRAC1	95.4	22.9	0.927	3.85	47.4	0.998	9.20	30.5	0.965
CRAC5	1.50	37.5	0.999	5.37	45.5	1.00	1.26	29.8	0.964

The adsorption of methane and propane on HY generally increased with increasing coke content (Figures 5.35a and b) according to the R_x model, although there was considerable scatter in the data. The R_xK_y model yielded lower values of K_c for CRAC1 and CRAC5. For methane, the latter model gave a lower value of K_c than before deactivation. For propane, the R_xK_y model gave a smaller increase in K_c with increasing coke content than the R_x model. The heat of sorption of propane (Figure 5.35c) increased with increasing coke content, although the R_xK_y model predicted higher values than the R_x model. The two data points at 0% coke in the above figures indicate that the regeneration in air (REGEN8) was able to restore spent catalyst to its initial sorption properties.

Methane diffusional resistance in HY became significant above 10% coke and D_c decreased by two orders of magnitude from 10.6% coke to 13.9% coke. Similarly diffusional resistance for propane was found to increase rapidly with a slight increase in coke content above a critical coke content as seen in Figure 5.36a. The diffusional resistance became sufficiently large to enable diffusivity estimation at about 8% coke. D_c decreased by an order of magnitude between 9 and 11% coke using the R_x model, and by two orders of magnitude over the same range using the R_xK_y model. Diffusional activation energy shown in Figure 5.36b increased with coke content when the R_x model was used while it decreased when the R_xK_y model was used. The scatter observed between 8-9% coke was due to the inaccuracy in determining D_c for relatively small diffusional resistance, particularly at the higher temperatures.

In the case of HM only the R_xK_y model was applicable. The parameter estimation showed that K_c and D_c decreased upon coking. In contrast to HY, the adsorption of propane on coked HM decreased. Diffusivities followed the same trend as HY in that they decreased by two orders of magnitude. The diffusional resistance in HM was large and clearly the critical coke content was probably well below 3%. The diffusivities determined were subject to variations due to inaccurate measurements of response curve tailing.

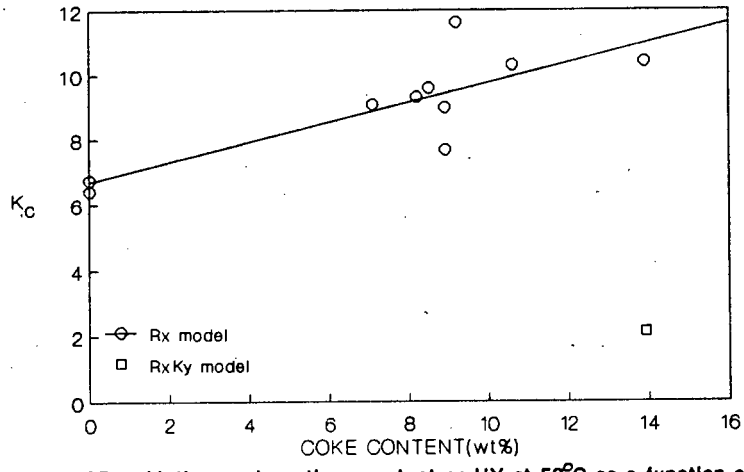

Figure 5.35a : Methane adsorption constant on HY at 50°C as a function of coke content after hexane cracking.

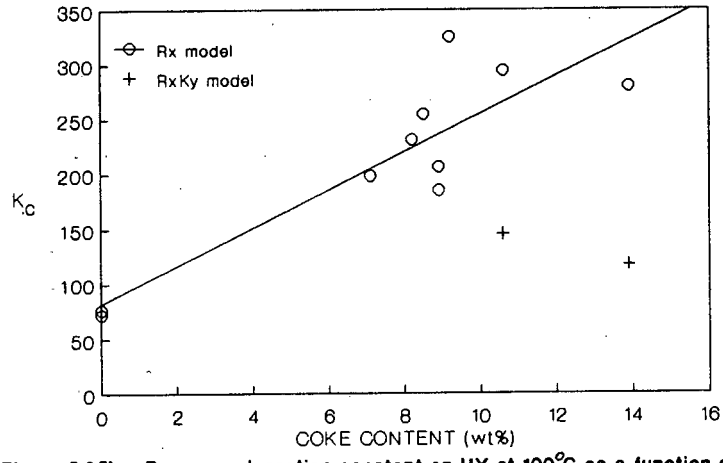

Figure 5.35b : Propane adsorption constant on HY at 100°C as a function of coke content after hexane cracking.

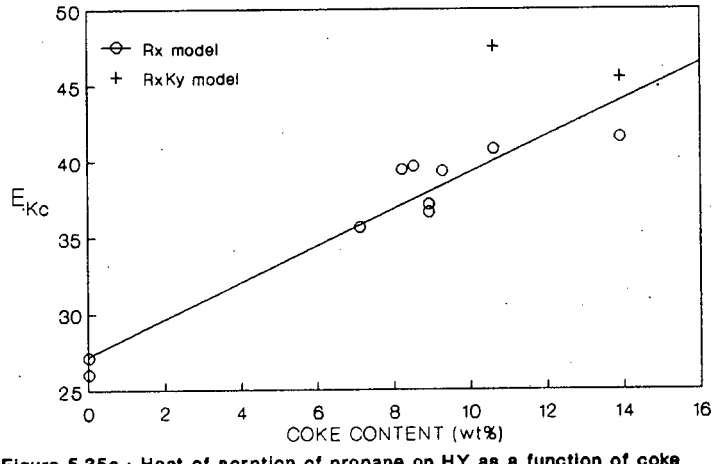

Figure 5.35c : Heat of sorption of propane on HY as a function of coke content after hexane cracking.

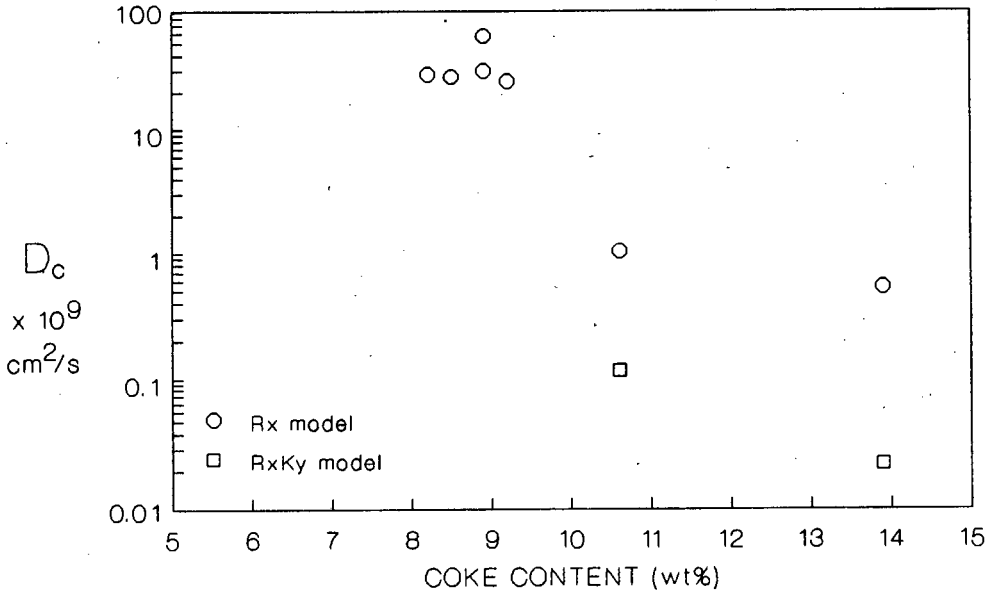

Figure 5.36a : Diffusivity of propane in HY at 100°C as a function of coke content after hexane cracking.

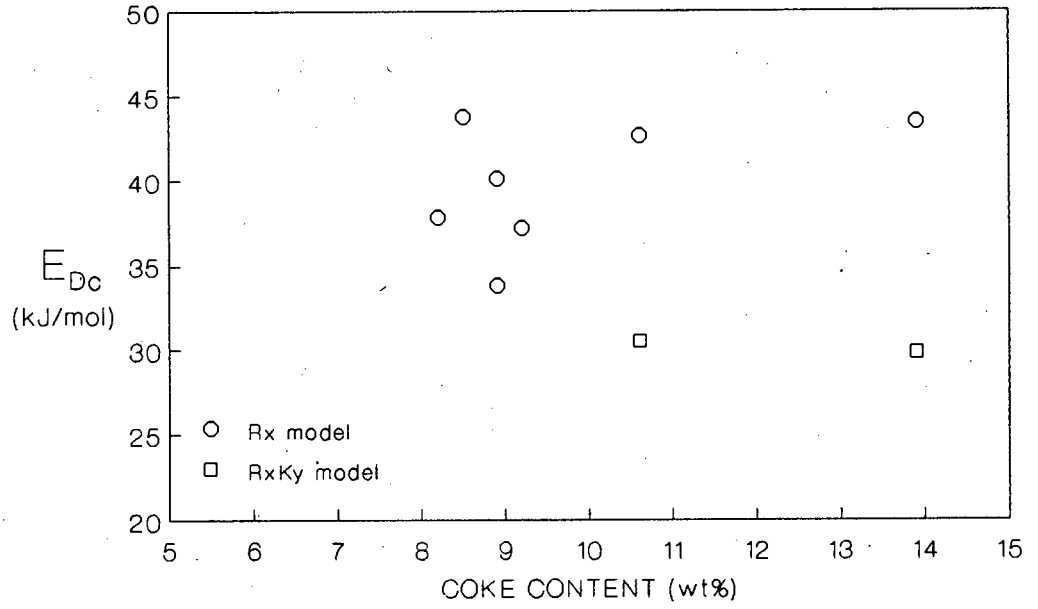

Figure 5.36b : Diffusional activation energy of propane in HY as a function of coke content after hexane cracking.

5.6.5 Adsorption and diffusion in HY and HM after propene oligomerisation

Experimental data for the adsorption and diffusion of methane, propane, n-butane and i-butane in HY and HM after propene oligomerisation are shown in Tables C13 to C31 in Appendix C. Most of the response curves showed severe tailing which affected the accuracy of the estimated parameters. Hence the effect of coke generated by oligomerisation on the catalyst adsorption and diffusion properties was difficult to ascertain. Because of erratic variation of K_c with increasing flow rate, it was also difficult to conclude if the system was in the linear regime.

In the case of HY, K_c and D_c of propane and n-butane showed more variation with velocity than those of methane and i-butane. Increases in D_c with increasing velocity of up to an order of magnitude was observed in some runs while in other cases D_c was approximately constant. Increases in D_c were often accompanied by decreases in K_c. However, D_c also increased for constant values of K_c. Data as a function of flowrate, which yielded a broad band of error values, contributed to the variation of parameters with flowrate.

In the case of HM, the rapid response of the system ($\approx$ 1s), particularly for methane in some runs (e.g., OLIG6, OLIG7), led to difficulty in estimating model parameters using frequency analysis. These fast responses were not observed in HY. Given the extremely short residence time of the tracer gas in the column, data recording was not as accurate as in previous runs. Variations with velocity in K_c of a factor of two and in D_c of an order of magnitude were observed. Butanes in some runs (e.g., OLIG8, OLIG7), however, had sufficiently long residence time for the purpose of data capture and analysis, although large variations with velocity were still observed.

Tables 5.17 to 5.20 summarise the estimated parameters for each model with an indication of the accuracy of the model prediction based on the squared error criterion (see section 5.4). Where possible, heats of sorption and diffusional activation energies were calculated. Coke contents and reaction conditions are shown for the purpose of comparison. The values in these tables were taken at approximately the same velocity (±20%) in an attempt to eliminate some of the effects discussed above.

Singling out the effect of reaction temperature and pressure on model parameters was not possible because of differences in other reaction

Table 5.17 : ADSORPTION AND DIFFUSION IN HY AND HM AFTER PROPENE OLIGOMERISATION USING THE R_M MODEL.

Tracer : Methane

Run ID	T_{reac} °C	P_{reac} atm	T_{max} °C	total coke wt%	hbph wt%	graphitic coke wt%	MP	K_c 50 °C	$D_c \times 10^6$ cm^2/sec
OLIGT	200	53	243	19.1	5.4	13.7	F	4.33	6.22
1	200	52	278	17.3	4.3	13.0	G	7.06	38.1
2	200	52	270	18.4	5.2	13.2	G	3.56	6.96
3	350	50	360	23.0	1.3	21.7	P	6.13	0.223
4	100	53	106	14.8	7.9	6.9	E	3.28	555
5	200	50	320	21.1	4.4	16.7	F	2.33	5.94
6*	250	52	-	12.1	5.4	6.7	F	0.388	480
7*	300	52	-	12.2	2.2	10.0	G	0.456	188
8*	350	53	-	11.1	0.5	10.6	F	0.287	32.8
9	250	30	330	22.4	3.3	19.1	P	1.43	2.14
10	250	30	262	15.7	3.5	12.2	F	3.27	4.41
11	250	64	262	24.1	5.3	18.8	P	1.61	7.64
12	100	50	110	13.7	6.7	7.0	E	3.90	451
13*	300	64	-	10.7	1.9	8.8	G	0.183	30.1
14*	300	64	-	10.0	1.8	8.2	G	0.139	26.2
15*	300	30	-	8.1	0	8.1	F	0.118	43.0
16*	300	50	-	8.1	0	8.1	G	0.231	26.8
17*	300	50	-	8.7	0	8.7	F	0.667	527
18	200	50	255	21.2	4.3	16.9	G	2.08	1.72

* HM; all others HY
hbph - high boiling point hydrocarbons
MP-Model Prediction; P: error > 0.2;
F: 0.05 <error< 0.2;
G: 0.01 <error< 0.05;
E: error < 0.01
OLIG16, OLIG17-regenerated in flowing N_2 at 350 °C
OLIG18-regenerated in flowing N_2 and then reacted again at the same conditions.

Tracer : Propane

Run ID	MP	K_c			$D_c \times 10^{10}$			K_{c_o} x10^4	E_{Kc} kJ/ mol	r^2	D_{c_o} x10^3	E_{Dc} kJ/ mol	r^2
		50°C	100°C	150°C	50°C	100°C	150°C						
OLIGT	G	414	51.7	11.7	0.651	9.42	86.1	1.12	40.6	1.00	57.4	55.4	1.00
1	G	1097	158	38.9	6.93	103	485	7.81	38.0	1.00	53.5	48.6	1.00
2	F	301	41.8	10.7	0.330	6.53	90.4	2.11	38.0	1.00	593	63.6	1.00
3	P	325	51.1	12.9	0.609	2.31	11.7	3.79	36.7	1.00	0.013	33.2	0.99
4	G	207	38.2	-	170	863	-	6.93	33.9	-	3.12	32.5	-
5	F	163	24.9	6.85	0.515	7.92	111	2.32	36.1	1.00	311	60.7	1.00
6*	P	0.635	0.809	0.585	7430	6940	67800	5435	0.6	0.17	3.57	23.8	0.81
7*	P	0.379	0.449	0.444	3960	8700	17600	7805	-1.9	0.88	0.209	16.9	1.00
8*	P	6.62	1.07	0.452	58.2	736	3400	0.634	30.8	0.99	201	46.4	1.00
9	P	41.3	6.64	2.14	34.5	281	939	1.37	33.8	1.00	4.70	37.8	1.00
10	G	381	53.0	12.5	0.323	3.00	26.7	1.97	38.9	1.00	3.47	49.9	1.00
11	P	40.0	6.33	2.64	216	146	758	3.32	31.2	0.99	21E-4	13.1	0.68
12	G	234	40.9	-	154	836	-	5.23	34.9	-	4.66	33.8	-
13*	P	0.825	0.578	0.470	287	4660	10700	745	6.4	1.00	207	41.8	0.98
14*	P	0.395	0.212	0.117	65.7	2730	1850	24.0	13.8	1.00	30.0	39.8	0.86
15*	F	1.55	0.297	0.241	276	1230	3810	3.98	21.7	0.94	1.84	29.8	1.00
16*	P	3.71	0.717	0.361	25.8	361	1120	1.57	26.8	0.99	30.4	43.3	0.99
17*	P	3.05	1.03	0.724	254	4550	25800	58.2	16.6	0.98	9331	52.8	1.00
18	P	54.3	15.4	5.01	2.05	2.96	9.23	24.2	27.0	1.00	86E-6	16.6	0.93

Tracer : n-butane

Run ID	MP	K_c			$D_c \times 10^{10}$			K_{c_o} x10^5	E_{Kc} kJ/ mol	r^2	D_{c_o} x10^3	E_{Dc} kJ/ mol	r^2
		50°C	100°C	150°C	50°C	100°C	150°C						
OLIGT	G	-	296	42.2	-	1.89	17.3	2.06	51.1	-	25.8	58.1	-
1	E	-	1010	177	-	14.0	102	40.3	45.7	-	27.7	52.1	-
2	F	-	238	35.7	-	1.10	22.0	2.55	49.8	-	11171	78.6	-
3	P	-	327	47.8	-	0.486	3.25	2.81	50.4	-	0.466	49.9	-
4	G	1604	200	-	28.3	162	-	28.2	41.7	-	1.27	35.0	-
5	F	-	124	20.8	-	1.72	27.3	3.42	46.8	-	2471	72.5	-
6*	P	1.25	0.880	0.627	1720	5850	10100	6934	7.8	1.00	0.356	20.3	0.99
7*	P	0.703	0.961	0.439	2840	30700	9380	14085	4.8	0.53	0.138	15.3	0.57
8*	P	50.1	3.56	0.806	10.1	135	1500	0.106	47.2	1.00	1321	56.6	1.00
9	P	344	29.5	5.76	9.05	73.3	489	0.964	46.6	1.00	17.2	45.1	1.00
10	F	-	297	49.0	-	0.591	4.85	7.12	47.3	-	3.20	55.2	-
11	P	-	27.5	6.30	-	39.4	361	10.6	38.7	-	542	58.1	-
12	F	1672	203	-	-	145	-	24.6	42.2	-	-	-	-
13*	P	2.69	0.627	0.454	21.9	989	5500	108	20.7	0.96	48629	63.5	0.99
14*	P	1.11	0.341	0.198	24.5	861	4290	66.1	19.8	0.99	11475	59.3	0.99
15*	P	10.3	0.869	0.336	37.7	351	2750	0.373	39.4	0.99	251	48.5	1.00
16*	P	40.6	2.74	0.659	2.26	40.0	344	0.086	47.2	1.00	392	57.1	1.00
17*	P	18.6	2.41	1.01	22.6	361	9030	6.38	33.5	0.99	1.5e6	67.4	0.99
18	P	457	56.1	13.8	0.532	3.08	3.08	25.8	39.9	1.00	99E-6	20.1	1.00

Tracer : i-butane

Run ID	MP	K_c			$D_c \times 10^{10}$			K_{c_0} x10^3	E_{Kc} kJ/ mol	r^2	D_{c_0} x10^3	E_{Dc} kJ/ mol	r^2
		50°C	100°C	150°C	50°C	100°C	150°C						
OLIGT	P	-	159	28.0	-	0.325	4.34	6.62	45.6	-	108	68.0	-
1	F	-	801	150	-	4.85	41.8	56.1	44.0	-	39.8	56.5	-
2	P	-	115	24.3	-	0.704	8.06	22.4	40.8	-	63.8	64.0	-
3	P	-	74.3	13.5	-	17.5	113	4.03	44.7	-	12.5	48.9	-
4	G	1169	163	-	23.9	170	-	48.4	39.5	-	5.43	39.3	-
5	P	-	47.7	13.3	-	2.09	13.9	96.8	33.5	-	1.91	49.7	-
6*	P	0.896	0.678	0.594	2180	7570	28100	15276	4.7	0.99	9.46	28.8	1.00
7*	P	0.653	0.530	0.404	-	65200	11400	8935	5.4	0.99	-	-	-
8*	P	21.9	2.25	0.596	3.06	60.4	1190	0.450	41.2	1.00	21180	67.3	1.00
9	G	152	16.6	4.02	9.06	40.4	170	2.91	41.4	1.00	0.197	33.1	1.00
10	P	-	100	24.7	-	0.320	1.97	72.8	36.7	-	0.152	47.7	-
11	P	-	14.8	4.25	-	3.74	94.0	38.5	32.7	-	2.6E5	84.6	-
12	G	1281	178	-	19.7	161	-	51.7	39.5	-	12.6	42.1	-
13*	P	0.648	0.499	0.425	2160	4430	9440	10723	4.8	1.00	0.102	16.6	1.00
14*	P	0.219	0.233	0.133	3840	5260	3120	3338	5.3	0.76	21E-8	1.9	0.32
15*	P	3.70	0.477	0.234	75.7	675	3980	2.28	31.8	0.98	138	44.9	1.00
16*	P	2.99	0.748	0.285	173	1880	1360	13.9	26.8	1.00	0.238	24.6	0.84
17*	P	6.46	1.38	0.761	31.8	8960	8960	61.1	24.6	0.99	80239	64.2	1.00
18	P	134	17.9	3.99	6.76	113	113	4.63	39.9	1.00	0.109	32.1	1.00

Table 5.18 : ADSORPTION AND DIFFUSION IN HM AFTER PROPENE OLIGOMERISATION USING THE MACRO-MODEL.

Tracer : methane

Run ID	MP	K_y at 50°C	$D_y \times 10^3$ at 50°C
OLIG6	P	0.903	14.9
7	G	1.05	6.65
8	P	0.649	1.58
13	F	0.417	1.74
14	F	0.317	2.02
15	P	0.278	3.28
16	F	0.520	1.48
17	F	1.54	14.5

Tracer : propane

Run ID	MP	K_y			$D_y \times 10^3$			$K_{y\,o}$ $\times 10^3$	E_{Ky} kJ/mol	r^2	$D_{y\,o}$ $\times 10^2$	E_{Dy} kJ/mol	r^2
		50°C	100°C	150°C	50°C	100°C	150°C						
OLIG6	P	1.45	1.84	1.35	2.84	2.71	21.1	-	-	-	626	21.6	0.81
7	P	0.856	1.02	1.03	1.88	3.32	5.76	1960	-2.2	0.92	20.5	12.7	1.00
8	P	13.6	2.27	1.01	0.173	0.521	1.60	0.185	29.9	0.99	0.019	5.1	0.80
13	P	1.61	1.30	1.08	0.299	1.97	3.72	300	4.5	1.00	1730	29.1	0.98
14	P	0.524	0.476	0.259	0.269	1.88	2.24	32.5	7.7	0.89	344	24.8	0.93
15	P	3.17	0.625	0.543	0.288	0.965	2.11	1.20	20.7	0.93	138	22.7	1.00
16	P	6.74	1.40	0.751	0.084	0.367	0.859	0.505	25.3	0.99	178	26.6	1.00
17	P	6.45	2.33	1.67	0.333	2.11	8.05	18.0	15.6	0.98	24300	36.2	1.00

Tracer : n-butane

Run ID	MP	K_y			$D_y \times 10^4$			$K_{y\,o}$ $\times 10^3$	E_{Ky} kJ/mol	r^2	$D_{y\,o}$ $\times 10^2$	E_{Dy} kJ/mol	r^2
		50°C	100°C	150°C	50°C	100°C	150°C						
OLIG6	P	2.77	1.99	1.43	9.79	25.0	36.9	174	7.5	1.00	30.3	15.3	0.99
7	P	1.56	2.21	1.01	14.1	102	34.5	368	4.3	0.49	16.5	11.6	0.52
8	P	105	7.34	1.74	1.82	2.32	8.85	25E-4	46.9	1.00	9.49	17.3	0.90
13	P	4.47	1.31	1.03	0.752	7.20	23.2	6.92	17.1	0.96	18500	39.3	1.00
14	P	1.47	0.695	0.451	10.0	7.91	27.0	9.42	13.5	1.00	3.94	10.5	0.71
15	P	21.1	1.71	0.740	1.69	3.51	15.6	98E-4	38.7	0.98	144	24.7	0.96
16	P	75.9	4.95	1.25	0.599	1.06	3.89	17E-4	47.0	0.99	11.8	20.8	0.96
17	P	38.4	5.09	2.30	1.70	4.07	36.1	0.195	32.4	0.99	3950	33.8	0.95

Tracer : i-butane

Run ID	MP	K_y			D_y x 10^4			K_{ye} x10^3	E_{Ky} kJ/ mol	r^2	D_{ye} x10^2	E_{Dy} kJ/ mol	r^2
		50°C	100°C	150°C	50°C	100°C	150°C						
OLIG6	P	1.99	1.54	1.37	11.1	29.2	93.6	398	4.3	1.00	781	24.0	0.99
7	F	1.51	1.23	0.930	3.47	177	38.4	204	5.4	0.99	4960	29.9	0.67
8	P	39.0	4.15	1.26	0.510	1.24	7.74	0.016	39.3	1.00	328	30.2	0.96
13	P	1.43	1.12	0.975	11.6	19.3	34.9	278	4.4	1.00	11.3	12.4	0.99
14	P	0.500	0.533	0.303	22.3	28.6	26.7	75.7	5.3	0.76	0.526	2.2	0.75
15	P	7.38	0.961	0.529	1.63	5.99	23.2	0.074	30.5	0.97	1080	30.0	1.00
16	P	6.25	1.64	0.602	2.39	10.5	10.3	0.312	26.6	1.00	17.8	17.3	0.90
17	P	12.7	2.96	1.73	1.18	6.55	33.9	2.23	23.0	0.98	15300	38.0	1.00

Table 5.19 : ADSORPTION AND DIFFUSION IN HY AND HM AFTER PROPENE OLIGOMERISATION USING THE R_xK_y MODEL.

Tracer : methane

Run ID	MP	K_y at 50°C	K_c at 50°C	D_c x 10^{10} at 50°C
OLIG3	E	3.86	4.80	3.52
6*	F	0.851	0.032	43.4
9	G	1.48	0.927	5.72
11	E	2.00	0.560	20.8
15*	G	0.193	0.045	207

Tracer : propane

Run ID	MP	K_y			K_c			D_c x 10^{10}		
		50°C	100°C	150°C	50°C	100°C	150°C	50°C	100°C	150°C
OLIGT	E	51.7	15.5	7.01	387	43.1	7.69	0.530	5.94	33.8
2	E	71.1	14.3	5.39	272	34.5	7.63	0.189	3.42	40.0
3	G	196	43.1	9.06	241	47.8	12.0	0.133	0.181	0.778
5	G	51.9	10.3	4.00	146	20.2	4.65	0.214	3.11	40.4
6*	F	1.31	1.61	1.30	0.176	0.192	4.15	15.4	49.3	-
7*	G	0.741	0.776	0.937	0.251	0.127	0.067	4.77	589	55.4
8*	E	5.08	1.33	0.594	5.03	0.614	0.212	16.4	84.3	577
9	G	50.6	8.60	2.87	14.9	2.37	0.704	0.990	4.00	8.89
11	G	38.2	7.22	3.54	19.5	3.07	1.00	2.57	3.97	5.36
13*	F	0.900	1.13	0.973	0.783	0.194	0.133	14.4	24.8	17.0
14*	F	0.163	0.367	0.127	0.560	0.120	0.073	8.98	25.4	322
15*	G	1.64	0.369	0.228	1.11	0.186	0.147	32.4	106	1360
16*	G	2.33	0.815	0.343	4.48	0.712	0.244	2.81	14.1	245
17*	G	3.88	1.92	1.60	1.89	0.281	0.784	19.3	107	0.110
18	G	56.0	11.3	3.21	50.2	21.0	6.00	0.109	0.159	0.884

Tracer : n-butane

Run ID	MP	K_y			K_c			$D_e \times 10^{10}$		
		50°C	100°C	150°C	50°C	100°C	150°C	50°C	100°C	150°C
OLIGT	F	-	2.42	4.01	-	294	39.9	-	1.87	15.4
1	E	-	7.60	-	-	1006	-	-	14.0	-
2	G	-	108	7.56	-	185	31.4	-	0.428	16.5
3	G	-	210	30.7	-	267	41.0	-	0.0626	0.362
5	F	-	24.7	5.4	-	112	17.8	-	1.19	18.5
6*	G	2.10	1.78	1.29	0.460	0.306	0.146	67.8	12.7	31.2
7*	F	1.32	2.10	0.920	0.355	0.125	0.223	11.4	14.2	3.15
8*	E	38.3	2.67	1.12	36.9	2.65	0.404	3.24	43.2	134
9	G	315	36.6	7.55	157	9.53	1.65	2.26	2.57	10.5
11	F	-	29.0	7.96	-	12.5	2.09	-	2.79	8.82
13*	F	1.31	0.873	0.871	3.80	0.445	0.179	2.46	32.6	26.0
14*	G	0.421	0.473	0.359	2.43	0.343	0.098	1.36	12.9	30.6
15*	E	9.63	0.871	0.484	7.86	0.714	0.158	5.72	34.5	226
16*	F	16.6	1.41	0.668	40.8	2.84	0.663	0.738	8.99	19.6
17*	G	18.0	3.13	2.00	14.0	1.50	0.189	3.19	25.2	143
18	F	439	51.3	8.81	308	55.2	18.2	0.0984	0.115	0.234

Tracer : i-butane

Run ID	MP	K_y			K_c			$D_e \times 10^{10}$		
		50°C	100°C	150°C	50°C	100°C	150°C	50°C	100°C	150°C
OLIGT	F	-	54.8	6.88	-	159	25.0	-	0.0845	2.49
1	G	-	753	122	-	356	76.2	-	1.05	14.1
2	G	-	49.0	11.8	-	107	19.5	-	0.161	2.35
3	G	-	79.9	14.5	-	32.4	5.50	-	1.15	4.99
5	G	-	23.9	7.42	-	42.8	10.6	-	0.388	2.99
6*	G	1.58	1.33	1.29	0.336	0.165	0.086	44.0	71.0	20.3
7*	F	1.48	1.18	0.830	0.371	0.449	0.083	0.0051	0.0822	51.4
8*	G	2.44	1.34	0.730	21.7	2.15	0.350	2.35	13.9	138
10	G	-	24.3	6.81	-	103	24.2	-	0.116	0.708
11	G	-	3.60	2.27	-	14.1	3.07	-	1.70	33.0
13*	G	1.21	0.902	0.886	0.722	0.166	0.216	1.87	87.5	4.01
14*	F	0.415	0.432	0.185	0.124	0.086	0.065	11.0	53.5	264
15*	G	3.50	0.542	0.375	3.22	0.364	0.096	7.63	51.4	196
16*	F	4.18	1.27	0.113	3.46	0.389	0.241	1.63	27.7	874
17*	F	5.80	2.23	1.59	6.92	0.869	0.267	2.14	12.3	6.75
18	F	178	25.2	6.00	63.2	9.05	2.88	0.875	2.26	1.64

Table 5.20 : HEATS OF SORPTION AND DIFFUSIONAL ACTIVATION ENERGY FOR HY AND HM AFTER PROPENE OLIGOMERISATION USING THE R_xK_y MODEL.

Tracer : propane

Run ID	K_{ye} x 10^3	E_{Ky} kJ/mol	r^2	K_{ce} x 10^4	E_{Kc} kJ/mol	r^2	D_{ce} x 10^3	E_{Dc} kJ/mol	r^2
OLIGT	10.5	22.8	1.00	0.249	44.5	1.00	2.37	47.3	1.00
2	1.18	29.4	1.00	0.722	40.6	1.00	118	60.7	1.00
3	0.440	34.9	1.00	7.85	34.0	1.00	1.48E-5	19.4	0.91
5	0.911	29.3	1.00	0.669	39.2	1.00	74.6	59.2	1.00
6*	-	-	-	3.64E7	-34.2	0.84	9.06E-3	23.3	-
7*	1888	-2.6	0.92	9.84	14.9	1.00	0.0148	31.3	0.57
8*	0.534	24.5	1.00	0.0625	36.3	0.99	4.43	40.1	0.99
9	0.246	32.7	1.00	0.343	34.8	1.00	1.18E-3	25.1	1.00
11	1.32	27.3	0.99	0.611	33.9	1.00	5.83E-6	8.4	1.00
13*	-	-	-	3.36	20.5	0.97	3.91E-6	2.3	0.37
14*	-	-	-	0.784	23.5	0.98	1.75	39.7	0.95
15*	0.304	22.8	0.98	1.40	23.6	0.94	12.8	41.5	0.96
16*	0.721	21.7	1.00	0.178	33.2	1.00	24.7	49.8	0.97
17*	80.1	10.3	0.97	-	-	-	0.683	34.3	-
18	0.318	32.5	1.00	78.4	23.8	0.98	4.46E-5	23.0	0.91

Tracer : n-butane

Run ID	K_{ye} X 10^3	E_{Ky} kJ/mol	r^2	K_{ce} x 10^5	E_{Kc} kJ/mol	r^2	D_{ce} x 10^3	E_{Dc} kJ/mol	r^2
OLIGT	174000	-13.2	-	1.35	52.4	-	10.4	55.3	-
2	1.83E-5	69.8	-	5.64	46.5	-	1.12E6	95.8	-
3	0.0181	50.4	-	3.49	49.2	-	0.0175	46.0	-
5	0.0641	39.9	-	1.96	48.3	-	1430	72.0	-
6*	288	5.4	0.97	421	12.8	0.97	1.13E-7	-10.1	0.53
7*	447	3.4	0.37	2960	6.1	0.51	9.27E-9	-13.7	0.74
8*	8.02E-3	40.8	0.98	0.0179	51.4	1.00	3.07	42.8	0.99
9	0.0430	42.4	1.00	0.0581	52.0	1.00	9.17E-5	16.7	0.87
11	0.516	33.9	-	51.6	33.9	-	4.73E-3	30.2	-
13*	208	4.8	0.90	0.705	35.1	0.99	0.0121	28.0	0.87
14*	246	1.6	0.51	0.280	36.6	1.00	0.0983	35.9	0.99
15*	0.0193	34.7	0.97	0.0463	44.6	1.00	2.68	41.5	1.00
16*	0.0136	37.1	0.98	0.0887	47.1	1.00	0.119	37.9	0.98
17*	1.19	25.5	0.97	0.0198	48.7	1.00	2.91	43.1	1.00
18	0.0303	44.3	1.00	182	32.2	1.00	3.08E-7	9.5	0.91

Tracer : i-butane

Run ID	K_{ye} x 10^3	E_{Ky} kJ/mol	r^2	K_{ce} x 10^5	E_{Kc} kJ/mol	r^2	D_{ce} x 10^3	E_{Dc} kJ/mol	r^2
OLIGT	1.30E-3	54.4	-	2.54	48.5	-	22800	88.8	-
1	0.155	47.7	-	77.2	40.4	-	367	68.1	-
2	0.288	37.4	-	5.95	44.7	-	134	70.3	-
3	0.0429	44.8	-	0.988	46.5	-	0.0284	38.5	-
5	1.20	30.7	-	31.9	36.6	-	1.23	53.6	-
6*	645	2.4	0.95	110	15.4	1.00	3.12E-7	7.8	0.55
7*	137	6.5	0.98	131	16.0	0.76	8.47E6	102.2	0.95
8*	15.7	13.6	1.00	0.0579	46.9	1.00	5.01	45.7	0.99
10	0.515	33.4	-	49.1	38.0	-	0.0513	47.5	-
11	72.8	12.1	-	3.53	40.0	-	13400	77.8	-
13*	300	3.7	0.92	260	14.5	0.82	4.52E-5	12.1	0.26
14*	18.9	8.7	0.80	807	7.3	1.00	0.655	35.9	1.00
15*	0.186	26.0	0.96	0.100	40.1	1.00	0.733	36.9	1.00
16*	1.72E-3	40.2	0.96	2.82	30.9	0.96	35200	70.0	0.99
17*	21.0	14.9	0.98	0.623	37.2	1.00	5.71E-5	14.2	0.70
18	0.103	38.5	1.00	11.8	35.3	1.00	1.89E-6	7.7	0.71

parameters (e.g., WHSV, temperature runaway, total time on stream). One parameter which incorporated the effect of varying reaction conditions is the coke content. As discussed in Chapter 3 "coke" deposited during oligomerisation was broadly classified into two catogories, viz., high boiling point hydrocarbons and graphitic coke. To facilitate comparison with the data obtained from cracking, the estimated adsorption and diffusion parameters were plotted against wt% graphitic coke. In this way the effect of high boiling point hydrocarbons on the transport properties was more easily seen. It should be recalled, however, that the amount of graphitic coke computed from TG/DTA spectra could be an overestimation.

Considering first the model predictions in HY, the R_x model was found to apply to methane diffusion in most cases (Figures 5.37a and b), except at high graphitic coke content for which the R_xK_y model was necessary (Figure 5.37c). The figures show that the model prediction was acceptable. In the case of propane, Figure 5.38a shows that the R_xK_y model was necessary to predict the response curves, and that only at lower graphitic coke contents which had larger D_c did the R_xK_y model degenerate into the R_x model (Figure 5.38b) and lead to a poor determination of K_y. The same phenomena were observed for n- and i-butane shown in Figures 5.39a-c and 5.40a and b. The analysis of the data showed that the R_xK_y model had to be applied to successively lower critical graphitic coke contents (viz., the graphitic coke levels at which K_y had to be introduced for good curve fits) as the tracer gas molecules became larger. However, i-butane showed anomalous behaviour in that OLIG9 (19.1% graphitic coke) was well predicted by the R_x model while OLIG10 (12.2%) required the use of the R_xK_y model. This was not observed in the case of n-butane or propane. In some cases such as those shown in Figure 5.39c and 5.40b no model was able to fit the data well. Considering the difficulty involved in measuring transport properties inside deactivated catalyst samples using the GC technique, it was felt that the agreement between theory and experiment was sufficient for the determination of marked trends.

The methane adsorption constant in HY decreased with an increase in coke content (Figure 5.41a) except for OLIG1 (13.7%) and OLIG3 (21%) which showed greater adsorption than the rest. Figure 5.41b shows that D_c decreased by four orders of magnitude in the range of coke content examined. The R_xK_y model, which predicted the experimental data well (when applicable), gave considerably lower values of K_c and D_c. Similar trends in K_c were observed for propane, n- and i-butane shown in Figures 5.42a, 5.44a and 5.46a, respectively. The variation of K_c in coked catalyst relative to K_c in fresh

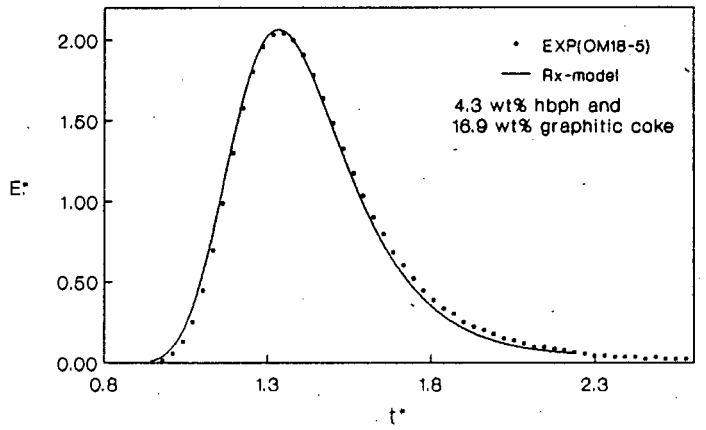

Figure 5.37a : E* vs t* of experimental data and model predictions for methane in HY at 50°C after propene oligomerisation (OLIG18); run OM18-5.

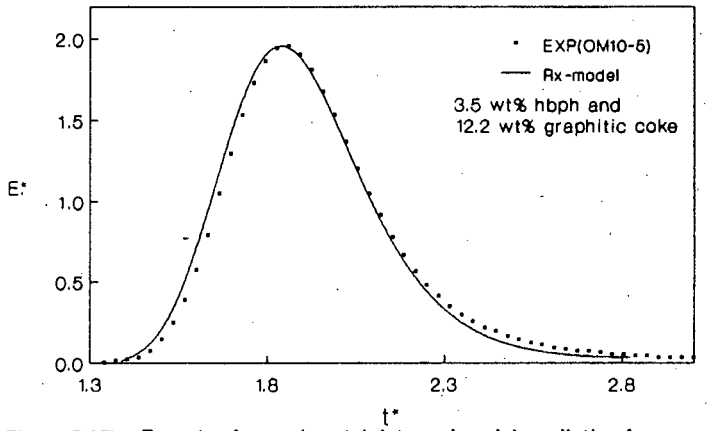

Figure 5.37b : E* vs t* of experimental data and model prediction for methane in HY at 50°C after propene oligomerisation (OLIG10); run OM10-5.

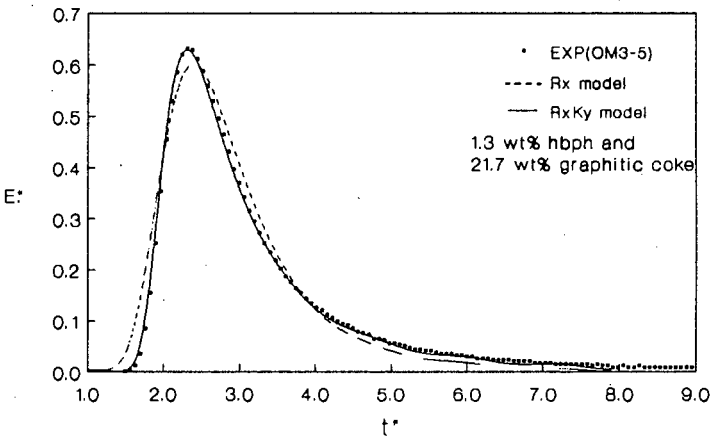

Figure 5.37c : E* vs t* of experimental data and model prediction for methane in HY at 50°C after propene oligomerisation; run OM3-5.

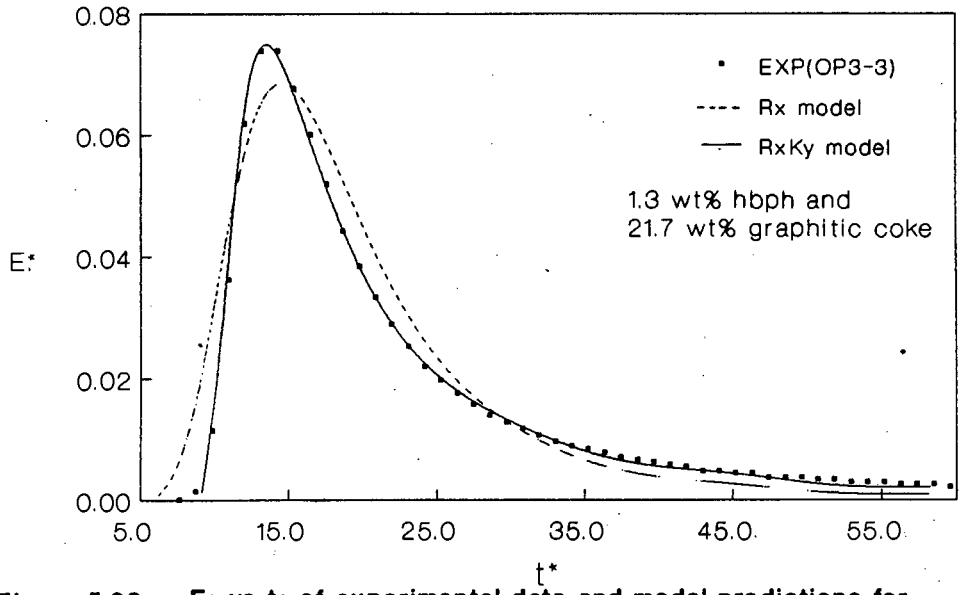

Figure 5.38a : E* vs t* of experimental data and model predictions for propane in HY at 100°C after propene oligomerisation (OLIG3); run OP3-3.

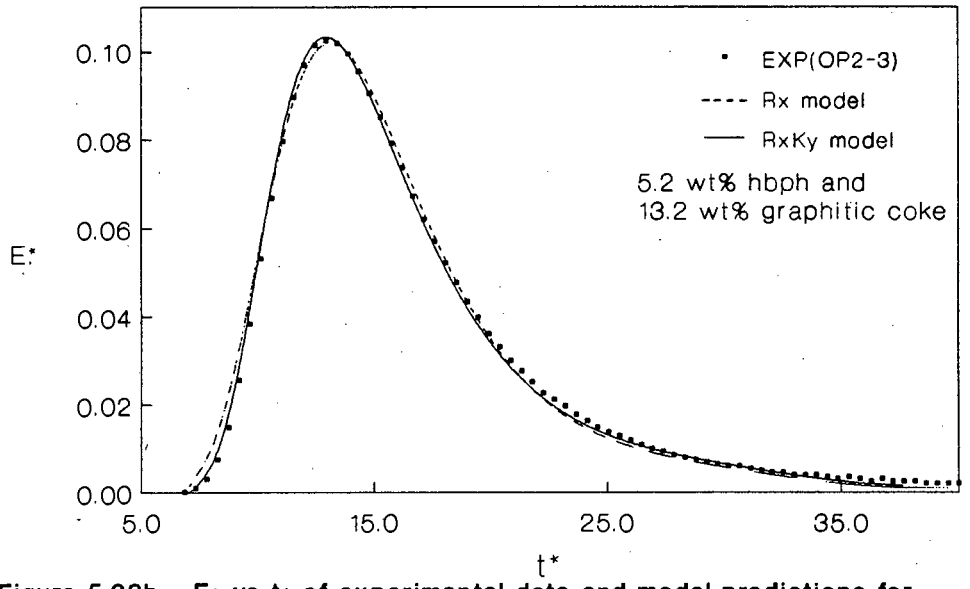

Figure 5.38b : E* vs t* of experimental data and model predictions for propane in HY at 100°C after propene oligomerisation (OLIG2); run OP2-3.

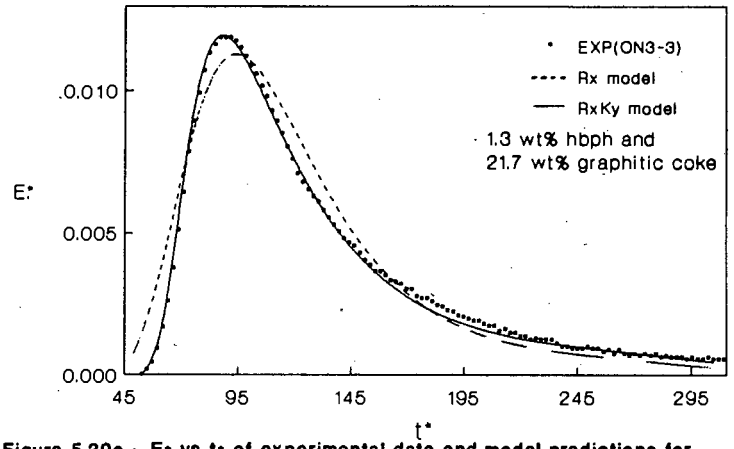

Figure 5.39a : E* vs t* of experimental data and model predictions for n-butane in HY at 100°C after propene oligomerisation (OLIG3); run ON3-3.

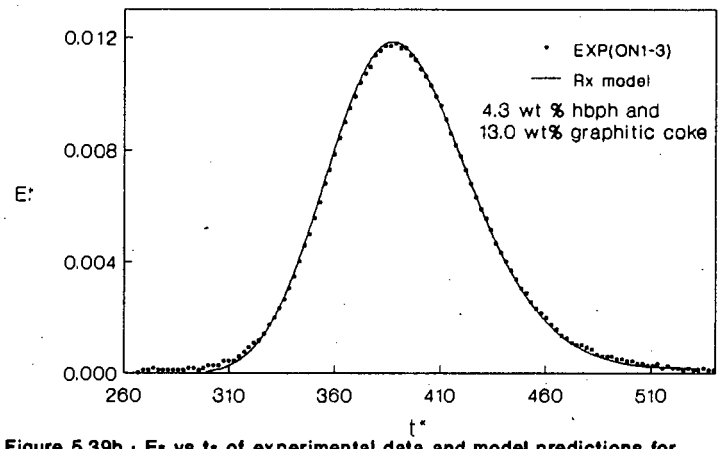

Figure 5.39b : E* vs t* of experimental data and model predictions for n-butane in HY at 100°C after propene oligomerisation (OLIG1); run ON1-3.

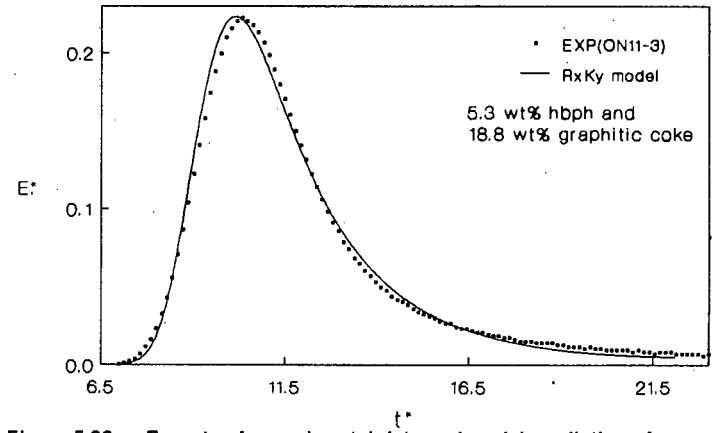

Figure 5.39c : E* vs t* of experimental data and model predictions for n-butane in HY at 100°C after propene oligomerisation (OLIG11); run ON11-3.

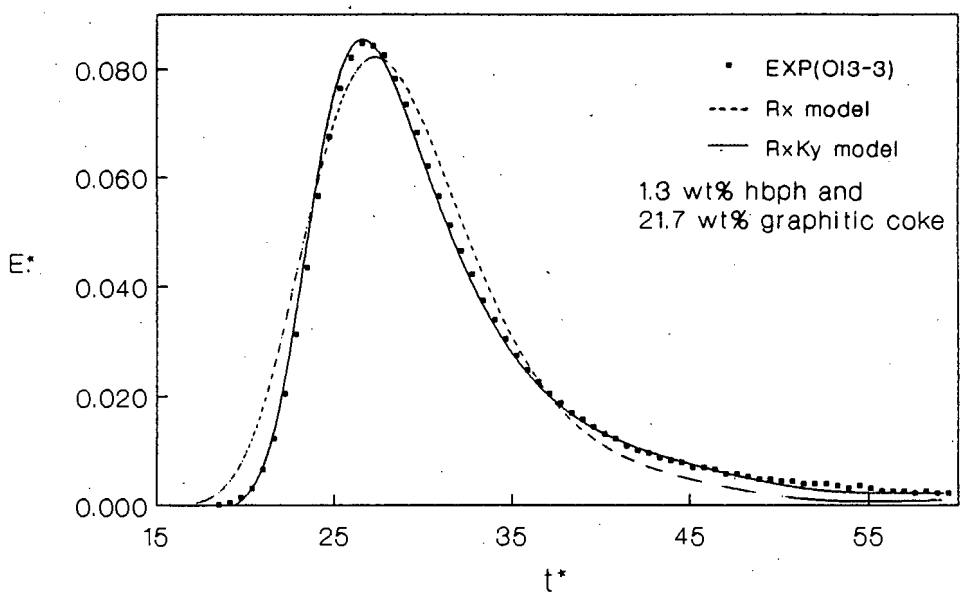

Figure 5.40a : E* vs t* of experimental data and model predictions for i-butane in HY at 100°C after propene oligomerisation (OLIG3); run OI3-3.

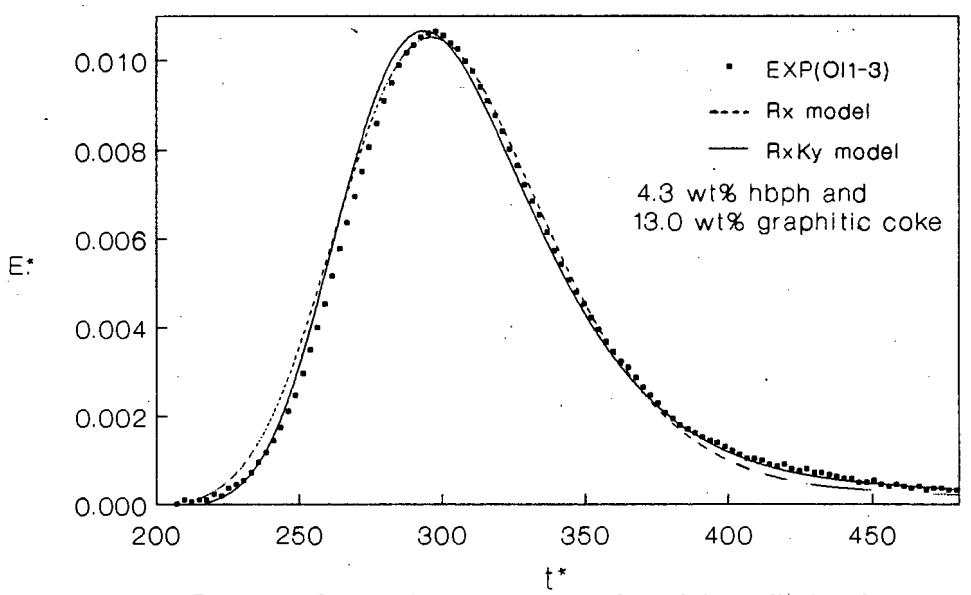

Figure 5.40b : E* vs t* of experimental data and model prediction for i-butane in HY at 100°C after propene oligomerisation (OLIG1); run OI1-3.

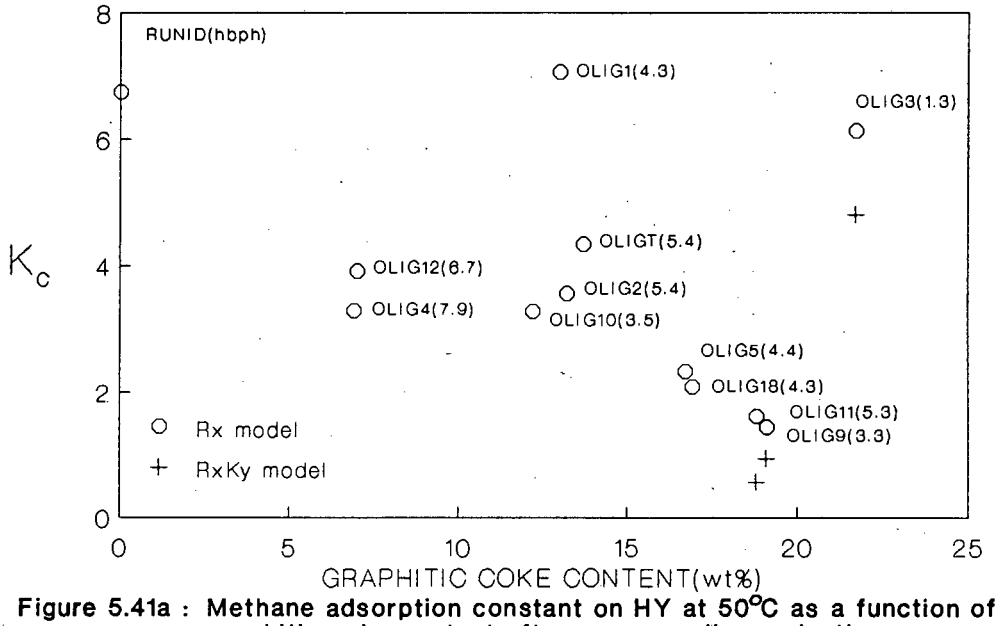

Figure 5.41a : Methane adsorption constant on HY at 50°C as a function of graphitic coke content after propene oligomerisation.

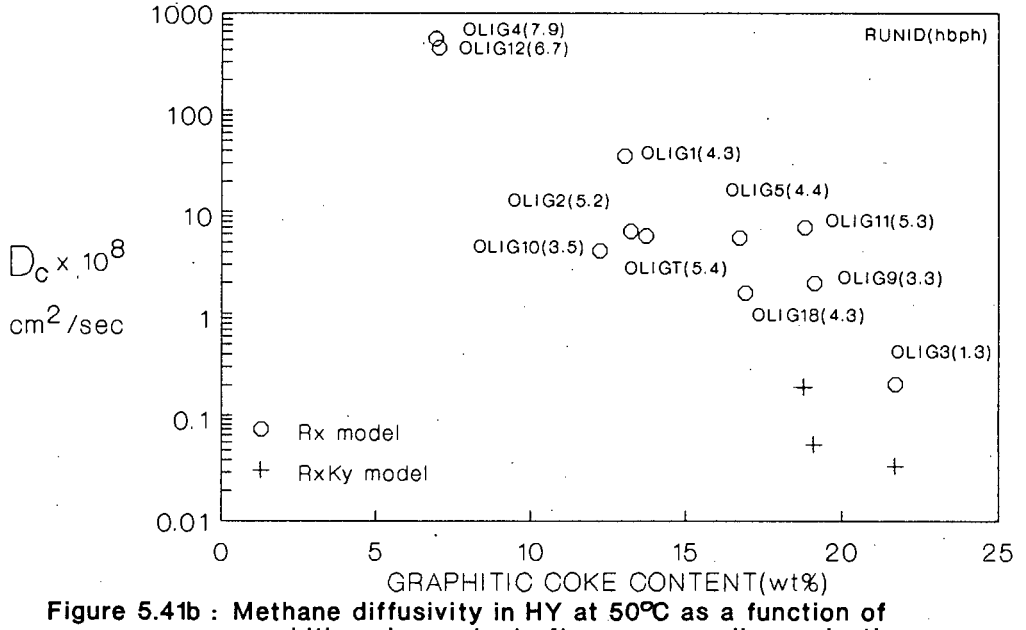

Figure 5.41b : Methane diffusivity in HY at 50°C as a function of graphitic coke content after propene oligomerisation.

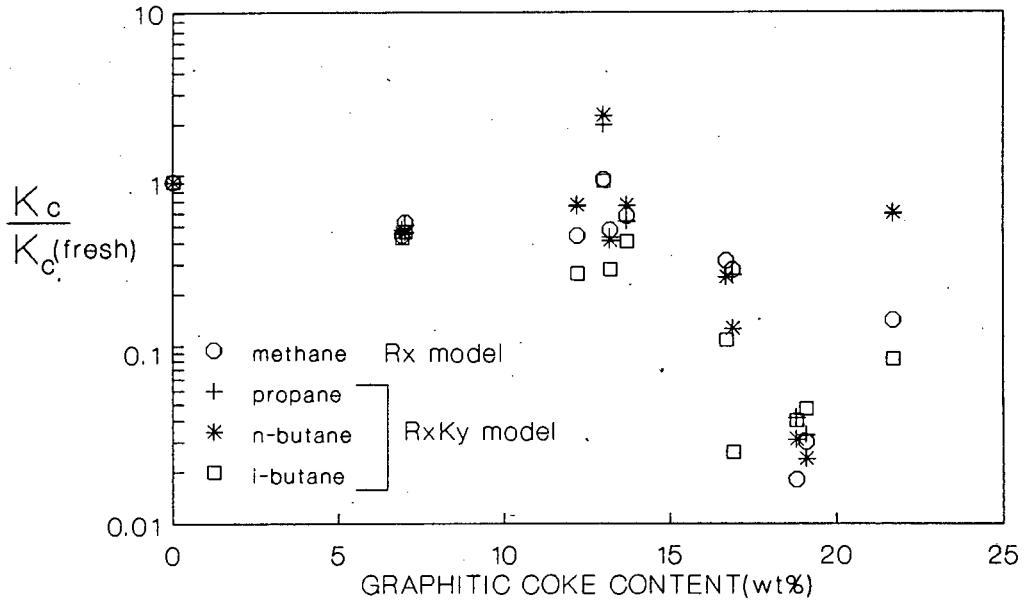

Figure 5.41C : Relative adsorption constant in HY as a function of graphitic coke content after propene oligomerisation.

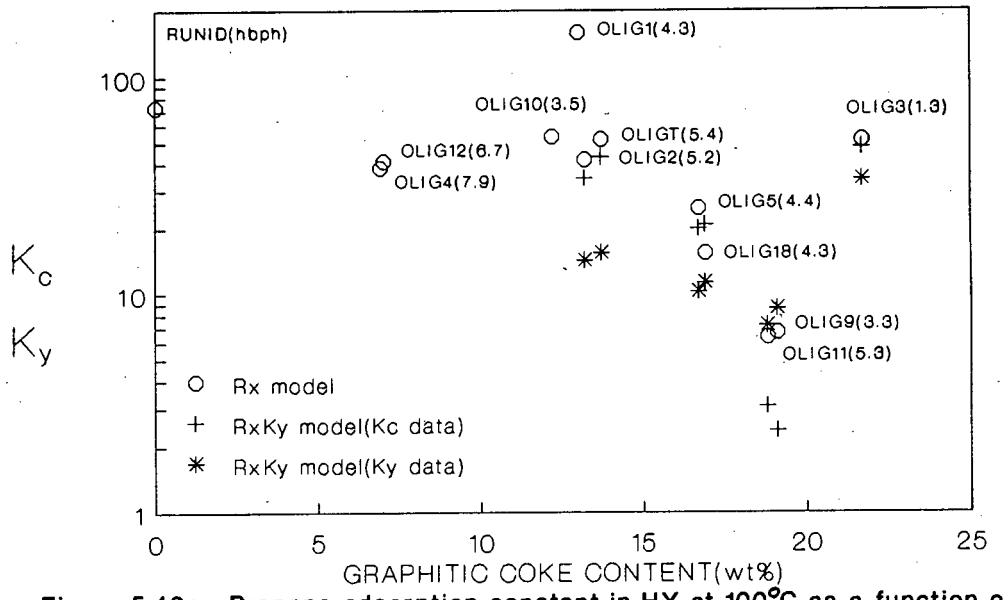

Figure 5.42a : Propane adsorption constant in HY at 100°C as a function of graphitic coke content after propene oligomerisation.

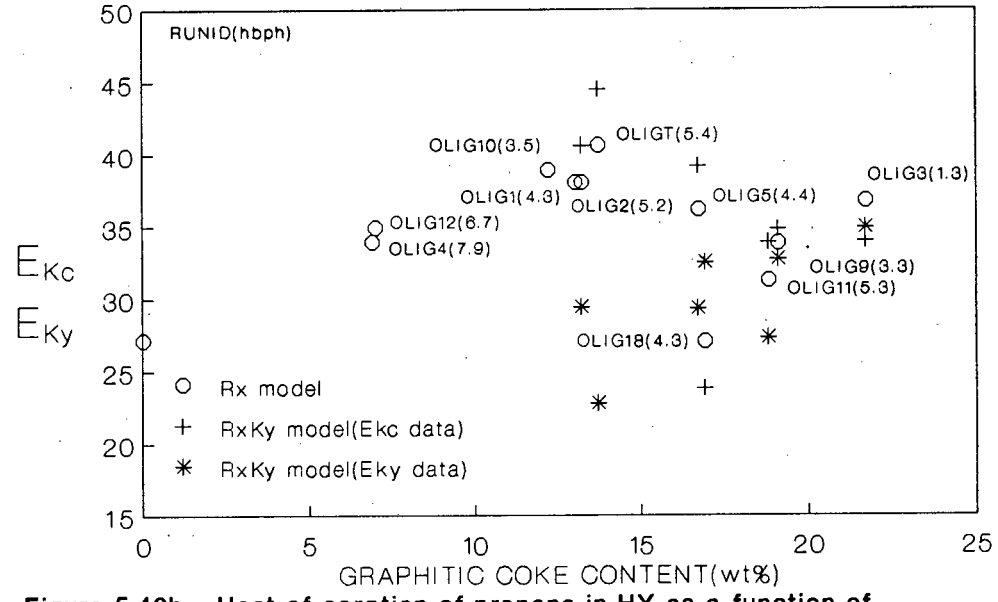

Figure 5.42b : Heat of sorption of propane in HY as a function of graphitic coke content after propene oligomerisation.

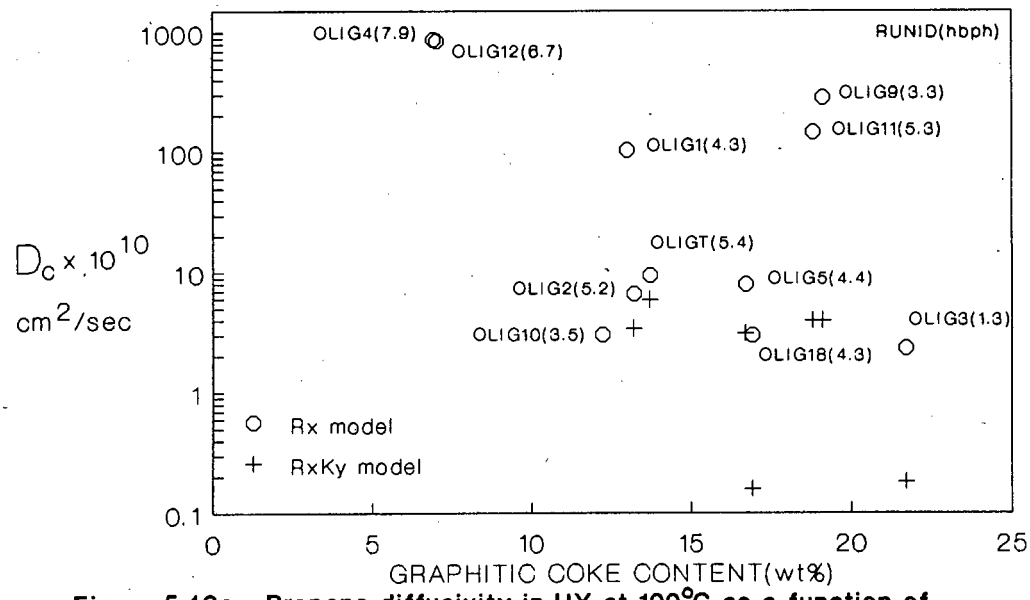

Figure 5.43a : Propane diffusivity in HY at 100°C as a function of graphitic coke content after propene oligomerisation.

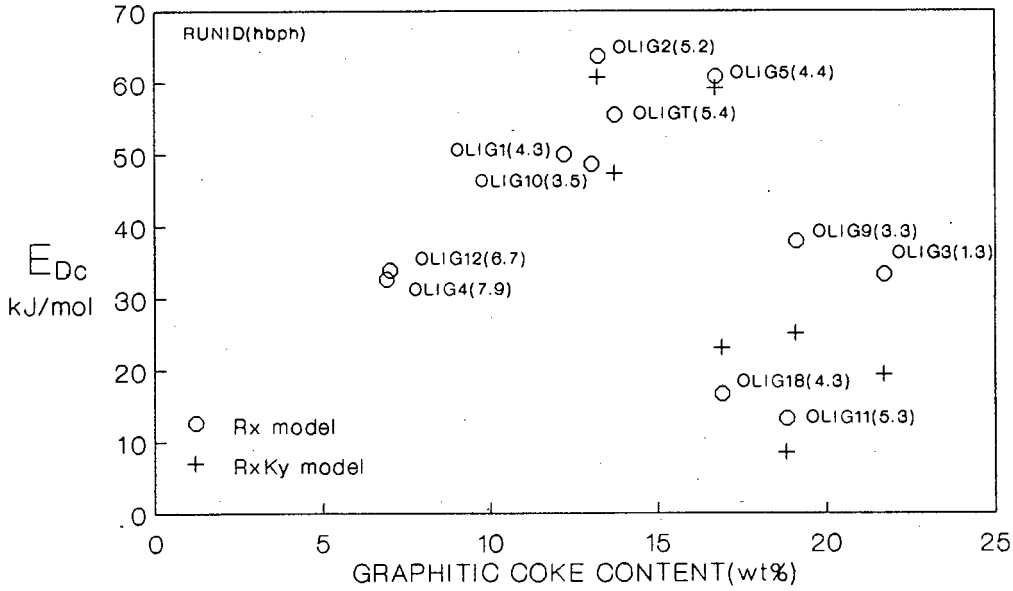

Figure 5.43b : Diffusional activation energy of propane in HY as a function of graphitic coke content after propene oligomerisation.

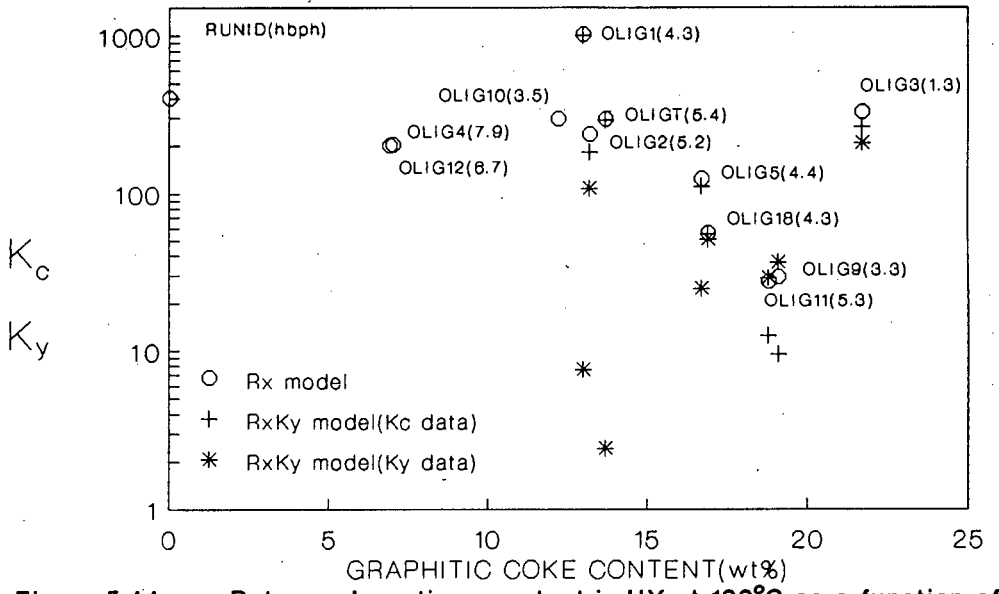

Figure 5.44a : n-Butane adsorption constant in HY at 100°C as a function of graphitic coke content after propene oligomerisation.

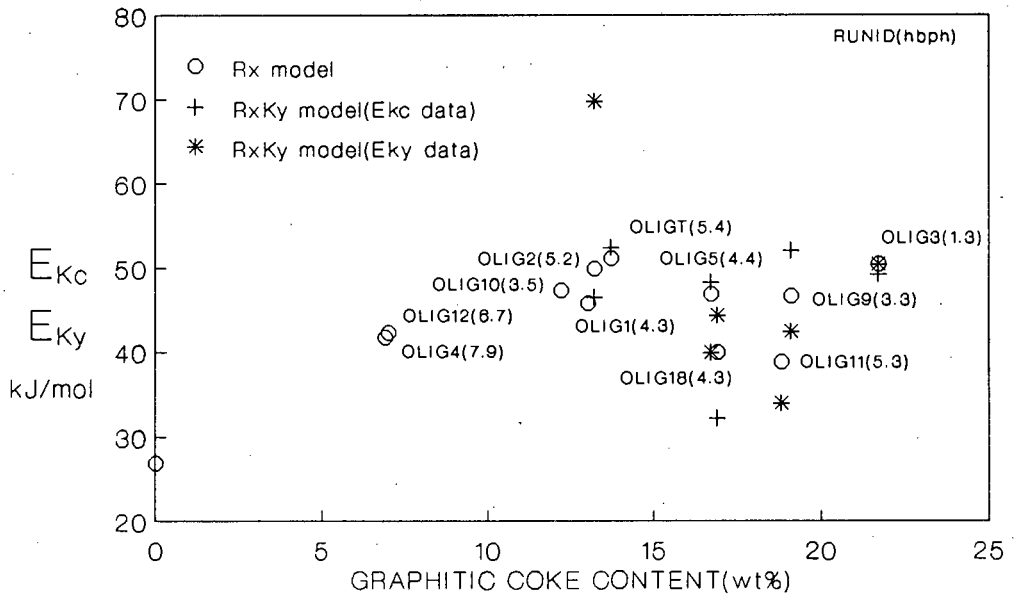

Figure 5.44b : Heat of sorption of n-butane in HY as a function of graphitic coke content after propene oligomerisation.

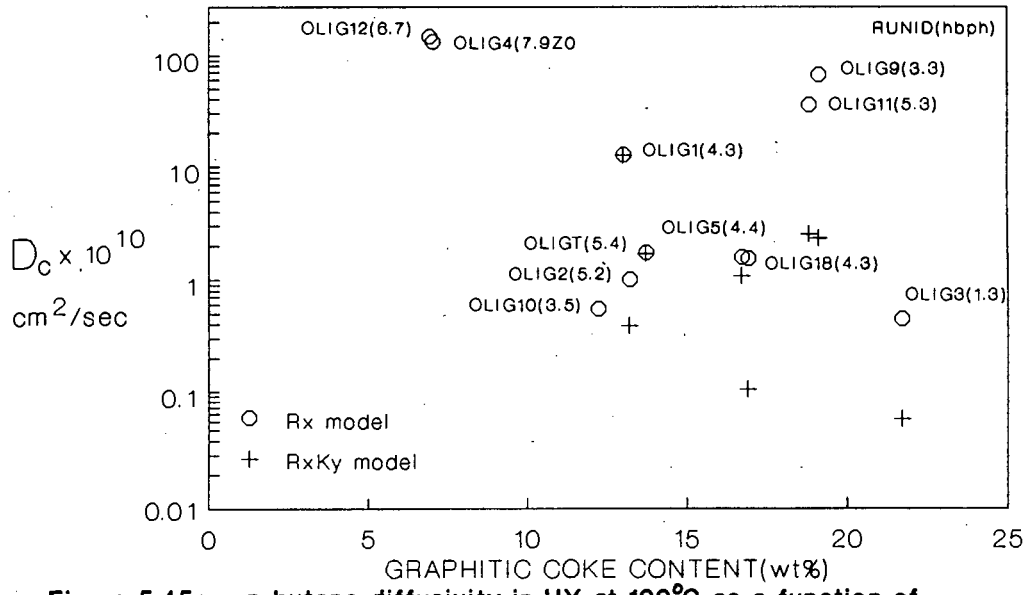

Figure 5.45a : n-butane diffusivity in HY at 100°C as a function of graphitic coke content after propene oligomerisation.

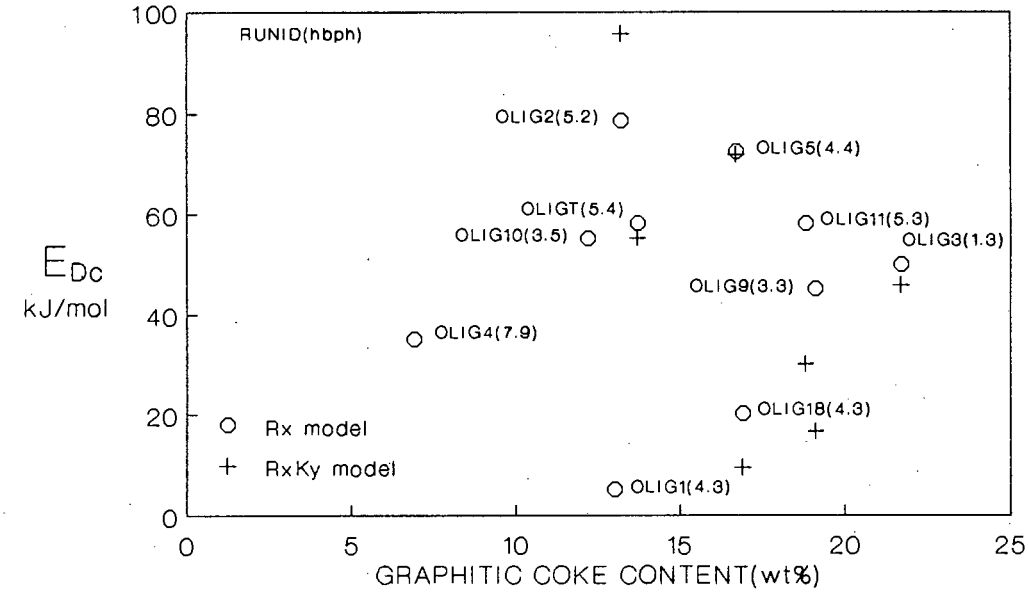

Figure 5.45b : Diffusional activation energy of n-butane in HY as a function of graphitic coke content after propene oligomerisation.

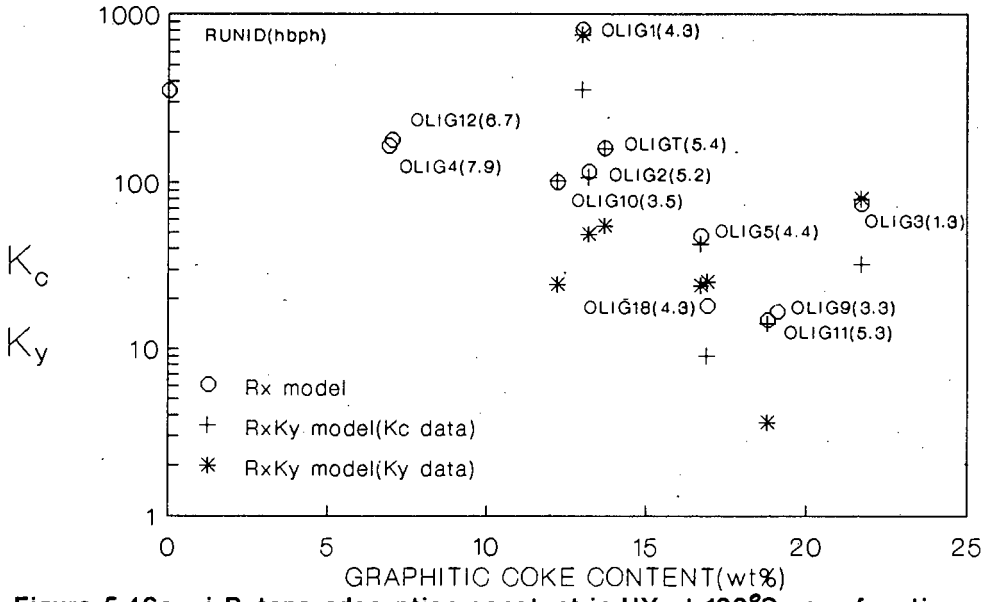

Figure 5.46a : i-Butane adsorption constant in HY at 100°C as a function of graphitic coke content after propene oligomerisation.

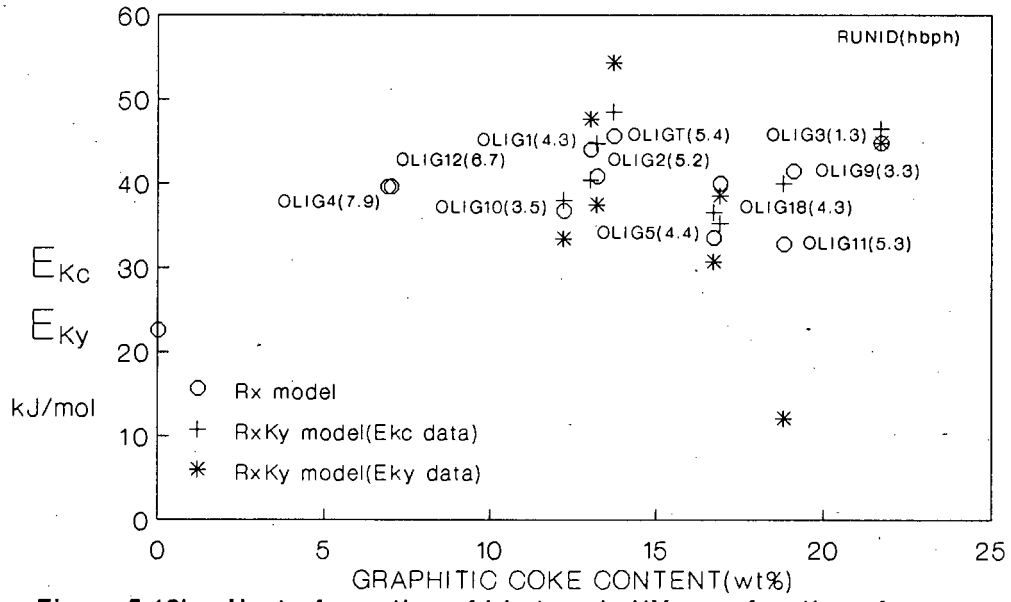

Figure 5.46b : Heat of sorption of i-butane in HY as a function of graphitic coke content after propene oligomerisation.

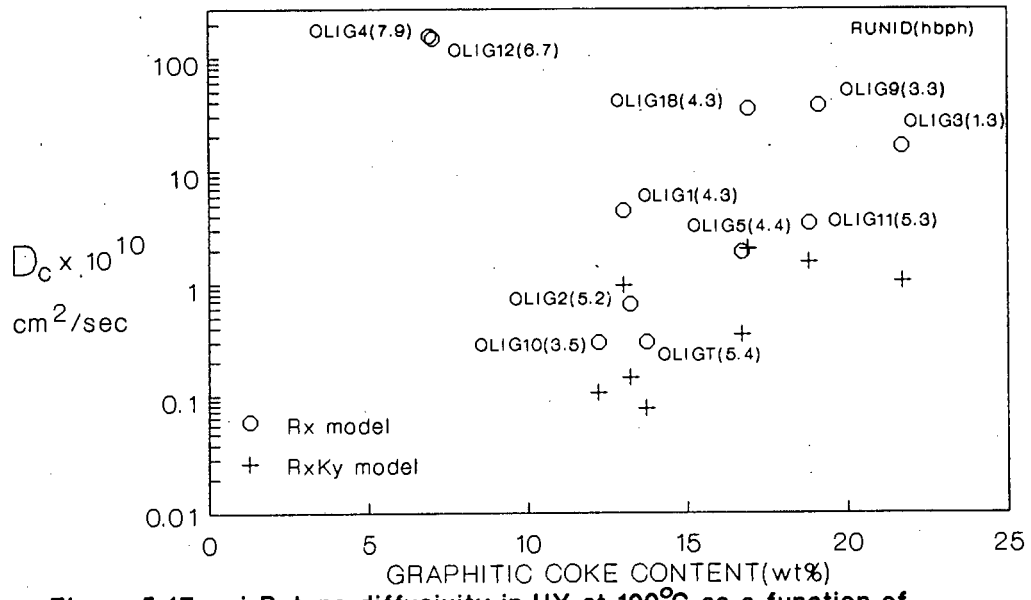

Figure 5.47a : i-Butane diffusivity in HY at 100°C as a function of graphitic coke content after propene oligomerisation.

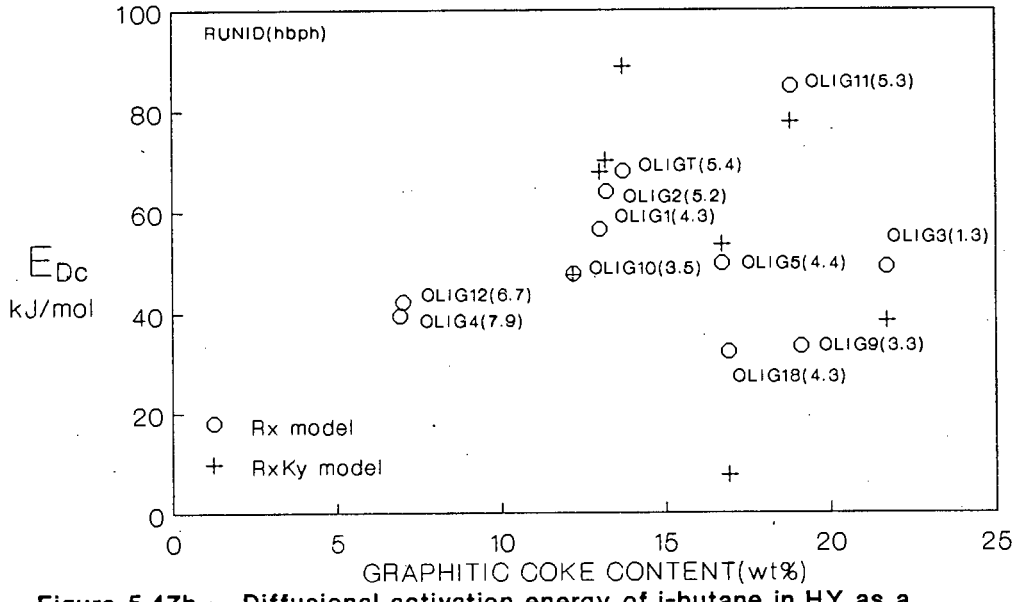

Figure 5.47b : Diffusional activation energy of i-butane in HY as a function of graphitic coke content after propene oligomerisation.

catalyst, as a function of graphitic coke content, was similar for all the tracer gases studied with the same anomalous behaviour for OLIG1 and OLIG3 (Figure 5.41c). Heats of sorption (Figures 5.42b, 5.44b and 5.46b) were found to increase with increasing graphitic coke content, and in the case of propane appeared to have a maximum value at 14 wt% coke. Although the values of K_c were fairly independent of velocity, for each run the data still showed substantial scatter at the same coke content, perhaps due to differences in the position and nature of coke. OLIG18 was found to have low values of E_{Kc} for propane and n-butane.

D_c in HY decreased with increasing graphitic coke, by four orders of magnitude for propane and three orders of magnitude for i- and n-butane (Figures 5.43a, 5.45a and 5.47a), respectively. Clearly D_c became smaller with increasing molecular weight. In the case of i-butane, D_c appeared to go through a minimum at 14% graphitic coke above which the diffusivity became greater than that of n-butane. Diffusional activation energy for propane went through a maximum (Figure 5.43b) while the data for n- and i-butane showed considerable scatter (Figures 5.45b and 5.47b). The values of E_{Dc} were strongly dependent on variations in D_c due to velocity, resulting in the scatter.

Model predictions of methane in coked HM (Figures 5.48a and b) showed that the macro model adequately represented the data. As seen in Appendix C, the error criterion showed that the R_x model would be expected to predict the data better. As the response peak tailed considerably (not all of the tail is shown in the graphs), the R_x model would fit this portion of the graph better than the macro model. However, as only a few data points were obtained for these response peaks, the frequency domain analysis used here was not accurate to make a conclusive distinction between the different models. For the larger hydrocarbons more data points from the response peaks were recorded which led to a more accurate analysis. In all these cases it was found that the R_xK_y model predicted the experimental data best (Figures 5.49a and b, 5.50a-c, 5.51a-c). The macro model was not able to fit these data due to severe tailing and skewing, which also limited the accuracy of the R_x model. These effects were more pronounced with samples which had little or no high boiling point hydrocarbons and with larger tracer molecules. For some cases, however, even the R_xK_y model was not able to predict the data as well as would be required for good analysis (Figures 5.50b and 5.51c). Examples of exceptionally good curve fits are shown in Figures 5.50a, 5.51b and 5.49b.

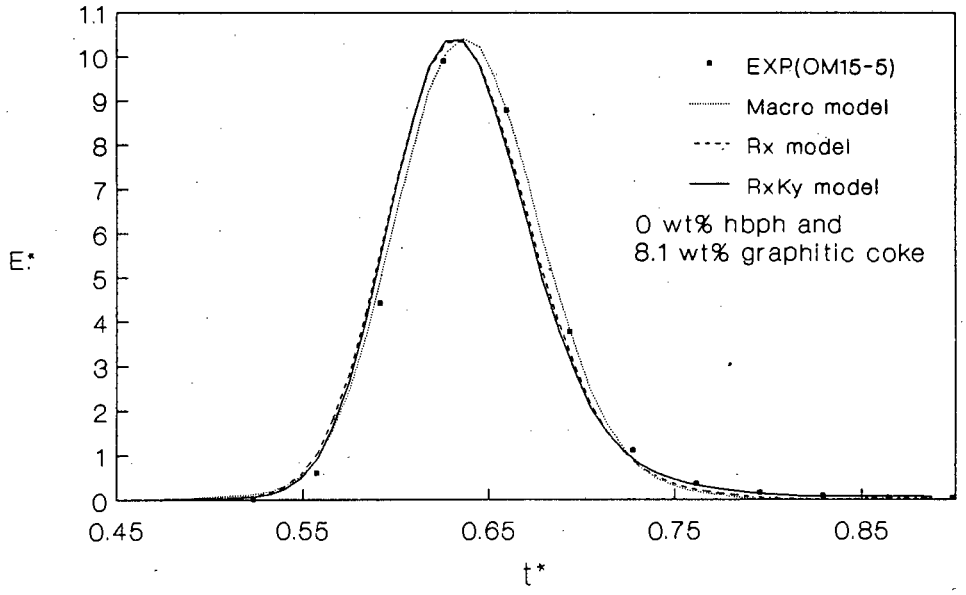

Figure 5.48a : E* vs t* of experimental data and model predictions for methane in HM at 50°C after propene oligomerisation (OLIG15); run OM15-5.

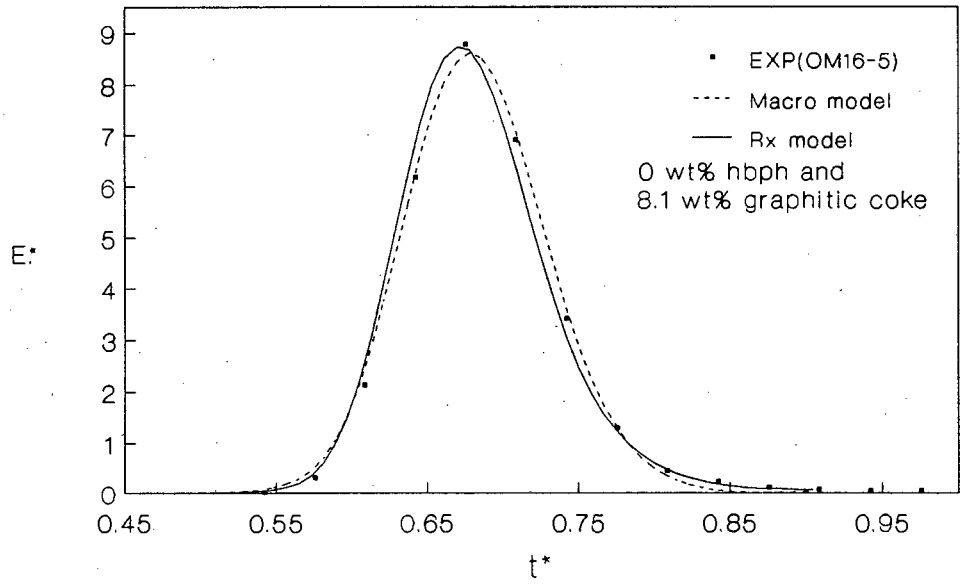

Figure 5.48b : E* vs t* of experimental data and model predictions of methane in HM at 50°C after propene oligomerisation (OLIG16); run OM16-5.

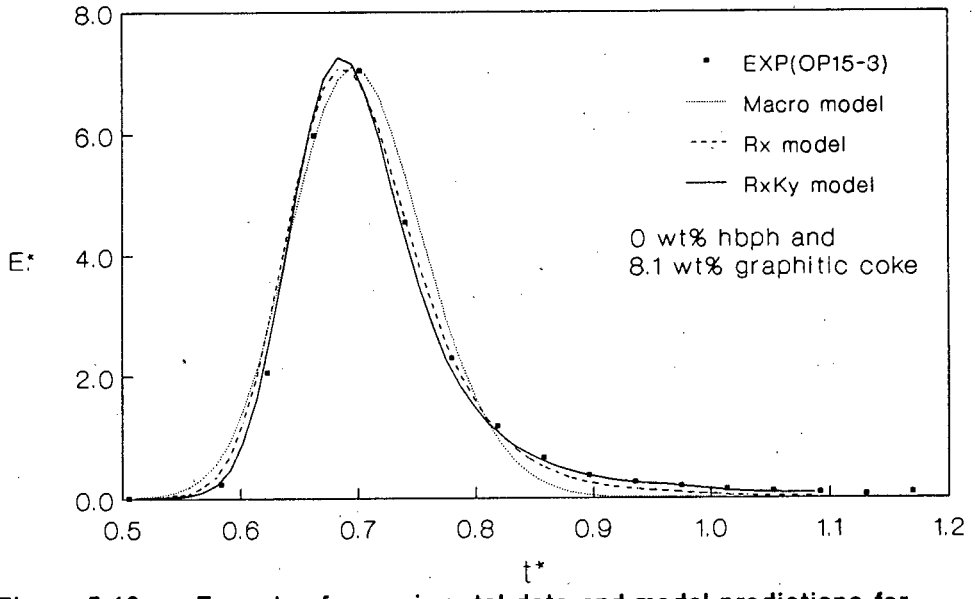

Figure 5.49a : E* vs t* of experimental data and model predictions for propane in HM at 100°C after propene oligomerisation (OLIG15); run OP15-3.

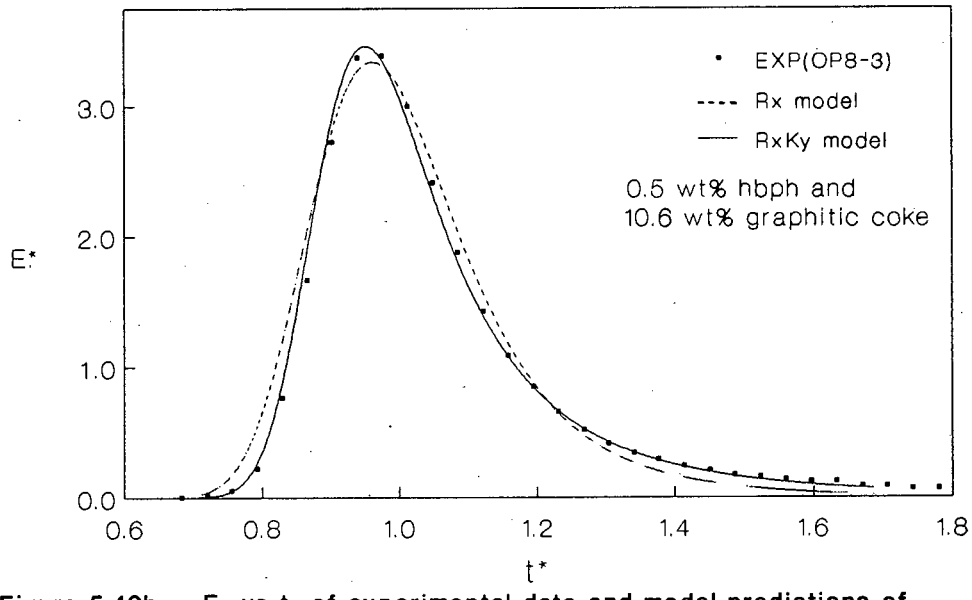

Figure 5.49b : E* vs t* of experimental data and model predictions of propane in HM at 100°C after propene oligomerisation (OLIG8); run OP8-3.

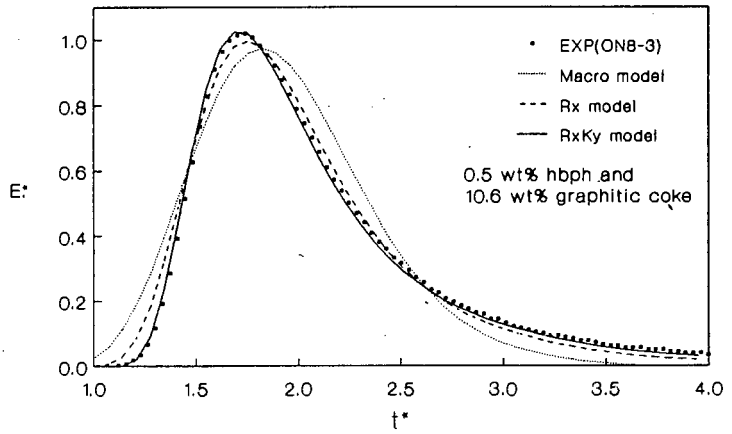

Figure 5.50a : E* vs t* of experimental data and model predictions for n-butane in HM at 100°C after propene oligomerisation (OLIG8); run ON8-3.

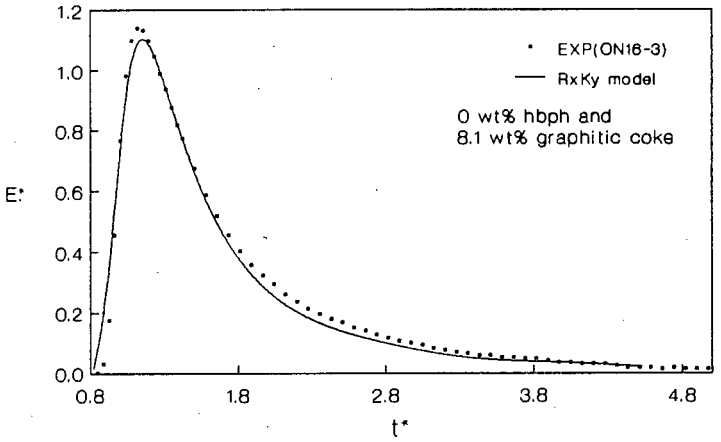

Figure 5.50b : E* vs t* of experimental data and model predictions for n-butane in HM at 100°C after propene oligomerisation (OLIG16); run ON16-3.

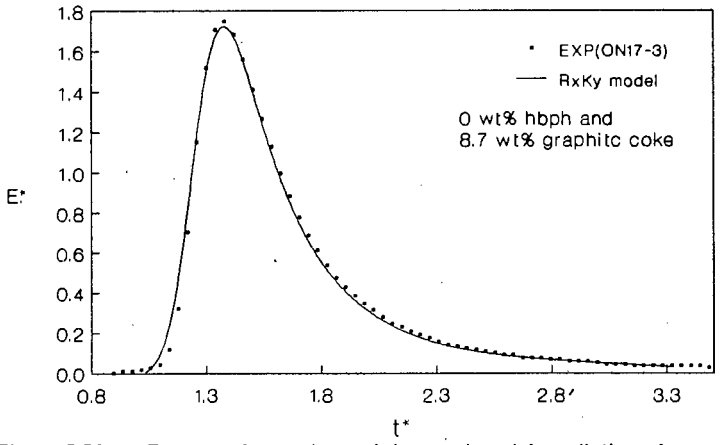

Figure 5.50c : E* vs t* of experimental data and model predictions for n-butane in HM at 100°C after propene oligomerisation (OLIG17); run ON17-3.

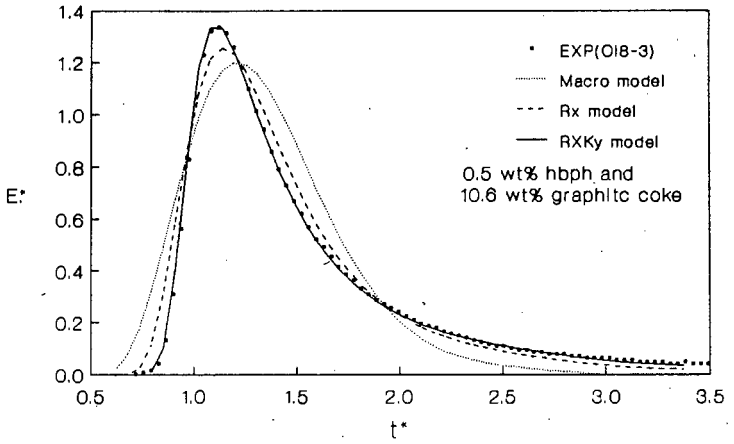

Figure 5.51a : E• vs t• of experimental data and model predictions for i-butane in HM at 100°C after propene oligomerisation (OLIG8); run OI8-3.

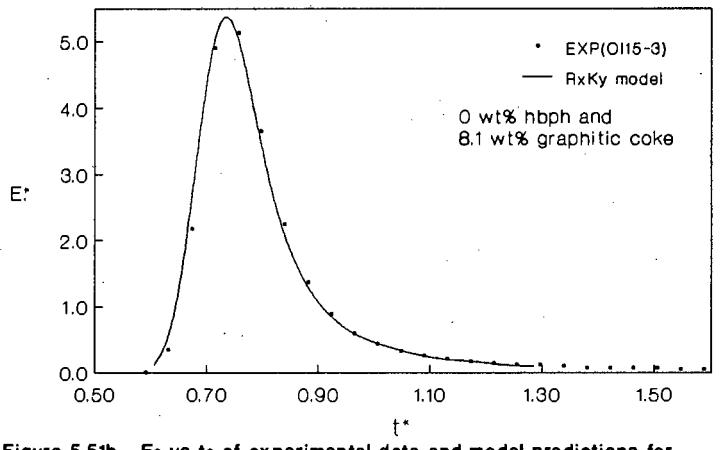

Figure 5.51b : E• vs t• of experimental data and model predictions for i-butane in HM at 100°C after propene oligomerisation (OLIG15); run OI15-3.

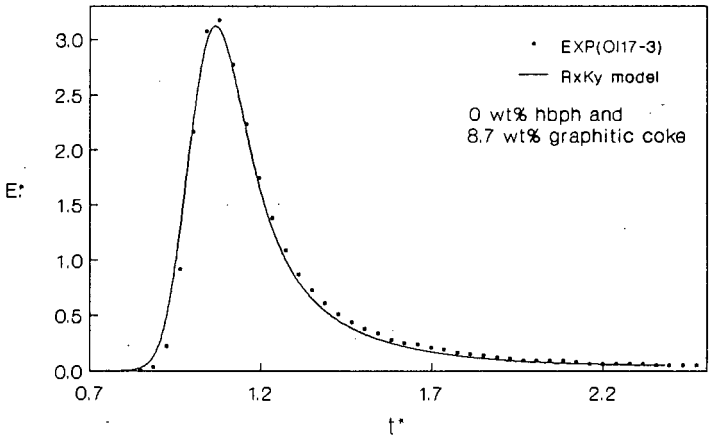

Figure 5.51c : E• vs t• of experimental data and model predictions for i-butane in HM at 100°C after propene oligomerisation (OLIG17); run OI17-3.

Methane adsorption constant at 50°C in HM (Figure 5.52a) decreased from 30 for fresh HY to between 1 and 0.1 for coked samples, but showed erratic variation with coke content. As expected the macro and R_x models followed the same trend. There appeared to be no marked effect of high boiling point hydrocarbons on the adsorption constant. Diffusivities greater than 10^{-7} cm^2/s were too high to measure accurately, and methane diffusion for fresh HM was not determined. Thus it was not clear if the diffusivity increased or decreased in the coked samples. Diffusivity computed using a given model (Figure 5.52b) varied within a band covering an order of magnitude with no systematic variation as a function of coke content, either graphitic or high boiling point hydrocarbons.

A trend in K_c similar to that of methane was observed for propane, n- and i-butane (Figures 5.53a, 5.55a and 5.57a). The values of K_c for all gases were in the range 0.1 to 10 and was not a strong function of graphitic coke content. K_c tended to be lower for samples which contained substantial amounts of high boiling point hydrocarbons. The relative decrease in K_c increased with increasing molecular size (Figures 5.52c). The decrease in K_c after deactivation was about three orders of magnitude greater in HM than in HY. The K_y values of the R_xK_y model were close to the K_y values determined from the macro model. The scatter observed in the adsorption data was insignificant when compared to differences in adsorption constants of fresh and deactivated samples. Heats of sorption tended to decrease with increasing graphitic coke content although the data showed considerable scatter (Figures 5.53b, 5.55b and 5.57b). E_{Kc} values for some samples were found to be negative which indicated errors in the measurements. It appeared that samples with high boiling point hydrocarbons had lower heats of sorption than the samples with little or no high boiling point hydrocarbons. The lower E_{Kc} values also appeared to correspond to the lower values of K_c. The values of E_{Ky} of the R_xK_y model were lower than the E_{Kc} values. From the low heats of sorption it is clear that temperature dependence of some samples was negligible over the range studied.

Considering the R_xK_y model, diffusivity showed an order of magnitude decrease for propane (Figure 5.54a), and an order of magnitude increase for n-butane (Figures 5.56a) and i-butane (Figure 5.58a). The order of magnitude variation of the data with graphitic coke content was within the accuracy of the parameter determination. D_c of the R_xK_y model was an order of magnitude lower than that from the R_x model. D_c showed no dependence on high boiling point hydrocarbons as observed in the case of K_c. Unexpectedly, D_c appeared to be of the same order of magnitude for propane, n- and i-butane. It is

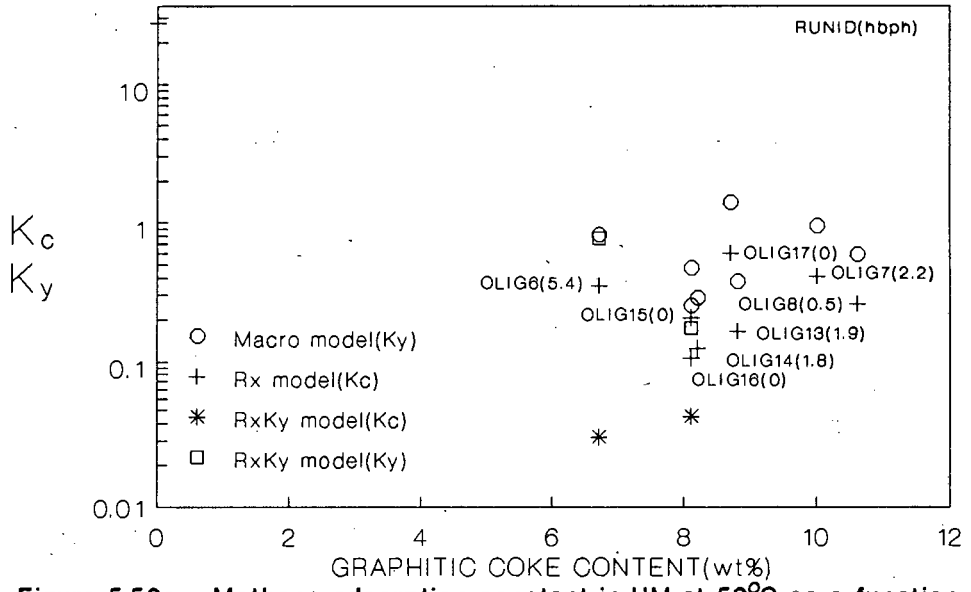

Figure 5.52a : Methane adsorption constant in HM at 50°C as a function of graphitic coke content after propene oligomerisation.

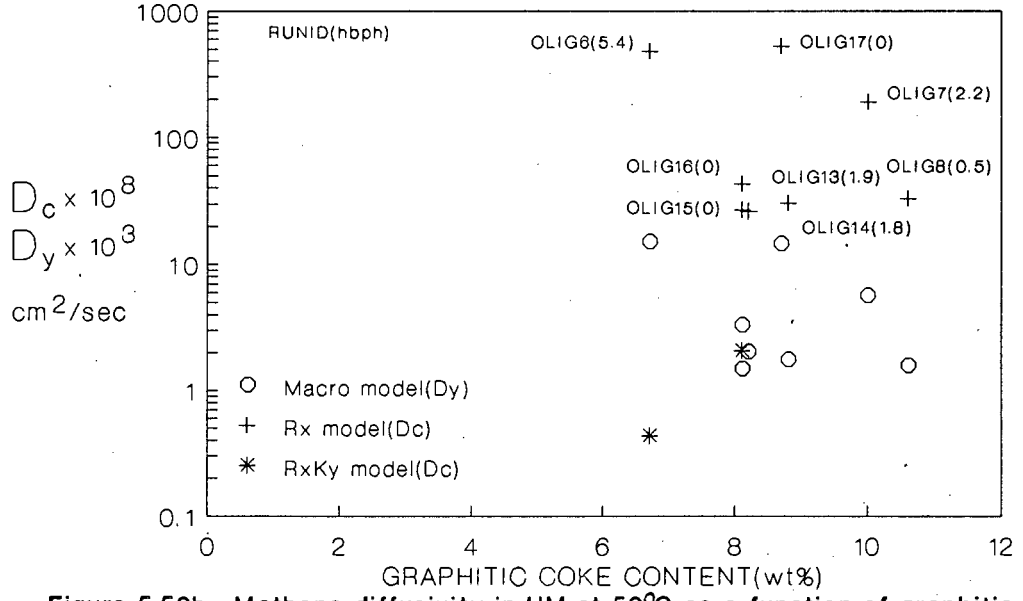

Figure 5.52b : Methane diffusivity in HM at 50°C as a function of graphitic coke content after propene oligomerisation.

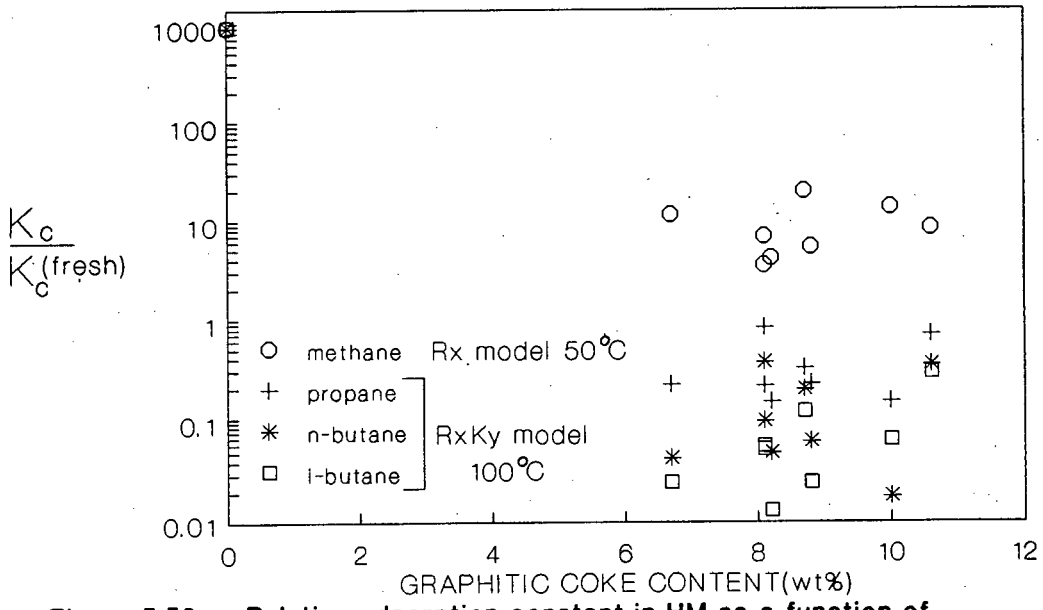

Figure 5.52c : Relative adsorption constant in HM as a function of graphitic coke content after propene oligomerisation.

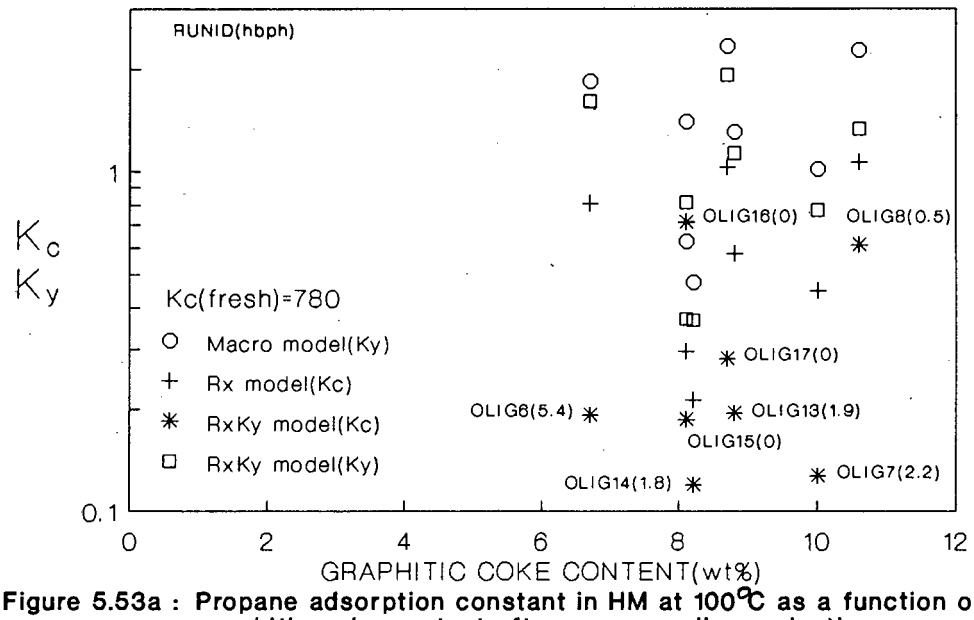

Figure 5.53a : Propane adsorption constant in HM at 100°C as a function of graphitic coke content after propene oligomerisation.

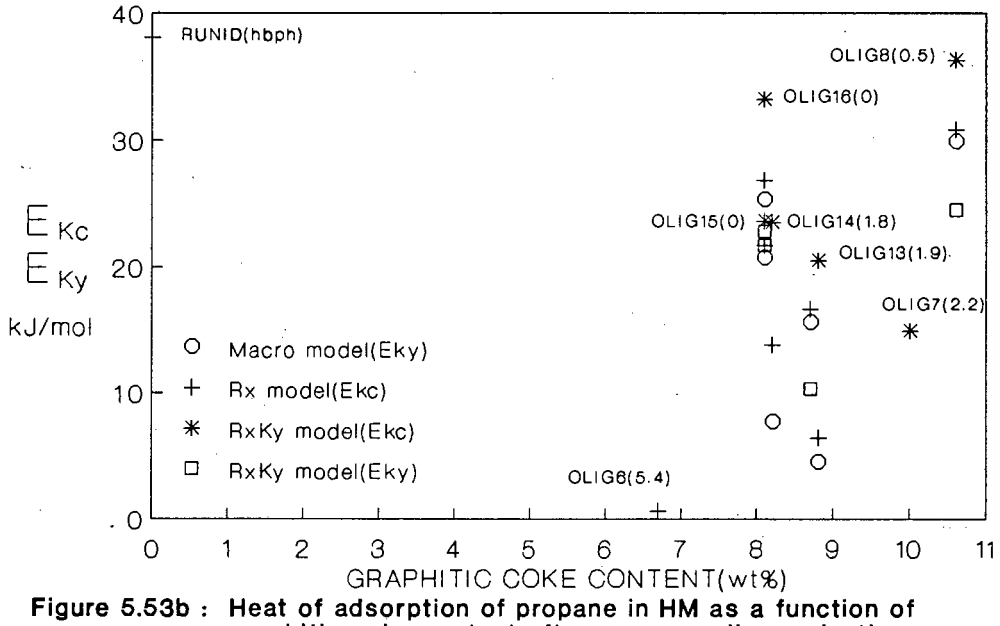

Figure 5.53b : Heat of adsorption of propane in HM as a function of graphitic coke content after propene oligomerisation.

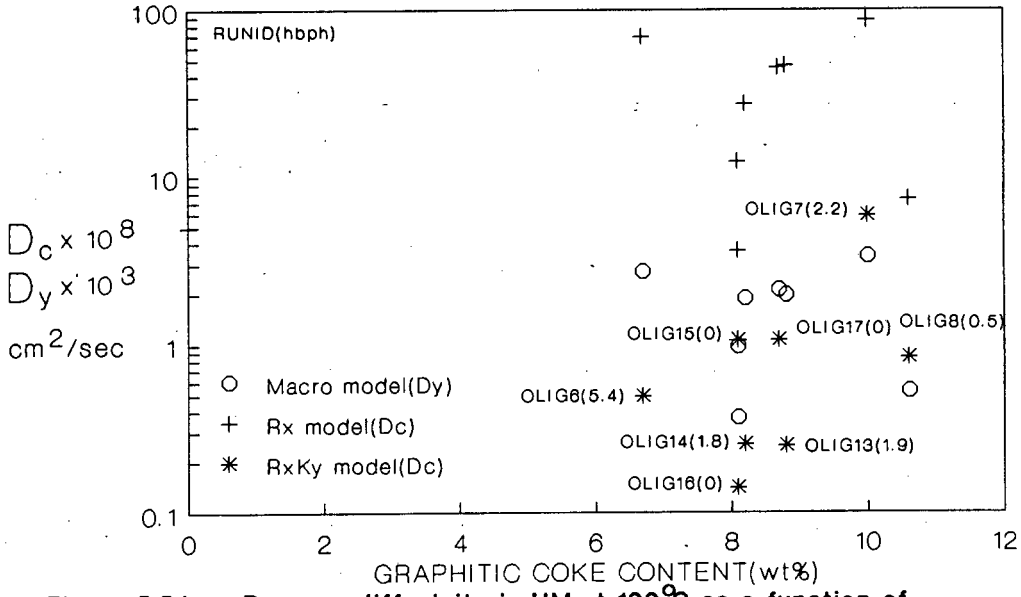

Figure 5.54a : Propane diffusivity in HM at 100°C as a function of graphitic coke content after propene oligomerisation.

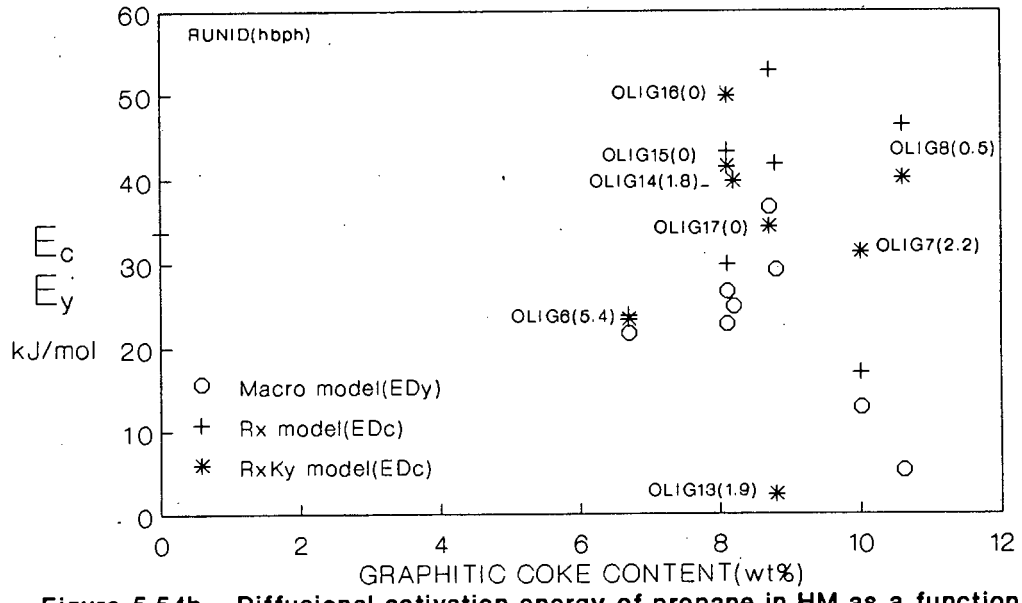

Figure 5.54b : Diffusional activation energy of propane in HM as a function of graphitic coke after propene oligomerisation.

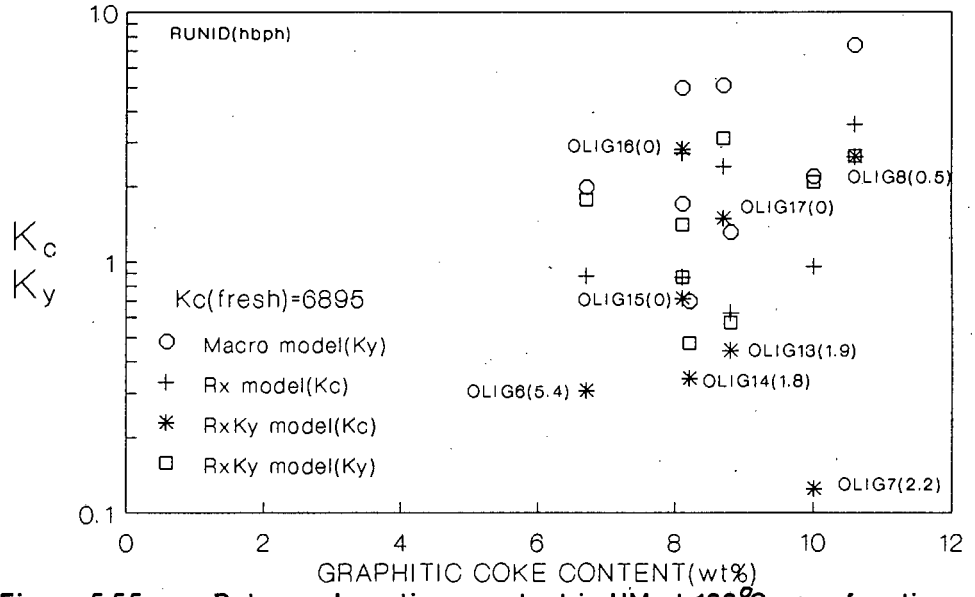

Figure 5.55a : n-Butane adsorption constant in HM at 100°C as a function of graphitic coke content after propene oligomerisation.

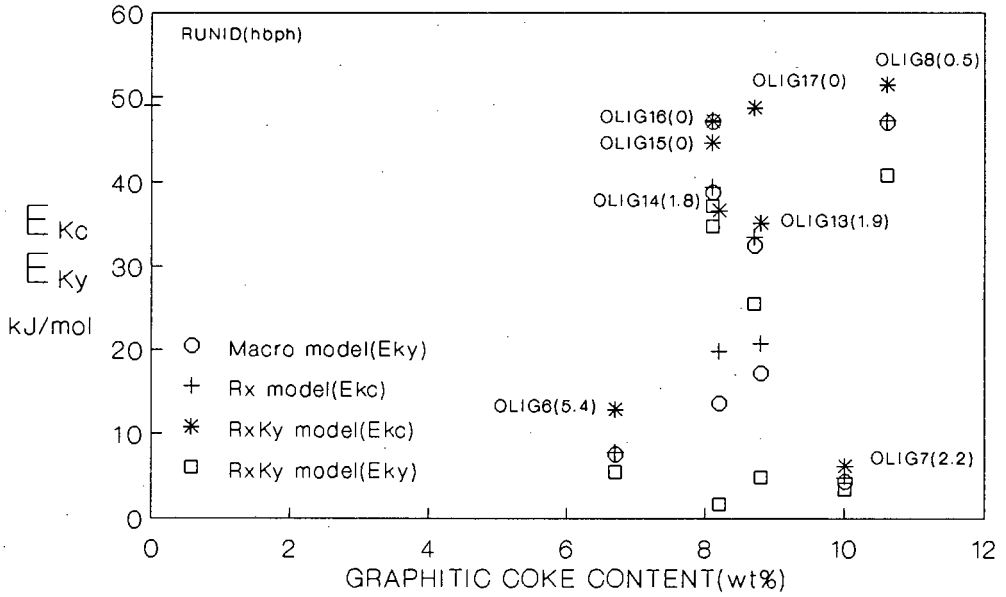

Figure 5.55b : Heat of sorption of n-butane on HM as a function of graphitic coke content after propene oligomerisation.

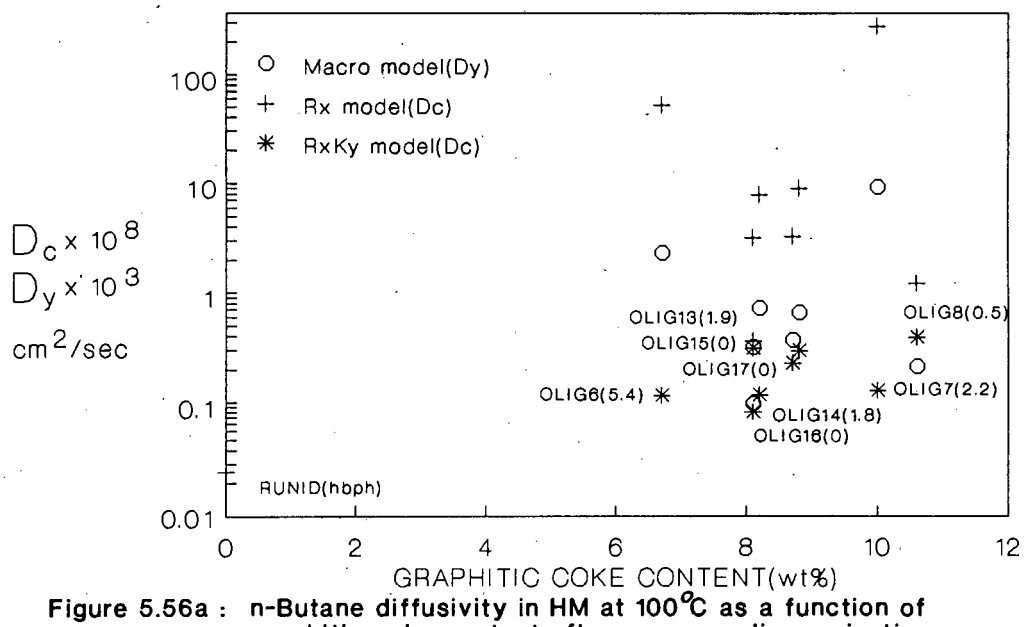

Figure 5.56a : n-Butane diffusivity in HM at 100°C as a function of graphitic coke content after propene oligomerisation.

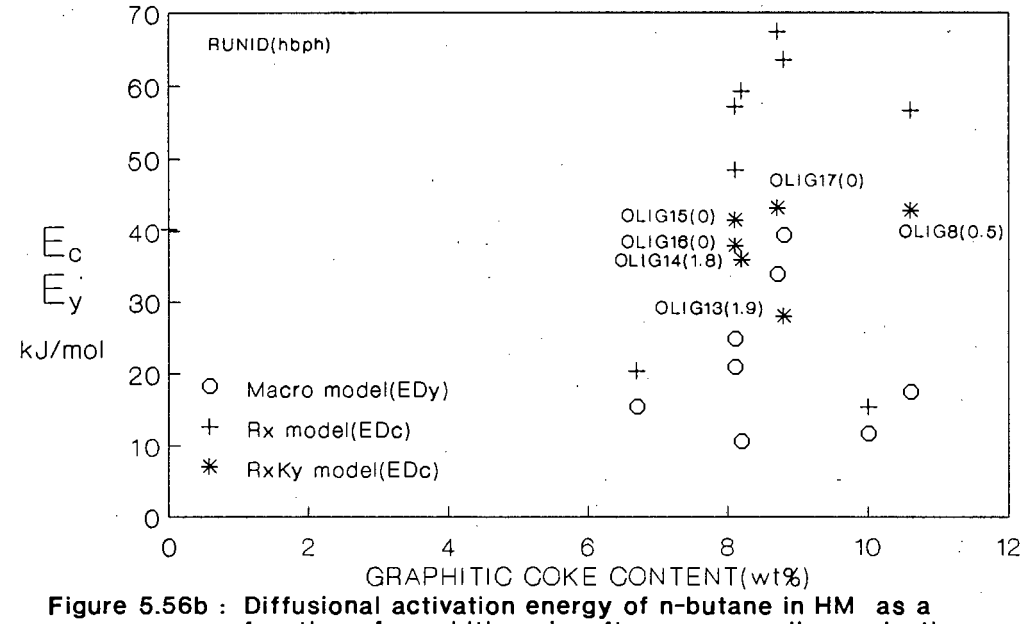

Figure 5.56b : Diffusional activation energy of n-butane in HM as a function of graphitic coke after propene oligomerisation.

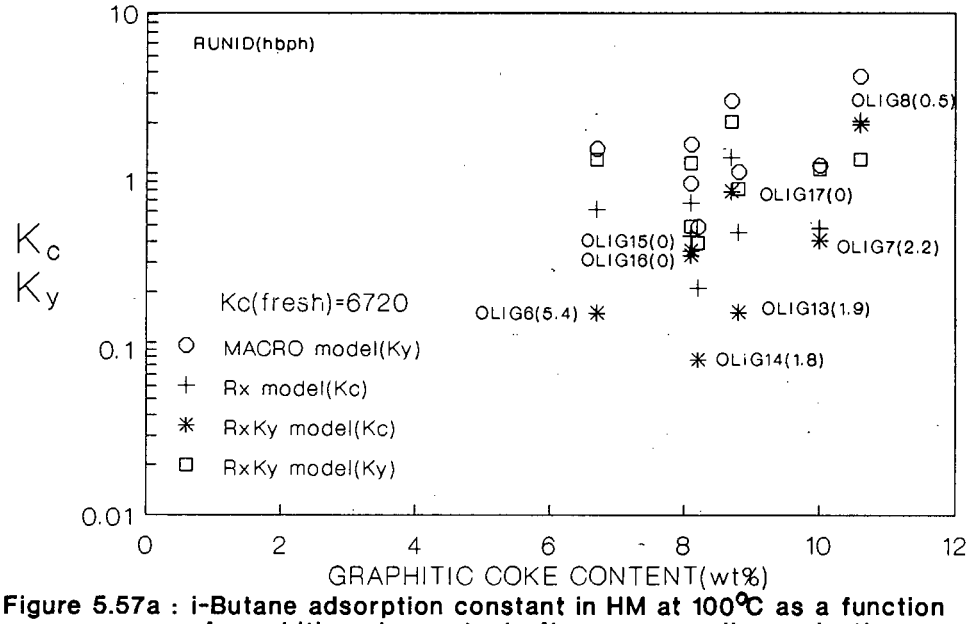

Figure 5.57a : i-Butane adsorption constant in HM at 100°C as a function of graphitic coke content after propene oligomerisation.

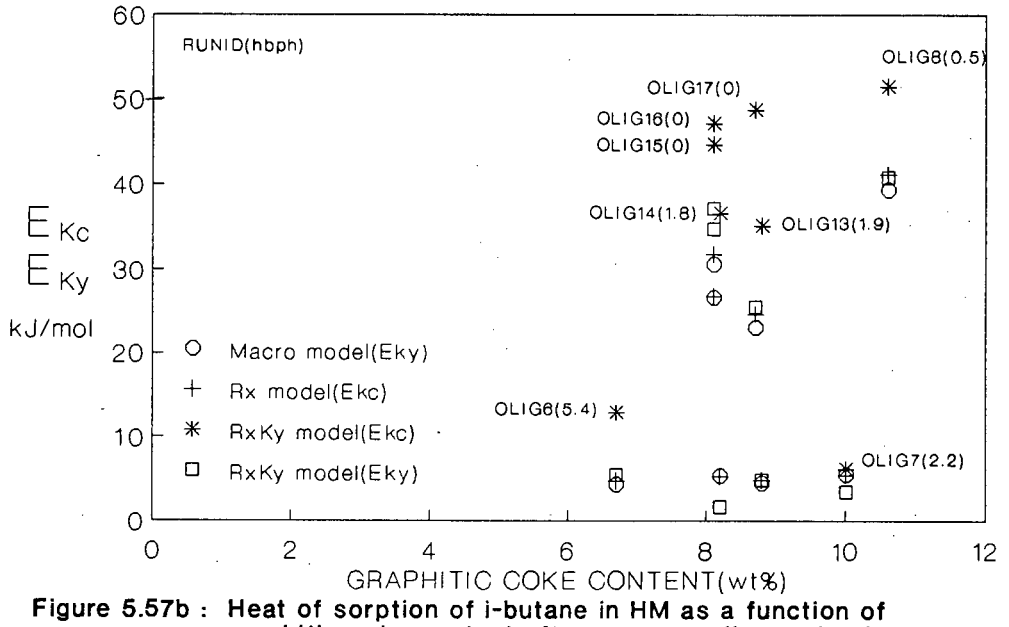

Figure 5.57b : Heat of sorption of i-butane in HM as a function of graphitic coke content after propene oligomerisation.

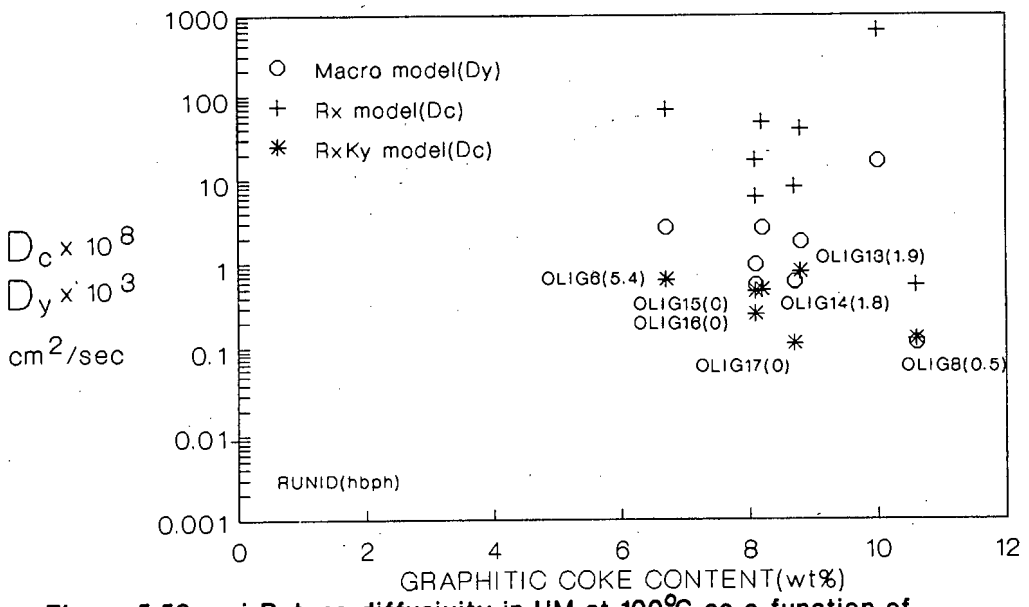

Figure 5.58a : i-Butane diffusivity in HM at 100°C as a function of graphitic coke content after propene oligomerisation.

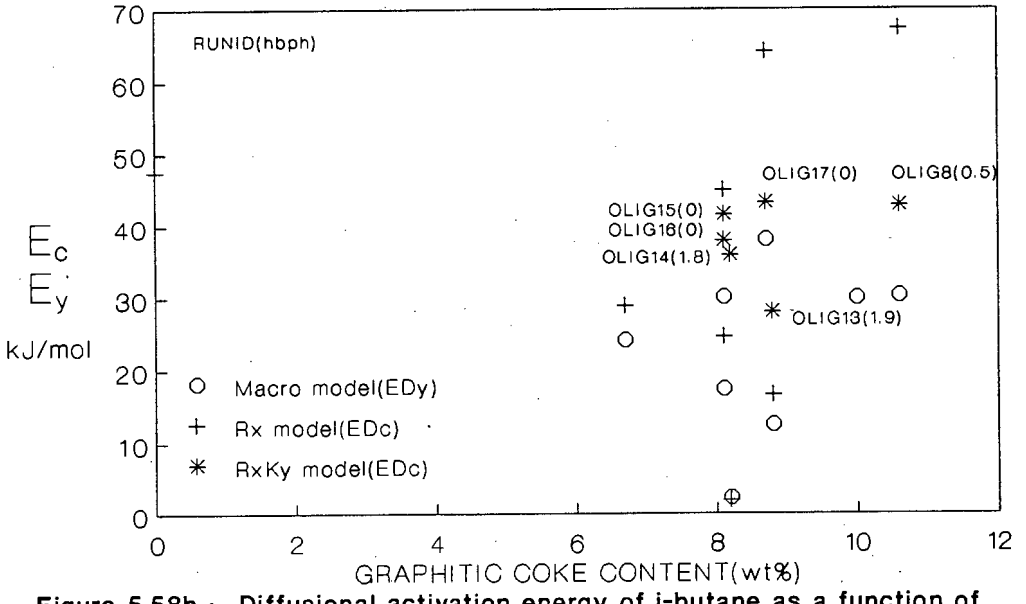

Figure 5.58b : Diffusional activation energy of i-butane as a function of graphitic coke after propene oligomerisation.

possible to conclude from the figures that the values of D_c decreased on average C_3 > n-C_4 > i-C_4, but the differences are within experimental error. Diffusional activation energies of the R_xK_y model increased for propane (Figure 5.54b), did not change for n-butane (Figure 5.56b) and decreased for i-butane (Figure 5.58b) with increasing graphitic coke content. These trends are only approximate as D_c varied by an order of magnitude with velocity, which would significantly affect the values of E_{Dc}.

5.7 DISCUSSION

The results clearly showed that for diffusion of methane, propane and i-butane in fresh HY, diffusivity was too large to be measured. The dispersion correlation could adequately predict the data within experimental error. In the case of n-butane the determination of diffusivity was difficult and only an order of magnitude estimate was possible, although the responses curves tailed, indicating significant diffusional resistance. The curve-fitting of n-butane response curves with unreasonably low axial dispersion was also observed by Hsu and Haynes (1981) for NaY. They attributed this behaviour to non-linear adsorption isotherm. The results of this work showed that the adsorption constant did not vary systematically with pulse size and therefore it was not clear that non-linear behaviour was responsible for the above difficulty. Fu et al. (1986), by reducing the pulse size to 4-25 $\mu\ell$ for the above NaY system, were able to fit the response curves well. The model parameters determined by Hsu and Haynes (1981) (K_c = 700, D_c = 2.4 x 10^{-8} cm^2/s at 100°C and E_{Kc} = 37 kJ/mol) were quite different from the values extrapolated from the work of Fu et al. (K_c = 3300, D_c = 5.05 x 10^{-12} at 100°C, E_{Kc} = 43 kJ/mol). Forni and Viscardi (1986), using the benzene/HY system, were unable to obtain conclusive results due to non-linear adsorption isotherm even at the lowest concentration. Their data also showed that the apparent adsorption on HY was much smaller than that on NaY, although HY had stronger acid sites. Similarly n-butane adsorption measured in this work was less than that reported by Fu et al. (1986). In light of the above observation and the fact that E_{Kc} decreased in the order C_3 > n-C_4 > i-C_4, the possibility that non-linearities were present in our system cannot be excluded. Alternatively, it is possible that in the case of linear hydrocarbons such as propane and n-butane, a fraction of the molecules which enter the micro-pores adsorb on two or more acid sites. Such a configuration would stablize the adsorbed phase, increase the residence time, and cause the tailing. The model would not be able to predict the response curve because D_c is no longer a constant.

Adsorption and diffusional resistance were much greater in HM than in HY. The greater adsorption in HM was expected in view of the large number of strong acid sites which was the dominant factor, although HY had theoretically 50% more acid sites and more surface area. Eberly (1969) showed that the effective diffusional resistance (including macro and micropores) of Ar, Kr and SF_6 followed the order NaM > HM > 5A > NaY using the GC/HETP technique. A similar observation was made by Ma and Mancel (1972) where the effective diffusional resistance of CO_2, NO, NO_2 and SO_2 decreased as natural M > NaM > HM > 13X, 5A, also using the GC/HETP method. These results show that although HM has larger pores than 5A, the one-dimensional structure causes significant diffusional resistance. Comparison of the data in this work however shows that the diffusivity of propane is three orders of magnitude larger in HM than in 5A molecular sieves. The above workers however did not take into account the crystallite size distribution and determined instead overall effective diffusivity. The tracer gases used in the above cases were considerably more weakly adsorbed than hydrocarbons.

The sorption isotherms for methane, ethane, propane and n-butane determined gravimetrically up to 140°C in NaM by Satterfield and Frabetti (1967) showed that Henry's law was valid for methane to a partial pressure of 20 cm Hg, while for propane and n-butane Henry's law applied only at partial pressures of less than 1 cm Hg. However, the linear region grew with increasing temperature, most significantly in the case of propane. Assuming an injection time of 0.2 s for a 5 $\mu\ell$ sample injection gives an initial pulse concentration of approximately 2 cm Hg, which is clearly in the non-linear range. However, Schneider and Smith (1968b) have shown that concentration drops rapidly with column length ($C/C_0 \approx 3\%$ 1 cm into a 13 cm column, $K_c \approx 50$) with fractional surface coverages of the order 10^{-4} for propane on silica gel. This suggests that pulse concentration would more likely be of the order 0.1 cm Hg which is in the linear range for NaM. Non-linear effects in the initial section are not likely to be significant. The above applies to NaM and silica gel, while HY and HM were used in this study. Use of different pulse sizes did not show much evidence for non-linearity in the fresh catalyst samples.

Satterfield and Frabetti (1967) also observed large differences in diffusivities of the same hydrocarbons depending on the size fraction of mordenite used. Diffusivities for methane, propane and n-butane at 50°C measured from desorption, which would be expected to have less heat effects, were 1.2×10^{-9}, 7×10^{-11} and 1.8×10^{-11} cm^2/s, respectively. When our

data were extrapolated to 50°C, values were of the same order of magnitude. Boniface and Ruthven (1985) observed highly skewed peaks for O_2 diffusion in HM and could not determine model parameters due to adsorption isotherm non-linearity observed by increasing retention time with decreasing pulse size. Regeneration time length and temperature were found to affect the response peaks, with retention time increasing with increased regeneration time. The results of this work did not show such trends.

5.7.1 Adsorption and diffusion in HY and HM after hexane cracking

The increase in K_c with increasing coke content obtained using the R_x model was not expected as this suggests stronger sorption sites and/or a larger surface area. Hexane cracking was expected to deactivate the strong acid sites first while the coke build-up would reduce the surface area resulting in a lower K_c. BET data showed that surface area was indeed reduced as a result of the coke deposition. The R_xK_y model, which predicted the high coke content response curves well, showed a smaller increase in K_c for propane than the R_x model, and a decrease in K_c in HY for methane after deactivation. BET data and mercury porosimetry data showed that micro-pore surface area was significantly reduced, especially at high coke content, while the total macro-pore surface area (meso- and macro-pores) showed a 20% decrease for all coke levels. In the case of fast diffusion it was not possible to separate K_y and K_c, but for slow diffusion where not all of the diffusing molecules would be expected to enter the micro-pores, K_y and K_c were estimated separately. Tailing of these reponse curves affected the accuracy of the estimation of K_c and D_c. K_y was expected to be considerably smaller than K_c due to smaller surface area in the macro-pores. To compare K_y on a similar basis as K_c, multiplication by the factor $\theta_y/(1 + \theta_y)$ was necessary. This gave K_y values larger than K_c of uncoked HY, suggesting that not only K_c but also K_y increased with coking and that graphitic coke has adsorption properties. The relative increase of K_c (based on fresh HY) was between two to three times greater for propane than for methane. It is not likely, however, that propane accessed more adsorption sites than methane, as methane is smaller than propane. TPD showed that more than 80% of the acid sites were still accessible to ammonia. The reduction of BET surface area indicates that access to molecules greater than N_2 is severely restricted. One possible explanation for the larger increase of K_c for propane which is much bigger than ammonia is that graphitic coke stabilizes propane more than methane. Propane, being larger and adsorbing more readily than methane,

would be stabilized more by the adjacent coke molecules within the reduced diameter of the coked pore.

Diffusivity decreased with an increase in coke content as expected. This decrease, however, was measurable only above the critical graphitic coke content of 8 wt%. Above 8 wt% graphitic coke the diffusivity decreased rapidly. This critical coke content was higher for methane than for propane as expected, since methane is able to diffuse through smaller channels. This as in accordance with the observations of Sarma and Haynes (1974) for the diffusion of argon in 3A, 4A and 5A molecular sieves in which the smaller channels were obtained by cation exchange as opposed to coking. This was also shown by the BET surface area measurements which decreased with increasing coke content, while the pore volume showed a much smaller change, indicating that the access of nitrogen was hindered by the smaller pores. Helium in helium pycnometry would not be affected as much by effective pore diameter reduction.

When the R_x and R_xK_y models were compared for the cases of severe coking, it became clear that the latter model had to be used. This suggested that the ratio of macro-pore to micro-pore surface area as well as micro-pore diffusional resistance was considerably enhanced. In the case of fresh HY micro-pore diffusion was fast, and separation of K_y and K_c was not possible although macro-pore adsorption may have been high. In Chapter 3 it was shown that macro-pore surface area does contribute significantly to total surface area in HY, but its contribution to the total surface area became large in the case of coked samples. A more accurate determination of K_c in fresh HY was hence not feasible, nor was it possible to quantifying the variation of K_c with coke content other than that K_c increased with coke content, at least for propane. In the case of diffusion the trend was well established and the only difference between the R_xK_y and R_x models was that the former predicted smaller diffusivities.

Heats of sorption increased with coke content which indicated that changes in adsorption had occurred. Higher E_{Kc} meant that the adsorbed species were more stable. Coke appeared to stabilize the adsorbed species sufficiently to increase K_c notwithstanding the reduction in the amount of acid sites and surface area. Diffusional activation energy appeared to increase with coke content according to the R_x model. The scatter in the data in the 8-9 wt% coke region was due to measurement difficulties.

Lastly, HY regenerated in air at 400°C regained its initial adsorption properties. It follows that coking had no permanent effect on the mass transfer properties of this catalyst.

In the case of hexane cracking over HM, the R_xK_y model was necessary to predict the response curves. Moreover, even the R_xK_y model did not simulate the experimental curves well as seen from the large squared error values, particularly in the case of propane diffusion. Both adsorption constants and diffusivities decreased after deactivation. However, K_y, K_c and D_c were found to vary significantly with velocity. At sufficiently large diffusional resistance most of the tracer would pass through the catalyst bed undergoing only macro-pore adsorption, while a small portion would enter the micro-pores and cause the severe tailing observed. It has been shown by Fu et al. (1986) that diffusion and surface barrier models could not be distinguished in their systems. Simulations incorporating the adsorption rate to the outer crystallite surface (k_a) into the R_xK_y model showed that the adsorption rate could be separated from micro-pore diffusion under severe diffusional limitation. However, it became immediately clear that in the case of HM deactivated by cracking the surface barrier model could not fit the response curves. Thus adsorption to the crystallite outer surface could not be responsible for variations in K_c with velocity. On the other hand if the surface area was reduced sufficiently, as suggested by BET and porosimetry measurements of oligomerisation samples, so that the injection pulse was large enough to cause saturation (i.e., well outside the linear range), then at higher velocities (viz., higher pulse concentration) a greater proportion of the diffusing species would undergo only macro-pore adsorption, resulting in a decrease in the amount of tailing and hence also K_c. The R_xK_y model parameters in this case required accurate measurements of tailing which may have been a significant source of error. These data therefore give only an approximation of the transport processes in coked HM.

The large decrease in diffusivity suggested that the pores were severely restricted. The decrease in K_c most probably resulted from a large decrease in surface area, as in the case of pore blockage. It is possible that at low velocity more time is allowed for the tracer to reach the adsorption sites. Under these conditions, where time required for reaching adsorption equilibrium is of the same order as the residence time inside the pores, K_c would increase with decreasing velocity. Nevertheless, this would also be consistent with the postulate that saturation occurred at very low concentrations.

Butt et al. (1975) studied cumene cracking over HM and found that the effective diffusivity (macro and micro)-pore of SF_6 decreased by a factor of two using the HETP method. Effective diffusivity was found to be non-linearly related to coke content, but independent of the coking temperature. In this work the diffusivity was found to decrease by three orders of magnitude.

Comparison of K_y between HM and HY shows that the macro-pore contribution in HY was much greater than in HM. This was expected owing to its macro-pore surface area which was five times larger in HY than in HM, although the latter had stronger acid sites. Comparison of K_c and D_c between HM and HY shows that deactivation mechanisms due to cracking were probably different. In the case of HY the decrease in D_c and increase in K_c meant that the channels were smaller offering more resistance but also that enough sites were available to increase adsorption with the help of stabilization of the adsorbed phase by graphitic coke in the smaller channels. In addition, if graphitic coke were to have an adsorption capacity of its own for the hydrocarbons, this would also slow down diffusion. It has been increasingly accepted in the literature recently that molecules in zeolite pores are located very close to the pore walls, even if molecular dimensions are much smaller than the pore diameter, and that the molecules move from one region of low chemical potential to another as they diffuse. Hence if a molecule is strongly held, it will spend more time in each region of lowest chemical potential, thereby slowing its diffusion rate. An example of such a phenomenon is the diffusion of benzene and pyridine in HM (Drachsel and Becker, 1980). The diffusivity of pyridine, a much stronger base than benzene, was found to be orders of magnitude smaller than that of benzene in HM, although their molecular dimensions are essentially identical.

Hexane being larger than propane, it would encounter far greater diffusional limitation in accessing the active sites. It may be postulated that during hexane cracking severe diffusional limitations are introduced by coke build-up. Whether or not greater propane adsorption constants imply that hexane is much more strongly adsorbed is not clear.

For HM the decrease of both D_c and K_c suggests that even methane encountered enormous steric hindrance and resulting reduction in effective surface area after deactivation. This is in accordance with the BET surface area measurement of oligomerisation samples, which showed little surface area accessible to N_2. In contrast, ammonia was still able to reach over 85% of the acid sites initially present on the catalyst. The larger hexane molecule

would therefore be unable to diffuse into such small channels, suggesting that pore blockage may be prevalent. The fact that severe diffusional limitation occurred at 3.1% coke in HM suggests pore blocking, as opposed to HY in which coke contents of up to 10% did not introduce severe diffusion limitations, and even at 13% coke diffusivities were still greater than in HM. The same reasoning holds for the large reduction in K_c for HM which must have occurred from large reduction of surface area by pore blockage at low coke content.

Reaction profiles showed that the pore blockage which occurred in HM caused faster deactivation than the partial pore blockage which occurred in HY. This is expected from the one-dimensional pore structure of HM. In the case of HY pore blockage would only increase the diffusional resistance as access from other directions would still be possible. In addition, the greater number of strong acid sites as demostrated by ammonia TPD from HM would enhance the probability of coking.

5.7.2 Adsorption and diffusion in HY and HM after propene oligomerisation

The interpretation of oligomerisation data is made more difficult by the fact that there were two types of coke present on the catalyst. In this respect it is illuminating to compare OLIG12, CRAC5 and CRAC7. OLIG12 and CRAC5 had the same total amount of coke. However, in the case of OLIG12, of the 13.7 wt% total coke, 6.7 wt% was due to high boiling point hydrocarbons, the remaining 7.0 wt% consisting of graphitic coke. In contrast, CRAC5 had 13.9 wt% graphitic coke. It is immediately clear from Tables 5.13, 5.14 and 5.17 that high boiling point hydrocarbons introduced far less diffusional limitation, and methane and propane diffusivities were found to be orders of magnitude larger in OLIG12 than in CRAC5. Although in theory high boiling point hydrocarbons should take up twice as much volume, the effective ratio of micro-pore to macro-pore surface area was much smaller in CRAC5, as evident from the fact that the R_x model was adequate for OLIG12 but K_y had to be introduced for CRAC5.

Another instructive comparison is that of OLIG12 and CRAC7. CRAC7 had 7.1 wt% graphitic coke and no high boiling point hydrocarbons. The adsorption constants of methane and propane were much smaller in OLIG12 than in CRAC7, indicating that high boiling point hydrocarbons lowered adsorption

capacities. At the same time, diffusivities were also much lower in OLIG12 and were measurable.

One model which incorporates many of the above features is that a large fraction of the high boiling point hydrocarbons are located in the meso-pores, having no effect on micro-pore diffusivity. The remaining high boiling point hydrocarbons are in the micro-pores, reducing the effective pore dimensions and hence the micro-pore diffusivity.

The high boiling point hydrocarbons decrease K_c, partly by covering adsorption sites, but also by completely blocking pore mouths, even to N_2, thereby decreasing the surface area. The latter process is inferred from comparing the BET surface area measurements of CRAC7 and OLIG4 samples. They had 7.1 and 6.9 wt% graphitc coke, respectively. In addition the latter contained 7.9 wt% high boiling point hydrocarbons. The BET surface area in OLIG4 was approximately four times smaller, indicating that nitrogen accesses far less area. The high boiling point hydrocarbons in the meso-pores can easily be flushed in flowing nitrogen, and REGEN8 showed that indeed this treatment appeared to "unblock" pore mouths. The location of high boiling point hydrocarbons in the meso-pores is also supported by the fact that the meso-pore volume was found to decrease by 30% after oligomerisation.

At high graphitic coke contents, where the diffusivity was small enough to allow separation of K_y and K_c in the R_xK_y model, much lower K_c and D_c parameters were obtained. This suggests that the diffusivity was probably smaller in samples in which K_y and K_c could not be separated than that given by the R_x model. As observed with hexane cracking, the higher heats of sorption indicated a more stable adsorbed phase which must be due to stabilization effects of coke. During the oligomerization over nitrogen regenerated HY (OLIG18), the same temperature rise during the sorption of propene feed was observed as in the case of fresh catalyst, as well as a comparable temperature runaway. Slight variations in reaction conditions (e.g., WHSV, temperature runaway) could cause a small variation in the nature of the coke, although the reactions yielded similar coke contents. The TG/DTA method would not be able to differentiate small variations in the nature of coke in terms of the high boiling point hydrocarbons and graphitic coke groupings. Assuming that coke stabilises the adsorbed phase, slight variations in reaction conditions would cause variations in K_y, K_c and the diffusivity.

The results of samples with 13-14% graphitic coke appear to support the above postulate. The samples from OLIGT, OLIG1 and OLIG2, tested under similar reaction conditions, had essentially the same coke compositions. OLIGT and OLIG2 gave comparable K_y, K_c and D_c values for all molecules except K_y for n-butane at 100°C. The results obtained in OLIG1, however, were markedly different, indicating that the location of coke, and possibly its nature, were different. In particular, the adsorption constants in OLIG1 were much higher than in OLIGT and OLIG2. One possible explanation is that the high boiling point hydrocarbons in OLIG1 (which might be more than the 4.3 wt% indicated by TG/DTA) were located predominantly in the meso-pores without closing the mouths of the micro-pores. OLIG1 was the only deactivated sample where the adsorption constants were much higher than those of fresh HY.

The critical coke content above which the R_xK_y model was required decreased with increasing molecular size as expected. However, the critical graphitic coke content in hexane cracking (ca. 10% for propane, 14% for methane) was lower than for oligomerisation (ca. 16% for propane, 19% for methane). This may well be a consequence of the TG/DTA method of analysis of determining coke, because the amount of graphitic coke in oligomerisation samples may well be much lower than that calculated from TG/DTA spectra. K_c of cracking samples increased and that of oligomerization samples decreased while the heat of sorption showed similar increases for both samples with increasing graphitic coke content. The similar heats of sorption suggest that graphitic coke probably offered the same amount of stabilization to the adsorbed phase.

Because of the small K_c and extremely short residence time in coked HM relative to uncoked HM, it would be expected that the micro-pores were essentially blocked and that the macro model applied, as suggested by the BET results. The macro model, however, gave the poorest correlation. The larger hydrocarbons in particular required the R_xK_y model to predict the skewed, severely tailing response curves. This suggested that two-pore systems still existed. Methane diffusion in the coked samples must be too fast to allow separation of K_y and K_c. Typically, methane diffusivity was approximately two orders of magnitude larger than all the other diffusivities which were comparable in magnitude. K_y and K_c were, however, separated using the R_xK_y model under diffusion limiting conditions. It was therefore more likely that a second pore system with small K_c and D_c existed. The latter may be a small fraction of the micro-pores which were not blocked. This in turn is consistant with the residual activity of the catalyst at time of the termination of the run, which was much larger than that suggested by the marked decrease in the BET surface area or micro-pore voidage. It appears

that these surface characterization techniques have limitations for zeolites with carbonaceous deposits. The extremely small K_c observed suggested very low surface areas for adsorption. Skewing and tailing was more severe in the absence of high boiling point hydrocarbons. Overall adsorption also increased with a reduction in high boiling point hydrocarbons, particularly noticeable at 50°C (see HM diffusion data of coked samples in Appendix C), possibly indicating the availability of greater surface area or better stabilization.

The increasing proportional reduction in K_c with increasing molecular size suggests that the available surface area for adsorption decreased with increasing molecular size. This in turn suggests that pore shrinkage was taking place. Methane being the smallest molecule would be able to access the most adsorption sites and hence showed the smallest relative decrease in K_c. It is also possible that the structure of the coked pore system stabilized the adsorption of methane more than the others, but this would not account for the large difference in diffusivity between methane and the other hydrocarbons.

The diffusivity in HM did not show the three orders of magnitude decrease with coke as observed in HY, but instead showed an order of magnitude decrease for propane, no change for n-butane and an increase for i-butane. Although the range of graphitic coke content was narrow, no systematic variation was observed in K_c and D_c as was the case in HY. The diffusion in uncoked HY was faster than in uncoked HM, while for the coked samples the opposite was seen. It is also interesting to note that the propane diffusivity after oligomerisation was much higher than after cracking, although the amount of coke in samples deactivated by oligomerisation was considerably higher. A heulistical argument gives that lowering K_c increases D_c only if sorption sites are poisoned without introducing substantial steric hindrance. In such a case the interaction between the diffusing molecules and the pore wall is reduced, facilitating surface diffusion. Given the dramatic decrease in K_c after oligomerisation and the seeming accessibilty of ammonia to more than one half of the acid sites initially present in HM, it seems unlikely that the absence of large decrease in D_c is due to lowered K_c resulting from site poisoning. In order to measure D_c accurately at the mean residence time of a matter of a few seconds, the tail of the response curve must be precisely recorded. The surprisingly large values of diffusivities in coked HM may in part be due to the difficulty presented by the need for more accurate data capturing.

In HM, adsorption after cracking was found to be larger than after oligomerisation. This was possibly due to the lower coke content of the cracking sample (3.1%) as opposed to the oligomerisation samples (≈ 10%) and therefore more surface area was available for adsorption. However, in the cracking sample K_c was found to decrease with increasing velocity, particularly for propane, while in oligomerisation no such trend was observed although the data scattered by two-fold. This is inconsistent with the hypothesis of saturated sorption as discussed for cracking, as the saturation levels for oligomerisation were expected to be considerably lower than for cracking catalysts. On the other hand, the fact that K_c was almost invariant with temperature for the oligomerisation samples containing high boiling point hydrocarbons may mean that saturation has taken place. However, for samples with no high boiling point hydrocarbons large variations in K_c with temperature were observed. To clarify these points it would be necessary to make accurate isotherm measurements on these samples to test the linearity and saturation levels.

The HM samples regenerated in nitrogen removing most of high boiling point hydrocarbons had slightly higher adsorption constants than the other samples and tended to behave more like the cracking samples. These HM samples were active before regeneration, and therefore a larger portion of coke than expected must have been higher boiling point hydrocarbons. The reaction could have been slowed down by severe diffusion limitation and strong adsorption of product. During regeneration these molecules, due to the diffusional limitation and lower pressure, were rather cracked to smaller fractions than boiled off, producing much more graphitic coke (the TG/DTA method of coke analysis would not detect this). This would result in an inactive catalyst, similar to that produced after cracking, the lower K_c being due to the higher graphitic coke content. In contrast, during the regeneration in HY, the lower diffusional resistance would allow the heavier fractions to boil off before further transformation in acid sites, resulting in a catalyst which was still active with high sorption but lower diffusivity.

No systematic variations of K_c and D_c with reaction temperature, pressure and time were observed, but rather changes could be correlated indirectly with coke content. It was clear that in the case of hexane cracking with essentially constant pressure and temperature, time on stream should be a relevant parameter. However, any fluctuations in WHSV or temperature overshoot and the variation of product distribution would affect the nature of the coke and therefore K_c and D_c, as was observed by variations at

approximately constant coke content. In the case of oligomerisation, where temperature and pressure were varied together with WHSV, temperature runaway, activity, start-up procedure and the change in product spectrum would affect not only the coke content, but the nature of the coke which yielded scattered results at similar coke levels. This work shows that a knowledge of high boiling point hydrocarbons and graphitic coke as determined by TG/DTA alone was not enough to asses systematically trends in K_c and D_c, but that a more detailed analysis of the nature and position of the coke would be required together with the history of its formation.

5.8 SUMMARY

Modelling showed that macro-pore adsorption in the presence of severe diffusional resistance can result in RTD curves with long tails. Axial dispersion could not be determined from coked catalyst samples but had to be estimated from dispersion correlations of methane diffusion in fresh HY and HM. Methane and propane diffusion in Linde 5A molecular sieves was adequately represented by the R_x model, the results comparing favourably with those in the literature.

The diffusivities of light hydrocarbons in fresh HY were too large to measure. In fresh HM the diffusion of methane was fast, but propane, n- and i-butane diffusional resistance was significant. Diffusivity decreased and adsorption constants increased with increasing molecular size. The adsorption constants in HM were much larger than in HY, indicating that HM had much stronger acid sites. The diffusional resistance in HM was much larger than in HY, reflecting the steric hindrance owing to the one-dimensional pore structure of HM. The meso-pores in HY, which effectively gave HY tri-disperse pore structure, contributed significantly to the macro-pore surface area, but its effect could not be quantified.

Following hexane cracking over HY the adsorption constants and the heats of sorption increased with increasing coke content. The adsorbed phase appeared to be more stable, suggesting that coke must offer stabilization to the adsorbing molecules. The R_xK_y model was neccessary to predict the response curves at above 10 and 13 wt% graphitic coke for propane and methane respectively, thus illustrating the significance of the contribution of the macro-pore surface area. Diffusivity decreased by approximately three orders of magnitude with an increase of graphitic coke up to 14 wt%. Below 8 and 10

wt% graphitic coke the diffusivities of propane and methane, repectively, was too large to measure.

After hexane cracking over HM the R_xK_y model was neccesary to predict the response curves at 3.1 wt% graphitic coke. Large decreases in adsorption constant and diffusivity were observed, the latter by three orders of magnitude. Parameters showed large variations with velocity. Pore blockage was the dominant mechanism causing deactivation with severe diffusional limitation.

The macro-pore contribution to the adsorption constant in HY was much greater than in HM, corresponding to the five-fold greater surface area observed in the former. Diffusional resistance in HM at 3 wt% graphitic coke was greater than that of HY at 14 wt% coke. The results suggest that partial pore blockage was the dominant mechanism of deactivation in HY in contrast to HM. In addition, active site poisoning also occurred in both HY and HM as demontrated by ammonia TPD

In HY after oligomerisation, adsorption constant and diffusivity decreased while heats of sorption increased with increasing coke content. The changes in the adsorption constants in HY after oligomerisation taken relative to those of fresh HY were similar for all the hydrocarbons, indicating that all the gases accessed a comparable surface area, although the relative change for i-butane was slightly larger. The R_xK_y model had to be applied at successively lower graphitic coke content as the molecular size of the tracer gas increased. The diffusivities at similar total coke contents were orders of magnitude greater than that in HY after hexane cracking. The dominant deactivation mechanism appeared to be partial pore blockage with a large reduction in accessible surface area.

For methane diffusion in HM after oligomerisation, the R_x model proved to be adequate. For the larger hydrocarbons R_xK_y model was neccessary to predict all the response curves, indicating that the micro-pore system must still exist contrary to BET and porosimetry data. The diffusivity of methane was large when compared to those of the higher hydrocarbons for which diffusional resistance was substantial. The change in the relative adsorption constant increased with increasing molecular size, suggesting that the available surface area decreased with increasing molecular size. Diffusivity decreased by an order of magnitude for propane, showed no change for n-butane and increased for i-butane in coked samples. However no systematic variation of adsorption constant and diffusivity with increasing coke content was

observed. The diffusivities in HM were much greater than the diffusivities in HY after oligomerisation, in contrast to the case after cracking or in fresh catalysts. The deactivation mechanism in HM appeared to be primarily total pore blockage in the one dimesional pore structure causing severe reduction in surface area.

6 CONCLUSIONS

This chapter considers all the findings of the experiments completed in this work. These findings are integrated in an effort to postulate a deactivation mechanism for hexane cracking and propene oligomerisation.

6.1 Adsorption and diffusion in fresh HY and HM

The application of the GC technique using the bidisperse pore model in combination with Fourier analysis was shown to adequately represent the diffusion of methane and propane in 5A molecular sieves. The crystallite size distribution was needed to predict the data accurately. The adsorption (K_c = 54) and the diffusivity (D_c = 1.5 x 10^{-9} cm^2/s) at 200°C as well as the heat of sorption (E_{Kc} = 33.2 kJ/mol) and diffusion activation energy (E_{Dc} = 21.1 kJ/mol) for propane compared favourably with the values reported in the literature.

In HY the adsorption constant increased with increasing molecular size, the order at 100°C given by methane (4.1) < propane (72.4) < i-butane (350) < n-butane (399), while the heats of sorption followed the order methane (9.6 kJ/mol) < i-butane (22.5) < n-butane (26.8) ≈ propane (27.1). The diffusivity in the temperature range 50-150°C was too large to measure, with the response curves for methane and i-butane being well predicted by the dispersion model. However, tailing of the propane and n-butane response curves suggested that diffusional resistance was large. The higher heats of sorption for the non-symmetrical molecules indicate a more stable adsorbed phase. It may thus be proposed that due to the high acid site density of HY, some of these non-symmetrical molecules adsorb on two sites, thereby causing the long tail and inability of the model to predict the tail. Pore size distribution data showed a tri-disperse pore system, which might limit the applicability of the bidisperse pore model. It may well be that the surface skin effects on the extrudates (due to the binder) are being observed as the meso-pore system (60 Å) in the crushed samples.

From BET and porosity data it was clear that the macro-pore surface area (primarily due to the meso-pores) constituted nearly 20% of the total surface area. This would therefore be expected to contribute to the total adsorption, although this effect could not be quatified. The adsorption properties of this region is not clearly understood, but the meso-pore adsorption may affect the transport properties of the tracer gas.

The adsorption constants of HM were much larger than those of HY and also increased with molecular size, following the order methane (9.1) < propane (784) < i-butane (6720) < n-butane (6895) at 100°C. Heats of sorption followed the order methane (24 kJ/mol) < propane (38) < n-butane (49) ≈ i-butane (50), the larger values than HY showing a more stable adsorbed phase. This was substantiated by the greater number of strong acid sites observed from TPD, although HY had 50% more maximum theoretical Brønsted acid sites. The diffusivity of methane in HM was too large to determine, while that for the other hydrocarbons followed the order propane (4.9 x 10-8 cm^2/s) > n-butane (1.11 x 10^{-9}) > i-butane (5.1 x 10^{-10}) at 100°C. The bidisperse pore model was shown to fit the data well. It was found that the diffusivity in HM was three orders of magnitude greater than in 5A molecular sieves, which is at variance with the values reported in the literature. This was attributed in part to the fact that in this work intracrystalline diffusivity was measured and in addition the crystallite size distribution was taken into account, whereas previous data found in the literature considered only constant crystallite size and measured overall effective diffusivity.

6.2 Hexane cracking

The rapid decrease in the catalyst activity (i.e., most of the deactivation took place within the first hour) was paralleled by a rapid increase in coke content. The olefin to paraffin ratio increased from 0.1 to 1.0 while the C_4 to C_3 ratio decreased with increasing coke content. Langmuir kinetics using the Wojciechowski (1968) decay function predicted the data well. Modelling showed that the reaction was inhibited by the strong adsorption of olefinic products. HM lost 2 active sites per decay event while HY lost 1.5. Nevertheless HY lost active sites at a greater rate than HM, although HY deactivated more slowly. These estimations suggest that pore blockage was the dominant mechanism in HM. HY must have considerably more accessible active sites for hexane cracking than HM because of its slower deactivation rate. This was also supported by the fact that HM deactivated at very low coke levels.

The TG/DTA analysis indicated the presence of one type of coke on hexane cracking samples with an exotherm at approximately 500°C. Skeleton density of HY decreased while the bulk density increased with increasing coke content on account of the volume occupied by coke. Macro- and meso-pore volume showed very little change while the micro-pore volume decreased with

increasing coke content. This trend was complemented by the decrease in BET surface area, although the change was much greater than that for the micro-pore volume. The decrease in the macro-pore surface area was not in accordance with the negligible change in macro- and meso-pore volume. The actual decrease in micro-pore volume was always greater than the estimated volume of coke.

The above analytical techniques however do have limitations. In the case of hexane cracking the TG/DTA quantified reasonably well the graphitic coke content of the catalyst, but gave no indication as to the actual species constituting the coke. Thus the volume of coke could not be accurately estimated. The skeleton and bulk densities were subject only to experimental error. However, porosity and macro-pore surface area measurements rested on the assumption that the contact angle of mercury was 130° and that all the pores were perfectly cylindrical. The method cannot account for phenomena such as skin effects (bottle neck pores). This was seen by changes in macro-pore surface area, which must be due to subtle changes in the meso-pore distribution which was the primary contributor to the total macro-pore surface area. The effect that coke has on the BET technique is not known, but it is clear that the nitrogen molecule cannot access all the avaliable surface area due to pore restrictions caused by coke. For the purpose of assessing the effect of changing surface area in hexane cracking it would be of interest to measure hexane adsorption capacities of coked samples.

Nevertheless, it may be proposed that almost all the coke formed during hexane cracking was in the micro-pores. Both hexane cracking and coking effectively took place in the micro-pores, the hexane cracking rate being slowed down by pore diffusional resistance and loss of surface area due to the inability of the reactant to reach the remaining active sites.

Ammonia TPD showed that the number of acid sites decreased by 20% for HY and 10% for HM, the changes in the h-peak being twice as large. These changes were much smaller than the changes in BET surface area or the micro-pore voidage. The decrease in acid sites was much smaller than the decrease in activity, while the amount of acid sites decreased faster in HM than in HY as was observed with their respective activities. Ammonia TPD was limited by the poor seperation of the l- and h-peak in the case of HY, which had to be somewhat arbitrarily chosen. In addition ammonia being a small basic molecule, would be able to adsorb on sites which might not be accessible to reactant molecules. Even on fresh HM, ammonia may access considerably more acid sites than are actually available to hexane.

TPD showed that hexane cracking eliminated strong acid sites preferentially to the weaker acid sites. It would be expected that the strong acid sites would be the place where coke would most likely form. Based on the above discussion it is clear that hexane would only be able to access a small fraction of the active sites measured by ammonia TPD. Hence deactivation occurs both as a result of elimination of the most active sites by site poisoning and by partial blockage which renders some of the remaining sites inaccessible to hexane.

Diffusion experiments in HY showed an increase in adsorption constant for methane and propane with increasing coke content using the R_x model. However, high coke contents required the addition of the macro-pore adsorption term, i.e., R_xK_y model, to predict the data. The R_xK_y model predicted a decrease for methane and a smaller increase for propane adsorption constant with increasing coke content. The diffusivity decreased by three orders of magnitude with increasing coke content, diffusional resistance becoming significant at the critical coke contents of 8% for propane and 10% for methane in HY. Heats of sorption increased with coke content. Regeneration of HY in air restored its initial adsorption properties.

Diffusion experiments on HM necessitated the use of the R_xK_y model to predict the data. Adsorption and diffusivity decreased markedly with coke content.

This technique was hampered by the possibilities of non-linear system response for the coked samples, particularly in the case of HM in which the parameters showed large variations with velocity. The inability to separate the macro-pore adsorption under conditions of fast diffusion could have caused the diffusivity to be an order of magnitude too large, as well as yielding an incorrect trend of adsorption constant with coke content.

It may be proposed that increases in coke content under certain conditions can stabilise the adsorption of hydrocarbons on catalysts as shown by the HY data. The decrease in diffusivity in HY with increasing coke levels shows that coke provides increased diffusional limitations to reactant as opposed to complete pore blockage. Thus the reaction would be expected to become diffusion limited. This analysis is only approximate as propane and not hexane was used as the tracer. The use of hexane was infeasible on account of the higher temperatures required to carry out the experiments with reasonable residence time. This in turn led to cracking of hexane. The

behaviour of HM at only 3% coke suggests that the tracer gas was not able to access a large portion of the pores, that there were large diffusional limitations, and that in this case deactivation must be due to the inability of hexane to reach the acid sites. The fact that coke increased the adsorption properties in HY may well indicate that olefinic products adsorb strongly, but not necessarily take part in the reaction. The remaining acid sites would be catalytically weaker as demonstrated by TPD, but due to the influence of adjacent coke molecules they would adsorb hydrocarbons strongly.

From the above conclusions it is proposed that the cracking reaction as well as the coke formation takes place almost entirely in the micro-pores. During the initial reaction stages in HY, the diffusion of reactant and product in the supercages is fast. The high acid site concentration and the large amount of hexane which can access the acid sites cause a high reaction rate, which is paralled by a high coking rate. The secondary reaction rates, alkylation and hydride transfer to the olefins, are high so as to provide the high initial paraffin to olefin ratios. The coke precursors must therefore be the olefins which adsorb strongly on acid sites. Once these strongly adsorbed olefins become hydrogen deficient and undergo addition reactions their adsorption is almost permanent.

These adsorbed coke molecules reduce the pore dimensions and even block pore openings partially. Thus the access of reactant is retarded by diffusion limitations. These coke molecules tend to remove the strong acid sites preferentially. The available acid sites would still be able to crack hexane. The remaining weaker acid sites are able to adsorb hydrocarbons strongly with additional stabilisation of adjacent coke molecules, but these sites are less catalytically active for the promotion of the secondary transformations. Secondary transformations also have bulky intermediates, the formation of which are not favoured in the smaller pores. Hence the paraffin to olefin ratio decreases with increased coke content. The primary cracking step is retarded due to diffusion limitations and inability of the reactant to access the acid sites. The secondary transformations are retarded by the predominance of weaker acid sites, steric constraints of the coked pores and diffusional limitations. Clearly hexane cracking should have negligible effect on the meso- and macro-pores, in accordance with the porosimetry data.

In the case of HM a similar mechanism may be proposed. Due to the high concentration of strong acid sites it was expected that the reaction rate would be faster. However, these strong acid sites would also accelerate the

secondary transformations as well as the coking reactions, thus causing rapid deactivation. Indeed, rapid deactivation of HM lowered the activity to below that of HY within minutes on stream. It follows therefore that the initial coking rate of HM is high due to the strong acid sites.

Because of the one dimensional pore structure in HM a small amount of coke would make the acid sites inaccessible to reactant and products as shown by the severe diffusional resistance of tracer gases at only 3% coke. However these sites are still accessible to ammonia. Therefore, the activity in HM is reduced much more rapidly than in HY because the pores are rapidly blocked and the blockage prevents hexane from reaching active sites, while for HY the pores first undergo a stage of enhanced diffusional resistance before becoming blocked towards reactant and product.

6.3 Propene oligomerisation

In HY increasing WHSV caused increased coking and decreased activity. Thus there will be an optimum WHSV which produces the highest LPR and the largest amount of liquid per g of catalyst. Temperature runaway, particularly above 300°C, caused a rapid build-up of graphitic coke and modified the selectivity of the catalyst to favour heavier fractions. No temperature runaway was observed for HM. HY had a five-fold higher temperature rise due to the heat of sorption of propene during start-up and was overall more active than HM. Clearly, propene being olefinic adsorbs more readily on acid sites than aliphatics, and the larger number of acid sites on HY is an important parameter determining the amount of heat generated. At the same time, the smaller diffusional restrictions in HY than in HM allows rapid diffusion of propene into the pores. Increasing time on stream favoured the production of heavier liquid fractions at the expense of dimer over HY and at reaction temperatures above 300°C over HM. Graphitic coke contents were much higher in HY than in HM at similar residual activity.

For HY, a reaction temperature of 350°C produced high graphitic coke content, with lighter liquid fractions being favoured at small time on stream. At 100°C the composition was almost invariant with time on stream, suggesting that the high boiling point hydrocarbons responsible for the deactivation had no significant effect on the product distribution. HM was inactive below 200°C while HY was active below 100°C. At 250°C HM favoured the formation of heavier fractions with time on stream while at 350°C the opposite was observed. Graphitic coke content increased with reaction temperature.

Oligomerisation has a much lower activation energy than cracking, requiring weaker acid sites and lower temperatures. This is seen from the longer lifetime of the oligomerisation notwithstanding the removal of strong acid sites by the formation of graphitic coke.

High pressure increased LPR and lifetime but appeared to favour lighter fractions, perhaps because longer chain length products are less volatile at high pressure and do not desorb as readily. The activity of HY increased more rapidly with an increase in pressure than HM. The graphitic coke content in HY increased with reaction pressure, while in HM no significant change was observed. For HY the graphitic coke content dictated the product composition above temperature and pressure. Regeneration of HY in flowing nitrogen at 350°C restored its initial activity with a slightly heavier product fraction, while HM became inactive after treatment with nitrogen.

TG/DTA performed in flowing air gave two exotherms (due to the combustion of coke) at 350 and 500°C, assigned to high boiling point hydrocarbons and graphitic coke, respectively. This allowed the estimation of the amount of each fraction as well as the volume occupied by coke. The magnitude of the exotherms was proportional to the amount of coke on the catalyst. This technique was limited by the fact that high boiling point hydrocarbons crack during the temperature programming of the sample and be transformed to graphitic coke. The cracking reactions, being endothermic, would also be promoted by the combustion exotherms. This clearly would yield an overestimation of the graphitic coke content. This limitation applies equally to the definition of coke used in this study. To isolate coke the deactivated catalyst was flushed in flowing nitrogen at the reaction temperature and 1 atm. This is valid only if the long chainlength hydrocarbons trapped inside the zeolite pores can be rapidly removed without further transformation. However, particularly in the case of HM where the reaction temperature (and hence temperature at which nitrogen was passed over the deactivated sample) was typically higher, diffusional limitations larger on account of its one dimensional pore structure, and acid sites generally stronger than in the case of HY, the residual heavier fractions can crack and convert to graphitic coke, premanently blocking the main channels. This possibility must be borne in mind in interpreting the experimental data. The estimated volume of coke was always greater than the volume of coke determined from porosimetry measurements.

For samples reacted at 100°C, additional error is introduced in the estimation of high boiling point hydrocarbons due to the difficulty in

seperating the desorption of water from high boiling point hydrocarbons below 200°C. The nature of the high boiling point hydrocarbons, which could yield different cracking rates and thus different amounts of graphitic coke, is also not known.

Porosimetry showed that the total pore volume decreased with coking. The coke after oligomerisation appeared to affect the meso-pore fraction as well as the micro-pores in HY. The macro-pore surface area decreased by 50% in HY due to the large meso-pore fraction, while in HM, because of the order of magnitude larger macro-pore diameter, the macro-pore surface area showed little vatiation. BET suface area showed much more rapid decrease than the micro-pore volume fraction or the amount of sites accessible to ammonia, particularly in the case of HM, suggesting that the pore diameter restrictions were so large that only molecules as small as ammonia could enter the mordenite main channels.

The presence of high boiling point hydrocarbons appeared to render the applications of the surface characterization techniques rather limited. In the case of mercury porosimetry, a long time was required to reach the equilibrium at each incremental step. Deactivated HM samples even gave inconsistent results in that the total porosity computed from skeleton and bulk densities was smaller than the sum of the macro- and meso-pore volumes. It is not clear what effect the presence of carbonaceous material has on the adsorption of nitrogen in BET, nor if high boiling point hydrocarbons can move from macro-pores to micro-pores with increasing pressure in the mercury porosimetry, distorting the pore size distribution.

The reduction of the total number of acid sites, as measured by ammonia TPD, is 40% in HY and 25% in HM. The number of acid sites decreased with increasing coke content. The decrease in the number of acid sites was greater at the same wt% coke than in the case of cracking in HY, while HM followed a similar trend as that of cracking.

These results were limited because any attempt to separate the l- and h-peaks was hampered by the desorption of high boiling point hydrocarbons. Accounting for the high boiling point hydrocarbons using baseline correction runs was not possible as ammonia interfered with the desorption of high boiling point hydrocarbons, shifting the desorption spectrum. Additionally the amount of adsorbed ammonia was small while the desorption of high boiling point hydrocarbons was large, which led to the magnification of errors upon baseline subtraction. These problems were due to the use of the TCD as the

detector. The use of a mass spectrometer or an infra-red analyser would eliminate many of these problems, but might introduce new difficulties. These problems prevented drawing firm conculsions as regards the strength of the acid sites after propene oligomerisation. However, titration values were independent of the desorption of high boiling point hydrocarbons and clearly indicated that the number of acid sites adsorbing ammonia decreased.

Adsorption and diffusion experiments in HY showed that the R_xK_y model was necessary to predict the response of methane, propane, n- and i-butane. However the R_xK_y model degenerated into the R_x model (due to increasing diffusivity) at successively lower levels of graphitic coke content with increasing molecular size of the tracer gas. Adsorption constants decreased as a result of deactivation. The change in the adsorption constant, when taken relative to the adsorption constant in fresh HY, was essentially the same for all the tracer gas molecules. At the same time heats of sorption were found to increase with increasing graphitic coke content.

On the other hand, diffusivity decreased by three orders of magnitude for the tracer gases, with the absolute values being orders of magnitude greater than those after cracking at similar total coke contents. For reaction at 350°C the transport properties tended to those of cracking, except that the coke content was higher. Comparison of diffusion data of various HY samples with similar graphitic coke levels, as well as those with the same total coke mass but different coke compositions, indicated that high boiling point hydrocarbons reduced the adsorption constant and at the same time presented much less diffusional restriction than the equivalent amount of graphitic coke. It is proposed that a large fraction of high boiling point hydrocarbons is present in the meso-pores, blocking the pore mouths. These high boiling point hydrocarbons which are outside the micro-pores should not affect the micro-pore diffusivity. When two HY samples, one with only graphitic coke and the other with the same amount of graphitic coke but in addition containing high boiling point hydrocarbons, were compared, it was evident that high boiling point hydrocarbons lowered diffusivities, although not nearly as much as the equivalent mass of graphitic coke. Hence high boiling point hydrocarbons also occupy volume within the micro-pores and present some steric hindrance. These high boiling point hydrocarbons do not stabilize the adsorbed phase of the hydrocarbons. Whether in meso-pores or micro-pores, they block pore mouths and reduce the micro-pore surface area, thereby reducing the adsorption constant. Moreover, they may cover sorption sites inside the micro-pores, lowering adsorption. The high boiling point hydrocarbons in the meso-pores are easily flushed out of HY in flowing

nitrogen at an elevated temperature, restoring the activity of HY for oligomerisation. The reaction at 200°C appears to deposit little coke permanently and the activity was fully restored after the nitrogen treatment at 350°C. This regeneration also suggests that the amount of graphitic coke determined by TG/DTA is most likely an overestimation.

The same experiments in HM showed that the R_x model predicted the transport properties of methane. However, the R_xK_y model was necessary to predict the response curves of all the other tracer gases. This clearly showed the presence of a small fraction of micro-pores. The adsorption constants of all the tracer gases at 100°C were between 0.1 and 10 and showed no marked trend with graphitic coke. Samples containing high boiling point hydrocarbons had slightly lower adsorption constants, while the heats of sorption were almost negligible over the range of temperatures studied. The change in adsorption constants after oligomerisation, relative to the adsorption constant in fresh HM, showed a decrease with increasing molecular size, which meant that the surface area accessed by each tracer gas must have been different.

When compared to the diffusivity in fresh HM, the diffusivities in deactivated samples showed an order of magnitude decrease for propane, no change for n-butane and an increase for i-butane. Diffusivities showed no marked trend with graphitic coke content, but the diffusivity of samples after oligomerisation was three orders of magnitude greater than in samples after hexane cracking. The diffusivities of propane, n-and i-butane were of the same order of magnitude.

The significant reduction in the BET surface area and the adsorption constant following oligomerisation in HM suggest that nearly all of the micro-porosity is not available to nitrogen or the hydrocarbons. However, ammonia is still able to enter the mordenite main channels. Hence a very severe reduction in pore diameter has occurred. That the diffusivities of butanes determined using the R_xK_y model were as large as those measured using fresh HM indicates that a small fraction of the pores were unaffected by deactivation, were fully accessible to the hydrocarbons, and small site poisoning might have occurred, facilitating diffusion.

Such a large reduction in the surface area of HM is not consistent with the activity of the catalyst at the end of the run, which was by no means negligibly small. A plausible explanation is that the high boiling point hydrocarbons are trapped more easily in the HM pores on account of its one dimensional channel structure. Upon flushing the catalyst in nitrogen at the

reaction temperature and 1 atm after the reaction, these high boiling point hydrocarbons are not easily removed, and particularly in light of relatively high reaction temperatures (all but one oligomerisation run over HM were performed at or above 300°C), they crack over acid sites and are transformed into graphitic coke, blocking pores. This also explains why passing nitrogen over spent HM at 350°C not only failed to restore its initial activity, but eliminated altogether the residual activity of the catalyst. This in turn suggests that the pore structure of HM when the catalyst is taken out of the reactor is different from that under the reaction conditions. In contrast, in the case of HY, its open pore structure enables the high boiling point hydrocarbons to desorb more readily, and its weaker acid sites should also lower the extent of hydrocarbon transformation.

One limitation of the diffusion technique lay in the difficulty of fitting the severe tailing of the response curves which could have contributed to the scatter in the data. It is also possible that the response of coked samples was non-linear. It would be necessary to determine adsorption isotherms for the coked samples to establish saturation levels and the linear response range. The inability to separate K_y and K_c in all cases would lead to incorrect trends with coke content. The classification of coke as high boiling point hydrocarbons and graphitic coke was not sufficient to establish exact trends as the nature and position of this coke would also have an effect on the transport properties.

From these conclusions the following mechanism may be proposed. When propene is introduced into HY at 25°C and 8 atm (i.e., gas phase), the heat of sorption causes a high temperature rise, both on account of the large number of acid sites and the negligible diffusional resistance presented to propene by the open pore structure of HY. The temperature rise of the catalyst of approximately 50-120°C is also aided by some heat of reaction, the liquid product of which (only a few drops) appears once the system has been pumped to pressure (liquid phase). This heat of sorption/reaction lasts only a few minutes and is not expected to cause coking. When the system is then heated at 50 atm to just beyond the flash point of the feed, the reactant molecules become highly mobile under negligible diffusional resistance, and in the presence of a high concentration of acid sites, rapid reaction takes place. The reaction, being exothermic, causes an uncontrollable temperature runaway. The high temperature together with the high concentration of olefins (coke precursors) produces a high coking rate. Cracking of oligomers (although not favoured by high pressure) as well as secondary transformation (favoured by the high concentration of olefins) take place causing coke build-up.

Catalyst deactivation proceeds via the strong adsorption of large product molecules blocking pores and reducing the effective surface area, aided by the gradual formation of graphitic coke. These reactions essentially occur in the micro-pores under the infuence of strong acid sites. The oligomers are mobile and migrate into the meso-pores, where they block the mouths of the micro-pores. The formation of oligomers in the supercages, which are too large to leave, are also responsible for deactivation. This would constitute a blocked pore in the case of hydrocarbons, but ammonia would still be able to access the remaining acid sites.

Initially the concentration of strong acid sites is high (favouring cracking) and the diffusional resistance is low; thus oligomers which are formed are able to diffuse rapidly out of the catalyst, while the larger oligomers are easily cracked. As graphitic coke builds up, cracking reactions become less likely, simultanously the diffusional resistance becomes appreciable, and the oligomers spend more time in the catalyst, producing heavier fractions. Increasing graphitic coke reduces the number of strong acid sites.

Increasing temperature promotes cracking reactions and thus the graphitic coke formation. The coking rate will initially be fast, but will decrease rapidly. Oligomerisation which requires weaker acid sites will decrease more slowly, being hindered primarily by the diffusional resistance due to the presence of graphitic coke and pore mouth blockage. At low temperatures, cracking activity is negligible, and therefore little graphitic coke build-up is expected. Deactivation is caused by the strong adsorption of product oligomers which cannot desorb at these low temperatures. Increasing pressure promotes the oligomerisation reaction and reduces cracking. This will result in the high LPR observed. Low pressure alternatively promotes cracking. Because of the large concentration of olefins, coke formation is probably dictated largely by the temperature and the availability of strong acid sites.

For HM a similar mechanism may be proposed, but the results are different due to the one-dimensional pore structure and a larger number of stronger acid sites. When propene is introduced into the reactor at 25°C, the smaller temperature rise due to the heat of sorption (5-25°C) is observed because of the significant diffusional resistance. Because of the strong acid sites, feed and product adsorb very strongly at low temperature, making the catalyst inactive. No liquid was observed when the system was pumped to pressure. Heating to just beyond the flash point does not produce temperature runaway,

due to strong adsorption and diffusion limitations. Therefore no premature coking occurs in HM.

Reaction temperatures above 200°C allow the desorption of reactant and product, and therefore the catalyst becomes active. The higher reaction temperature required to obtain activity also favours cracking which is promoted by strong acid sites. The cracking reactions in this case causes predominantly pore blockage. The diffusion to the remaining acid sites is also severely restricted. Due to the higher reaction temperatures the high boiling point hydrocarbons are not as strongly adsorbed, so that deactivation is primarily due to graphitic coke. Increasing the pressure still caused the deactivation to be dominated by cracking reactions which form graphitic coke. The slower desorption of the oligomers due to severe diffusional resistance also favours the formation of coke.

As mentioned earlier, during regeneration in nitrogen after oligomerisation at 200°C over HY, all the high boiling point hydrocarbons in the meso-pores are readily desorbed, "unblocking" the pore mouths. The high boiling point hydrocarbons in the micro-pores may also diffuse out of the pores without undergoing further transformation on acid sites. Although some of the strong acid sites are likely to be permanently poisoned, the acid sites needed for oligomerisation are not as strong as those needed for hexane cracking, and the activity of fresh HY is restored. In contrast, in the case of HM, a difference of 50°C between regeneration (350°C) and reaction (300°C), as opposed to 150°C in the case of HY, is not high enough to desorb high boiling point hydrocarbons, almost all of which are in the micro-pores. Far greater graphitic coke is deposited in HM than in HY, on account of the higher reaction temperature and stronger acid sites. This, together with the one dimensional pore structure, introduces significant steric hindrances, permanently trapping the high boiling point hydrocarbons which are converted to graphitic coke, eliminating any residual activity.

It is clear from the foregoing discussion that the zeolite pore structure, reactant and product molecules, pressure and temperature all play a role in determining the mode of deactivation and how the carbonaceous material in turn affects the acidity and the porosity of the zeolite. The definition of coke has also been found to be critical, since altering the pressure subsequent to reaction may introduce further changes in the catalyst pore structure. Diffusion experiments were able to give some indication of the location of the carbonaceous material after reaction. While each technique was shown to have limitations, combining the results from TPD, TG/DTA,

porosimetry, BET and diffusion experiments enabled the construction of reasonably consistent models outlining the deactivation of zeolite-Y and H-mordenite due to hexane cracking and high pressure propene oligomerisation.

7. REFERENCES

Abbot, J. and Wojciechowski, B.W., J. Catal., 1987, 104, 80

Ahn, B.-J., Zoulalian, A. and Smith, J.M., A.I.Ch.E. J., 1986, 32, 170

Anderssen, A.S. and White, E.T., Chem. Eng. Sci., 1970, 25, 1015

Androutsopolous, G.P. and Mann, R., Chem. Eng. Sci., 1976, 31, 1131

Appleby, W.G., Gibson, J.W. and Good, G.M., I&EC Proc. Des. Dev., 1962, 1, 102

Beeckman, J.W. and Froment, G.F., Chem. Eng. Sci., 1980, 35, 805

Beeckman, J.W. and Froment, G.F., I&EC Fund., 1979, 18, 3, 245

Beeckman, J.W. and Froment, G.F., I&EC Fund., 1982, 21, 243

Best, D.A., Pachovsky, R.A. and Wojciechowski, B.W., Can. J. Chem. Eng., 1973, 49, 809

Beuther, H., Larsen, O.A. and Perrotta, A.J., Catalyst Deactivation, B Delmon and G.F. Forment (Ed.), 1980, 104

Biswas, J., Do, D.D., Greenfield, P.F. and Smith, J.M., Appl. Catal., 1987a, 32, 217

Biswas, J., Do, D.D., Greenfield, P.F. and Smith, J.M., Appl. Catal., 1987b, 32, 235

Blackmond, D.G., Goodwin, J.G. and Lester, J.E., J. Catal., 1982, 78, 34

Boersma-Klein, W. and Moulijn, J.A., Chem. Eng. Sci., 1979, 34, 959

Boniface, H.A. and Ruthven, D.M., Chem. Eng. Sci., 1985, 40, 1401

Brenner, A. and Hucul, D.A., J. Catal., 1979, 56,134

Burghardt, A. and Smith, J.M., Chem. Eng. Sci., 1979, 34, 267

Butt, J.B., ACS Symp. Ser., 1978, 102, 288

Butt, J.B., Delgado-Diaz, S. and Muno, W.E., J. Catal., 1975, 37, 158

Carg, D.R. and Ruthven, D.M., Chem. Eng. Sci., 1974, 29, 571

Carleton, F.B., Kershenbaum, L.S. and Wakeham, W.A., Chem. Eng. Sci., 1978, 33, 1239

Cerro, R.L. and Smith, J.M , A.I.Ch.E. J., 1970, 16, 1035

Cerro, R.L. and Smith. J.M., I&EC Fund., 1969, 8, 796

Chiang, A.S., Dixon, A.G. and Ma, Y.H., Chem. Eng. Sci., 1984a, 39, 1451

Chiang, A.S., Dixon, A.G. and Ma, Y.H., Chem. Eng. Sci., 1984b, 39, 1461

Chihara, K., Suzuki, M. and Kawazoe, K., Chem. Eng. Sci., 1976, 31, 505

Choudary, V.R., J. Chrom., 1974, 98, 491

Chu, C., I&EC Fund., 1968, 7, 3, 509

Cvetanovic, R.J. and Amenomiya, Y., Adv. Catal., 1967, 17, 103

Dadyburjor, D., J Catal., 1983, 79, 222

Dankwerts, P.V., Chem. Eng. Sci., 1953, 2, 1

Dejaifve, P., Auroux, A., Gravelle, P.C., Vedrine, J.C., Gabelica, Z. and Derouane, E.G., J. Catal., 1981, 70, 123

Derrah, R.I., Loughlin, K.F. and Ruthven, D.M., J. Chem. Soc. Faraday Trans. I, 1972, 68, 1947

Do, D.D. and Smith, J.M., Chem. Eng. Sci., 1984, 39, 1689

Dogu, G. and Ercan, C., Can. J. Chem. Eng., 1983, 61, 660

Dogu, G. and Smith, J.M., A.I.Ch.E. J., 1975, 21, 58

Dogu, G. and Smith, J.M., Chem. Eng. Sci., 1976, 31, 123

Drachsel, W. and Becker, K.A., Z. Phys. Chem. Neue Folge, 1980, 122, 91

Eberly, P.E.,Jr., I&E.C Fund., 1969, 8, 25

Eberly, P.E.,Jr., Kimberlin, C.N.,Jr., Millar, W.H. and Drushel, H.V., I&EC Proc. Des. Dev., 1966, 5, 193

Edwards, M.F. and Richardson, J.F., Chem. Eng. Sci., 1968, 23, 109

Eisenbach, D. and Gallei, E., J Catal., 1979, 56, 377

Fahim, M.A., and Wakao, N., Chem. Eng. J., 1982, 25, 1

Fasol, R.E., MSc Thesis, 1983, University of Cape Town

Fetting, F., Gallei, E. and Kredel, P., Ger. Chem. Eng., 1984, 7, 32

Forni, L., Viscardi, C.F. and Olivia, C., J. Catal., 1986a, 97, 469

Forni, L., Viscardi, C.F. and Olivia, C., J. Catal., 1986b, 97, 480

Froment, G.,F. and Bischoff, K.B., Chem. Eng. Sci.,1961, 16, 189

Froment, G.F., Catalyst Deactivation, B. Delmon and G.F. Froment (Ed.), 1980, 1

Froment, G.F., Proc. 7th ICC, The Chemical Society, London, 1976, 1, 10

Froment, G.F., Progress in Catalysis Deactivation, J.L. Figueriredo (Ed.), NATO Advanced Study Institutes Series, E54, 1982, 103

Fu, C.-C., Ramesh, M.S.P., Haynes, H.W.,Jr., A.I.Ch.E. J., 1986, 32, 1848

Fuller, E.N., Schettler, P.D. and Giddings, J.C., I&EC, 1966, 58, 19

Furimsky, E. I&EC Prod. Res. Dev., 1979, 18, 206

Furimsky, E., I&EC Prod. Res. Dev., 1978, 17, 329

Furusawa, T. and Smith, J.M., J. Chem. Eng. Japan, 1974, 7, 470

Gangwal, S.K., Hudgins, R.R. and Silverston, P.L., Can. J. Chem. Eng., 1978, 56, 554

Gangwal, S.K., Hudgins, R.R. and Silverston, P.L., Can. J. Chem. Eng., 1979, 57, 609

Gangwal, S.K., Hudgins, R.R. and Silverston, P.L., Can. J. Chem. Eng., 1980, 58, 33

Gangwal, S.K., Hudgins, R.R., Bryson, A.W. and Silverston, P.L., Can. J. Chem. Eng., 1971, 79, 113

Goddard, M. and Ruthven, D.M., Zeolites, 1986, 6, 445

Gorte, R.J., J. Catal., 1982, 75, 113

Abramovitz, M. and Stegun, I.A., Handbook of Mathematical Formulas, Graphs and Mathematical Tables, 1965, Dover Publications Inc., NY

Haq, N. and Ruthven, D.M., J. Colloid Int. Sci., 1986a, 112, 154

Haq, N. and Ruthven, D.M., J. Colloid Int. Sci., 1986b, 112, 164

Hashimoto, N. and Smith, J.M., A.I.Ch.E. J., 1976, 22, 945

Hashimoto, N. and Smith, J.M., I&E.C Fund., 1973, 12, 353

Hashimoto, N. and Smith, J.M., I&E.C Fund., 1974, 13, 115

Hashimoto, N., Moffat, A.J. and Smith, J.M., A.I.Ch.E. J., 1976, 22, 944

Haynes, H.W.,Jr. and Sarma, P.N.,A.I.Ch.E. J., 1973, 19, 1042

Haynes, H.W.,Jr., A.I.Ch.E. J., 1986, 32, 1750

Haynes, H.W.,Jr., Chem. Eng. Sci., 1975, 30, 955

Hays, J.R., Clements, W.C. and Harris, T.R., A.I.Ch.E. J., 1967, 13, 374

Henry, J.P., Chennakesavan, B. and Smith, J.M., A.I.Ch.E.J., 1961, 7, 10

Hildalgo, C.V., Itoh, H., Hattori, T., Niwa, M. and Murakami, Y., J. Catal., 1984, 85, 362

Hsiang, T.C. and Haynes, H.W.,Jr., Chem. Eng. Sci., 1977, 32, 678

Hsu, L.-K.P. and Haynes, H.W.,Jr., A.I.Ch.E. J., 1981, 27, 81

Itoh, H., Hidalgo, C.V., Hattori, T., Niwa, M. and Murakami, Y., J. Catal., 1984, 85, 521

Jones, D.M. and Giffin, G.L., J. Catal., 1983, 80, 40

Karge, H.G., Proceeding of the Fourth Int. Conf. on Molecular Sieves, Chicago, 1977, J. Katzer (Ed.), A.C.S. Symp. Ser., 40, 584

Karge, H.G., Abke, W., Boldingh, E.P. and Laniecki, M., IX Iberoamerican Symposium on Catalysis, 1984, 582

Kärger, J., A.I.Ch.E. J., 1982, 28, 417

Kärger, J., Pfeiffer, H. and Heink, W., Proc. 6th Int. Zeolite Conf., 1983, 184

Kelly, J.F. and Fuller, O.M., I&E.C Fund., 1980, 19, 11

Kmiotek, S.J., Wu, P. and Ma, Y.H., A.I.Ch.E. Symp. Ser., 219, 1982, 78, 83

Kojima, M., Rautenbach, M.W. and O'Connor, C.T., J. Catal., 1988a, 112, 495

Kojima, M., Rautenbach, M.W. and O'Connor, C.T., J. Catal., 1988b, 112, 505

Kubelkova, L., Novakova, J., Tupa, M. and Tvaruzkova, Z., ACTA Phys. Chem., 1985, 31, 235

Kucèra, E., J. Chrom., 1965, 19, 235

Langner, B.E. and Meyer, S., Catalyst Deactivation, B. Delmon and G.F. Froment (Ed.), 1980, 91

Langner, B.E., App. Catal., 1982, 2, 289

Langner, B.E., I&EC Proc. Des. Dev., 1981, 20, 326

Langner, B.E., J. Catal., 1980, 65, 416

Lee, L.-K. and Ruthven, D.M., Can. J. Chem. Eng., 1979, 57, 65

Lee, L.-K. and Ruthven, D.M., J. Chem. Soc. Faraday Trans. I, 1979, 75, 2406

Lee, L.-K., Yucel, H. and Ruthven, D.M., Can. J. Chem. Eng., 1979,, 57, 71

Leung, K. and Haynes, H.W.,Jr., Chem. Eng. Sci., 1984, 39, 1815

Levenspiel, O., Chemical Reaction Engineering, 1972, Wiley International Edition

Levenspiel, O., The Chemical Reactor Omnibook, 1979, OSU Book Stores

Lin, C.-C., Park, S.W. and Hatcher, W.J.,Jr., I&EC Proc. Des. Dev., 1983, 22, 609

Loughlin, K.F. and Ruthven, D.M., Chem. Eng. Sci., 1972, 27, 1401

Loughlin, K.F., Derrah, R.I. and Ruthven, D.M., Can. J. Chem. Eng., 1971, 49, 67

Ma, Y.H. and Mancel, C., A.I.Ch.E. J., 1972, 18, 1148

MacDonald, W.R. and Habgood, H.W., Can. J. Chem. Eng., 1972, 50, 462

Magnoux, P., Cartraud, P., Mignard, S. and Guisnet, M., J. Catal., 1987a, 106, 235

Magnoux, P., Cartraud, P., Mignard, S. and Guisnet, M., J. Catal., 1987b, 106, 242

Mann, R. and Thompson, G., Chem. Eng. Sci., 1987, 42, 555

McLellan, G.D., Howe, R.F., Parker, L.M. and Bibby, D.M., J. Catal., 1986, 99, 486

Mingle, J.O. and Smith, J.M., A.I.Ch.E. J., 1961, 7, 243

Niwa, M., Iwamoto, M. and Segawa, K.-I., Bull. Chem. Soc. Japan, 1986, 59, 3735

Oliverous, G. and Smith, J.M., A.I.Ch.E. J., 1982, 28, 751

Ozawa, Y. and Bischoff, K.B., I&EC Proc. Des. Dev., 1968a, 7, 68

Ozawa, Y. and Bischoff, K.B., I&EC Proc. Des. Dev., 1968b, 7, 72

Pachovsky, R.A. and Wojciechowski, B.W., Can. J. Chem. Eng., 1971, 49, 365

Pachovsky, R.A., Best, D.A. and Wojciechowski, B.W., I&EC Proc. Des. Dev., 1973, 21, 254

Park, S.H. and Kim, Y.G., Chem. Eng. Sci., 1984a, 39, 523

Park, S.H. and Kim, Y.G., Chem. Eng. Sci., 1984b, 39, 549

Pillai, K.K., Chem. Eng. Sci., 1977, 32, 59

Post, J.G. and van Hoof, J.H.C., Zeolites, 1984, 4, 9

Raghavan, N.S. and Ruthven, D.M., Chem. Eng. Sci., 1985, 40, 699

Raja Rao, M., Wakao, N. and Smith, J.M., I&EC Fund., 1964, 3, 127

Rautenbach, M.W., PhD Thesis, 1986, University of Cape Town

Rieck, J.S. and Bell, A.T., J. Catal., 1984, 85, 143

Rodrigues, A.F., Ahn, B.-J. and Zoulalian, A., A.I.Ch.E. J., 1982, 28, 541

Rollmann, L.D. and Walsh, D.E., J. Catal., 1979, 56, 139

Rollmann, L.D., J. Catal., 1977, 47, 113

Ruckenstein, E., Vaidyanathan, A.S. and Youngquist, G.R., Chem. Eng. Sci., 1971, 26, 1305

Ruthven, D.M. and Derrah, R.I., J. Chem. Soc. Faraday Trans. I, 1975, 71, 2031

Ruthven, D.M. and Doetsch, I.H., A.I.Ch.E. J., 1976, 22, 883

Ruthven, D.M. and Kumar, R., Can. J. Chem. Eng., 1979, 57, 342

Ruthven, D.M. and Loughlin, K.F., Chem. Eng. Sci., 1971a, 26, 577

Ruthven, D.M. and Loughlin, K.F., Chem. Eng. Sci., 1971c, 26, 1145

Ruthven, D.M. and Loughlin, K.F., J. Chem. Soc. Faraday Trans. I, 1972, 68, 696

Ruthven, D.M. and Loughlin, K.F., J. Chem. Soc. Faraday Trans. I, 1971b, 67, 1661

Ruthven, D.M., Lee, L.-K. and Yucel, H., A.I.Ch.E. J., 1980, 26, 16

Ruthven, D.M., A.I.Ch.E. J., 1976, 22, 753

Sarma, P.N. and Haynes, W.H.,Jr., Adv. Chem., 1974, 133, 205

Satterfield, C.N. and Frabetti, A.J., A.I.Ch.E. J., 1967, 13, 731

Schneider, P. and Smith, J.M., A.I.Ch.E. J., (1968a), 14, 762

Schneider, P. and Smith, J.M., A.I.Ch.E. J., (1968b), 14, 886

Scott, D.S., Lee, W. and Papa, J., Chem. Eng. Sci., 1974, 29, 2155

Shah, D.B. and Ruthven, D.M., A.I.Ch.E. J., 1977, 23, 804

Shah, N. and Ottino, J.M., Chem. Eng. Sci., 1987, 42, 73

Shiring, F.J., Venkatadri, R, and Goodwin, J.G.,Jr., Can. J. Chem. Eng., 1983, 61, 218

Staneck, V. and Eckert, V., Chem. Eng. Sci., 1979, 34, 933

Suzuki, M. and Smith, J.M., Chem. Eng. J., 1972, 3, 256

Suzuki, M. and Smith, J.M., Chem. Eng. Sci., 1971, 26, 221

Topsøe, N.-Y., Pedersen, K. and Derouane, E.G., J. Catal., 1981, 70, 41

Trimm, D.L., App. Catal., 1982, 5, 263

Tronconi, E. and Forzatti, P., Chem. Eng. Sci., 1988, 41, 2541

Tronconi, E. and Forzatti, P. J. Catal., 1985, 93, 197

Urban, J.C. and Gomezplata, A., Can. J. Chem. Eng., 1969, 47, 353

van Deemter, J.J., Zuiderweg, F.J. and Klinkenberg, A., Chem. Eng. Sci., 1956, 5, 271

Voorhies, A.,Jr., I&EC, 1945, 37, 318

Wakao, N. and Smith, J.M., I&EC Fund., 1964, 3, 123

Wakao, N. and Smith, J.M.,Chem. Eng. Sci., 1962, 17, 825

Wakao, N. and Tanaka, K., J. Chem. Eng. Japan, 1974, 7, 472

Wakao, N. and Tanaka, K., J. of Chem. Eng. Japan, 1973, 6, 338

Wakao, N., Kaguei, S. and Nagai, H., Chem. Eng. Sci., 1978, 33, 183

Wakao, N., Kaguei, S. and Smith, J.M., I&EC Fund., 1980, 19, 363

Wakao, N., Kaguei, S. and Smith, J.M., J. Chem. Eng. Japan, 1979, 12, 481

Wakao, N., Oshima, T. and Yagi, S., Chem. Eng. Japan, 1958, 22, 780

Walsh, D.E. and Rollmann, L.D., J. Catal., 1977, 49, 369

Weisz, P.B. and Goodwin, R.D., J. Catal., 1963, 2, 397

Weisz, P.B. and Schwartz, A.B., J. Catal., 1962, 1, 399

Weisz, P.B., Z. Phys. Chem., Neue Folge, 1957, 11, 1

Wicke, E.and Kallenbach, R., Kolloid-Z., 1941, 97, 135

Wojciechowski, B.W., Can. J. Chem. Eng., 1968, 46, 48

Wukasch, J.E. and Rase, H.F., I&EC Proc. Res. Dev., 1982, 21, 558

Yucel, H. and Ruthven, D. M., J. Chem. Soc. Faraday Trans. I, 1980a, 76, 60

Yucel, H. and Ruthven D. M., J. Chem. Soc. Faraday Trans. I, 1980b, 76, 71

APPENDIX A

TABLE A1 : SUMMARY OF HEXANE CRACKING CONVERSION AND PRODUCT DISTRIBUTION (in mole%) DATA

Run ID : CRACT
Catalyst : HY
Mass : 5.65g
Pretreatment : Calcined in air overnight at 400°C
Reaction : Hexane cracking at 400°C, 1 atm
WHSV : 0.89 g(hex)/g(cat)/h
N_2 Flow rate : 150 ml/min at 20°C
Coke Content : 9.2 wt%

Time on Stream h	Conversion %	Comments
0.0	93.2	Heat of Reaction to 410°C
0.67	56.2	
1.75	31.2	
3.0	16.1	
4.0	21.9	
5.0	19.4	
6.0	12.8	

Run ID : CRAC1
Catalyst : HY
Mass : 5.97g
Pretreatment : Calcined in air overnight at 400°C
Reaction : Hexane cracking at 400°C, 1 atm
WHSV : 1.96 g(hex)/g(cat)/h
N_2 Flow rate : 337 ml/min at 20°C
Coke Content : 10.6 wt%

Time on Stream h	Conversion %	Comments
0.0	--	Heat of Reaction 430°C undershoot to 390°C
1.0	24.3	GC analysis not good
2.33	26.9	GC analysis not good
3.25	22.4	
4.5	19.7	
5.5	20.2	
6.5	19.1	
11.0	12.6	
12.0	17.0	

Run ID : CRAC2
Catalyst : HY
Mass : 6.04g
Pretreatment : Calcined in air overnight at 400°C
Reaction : Hexane Cracking at 400°C, 1 atm
WHSV : 1.97 g(hex)/g(cat)/h
N_2 Flow rate : 345 ml/min at 20°C
Coke Content : 8.5 wt%

Time on Stream h	Conversion %	Comments
0.0	49.4	Heat of Reaction 420°C
1.17	34.6	
2.5	26.6	
3.5	15.0	
5.5	17.1	
6.0	17.4	

Run ID : CRAC3
Catalyst : HM
Mass : 6.48g
Pretreatment : Calcined in air overnight at 400°C
Reaction : Hexane cracking at 400°C, 1 atm
WHSV : 1.99 g(hex)/g(cat)/h
N_2 Flow rate : 374 ml/min at 20°C
Coke Content : 3.1 wt%

Time on Stream h	Conversion %	Comments
0.0	47.9	Heat of Reaction 460°C undershoot to 360°C
0.83	16.5	
2.83	7.0	
4.67	3.0	
5.5	5.0	

Run ID : CRAC4
Catalyst : HY
Mass : 5.66g
Pretreatment : Calcined in air overnight at 400°C
Reaction : Hexane cracking at 400°C, 1 atm
WHSV : 2.09 g(hex)/g(cat)/h
N_2 Flow rate : 350 ml/min at 20°C
Coke Content : 8.9 wt%

Time on Stream h	Conv %	C_1 %	C_2 %	C_3 %	C_3= %	C_4 %	C_4= %	C_5 %	Comments
0.0	89.1	0.5	3.9	54.0	2.3	31.8	6.2	1.1	T overshoot to 420 °C
0.58	38.2	1.8	6.0	55.8	10.2	17.2	8.0	0.6	down to 380°C
1.08	16.7	1.9	5.5	50.1	11.8	16.8	12.1	1.6	
2.17	13.5	2.1	5.5	49.8	15.0	15.8	10.5	1.0	
2.75	31.0	1.1	2.9	28.9	56.6	5.8	4.0	0.4	Bad GC sample
3.08	13.4	2.0	5.2	45.2	15.9	13.5	12.3	5.6	

Run ID : CRAC5
Catalyst : HY
Mass : 5.77g
Pretreatment : Calcined in air overnight at 400°C
Reaction : Hexane cracking at 400°C, 1 atm
WHSV : 2.00 g(hex)/g(cat)/h
N_2 Flow rate : 351 ml/min at 20°C
Coke Content : 13.9 wt%

Time on Stream h	Conv %	C_1 %	C_2 %	C_3 %	C_3= %	C_4 %	C_4= %	C_5 %	Comments
0.0	78.3	0.5	4.0	51.7	2.9	30.4	7.7	2.6	T overshoot 410 °C
1.08	15.2	1.5	4.7	45.2	11.5	15.9	18.8	2.1	
2.25	16.5	1.8	4.9	43.2	13.4	14.6	12.5	9.4	
6.08	9.5	2.1	5.3	44.4	21.3	12.1	12.4	2.1	
9.17	9.4	1.8	4.9	43.2	21.5	14.3	10.8	3.1	add hexane to bubbler
18.75	6.3	2.6	6.0	44.5	29.4	8.6	7.6	0.9	add hexane to bubbler
20.92	3.4	2.4	6.0	40.0	31.4	9.2	9.3	1.4	
24.0	1.4	4.0	7.3	40.3	32.4	6.5	8.4	0.8	

Run ID : CRAC6
Catalyst : HY
Mass : 5.69g
Pretreatment : Calcined in air overnight at 400°C
Reaction : Hexane cracking at 400°C, 1 atm
WHSV : 2.52 g(hex)/g(cat)/h
N_2 Flow rate : 350 ml/min at 20°C
Coke Content : 8.9 wt%

Time on Stream h	Conv %	C_1 %	C_2 %	C_3 %	C_3= %	C_4 %	C_4= %	C_5 %	Comments
0.0	83.6	0.1	3.8	49.8	2.5	32.1	8.3	3.2	T overshoot 430°C
0.5	29.6	1.6	4.8	43.4	9.5	15.3	8.9	16.2	undershoot 380°C
1.42	25.8	2.3	5.5	41.1	13.1	11.5	6.4	19.9	
2.17	25.7	2.2	5.0	40.4	14.4	11.0	9.0	14.5	
3.0	14.7	2.1	5.0	36.5	14.9	10.1	7.0	24.0	

Run ID : CRAC7
Catalyst : HY
Mass : 5.50g
Pretreatment : Calcined in air overnight at 400°C
Reaction : Hexane cracking at 400°C, 1 atm
WHSV : 2.32 g(hex)/g(cat)/h
N_2 Flow rate : 310 ml/min at 20°C
Coke Content : 7.1 wt%

Time on Stream h	Conv %	C_1 %	C_2 %	C_3 %	C_3= %	C_4 %	C_4= %	C_5 %	Comments
0.0	94.4	0.9	4.7	55.3	2.1	31.1	4.8	0.9	T overshoot 430°C
0.5	43.8	2.0	5.6	48.3	9.6	16.6	8.0	9.7	
1.0	29.9	2.5	5.9	45.5	11.3	13.6	6.9	14.1	

Run ID : CRAC8
Catalyst : HY
Mass : 5.75g
Pretreatment : Calcined in air overnight at 400°C
Reaction : Hexane cracking at 400°C, 1 atm
WHSV : 2.04 g(hex)/g(cat)/h
N_2 Flow rate : 302 ml/min at 20°C
Coke Content : 8.2 wt%

Time on Stream h	Conv %	C_1 %	C_2 %	C_3 %	C_3= %	C_4 %	C_4= %	C_5 %	Comments
0.0	83.6	0.5	3.6	48.6	2.4	32.2	8.5	3.9	T overshoot to 420°C
1.0	26.4	1.9	5.0	42.8	11.6	13.6	8.4	16.4	undershoot to 380°C
2.17	16.6	1.9	4.8	36.5	15.3	11.5	7.7	21.9	
3.0	15.3	1.7	4.4	32.6	15.2	11.7	7.9	26.4	
4.0	11.3	0.9	4.1	32.9	15.9	9.7	7.3	29.0	
6.0	11.2	2.0	4.5	33.0	17.0	9.2	7.0	27.1	

TABLE A2 : HEXANE CRACKING MODELLING OF CONVERSION DATA USING THE TIME ON STREAM DECAY FUNCTION OF WOJCIECHOWSKI (1968).

Langmuir Kinetics : $$\frac{dX}{d\tau} = (1+Gt)^{-N} \left[\frac{A(1-X)/(1+\epsilon X)}{1+B*(1-X)/(1+\epsilon X)}\right]$$

Run ID	Catalyst	WHSV g(hex)/gcat.h	Coke wt%	G h^{-1}	N	A g(hex)/gcat.h	B	SQRD ERROR
CRACT	HY	0.89	9.2	5.22	0.842	2.95	0.231	7.4E-3
CRAC1	"	1.96	10.6	0.532	0.382	0.695	-0.052	3.2E-3
CRAC2	"	1.97	8.5	0.849	0.889	0.953	-0.453	4.6E-3
CRAC3	HM	1.99	3.1	4.29	0.875	1.53	0.156	3.5E-4
CRAC4	HY	2.09	8.9	2.09	3.78	3.26	-1.07	3.0E-3
CRAC5	"	2.00	13.9	13.6	0.601	9.05	3.03	6.9E-3
CRAC6	"	2.52	8.9	3.46	3.99	2.85	-1.14	7.8E-3
CRAC7	"	2.32	7.1	3.03	3.51	5.29	-1.15	2.2E-5
CRAC8	"	2.04	8.2	1.66	3.58	2.20	-1.07	6.6E-4

First Order Kinetics : $$\frac{dX}{d\tau} = K(1+Gt)^{-N} \left[\frac{1-X}{1+\epsilon X}\right]$$

Run ID	Catalyst	WHSV g(hex)/gcat.h	Coke wt%	G h^{-1}	N	K g(hex)/gcat.h	SQRD ERROR
CRACT	HY	0.89	9.2	5.31	0.874	2.72	7.5E-3
CRAC1	"	1.96	10.6	0.223	0.553	0.679	2.9E-3
CRAC2	"	1.97	8.5	0.836	0.805	1.40	4.5E-3
CRAC3	HM	1.99	3.1	3.81	0.940	1.40	3.7E-4
CRAC4	HY	2.09	8.9	9.32	0.952	5.39	6.1E-3
CRAC5	"	2.00	13.9	434	0.462	6.99	3.9E-3
CRAC6	"	2.52	8.9	200	0.426	7.64	6.5E-3
CRAC7	"	2.32	7.1	6.10	1.16	7.53	1.0E-3
CRAC8	"	2.04	8.2	22.5	0.615	4.38	4.4E-4

Overall model based on WHSV = 2.0, using data from CRAC1, 2, 3, 4, 5, 8.

Langmiur kinetics	First order kinetics
G = 5.26 h^{-1}	G = 96.8 h^{-1}
N = 1.89	N = 0.414
A = 1.41 g(hex)/gcat.h	K = 4.20 g(hex)/gcat.h
B = -1.09	

ϵ = 0.1 calculated from product distribution data
τ = space time = gcat.h/g(hex)
X = fractional conversion

TABLE A3 : FEED GAS ANALYSIS

Compound	mass%
Methane	0.005
Ethane	10.36
Propane	10.58
Propene	79.03
i-Butane	0.043

TABLE A4 : TAIL GAS ANALYSIS

Compound	mass % for four different samples			
Methane	-	0.004	0.077	0.004
Ethane	7.90	7.09	9.01	8.99
Propane	33.11	27.37	35.93	26.92
Propene	55.38	50.27	38.20	56.90
i-Butane	0.90	5.24	4.51	0.79
n-Butane	0.56	0.90	0.84	0.42
n-Butene	0.18	0.32	0.54	0.13
i-Butene	0.14	0.02	1.22	0.12
t2-Butene	0.76	0.36	1.21	0.63
c2-Butene	0.40	0.33	0.78	0.33
C_5 group	0.48	4.64	4.82	1.72
C_6 group	0.20	3.98	2.86	3.05

Average density of tail gas based on the above samples
= 1.784±0.040 g/l
at 1 atm, 20°C, ideal gas.

TABLE A5 : PROPENE OLIGOMERISATION; CONVERSION AND PRODUCT DISTRIBUTION DATA

Run ID : OLIGT
Catalyst : HY
Mass catalyst : 6.25 g
Pretreatment : calcined at 400°C in air overnight
Reaction Conditions : 200°C, 50 atm
WHSV(ave) : 1.1 ± 0.1 g/gcat/h
Coke Content : high b.p. hydrocarbons = 5.4%, graphitic = 13.7%

Time h	Temp °C	Tail gas(g)	Liquid (g)	Total (g)	WHSV C_3	Conv %	LPR g/g/h	Comments
0.00	24	-	-	-	-	-	-	feed in
0.10	40	-	-	-	-	-	-	pump on
0.35	28	-	-	-	-	-	-	heat, pump off
0.75	200	13.4	-	13.4	-	-	-	pump off, liq
0.83	211	0.5	1.7	2.2	2.9	13	0.32	pump on, T=243
1.33	220	2.7	-	2.7	-	-	-	T high
1.83	202	1.8	1.6	3.4	0.94	33	0.31	200<T<230
2.83	198	2.3	3.2	5.6	0.87	74	0.64	200<T<210
3.83	203	2.1	4.3	6.5	1.0	85	0.86	T stable
6.83	205	9.0	13.0	22.0	1.2	75	0.86	Steady LPR
7.83	205	3.4	4.3	7.7	1.2	71	0.86	
8.83	205	3.4	4.4	7.8	1.2	71	0.87	
9.00	205	0.5	-	0.5	-	-	-	pump rate up
9.83	204	17.5	13.5	31.0	4.9	55	2.7	residual liq
10.83	203	24.3	2.7	26.9	4.2	13	0.53	
		11.3	-	11.3	-	-	-	purge
			48.7	140.8				

Run ID : OLIG1
Catalyst : HY
Mass catalyst : 5.11 g
Pretreatment : calcined at 400°C in air overnight
Reaction Conditions : 200°C, 53 atm
WHSV(ave) : 2.7 ± 0.1 g/gcat/h
Coke Content : high b.p. hydrocarbons = 4.3%, graphitic = 17.3%

Time h	Temp °C	Tail gas(g)	Liquid (g)	Total (g)	WHSV	Conv %	LPR g/g/h	Comments
0.0	24	-	-	-	-	-	-	feed in
0.12	54	-	-	-	-	-	-	pump on
0.38	29	-	-	-	-	-	-	heat, pump off
1.0	198	11.4	2.6	14.0	2.2	23	0.51	T=278, pump on
2.0	198	14.5	3.0	17.4	2.7	22	0.58	T stable
3.0	199	15.9	1.4	17.3	2.7	10	0.27	not active
4.0	202	16.6	1.2	17.8	2.8	9	0.24	
5.0	202	15.2	0.8	16.0	2.5	7	0.16	
		10.3	-	10.3	-	-	-	purge
			9.0	92.8				

Run ID : OLIG2
Catalyst : HY
Mass catalyst : 5.03 g
Pretreatment : calcined at 400°C in air overnight
Reaction Conditions : 200°C, 53 atm
WHSV(ave) : 1.5 ± 0.1 g/gcat/h
Coke Content : high b.p. hydrocarbons = 5.2%, graphitic = 18.4%

Time h	Temp °C	Tail gas(g)	Liquid (g)	Total (g)	WHSV	Conv %	LPR g/g/h	Comments
0.0	27	-	-	-	-	-	-	feed in
0.28	50	-	-	-	-	-	-	pump on
0.83	32	-	-	-	-	-	-	heat
1.17	-	-	-	-	-	-	-	T=270 from 110
1.42	215	20.2	1.9	22.0	2.4	11	0.26	
2.42	202	6.2	2.9	9.1	1.4	40	0.57	
3.42	204	4.6	3.7	8.4	1.3	56	0.74	
4.42	200	5.2	4.5	9.6	1.5	59	0.89	
5.42	205	6.1	4.3	10.3	1.6	52	0.85	
6.42	204	6.4	4.1	10.5	1.7	49	0.82	
7.42	203	7.0	3.7	10.7	1.7	44	0.74	
		8.6	3.6	12.2				purge
			28.6	92.8				

Run ID : OLIG3
Catalyst : HY
Mass catalyst : 5.07 g
Pretreatment : Calcined at 400°C in air overnight
Reaction Conditions : 350°C, 51 atm
WHSV(ave) : 2.7 ± 0.1 g/gcat/h
Coke Content : high b.p. hydrocarbons = 1.3%, graphitic = 21.7%

Time h	Temp °C	Tail gas(g)	Liquid (g)	Total (g)	WHSV	Conv %	LPR g/g/h	Comments
0.0	28	-	-	-	-	-	-	feed in
0.17	55	-	-	-	-	-	-	pump on
0.58	29	-	-	-	-	-	-	heat
0.83	-	-	-	-	-	-	-	T=274/310/360
1.42	348	25.1	4.8	30.8	3.4	20	0.51	T fluctuates
2.42	351	8.9	8.0	17.0	2.7	60	1.22	
3.42	352	12.8	4.6	17.5	2.7	34	0.70	T stable
4.42	350	14.5	3.5	17.9	2.8	25	0.53	
5.42	349	14.8	2.4	17.2	2.7	18	0.37	
		8.6	-	8.6	-			purge
			23.3	109.0				

Run ID : OLIG4
Catalyst : HY
Mass catalyst : 5.18 g
Pretreatment : calcined at 400°C in air overnight
Reaction Conditions : 100 °C, 54 atm
WHSV(ave) : 1.8 ± 0.2 g/gcat/h
Coke Content : high b.p. hydrocarbons = 7.9%, graphitic = 6.9%

Time h	Temp °C	Tail gas(g)	Liquid (g)	Total (g)	WHSV	Conv %	LPR g/g/h	Comments
0.0	25	-	-	-	-	-	-	feed in, pump
0.42	30	-	-	-	-	-	-	T=76, heat
1.42	100	13.6	3.6	17.2	1.9	27	0.50	T=106, stable
2.42	101	7.1	3.0	10.2	1.6	38	0.58	
4.42	100	16.6	5.9	22.4	1.7	33	0.57	
6.42	97	17.8	4.7	22.5	1.7	26	0.45	
11.58	95	56.4	5.7	62.1	1.9	12	0.22	
12.42	99	11.6	-	11.6	2.1	0	0	dead
		38.2	-	38.2	-	-	-	purge
			22.9	184.2				

Run ID : OLIG5
Catalyst : HY
Mass catalyst : 5.20 g
Pretreatment : calcined at 400°C in air overnight
Reaction Conditions : 200°C, 51 atm
WHSV(ave) : 2.6 ± 0.2 g/gcat/h
Coke Content : high b.p. hydrocarbons = 4.4%, graphitic = 16.7%

Time h	Temp °C	Tail gas(g)	Liquid (g)	Total (g)	WHSV	Conv %	LPR g/g/h	Comments
0.0	27	-	-	-	-	-	-	feed in T=72
0.28	48	-	-	-	-	-	-	pump on
0.62	31	-	-	-	-	-	-	heat
1.62	102	-	-	-	-	-	-	T=320
1.87	211	36.8	5.3	42.1	3.4	16	0.54	T unstable
3.37	198	20.0	3.3	23.3	2.4	18	0.42	
4.87	201	23.6	2.6	26.2	2.7	13	0.28	dying
6.87	201	25.9	1.9	27.7	2.8	9	0.18	
		11.0	-	11.0	-	-	-	purge
			13.1	130.3				

Product distribution

Time h	Dimer mole%	Trimer mole%	Tetramer mole%	Pentamer mole%	Hexamer mole%	Heptamer mole%
1.87	6.5	45.5	27.6	9.3	4.3	6.7
3.37	5.9	44.9	30.6	10.4	3.9	4.3

Run ID : OLIG6
Catalyst : HM
Mass catalyst : 6.53 g
Pretreatment : calcined at 350°C in air overnight
Reaction Conditions : 200-250°C, 53 atm
WHSV(ave) : 1.7 ± 0.1 g/gcat/h
Coke Content : high b.p. hydrocarbons = 5.4%, graphitic = 6.7%

Time h	Temp °C	Tail gas(g)	Liquid (g)	Total (g)	WHSV	Conv %	LPR g/g/h	Comments
0.0	27	-	-	-	-	-	-	feed in T=51
0.27	27	-	-	-	-	-	-	pump on
0.45	29	-	-	-	-	-	-	heat
1.20	200	-	-	-	-	-	-	
1.87	199	41.9	-	41.9	2.9	0	0	few drops liq
2.87	198	15.2	1.3	16.4	1.8	10	0.18	
4.87	200	27.8	1.5	29.3	1.8	6	0.11	heat to 250
6.87	250	23.6	4.3	27.3	1.7	20	0.33	LPR better
10.37	250	43.5	6.0	49.6	1.7	15	0.26	
12.37	250	25.9	2.0	27.8	1.7	9	0.15	
		10.9	-	10.9	-	-	-	purge
			15.0	203.2				

Product distribution

Time h	Dimer mole%	Trimer mole%	Tetramer mole%	Pentamer mole%	Hexamer mole%	Heptamer mole%
6.87	10.8	36.3	27.7	13.9	5.9	5.1
10.37	12.1	30.4	25.7	14.7	6.6	10.3
12.37	8.7	26.9	26.2	16.5	7.5	13.9

Run ID : OLIG7
Catalyst : HM
Mass catalyst : 6.25 g
Pretreatment : calcined at 350°C in air overnight
Reaction Conditions : 300°C, 53 atm
WHSV(ave) : 1.6 ± 0.3 g/gcat/hr
Coke Content : high b.p. hydrocarbons = 2.2%, graphitic = 10.0%

Time h	Temp °C	Tail gas(g)	Liquid (g)	Total (g)	WHSV	Conv %	LPR g/g/h	Comments
0.0	25	-	-	-	-	-	-	feed in, T=48
0.5	26	-	-	-	-	-	-	pump on
0.57	27	-	-	-	-	-	-	heat
1.17	308	27.7	-	27.7	3.0	-	-	T unstable
2.17	298	8.6	4.9	13.4	1.7	46	0.78	
3.17	298	8.6	6.3	14.8	1.9	54	1.00	
4.17	300	9.5	5.2	14.7	1.9	45	0.83	
5.17	298	10.9	4.7	15.6	2.0	38	0.76	
7.17	301	21.4	6.4	27.8	1.8	29	0.51	
11.17	305	36.2	9.9	46.0	1.5	27	0.39	catalyst dying
13.17	306	15.3	3.3	18.6	1.2	26	0.26	
		8.4	-	8.4	-	-	-	purge
			41.3	187.0				

Product distribution

Time h	Dimer mole%	Trimer mole%	Tetramer mole%	Pentamer mole%	Hexamer mole%	Heptamer mole%
2.17	23.8	29.5	21.7	9.7	4.1	10.9
3.17	27.5	30.7	22.9	10.3	4.2	4.2
4.17	24.4	29.5	23.5	11.2	4.6	6.5
5.17	23.3	29.4	23.7	11.4	4.6	7.4
7.17	26.0	29.6	22.2	10.5	4.1	7.3
11.17	31.4	32.1	21.3	8.9	3.0	3.0
13.17	18.8	31.8	25.3	12.2	4.7	6.9

Run ID : OLIG8
Catalyst : HM
Mass catalyst : 6.19 g
Pretreatment : calcined at 350°C in air overnight
Reaction Conditions : 350°C, 54 atm
WHSV(ave) : 0.96 ± 0.3 g/gcat/h
Coke Content : high b.p. hydrocarbons = 0.5%, graphitic = 10.6%

Time h	Temp °C	Tail gas(g)	Liquid (g)	Total (g)	WHSV	Conv %	LPR g/g/h	Comments
0.0	27	-	-	-	-	-	-	feed in, T=45
0.17	29	-	-	-	-	-	-	pump on
0.36	29	-	-	-	-	-	-	heat
1.50	277	-	-	-	-	-	-	bed lag 50
2.00	345	-	-	-	-	-	-	LPR low, liq
2.33	350	31.8	2.6	34.3	1.9	9	0.18	looks like
3.33	347	2.3	3.7	6.0	0.76	78	0.59	heavy fraction
4.33	348	1.8	4.8	6.6	0.84	92	0.78	
5.83	353	2.7	5.3	8.0	1.0	84	0.57	
7.33	350	3.2	4.7	7.9	0.67	75	0.50	pump erratic
11.83	353	10.4	9.0	19.4	0.55	59	0.42	increase flow
12.83	352	8.7	2.7	11.4	1.5	30	0.43	
13.83	350	10.4	0.9	11.3	1.4	10	0.15	
		8.2	0.5	8.7				purge
			34.0	113.4				

Product distribution

Time h	Dimer mole%	Trimer mole%	Tetramer mole%	Pentamer mole%	Hexamer mole%	Heptamer mole%
2.33	6.5	30.1	24.0	12 3	7.3	19.6
3.33	16.4	29.6	25.9	11.9	5.3	10.7
4.33	26.2	29.5	21.7	9.4	4.2	8.7
5.83	30.6	32.9	22.0	7.7	2.8	3.8
7.33	26.2	36.4	23.5	7.9	2.7	3.0
11.83	45.2	36.5	14.9	3.1	0.0	0.0
12.83	27.3	41.7	20.0	7.1	2.1	1.5

Run ID : OLIG9
Catalyst : HY
Mass catalyst : 5.00 g
Pretreatment : calcined at 400°C in air overnight
Reaction Conditions : 200-300°C, 30 atm
WHSV(ave) : 13.6 g/gcat/h
Coke Content : high b.p. hydrocarbons = 3.3%, graphitic = 19.1%

Time h	Temp °C	Tail gas(g)	Liquid (g)	Total (g)	WHSV	Conv %	LPR g/g/h	Comments
0.0	25	-	-	-	-	-	-	feed in T=150
0.17	33	-	-	-	-	-	-	pump on
0.28	38	-	-	-	-	-	-	heat
0.75	330	-	-	-	-	-	-	T 80 to 330
1.17	209	74.0	3.1	77.2	10.4	5.1	0.53	WHsv very high
1.67	205	-	-	-	-	-	-	due to low P
2.67	250	-	-	-	-	-	-	
3.03	308	280.3	1.6	281.9	16.8	0.7	0.12	
		6.4	-	6.4	-	-	-	purge
			4.8	365.5				

Product distribution

Time h	Dimer mole%	Trimer mole%	Tetramer mole%	Pentamer mole%	Hexamer mole%	Heptamer mole%
1.17	15.2	47.3	25.3	6.2	2.7	3.1
3.03	10.8	42.0	27.8	9.0	4.0	6.2

Run ID : OLIG10
Catalyst : HY
Mass catalyst : 4.86 g
Pretreatment : calcined at 400°C in air overnight
Reaction Conditions : 250°C, 30 atm
WHSV(ave) : 2.22 g/gcat/h
Coke Content : high b.p. hydrocarbons = 3.5%, graphitic = 12.2%

Time h	Temp °C	Tail gas(g)	Liquid (g)	Total (g)	WHSV	Conv %	LPR g/g/h	Comments
0.0	27	-	-	-	-	-	-	feed in T=116
0.42	34	-	-	-	-	-	-	pump on
0.75	29	-	-	-	-	-	-	heat
1.42	262	44.2	-	44.2	5.1	-	-	T 80 to 262
1.75	260	3.0	-	3.0	1.5	-	-	
2.75	249	10.0	3.5	13.5	2.2	33	0.26	
4.25	254	17.8	2.9	20.7	2.3	18	0.40	
5.75	253	18.7	1.8	20.5	2.2	11	0.24	
		6.8	-	-	-		-	purge
			8.2	102.0				

Product distribution

Time h	Dimer mole%	Trimer mole%	Tetramer mole%	Pentamer mole%	Hexamer mole%	Heptamer mole%
2.75	26.9	39.8	22.7	6.5	1.9	2.0
4.25	18.7	39.9	21.7	9.5	4.9	5.1

Run ID : OLIG11
Catalyst : HY
Mass catalyst : 5.10 g
Pretreatment : calcined dt 400°C in air overnight
Reaction Conditions : 250°C, 65 atm
WHSV(ave) : 1.6 ± 0.1 g/gcat/h
Coke Content : high b.p. hydrocarbons = 5.3%, graphitic = 18.8%

Time h	Temp °C	Tail gas(g)	Liquid (g)	Total (g)	WHSV	Conv %	LPR g/g/h	Comments
0.0	25	-	-	-	-	-	-	feed in T=123
0.33	31	-	-	-	-	-	-	pump on
0.47	27	-	-	-	-	-	-	heat
1.60	265	-	-	-	-	-	-	T 110 to 262
2.00	249	23.9	2.8	26.8	2.1	13	0.28	
3.00	249	4.3	5.9	10.2	1.6	73	1.2	T stable
4.00	249	3.8	6.4	10.1	1.6	80	1.3	pump slow
5.00	250	3.9	6.5	10.4	1.6	79	1.3	
6.00	247	4.1	6.2	10.1	1.6	78	1.2	
7.00	250	4.6	6.0	10.6	1.7	71	1.2	
10.50	247	22.8	16.3	39.1	1.7	53	0.91	
12.00	252	13.7	3.1	16.8	1.7	23	0.40	
13.00	251	9.1	1.7	10.8	1.7	20	0.34	
		10.0	-	10.0	-	-	-	purge
			54.9	155.0				

Product distribution

Time h	Dimer mole%	Trimer mole%	Tetramer mole%	Pentamer mole%	Hexamer mole%	Heptamer mole%
2.00	14.0	44.0	21.1	6.1	3.5	11.0
3.00	35.3	35.7	17.4	6.0	2.2	3.2
4.00	30.5	33.6	19.9	8.1	3.5	4.2
5.00	27.2	34.6	21.3	8.7	3.7	4.2
6.00	28.3	35.6	20.9	8.2	3.4	3.4
7.00	27.9	36.3	20.9	8.1	3.3	3.2
10.50	29.3	38.8	19.1	7.1	2.8	2.6
12.00	25.2	46.4	19.4	5.0	0.7	3.0
13.00	16.3	49.3	23.5	6.5	1.2	2.9

Run ID : OLIG12
Catalyst : HY
Mass catalyst : 5.68 g
Pretreatment : calcined at 400°C in air overnight
Reaction Conditions : 100°C, 51 atm
WHSV(ave) : 2.94 g/gcat/h
Coke Content : high b.p. hydrocarbons = 6.7%, graphitic = 7.0%

Time h	Temp °C	Tail gas(g)	Liquid (g)	Total (g)	WHSV	Conv %	LPR g/g/h	Comments
0.0	27	-	-	-	-	-	-	feed in T=74
0.33	44	-	-	-	-	-	-	pump on
0.50	31	-	-	-	-	-	-	heat
1.33	110	-	-	-	-	-	-	T runaway
1.67	101	34.6	2.3	36.9	3.1	8	0.24	LPR low
3.67	102	39.8	2.5	42.3	2.9	8	0.22	
5.67	100	38.9	1.4	40.3	2.8	4	0.12	
		56.6	-	56.6				purge+last Sam
			6.2	176.1				

Product distribution

Time h	Dimer mole%	Trimer mole%	Tetramer mole%	Pentamer mole%	Hexamer mole%	Heptamer mole%
1.67	8.4	57.0	25.0	6.2	1.5	1.6
3.67	5.7	45.0	28.7	8.8	4.2	7.2
5.67	6.2	49.8	28.0	8.6	3.1	4.1

Run ID : OLIG13
Catalyst : HM
Mass catalyst : 6.48
Pretreatment : calcined at 350°C in air overnight
Reaction Conditions : 300°C, 65 atm
WHSV(ave) : --- g/gcat/hr
Coke Content : high b.p. hydrocarbons = 1.9%, graphitic = 8.8%

Time h	Temp °C	Tail gas(g)	Liquid (g)	Total (g)	WHSV	Conv %	LPR g/g/h	Comments
0.0	27	-	-	-	-	-	-	feed in T=35
0.33	27	-	-	-	-	-	-	pump on
0.50	27	-	-	-	-	-	-	heat
1.91	304	27.5	-	27.5	1.8	-	-	no liquid
2.91	299	6.6	3.4	10.0	1.2	43	0.18	
4.41	295	5.7	8.7	14.4	1.2	76	0.89	
5.66	297	6.4	8.8	15.3	1.5	73	1.1	
6.41	299	7.3	6.3	13.6	2.2	59	1.3	coolant pump
10.41	301	151.6	13.4	165.1	5.0	10	0.52	fails, fix,
12.41	300	15.5	2.6	18.1	1.1	18	0.20	causes ±WHSV
13.41	303	10.7	2.7	13.4	1.6	26	0.42	
		12.0	1.0	13.0				purge
			46.9	290.2				

Product distribution

Time h	Dimer mole%	Trimer mole%	Tetramer mole%	Pentamer mole%	Hexamer mole%	Heptamer mole%
2.91	26.0	32.5	22.4	9.2	4.2	5.4
4.41	31.5	32.4	19.4	8.6	3.5	4.3
5.66	31.8	33.4	18.7	8.4	3.4	4.0
6.41	28.3	31.0	24.8	7.9	3.2	4.4
10.41	23.7	31.6	23.0	10.4	3.8	7.3
12.41	26.1	32.0	22.8	10.8	3.8	4.2
13.41	28.3	35.0	20.4	9.6	3.3	3.1

Run ID : OLIG14
Catalyst : HM
Mass catalyst : 6.62 g
Pretreatment : calcined at 350°C in air overnight
Reaction Conditions : 300°C, 64 atm
WHSV(ave) : 1.6 ± 0.1 g/gcat/h
Coke Content : high b.p. hydrocarbons = 1.8%, graphitic = 8.2%

Time h	Temp °C	Tail gas(g)	Liquid (g)	Total (g)	WHSV	Conv %	LPR g/g/h	Comments
0.0	27	-	-	-	-	-	-	feed in T=37
0.25	27	-	-	-	-	-	-	pump on
0.50	28	-	-	-	-	-	-	heat
2.00	297	39.1	-	39.1	2.3	-	-	drop of liq
3.00	299	5.9	8.5	14.3	1.7	75	1.3	
4.00	299	6.4	8.3	14.7	1.8	71	1.3	
6.00	299	17.5	9.1	26.5	1.6	43	0.68	
7.00	302	9.8	3.2	13.0	1.6	31	0.48	
		10.0	1.0	11.0	-	-	-	purge
			30.0	118.6				

Product distribution

Time h	Dimer mole%	Trimer mole%	Tetramer mole%	Pentamer mole%	Hexamer mole%	Heptamer mole%
3.00	31.2	31.6	19.9	8.1	3.5	5.5
4.00	32.2	31.4	18.8	9.5	2.2	5.6
6.00	42.1	34.7	16.5	5.7	0.3	0.4
7.00	32.6	36.8	20.2	9.1	0.3	0.7

Run ID : OLIG15
Catalyst : HM
Mass catalyst : 6.94 g
Pretreatment : calcined at 350°C in air overnight
Reaction Conditions : 300°C, 30 atm
WHSV(ave) : 1.83 g/gcat/h
Coke Content : high b. p. hydrocarbons = 0%, graphitic = 8.1%

Time h	Temp °C	Tail gas(g)	Liquid (g)	Total (g)	WHSV	Conv %	LPR g/g/h	Comments
0.0	27	-	-	-	-	-	-	feed in T=31
0.33	27	-	-	-	-	-	-	pump on
0.50	27	-	-	-	-	-	-	heat
1.25	297	28.2	-	28.2	2.6	-	-	no liqiud
2.00	300	10.0	2.1	12.1	1.8	22	0.41	
4.00	299	29.1	3.4	32.5	1.9	13	0.24	
6.00	304	30.9	1.2	32.1	1.8	5	0.09	
		7.9	-	7.9	-	-	-	purge
			6.7	112.7				

Product distribution

Time h	Dimer mole%	Trimer mole%	Tetramer mole%	Pentamer mole%	Hexamer mole%	Heptamer mole%
2.00	11.8	26.8	23.7	13.1	7.4	16.8
4.00	12.0	27.7	26.5	16.7	4.9	12.0
6.00	7.0	22.6	31.1	20.8	6.5	11.8

Run ID : OLIG16
Catalyst : HM
Mass catalyst : 6.56 g
Pretreatment : calcined at 350°C in air overnight
Reaction Conditions : 300°C, 51 atm
WHSV(ave) : 2.75 g/gcat/h
Coke Content : graphitic = 8.1%

Time h	Temp °C	Tail gas(g)	Liquid (g)	Total (g)	WHSV	Conv %	LPR g/g/h	Comments
0.0	28	-	-	-	-	-	-	feed in T=33
0.33	28	-	-	-	-	-	-	pump on
0.50	29	-	-	-	-	-	-	heat
1.25	302	26.4	-	26.4	2.5	-	-	
2.17	302	5.9	3.6	9.5	1.2	48	0.60	
3.17	301	12.7	8.5	21.1	2.5	51	1.3	
5.67	300	51.4	7.1	58.4	2.8	15	0.43	
7.00	302	29.8	2.1	31.9	2.9	8	0.24	
		8.7		8.7				purge
			21.2	156.1				

After regeneration in N_2 at 500 °C overnight , the catalyst was found to be inactive.

Product distribution

Time h	Dimer mole%	Trimer mole%	Tetramer mole%	Pentamer mole%	Hexamer mole%	Heptamer mole%
2.17	28.9	35.0	20.7	8.9	2.5	3.9
3.17	33.7	31.3	18.2	7.7	3.4	5.5
5.67	22.3	31.2	23.8	11.6	3.6	7.2
7.00	18.2	29.6	28.8	14.9	3.3	4.9

Run ID : OLIG17
Catalyst : HM
Mass catalyst : 6.58 g
Pretreatment : calcined at 350°C in air overnight
Reaction Conditions : 300°C, 52 atm
WHSV(ave) : 2.43 g/gcat/h
Coke Content : graphitic = 8.7%

Time h	Temp °C	Tail gas(g)	Liquid (g)	Total (g)	WHSV	Conv %	LPR g/g/h	Comments
0.0	26	-	-	-	-	-	-	feed in T=39
0.17	26	-	-	-	-	-	-	pump on
0.25	27	-	-	-	-	-	-	heat
1.00	310	35.7	-	35.7	4.3	-	-	
2.00	296	14.6	6.5	21.1	2.5	39	0.98	
4.00	300	34.1	6.4	40.5	2.4	20	0.49	
6.00	299	35.3	3.7	39.0	2.3	12	0.28	
		9.1		9.1				purge
			16.5	145.3				

After regeneration in N_2 at 350 °C overnight , the catalyst was found to be inactive.

Product distribution

Time h	Dimer mole%	Trimer mole%	Tetramer mole%	Pentamer mole%	Hexamer mole%	Heptamer mole%
2.00	32.8	32.1	18.2	7.7	3.3	5.6
4.00	32.2	32.1	19.8	8.9	3.2	3.4
6.00	27.1	32.2	22.7	11.2	2.6	3.8

Run ID : OLIG18
Catalyst : HY
Mass catalyst : 5.09 g
Pretreatment : calcined at 400°C in air overnight
Reaction Conditions : 200°C, 50 atm
WHSV(ave) : 4.40 g/gcat/h
Coke Content : see OLIG18(regen)

Time h	Temp °C	Tail gas(g)	Liquid (g)	Total (g)	WHSV	Conv %	LPR g/g/h	Comments
0.0	26	-	-	-	-	-	-	feed in T=77
0.33	33	-	-	-	-	-	-	pump on
0.42	250	-	-	-	-	-	-	heat
1.25	200	37.6	-	37.6	4.7	-	-	T runaway
2.00	198	20.2	6.0	26.1	5.4	28	0.59	
4.00	200	56.2	1.9	58.1	4.5	4	0.18	
6.00	199	54.2	1.0	55.2	4.3	2	0.10	
		10.4	-	10.4				purge
			8.9	187.4				

Product distribution

Time h	Dimer mole%	Trimer mole%	Tetramer mole%	Pentamer mole%	Hexamer mole%	Heptamer mole%
2.00	25.4	45.1	19.2	6.0	1.9	2.1
4.00	11.8	46.5	22.0	7.9	3.0	8.4
6.00	8.1	41.4	28.7	10.8	4.0	6.8

Run ID : OLIG18 regen
Catalyst : HY
Mass catalyst : 5.09 g
Pretreatment : regeneration in N_2 at 350°C overnight
Reaction Conditions : 200°C, 50 atm
WHSV(ave) : 4.06 g/gcat/h
Coke Content : high b.p. hydrocarbons = 4.3% , graphitic = 16.9%

Time h	Temp °C	Tail gas(g)	Liquid (g)	Total (g)	WHSV	Conv %	LPR g/g/h	Comments
0.0	27	-	-	-	-	-	-	feed in T=55
0.50	30	-	-	-	-	-	-	pump on
0.58	30	-	-	-	-	-	-	heat
1.50	206	-	-	-	-	-	-	T=255
2.50	199	53.7	7.2	60.9	3.8	15	0.57	
5.50	201	49.2	3.1	52.3	4.1	7	0.30	
6.50	199	51.4	1.0	52.4	4.1	2	0.10	
		8.9	-	8.9				purge
			11.3	174.5				

Product distribution

Time h	Dimer mole%	Trimer mole%	Tetramer mole%	Pentamer mole%	Hexamer mole%	Heptamer mole%
2.50	21.2	47.0	20.7	6.8	1.6	2.5
4.50	16.0	46.9	20.3	7.3	3.2	6.0
6.50	12.1	43.2	24.9	8.6	3.2	7.6

TABLE A6 : SUMMARY OF OLIGOMERISATION DATA.

Run ID	Cat	mass Cat g	T°C over shoot	T °C	P atm	Run Time h	WHSV g/g/h	Total liq g	LPR ave g/g/h	Coke wt%	
										hbph	gc
OLIGT	HY	6.25	243	200	50	10.8	1.1	48.7	0.72	5.4	13.7
OLIG1	"	5.11	278	200	53	5.0	2.7	9.0	0.35	4.3	17.3
OLIG2	"	5.03	270	200	53	7.4	1.5	28.6	0.77	5.2	18.4
OLIG3	"	5.07	360	350	51	5.4	2.7	23.3	0.85	1.3	21.7
OLIG4	"	5.18	106	100	54	12.4	1.8	22.9	0.36	7.9	6.9
OLIG5	"	5.20	320	200	51	6.8	2.6	13.1	0.37	4.4	16.7
OLIG6	HM	6.53		250	53	12.3	1.7	15.0	0.30	5.4	6.7
OLIG7	"	6.25		300	53	13.1	1.7	41.3	0.50	2.2	10.0
OLIG8	"	6.19		350	54	13.8	0.96	34.0	0.40	0.5	10.6
OLIG9	HY	5.00	330	250	30	3.0	13.6	4.8	0.31	3.3	19.1
OLIG10	"	4.86	262	250	30	5.7	2.2	8.2	0.29	3.5	12.2
OLIG11	"	5.10	262	250	65	13.0	1.6	54.9	0.83	5.3	18.8
OLIG12	"	5.68	110	100	51	5.6	2.9	6.2	0.19	6.7	7.0
OLIG13	HM	6.48		300	65	13.4	--	46.9	0.54	1.9	8.8
OLIG14	"	6.62		300	64	7.0	1.7	30.0	0.65	1.8	8.2
OLIG15	"	6.94		300	30	6.0	1.8	6.7	0.16	0.0	8.1
OLIG16	"	6.56		300	51	7.0	2.8	21.2	0.46	-	8.1
OLIG17	"	6.58		300	52	6.0	2.4	16.5	0.42	-	8.7
OLIG18	HY	5.09	250	200	50	6.0	4.4	8.8	0.29	-	-
REGN18	"	5.09	255	200	50	6.5	4.1	11.3	0.34	4.3	16.9

hbph=high b.p. hydrocarbons, gc=graphitic coke
LPR(ave) = (Total mass of liquid)/(mass of catalyst)/(total run time)

APPENDIX B

TABLE B1 : BLANK COLUMN PULSE DATA.

Run ID : BLK1-i
Pulse Size : 1 µL

V cm/sec	$\left[\frac{D}{vL}\right]_{out} \times 10^3$	$\left[\frac{D}{vL}\right]_{in} \times 10^4$	SQRD ERROR	TMEAN (sec)	TOTAL Volume (ml)	DEAD Volume (ml)
1.03	7.08	-1.91	0.184	35.7	10.42	2.36
1.03	6.90	-3.79	0.142	36.4	10.65	2.59
1.34	5.36	5.36	0.307	24.3	9.16	1.10
1.34	5.27	-5.43	0.291	24.1	9.10	1.05
1.70	4.17	-5.99	0.262	19.4	9.35	1.29
1.70	4.13	-6.46	0.403	19.5	9.41	1.35
2.17	4.38	3.96	0.304	14.8	9.10	1.04
2.17	4.27	2.81	0.231	14.8	9.08	1.02
2.11	4.33	2.63	0.189	14.9	8.90	0.84
2.11	4.43	3.65	0.219	14.9	8.88	0.82
2.77	2.81	-6.83	4.94	12.3	9.67	1.61
2.77	2.97	-5.26	5.40	12.3	9.61	1.55
3.39	2.47	-7.55	1.43	9.94	9.54	1.48
3.39	2.61	-6.12	2.69	9.97	9.57	1.51
4.14	2.94	-1.23	0.049	8.64	10.10	2.04
4.14	3.02	-0.47	0.022	8.38	9.80	1.74
5.26	3.01	-5.27	0.034	6.71	9.98	1.92
5.26	3.22	1.63	0.154	6.64	9.88	1.82
6.12	3.20	0.62	0.072	5.30	9.17	1.11
6.12	3.12	-0.27	0.113	5.32	9.21	1.15
7.50	3.44	0.71	0.113	4.42	9.38	1.32
7.50	3.68	3.14	0.209	4.27	9.05	1.00
					9.50±0.47	

Run ID : BLK2-i
Pulse Size : 2 µL

V cm/sec	$\left[\frac{D}{vL}\right]_{out} \times 10^3$	$\left[\frac{D}{vL}\right]_{in} \times 10^4$	SQRD ERROR	TMEAN (sec)	TOTAL Volume (ml)	DEAD Volume (ml)
1.02	7.61	2.76	0.144	37.1	10.70	2.64
1.49	4.72	-6.05	0.383	21.8	9.19	1.13
1.92	4.44	1.02	0.157	16.3	8.86	0.80
2.69	3.03	-5.20	4.69	12.8	9.74	1.67
3.48	2.97	-2.12	0.110	9.69	9.53	1.47
4.44	2.85	-2.08	0.029	8.16	10.23	2.18
5.49	3.02	-0.52	0.150	6.13	9.52	1.46
7.49	3.35	-0.25	0.102	4.33	9.17	1.11
8.28	3.98	4.55	0.079	3.66	8.58	0.52
					9.50±0.62	

Run ID : BLK3-i
Pulse Size : 3 µl

V cm/sec	$[\frac{D}{VL}]_{out} \times 10^3$	$[\frac{D}{VL}]_{in} \times 10^4$	SQRD ERROR	TMEAN (sec)	TOTAL Volume (ml)	DEAD Volume (ml)
1.30	4.52	-14.5	0.469	22.6	8.34	0.28
1.77	3.95	-6.90	0.032	16.6	8.31	0.25
2.63	2.53	-10.60	1.60	11.5	8.58	0.52
3.88	2.89	-2.09	0.039	8.58	9.42	1.36
5.26	2.93	-1.28	0.079	6.05	9.00	0.94
7.18	3.37	0.55	0.115	4.47	9.08	1.02
					8.79±0.41	

Run ID : BLK4-i
Pulse Size : 4 µl

V cm/sec	$[\frac{D}{VL}]_{out} \times 10^3$	$[\frac{D}{VL}]_{in} \times 10^4$	SQRD ERROR	TMEAN (sec)	TOTAL Volume (ml)	DEAD Volume (ml)
1.07	6.40	-6.93	0.039	29.2	8.82	0.76
1.75	4.26	-4.09	0.015	16.6	8.23	0.17
2.92	3.64	2.57	0.931	12.7	10.47	2.41
3.96	2.95	-1.36	0.087	8.17	9.15	1.09
5.48	2.93	-1.45	0.097	5.91	9.16	1.10
7.37	3.14	-2.13	0.655	4.41	9.19	1.13
					9.17±0.67	

Run ID : BLK5-i
Pulse Size : 5 µl

V cm/sec	$[\frac{D}{VL}]_{out} \times 10^3$	$[\frac{D}{VL}]_{in} \times 10^4$	SQRD ERROR	TMEAN (sec)	TOTAL Volume (ml)	DEAD Volume (ml)
1.12	5.75	-10.8	0.126	27.1	8.54	0.49
1.12	5.76	-10.7	0.122	27.0	8.53	0.47
2.27	3.46	-4.39	1.32	13.2	8.48	0.42
3.96	2.97	-1.15	0.030	8.40	9.41	1.35
5.32	2.91	-1.53	0.015	6.10	9.17	1.11
7.67	3.41	0.031	0.208	4.16	9.02	0.96
					8.86±0.36	

Run ID : BLK6-i
Pulse size : 6 µl

V cm/sec	$\left[\frac{D}{VL}\right]_{out} \times 10^3$	$\left[\frac{D}{VL}\right]_{in} \times 10^4$	SQRD ERROR	TMEAN (sec)	TOTAL Volume (ml)	DEAD Volume (ml)
1.12	5.84	-9.91	0.091	27.6	8.71	0.65
1.88	4.31	-1.12	0.072	15.1	8.00	-0.06
3.18	2.32	-9.76	2.05	10.3	9.31	1.25
4.15	3.10	0.34	0.091	7.15	8.38	0.32
6.04	3.04	-0.97	0.037	5.39	9.20	1.15
7.41	3.43	0.79	0.061	4.30	9.01	0.96
					8.77±0.46	

Run ID : BLK7-i
Pulse Size : 7 µl

V cm/sec	$\left[\frac{D}{VL}\right]_{out} \times 10^3$	$\left[\frac{D}{VL}\right]_{in} \times 10^4$	SQRD ERROR	TMEAN (sec)	TOTAL Volume (ml)	DEAD Volume (ml)
1.13	5.80	-9.73	0.082	26.3	8.36	0.30
1.88	4.35	-0.73	0.037	16.1	8.54	0.48
3.12	1.98	-13.5	4.51	10.3	9.12	1.07
4.05	2.99	-0.85	0.051	7.01	8.03	-0.03
5.93	3.20	0.81	0.107	5.31	8.90	0.85
7.69	3.49	0.77	0.011	4.10	8.91	0.86
					8.65±0.37	

Run ID : BLK8-i
Pulse Size : 8 µl

V cm/sec	$\left[\frac{D}{VL}\right]_{out} \times 10^3$	$\left[\frac{D}{VL}\right]_{in} \times 10^4$	SQRD ERROR	TMEAN (sec)	TOTAL Volume (ml)	DEAD Volume (ml)
1.16	6.82	2.95	0.042	32.1	10.54	2.48
2.38	4.00	2.29	0.049	14.5	9.74	1.69
3.88	3.04	-0.58	0.036	8.98	9.86	1.81
4.11	3.06	-0.39	0.040	5.59	9.01	0.95
7.93	3.39	-0.73	0.011	4.14	9.30	1.24
					9.69±0.53	

Run ID : BLK9-i
Pulse Size : 9 µl

V cm/sec	$\left[\frac{D}{VL}\right]_{out} \times 10^3$	$\left[\frac{D}{VL}\right]_{in} \times 10^4$	SQRD ERROR	TMEAN (sec)	TOTAL Volume (ml)	DEAD Volume (ml)
1.20	5.83	-5.44	0.079	25.7	8.74	0.68
2.49	2.70	-10.1	2.52	12.6	8.86	0.81
3.68	2.97	-1.62	0.064	8.72	9.08	1.02
5.48	3.17	1.00	0.003	5.70	8.84	0.78
7.36	3.34	-0.08	0.013	4.35	9.05	0.99
					8.91±0.13	

Run ID : BLK10-i
Pulse Size : 10 µl

V cm/sec	$\left[\frac{D}{VL}\right]_{out} \times 10^3$	$\left[\frac{D}{VL}\right]_{in} \times 10^4$	SQRD ERROR	TMEAN (sec)	TOTAL Volume (ml)	DEAD Volume (ml)
1.07	6.11	-9.67	0.067	29.0	8.78	0.72
1.67	5.11	3.00	0.604	18.2	8.60	0.54
1.67	4.31	-5.24	0.211	18.4	8.69	0.64
2.50	2.71	-9.94	3.96	12.6	8.90	0.84
3.46	3.07	-1.20	0.062	9.40	9.20	1.14
4.98	3.16	1.23	0.073	6.46	9.09	1.03
6.51	3.38	1.85	0.050	4.87	8.97	0.91
7.50	3.59	2.23	0.021	4.17	8.84	0.78
					8.88±0.19	

TABLE B2 : GLASSBEAD COLUMN PULSE DATA.

Run ID : GB1-i
Pulse Size : 1 µl

V cm/sec	P_{ave} kPa	N_1	θ_z	D_z cm^2/sec	SQRD ERROR
1.04	102.5	242	0.421	0.122	1.83
1.52	102.9	340	0.336	0.127	8.06
2.44	103.8	410	0.359	0.169	5.84
4.09	105.2	504	0.511	0.231	3.01
5.64	106.5	442	0.542	0.363	3.73

0.434±0.081

Run ID : GB2-i
Pulse Size : 2 µl

V cm/sec	P_{ave} kPa	N_1	θ_z	D_z cm^2/sec	SQRD ERROR
1.06	102.5	237	0.411	0.127	2.12
1.52	102.9	361	0.343	0.120	3.32
2.58	103.9	443	0.391	0.166	6.49
3.36	104.6	420	0.351	0.227	6.82
4.88	105.8	391	0.356	0.356	5.75
5.95	106.7	340	0.355	0.500	7.04

0.368±0.025

Run ID : GB3-i
Pulse Size : 3 µl

V cm/sec	P_{ave} kPa	N_1	θ_z	D_z cm^2/sec	SQRD ERROR
0.98	102.4	236	0.386	0.118	1.65
1.34	102.8	353	0.322	0.108	3.08
1.92	103.3	401	0.332	0.137	6.39
3.15	104.4	459	0.346	0.196	3.90
4.64	105.6	409	0.331	0.323	1.66
5.67	106.5	425	0.324	0.380	1.14

0.340±0.022

Run ID : GB4-i
Pulse Size : 4 µl

V cm/sec	P_{ave} kPa	N_1	θ_z	D_z cm^2/sec	SQRD ERROR
1.06	102.5	241	0.372	0.125	1.97
1.59	103.0	366	0.356	0.124	2.60
2.33	103.7	421	0.369	0.158	5.72
3.65	104.8	394	0.369	0.264	0.92
5.13	106.0	349	0.333	0.418	1.12
6.06	106.8	460	0.329	0.375	1.40

0.355±0.018

Run ID : GB5-i
Pulse Size : 5 µl

V cm/sec	P_{ave} kPa	N_1	θ_z	D_z cm^2/sec	SQRD ERROR
1.01	102.5	249	0.377	0.115	1.15
1.62	103.2	373	0.367	0.124	2.41
2.38	103.7	410	0.358	0.166	4.18
4.74	104.5	367	0.331	0.368	2.32
5.74	106.5	390	0.340	0.420	1.36

0.355±0.017

Run ID : GB6-i
Pulse Size : 6 µl

V cm/sec	P_{ave} kPa	N_1	θ_z	D_z cm^2/sec	SQRD ERROR
1.06	102.5	251	0.405	0.121	1.53
1.46	102.9	353	0.337	0.118	5.34
2.71	104.0	413	0.327	0.187	4.67
3.38	104.6	376	0.315	0.256	3.33
4.90	105.9	421	0.359	0.332	1.49
5.87	106.7	353	0.345	0.474	0.65

0.348±0.029

Run ID : GB7-i
Pulse Size : 7 µl

V cm/sec	P_{ave} kPa	N_1	θ_z	D_z cm^2/sec	SQRD ERROR
1.06	102.5	256	0.409	0.118	2.20
2.12	103.5	406	0.344	0.149	4.60
3.16	104.4	433	0.340	0.208	3.34
4.27	105.3	354	0.324	0.344	3.32
5.75	106.6	275	0.334	0.596	0.37

0.350±.0.030

Run ID : GB8-i
Pulse Size : 8 µl

V cm/sec	P_{ave} kPa	N_1	θ_z	D_z cm^2/sec	SQRD ERROR
1.10	102.6	266	0.369	0.118	2.46
1.65	103.1	380	0.335	0.124	6.35
2.64	104.0	455	0.379	0.166	4.06
4.45	105.5	459	0.411	0.276	1.74
5.64	106.5	276	0.342	0.582	1.61

0.367±0.027

Run ID : GB9-i
Pulse Size : 9 µl

V cm/sec	P_{ave} kPa	N_1	θ_z	D_z cm^2/sec	SQRD ERROR
1.00	102.5	237	0.400	0.121	1.72
1.60	103.0	378	0.329	0.121	6.30
2.80	104.1	399	0.326	0.200	5.88
4.64	105.6	353	0.364	0.375	1.11
5.85	106.6	235	0.328	0.709	2.06

0.349±0.029

Run ID : GB10-i
Pulse Size : 10 µl

V cm/sec	P_{ave} kPa	N_1	θ_z	D_z cm^2/sec	SQRD ERROR
1.01	102.5	240	0.359	0.120	2.46
1.78	103.2	395	0.324	0.129	6.25
3.00	104.3	426	0.346	0.201	3.89
4.14	105.2	334	0.354	0.354	2.06
5.83	106.6	295	0.356	0.563	0.86

0.348±0.013

TABLE : B3
Catalyst : 30/40 mesh 5A Molecular Sieves
Reaction :
Coke Content :
Column length : 28.0 cm Column Diameter : 0.60 cm
Particle Diameter : 0.0508 cm Bed Porosity : 0.374

											Dx(constant)			Dx-model			Dx(constant,Dy)		
Run ID	T C	Tracer gas	Pulse Size	Pressure kPa	Velocity cm/sec	mu	sigma	HETP/2V	1/V/V	Dx	Kc	Dc	error	Kc	Dc	error	Dy	Kc	Dc	error
MS5-0	100	Methane	5 uL	102.9	1.43	3.48	0.0756	0.0612	0.489	0.125	6.82	8.69E-02	0.057							
MS5-1				103.3	1.91	3.39	0.0579	0.0369	0.274	0.139	6.62	2.25E-01	0.047							
MS5-2				104.2	2.87	3.48	0.0572	0.0230	0.122	0.183	6.83	1.52E-01	0.035							
MS5-3				104.9	3.79	3.63	0.0523	0.0147	0.0700	0.237	7.19	2.24E-01	0.541							
MS5-4				105.7	4.72	3.61	0.0543	0.0123	0.0450	0.301	7.10	5.26E+00	0.701							
MS5-5				106.8	6.09	3.76	0.0669	0.0110	0.0270	0.403	7.50	7.11E-02	0.016							
MS5-6				107.6	6.98	3.81	0.0767	0.0106	0.0210	0.484	7.58	6.77E-04	0.014							
MS5-7				108.3	7.89	3.70	0.0757	0.0098	0.0160	0.566	7.31	1.39E-04	0.015							
MS200-0	200	Propane	5 uL	104.0	2.66	22.0	18.3	0.199	0.141	0.168	49.1	6.62E-10	0.243	50.1	1.42E-09	0.015	61.7	21.0	2.37E-10	0.036
MS200-1				105.3	4.21	23.9	26.1	0.153	0.0570	0.271	53.3	6.86E-10	0.242	54.7	1.50E-09	0.007	61.2	25.7	2.94E-10	0.030
MS200-2				106.5	5.72	23.4	31.2	0.139	0.0310	0.394	52.2	7.54E-10	0.223	53.9	1.57E-09	0.003	54.1	28.0	3.60E-10	0.029
MS200-3				108.2	7.82	24.4	45.2	0.136	0.0160	0.588	54.1	7.64E-10	0.256	56.3	1.51E-09	0.003	52.2	31.1	3.86E-10	0.044
MS200-4				109.8	9.76	24.2	52.5	0.128	0.0100	0.788	53.7	7.98E-10	0.222	56.2	1.50E-09	0.003	46.1	33.5	4.40E-10	0.033
MS250-0	250			106.5	5.72					0.374	24.2	1.25E-09	0.238	25.2	2.45E-09	0.002	22.8	14.1	1.46E-10	0.039
MS150-0	150			106.5	5.72					0.412	150	3.54E-10	0.238	153	7.79E-10	0.009	176	70.0	6.46E-10	0.030

TABLE : B4
Catalyst : 45/60 mesh 5A Molecular Sieves
Reaction :
Coke Content :
Column length : 28.0 cm Column Diameter : 0.60 cm
Particle Diameter : 0.0302 cm Bed Porosity : 0.374

											Dx(constant)			Dx-model			Dx(constant,Dy)		
Run ID	T C	Tracer gas	Pulse Size	Pressure kPa	Velocity cm/sec	mu	sigma	HETP/2V	1/V/V	Dx	Kc	Dc	error	Kc	Dc	error	Dy	Kc	Dc	error
MSM-0	100	Methane	5 uL	102.8	1.40	3.51	0.0754	0.0612	0.510	0.121	6.88	3.46E-02	0.014							
MSM-1				103.4	1.98	3.55	0.0640	0.0359	0.255	0.139	6.98	7.40E-02	0.034							
MSM-2				104.2	2.87	3.57	0.0571	0.0219	0.121	0.178	7.02	4.29E-01	0.041							
MSM-3				104.8	3.61	3.82	0.0633	0.0168	0.0770	0.217	7.59	4.09E-02	0.224							
MSM-4				105.7	4.68	3.69	0.0610	0.0134	0.0460	0.284	7.26	3.20E-02	0.367							
MSM-5				106.7	5.91	3.84	0.0615	0.0099	0.0290	0.371	7.66	4.06E-02	0.204							
MSM-6				107.6	7.06	3.56	0.0845	0.0113	0.0200	0.461	7.66	8.37E-05	0.092							
MSM-7				109.1	8.91	3.83	0.0723	0.0077	0.0130	0.619	7.55	1.33E-01	1.55							
MSM20-0	200	Propane	5 uL	103.7	2.37	22.8	29.3	0.332	0.178	0.146	50.1	4.12E-10	0.482	51.4	8.81E-10	0.0808	65.2	21.1	1.41E-10	0.0830
MSM20-1				104.9	3.78	24.9	40.1	0.239	0.0700	0.229	54.7	4.69E-10	0.495	56.6	9.62E-10	0.0646	66.3	25.6	1.77E-10	0.0710
MSM20-2				106.0	5.01	22.8	46.8	0.251	0.0400	0.318	49.6	5.21E-10	0.446	51.7	1.00E-09	0.0342	53.2	26.5	2.28E-10	0.0850
MSM20-3				108.1	7.71	27.3	63.5	0.204	0.0170	0.546	56.9	5.65E-10	0.512	61.8	1.04E-09	0.0456	61.5	32.8	2.49E-10	0.0900
MSM20-4				109.6	9.84	26.7	78.3	0.155	0.0100	0.718	58.2	6.23E-10	0.395	61.3	1.12E-09	0.0133	54.4	35.1	3.09E-10	0.0640
MSM25-0	250			105.9	4.96					0.304	24.7	9.59E-10	0.443	25.8	1.82E-09	0.0295	25.6	13.6	4.35E-10	0.0830
MSM15-0	150			105.9	4.96					0.330	146	2.55E-10	0.487	150	5.35E-10	0.0694	182	65.4	9.30E-11	0.0700

APPENDIX C

TABLE : C1
Catalyst : HY
Reaction :
Coke Content :
Column length : 28.0 cm Column Diameter : 0.60 cm
Particle Diameter : 0.0375 cm Bed Porosity : 0.440

Run ID	T C	Tracer gas	Pulse Size	Pressure kPa	Velocity cm/sec	mu	sigma	HETP/2V	1/V/V	Dz	Rx(constant) Kc	Rx(constant) Dc	Rx(constant) error	Rx-model Kc	Rx-model Dc	Rx-model error
LZYM-0	50	Methane	5 uL	102.7	1.24	2.42	0.0309	0.0596	0.650	0.0920	5.09	5.07E-04	0.003	5.10	1.79E-04	0.003
LZYM-1				103.3	1.89	3.20	0.0210	0.0294	0.280	0.110	4.77	1.04E-03	0.087	4.77	3.36E-04	0.092
LZYM-2				104.4	2.84	2.50	0.0254	0.0200	0.124	0.143	5.34	1.70E-07	0.004	5.34	1.86E-06	0.804
LZYM-3				104.8	3.80	2.46	0.0195	0.0125	0.0772	0.174	5.22	1.28E-02	0.889	5.22	9.39E-04	0.915
LZYM-4				105.6	4.64	2.58	0.0332	0.0150	0.0465	0.223	5.52	2.68E-07	0.040	5.52	3.07E-06	0.038
LZYM-5				106.4	5.55	2.56	0.0270	0.0102	0.0325	0.270	5.56	2.71E-07	0.014	5.57	2.98E-06	0.013
LZYM-6				107.4	6.68	2.62	0.0219	0.0067	0.0224	0.333	5.64	2.41E-02	2.550	5.64	2.08E-03	2.570
LZYM-7				108.3	7.89	2.63	0.0239	0.0061	0.0161	0.404	5.73	2.03E-03	0.018	5.73	2.31E-03	0.017
M50-0	50	Methane	5 uL	102.8	1.32	2.66	0.0332	0.0498	0.574	0.0940	5.77	2.31E-04	0.067	5.77	1.20E-04	0.068
M50-1				104.9	3.81	2.72	0.0307	0.0152	0.0689	0.184	6.52	1.06E-02	0.466	6.52	1.64E-03	0.481
M50-2				106.2	5.29	2.94	0.0295	0.0090	0.0357	0.257	7.34	1.40E-03	0.025	7.34	8.85E-04	0.026
M50-3				107.4	6.77	3.21	0.0361	0.0072	0.0218	0.338	7.81	2.10E-03	0.020	7.82	1.48E-04	0.021
M100-0	100	Methane	5 uL	102.9	1.46	1.78	0.0168	0.0508	0.469	0.116	3.24	4.04E-04	0.196	3.24	1.60E-03	0.204
M100-1				104.1	2.81	1.87	0.0105	0.0150	0.127	0.153	3.51	7.01E-03	1.810	3.51	4.75E-03	1.840
M100-2				105.3	4.22	1.92	0.0186	0.0167	0.0562	0.206	3.61	7.20E-07	0.041	3.61	7.88E-06	0.048
M100-3				106.6	5.85	2.13	0.0105	0.0055	0.0292	0.282	4.22	1.61E-02	5.860	4.23	2.95E-02	5.890
M100-4				108.1	7.62	2.35	0.0218	0.0073	0.0172	0.375	4.85	4.32E-04	0.162	4.86	6.38E-04	0.166
M150-0	150	Methane	5 uL	103.1	1.67	1.38	0.0116	0.0511	0.358	0.141	2.10	5.20E-07	0.001	2.10	6.61E-06	0.001
M150-1				104.0	2.75	1.40	0.0101	0.0262	0.132	0.167	2.15	4.39E-07	0.032	2.15	5.17E-04	0.032
M150-2				105.0	3.85	1.28	0.0050	0.0111	0.0675	0.202	2.34	6.83E-03	4.380	2.34	2.05E-02	4.330
M150-3				106.5	5.69	1.47	0.0073	0.0084	0.0309	0.276	2.93	6.27E-02	0.146	2.93	2.34E-02	0.149
M150-4				107.9	7.45	1.60	0.0098	0.0065	0.0180	0.359	3.38	2.29E-02	0.200	3.38	2.44E-02	0.203
MM50-0	50	Methane	5 uL	102.7	1.28	2.98	0.0493	0.0607	0.610	0.0930	6.70	4.66E-08	0.001	6.70	5.12E-07	0.001
MM50-1				103.6	2.27	2.93	0.0323	0.0232	0.194	0.122	6.54	4.18E-04	0.172	6.55	4.40E-04	0.178
MM50-2				104.6	3.43	3.08	0.0327	0.0141	0.085	0.167	7.00	8.12E-04	0.004	7.00	4.66E-05	0.004
MM50-3				106.1	5.21	3.40	0.0380	0.0088	0.0368	0.253	7.92	5.48E-03	0.355	7.93	1.72E-03	0.361
MM50-4				107.5	6.95	3.42	0.0481	0.0063	0.0207	0.349	7.94	7.14E-06	0.018	7.94	4.96E-05	0.018
MM100-0	100	Methane	5 uL	102.9	1.50	2.06	0.0256	0.0413	0.444	0.117	4.06	9.36E-08	0.008	4.06	1.05E-06	0.008
MM100-1				103.8	2.51	1.86	0.0121	0.0195	0.159	0.143	3.45	1.72E-03	0.778	3.45	9.68E-04	0.800
MM100-2				104.9	3.80	2.01	0.0162	0.0148	0.0693	0.189	3.91	1.96E-04	0.016	3.91	3.08E-03	0.016
MM100-3				106.6	5.81	2.27	0.0145	0.0068	0.0296	0.280	4.64	1.80E-02	4.660	4.64	1.43E-02	4.660
MM100-4				108.2	7.77	2.38	0.0198	0.0060	0.0166	0.383	4.97	1.34E-02	0.237	4.97	7.28E-03	0.246
MM150-0	150	Methane	5 uL	103.2	1.79	1.58	0.0140	0.0439	0.312	0.143	2.67	3.92E-05	0.029	2.67	3.96E-04	0.031
MM150-1				104.4	3.16	1.54	0.0106	0.0198	0.100	0.179	2.53	3.68E-07	0.013	2.53	3.98E-06	0.013
MM150-2				105.8	4.79	1.65	0.0073	0.0079	0.0436	0.237	2.88	4.80E-03	2.610	2.88	2.38E-02	2.620
MM150-3				107.5	6.94	1.78	0.0115	0.0073	0.0208	0.334	3.24	1.45E-04	0.158	3.24	4.37E-03	0.164
MM150-4				108.7	8.46	1.87	0.0125	0.0059	0.0140	0.411	3.48	9.44E-03	0.226	3.49	1.12E-02	0.232

TABLE : C1 continued

Run ID	T C	Tracer gas	Pulse Size	Pressure kPa	Velocity cm/sec	nu	sigma	HETP/2V	1/V/V	Dz	Rx(constant) Kc	Rx(constant) Dc	Rx(constant) error	Rx-model Kc	Rx-model Dc	Rx-model error
M1-0	50	Methane	1 uL	102.8	1.40	2.95	0.0437	0.0502	0.510	0.0960	6.61	1.80E-07	0.001	6.61	2.12E-06	0.001
M1-1				103.7	2.32	2.61	0.0254	0.0225	0.186	0.124	5.61	1.78E-04	0.081	5.61	3.22E-04	0.090
M1-2				105.2	4.14	2.80	0.0207	0.0089	0.0583	0.199	6.19	8.12E-03	1.750	6.19	4.34E-03	1.790
M1-3				106.9	6.22	2.82	0.0300	0.0085	0.0259	0.307	6.23	2.07E-06	0.011	6.24	1.91E-05	0.011
M3-0	50	Methane	3 uL	102.8	1.34	2.90	0.0449	0.0558	0.557	0.095	6.46	7.40E-08	0.012	6.47	8.09E-07	0.012
M3-1				103.7	2.36	2.61	0.0238	0.0207	0.180	0.125	5.62	5.27E-02	0.295	5.62	9.12E-03	0.309
M3-2				105.1	3.96	2.72	0.0216	0.0103	0.0638	0.191	5.94	5.55E-02	1.270	5.94	1.05E-02	1.300
M3-3				106.7	5.89	2.73	0.0286	0.0091	0.0288	0.289	5.98	4.78E-06	0.015	5.98	5.08E-06	0.015
M5-0	50	Methane	5 uL	102.8	1.31	2.75	0.0383	0.0534	0.581	0.0940	6.05	1.79E-06	0.000	6.05	6.91E-06	0.001
M5-1				103.7	2.33	2.56	0.0236	0.0215	0.186	0.124	5.46	1.07E-03	0.235	5.46	9.18E-05	0.250
M5-2				105.0	3.82	2.60	0.0196	0.0105	0.0680	0.184	5.62	1.06E-03	1.430	5.62	1.48E-02	1.460
M5-3				106.9	6.16	2.63	0.0243	0.0079	0.0260	0.304	5.63	2.14E-02	0.388	5.63	2.03E-03	0.410
M10-0	50	Methane	10 uL	102.8	1.37	2.83	0.0407	0.0519	0.533	0.0950	6.28	1.07E-07	0.000	6.28	1.03E-06	0.001
M10-1				103.8	2.43	2.70	0.0260	0.0206	0.169	0.127	5.87	3.19E-03	0.099	5.87	5.90E-05	0.106
M10-2				105.0	3.82	2.58	0.0201	0.0111	0.0685	0.184	5.56	4.27E-03	1.240	5.57	3.54E-03	1.270
M10-3				106.8	6.06	2.62	0.0233	0.0078	0.0272	0.298	5.64	8.43E-03	0.192	5.64	1.12E-02	0.203
ZM-0	50	Methane	5 uL	102.8	1.31	3.19	0.0623	0.0645	0.581	0.095	7.32	1.36E-08	0.002	7.33	1.43E-07	0.000
ZM-1				103.0	1.58	3.17	0.0539	0.0471	0.400	0.101	7.25	1.77E-08	0.003	7.26	1.84E-07	0.002
ZM-2				103.6	2.21	3.93	0.0754	0.0306	0.204	0.120	9.43	2.12E-08	0.005	9.44	2.21E-07	0.001
ZM-3				104.1	2.85	3.91	0.0713	0.0227	0.123	0.142	9.36	3.61E-08	0.027	9.37	3.82E-07	0.021
ZM-4				104.5	3.22	3.56	0.0464	0.0158	0.0966	0.157	8.35	4.66E-04	0.086	8.35	8.26E-05	0.086
ZM-5				105.3	4.19	3.38	0.0457	0.0132	0.0570	0.199	7.82	1.02E-07	0.068	7.82	1.05E-06	0.063
ZM-6				106.4	5.52	3.27	0.0411	0.0096	0.0328	0.266	7.54	1.33E-07	0.004	7.54	1.43E-06	0.002
ZM-7				107.2	6.55	3.04	0.0387	0.0089	0.0233	0.322	6.86	1.12E-07	0.009	6.86	1.17E-06	0.004
LZYP-0	100	Propane	5 uL	103.7	2.37	23.6	2.24	0.0238	0.178	0.116	65.8	2.42E-04	0.252	65.8	5.58E-05	0.261
LZYP-1				104.7	3.51	24.2	2.25	0.0153	0.0812	0.170	67.6	9.82E-04	0.081	67.7	4.25E-04	0.086
LZYP-2				105.5	4.50	24.4	2.46	0.0129	0.0494	0.224	68.4	3.74E-03	0.172	68.5	1.25E-03	0.178
LZYP-3				107.0	6.24	25.6	2.66	0.0091	0.0257	0.327	71.8	9.67E-04	0.044	71.8	5.87E-04	0.046
LZYP-4				108.4	8.03	25.1	2.90	0.0080	0.0155	0.440	70.4	6.67E-08	0.017	70.4	7.40E-07	0.016
LZYPL-0	50			105.5	4.50					0.232	258	6.85E-05	0.158	256	9.27E-05	0.164
LZYPH-0	150			105.5	4.48					0.217	24.3	1.72E-05	0.151	24.3	2.20E-04	0.154
P100-0	100	Propane	5 uL	103.5	2.07	24.2	2.19	0.0253	0.233	0.103	67.5	3.36E-04	0.307	67.5	8.21E-05	0.315
P100-1				104.9	3.79	27.2	2.44	0.0122	0.070	0.184	76.3	9.90E-04	0.421	76.3	2.36E-04	0.431
P100-2				105.8	4.82	27.4	2.73	0.0106	0.0430	0.241	76.7	3.78E-03	0.478	76.7	1.49E-03	0.485
P100-3				106.8	6.09	28.9	2.98	0.0082	0.0270	0.317	81.1	2.69E-03	0.186	81.1	1.38E-03	0.189
P100-4				108.0	7.56	30.6	3.44	0.0068	0.0175	0.408	86.1	5.52E-02	0.114	86.1	9.15E-04	0.115
P50-0	50			105.8	4.79					0.249	336	1.41E-04	0.419	336	1.72E-04	0.428
P150-0	150			105.8	4.79					0.233	28.0	6.04E-03	0.036	28.0	3.34E-04	0.036

TABLE : C1 continued

Run ID	T C	Tracer gas	Pulse Size	Pressure kPa	Velocity cm/sec	mu	sigma	HETP/2Y	1/Y/Y	Dz	Rx(constant) Kc	Dc	error	Rx-model Kc	Dc	error
PP100-0	100	Propane	5 uL	103.8	2.51	26.0	4.20	0.0347	0.159	0.122	72.2	1.96E-08	0.169	72.2	2.02E-07	0.168
PP100-1				105.1	3.99	28.7	4.33	0.0185	0.0628	0.195	80.0	6.71E-04	0.141	80.0	3.28E-04	0.146
PP100-2				106.1	5.25	28.7	3.97	0.0129	0.0363	0.266	80.3	6.42E-04	0.237	80.4	6.29E-04	0.246
PP100-3				107.3	6.64	30.4	3.50	0.0080	0.0227	0.350	85.3	1.40E-03	0.218	85.3	8.35E-04	0.225
PP100-4				108.7	8.36	30.6	3.92	0.0070	0.0143	0.460	86.1	2.72E-04	0.062	86.1	1.98E-04	0.066
PP50-0	50			106.1	5.21					0.275	335	1.18E-04	0.322	334	2.37E-04	0.328
PP150-0	150			106.1	5.25					0.258	29.7	2.59E-03	0.087	29.7	6.67E-05	0.090
P1-0	100	Propane	1 uL	103.0	1.58	25.2	2.57	0.0359	0.401	0.0840	70.4	1.07E-08	0.025	70.4	1.17E-07	0.025
P1-1				103.9	2.55	22.6	1.89	0.0203	0.154	0.123	63.1	7.57E-05	0.052	63.1	2.09E-05	0.053
P1-2				105.7	4.65	23.6	2.04	0.0110	0.0463	0.235	65.9	1.01E-03	0.244	66.0	1.35E-03	0.249
P1-3				107.6	7.01	25.4	2.32	0.0072	0.0204	0.375	71.2	1.27E-02	0.358	71.2	3.75E-05	0.370
P3-0	100	Propane	3 uL	102.9	1.51	24.4	3.16	0.0492	0.439	0.0820	68.0	6.36E-09	0.138	68.0	6.55E-08	0.132
P3-1				104.0	2.67	23.3	2.35	0.0227	0.140	0.129	64.9	5.55E-05	0.079	64.9	2.14E-05	0.082
P3-2				105.9	4.92	24.4	3.62	0.0173	0.0413	0.248	67.9	4.70E-04	0.133	67.9	7.76E-04	0.139
P3-3				107.6	7.01	25.9	2.36	0.0070	0.0204	0.375	72.5	1.93E-04	0.354	72.6	8.18E-04	0.361
P5-0	100	Propane	5 uL	103.0	1.58	25.9	5.25	0.0685	0.401	0.0840	71.8	3.21E-09	0.205	71.8	3.25E-08	0.181
P5-1				104.0	2.67	23.4	2.52	0.0239	0.140	0.129	64.9	5.19E-05	0.179	64.9	2.54E-04	0.186
P5-2				105.7	4.76	24.9	2.18	0.0103	0.0442	0.238	69.6	4.87E-04	0.296	69.6	9.36E-04	0.301
P5-3				107.7	7.14	27.3	2.78	0.0072	0.0196	0.383	76.6	1.83E-03	0.158	76.6	3.87E-04	0.163
LP5-0	50			105.7	4.66					0.219	336	3.18E-04	0.362	336	4.52E-04	0.373
HP5-0	150			105.5	4.51					0.242	36.9	1.62E-05	0.100	36.9	6.97E-04	0.103
P10-0	100	Propane	10 uL	103.1	1.65	26.6	3.62	0.0434	0.367	0.0870	74.1	5.75E-09	0.137	74.2	6.14E-08	0.129
P10-1				104.0	2.67	23.1	2.26	0.0222	0.140	0.129	64.2	2.21E-05	0.243	64.2	7.59E-05	0.251
P10-2				105.4	4.29	23.3	4.44	0.0267	0.0543	0.212	64.7	1.47E-05	0.078	64.8	5.73E-05	0.082
P10-3				107.8	7.32	23.2	2.01	0.0071	0.0187	0.394	77.6	1.18E-03	0.118	77.6	9.53E-04	0.124
ZN1-0	100	n-Butane	1 uL	104.0	2.71	136	120	0.0333	0.136	0.129	388	2.72E-10	0.214	390	2.46E-09	0.131
ZN1-1				105.1	3.99	145	210	0.0348	0.0628	0.197	405	3.91E-10	1.900	407	3.19E-09	1.470
ZN1-2				106.4	5.58	160	84.5	0.0082	0.0321	0.291	418	4.47E-10	4.280	421	3.39E-09	3.800
ZN1-3				107.9	7.39	137	67.9	0.0068	0.0183	0.406	391	1.18E-04	0.265	391	3.25E-04	0.273
ZN3-0	100	n-Butane	3 uL	103.9	2.55	144	166	0.0434	0.154	0.121	406	4.20E-10	0.967	407	3.79E-09	0.777
ZN3-1				104.9	3.80	139	74.0	0.0140	0.0694	0.186	397	6.18E-09	0.150	397	6.49E-09	0.157
ZN3-2				106.8	6.04	146	192	0.0206	0.0274	0.320	410	1.57E-09	0.808	411	1.47E-08	0.749
ZN3-3				108.1	7.64	134	165	0.0166	0.0171	0.423	378	2.74E-09	0.473	379	2.68E-08	0.437
ZN5-0	100	n-Butane	5 uL	103.9	2.55	147	108	0.0272	0.154	0.121	418	6.36E-10	0.381	418	6.11E-09	0.310
ZN5-1				104.9	3.80	145	169	0.0295	0.0694	0.186	406	9.36E-10	0.854	407	8.71E-09	0.755
ZN5-2				106.5	5.70	147	121	0.0137	0.0308	0.298	418	3.91E-09	0.329	418	3.96E-08	0.319
ZN5-3				108.3	7.90	136	282	0.0269	0.0160	0.440	378	3.71E-09	0.446	378	3.81E-08	0.425
ZNL5-0	50			106.1	5.21					0.281	1217	4.27E-07	0.424	1216	2.06E-07	0.437
ZNH5-0	150			106.3	5.43					0.272	112	2.07E-08	0.112	112	2.25E-07	0.109

TABLE : C1 continued

Run ID	T C	Tracer gas	Pulse Size	Pressure kPa	Velocity cm/sec	mu	sigma	HETP/2V	1/V/V	Dz	Rx(constant) Kc	Dc	error	Rx-model Kc	Dc	error
ZN10-0	100	n-Butane	10 uL	104.0	2.71	142	116	0.0296	0.136	0.129	402	6.46E-10	0.519	402	6.11E-09	0.427
ZN10-1				105.1	3.99	140	106	0.0188	0.0628	0.197	397	1.95E-09	0.436	397	1.89E-08	0.409
ZN10-2				106.6	5.81	140	103	0.0125	0.0296	0.305	397	6.92E-09	0.348	397	7.44E-08	0.248
ZN10-3				108.2	7.77	127	83.7	0.0093	0.0166	0.432	361	6.34E-09	0.176	361	6.43E-08	0.170
ZI1-0	100	i-Butane	1 uL	103.9	2.55	112	30.9	0.0133	0.153	0.121	322	2.54E-05	0.895	322	3.10E-04	0.866
ZI1-1				105.0	3.89	119	45.4	0.0115	0.0660	0.191	340	1.44E-04	0.133	340	2.16E-07	0.187
ZI1-2				106.4	5.58	122	47.1	0.0079	0.0321	0.291	350	3.56E-05	0.269	350	4.78E-04	0.269
ZI1-3				108.1	7.64	120	55.4	0.0070	0.0171	0.423	343	5.18E-05	0.020	343	1.28E-04	0.021
ZI3-0	100	i-Butane	3 uL	103.9	2.55	124	49.7	0.0177	0.154	0.121	354	1.85E-05	0.019	354	1.62E-06	0.021
ZI3-1				105.0	3.89	121	47.2	0.0116	0.0660	0.191	346	4.46E-06	0.112	345	2.06E-05	0.116
ZI3-2				106.5	5.70	127	53.8	0.0081	0.0308	0.298	365	9.82E-05	0.213	365	5.90E-05	0.218
ZI3-3				107.9	7.37	118	51.0	0.0069	0.0183	0.406	337	5.68E-05	0.098	337	2.88E-04	0.100
ZI5-0	100	i-Butane	5 uL	103.8	2.47	121	49.0	0.0188	0.164	0.117	347	2.60E-06	0.021	347	2.36E-05	0.023
ZI5-1				105.4	4.29	131	57.8	0.0109	0.0543	0.214	375	1.25E-04	0.246	375	3.48E-05	0.248
ZI5-2				106.5	5.70	128	54.1	0.0081	0.0308	0.298	366	1.11E-05	0.215	366	1.94E-05	0.220
ZI5-3				108.0	7.52	121	54.1	0.0068	0.0177	0.415	347	1.79E-04	0.095	347	4.40E-05	0.097
ZIL5-0	50			106.1	5.16					0.278	792	5.89E-06	0.514	791	1.23E-04	0.529
ZIH5-0	150			106.3	5.43					0.271	106	1.94E-06	0.031	106	6.40E-05	0.031
ZI10-0	100	i-Butane	10 uL	103.9	2.55	123	49.6	0.0180	0.154	0.121	351	1.45E-05	0.021	351	8.12E-05	0.022
ZI10-1				104.9	3.83	121	46.8	0.0117	0.0694	0.186	346	1.79E-05	0.118	346	1.65E-05	0.119
ZI10-2				106.5	5.70	128	55.8	0.0082	0.0308	0.298	368	6.98E-05	0.172	368	9.12E-06	0.178
ZI10-3				107.9	7.39	118	51.6	0.0069	0.0183	0.406	339	1.18E-04	0.073	339	2.59E-04	0.074

TABLE : C2
Catalyst : HM
Reaction :
Coke Content :
Column length : 28.0/32.4 cm Column Diameter : 0.60(runs HMR,PMR)/0.46(all others) cm
Particle Diameter : 0.0375 cm Bed Porosity : 0.390/0.396

Run ID	T C	Tracer gas	Pulse Size	Pressure kPa	Velocity cm/sec	mu	sigma	HETP/2V	1/V/V	Ds	Rx(constant) Kc	Rx(constant) Dc	Rx(constant) error	Rx-model Kc	Rx-model Dc	Rx-model error
HMR-0	50	Methane	5 uL	102.8	1.32	14.0	1.14	0.0606	0.571	0.0950	31.8	1.40E-08	0.081	31.8	1.00E-07	0.001
HMR-1				103.2	1.74	12.6	0.670	0.0338	0.331	0.105	28.3	2.71E-07	0.003	28.3	1.86E-06	0.003
HMR-2				103.6	2.21	11.8	0.517	0.0231	0.204	0.120	26.6	4.03E-06	0.072	26.6	2.86E-03	0.071
HMR-3				104.5	3.30	14.1	0.664	0.0140	0.0818	0.160	32.0	2.86E-04	0.074	32.0	3.95E-04	0.008
HMR-4				105.2	4.14	13.9	0.613	0.0106	0.0583	0.197	31.4	5.21E-03	0.037	31.4	1.29E-03	0.037
HMR-5				106.0	5.06	13.7	0.586	0.0084	0.0390	0.242	31.3	1.90E-03	0.059	31.3	2.40E-03	0.057
HMR-6				106.7	5.95	13.7	0.604	0.0076	0.0283	0.288	30.9	1.10E-03	0.047	31.9	5.36E-05	0.051
HMR-7				107.7	7.12	13.2	0.584	0.0066	0.0197	0.354	29.9	1.93E-03	0.020	29.9	1.99E-05	0.029
PMR-0	100	Propane	5 uL	104.1	2.80	298	315	0.0175	0.128	0.133	702	8.32E-09	0.017	703	6.13E-08	0.017
PMR-1				105.2	4.14	351	477	0.0129	0.0584	0.201	826	6.04E-09	0.024	826	4.46E-08	0.023
PMR-2				106.6	5.81	351	583	0.0097	0.0296	0.297	826	7.34E-09	0.020	826	5.31E-08	0.019
PMR-3				108.6	8.23	331	536	0.0088	0.0148	0.449	778	5.61E-09	0.029	779	4.02E-08	0.025
PMRL-0	50			106.8	6.06					0.326	5280	6.74E-10	0.027	5283	4.83E-09	0.034
PMRH-0	150			106.6	5.80					0.286	185	1.26E-08	0.501	185	8.82E-08	0.040
HMMP-0	100	Methane	1 uL	104.8	6.11	4.41	0.0808	0.0110	0.0268	0.292	9.10	1.31E-07	0.030	9.06	8.99E-07	0.013
HMMP-1			3 uL	104.0	6.11	4.44	0.0870	0.0117	0.0268	0.292	9.17	1.08E-07	0.051	9.11	7.32E-07	0.023
HMMP-2			5 uL	104.0	6.11	4.44	0.0937	0.0126	0.0268	0.292	9.17	9.62E-08	0.067	9.10	6.43E-07	0.031
HMMP-3			10 uL	104.0	6.11	4.46	0.0911	0.0121	0.0268	0.292	9.21	9.57E-08	0.076	9.15	6.40E-07	0.036
HMMP-4			20 uL	104.0	6.11	4.47	0.0973	0.0129	0.0268	0.292	9.22	8.72E-08	0.108	9.17	5.75E-07	0.050
HMPP-0	100	Propane	1 uL	104.0	6.11	324	970	0.0245	0.0268	0.314	766	3.83E-10	0.186	766	2.23E-09	0.027
HMPP-1			3 uL	104.0	6.11	323	898	0.0228	0.0268	0.314	764	3.91E-10	0.179	764	2.28E-09	0.029
HMPP-2			5 uL	104.0	6.11	312	893	0.0243	0.0268	0.314	736	4.13E-10	0.235	736	2.40E-09	0.047
HMPP-3			10 uL	104.0	6.11	315	1139	0.0304	0.0268	0.314	739	3.63E-10	0.312	741	2.08E-09	0.073
HMPP-4			20 uL	104.0	6.11	316	1244	0.0329	0.0268	0.314	739	3.46E-10	0.354	741	1.94E-09	0.087
HMNP-1	100	n-Butane	3 uL	104.0	6.11	2961	77900	0.0236	0.0268	0.322	7003	4.59E-11	0.159	7006	2.71E-10	0.022
HMNP-2			5 uL	104.0	6.11	2924	84800	0.0268	0.0268	0.322	6888	4.39E-11	0.235	6895	2.56E-10	0.048
HMNP-3			10 uL	104.0	6.11	2956	97300	0.0295	0.0268	0.322	6942	4.13E-11	0.318	6952	2.38E-10	0.085
HMIP-1	100	i-Butane	3 uL	104.0	6.11	2912	158000	0.0494	0.0268	0.322	6781	2.02E-11	0.555	6852	1.01E-10	0.103
HMIP-2			5 uL	104.0	6.11	2812	146000	0.0489	0.0268	0.322	6640	1.85E-11	0.288	6720	9.10E-11	0.040
HMIP-3			10 uL	104.0	6.11	2540	88200	0.0362	0.0268	0.322	5900	4.54E-11	0.836	5914	2.54E-10	0.390
HMH-1	150	n-Butane	5 uL	103.3	4.65	390	1870	0.0427	0.0460	0.277	917	1.78E-10	0.272	921	9.75E-10	0.035
HMH-2				104.4	6.90	389	2480	0.0386	0.0210	0.358	910	1.99E-10	0.345	917	1.04E-09	0.041
HMH-3				106.0	9.93	393	2816	0.0297	0.0101	0.552	921	2.33E-10	0.256	931	1.17E-09	0.012
HMH-4				107.7	13.6	416	3450	0.0237	0.0054	0.802	976	2.58E-10	0.228	988	1.26E-09	0.006
HMHH-0	200			105.6	9.17					0.484	244	7.92E-10	0.216	247	3.98E-09	0.012
HMI-1	150	i-Butane	5 uL	103.3	4.66	367	3788	0.0978	0.0460	0.227	841	8.17E-11	1.040	857	3.66E-10	0.257
HMI-2				104.3	6.74	355	4056	0.0774	0.0220	0.348	816	1.03E-10	0.701	834	4.46E-10	0.089
HMI-3				106.2	10.3	370	4538	0.0520	0.0094	0.578	854	1.36E-10	0.504	875	5.79E-10	0.028
HMI-4				107.7	13.4	375	4972	0.0427	0.0056	0.786	869	1.57E-10	0.391	892	6.50E-10	0.007
HMIH-0	200			105.6	9.17					0.484	222	5.24E-10	0.258	226	2.33E-09	0.060

TABLE : C3
Catalyst : CRACT, HY
Reaction : Hexane cracking over HY at 400 C, 1 atm, 6 h
Coke Content : 9.2 wt% graphitic
Column length : 28.0 cm Column Diameter : 0.60 cm
Particle Diameter : 0.0375 cm Bed Porosity : 0.407

Run ID	T C	Tracer gas	Pulse Size	Pressure kPa	Velocity cm/sec	mu	sigma	HETP/2V	1/V/V	Dz	Rx(constant) Kc	Rx(constant) Dc	Rx(constant) error	Rx-model Kc	Rx-model Dc	Rx-model error
CHT-0	50	methane	5 uL	102.8	1.37	4.83	0.131	0.0567	0.533	0.0960	12.0	1.79E-08	0.004	12.0	1.96E-07	0.002
CHT-1				103.4	1.97	4.34	0.0729	0.0273	0.258	0.112	10.6	1.86E-04	0.036	10.6	8.10E-04	0.037
CHT-2				104.3	3.05	4.80	0.0834	0.0164	0.107	0.150	12.0	2.00E-06	0.008	12.0	1.82E-05	0.009
CHT-3				105.6	4.57	5.11	0.0902	0.0105	0.0480	0.217	12.8	4.19E-08	0.208	12.8	3.55E-03	0.214
CHT-4				106.7	5.89	4.58	0.0726	0.0081	0.0288	0.286	11.2	2.91E-05	0.193	11.3	1.85E-03	0.193
CHT-5				107.7	7.12	4.49	0.0763	0.0073	0.0197	0.354	11.1	1.40E-07	0.005	11.1	1.53E-06	0.007
CPT-0	100	propane	5 uL	103.7	2.31	103	43.4	0.0245	0.188	0.112	277	2.76E-09	0.047	278	2.96E-08	0.044
CPT-1				104.8	3.61	118	60.7	0.0168	0.0769	0.173	318	2.80E-09	0.057	318	2.99E-08	0.050
CPT-2				106.6	5.81	121	73.7	0.0121	0.0296	0.297	325	2.56E-09	0.039	325	2.70E-08	0.029
CPT-3				108.3	7.90	118	79.4	0.0100	0.0160	0.428	319	1.88E-09	0.021	320	1.88E-08	0.006
CPTL-0	50			106.9	6.00					0.323	2313	4.68E-10	0.039	2315	4.96E-09	0.031
CPTH-0	150			106.8	6.11					0.304	72.7	1.25E-08	0.025	72.8	1.33E-07	0.017

TABLE : C4
Catalyst : CRAC1, HY
Reaction : Hexane cracking over HY at 400 C, 1 atm, 12 h
Coke Content : 10.6 wt% graphitic
Column length : 28.0 cm Column Diameter : 0.60 cm
Particle Diameter : 0.0375 cm Bed Porosity : 0.414

Run ID	T C	Tracer gas	Pulse Size	Pressure kPa	Velocity cm/sec	mu	sigma	HETP/2V	1/V/V	Dz	Rx(constant) Kc	Rx(constant) Dc	Rx(constant) error	Rx-model Kc	Rx-model Dc	Rx-model error	RxKy-model Ky	RxKy-model Kc	RxKy-model Dc	RxKy-model error
CH1-0	50	methane	5 uL	102.8	1.31	4.47	0.136	0.0719	0.581	0.0950	10.5	6.31E-09	0.031	10.5	6.20E-08	0.011				
CH1-1				103.3	1.94	3.99	0.117	0.0527	0.267	0.111	9.14	8.28E-09	0.098	9.17	7.69E-08	0.049				
CH1-2				104.2	2.89	4.20	0.108	0.0293	0.120	0.144	9.73	1.38E-08	0.119	9.77	1.29E-07	0.054				
CH1-3				105.1	3.96	4.42	0.118	0.0212	0.0639	0.189	10.3	1.72E-08	0.205	10.3	1.56E-07	0.106				
CH1-4				106.1	5.16	4.67	0.153	0.0188	0.0375	0.247	11.0	1.34E-08	0.040	11.1	1.18E-07	0.006				
CH1-5				106.9	6.22	4.57	0.148	0.0158	0.0258	0.303	10.7	2.07E-08	0.186	10.8	1.87E-07	0.086				
CH1-6				107.7	7.12	4.44	0.144	0.0142	0.0197	0.354	10.4	1.64E-08	0.022	10.5	1.42E-07	0.012				
CP1-0	100	propane	5 uL	103.7	2.39	93.5	131	0.0867	0.176	0.115	250	1.16E-10	0.630	254	8.22E-10	0.146	265	95.7	1.50E-10	0.017
CP1-1				105.3	4.24	105	224	0.0661	0.0556	0.206	280	1.40E-10	0.634	285	9.26E-10	0.116	258	132	2.34E-10	0.006
CP1-2				107.2	6.58	109	287	0.0512	0.0231	0.344	288	1.81E-10	0.636	294	1.14E-09	0.090	250	146	3.20E-10	0.004
CP1-3				108.7	8.43	104	268	0.0407	0.0141	0.462	275	2.27E-10	0.638	282	1.42E-09	0.090	233	144	4.10E-10	0.006
CPL1-0	50			107.3	6.67					0.366	2100	2.39E-11	0.418	2148	1.53E-10	0.096	400	1907	1.28E-11	0.094
CPB1-0	150			107.1	6.42					0.322	58.4	9.98E-10	0.507	59.5	6.60E-09	0.058	49.8	29.9	1.99E-09	0.002

TABLE : C5
Catalyst : CRAC2, HY
Reaction : Hexane cracking over HY at 400 C, 1 atm, 6 h
Coke Content : 8.5 wt% graphitic
Column length : 28.0 cm Column Diameter : 0.60 cm
Particle Diameter : 0.0375 cm Bed Porosity : 0.419

		Tracer	Pulse	Pressure	Velocity						Rx(constant)			Rx-model		
Run ID	T C	gas	Size	kPa	cm/sec	mu	sigma	HETP/2V	1/V/V	Dz	Kc	Dc	error	Kc	Dc	error
CM2-0	50	methane	5 uL	102.8	1.31	4.26	0.101	0.0589	0.581	0.0950	10.0	2.42E-08	0.004	10.0	2.64E-07	0.003
CM2-1				103.2	1.76	3.54	0.0553	0.0346	0.321	0.106	8.05	9.75E-07	0.002	8.06	1.19E-05	0.003
CM2-2				104.0	2.66	4.07	0.0600	0.0189	0.142	0.135	9.52	4.22E-07	0.003	9.53	4.16E-06	0.004
CM2-3				105.0	3.87	4.55	0.0787	0.0136	0.0669	0.185	10.8	8.35E-08	0.037	10.8	8.86E-07	0.034
CM2-4				105.7	4.76	4.23	0.0713	0.0116	0.0441	0.227	9.95	7.18E-08	0.008	9.96	7.65E-07	0.004
CM2-5				106.3	5.42	4.10	0.0546	0.0083	0.0341	0.260	9.55	2.37E-02	0.466	9.56	6.96E-03	0.490
CM2-6				107.1	6.44	4.23	0.0790	0.0087	0.0241	0.316	9.96	2.81E-07	0.047	9.97	3.36E-06	0.050
CM2-7				107.8	7.30	3.84	0.0735	0.0095	0.0188	0.364	8.86	6.06E-08	0.021	8.87	6.06E-07	0.008
CP2-0	100	propane	5 uL	103.7	2.31	80.2	24.2	0.0226	0.188	0.112	220	5.43E-09	0.024	220	5.95E-08	0.022
CP2-1				105.1	3.99	92.1	37.1	0.0152	0.0628	0.193	253	2.99E-09	0.027	253	3.29E-08	0.019
CP2-2				106.9	6.16	92.3	39.7	0.0105	0.0264	0.318	254	2.82E-09	0.022	254	2.93E-08	0.010
CP2-3				108.3	7.90	84.5	40.5	0.0100	0.0160	0.428	232	2.25E-09	0.014	233	2.22E-08	0.001
CPL2-0	50			106.9	6.16					0.333	2014	3.13E-10	0.042	2017	3.20E-09	0.025
CPH2-0	150			107.0	6.30					0.315	62.5	1.42E-08	0.018	62.6	1.49E-07	0.010

TABLE : C6
Catalyst : CRAC3, HM
Reaction : Hexane cracking over HM at 400 C, 1 atm, 5.5 h
Coke Content : 3.1 wt% graphitic
Column length : 28.0 cm Column Diameter : 0.60 cm
Particle Diameter : 0.0375 cm Bed Porosity : 0.415

		Tracer	Pulse	Pressure	Velocity						Rx-model			RxKy-model			
Run ID	T C	gas	Size	kPa	cm/sec	mu	sigma	HETP/2V	1/V/V	Dz	Kc	Dc	error	Ky	Kc	Dc	error
CM3-0	50	methane	5 uL	103.0	1.58	13.3	59.6	2.95	0.401	0.101	31.9	9.53E-11	0.494	16.4	32.3	2.31E-11	0.107
CM3-1				103.8	2.43	9.72	43.5	2.63	0.170	0.127	20.1	2.77E-10	0.765	13.9	21.8	3.47E-11	0.038
CM3-2				104.5	3.30	10.8	59.0	2.12	0.0918	0.160	21.7	3.77E-10	0.801	16.0	23.6	4.17E-11	0.045
CM3-3				105.5	4.47	9.53	50.1	1.71	0.0501	0.213	18.6	6.66E-10	0.692	13.7	19.0	8.59E-11	0.073
CM3-4				106.3	5.42	7.91	29.2	1.19	0.0341	0.260	16.0	1.01E-09	0.450	10.7	14.9	2.04E-10	0.065
CM3-5				107.2	6.56	7.64	31.1	1.13	0.0233	0.322	15.2	1.24E-09	0.383	9.33	14.0	3.07E-10	0.113
CP3-0	100	propane	5 uL	103.9	2.59	9.05	68.5	4.48	0.149	0.124	49.8	4.46E-12	0.376	0.103	53.7	3.75E-12	0.363
CP3-1				104.9	3.80	6.56	39.2	3.32	0.0694	0.182	12.7	1.07E-10	1.890	3.33	46.3	2.47E-12	0.254
CP3-2				106.9	6.16	5.21	28.7	2.38	0.0264	0.318	5.49	1.63E-10	3.220	4.13	22.4	8.60E-12	0.174
CP3-3				108.5	8.16	3.11	7.75	1.36	0.0150	0.444	3.41	8.83E-09	2.590	3.87	12.9	1.93E-11	0.017

TABLE : C7
Catalyst : CRAC4, HY
Reaction : Hexane cracking over HY at 400 C, 1 atm, 3 h
Coke Content : 8.9 wt% graphitic
Column length : 28.0 cm Column Diameter : 0.60 cm
Particle Diameter : 0.0375 cm Bed Porosity : 0.433

Run ID	T C	Tracer gas	Pulse Size	Pressure kPa	Velocity cm/sec	mu	sigma	HETP/2Y	1/Y/Y	Dz	Rx(constant) Kc	Rx(constant) Dc	Rx(constant) error	Rx-model Kc	Rx-model Dc	Rx-model error
CM4-0	50	methane	5 uL	103.1	1.34	3.16	0.0458	0.0386	0.371	0.103	7.14	2.40E-07	0.008	7.14	2.74E-06	0.008
CM4-1				103.3	1.64	3.11	0.0428	0.0316	0.267	0.111	6.99	6.95E-07	0.017	7.00	1.11E-05	0.019
CM4-2				103.8	2.51	3.03	0.0362	0.0219	0.159	0.130	6.76	1.21E-07	0.007	6.77	1.41E-06	0.009
CM4-3				104.7	3.47	3.54	0.0447	0.0142	0.0830	0.167	8.20	9.98E-05	0.109	8.21	5.68E-04	0.116
CM4-4				105.3	4.28	3.64	0.0520	0.0127	0.0546	0.204	8.49	8.28E-08	0.015	8.49	8.82E-04	0.010
CM4-5				106.0	5.06	3.59	0.0468	0.0100	0.0390	0.242	8.33	1.79E-04	0.307	8.33	8.61E-04	0.324
CM4-6				107.0	6.33	3.36	0.0517	0.0101	0.0250	0.309	7.67	8.28E-08	0.023	7.68	8.62E-07	0.013
CM4-7				107.6	7.01	3.43	0.0536	0.0091	0.0204	0.348	7.90	7.89E-08	0.017	7.91	8.10E-07	0.007
CP4-0	100	propane	5 uL	103.7	2.39	59.0	13.7	0.0228	0.176	0.115	166	1.66E-08	0.037	166	1.78E-07	0.037
CP4-1				105.0	3.89	66.5	17.1	0.0137	0.0660	0.188	187	1.41E-08	0.017	188	1.57E-07	0.017
CP4-2				106.9	6.16	65.8	20.0	0.0104	0.0264	0.318	185	5.85E-09	0.012	185	6.25E-08	0.007
CP4-3				108.4	8.03	64.4	20.5	0.0085	0.0155	0.436	181	4.69E-09	0.008	181	4.85E-08	0.002
CPL4-0	50			106.9	6.22					0.337	1255	1.70E-09	0.032	1256	1.98E-08	0.034
CPH4-0	150			106.9	6.17					0.307	48.3	3.64E-08	0.005	48.4	4.09E-07	0.005

TABLE : C8
Catalyst : CRAC5, HY
Reaction : Hexane cracking over HY at 400 C, 1 atm, 24 h
Coke Content : 13.9 wt% graphitic
Column length : 28.0 cm Column Diameter : 0.60 cm
Particle Diameter : 0.0375 cm Bed Porosity : 0.436

Run ID	T C	Tracer gas	Pulse Size	Pressure kPa	Velocity cm/sec	mu	sigma	HETP/2Y	1/Y/Y	Dz	Rx(constant) Kc	Rx(constant) Dc	Rx(constant) error	Rx-model Kc	Rx-model Dc	Rx-model error	RxKy-model Ky	RxKy-model Kc	RxKy-model Dc	RxKy-model error
CM5-0	50	methane	5 uL	102.9	1.49	4.09	0.322	0.179	0.451	0.0990	9.47	2.20E-09	0.643	9.56	1.61E-08	0.279	13.2	1.86	4.73E-10	0.004
CM5-1				103.6	2.28	4.81	0.283	0.0742	0.192	0.122	11.6	2.95E-09	0.426	11.8	2.22E-08	0.115	13.7	3.59	2.92E-09	0.004
CM5-2				104.3	3.09	4.45	0.244	0.0553	0.105	0.152	10.6	4.15E-09	0.619	10.7	3.03E-08	0.201	13.2	2.90	2.73E-09	0.015
CM5-3				105.1	3.96	4.34	0.233	0.0433	0.0638	0.189	10.3	5.02E-09	0.729	10.4	3.63E-08	0.252	12.8	2.86	3.09E-09	0.032
CM5-4				105.7	4.76	4.31	0.255	0.0399	0.0441	0.227	10.2	5.52E-09	0.545	10.4	3.87E-08	0.127	14.2	2.31	7.02E-10	0.268
CM5-5				106.4	5.58	4.43	0.268	0.0340	0.0322	0.268	10.5	7.20E-09	1.120	10.6	5.14E-08	0.505	15.3	2.09	3.61E-10	0.154
CM5-6				106.9	6.22	4.24	0.245	0.0303	0.0258	0.303	10.0	8.97E-09	0.538	10.1	6.55E-08	0.184	13.7	2.15	2.03E-09	0.080
CM5-7				107.7	7.18	4.17	0.244	0.0270	0.0194	0.358	9.83	7.36E-09	0.523	10.0	5.05E-08	0.111	9.50	4.34	1.17E-08	0.024
CP5-0	100	propane	5 uL	104.0	2.67	89.8	293	0.188	0.140	0.127	241	6.34E-11	1.480	249	3.54E-10	0.407	265	99.5	3.71E-11	0.024
CP5-1				105.4	4.29	99.3	439	0.144	0.0543	0.209	265	8.51E-11	1.490	274	4.64E-10	0.394	287	113	4.90E-11	0.010
CP5-2				107.1	6.40	103	695	0.142	0.0244	0.333	269	1.12E-10	1.550	279	5.85E-10	0.420	294	117	5.50E-11	0.004
CP5-3				108.4	8.10	93.9	404	0.0784	0.0153	0.441	252	1.55E-10	1.060	261	8.26E-10	0.186	229	130	1.71E-10	0.011
CPL5-0	50			107.1	6.44					0.351	2150	1.43E-11	1.190	2226	7.75E-11	0.303	1707	1236	2.25E-11	0.167
CPH5-0	150			107.1	6.42					0.322	55.7	6.43E-10	1.350	57.5	3.57E-09	0.350	62.0	22.8	3.29E-10	0.013

TABLE : C9
Catalyst : CRAC6, HY
Reaction : Hexane cracking over HY at 400 C, 1 atm, 3 h
Coke Content : 8.9 wt% graphitic
Column length : 28.0 cm Column Diameter : 0.60 cm
Particle Diameter : 0.0375 cm Bed Porosity : 0.446

		Tracer	Pulse	Pressure	Velocity						Rx(constant)			Rx-model		
Run ID	T C	gas	Size	kPa	cm/sec	mu	sigma	HETP/2Y	1/Y/Y	Dz	kc	Dc	error	kc	Dc	error
CH6-0	50	methane	5 uL	103.2	1.80	3.75	0.0672	0.0367	0.308	0.107	9.01	3.09E-08	0.000	9.01	3.38E-07	0.001
CH6-1				103.5	2.18	3.44	0.0525	0.0282	0.211	0.119	8.09	5.73E-08	0.007	8.09	6.34E-07	0.007
CH6-2				104.3	3.05	3.88	0.0636	0.0191	0.107	0.150	9.39	6.58E-08	0.021	9.39	7.41E-07	0.028
CH6-3				105.2	4.09	3.93	0.0583	0.0128	0.0596	0.195	9.53	1.19E-07	0.029	9.53	1.37E-06	0.040
CH6-4				105.7	4.66	3.88	0.0631	0.0125	0.0460	0.222	9.35	4.80E-08	0.020	9.36	4.34E-07	0.010
CH6-5				106.4	5.58	3.81	0.0531	0.0091	0.0322	0.268	9.19	8.12E-05	0.134	9.19	3.76E-03	0.154
CH6-6				107.1	6.44	3.71	0.0612	0.0096	0.0241	0.316	8.88	5.78E-08	0.004	8.89	5.92E-07	0.000
CH6-7				107.8	7.24	3.54	0.0621	0.0095	0.0191	0.361	8.36	5.00E-08	0.006	8.38	4.94E-07	0.001
CP6-0	100	propane	5 uL	103.8	2.47	61.7	15.4	0.0227	0.164	0.118	177	3.40E-09	0.024	177	3.65E-08	0.019
CP6-1				105.0	3.89	69.7	21.3	0.0156	0.0660	0.188	201	3.31E-09	0.017	201	3.49E-08	0.010
CP6-2				107.7	6.40	71.4	26.5	0.0112	0.0244	0.333	206	3.17E-09	0.010	206	3.27E-08	0.004
CP6-3				108.4	8.03	67.3	23.8	0.0091	0.0155	0.436	194	3.57E-09	0.007	194	3.63E-08	0.000
CPL6-0	50			107.2	6.61					0.362	1303	4.89E-10	0.035	1304	4.99E-09	0.016
CPH6-0	150			107.2	6.55					0.330	52	1.63E-08	0.002	52.0	1.72E-07	0.002

TABLE : C10
Catalyst : CRAC7, HY
Reaction : Hexane cracking over HY at 400 C, 1 atm, 1 h
Coke Content : 7.1 wt% graphitic
Column length : 28.0 cm Column Diameter : 0.60 cm
Particle Diameter : 0.0375 cm Bed Porosity : 0.436

		Tracer	Pulse	Pressure	Velocity						Rx(constant)			Rx-model		
Run ID	T C	gas	Size	kPa	cm/sec	mu	sigma	HETP/2Y	1/Y/Y	Dz	kc	Dc	error	kc	Dc	error
CH7-0	50	methane	5 uL	103.0	1.55	5.46	0.206	0.0616	0.416	0.100	13.7	4.46E-09	0.011	13.8	4.21E-08	0.001
CH7-1				103.5	2.07	4.40	0.0959	0.0330	0.233	0.115	10.7	2.13E-08	0.006	10.7	2.24E-07	0.004
CH7-2				104.1	2.81	4.10	0.0642	0.0188	0.126	0.141	9.83	1.37E-06	0.049	9.83	1.26E-05	0.052
CH7-3				104.7	3.57	3.82	0.0510	0.0138	0.0810	0.169	9.02	1.04E-03	0.216	9.02	1.94E-04	0.234
CH7-4				105.6	4.57	3.71	0.0500	0.0110	0.0479	0.217	8.72	1.01E-06	0.039	8.72	1.11E-05	0.040
CH7-5				106.3	5.42	3.66	0.0402	0.0077	0.0341	0.260	8.62	1.73E-02	0.793	8.62	4.64E-03	0.810
CH7-6				107.2	6.55	3.56	0.0513	0.0085	0.0233	0.322	8.31	4.68E-07	0.013	8.31	5.28E-06	0.013
CH7-7				107.9	7.36	3.56	0.0501	0.0074	0.0185	0.368	8.31	2.81E-07	0.008	8.31	3.08E-06	0.007
CP7-0	100	propane	5 uL	103.7	2.39	66.3	16.7	0.0220	0.176	0.115	187	1.52E-07	0.034	187	1.22E-05	0.037
CP7-1				104.9	3.80	69.8	16.7	0.0125	0.0694	0.183	197	1.46E-06	0.115	197	4.48E-05	0.118
CP7-2				106.9	6.24	70.2	18.9	0.0085	0.0257	0.323	198	8.66E-05	0.064	198	2.70E-04	0.067
CP7-3				108.6	8.28	66.6	18.4	0.0069	0.0145	0.453	188	7.46E-08	0.008	188	8.83E-07	0.008
CPL7-0	50			106.8	6.00					0.323	1164	1.74E-06	0.383	1164	4.30E-05	0.389
CPH7-0	150			106.8	6.04					0.300	50.7	3.52E-04	0.021	50.7	1.93E-05	0.024

TABLE : C14
Catalyst : HY, OLIG1
Reaction : Propene Oligomerisation for 5.0 h, 200 C, 52 atm
Coke Content : 4.3% high boiling point hydrocarbons, 13.0% graphitic coke
Column length : 32.4 cm Column Diameter : 0.46 cm
Particle Diameter : 0.0375 cm Bed Porosity : 0.374

Run ID	T C	Tracer gas	Pulse Size	Pressure kPa	Velocity cm/sec	mu	sigma	HETP/2Y	1/Y/Y	Dz	Rx model Kc	Dc	error	RxRy model Ky	Kc	Dc	error
OH1-0	50	Methane	5 uL	102.2	2.19	3.49	0.0559	0.0338	0.208	0.120	7.35	2.22E-07	0.011				
OH1-1				102.4	2.55	3.25	0.0455	0.0275	0.154	0.132	6.70	2.75E-07	0.026				
OH1-2				102.9	3.55	3.62	0.0508	0.0177	0.0795	0.171	7.68	2.93E-07	0.008				
OH1-3				103.6	5.09	3.78	0.0688	0.0154	0.0387	0.243	8.06	3.45E-07	0.012				
OH1-4				104.2	6.23	3.51	0.0588	0.0124	0.0257	0.303	7.41	9.24E-07	0.068				
OH1-5				104.8	7.32	3.39	0.0755	0.0146	0.0187	0.364	7.06	3.81E-07	0.022				
OH1-6				105.8	8.99	3.22	0.0492	0.0086	0.0124	0.463	6.56	6.63E-06	0.596				
OH1-7				106.6	10.4	3.28	0.0401	0.0058	0.0092	0.551	6.83	9.93E-05	0.671				
OP1-0	100	Propane	5 uL	102.6	2.94	59.3	18.5	0.0289	0.116	0.140	150	8.65E-09	0.042				
OP1-1				103.1	3.95	63.2	22.0	0.0226	0.0641	0.190	160	9.64E-09	0.032				
OP1-2				104.0	5.85	67.4	31.2	0.0190	0.0292	0.298	170	9.67E-09	0.036				
OP1-3				105.4	8.40	62.3	31.6	0.0157	0.0142	0.458	158	1.03E-08	0.011				
OP1-4				106.8	10.7	59.5	38.5	0.0165	0.0087	0.610	150	9.46E-09	0.011				
OPL1-0	50			105.9	8.87					0.376	1097	6.93E-10	0.013				
OPH1-0	150			104.6	6.85					0.469	38.9	4.85E-08	0.010				
ON1-0	100	n-Butane	5 uL	102.8	3.43	434	751	0.0118	0.0851	0.165	1110	2.02E-09	0.022	1446	227	2.71E-10	0.066
ON1-1				103.3	4.50	423	945	0.0190	0.0493	0.225	1080	1.48E-09	0.023	1321	276	2.30E-10	0.023
ON1-2				104.7	7.16	433	1460	0.0177	0.0195	0.390	1104	1.42E-09	0.015	1352	285	1.92E-10	0.035
ON1-3				105.6	8.59	394	1325	0.0161	0.0136	0.483	1010	1.40E-09	0.007	7.60	1006	1.40E-09	0.007
ON1-4				106.7	10.5	383	1403	0.0148	0.0091	0.612	984	1.39E-09	0.007	0.750	983	1.41E-09	0.008
ONh1-0	150			105.7	8.87					0.483	177	1.02E-08	0.008				
OI1-0	100	i-Butane	5 uL	102.7	3.30	300	1572	0.0857	0.197	0.159	754	3.03E-10	0.366	935	206	2.10E-11	0.030
OI1-1				103.7	5.23	298	1800	0.0627	0.0365	0.269	750	4.09E-10	0.271	879	232	4.17E-11	0.027
OI1-2				104.3	6.33	294	1698	0.0503	0.0250	0.337	744	4.43E-10	0.150	743	304	8.66E-11	0.014
OI1-3				105.9	9.14	319	2942	0.0512	0.0120	0.521	801	4.85E-10	0.141	753	356	1.05E-10	0.019
OI1-4				106.8	10.7	302	2167	0.0360	0.0087	0.626	767	5.53E-10	0.081	603	409	1.78E-10	0.012
OIH1-0	150			105.7	8.87					0.483	150	4.18E-09	0.050	122	76	1.41E-09	0.003

TABLE : C15
Catalyst : HY, OLIG2
Reaction : Propene Oligomerisation for 7.4 h, 200 C, 52 atm
Coke Content : 5.2% high boiling point hydrocarbons, 13.2% graphitic coke
Column length : 32.4 cm Column Diameter : 0.46 cm
Particle Diameter : 0.0375 cm Bed Porosity : 0.385

Run ID	T C	Tracer gas	Pulse Size	Pressure kPa	Velocity cm/sec	mu	sigma	HETP/2V	1/V/V	Dz	Rx model Kc	Rx model Dc	Rx model error	RxRy model Ky	RxRy model Kc	RxRy model Dc	RxRy model error
OH2-0	50	Methane	5 uL	102.1	2.05	2.10	0.0456	0.0821	0.238	0.115	3.81	4.61E-08	0.028				
OH2-1				102.3	2.34	1.92	0.0324	0.0611	0.182	0.125	3.35	5.26E-08	0.014				
OH2-2				102.5	2.92	1.85	0.0346	0.0563	0.117	0.145	3.17	5.41E-08	0.017				
OH2-3				102.9	3.67	1.80	0.0387	0.0528	0.0744	0.176	3.04	5.83E-08	0.020				
OH2-4				103.5	4.81	1.88	0.946	0.0432	0.0432	0.229	3.27	6.24E-08	0.016				
OH2-5				104.2	6.09	1.99	0.0480	0.0322	0.0272	0.295	3.56	6.94E-08	0.013				
OH2-6				105.0	7.64	1.97	0.0611	0.0334	0.0171	0.383	3.50	6.48E-08	0.012				
OH2-7				105.9	9.16	1.97	0.0820	0.0374	0.0119	0.473	3.48	6.05E-08	0.013				
OP2-0	100	Propane	5 uL	102.6	2.94	18.5	20.9	0.337	0.116	0.140	46.8	5.38E-10	0.038	16.3	37.6	3.21E-10	0.012
OP2-1				103.0	3.82	17.8	32.2	0.431	0.0687	0.183	44.1	5.14E-10	0.071	20.2	33.3	2.30E-10	0.007
OP2-2				103.9	5.54	17.3	34.2	0.334	0.0326	0.280	43.3	5.92E-10	0.054	16.7	34.5	2.95E-10	0.005
OP2-3				105.2	8.04	16.7	39.9	0.288	0.0155	0.435	41.8	6.53E-10	0.055	14.3	34.5	3.42E-10	0.005
OP2-4				106.7	10.5	16.1	42.2	0.251	0.0091	0.596	40.7	7.10E-10	0.050	12.5	34.5	3.87E-10	0.006
OPL2-0	50			104.7	7.00					0.386	301	3.30E-11	0.063	71.1	272	1.89E-11	0.020
OPH2-0	150			105.9	9.27					0.494	10.7	9.04E-09	0.044	5.39	7.63	4.00E-09	0.004
ON2-0	100	n-Butane	5 uL	102.5	2.82	93.7	423	0.277	0.126	0.134	249	1.05E-10	0.085	21.4	236	9.44E-11	0.083
ON2-1				103.0	3.82	84.8	496	0.293	0.0687	0.186	224	1.11E-10	0.042	28.4	208	9.27E-11	0.036
ON2-2				103.9	5.69	90.1	850	0.298	0.0308	0.297	236	9.78E-11	0.123	96.4	187	4.52E-11	0.053
ON2-3				105.0	7.69	92.1	1186	0.295	0.0169	0.424	238	1.10E-10	0.140	108	185	4.28E-11	0.034
ON2-4				106.8	10.7	83.2	930	0.203	0.0087	0.626	221	1.31E-10	0.093	68.3	188	7.09E-11	0.047
ONH2-0	150			106.0	9.27					0.509	35.7	2.20E-09	0.019	7.56	31.4	1.65E-09	0.011
OI2-0	100	i-Butane	5 uL	102.5	2.82	42.0	211	0.687	0.126	0.134	115	5.41E-11	0.185	8.19	111	4.76E-11	0.183
OI2-1				103.1	4.08	43.7	327	0.679	0.0600	0.201	119	5.35E-11	0.178	32.2	105	2.85E-11	0.119
OI2-2				103.9	5.69	47.0	495	0.637	0.0308	0.297	124	6.13E-11	0.251	48.2	108	2.04E-11	0.077
OI2-3				105.2	8.04	46.8	884	0.813	0.0155	0.447	115	7.04E-11	0.306	49.0	107	1.61E-11	0.011
OI2-4				106.9	10.9	43.3	815	0.646	0.0084	0.640	105	8.35E-11	0.510	48.1	108	1.26E-11	0.051
OIH2-0	150			106.0	9.27					0.509	24.3	8.06E-10	0.177	11.8	19.5	2.35E-10	0.019

TABLE : C16
Catalyst : HY, OLIG3
Reaction : Propene Oligomerisation for 5.4 h, 350 C, 50 atm
Coke Content : 1.3% high boiling point hydrocarbons, 21.7% graphitic coke
Column length : 32.4 cm Column Diameter : 0.46 cm
Particle Diameter : 0.0375 cm Bed Porosity : 0.361

		Tracer	Pulse	Pressure	Velocity						Rx model			RxRy model			
Run ID	T C	gas	Size	kPa	cm/sec	mu	sigma	HETP/2V	1/V/V	Dz	Kc	Dc	error	Ky	Kc	Dc	error
OH3-0	50	Methane	5 uL	102.2	2.24	3.53	1.80	1.04	0.199	0.121	6.99	9.93E-10	0.286	4.44	5.03	2.04E-10	0.006
OH3-1				102.5	2.76	3.34	1.56	0.823	0.131	0.139	6.55	1.24E-09	0.295	4.08	4.78	2.55E-10	0.007
OH3-2				102.7	3.20	3.22	1.63	0.797	0.0978	0.156	6.22	1.33E-09	0.331	3.88	4.66	2.52E-10	0.008
OH3-3				103.3	4.42	3.88	2.57	0.627	0.0513	0.210	7.65	1.52E-09	0.514	5.30	5.69	2.06E-10	0.021
OH3-4				103.7	5.22	3.57	1.97	0.480	0.0366	0.250	7.04	2.06E-09	0.374	4.61	5.17	3.54E-10	0.008
OH3-5				104.3	6.39	3.26	2.26	0.541	0.0245	0.311	6.13	2.23E-09	0.407	3.86	4.80	3.52E-10	0.004
OH3-6				105.0	7.64	3.18	2.51	0.525	0.0171	0.383	5.85	2.52E-09	0.453	3.67	4.72	3.60E-10	0.004
OH3-7				105.9	9.16	2.87	1.90	0.408	0.0119	0.473	5.21	3.02E-09	0.422	3.11	4.30	4.66E-10	0.005
OP3-0	100	Propane	5 uL	102.4	2.59	30.7	234	1.56	0.150	0.124	72.7	5.39E-11	0.561	41.8	63.0	7.96E-12	0.052
OP3-1				103.2	4.22	22.7	133	0.990	0.0561	0.205	52.5	1.41E-10	0.580	30.8	44.4	1.77E-11	0.029
OP3-2				103.9	5.69	24.0	204	1.01	0.0308	0.289	52.4	1.74E-10	0.760	34.4	47.3	1.57E-11	0.015
OP3-3				105.1	7.86	24.9	311	1.04	0.0162	0.423	51.1	2.31E-10	0.863	34.1	47.8	1.81E-11	0.017
OP3-4				107.1	11.1	20.4	157	0.549	0.0081	0.637	43.9	4.45E-10	0.752	29.2	37.6	4.45E-11	0.019
OPL3-0	50			104.6	7.00					0.386	325	6.09E-11	0.354	196	241	1.33E-11	0.064
OPH3-0	150			105.8	9.07					0.482	12.9	1.17E-09	0.920	9.06	12.0	7.78E-11	0.021
ON3-0	100	n-Butane	5 uL	102.5	2.82	179	2881	0.518	0.126	0.134	464	1.96E-11	0.593	219	357	7.26E-12	0.439
ON3-1				103.3	4.36	139	2297	0.450	0.0526	0.217	350	3.55E-11	0.325	177	268	1.11E-11	0.142
ON3-2				104.3	6.33	151	4301	0.485	0.0250	0.337	372	3.25E-11	0.541	212	299	6.20E-12	0.101
ON3-3				105.3	8.22	140	5293	0.536	0.0148	0.459	327	4.86E-11	0.568	210	267	6.26E-12	0.024
ON3-4				106.9	10.9	122	2808	0.279	0.0084	0.640	299	8.48E-11	0.397	179	230	1.64E-11	0.041
ONH3-0	150			105.8	9.07					0.496	47.8	3.25E-10	0.651	30.7	41.0	3.62E-11	0.027
OI3-0	100	i-Butane	5 uL	102.4	2.70	44.3	131	0.400	0.137	0.128	103	4.67E-10	1.120	121	42.0	1.48E-11	0.030
OI3-1				103.2	4.22	31.9	57.7	0.218	0.0561	0.209	74.6	1.12E-09	0.866	86.5	29.1	4.92E-11	0.021
OI3-2				104.3	6.33	32.3	68.8	0.169	0.0250	0.337	75.5	1.46E-09	0.706	83.2	31.1	9.18E-11	0.010
OI3-3				105.6	8.71	32.1	89.3	0.161	0.0132	0.491	74.3	1.75E-09	0.595	79.9	32.4	1.15E-10	0.009
OI3-4				106.8	10.7	31.8	135	0.202	0.0087	0.626	72.2	1.93E-09	0.544	74.4	33.4	1.52E-10	0.024
OIH3-0	150			105.8	9.07					0.496	13.5	1.13E-08	0.711	14.5	5.50	4.99E-10	0.029

TABLE : C17
Catalyst : HY, OLIG4
Reaction : Propene Oligomerisation for 12.4 h, 100 C, 53 atm
Coke Content : 7.9% high boiling point hydrocarbons, 6.9% graphitic coke
Column length : 32.4 cm Column Diameter : 0.46 cm
Particle Diameter : 0.0375 cm Bed Porosity : 0.409

Run ID	T C	Tracer gas	Pulse Size	Pressure kPa	Velocity cm/sec	mu	sigma	HETP/2V	1/V/V	Dx	Rx model Kc	Dc	error
OM4-0	50	Methane	5 uL	102.1	2.05	1.96	0.0146	0.0300	0.238	0.115	3.58	7.24E-07	0.002
OM4-1				102.4	2.55	1.86	0.0118	0.0217	0.154	0.132	3.33	1.68E-06	0.002
OM4-2				102.7	3.31	1.89	0.0107	0.0146	0.0911	0.161	3.40	2.70E-05	0.000
OM4-3				103.1	4.10	1.83	0.0103	0.0122	0.0596	0.195	3.23	8.08E-06	0.002
OM4-4				103.7	5.15	1.85	0.0102	0.0094	0.0376	0.246	3.30	3.11E-05	0.000
OM4-5				104.6	6.85	1.85	0.0113	0.0078	0.0213	0.337	3.28	5.55E-06	0.003
OM4-6				105.1	7.70	1.92	0.0123	0.0070	0.0169	0.386	3.46	5.96E-06	0.002
OM4-7				105.8	8.99	1.84	0.0118	0.0063	0.0124	0.463	3.25	3.22E-06	0.001
OP4-0	100	Propane	5 uL	102.4	2.59	14.8	0.810	0.0232	0.150	0.124	38.5	7.93E-08	0.000
OP4-1				103.1	4.08	17.5	1.10	0.0142	0.0600	0.198	45.9	1.17E-07	0.002
OP4-2				103.9	5.54	14.5	0.889	0.0124	0.0326	0.280	37.8	1.05E-07	0.006
OP4-3				105.4	8.40	14.7	1.14	0.0102	0.0142	0.458	38.2	8.63E-08	0.021
OP4-4				106.8	10.7	14.2	1.32	0.0099	0.0087	0.610	37.0	6.99E-08	0.035
OPL4-0	50			104.7	7.00					0.386	207	1.70E-08	0.010
ON4-0	100	n-Butane	5 uL	102.4	2.59	72.8	19.1	0.0226	0.150	0.123	196	1.89E-08	0.013
ON4-1				103.2	4.22	74.7	21.9	0.0151	0.0561	0.209	201	2.27E-08	0.029
ON4-2				104.5	6.66	78.6	31.1	0.0122	0.0225	0.357	212	1.63E-08	0.024
ON4-3				105.4	8.40	74.1	30.0	0.0105	0.0142	0.471	200	1.62E-08	0.054
ON4-4				106.8	10.7	74.1	34.5	0.0095	0.0087	0.626	200	1.46E-08	0.067
ONL4-0	50			104.7	7.00					0.397	1604	2.83E-09	0.016
OI4-0	100	i-Butane	5 uL	102.4	2.59	55.1	15.3	0.0316	0.150	0.123	147	1.36E-08	0.098
OI4-1				103.1	3.95	52.5	12.1	0.0180	0.0641	0.194	142	1.86E-08	0.005
OI4-2				104.2	6.17	58.5	16.9	0.0130	0.0263	0.326	157	1.86E-08	0.017
OI4-3				105.4	8.40	60.4	20.9	0.0110	0.0142	0.471	163	1.70E-08	0.055
OI4-4				106.9	10.9	60.2	26.9	0.0110	0.0084	0.640	163	1.37E-08	0.105
OIL4-0	50			104.7	7.00					0.397	1169	2.39E-09	0.013

TABLE : C18
Catalyst : HY, OLIG5
Reaction : Propene Oligomerisation for 6.9 h, 200 C, 50 atm
Coke Content : 4.4% high boiling point hydrocarbons, 16.7% graphitic coke
Column length : 32.4 cm Column Diameter : 0.46 cm
Particle Diameter : 0.0375 cm Bed Porosity : 0.368

Run ID	T C	Tracer gas	Pulse Size	Pressure kPa	Velocity cm/sec	mu	sigma	HETP/2V	1/V/V	Rx model Dz	Kc	Dc	error	RxKy model Ky	Kc	Dc	error
OH5-0	50	Methane	5 uL	102.2	2.15	1.41	0.0227	0.105	0.217	0.118	2.00	4.14E-08	0.055				
OH5-1				102.4	2.60	1.37	0.0224	0.0750	0.148	0.133	1.89	4.38E-08	0.031				
OH5-2				102.6	3.08	1.37	0.0309	0.0868	0.105	0.152	1.88	4.24E-08	0.041				
OH5-3				103.2	4.16	1.49	0.0424	0.0746	0.0577	0.198	2.17	5.16E-08	0.054				
OH5-4				103.5	4.81	1.51	0.0325	0.0478	0.0432	0.229	2.26	5.79E-08	0.032				
OH5-5				104.2	6.09	1.54	0.0362	0.0408	0.0270	0.295	2.33	5.94E-08	0.028				
OH5-6				105.1	7.80	1.60	0.0459	0.0371	0.0164	0.392	2.50	6.15E-08	0.025				
OH5-7				105.9	9.16	1.58	0.0529	0.0375	0.0119	0.473	2.43	6.22E-08	0.026				
OP5-0	100	Propane	5 uL	102.3	2.24	10.7	9.49	0.556	0.199	0.116	25.5	5.54E-10	0.062	11.3	19.4	2.56E-10	0.010
OP5-1				102.9	3.68	9.5	9.06	0.439	0.0738	0.177	22.8	6.65E-10	0.056	7.62	18.8	3.70E-10	0.016
OP5-2				104.0	5.85	11.2	16.1	0.356	0.0293	0.298	27.0	7.30E-10	0.079	10.5	21.7	3.43E-10	0.011
OP5-3				105.4	8.40	10.6	22.0	0.377	0.0142	0.458	24.9	7.92E-10	0.109	10.3	20.2	3.11E-10	0.004
P5-4				106.7	10.5	9.5	16.4	0.279	0.0091	0.597	22.8	9.37E-10	0.086	8.32	19.1	4.03E-10	0.014
OPL5-0	50			104.7	7.00					0.386	163	5.15E-11	0.129	51.9	146	2.14E-11	0.049
OPH5-0	150			105.8	9.07					0.482	6.85	1.11E-08	0.085	3.98	4.65	4.04E-09	0.005
ON5-0	100	n-Butane	5 uL	102.3	2.36	43.5	126	0.456	0.179	0.113	112	1.19E-10	0.099	17.2	102	9.54E-11	0.093
ON5-1				103.3	4.36	48.0	277	0.446	0.0525	0.217	122	1.21E-10	0.068	41.0	101	6.45E-11	0.026
ON5-2				104.6	6.83	51.2	317	0.287	0.0214	0.368	132	1.52E-10	0.059	26.8	119	1.06E-10	0.043
ON5-3				105.4	8.31	48.0	305	0.258	0.0145	0.465	124	1.72E-10	0.064	24.7	112	1.19E-10	0.046
ON5-4				106.8	10.7	43.2	298	0.242	0.0087	0.626	112	1.96E-10	0.066	24.8	100	1.25E-10	0.039
ONH5-0	150			105.8	9.07					0.496	20.8	2.73E-09	0.038	5.39	17.8	1.85E-09	0.024
OI5-0	100	i-Butane	5 uL	102.4	2.53	29.4	308	2.28	0.157	0.120	69.5	3.39E-11	0.666	35.6	69.8	4.35E-12	0.078
OI5-1				102.9	3.68	18.7	89.0	1.12	0.0738	0.179	45.6	1.00E-10	0.372	21.4	40.3	2.24E-11	0.052
OI5-2				103.7	5.23	18.8	91.5	0.801	0.0365	0.269	45.7	1.51E-10	0.332	21.6	39.8	3.49E-11	0.036
OI5-3				105.3	8.22	20.3	133	0.636	0.0148	0.459	47.7	2.09E-10	0.402	23.9	42.8	3.88E-11	0.020
OI5-4				106.7	10.5	17.9	98.5	0.474	0.0091	0.612	42.1	3.19E-10	0.365	21.0	37.2	6.31E-11	0.020
OIH5-0	150			105.8	9.07					0.496	13.3	1.39E-09	0.289	7.42	10.6	2.99E-10	0.004

TABLE : C19
Catalyst : HM, OLIG6
Reaction : Propene Oligomerisation for 12.4 h, 250 C, 52 atm
Coke Content : 5.4% high boiling point hydrocarbons, 6.7% graphitic coke
Column length : 32.4 cm Column Diameter : 0.46 cm
Particle Diameter : 0.0375 cm Bed Porosity : 0.391

Run ID	T C	Tracer gas	Pulse Size	Pressure kPa	Velocity cm/sec	mu	sigma	HETP/2V	1/V/V	Ds	macro-model Ky	macro-model Dy	macro-model error	Rx model Kc	Rx model Dc	Rx model error	RxRy model Ky	RxRy model Kc	RxRy model Dc	RxRy model error
OM6-0	50	Methane	5 uL	102.1	1.96	0.767	0.0036	0.0507	0.261	0.112	0.995	6.44E-04	0.073	0.436	1.77E-07	0.005	0.736	0.128	1.49E-08	0.036
OM6-1				102.4	2.55	0.708	0.0027	0.0336	0.154	0.132	0.676	1.11E-03	0.079	0.293	2.91E-07	0.016	0.437	0.108	4.74E-08	0.002
OM6-2				102.7	3.20	0.747	0.0028	0.0250	0.0977	0.156	0.881	2.19E-03	0.116	0.381	6.71E-07	0.059	0.617	0.114	1.01E-07	0.018
OM6-3				103.0	3.91	0.702	0.0024	0.0204	0.0654	0.187	0.638	2.92E-03	0.146	0.274	8.16E-07	0.087	0.539	0.049	1.78E-08	0.009
OM6-4				104.0	5.80	0.816	0.0060	0.0250	0.0298	0.280	1.21	1.77E-02	0.161	0.523	6.39E-06	0.154	1.14	0.027	2.24E-08	0.076
OM6-5				104.5	6.77	0.754	0.0030	0.0126	0.0218	0.333	0.903	1.49E-02	0.219	0.388	4.80E-06	0.204	0.851	0.032	4.34E-09	0.085
OM6-6				104.9	7.48	0.751	0.0030	0.0115	0.0179	0.373	0.891	4.60E-02	0.139	0.382	1.56E-06	0.137	0.845	0.017	1.35E-08	0.084
OM6-7				105.9	9.16	0.683	0.0029	0.0111	0.0119	0.473	0.520	4.76E-03	0.108	0.228	1.13E-06	0.051	0.421	0.054	4.28E-08	0.042
OP6-0	100	Propane	5 uL	102.3	2.37	0.889	0.0098	0.0851	0.179	0.114	1.56	1.76E-03	0.463	0.679	5.35E-07	0.348	1.45	0.122	6.00E-10	0.014
OP6-1				103.1	3.95	0.805	0.0118	0.0747	0.0640	0.190	1.08	1.92E-03	0.651	0.473	5.14E-07	0.441	0.969	0.126	1.36E-09	0.022
OP6-2				104.0	5.70	0.973	0.0153	0.0460	0.0308	0.289	1.96	5.29E-03	0.651	0.854	1.55E-06	0.541	1.86	0.191	4.00E-10	0.060
OP6-3				105.2	8.03	0.946	0.0136	0.0306	0.0155	0.434	1.84	2.71E-03	0.500	0.809	6.94E-07	0.242	1.61	0.192	4.93E-09	0.033
OP6-4				106.9	10.7	0.905	0.0116	0.0210	0.0084	0.611	1.25	1.21E-03	0.800	0.581	2.09E-07	0.245	0.709	0.317	3.14E-08	0.133
OPL6-0	50			104.4	6.53					0.355	1.45	2.84E-03	0.880	0.635	7.43E-07	0.599	1.31	0.176	1.54E-09	0.052
OPH6-0	150			105.5	8.46					0.444	1.35	2.11E-02	0.316	0.585	6.78E-06	0.300	1.30	4.15	2.53E-13	0.132
ON6-0	100	n-Butane	5 uL	102.2	2.26	0.990	0.0096	0.0705	0.196	0.108	2.09	1.11E-03	0.763	0.916	2.88E-07	0.488	1.88	0.169	1.62E-09	0.026
ON6-1				103.1	4.01	1.01	0.0228	0.0903	0.0621	0.197	2.09	2.44E-03	1.120	0.917	6.32E-07	0.872	1.95	0.244	4.23E-10	0.089
ON6-2				104.3	6.33	1.07	0.0163	0.0364	0.0250	0.336	2.45	4.48E-03	1.010	1.07	1.15E-06	0.800	2.30	0.224	7.89E-10	0.114
ON6-3				105.3	8.22	0.996	0.0294	0.0584	0.0148	0.459	1.99	2.50E-03	1.130	0.880	5.85E-07	0.678	1.78	0.306	1.27E-09	0.021
ON6-4				107.1	11.1	0.896	0.0242	0.0440	0.0081	0.654	1.48	1.64E-03	0.942	0.673	3.18E-07	0.291	1.04	0.284	2.10E-08	0.010
ONL6-0	50			104.4	6.53					0.365	2.77	9.79E-04	1.450	1.25	1.72E-07	0.576	2.10	0.460	6.78E-09	0.009
ONH6-0	150			105.5	8.46					0.457	1.43	3.69E-03	0.489	0.627	1.01E-06	0.301	1.29	0.146	3.12E-09	0.009
OI6-0	100	1-Butane	5 uL	102.2	2.26	0.936	0.0075	0.0617	0.196	0.108	1.82	1.43E-03	0.556	0.794	4.09E-07	0.383	1.76	0.127	1.32E-09	0.026
OI6-1				103.0	3.82	0.912	0.0074	0.0376	0.0685	0.187	1.69	4.52E-03	0.662	0.735	1.35E-06	0.580	1.59	0.099	1.15E-09	0.150
OI6-2				104.3	6.33	0.855	0.0107	0.0375	0.0250	0.336	1.36	3.35E-03	0.655	0.592	9.26E-07	0.467	1.24	0.156	1.16E-09	0.030
OI6-3				105.7	8.78	0.890	0.0121	0.0282	0.0130	0.496	1.54	2.92E-03	0.568	0.678	7.57E-07	0.292	1.33	0.165	7.10E-09	0.005
OI6-4				106.9	10.9	0.696	0.0261	0.0801	0.0084	0.640	0.417	5.95E-04	0.722	0.271	2.14E-08	0.068		0.272	2.13E-08	0.068
OIL6-0	50			104.4	6.54					0.365	1.99	1.11E-03	1.370	0.896	2.18E-07	0.604	1.58	0.336	4.40E-09	0.005
OIH6-0	150			105.5	8.46					0.457	1.37	9.36E-03	0.490	0.594	2.81E-06	0.418	1.29	0.086	2.04E-09	0.129

TABLE : C20
Catalyst : HM, OLIG7
Reaction : Propene Oligomerisation for 13.2 h, 300 C, 52 atm
Coke Content : 2.2% high boiling point hydrocarbons, 10.0% grahitic coke
Column length : 32.4 cm Column Diameter : 0.46 cm
Particle Diameter : 0.0375 cm Bed Porosity : 0.391

											macro-model				Rx model			RxRy model			
Run ID	T C	Tracer gas	Pulse Size	Pressure kPa	Velocity cm/sec	mu	sigma	HETP/2V	1/V/V	Dz	Ky	Dy	error	Kc	Dc	error	Ky	Kc	Dc	error
OM7-0	50	Methane	5 uL	102.1	2.05	0.689	0.0027	0.0457	0.239	0.115	0.585	5.52E-04	0.039	0.257	1.18E-07	0.004				
OM7-1				102.4	2.55	0.621	0.0019	0.0320	0.154	0.132	0.218	6.51E-04	0.034	0.099	4.94E-08	0.024				
OM7-2				102.7	3.14	0.600	0.0017	0.0249	0.101	0.154	0.105	8.26E-04	0.043	0.056	1.36E-08	0.054				
OM7-3				103.0	3.91	0.615	0.0016	0.0173	0.0564	0.187	0.189	1.70E-03	0.053	0.081	1.38E-07	0.001				
OM7-4				103.6	5.09	0.657	0.0019	0.0142	0.0385	0.243	0.409	2.26E-03	0.037	0.176	4.46E-07	0.004				
OM7-5				104.9	7.48	0.779	0.0031	0.0111	0.0179	0.373	1.05	5.65E-03	0.042	0.458	1.88E-06	0.021				
OM7-6				105.7	8.82	0.747	0.0030	0.0100	0.0129	0.452	0.882	3.61E-03	0.068	0.385	1.03E-06	0.014				
OM7-7				104.5	6.77	0.788	0.0024	0.0094	0.0218	0.333	1.11	1.58E-02	0.049	0.479	5.98E-06	0.045				
OP7-0	100	Propane	5 uL	102.3	2.37	0.794	0.0031	0.0335	0.179	0.114	1.13	2.48E-03	0.196	0.487	8.13E-07	0.151	1.05	0.057	1.50E-09	0.016
OP7-1				102.9	3.68	0.641	0.0025	0.0267	0.0738	0.176	0.299	2.96E-03	0.222	0.125	4.51E-07	0.151	0.249	0.050	1.06E-09	0.028
OP7-2				103.6	4.93	0.615	0.0031	0.0272	0.0411	0.245	0.158	9.12E-04	0.240	0.090	2.09E-08	0.014	0.000	0.090	2.08E-08	0.014
OP7-3				104.8	7.34	0.809	0.0048	0.0163	0.0186	0.390	1.18	1.63E-02	0.317	0.507	5.18E-06	0.300	1.12	0.068	7.28E-10	0.120
OP7-4				106.2	9.72	0.780	0.0052	0.0142	0.0106	0.544	1.02	3.32E-03	0.253	0.449	8.70E-07	0.091	0.776	0.127	5.89E-08	0.007
OPL7-0	50			104.2	6.09					0.327	0.856	1.88E-03	1.160	0.379	3.96E-07	0.749	0.741	0.251	4.77E-10	0.054
OPH7-0	150			105.2	7.89					0.409	1.03	5.76E-03	0.190	0.444	1.76E-06	0.121	0.937	0.067	5.54E-09	0.032
ON7-0	100	n-Butane	5 uL	102.3	2.37	0.855	0.0086	0.0809	0.179	0.113	1.37	1.33E-03	0.674	0.598	3.76E-07	0.478	1.25	0.150	4.99E-10	0.027
ON7-1				102.9	3.56	0.644	0.0111	0.122	0.0789	0.173	0.287	9.68E-05	0.221	0.571	3.03E-10	2.390				
ON7-3				105.1	8.77	1.01	0.0124	0.0250	0.0162	0.599	2.21	1.02E-02	0.472	0.961	3.07E-06	0.408	2.10	0.125	1.42E-09	0.056
ON7-4				106.6	10.3	1.04	0.0166	0.0241	0.0094	0.382	2.40	1.23E-03	0.280	1.09	2.25E-07	0.009				
ONL7-0	50			104.2	6.79					0.420	1.56	1.41E-03	2.210	0.703	2.84E-07	1.360	1.32	0.355	1.14E-09	0.088
ONH7-0	150			105.2	7.89					0.244	1.01	3.45E-03	0.316	0.439	9.38E-07	0.163	0.921	0.223	3.15E-10	0.111
OI7-0	100	i-Butane	5 uL	102.3	2.48	0.681	0.0026	0.0362	0.163	0.118	1.56	7.40E-04	0.096	0.234	1.47E-07	0.013	0.294	0.115	2.72E-08	0.028
OI7-1				102.9	3.72	0.605	0.0039	0.0466	0.0722	0.181	0.095	1.23E-03	0.195	0.053	1.26E-08	0.011	0.0260	0.058	2.69E-09	0.003
OI7-2				103.6	4.93	0.582	0.0023	0.0225	0.0411	0.251	0.000	6.44E-04	0.086	0.565	3.49E-12	3.000				
OI7-3				105.2	7.95	0.814	0.0043	0.0128	0.0158	0.441	1.23	1.77E-02	0.155	0.530	6.52E-06	0.149	1.18	0.449	8.22E-12	0.038
OI7-4				106.7	10.5	0.738	0.0035	0.0099	0.0091	0.612	0.818	4.25E-03	0.126	0.356	1.16E-06	0.049	0.585	0.108	1.27E-07	0.019
OIL7-0	50			104.2	6.79					0.382	1.51	3.47E-04	0.195	0.653	1.00E-03	0.203	1.48	0.371	5.13E-13	0.195
OIH7-0	150			105.2	7.89					0.420	0.930	3.84E-03	0.143	0.404	1.14E-06	0.086	0.830	0.083	5.14E-09	0.042

TABLE : C21
Catalyst : HM, OLIG8
Reaction : Propene Oligomerisation for 13.8 h, 350 C, 53 atm
Coke Content : 0.5% high boiling point hydrocarbons, 10.6% graphitic coke
Column length : 32.4 cm Column Diameter : 0.46 cm
Particle Diameter : 0.0375 cm Bed Porosity : 0.393

		Tracer	Pulse	Pressure	Velocity						macro-model			Rz model			RxRy model			
Run ID	T C	gas	Size	kPa	cm/sec	mu	sigma	HETP/2V	1/V/V	Dz	Ky	Dy	error	Kc	Dc	error	Ky	Kc	Dc	error
OM8-0	50	Methane	5 uL	102.2	2.10	0.737	0.0044	0.0625	0.228	0.117	0.810	4.81E-04	0.133	0.360	1.09E-07	0.011				
OM8-1				102.3	2.44	0.692	0.0035	0.0483	0.168	0.128	0.571	5.57E-04	0.143	0.255	1.04E-07	0.009				
OM8-2				102.6	2.97	0.668	0.0038	0.0466	0.113	0.147	0.434	6.94E-04	0.191	0.195	1.01E-07	0.024				
OM8-3				102.9	3.67	0.627	0.0032	0.0364	0.0742	0.176	0.216	6.66E-04	0.194	0.110	3.06E-08	0.014				
OM8-4				103.4	4.55	0.652	0.0026	0.0220	0.0482	0.217	0.361	1.03E-03	0.133	0.164	1.26E-07	0.004				
OM8-5				104.1	5.94	0.712	0.0055	0.0298	0.0284	0.287	0.649	1.58E-03	0.193	0.287	3.28E-07	0.040				
OM8-6				104.9	7.48	0.710	0.0041	0.0178	0.0179	0.373	0.665	1.60E-03	0.101	0.297	3.21E-07	0.022				
OM8-7				106.0	9.34	0.770	0.0050	0.0146	0.0115	0.484	0.970	3.40E-03	0.175	0.425	9.19E-07	0.055				
OP8-0	100	Propane	5 uL	102.3	2.42	1.11	0.0508	0.276	0.171	0.116	2.47	2.77E-04	1.590	1.13	4.51E-08	0.530	1.72	0.515	2.61E-09	0.006
OP8-1				102.8	3.42	0.94	0.0512	0.273	0.0885	0.163	1.57	2.63E-04	1.660	0.750	3.65E-08	0.393	0.913	0.472	3.49E-09	0.017
OP8-2				103.5	4.86	0.95	0.0474	0.175	0.0423	0.241	1.64	3.46E-04	1.550	0.784	4.74E-08	0.302	0.349	0.487	4.58E-09	0.021
OP8-3				104.6	6.83	1.08	0.0694	0.141	0.0214	0.358	2.27	5.21E-04	1.550	1.07	7.36E-08	0.368	1.33	0.614	8.43E-09	0.014
OP8-4				106.0	9.34	1.18	0.120	0.150	0.0115	0.519	2.68	6.71E-04	1.610	1.26	8.88E-08	0.413	1.59	0.719	9.31E-09	0.019
OPL8-0	50			104.3	6.32					0.342	13.6	1.73E-04	1.590	6.62	5.82E-09	0.234	5.08	5.03	1.64E-09	0.004
OPH8-0	150			105.3	8.18					0.426	1.01	1.60E-03	0.452	0.452	3.40E-07	0.088	0.594	0.212	5.77E-08	0.007
ON8-0	100	n-Butane	5 uL	102.2	2.26	2.36	0.453	0.584	0.196	0.108	8.41	1.13E-04	1.940	3.96	7.27E-09	0.482	4.55	2.39	1.05E-09	0.008
ON8-1				102.8	3.42	1.94	0.314	0.395	0.0885	0.165	6.45	1.34E-04	1.630	3.10	9.13E-09	0.261	2.69	2.18	2.35E-09	0.009
ON8-2				103.7	5.23	2.09	0.418	0.296	0.0365	0.269	7.08	1.91E-04	1.560	3.41	1.19E-09	0.228	2.95	2.40	3.14E-09	0.011
ON8-3				104.6	6.83	2.14	0.458	0.237	0.0214	0.368	7.34	2.32E-04	1.460	3.56	1.35E-08	0.183	2.67	2.65	4.32E-09	0.006
ON8-4				106.1	9.52	2.35	0.593	0.183	0.0110	0.567	8.33	3.18E-04	1.430	4.03	1.70E-08	0.183	3.06	2.99	5.40E-09	0.005
ONL8-0	50			104.3	6.32					0.351	105	1.82E-04	1.520	50.1	1.01E-09	0.281	38.3	36.9	3.24E-10	0.073
ONH8-0	150			105.3	8.18					0.439	1.74	8.85E-04	1.230	0.806	1.50E-07	0.325	1.12	0.404	1.34E-08	0.007
OI8-0	100	i-Butane	5 uL	102.2	2.26	1.74	0.419	0.994	0.196	0.108	5.12	6.38E-05	1.950	2.55	4.05E-09	0.318	1.99	2.03	9.40E-10	0.004
OI8-1				102.9	3.56	1.51	0.453	0.904	0.0789	0.173	3.80	7.22E-05	2.050	2.03	3.92E-09	0.240	1.12	1.87	1.15E-09	0.003
OI8-2				103.7	5.23	1.43	0.472	0.714	0.0365	0.269	3.35	8.77E-05	2.060	1.89	4.05E-09	0.178	0.798	1.86	1.40E-09	0.003
OI8-3				104.6	6.83	1.66	0.796	0.685	0.0214	0.368	4.15	1.24E-04	2.350	2.25	6.04E-09	0.370	1.34	2.15	1.39E-09	0.007
OI8-4				106.2	9.72	1.60	0.571	0.372	0.0106	0.559	4.13	1.75E-04	2.248	2.24	8.50E-09	0.303	1.32	2.16	1.90E-09	0.008
OIL8-0	50			104.3	6.32					0.351	39.0	5.10E-05	0.316	21.9	3.06E-10	0.108	2.44	21.7	2.35E-10	0.094
OIH8-0	150			105.3	8.18					0.439	1.26	7.74E-04	1.150	0.596	1.19E-07	0.240	0.730	0.350	1.38E-08	0.018

TABLE : C22
Catalyst : HY, OLIG9
Reaction : Propene Oligomerisation for 3.0h, 200-300 C, 30 atm
Coke Content : 3.3% high boiling point hydrocarbons, 19.1% graphitic coke
Column length : 32.4 cm Column Diameter : 0.46 cm
Particle Diameter : 0.0375 cm Bed Porosity : 0.366

											Rx model			RxRy model			
Run ID	T C	Tracer gas	Pulse Size	Pressure kPa	Velocity cm/sec	mu	sigma	HETP/2V	1/V/V	Dz	Kc	Dc	error	Ky	Kc	Dc	error
ON9-0	50	Methane	5 uL	102.1	2.05	1.33	0.124	0.555	0.239	0.115	1.65	5.25E-09	0.551	1.49	1.03	3.62E-10	0.005
ON9-1				102.3	2.50	1.27	0.164	0.660	0.160	0.130	1.46	5.42E-09	0.646	1.28	1.03	3.12E-10	0.004
ON9-2				102.6	3.09	1.11	0.0834	0.355	0.105	0.152	1.15	6.83E-09	0.587	0.948	0.849	4.70E-10	0.010
ON9-3				103.0	3.91	1.13	0.133	0.431	0.0654	0.187	1.13	7.59E-09	0.714	0.945	0.930	3.53E-10	0.005
ON9-4				103.6	4.95	1.15	0.106	0.262	0.0407	0.236	1.19	1.19E-08	0.730	1.07	0.904	4.88E-10	0.008
ON9-5				104.2	6.23	1.26	0.116	0.190	0.0258	0.303	1.43	2.14E-08	0.969	1.48	0.927	5.72E-10	0.010
ON9-6				105.4	8.30	1.32	0.0911	0.102	0.0145	0.422	1.62	3.50E-08	0.900	1.75	0.903	9.96E-10	0.018
ON9-7				105.9	9.16	1.32	0.123	0.125	0.0119	0.473	1.58	3.84E-08	1.020	1.76	0.938	7.69E-10	0.011
OP9-0	100	Propane	5 uL	102.3	2.48	3.72	1.07	0.637	0.259	0.119	7.07	7.32E-09	1.580	9.16	3.01	6.25E-11	0.013
OP9-1				102.9	3.56	3.08	0.713	0.429	0.124	0.170	5.61	1.35E-08	1.430	7.29	2.29	1.25E-10	0.015
OP9-2				103.6	4.08	2.55	0.674	0.411	0.0600	0.198	4.31	1.55E-08	1.210	6.40	1.90	1.94E-10	0.029
OP9-3				105.1	7.86	3.54	1.17	0.236	0.0243	0.423	6.64	2.81E-08	1.020	8.60	2.37	4.00E-10	0.035
OP9-4				106.9	10.9	3.65	1.00	0.135	0.0122	0.624	7.06	2.81E-08	0.743	8.79	2.41	1.07E-09	0.041
OPL9-0	50			104.2	6.09					0.327	41.3	3.45E-09	0.925	50.6	14.9	9.90E-11	0.030
OPH9-0	150			105.2	7.89					0.409	2.14	9.39E-08	0.827	2.87	0.704	8.89E-10	0.010
ON9-0	100	n-Butane	5 uL	102.3	2.37	13.7	3.33	0.474	0.284	0.113	30.8	2.10E-09	1.370	39.8	10.8	3.14E-11	0.026
ON9-1				102.9	3.56	11.6	9.77	0.414	0.124	0.173	25.6	3.90E-09	1.230	33.2	8.83	5.66E-11	0.013
ON9-2				103.7	5.24	12.0	10.0	0.267	0.0564	0.269	26.6	5.59E-09	0.957	33.9	8.83	1.26E-10	0.021
ON9-3				104.7	7.16	13.0	9.22	0.152	0.0296	0.390	29.5	7.33E-09	0.723	36.6	9.53	2.57E-10	0.022
ON9-4				106.7	10.5	13.3	8.88	0.0936	0.0133	0.612	30.7	9.89E-09	0.446	35.4	10.8	6.86E-10	0.022
ONL9-0	50			104.2	6.09					0.336	344	9.05E-10	0.238	315	157	2.26E-10	0.127
ONH9-0	150			105.2	7.89					0.420	5.76	4.89E-08	0.689	7.55	1.65	1.05E-09	0.026
OI9-0	100	i-Butane	5 uL	102.4	2.26	7.33	1.79	0.302	0.314	0.108	16.7	3.77E-09	0.062	11.2	10.1	1.48E-09	0.010
OI9-1				102.9	3.62	6.33	1.80	0.252	0.120	0.176	14.4	3.86E-09	0.006	2.54	12.9	3.14E-09	0.004
OI9-2				104.0	5.70	6.78	2.50	0.192	0.0474	0.297	15.6	3.90E-09	0.002	0.070	15.6	3.87E-09	0.002
OI9-3				104.9	7.50	7.05	2.54	0.136	0.0268	0.412	16.6	4.04E-09	0.013				
OI9-4				107.0	11.0	7.61	3.66	0.112	0.0120	0.647	18.1	4.08E-09	0.016				
OIL9-0	50			104.2	6.09					0.336	152	9.06E-10	0.011	108	88.5	3.05E-10	0.042
OIH9-0	150			105.2	7.89					0.420	4.02	1.70E-08	0.037	1.45	3.20	1.01E-08	0.014

TABLE : C23
Catalyst : HY, OLIG10
Reaction : Propene Oligomerisation for 5.8 h, 250 C, 30 atm
Coke Content : 3.5% high boiling point hydrocarbons, 12.2% graphitic coke
Column length : 32.4 cm Column Diameter : 0.46 cm
Particle Diameter : 0.0375 cm Bed Porosity : 0.342

Run ID	T C	Tracer gas	Pulse Size	Pressure kPa	Velocity cm/sec	mu	sigma	HETP/2V	1/V/V	Rx model Dz	Kc	Dc	error	RxRy model Ky	Kc	Dc	error
OM10-0	50	Methane	5 uL	102.1	2.05	1.91	0.0450	0.0977	0.239	0.115	3.17	3.19E-08	0.049				
OM10-1				102.4	2.55	1.89	0.0490	0.0872	0.154	0.132	3.12	3.41E-08	0.053				
OM10-2				102.6	2.97	1.71	0.0390	0.0728	0.113	0.147	2.69	3.62E-08	0.040				
OM10-3				103.1	4.03	1.74	0.0640	0.0849	0.0615	0.192	2.73	3.54E-08	0.054				
OM10-4				103.6	4.95	1.89	0.0650	0.0595	0.0407	0.236	3.13	4.06E-08	0.039				
OM10-5				104.2	6.09	1.95	0.0710	0.0497	0.0270	0.295	3.27	4.41E-08	0.034				
OM10-6				104.7	7.00	1.99	0.0860	0.0503	0.0204	0.346	3.36	4.71E-08	0.036				
OM10-7				105.9	9.16	2.07	0.102	0.0421	0.0119	0.473	3.56	4.72E-08	0.021				
OP10-0	100	Propane	5 uL	102.3	2.37	22.5	39.1	0.529	0.179	0.114	54.2	2.46E-10	0.021				
OP10-1				102.9	3.42	20.0	54.6	0.647	0.0855	0.163	47.5	2.52E-10	0.017				
OP10-2				103.6	5.07	20.2	49.5	0.387	0.0388	0.253	49.5	2.85E-10	0.023				
OP10-3				104.7	6.99	21.8	75.6	0.369	0.0205	0.368	53.0	3.00E-10	0.011				
OP10-4				106.5	10.2	22.2	86.1	0.277	0.0081	0.576	55.0	3.36E-10	0.014				
OPL10-0	50			104.4	6.62					0.361	381	3.23E-11	0.087				
OPH10-0	150			105.5	8.57					0.451	12.5	2.67E-09	0.012				
ON10-0	100	n-Butane	5 uL	102.4	2.59	119	638	0.282	0.149	0.123	304	6.36E-11	0.327				
ON10-1				103.0	3.82	104	910	0.357	0.0685	0.187	266	5.09E-11	0.121				
ON10-2				103.8	5.39	107	1113	0.292	0.0435	0.278	275	5.65E-11	0.115				
ON10-3				105.0	7.68	115	1560	0.249	0.0169	0.423	297	5.91E-11	0.092				
ON10-4				107.1	11.1	122	2331	0.229	0.0081	0.654	316	5.92E-11	0.053				
ONH10-0	150			105.5	8.57					0.464	49.0	4.85E-10	0.033				
OI10-0	100	i-Butane	5 uL	102.3	2.48	62.3	1684	2.84	0.163	0.118	161	5.85E-12	0.460	44.7	178	1.48E-12	0.156
OI10-1				102.9	3.68	43.0	856	2.04	0.0738	0.179	107	1.72E-11	0.146	25.8	107	6.89E-12	0.022
OI10-2				103.9	5.54	41.1	871	1.51	0.0326	0.287	102	2.52E-11	0.148	24.2	103	9.71E-12	0.017
OI10-3				104.8	7.34	40.9	915	1.21	0.0185	0.401	100	3.20E-11	0.157	24.3	103	1.16E-11	0.016
OI10-4				106.9	10.9	38.3	730	0.740	0.0084	0.640	94.7	5.51E-11	0.133	21.9	94.7	2.24E-11	0.016
OIH10-0	150			105.5	8.57					0.464	24.7	1.97E-10	0.169	6.81	24.2	7.08E-11	0.016

TABLE : C24
Catalyst : HY, OLIG11
Reaction : Propene Oligomerisation for 13.0 h, 250 C, 64 atm
Coke Content : 5.3% high boiling point hydrocarbons, 18.8% graphitic coke
Column length : 32.4 cm Column Diameter : 0.46 cm
Particle Diameter : 0.0375 cm Bed Porosity : 0.364

Run ID	T C	Tracer gas	Pulse Size	Pressure kPa	Velocity cm/sec	mu	sigma	HETP/2V	1/V/V	Rx model Dz	Rx model Kc	Rx model Dc	Rx model error	RxRy model Ry	RxRy model Kc	RxRy model Dc	RxRy model error
OH11-0	50	Methane	5 uL	102.2	2.25	1.04	0.0300	0.200	0.198	0.121	1.02	1.86E-08	0.257	1.04	0.483	1.50E-09	0.006
OH11-1				102.5	2.81	1.04	0.0240	0.128	0.127	0.141	1.04	2.43E-08	0.232	1.03	0.493	2.45E-09	0.004
OH11-2				102.8	3.37	1.02	0.0240	0.111	0.0881	0.163	0.981	2.73E-08	0.295	0.985	0.472	2.26E-09	0.044
OH11-3				103.2	4.22	1.18	0.0340	0.0937	0.0561	0.201	1.37	4.68E-08	0.402	1.61	0.517	1.97E-09	0.005
OH11-4				104.1	5.94	1.31	0.0410	0.0652	0.0284	0.287	1.67	6.97E-08	0.478	2.11	0.573	1.53E-07	0.020
OH11-5				104.4	6.53	1.29	0.0450	0.0671	0.0235	0.319	1.61	7.64E-08	0.584	2.00	0.560	2.08E-09	0.007
OH11-6				105.0	7.56	1.20	0.0340	0.0506	0.0175	0.378	1.42	8.02E-08	0.406	1.64	0.544	4.01E-09	0.006
OH11-7				105.8	8.99	1.23	0.0430	0.0607	0.0124	0.463	1.23	7.00E-08	0.378	1.32	0.556	4.34E-09	0.003
OP11-0	100	Propane	5 uL	102.3	2.48	3.44	1.07	0.591	0.163	0.119	6.48	4.00E-09	1.260	7.36	3.32	9.54E-11	0.016
OP11-1				103.0	3.82	2.86	0.720	0.373	0.0685	0.184	5.13	7.82E-09	1.120	5.81	2.57	2.07E-10	0.017
OP11-2				104.0	5.86	3.19	1.13	0.307	0.0292	0.299	5.80	1.17E-08	1.030	6.71	2.83	2.66E-10	0.040
OP11-3				105.3	8.22	3.48	1.81	0.294	0.0158	0.446	6.33	1.46E-08	1.000	7.22	3.07	3.97E-10	0.059
OP11-4				106.7	10.5	3.39	1.51	0.203	0.0087	0.597	6.24	1.82E-08	0.768	6.90	2.97	6.99E-10	0.092
OPL11-0	50			104.5	6.77					0.371	40.0	2.16E-08	0.405	38.2	19.5	2.57E-10	0.052
OPH11-0	150			105.7	8.78					0.463	2.64	7.58E-08	1.060	3.54	1.00	5.36E-10	0.007
ON11-0	100	n-Butane	5 uL	102.4	2.53	12.5	16.5	0.677	0.157	0.120	27.4	1.11E-09	1.370	31.6	13.5	2.54E-11	0.021
ON11-1				103.2	4.22	10.8	13.1	0.431	0.0561	0.209	23.3	2.35E-09	1.020	26.5	10.7	7.72E-11	0.047
ON11-2				104.0	5.86	11.4	14.6	0.311	0.0292	0.307	24.8	3.17E-09	0.830	27.7	11.1	1.37E-10	0.056
ON11-3				105.2	7.95	12.3	15.2	0.205	0.0158	0.441	27.5	3.94E-09	0.599	29.0	12.5	2.79E-10	0.065
ON11-4				106.8	10.7	11.7	12.1	0.134	0.0087	0.626	26.7	5.14E-09	0.296	23.7	13.?	8.31E-10	0.059
ONH11-0	150			105.7	8.78					0.477	6.30	3.61E-08	0.784	7.96	2.09	8.82E-10	0.033
OI11-0	100	1-Butane	5 uL	102.3	2.37	6.65	13.7	2.12	0.179	0.113	14.8	2.38E-10	0.044	5.74	12.7	8.62E-11	0.030
OI11-1				102.9	3.68	5.64	7.42	1.03	0.0738	0.179	13.2	2.92E-10	0.039	2.17	12.4	1.95E-10	0.020
OI11-2				104.1	6.01	6.81	15.5	0.901	0.0277	0.316	15.8	3.30E-10	0.088	3.93	14.7	1.59E-10	0.016
OI11-3				105.0	7.68	6.39	14.6	0.754	0.0169	0.423	14.8	3.74E-10	0.154	3.60	14.1	1.70E-10	0.033
OI11-4				106.6	10.3	6.21	21.1	0.861	0.0094	0.599	13.4	4.30E-10	0.323	4.47	13.9	1.03E-10	0.025
OIH11-0	150			105.7	8.78					0.477	4.25	9.40E-09	0.116	2.27	3.07	3.30E-09	0.007

TABLE : C25
Catalyst : HY, OLIG12
Reaction : Propene Oligomerisation for 5.7 h, 100 C, 50 atm
Coke Content : 6.7% high boiling point hydrocarbons, 7.0% graphitic coke
Column length : 32.4 cm Column Diameter : 0.46 cm
Particle Diameter : 0.0375 cm Bed Porosity : 0.411

Run ID	T C	Tracer gas	Pulse Size	Pressure kPa	Velocity cm/sec	mu	sigma	HETP/2V	1/V/V	Dz	Rx model Kc	Dc	error
OM12-0	50	Methane	5 uL	102.3	2.35	1.85	0.0116	0.0234	0.182	0.125	3.29	1.84E-06	0.001
OM12-1				102.4	2.65	1.76	0.0104	0.0205	0.143	0.135	3.05	2.29E-06	0.001
OM12-2				102.7	3.31	1.68	0.0088	0.0153	0.0913	0.161	2.84	3.58E-06	0.000
OM12-3				103.2	4.16	1.87	0.0107	0.0119	0.0577	0.198	3.34	3.38E-06	0.000
OM12-4				103.5	4.81	1.94	0.0121	0.0108	0.0432	0.229	3.55	3.00E-06	0.001
OM12-5				104.2	6.09	2.07	0.0134	0.0083	0.0270	0.295	3.90	4.51E-06	0.000
OM12-6				104.9	7.48	2.09	0.0151	0.0075	0.0179	0.373	3.95	2.53E-06	0.001
OM12-7				105.9	9.17	2.00	0.0155	0.0069	0.0119	0.473	3.71	1.72E-06	0.002
OP12-0	100	Propane	5 uL	102.3	2.48	13.0	0.608	0.0235	0.163	0.119	33.8	9.89E-08	0.000
OP12-1				103.0	3.82	13.5	0.676	0.0157	0.0685	0.184	35.0	1.03E-07	0.008
OP12-2				103.6	5.07	13.5	0.784	0.0137	0.0388	0.253	35.0	8.71E-08	0.013
OP12-3				104.9	7.42	15.6	1.20	0.0108	0.0182	0.395	40.9	8.36E-08	0.019
OP12-4				106.7	10.5	15.2	1.41	0.0094	0.0091	0.597	39.9	7.14E-08	0.051
OPL12-0	50			104.7	7.08					0.391	234	1.54E-08	0.013
OM12-0	100	n-Butane	5 uL	102.4	2.59	65.4	14.6	0.0214	0.149	0.123	176	2.12E-08	0.011
OM12-1				102.9	3.56	66.0	17.2	0.0180	0.0789	0.173	178	1.69E-08	0.006
OM12-2				103.7	5.24	72.1	25.9	0.0154	0.0365	0.269	196	1.33E-08	0.054
OM12-3				104.7	6.99	74.8	28.9	0.0120	0.0186	0.379	203	1.45E-08	0.044
OM12-4				106.5	10.1	80.3	40.2	0.0100	0.0089	0.586	218	1.28E-08	0.075
OML12-0	50			104.7	7.08					0.402	1672	6.03E-05	23.100
OI12-0	100	i-Butane	5 uL	102.3	2.48	57.2	11.7	0.0234	0.163	0.118	154	2.11E-08	0.003
OI12-1				103.2	4.22	59.8	14.4	0.0155	0.0561	0.209	161	2.08E-08	0.027
OI12-2				103.7	5.24	58.7	16.3	0.0146	0.0365	0.269	159	1.66E-08	0.021
OI12-3				104.5	7.34	65.7	23.0	0.0118	0.0186	0.401	178	1.61E-08	0.044
OI12-4				106.8	10.6	65.8	28.4	0.0100	0.0089	0.619	179	1.45E-08	0.103
OIL12-0	50			104.7	7.00					0.397	1281	1.97E-09	0.040

TABLE : C26
Catalyst : HH, OLIG13
Reaction : Propene Oligomerisation for 13.4 h, 300 C, 64 atm
Coke Content : 1.9% high boiling point hydrocarbons, 8.8% graphitic coke
Column length : 32.4 cm Column Diameter : 0.46 cm
Particle Diameter : 0.0375 cm Bed Porosity : 0.407

		Tracer	Pulse	Pressure	Velocity					macro-model				Rx model			RxKy model			
Run ID	T C	gas	Size	kPa	cm/sec	mu	sigma	HETP/2Y	1/Y/Y	Dz	Ky	Dy	error	Kc	Dc	error	Ky	Kc	Dc	error
OH13-0	50	Methane	5 uL	102.2	2.25	0.635	0.0022	0.0386	0.198	0.121	0.243	4.77E-04	0.040	0.112	7.71E-08	0.030				
OH13-1				102.4	2.61	0.637	0.0025	0.0386	0.147	0.134	0.243	5.79E-04	0.051	0.112	4.47E-08	0.027				
OH13-2				102.6	3.09	0.619	0.0024	0.0328	0.105	0.152	0.141	6.67E-04	0.064	0.074	1.71E-08	0.048				
OH13-3				103.0	3.91	0.645	0.0018	0.0183	0.0650	0.187	0.300	1.26E-03	0.033	0.131	1.64E-07	0.005				
OH13-4				103.4	4.67	0.648	0.0019	0.0159	0.0458	0.222	0.314	1.52E-03	0.043	0.137	2.06E-07	0.002				
OH13-5				103.8	5.50	0.669	0.0025	0.0162	0.0331	0.264	0.417	1.74E-03	0.061	0.183	3.01E-07	0.012				
OH13-6				105.1	7.80	0.741	0.0028	0.0107	0.0164	0.392	0.825	3.19E-03	0.025	0.359	9.13E-07	0.023				
OH13-7				105.9	9.16	0.729	0.0027	0.0089	0.0119	0.473	0.756	2.71E-03	0.020	0.332	6.88E-07	0.024				
OP13-0	100	Propane	5 uL	102.4	2.64	0.757	0.0058	0.0623	0.144	0.126	0.837	8.34E-04	0.584	0.369	1.88E-07	0.286	0.699	0.126	1.69E-09	0.011
OP13-1				103.0	3.82	0.713	0.0051	0.0428	0.0738	0.184	0.599	1.09E-03	0.561	0.266	1.99E-07	0.241	0.465	0.111	3.42E-09	0.009
OP13-2				103.8	5.39	0.777	0.0071	0.0353	0.0345	0.271	0.930	1.50E-03	0.660	0.412	3.38E-07	0.308	0.756	0.138	5.31E-09	0.009
OP13-3				105.1	7.86	0.845	0.0080	0.0232	0.0162	0.423	1.30	1.97E-03	0.616	0.578	4.66E-07	0.247	1.13	0.194	2.48E-09	0.114
OP13-4				106.2	9.72	0.813	0.0078	0.0198	0.0106	0.544	1.31	2.23E-03	0.631	0.502	4.96E-07	0.246	0.934	0.207	3.58E-09	0.080
OPL13-0	50			104.4	6.53					0.355	1.61	2.99E-04	3.050	0.825	2.87E-08	0.862	0.900	0.783	1.44E-09	0.017
OPH13-0	150			105.5	8.46					0.444	1.08	3.72E-03	0.153	0.470	1.07E-06	0.059	0.973	0.133	1.70E-09	0.106
ON13-0	100	n-Butane	5 uL	102.4	2.59	0.894	0.0484	0.379	0.149	0.123	1.25	2.62E-04	2.320	0.593	3.78E-08	0.897	0.893	0.442	6.60E-10	0.005
ON13-1				102.9	3.68	0.817	0.0574	0.378	0.0738	0.179	0.788	2.68E-04	2.380	0.411	2.36E-08	0.652	0.446	0.406	1.12E-09	0.012
ON13-2				103.9	5.54	0.867	0.0410	0.160	0.0326	0.287	1.14	5.44E-04	2.180	0.546	7.52E-08	0.821	0.813	0.442	1.16E-09	0.009
ON13-3				105.6	8.59	0.895	0.0389	0.0916	0.0136	0.470	1.31	7.20E-04	1.990	0.627	9.89E-08	0.657	0.873	0.445	3.26E-09	0.015
ON13-4				106.5	10.1	1.10	0.277	0.433	0.0098	0.586	1.38	7.15E-04	2.190	0.672	8.92E-08	0.779	0.928	0.585	1.94E-09	0.064
ONL13-0	50			104.4	6.53					0.365	4.47	7.52E-05	3.210	2.690	2.19E-09	0.695	1.31	3.80	2.46E-10	0.009
ONH13-0	150			105.5	8.46					0.457	1.03	2.32E-03	0.423	0.454	5.50E-07	0.161	0.871	0.179	2.60E-09	0.090
OI13-0	100	i-Butane	5 uL	102.3	2.48	0.737	0.0072	0.0866	0.163	0.118	0.701	7.80E-04	0.732	0.310	1.57E-07	0.395	0.584	0.140	8.16E-10	0.016
OI13-1				102.9	3.68	0.668	0.0093	0.0914	0.0738	0.179	0.300	7.30E-04	0.774	0.146	4.81E-07	0.235	0.188	0.143	1.15E-09	0.006
OI13-2				104.0	5.86	0.761	0.0111	0.0530	0.0292	0.307	0.802	1.41E-03	0.718	0.358	2.82E-07	0.349	0.651	0.163	2.47E-09	0.007
OI13-3				105.3	8.13	0.819	0.0132	0.0392	0.0151	0.453	1.12	1.93E-03	0.575	0.499	4.43E-07	0.245	0.902	0.166	8.75E-09	0.013
OI13-4				106.6	10.3	0.792	0.0133	0.0333	0.0094	0.599	0.962	1.41E-03	0.682	0.442	2.45E-07	0.165	0.596	0.225	2.57E-08	0.022
OIL13-0	50			104.4	6.53					0.365	1.43	1.16E-03	2.330	0.648	2.16E-07	1.440	1.21	0.722	1.87E-10	0.032
OIH13-0	150			105.5	8.46					0.457	0.975	3.49E-03	0.284	0.425	9.44E-07	0.151	0.886	0.216	4.01E-10	0.060

TABLE : C27
Catalyst : HM, OLIG14
Reaction : Propene Oligomerisation for 7.0 h, 300 C, 64 atm
Coke Content : 1.8% high boiling point hydrocarbons, 8.2% graphitic coke
Column length : 32.4 cm Column Diameter : 0.46 cm
Particle Diameter : 0.0375 cm Bed Porosity : 0.404

		Tracer	Pulse	Pressure	Velocity						macro-model				Rx model			RxRy model			
Run ID	T C	gas	Size	kPa	cm/sec	mu	sigma	HETP/2Y	1/Y/Y	Dx	Ky	Dy	error	Kc	Dc	error	Ky	Kc	Dc	error
OM14-0	50	Methane	5 uL	102.2	2.25	0.678	0.0035	0.0543	0.198	0.121	0.467	5.61E-04	0.089	0.207	9.58E-08	0.012				
OM14-1				102.4	2.65	0.626	0.0018	0.0297	0.143	0.135	0.200	7.05E-04	0.057	0.091	4.63E-08	0.008				
OM14-2				102.7	3.31	0.607	0.0019	0.0259	0.0913	0.161	0.090	8.78E-04	0.078	0.054	7.03E-08	0.034				
OM14-3				103.2	4.16	0.619	0.0019	0.0191	0.0577	0.198	0.152	1.52E-03	0.090	0.068	7.03E-08	0.003				
OM14-4				103.6	4.95	0.630	0.0020	0.0162	0.0407	0.236	0.218	1.79E-03	0.069	0.095	1.57E-07	0.003				
OM14-5				104.2	6.23	0.650	0.0024	0.0150	0.0258	0.303	0.317	2.02E-03	0.097	0.139	2.62E-07	0.013				
OM14-6				105.2	7.97	0.695	0.0025	0.0107	0.0157	0.402	0.568	2.99E-03	0.097	0.247	6.78E-07	0.018				
OM14-7				105.9	9.16	0.705	0.0034	0.0121	0.0119	0.473	0.603	4.94E-03	0.105	0.260	1.27E-06	0.047				
OP14-0	100	Propane	5 uL	102.4	2.59	0.710	0.0049	0.0614	0.149	0.124	0.592	9.51E-04	0.570	0.260	1.85E-07	0.311	0.493	0.110	9.70E-10	0.025
OP14-1				102.9	3.56	0.649	0.0063	0.0683	0.0789	0.170	0.244	1.11E-03	0.572	0.112	7.37E-08	0.223	0.163	0.0990	1.10E-09	0.029
OP14-2				103.9	5.54	0.721	0.0109	0.0614	0.0292	0.279	0.596	2.34E-03	0.725	0.260	4.66E-07	0.482	0.516	0.195	3.19E-10	0.060
OP14-3				104.5	6.66	0.688	0.0044	0.0227	0.0186	0.347	0.476	1.88E-03	0.670	0.212	2.73E-07	0.298	0.367	0.120	2.54E-09	0.064
OP14-4				106.1	9.52	0.818	0.0170	0.0432	0.0102	0.531	1.10	2.53E-03	0.581	0.487	6.01E-07	0.293	0.947	0.207	1.96E-09	0.026
OPL14-0	50			104.2	6.23					0.336	0.524	2.69E-04	2.990	0.395	6.57E-09	0.298	0.163	0.560	8.98E-10	0.027
OPH14-0	150			105.3	8.08					0.420	0.259	2.24E-03	0.246	0.117	1.85E-07	0.044	0.127	0.0730	3.22E-08	0.015
ON14-0	100	n-Butane	5 uL	102.4	2.70	0.773	0.0217	0.218	0.137	0.128	0.747	3.92E-04	1.960	0.353	5.25E-08	0.845	0.554	0.315	4.41E-10	0.041
ON14-1				102.9	3.68	0.719	0.0194	0.165	0.0738	0.179	0.465	4.58E-04	1.910	0.239	3.32E-08	0.620	0.293	0.294	5.72E-10	0.049
ON14-2				104.0	5.86	0.740	0.0216	0.109	0.0292	0.307	0.579	6.32E-04	1.650	0.291	5.76E-08	0.470	0.361	0.275	1.74E-09	0.009
ON14-3				104.8	7.34	0.786	0.0487	0.174	0.0185	0.401	0.695	7.91E-04	1.790	0.341	8.61E-08	0.629	0.473	0.343	1.29E-09	0.006
OB14-4				106.3	9.91	0.803	0.0318	0.0806	0.0102	0.572	0.869	1.30E-03	1.620	0.407	1.89E-07	0.665	0.661	0.361	1.25E-09	0.025
ONL14-0	50			104.2	6.23					0.345	1.47	1.00E-03	4.540	1.11	2.45E-09	0.847	0.421	2.43	1.36E-10	0.037
ONH14-0	150			105.3	8.08					0.432	0.451	2.70E-03	0.433	0.198	4.29E-07	0.201	0.359	0.0980	3.06E-09	0.035
OI14-0	100	i-Butane	5 uL	102.4	2.70	0.716	0.0042	0.0492	0.137	0.128	0.631	3.36E-03	0.396	0.269	8.84E-07	0.348	0.580	0.0920	1.91E-10	0.106
OI14-1				103.2	4.22	0.653	0.0035	0.0311	0.0561	0.209	0.301	3.50E-03	0.437	0.127	4.42E-07	0.338	0.249	0.0750	5.52E-10	0.118
OI14-2				104.0	5.86	0.681	0.0036	0.0212	0.0290	0.307	0.448	4.54E-03	0.476	0.191	8.22E-07	0.368	0.388	0.0680	1.41E-09	0.141
OI14-3				105.0	7.68	0.697	0.0041	0.0176	0.0169	0.423	0.533	2.86E-03	0.492	0.233	5.26E-07	0.264	0.432	0.0860	5.35E-09	0.059
OI14-4				106.7	10.5	0.789	0.0053	0.0132	0.0091	0.612	1.07	2.26E-03	0.112	0.473	5.49E-07	0.045				
OIL14-0	50			104.2	6.23					0.345	0.500	2.23E-03	0.565	0.219	3.84E-07	0.319	0.415	0.124	1.10E-09	0.035
OIH14-0	150			105.3	8.08					0.432	0.303	2.67E-03	0.205	0.133	3.12E-07	0.052	0.185	0.0650	2.64E-08	0.026

TABLE : C28
Catalyst : HM, OLIG15
Reaction : Propene Oligomerisation for 6.0 h, 300 C, 30 atm
Coke Content : 8.1% graphitic coke
Column length : 32.4 cm Column Diameter : 0.46 cm
Particle Diameter : 0.0375 cm Bed Porosity : 0.409

		Tracer	Pulse	Pressure	Velocity					macro-model				Rx model			RxRy model			
Run ID	T C	gas	Size	kPa	cm/sec	mu	sigma	HETP/2V	1/V/V	Dx	Ky	Dy	error	Kc	Dc	error	Ky	Kc	Dc	error
OM15-0	50	Methane	5 uL	102.3	2.44	0.616	0.0062	0.108	0.168	0.128	0.0780	4.36E-04	0.137	0.0970	7.16E-10	0.113				
OM15-1				102.5	2.86	0.607	0.0019	0.0288	0.122	0.143	0.0750	6.51E-04	0.068	0.0610	2.33E-09	0.102				
OM15-3				103.2	4.16	0.633	0.0019	0.0187	0.0577	0.198	0.218	1.63E-03	0.080	0.0940	1.46E-07	0.006	0.0820	0.0620	5.02E-08	0.001
OM15-4				103.6	5.10	0.659	0.0089	0.0652	0.0385	0.243	0.291	1.89E-03	0.126	0.126	2.40E-07	0.576	0.224	0.0760	1.52E-09	0.048
OM15-5				104.3	6.39	0.645	0.0019	0.0116	0.0245	0.312	0.278	3.28E-03	0.129	0.118	4.30E-07	0.046	0.193	0.0450	2.07E-08	0.020
OM15-6				105.3	8.13	0.696	0.0045	0.0184	0.0151	0.411	0.521	3.67E-03	0.159	0.225	7.99E-07	0.070	0.404	0.0630	3.05E-08	0.016
OM15-7				106.0	9.42	0.692	0.0043	0.0155	0.0113	0.489	0.513	3.81E-03	0.087	0.221	8.43E-07	0.036	0.436	0.0810	2.88E-09	0.119
OP15-0	100	Propane	5 uL	102.5	2.82	0.751	0.0072	0.0732	0.126	0.134	0.775	8.88E-04	0.764	0.343	1.87E-07	0.404	0.143	0.132	1.45E-09	0.029
OP15-1				102.9	3.68	0.706	0.0061	0.0537	0.0738	0.176	0.537	8.76E-04	0.794	0.243	1.30E-07	0.318	0.402	0.130	2.22E-09	0.030
OP15-2				103.8	5.39	0.723	0.0067	0.0388	0.0345	0.271	0.626	9.26E-04	0.791	0.289	1.36E-07	0.217	0.411	0.156	7.98E-09	0.009
OP15-3				104.8	7.34	0.730	0.0116	0.0480	0.0186	0.390	0.625	9.65E-04	0.810	0.297	1.23E-07	0.174	0.369	0.186	1.06E-08	0.006
OP15-4				106.1	9.52	0.765	0.0125	0.0364	0.0098	0.531	0.821	1.01E-03	0.632	0.389	1.43E-07	0.064	0.339	0.267	4.02E-08	0.016
OPL15-0	50			104.5	6.69					0.366	3.17	2.88E-04	2.340	1.55	2.76E-08	0.575	1.64	1.11	3.24E-09	0.020
OPH15-0	150			105.6	8.67					0.456	0.543	2.11E-03	0.179	0.241	3.81E-07	0.037	0.228	0.147	1.36E-07	0.025
ON15-0	100	n-Butane	5 uL	102.5	2.82	1.06	0.0555	0.284	0.126	0.134	2.14	2.24E-04	2.530	1.01	3.19E-08	0.917	1.43	0.613	1.32E-09	0.041
ON15-1				103.1	3.95	1.02	0.112	0.441	0.0640	0.194	1.67	2.19E-04	2.770	0.830	2.44E-08	0.849	0.998	0.703	1.09E-09	0.013
ON15-2				103.8	5.39	1.06	0.108	0.289	0.0345	0.278	1.92	3.23E-04	2.600	0.935	3.86E-08	0.817	1.18	0.693	1.93E-09	0.011
ON15-3				105.0	7.68	1.02	0.112	0.227	0.0169	0.423	1.71	3.51E-04	2.330	0.869	3.51E-08	0.509	0.871	0.714	3.45E-09	0.004
ON15-4				106.5	10.1	1.12	0.122	0.156	0.0098	0.586	2.24	5.48E-04	2.090	1.09	6.36E-08	0.511	1.26	0.754	5.79E-09	0.003
ONL15-0	50			104.5	6.69					0.376	21.1	1.69E-04	2.270	10.3	3.77E-09	0.610	9.63	7.86	5.72E-10	0.032
ONH15-0	150			105.6	8.67					0.470	0.740	1.56E-03	0.528	0.336	2.75E-07	0.135	0.484	0.158	2.26E-08	0.005
OI15-0	100	i-Butane	5 uL	102.4	2.70	0.862	0.0349	0.282	0.137	0.128	1.15	4.28E-04	2.120	0.526	7.32E-08	1.050	0.901	0.347	5.42E-10	0.068
OI15-1				103.1	4.09	0.797	0.0239	0.149	0.0597	0.202	0.855	5.26E-04	1.940	0.404	7.28E-08	0.762	0.610	0.298	1.26E-09	0.055
OI15-2				104.0	5.86	0.860	0.0625	0.234	0.0292	0.307	1.04	6.20E-04	2.040	0.497	8.71E-08	0.761	0.737	0.374	1.63E-09	0.017
OI15-3				105.1	7.86	0.838	0.0553	0.162	0.0162	0.435	0.961	5.99E-04	1.720	0.477	6.75E-08	0.393	0.542	0.364	5.14E-09	0.011
OI15-4				106.7	10.5	0.943	0.0628	0.109	0.0097	0.612	1.52	9.23E-04	1.650	0.717	1.38E-07	0.519	1.00	0.433	6.61E-09	0.014
OIL15-0	50			104.5	6.69					0.376	7.38	1.63E-04	2.780	3.70	7.57E-09	0.821	3.50	3.22	7.63E-10	0.019
OIH15-0	150			105.6	8.67					0.470	0.529	2.32E-03	0.357	0.234	3.98E-07	0.113	0.375	0.0960	1.96E-08	0.016

TABLE : C29
Catalyst : HM, OLIG16
Reaction : Propene Oligomerisation, 300 C, 50 atm, regenerated in N2 at 350 C
Coke Content : 8.1% graphitic coke
Column length : 32.4 cm Column Diameter : 0.46 cm
Particle Diameter : 0.0375 cm Bed Porosity : 0.407

Run ID	T C	Tracer gas	Pulse Size	Pressure kPa	Velocity cm/sec	mu	sigma	HETP/2V	1/V/V	macro-model Dx	Dy	error	Rx model Kc	Dc	error	RxRy model Ky	Kc	Dc	error
OM16-0	50	Methane	5 uL	102.3	2.44	0.654	0.0039	0.0606	0.168	0.128	0.319	4.93E-04	0.117	0.147	4.95E-08	0.017			
OM16-1				102.5	2.81	0.659	0.0062	0.0821	0.127	0.141	0.321	5.29E-04	0.166	0.150	4.94E-08	0.040			
OM16-2				102.7	3.20	0.632	0.0022	0.0279	0.0977	0.156	0.216	6.37E-04	0.077	0.105	3.62E-08	0.030			
OM16-3				103.0	3.91	0.649	0.0031	0.0307	0.0654	0.187	0.298	8.56E-04	0.101	0.137	8.19E-08	0.016			
OM16-4				103.6	5.01	0.676	0.0030	0.0213	0.0398	0.239	0.451	1.29E-03	0.092	0.200	2.12E-07	0.010			
OM16-5				104.2	6.23	0.688	0.0030	0.0163	0.0258	0.303	0.520	1.48E-03	0.067	0.231	2.68E-07	0.013			
OM16-6				105.2	7.97	0.727	0.0064	0.0245	0.0157	0.402	0.691	1.80E-03	0.163	0.308	3.70E-07	0.018			
OM16-7				105.9	9.16	0.763	0.0076	0.0232	0.0119	0.473	0.901	2.08E-03	0.081	0.400	4.97E-07	0.082			
OP16-0	100	Propane	5 uL	102.3	2.48	1.040	0.156	0.943	0.163	0.119	1.67	1.16E-04	3.220	0.850	1.14E-08	0.984	0.962	0.843	4.47E-10	0.005
OP16-1				102.9	3.68	0.887	0.101	0.565	0.0738	0.176	0.970	1.48E-04	3.110	0.565	8.89E-09	0.582	0.426	0.688	6.98E-10	0.005
OP16-2				103.8	5.39	0.927	0.116	0.406	0.0345	0.271	1.13	2.35E-04	3.110	0.622	1.76E-08	0.753	0.578	0.734	8.87E-10	0.004
OP16-3				104.7	7.16	0.971	0.116	0.278	0.0195	0.379	1.40	3.67E-04	2.900	0.717	3.61E-08	0.827	0.815	0.712	1.41E-09	0.004
OP16-4				106.9	10.9	1.02	0.121	0.173	0.0084	0.624	1.71	5.08E-04	2.440	0.865	5.11E-08	0.583	0.942	0.744	3.28E-09	0.012
OPL16-0	50			104.3	6.32					0.342	6.74	8.35E-05	3.180	3.71	2.58E-09	0.937	2.33	4.48	2.81E-10	0.031
OPH16-0	150			105.3	8.18					0.426	0.751	8.59E-04	0.740	0.361	1.12E-07	0.111	0.343	0.244	2.45E-08	0.035
ON16-0	100	n-Butane	5 uL	102.4	2.70	2.48	1.69	1.65	0.137	0.128	7.97	3.72E-05	2.610	4.31	1.10E-09	0.615	2.60	4.55	1.83E-10	0.047
ON16-1				103.0	3.82	2.01	0.908	0.953	0.0685	0.187	6.06	5.42E-05	2.570	3.31	1.88E-09	0.555	1.85	3.47	3.61E-10	0.064
ON16-2				103.8	5.39	2.13	1.37	0.908	0.0345	0.278	6.14	7.43E-05	2.870	3.37	2.49E-09	0.692	2.06	3.83	3.39E-10	0.030
ON16-3				104.8	7.34	1.74	0.596	0.434	0.0186	0.401	4.95	1.06E-04	2.510	2.74	4.00E-09	0.473	1.41	2.84	8.99E-10	0.072
ON16-4				106.5	10.1	2.11	1.18	0.425	0.0098	0.586	6.13	1.69E-04	3.120	3.25	6.79E-09	0.894	2.48	3.59	6.36E-10	0.034
ONL16-0	50			104.3	6.32					0.352	75.9	5.99E-05	1.570	40.6	2.26E-10	0.408	16.6	40.8	7.38E-11	0.147
ONH16-0	150			105.3	8.18					0.439	1.25	3.89E-04	2.610	0.659	3.44E-08	0.625	0.668	0.663	1.96E-09	0.016
OI16-0	100	i-Butane	5 uL	102.4	2.70	0.896	0.0449	0.336	0.137	0.128	1.27	5.53E-04	2.630	0.576	1.03E-07	1.610	1.06	0.395	2.88E-10	0.271
OI16-1				103.0	3.82	0.804	0.0203	0.133	0.0685	0.187	0.918	6.39E-04	2.140	0.423	1.02E-07	1.070	0.704	0.281	9.77E-10	0.198
OI16-2				103.8	5.39	2.13	1.37	0.793	0.0263	0.278	3.53	1.37E-04	3.640	1.82	9.22E-09	1.280	1.75	1.97	4.95E-10	0.083
OI16-3				105.1	7.86	0.971	0.0700	0.153	0.0162	0.435	1.64	1.05E-03	1.780	0.748	1.88E-07	0.776	1.27	0.389	2.77E-09	0.022
OI16-4				106.7	10.5	1.05	0.0375	0.0525	0.0091	0.612	2.21	1.77E-03	1.670	0.994	3.37E-07	0.805	1.76	0.375	6.18E-09	0.070
OIL16-0	50			104.3	6.32					0.351	6.25	2.39E-04	4.380	2.99	1.73E-08	2.440	4.18	3.46	1.63E-10	0.189
OIH16-0	150			105.3	8.18					0.439	0.602	1.03E-03	0.345	0.285	1.36E-07	0.087	0.113	0.241	8.74E-08	0.084

TABLE : C30
Catalyst : HM, OLIG17
Reaction : Propene Oligomerisation, 300 C, 50 atm, regenerated in N2 at 350 C
Coke Content : 8.7% graphitic coke
Column length : 32.4 cm Column Diameter : 0.46 cm
Particle Diameter : 0.0375 cm Bed Porosity : 0.413

		Tracer	Pulse	Pressure	Velocity					macro-model				Rx model			RxRy model			
Run ID	T C	gas	Size	kPa	cm/sec	mu	sigma	HETP/2V	1/V/V	Dz	Ky	Dy	error	Kc	Dc	error	Ky	Kc	Dc	error
OM17-0	50	Methane	5 uL	102.3	2.44	0.696	0.0023	0.0319	0.168	0.128	0.562	9.94E-04	0.380	0.243	2.39E-07	0.0019				
OM17-1				102.6	2.97	0.705	0.0026	0.0280	0.113	0.147	0.606	1.18E-03	0.054	0.263	2.83E-07	0.0010				
OM17-2				102.9	3.67	0.743	0.0024	0.0189	0.0742	0.176	0.821	2.51E-03	0.043	0.354	7.82E-07	0.0137				
OM17-3				103.3	4.41	0.779	0.0028	0.0169	0.0514	0.210	1.02	3.36E-03	0.063	0.439	1.10E-06	0.0319				
OM17-4				103.6	4.95	0.805	0.0050	0.0252	0.0407	0.236	1.13	5.60E-03	0.082	0.488	1.96E-06	0.0613				
OM17-5				104.4	6.53	0.875	0.0035	0.0113	0.0235	0.319	1.54	1.45E-02	0.058	0.667	5.27E-06	0.0495				
OM17-6				104.9	7.48	0.825	0.0028	0.0089	0.0189	0.373	1.28	7.92E-03	0.019	0.554	2.85E-06	0.0146				
OM17-7				105.9	9.16	0.800	0.0026	0.0073	0.0119	0.473	1.13	6.30E-03	0.086	0.487	2.05E-06	0.0467				
OP17-0	100	Propane	5 uL	102.3	2.48	0.976	0.0102	0.0700	0.163	0.119	2.00	8.15E-04	0.871	0.883	1.94E-07	0.453	1.73	0.210	2.26E-09	0.031
OP17-1				103.1	3.95	0.872	0.0124	0.0669	0.0640	0.190	1.39	8.97E-04	1.020	0.621	1.96E-07	0.454	1.11	0.213	4.28E-09	0.013
OP17-2				103.8	5.39	0.955	0.0137	0.0452	0.0345	0.271	1.84	1.46E-03	1.030	0.817	3.32E-07	0.523	1.60	0.260	1.74E-09	0.055
OP17-3				105.4	8.40	1.04	0.0161	0.0287	0.0141	0.458	2.33	2.11E-03	0.967	1.03	4.55E-07	0.455	1.92	0.281	1.07E-08	0.014
OP17-4				106.5	10.1	0.995	0.0237	0.0384	0.0098	0.570	2.02	1.53E-03	0.832	0.914	2.98E-07	0.244	1.41	0.364	2.38E-08	0.010
OPL17-0	50			104.5	6.69					0.366	6.45	3.33E-04	2.530	3.05	2.54E-08	0.857	3.88	1.89	1.93E-09	0.031
OPH17-0	150			105.6	8.67					0.456	1.67	8.05E-03	0.144	0.724	2.58E-06	0.0959	1.60	0.783	1.10E-11	0.093
ON17-0	100	n-Butane	5 uL	102.4	2.70	1.66	0.193	0.421	0.137	0.128	5.09	1.95E-04	2.530	2.36	1.98E-08	0.951	3.40	1.26	1.09E-09	0.027
ON17-1				102.9	3.56	1.56	0.154	0.288	0.0789	0.173	4.62	2.34E-04	2.480	2.16	2.41E-08	0.871	2.96	1.22	1.57E-09	0.034
ON17-2				103.9	5.62	1.66	0.203	0.212	0.0317	0.292	5.10	3.47E-04	2.420	2.38	3.33E-08	0.826	3.22	1.36	2.29E-09	0.035
ON17-3				105.0	7.68	1.71	0.324	0.234	0.0169	0.423	5.09	4.07E-04	2.470	2.41	3.61E-08	0.807	3.13	1.50	2.52E-09	0.006
ON17-4				106.1	9.52	1.65	0.379	0.237	0.0110	0.546	4.71	4.48E-04	2.400	2.25	3.92E-08	0.716	2.75	1.49	3.17E-09	0.003
ONL17-0	50			104.5	6.69					0.376	38.4	1.70E-04	2.310	18.6	2.26E-09	0.685	18.0	14.0	3.19E-10	0.047
ONH17-0	150			105.6	8.67					0.470	2.30	3.61E-03	0.566	1.01	9.03E-07	0.309	2.00	0.189	1.43E-08	0.015
OI17-0	100	i-Butane	5 uL	102.4	2.70	1.20	0.0931	0.388	0.137	0.128	2.73	2.51E-04	3.040	1.27	3.55E-08	1.38	2.02	0.756	6.40E-10	0.054
OI17-1				103.1	4.09	1.15	0.0803	0.240	0.0597	0.202	2.49	3.67E-04	3.040	1.16	5.26E-08	1.36	1.82	0.715	9.95E-10	0.063
OI17-2				104.2	6.17	1.33	0.113	0.168	0.0263	0.326	3.34	7.19E-04	3.160	1.53	1.03E-07	1.68	2.63	0.813	1.19E-09	0.094
OI17-3				104.8	7.34	1.27	0.139	0.190	0.0186	0.401	2.96	6.55E-04	3.120	1.38	8.92E-08	1.47	2.23	0.869	1.23E-09	0.039
OI17-4				106.2	9.74	1.27	0.104	0.107	0.0105	0.561	3.12	6.86E-04	2.280	1.46	8.44E-08	0.775	2.05	0.853	4.41E-09	0.009
OIL17-0	50			104.5	6.69					0.376	12.7	1.18E-04	3.250	6.46	3.18E-09	1.18	5.80	6.92	2.14E-10	0.032
OIH17-0	150			105.6	8.67					0.470	1.73	3.39E-03	0.490	0.761	8.96E-07	0.260	1.59	0.267	6.75E-10	0.110

TABLE : C31
Catalyst : HY, OLIG18
Reaction : Propene Oligomerisation, 200 C, 50 atm, regenerated in N2 at 350 C
Coke Content : 4.3% high boiling point hyrocarbons, 16.9% graphitic coke
Column length : 32.4 cm Column Diameter : 0.46 cm
Particle Diameter : 0.0375 cm Bed Porosity : 0.387

		Tracer	Pulse	Pressure	Velocity					Rx model			RxRy model			
Run ID	T C	gas	Size	kPa	cm/sec	mu	sigma	HETP/2V	1/V/V	Ds	Kc	Dc	error	Ky	Kc	Dc	error
ON18-0	50	Methane	5 uL	102.2	2.25	1.34	0.0347	0.139	0.198	0.121	1.80	1.43E-08	0.002				
ON18-1				102.4	2.55	1.34	0.0369	0.131	0.154	0.132	1.80	1.41E-08	0.003				
ON18-2				102.6	2.87	1.29	0.0397	0.130	0.113	0.147	1.69	1.29E-08	0.003				
ON18-3				103.2	4.28	1.45	0.0553	0.0995	0.0545	0.204	2.07	1.65E-08	0.009				
ON18-4				103.5	4.88	1.48	0.0617	0.0934	0.0419	0.233	2.12	1.64E-08	0.008				
ON18-5				104.0	5.80	1.46	0.0635	0.0833	0.0298	0.280	2.08	1.72E-08	0.012				
ON18-6				104.9	7.48	1.61	0.107	0.0894	0.0179	0.373	2.42	1.84E-08	0.020				
ON18-7				105.7	8.82	1.57	0.119	0.0887	0.0129	0.452	2.32	1.80E-08	0.017				
OP18-0	100	Propane	5 uL	102.5	2.82	10.4	43.6	2.32	0.126	0.134	23.4	5.73E-11	0.459	11.2	25.4	1.16E-11	0.069
OP18-11				103.1	3.95	8.45	34.4	1.98	0.0640	0.190	18.6	1.15E-10	0.614	10.4	21.0	1.63E-11	0.046
OP18-2				103.8	5.39	7.85	23.8	1.16	0.0345	0.271	16.0	2.39E-10	0.775	10.9	17.7	2.45E-11	0.048
OP18-3				104.7	7.16	8.63	47.0	1.43	0.0195	0.378	15.4	2.96E-10	1.130	11.3	21.0	1.59E-11	0.014
OP18-4				106.3	9.91	7.96	28.3	0.756	0.0102	0.557	14.6	6.73E-10	1.190	12.8	17.5	3.10E-11	0.018
OPL18-0	50			104.2	6.23					0.336	54.3	2.05E-10	1.170	56.0	50.2	1.09E-11	0.053
OPH18-0	150			105.3	8.08					0.420	5.01	9.23E-10	0.709	3.21	6.03	8.84E-11	0.009
ON18-0	100	n-Butane	5 uL	102.5	2.77	35.1	272	1.29	0.131	0.132	87.1	2.50E-11	0.611	43.6	81.5	7.29E-12	0.347
ON18-1				103.1	4.09	31.7	306	1.21	0.0597	0.202	71.5	5.14E-11	0.699	50.2	70.6	6.88E-12	0.095
ON18-2				103.9	5.54	31.5	354	1.04	0.0326	0.287	66.9	8.31E-11	0.930	54.3	70.2	6.63E-12	0.053
ON18-3				104.7	7.16	27.2	255	0.780	0.0195	0.390	56.1	1.68E-10	1.000	51.3	55.2	1.15E-11	0.036
ON18-4				106.2	9.72	26.9	190	0.438	0.0106	0.559	56.6	3.10E-10	0.942	56.0	49.3	2.27E-11	0.042
ONL18-0	50			104.2	6.23					0.345	457	5.32E-11	0.512	439	386	9.84E-12	0.144
ONH18-0	150			105.3	8.08					0.432	13.8	3.08E-10	0.838	8.81	18.2	2.34E-11	0.009
OI18-0	100	i-Butane	5 uL	102.4	2.70	10.2	27.0	1.56	0.137	0.128	18.5	1.23E-09	1.640	29.3	11.6	1.62E-11	0.038
OI18-1				103.1	3.95	7.92	5.28	0.346	0.0640	0.194	16.1	2.90E-09	0.772	24.0	7.39	1.45E-10	0.019
OI18-2				104.4	6.49	9.29	11.4	0.330	0.0238	0.347	18.6	3.63E-09	0.683	26.9	8.94	2.12E-10	0.048
OI18-3				104.9	7.50	9.24	17.5	0.443	0.0178	0.412	17.9	3.76E-09	0.704	25.2	9.05	2.26E-10	0.081
OI18-4				106.4	10.0	9.53	13.4	0.239	0.0100	0.579	19.3	4.74E-09	0.467	25.0	9.92	5.04E-10	0.062
OIL18-0	50			104.2	6.23					0.345	134	6.76E-10	0.356	178	69.2	8.75E-11	0.017
OIH18-0	150			105.3	8.08					0.432	3.99	1.13E-08	1.390	6.00	2.88	1.64E-10	0.116

TABLE C1* : ADSORPTION AND DIFFUSION DATA FOR n-BUTANE IN HY USING D_z REDUCED BY A FACTOR OF 20 IN THE R_x MODEL.

Run ID	D_z	K_c	D_c x 10^9 cm^2/sec	error
ZN5-0	0.0061	422	1.17	0.024
ZN5-1	0.0093	411	1.70	0.234
ZN5-2	0.0149	422	2.85	0.030
ZN5-3	0.0220	382	3.84	0.178
ZNL5-0	0.0140	1227	0.982	0.040
ZNH5-0	0.0136	113	10.9	0.069
ZN10-0	0.0065	407	1.25	0.062
ZN10-1	0.0098	401	2.11	0.051
ZN10-2	0.0153	401	3.19	0.015
ZN10-3	0.0216	365	4.26	0.009

TABLE C2* : ADSORPTION AND DIFFUSION DATA FOR HM WITH D_z REDUCED BY 20% IN THE R_x MODEL.

Run ID	D_z	K_c	D_c x 10^9 cm^2/sec	error
MMR-0	0.076	31.8	40.9	0.004
MMR-1	0.084	28.3	121	0.004
MMR-2	0.096	26.6	308	0.001
MMR-3	0.128	32.0	308	0.004
MMR-4	0.158	31.4	488	0.003
MMR-5	0.193	31.3	627	0.010
MMR-6	0.231	30.9	663	0.025
MMR-7	0.283	29.9	778	0.001
PMR-0	0.107	703	9.69	0.013
PMR-1	0.161	827	10.6	0.016
PMR-2	0.238	827	13.8	0.012
PMR-3	0.359	780	15.5	0.016
PMRL-0	0.261	5286	1.77	0.027
PMRH-0	0.229	185	42.0	0.027

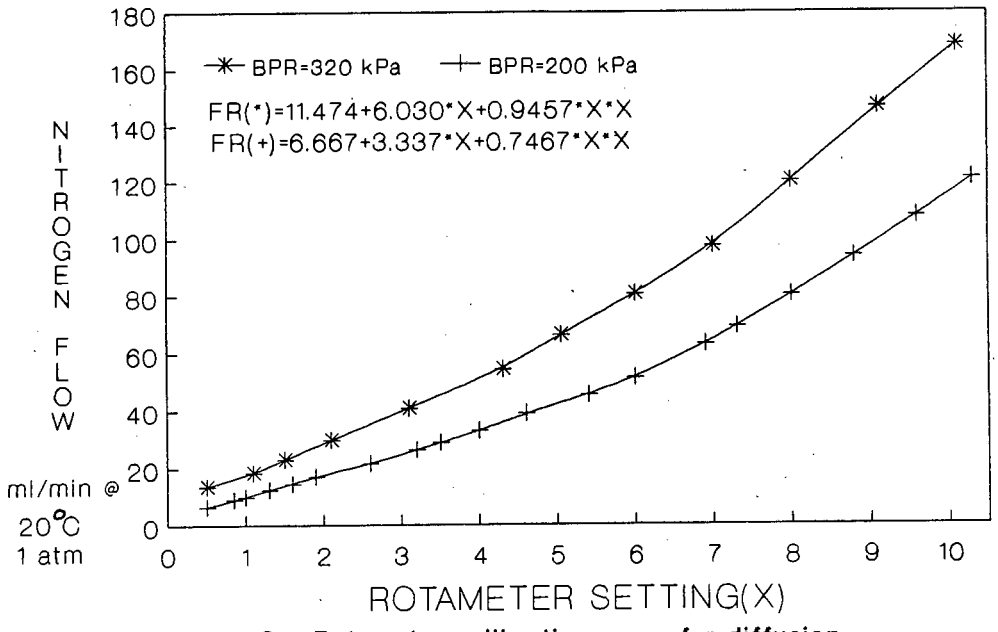

Figure C1 : Rotameter calibration curve for diffusion apparatus.

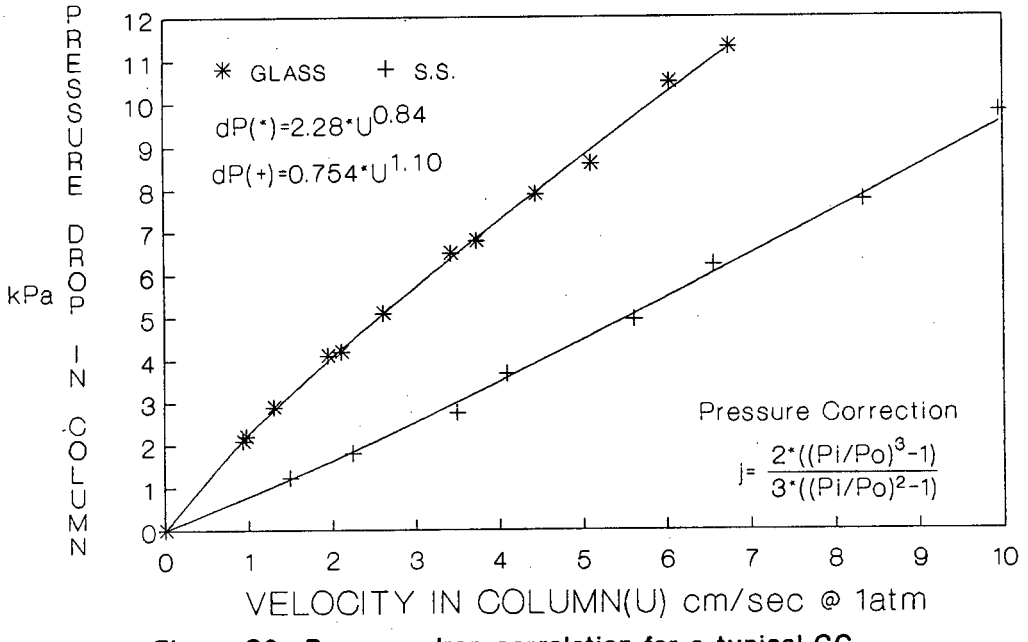

Figure C2 : Pressure drop correlation for a typical GC column

APPENDIX D

TABLE D1 : CALIBRATION OF NH_3/He FEED GAS.

No.	Time min	Flowrate ml/min	Volume H_2SO_4 ml	Volume NaOH ml	V_{gas} ml	mmol NH_3	mol% NH_3
1	30	61.0	100	70.45	1788	3.26	3.93
2	30	60.7	"	70.55	1779	3.34	4.04
3	30	60.8	"	42.65	1782	3.46	4.17
4	32	60.7	75	67.75	1898	3.58	4.06
5	30	60.7	100	68.15	1779	3.54	4.27
6	30	60.7	"	70.25	1779	3.34	4.04
7	30	60.7	"	70.05	1779	3.36	4.06
							4.08 ±0.10

V_{gas} corrected for saturated water vapour at 20°C(17.5mmHg)

$$V_{gas}=V_{gas}*(760-17.5)/760 = 0.977*V_{gas}$$

$$\%NH_3 = \frac{\text{mmol } NH_3}{V_{gas}/22.414 + \text{mmol } NH_3} \times 100$$

C_o=0.00182 mmol/ml

Concentration H_2SO_4 = 0.1N

Concentration NaOH = 0.095N